Matematisk-fysiske Meddelelser
udgivet af
Det Kongelige Danske Videnskabernes Selskab
Bind **32,** nr. 1

Mat. Fys. Medd. Dan. Vid. Selsk. **32,** no. 1 (1959)

# THE STRUCTURE OF CÆSIUM PLUMBO IODIDE $CsPbI_3$

BY

CHRISTIAN KN. MØLLER

København 1959
i kommission hos Ejnar Munksgaard

## Synopsis

$CsPbI_3$ is obtained from aqueous solutions as yellow, orthorhombic crystals belonging to space group No. 62 Pmnb. The unit cell contains 4 molecules, and $a = 4.797$ Å, $b = 10.46_2$ Å, $c = 17.78_8$ Å. Heated to 305—308° C. these crystals are transformed into a black modification which has a monoclinically distorted perovskite-like structure: $a = b = 6.15_2$ Å, $c = 6.22_8$ Å, $\beta = 88.^{\circ}1_5$. *X*-ray analysis by Fourier methods of the yellow crystals shows that distorted $PbI_6$-octahedra sharing I-atoms form one-dimensional, polynuclear complex ions, $(PbI_3^-)_n$, running parallel to the *a*-axis. The Pb-I distances vary from 3.01 Å to 3.42 Å. Nine I-atoms belonging to three different complex ions of this type are nearly di-trigonally arranged around each Cs-atom, with CsI-distances 3.87—4.19 Å. This structure is analogous to that of $M^1CdCl_3$.



Printed in Denmark
Bianco Lunos Bogtrykkeri A-S

## Introduction

Divalent lead is known to form complex ions with the halogen ions which together with alkali metal ions give compounds of the general compositions[1, 2]

$$M^{I}_{4}PbX_6, \quad M^{I}PbX_3, \quad \text{and} \quad M^{I}Pb_2X_5.$$

Some of these compounds crystallize with crystal water—apparently the size of the alkali metal ion is of importance in this connection—but the Cs-salts, as far as they are known, form crystals which do not contain water.

From an interest in the stereochemistry of divalent lead in simple compounds it was decided to investigate some of these crystals, as, with spherical anions all of the same kind and no water in the lattice, one might hope to discover the "intrinsic" symmetry of the $Pb^{++}$-ion and also obtain reliable interatomic distances.

It is true that the $PbX_2$-compounds have been investigated long ago,[3] but only $PbBr_2$ and $PbCl_2$ are similarly built, and they have rather unusual structures, from which it seems difficult to extract information about the symmetry of the electronic arrangement in the $Pb^{++}$-ion in general. Also compounds of the type $MPb_2X_5$ have been investigated by Powell and Tasker[4] and will not be discussed here; suffice it to say that these authors find that in crystals of $RbPb_2Br_5$ there are chains of $Rb^+$ and $Br^-$-ions, whereas the Pb-atoms tend to form molecules $PbBr_2$ with interatomic distances $r_{Pb-Br} = 2.89 \pm 0.04$ Å.

In this paper the structure of $CsPbI_3$ will be described. The structures of $CsPbCl_3$, $CsPbBr_3$, and $Cs_4PbCl_6$ will be dealt with in later publications.

[1] N. V. Sidgwick, *Chemical elements and their compounds.* Vol. I p. 626. Oxford Univ. Press.

[2] Gmelin-Kraut, *Handbuch d. anorg. Chemie.* IV. Band, 2. Teil, pp. 358, 376, 551, 555.

[3] See e. g. R. W. G. Wyckoff, *Crystal Structures.* Volume I. Interscience Publishers, New York 1948, where references can be found. See also A. F. Wells, *Structural inorganic chemistry.* Oxford 1945. Chapters 8 and 16.

[4] H. M. Powell and H. S. Tasker, *J. Chem. Soc.* London 1937, p. 113.

## Preparation

According to H. L. WELLS and coworkers[5] yellow crystals of composition $CsPbI_3$ can be obtained by dissolving $PbI_2$ in a hot aqueous solution of CsI and then leaving it to cool. As $PbI_2$ is only slightly soluble in a CsI solution only poor yields can be obtained in this way. Accidentally it was found that yellow crystals with composition $CsPbI_3$ can be obtained by the following procedure: $PbBr_2$ is dissolved in a hot, rather concentrated solution of CsBr and CsI (in about equal amounts, but apparently this is not important). On addition of water to this solution small yellow needle- or lath-shaped crystals precipitate. Qualitative tests on these crystals for Cs, Pb, and I were all positive. Instead of making a quantitative analysis the composition has been ascertained in the following way. Equimolar quantities of very pure CsI and $PbI_2$ after weighing have been fused in a crucible and cooled. The black reaction product changes to a yellow substance during some hours without change in weight, and the latter gives the same *X*-ray powder diagram as that obtained from powders of the yellow crystals precipitated in aqueous solution.

## Properties and polymorphism

The yellow $CsPbI_3$ crystals are very slowly decomposed by water under precipitation of $PbI_2$. Under the polarizing microscope they show birefringence and parallel extinction. When heated on a hot stage under the microscope they can be seen to undergo a phase change at 305—308° C.: the crystals become black and lose their transparency. When the product is left to cooling again the yellow crystals reappear, but only slowly, and in fact it has been possible to undercool the black substance to room temperature for several days before the yellow crystals appeared again.

When equimolar quantities of CsI and $PbI_2$ are fused together a deep purple liquid is obtained which solidifies to a black graphite-like mass. Left to itself in the open air this black substance changes to the yellow form of $CsPbI_3$, and no change in weight can be observed. When kept in a desiccator the black form can sometimes be preserved for several months so that it looks as if the humidity in the air has a catalytic effect on the transformation. If the black form is heated to temperatures a little above 310° C. it gradually changes to another yellow product, which has a different crystal structure, but it has not been further investigated.

[5] H. L. WELLS, *Z. anorg. Chem.* **3**, 195 (1893).

## *X*-ray examination. Unit cell dimensions

*X*-ray powder diagrams of crushed yellow $CsPbI_3$-crystals obtained from aqueous solutions and the low temperature yellow conversion product of black $CsPbI_3$ from the melt were taken in a Guinier type focusing camera with monochromatic $CuK_\alpha$-radiation and were found to be identical within the accuracy of our measurements. In order to obtain accurate $\sin^2\vartheta$-values powdered NaCl was added to the powder specimen and a calibration curve was drawn each time from which corrections to the measured $\sin^2\vartheta$-values could be obtained (Table 1). As the black form of $CsPbI_3$ is not very stable its *X*-ray powder diagram was obtained on a GE XRD-3 diffractometer. The substance was melted on a stainless steel holder, brought into position

TABLE 1. Observed and calculated $\sin^2\vartheta$-values for yellow $CsPbI_3$. $CuK_\alpha$-radiation

| Indices | Estimated intensity | $10^4\cdot\sin^2\vartheta$ obs. | $10^4\cdot\sin^2\vartheta$ calc. | Indices | Estimated intensity | $10^4\cdot\sin^2\vartheta$ obs. | $10^4\cdot\sin^2\vartheta$ calc. |
|---|---|---|---|---|---|---|---|
| 011 | m | 0072 | 0073 | 042 | vw? | 0943 | 0944.5 |
| 002 | m | 0075 | 0075 | 125 | | | 0944 |
| 012 | m-s | 0129 | 0129 | 035 | vw; diff. | 0959 | 0958 |
| 020 | vw? | 0217 | 0217 | 116 | w | 0988 | 0988 |
| 013 | vw | 0223 | 0223 | 200 | m; diff. | 1031 | 1033 |
| 021 | w | 0236 | 0236 | 134 | m | 1045 | 1047 |
| 022 | vw? | 0293 | 0292 | 027 | vw | 1137 | 1137 |
| 111 | s-m | 0332 | 0331 | 142 | w-m | 1202 | 1202 |
| 014 | m | 0355 | 0355 | 008 | | | |
| 023 | m-s | 0387 | 0386 | 117 | m-s | 1232 | 1232 |
| 120 | w | 0475 | 0475 | 143 | w | 1296 | 1296 |
| 113 | m-s | 0481 | 0481 | 037 | vw; diff. | 1412 | 1409 |
| 121 | s | 0494 | 0494 | 052 | vw | 1432 | 1433 |
| 024 | w-m | 0518 | 0518 | 118 | vw? | 1513 | 1514 |
| 015 | m | 0524 | 0524 | 215 | w-m, br | 1553 | 1551 |
| 122 | vs | 0550 | 0550 | 224 | | | 1556 |
| 123 | vw | 0644 | 0644 | 232 | vw | 1596 | 1597 |
| 105 | m-s, diff. | 0728 | 0727.5 | 145 | | | 1596.5 |
| 016 | | | 0730 | 216 | vw | 1760 | 1763 |
| 131 | vw | 0765 | 0766 | 154 | vw, br, diff. | 1918 | 1916 |
| 034 | (v)w | 0789 | 0789 | 241 | | | 1921 |
| 132 | m | 0821 | 0822 | 048 | w | 2068 | 2071 |
| 133 | vw | 0915 | 0916 | 313 | vw, br, diff | 2550 | 2548 |
| | | | | 322 | vw, br, diff | 2616 | 2615 |

br = broad, diff = diffuse, m = medium, s = strong, v = very, w = weak.

while still hot (~200° C.), and during the following hours several runs were made of the powder diagram of the same sample. Immediately after mounting, the specimen gave a very simple diagram, but this gradually changed and finally—usually after two hours—a diagram characteristic of the yellow $CsPbI_3$ was obtained. Simultaneously the colour of the specimen had changed from black to dirty yellow. From the accurate $\sin^2\vartheta$-values

TABLE 2. Observed and calculated $\sin^2\vartheta$-values for black $CsPbI_3$. $CuK_\alpha$-radiation

| Indices | Estimated intensity | $10^4 \cdot \sin^2\vartheta$ obs. | $10^4 \cdot \sin^2\vartheta$ calc. | Indices | Estimated intensity | $10^4 \cdot \sin^2\vartheta$ obs. | $10^4 \cdot \sin^2\vartheta$ calc. |
|---|---|---|---|---|---|---|---|
| 001 | s | 0164 | 0153 | 102 | vw | 0791 | 0785 |
| 100 | | | 0157 | 210 | | | 0790 |
| 101 | w-m | 0307 | 0300 | 112 | vw | 0912 | 0907 |
| 011 | | | 0310 | $11\bar{2}$ | vw | 0948 | 0947 |
| 110 | | | 0314 | 121 | | | |
| $10\bar{1}$ | (v)w | 0327 | 0320 | 202 | w-m | 1206 | 1201 |
| $\frac{1}{2}\,\frac{3}{2}\,\frac{1}{2}$ | (v)w | 0438 | 0431 | 022 | w-m | 1234 | 1241 |
| 111 | w-m | 0454 | 0457 | $20\bar{2}$ | w | 1285 | 1281 |
| $11\bar{1}$ | w-m | 0475 | 0477 | 212 | w | 1362 | 1358 |
| $\frac{1}{2}\,\frac{3}{2}\,1$ | (v)w | 0548 | 0546 | 222 | w-m | 1816 | 1829 |
| 002 | s | 0613 | 0613 | $22\bar{2}$ | w | 1899 | 1909 |
| 020 | vs | 0628 | 0628 | 004 | vw | 2445 | 2451 |
| $\frac{3}{2}\,\frac{3}{2}\,0$ | vw | 0714 | 0707 | 400 | vw | 2515 | 2512 |

obtained for the yellow $CsPbI_3$ in the Guinier camera a calibration was made for the diffractometer readings and so $\sin^2\vartheta$-values could be determined for the black variety, too. However, the accuracy of the latter $\sin^2\vartheta$-values is not high as the scanning had to be fast (Table 2).

Oscillation and Weissenberg diagrams were also taken of single crystals of the yellow $CsPbI_3$ and orthorhombic symmetry was established for these crystals. Preliminary values of the axes were determined from these photographs (camera diameter: 57.3 mm), and were used as basis of a first indexing of the powder photographs. By trial and error refined values were finally obtained from the quadratic form:

$$\sin^2\vartheta = 0.02583\, h^2 + 0.005430\, k^2 + 0.001878\, l^2, \qquad (1)$$

which gave satisfactory agreement between observed and calculated $\sin^2\vartheta$-values (Table 1).

The unit-cell dimensions derived from the coefficients in (1) are with $\lambda(\mathrm{CuK}_\alpha) = 1.5418$ Å:

$$a = 4.797 \pm 0.005 \text{ Å}; \quad b = 10.46_2 \pm 0.01 \text{ Å}; \quad c = 17.78_8 \pm 0.02 \text{ Å}.$$

Unit-cell volume: $892._3$ Å$^3$. Molar volume of unit cell: $892._3 10^{-24} \cdot 6.0228 \cdot 10^{23} = 537.4$ cm$^3$.

The strongest lines on the powder diagram of the black $CsPbI_3$ indicated a tetragonal lattice with cell dimensions $a = 6.15$ Å, $c = 6.23$ Å. But in order to account for the observed splittings of the weaker lines, it proved necessary to use a monoclinic quadratic form:

$$\sin^2\vartheta = 0.01570\,(h^2 + k^2) + 0.01532\,l^2 - 0.0010\,h\,l \qquad (2)$$

corresponding to a unit cell with dimensions:

$$a = b = 6.15_2 \pm 0.03 \text{ Å}; \quad c = 6.22_8 \pm 0.03 \text{ Å}; \quad \beta = 88.^\circ15 \pm 0.^\circ5.$$

Unit-cell volume: $235._6$ Å$^3$. Molar volume of unit cell: $235._6 \cdot 10^{-24} \cdot 6.0228 \cdot 10^{23} = 141._9$ cm$^3$.

Even so a few (very) weak lines still persisted and it seems only possible to include them in the above indexing by assuming a doubling of the cell dimensions. A similar doubling has also been found in the perovskite-like crystals of $CsPbBr_3$ and can there be explained in terms of a superstructure.[6] It seems reasonable that the same explanation applies to $CsPbI_3$ as well.

For convenience the black form of $CsPbI_3$ will be referred to the small monoclinic unit cell with the dimensions given above—although this monoclinic indexing is not quite without ambiguities, mainly due to inaccurate data. The weak lines, which require a doubling of cell dimensions, therefore appear with fractional indices in Table 2.

The molar volumes of CsI and $PbI_2$ calculated from the molecular weights and the density of the crystals of CsI and $PbI_2$ are 57.6 cm$^3$ and 74.8 cm$^3$, respectively. Assuming additivity of molar volumes, we should expect a crystal molar volume 132.4 cm$^3$ for $CsPbI_3$ or on an average a volume $132.4 \div 6.0228 \cdot 10^{23} = 219._8$ Å$^3$ per single molecule of $CsPbI_3$. From this we infer that the yellow $CsPbI_3$ has four molecules in the unit

[6] C. K. Møller, *Nature* **182**, 1436 (1958).

cell, whereas the black variety has only one in the small unit cell referred to above.

The black $CsPbI_3$ thus appears to have a monoclinically distorted perovskite structure and the intensity distribution on the powder diagram lends further support to this statement. As the general features of this type of structure will be discussed in another paper this modification will not be further considered here.

## Space group of the yellow $CsPbI_3$

Weissenberg diagrams were taken of a single crystal of yellow $CsPbI_3$, 45 $\mu$ thick, of nearly circular cross section, length 0.10 mm. Visually estimated intensities were obtained by a multiple film technique and by using an intensity scale, prepared by taken a series of photographs of a strong reflection with increasing exposure times. When taking diagrams for intensity measurements, care was taken to keep film material, temperature, developer, fixer, *X*-ray intensity, and speed of the Weissenberg goniometer as constant as possible. The absorption has been neglected, or rather, it has been included in the isotropic part of the temperature factor, as it turns out that these two factors nearly cancel for the zeroth layer line.[7] Otherwise the usual corrections for polarization and Lorentz-factors have been applied[8] and approximate relative $|F(hkl)|^2$-values thus obtained. With the orthorhombic unit cell given above it was found that reflections of the type h0l were only present for $h+l$ even and similarly hk0 only for $k$ even, whereas 0kl and hkl in general were not subjected to any systematic restrictions. These conditions are characteristic of space group No. 62 Pmnb and No. 33 $P2_1nb$.[9]

Furthermore, alternating layer lines taken about the $a$-axis were found to be identical, showing that $|F(h+2n, k, l)| = |F(hkl)|$, where $n$ is an integer. This shows that the scattering matter must lie in planes separated by the distance $\frac{a}{2}$. The space group No. 62, with 4 molecules per unit cell and with the atoms in special positions, does in fact require intensity relations of the type observed, whereas No. 33 does not. Hence there is strong evidence for space group No. 62 with all the atoms in special positions $a$, $b$, or $c$.

[7] Compare C. W. Bunn, *Chemical Crystallography*, p. 207. Oxford Univ. Press 1946.
[8] W. Cochran, *J. Sci. Instr.* **25**, No. 7 (1948).
[9] *Internat. Tables for X-Ray Cryst.* I. London 1952.

## Patterson and electron projections

A Patterson projection on the *bc*-plane was next calculated on a Hägg-Laurent Fourier machine[10] from the observed $|F(hkl)|^2$. The appearance of this projection showed that the special positions designated *a* and *b* in Ref. 9, p. 151, under space group No. 62 could be ruled out, as these po-

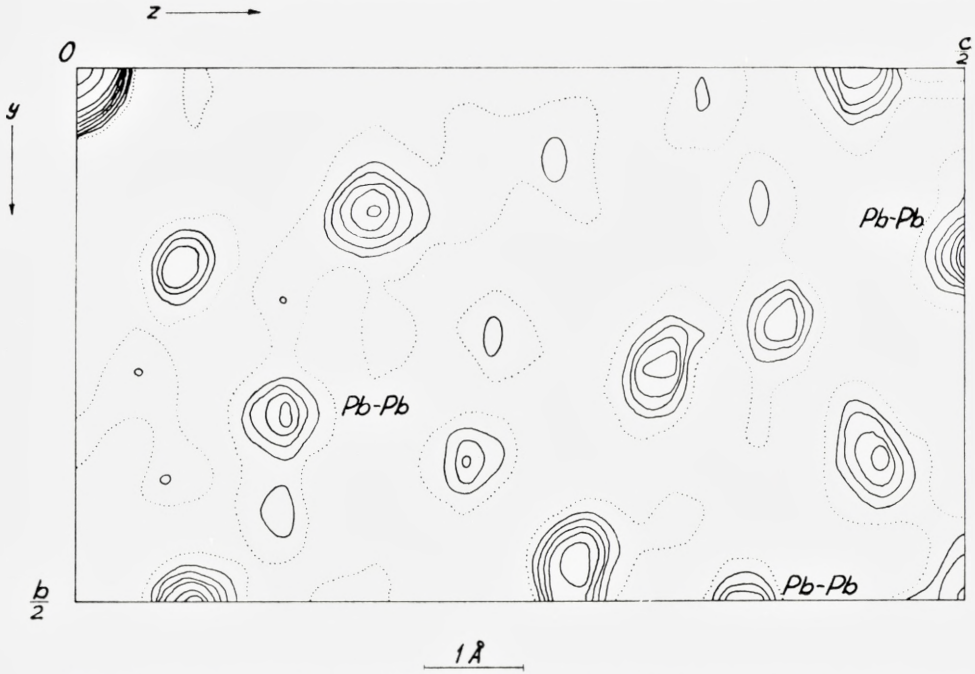


Fig. 1. Patterson projection of yellow $CsPbI_3$ on the *bc*-plane. Contour lines are drawn at the relative densities 0, 40, 60, 80, 100, 125, 150, 200, 600, 800.

sitions require high vector densities on the projection in places where either no such peaks appear or only rather small peaks show up. (Fig. 1).

We are thus left with the special positions *c*:

$$\left(\frac{1}{4}, y, z\right); \quad \left(\frac{3}{4}, \bar{y}, \bar{z}\right), \quad \left(\frac{3}{4}, \frac{1}{2}-y, \frac{1}{2}+z\right), \quad \left(\frac{1}{4}, \frac{1}{2}+y, \frac{1}{2}-z\right) \tag{3}$$

for the 5·4 atoms. It can easily be seen that e.g. four Pb-atoms in these positions give rise to vector peaks on the Patterson projection on the *bc*-plane in

[10] V. Frank, *J. Sci. Instr.* **34**, 210 (1957).

$$\left(0, \frac{1}{2}, \frac{1}{2} \pm 2z\right) \quad \left(0, \frac{1}{2} \pm 2y, \frac{1}{2}\right) \quad (0, 2y, \pm 2z). \tag{4}$$

Therefore the three strongest peaks on the Patterson projection which fulfil the relations expressed in (4), having been found, they were identified as Pb-Pb-maxima and the parameters $y$ and $z$ for the Pb-atoms could be determined straightforwardly, $(x, y, z) = \left(\pm\frac{1}{4}, 0.163, 0.059\right)$.

As the structure has a centre of symmetry in O, the structure factors all have phase angles 0 or $\pi$ so that $F(hkl) = \pm |F(hkl)|$. We must determine these signs before a calculation of an electron projection can be undertaken. Hence the following considerations.

The highest measured $|F|$-value is that of 039. With the Pb-parameters obtained above the contribution from Pb to this structure factor is found to be nearly maximum and positive. If we assume that all the atoms in the unit cell give nearly maximum positive contributions to this structure factor a rough estimate shows that all the structure factors not less than half of F (039) must have the same sign as the Pb-contribution alone, provided that the latter is appreciable. In this way signs were unambiguously determined for 16 structure factors. An electron projection calculated on the basis of these sixteen structure factors together with the Patterson projection gave the parameters of two I-atoms, and then signs could be obtained for 46 structure factors by a reasoning similar to that above. A second electron projection with these terms next revealed all the atoms so that all the parameters could now be determined and structure factors calculated. With signs obtained from this last calculation all the experimentally determined structure factors were finally used in a third calculation of the electron projection on the $yz$-plane (fig. 2).

New structure factors calculated from atomic scattering factors corrected for dispersion effects[11] and the atomic parameters from this last projection were brought on an absolute scale by plotting $\log_{10}\left|\frac{F_{obs.}}{F_{calc.}}\right|$ versus $\sin^2\vartheta$. As, theoretically,[12] $F(\vartheta)_{obs.} = A \cdot F(\vartheta)_{calc.} \cdot \exp(-B\sin^2\vartheta)$ this plotting should approximately give a straight line with slope -B and intersect the ordinate

[11] Atomic scattering factors were taken from W. H. Bragg and W. L. Bragg, *The Crystalline State* Vol. I, pp. 330—333 (London 1949), and corrections for dispersion effects from C. H. Dauben and D. H. Templeton, *Acta Cryst.* 8, 841 (1955). See also R. W. James, *Optical Principles of X-Rays*, p. 608 (London 1948).

[12] H. Lipson and W. Cochran, *Determination of Crystal Structures*, p. 61. London 1953.


Fig. 2. Electron projection of yellow $CsPbI_3$ on the *bc*-plane. Contour lines are drawn at the relative electron densities 0, 100, 200, 300, 400, 500, and 600.

axis in $\log A$, thus providing the conversion factor $\frac{1}{A}$. (It has then been assumed that the effect of absorption can be included in the exponential term, the "temperature factor".[13] For the zeroth layer line we find in this way $B \simeq 0$).

Having brought observed and calculated F's on the same absolute scale corresponding to $F(000) = 288.8$, a difference synthesis was calculated from $F(0\,kl)_{obs.} - F(0\,kl)_{calc.}$ and corrections to the atomic parameters obtained from

$$\Delta r = \left\{\frac{\partial\,(\varrho_{obs.} - \varrho_{calc.})}{\partial r}\right\}_{r=r_0} \Big/ \left\{\frac{\partial^2 \varrho_{obs.}}{\partial r^2}\right\}_{r=r_0},$$

[13] Ref. 7. See also B. JERSLEV, *Studier over Oximernes Struktur*, p. 25—26. Dissertation, Copenhagen 1958.

where approximate values for the denominators were estimated from the last electron projection ($\varrho_{obs.}$) and for the numerators from the difference projection ($\varrho_{obs.} - \varrho_{calc.}$). After these corrections had been applied to the atomic parameters, a definite improvement in the agreement between observed and calculated structure factors was obtained. (For the observed F-values $R$ decreased from 0.17 to 0.11). Further refinement was not attempted, as we did not consider our measured intensities accurate enough for this purpose.

In order to ascertain the $x$-parameters $\left(\pm\frac{1}{4}\right)$ the structure factors for the first layer line were also measured and calculated. Although a reasonably good agreement is obtained also in this case, it is not quite so good as for the zero-th layer line—presumably due to the neglect of absorption, which is more serious for the non-zero layer lines. (Table 3).

TABLE 3. Comparison of calculated and observed structure factors for yellow $CsPbI_3$

(brought on an absolute scale corresponding to F(000) = 289)

| Indices | | 0. layer line $h = 0$ | | 1. layer line $h = 1$ | | Indices | | 0. layer line $h = 0$ | | 1. layer line $h = 1$ | |
|---|---|---|---|---|---|---|---|---|---|---|---|
| $k$ | $l$ | $F_{calc.}$ | $\lvert F_{obs.}\rvert$ | $F_{calc.}$ | $\lvert F_{obs.}\rvert$ | $k$ | $l$ | $F_{calc.}$ | $\lvert F_{obs.}\rvert$ | $F_{calc.}$ | $\lvert F_{obs.}\rvert$ |
| 2 | 0 | $\overline{22}$ | 27 | 54 | 40 | 1 | 5 | $\overline{118}$ | 97 | $\overline{12}$ | |
| 4 | 0 | $\overline{49}$ | 39 | $\overline{52}$ | 45 | 1 | 6 | 85 | 73 | 53 | 43 |
| 6 | 0 | 77 | 83 | $\overline{22}$ | | 1 | 7 | $\overline{39}$ | 42 | $\overline{111}$ | 128 |
| 8 | 0 | $\overline{64}$ | 58 | 154 | 135 | 1 | 8 | $\overline{46}$ | 51 | 55 | 53 |
| 10 | 0 | $\overline{24}$ | 25 | 3 | | 1 | 9 | 13 | | $\overline{59}$ | 58 |
| 12 | 0 | 46 | 35 | $\overline{13}$ | | 1 | 10 | 0 | | $\overline{86}$ | 85 |
| 0 | 2 | 37 | 28 | | | 1 | 11 | $\overline{53}$ | 53 | $\overline{49}$ | 53 |
| 0 | 4 | 20 | 16 | | | 1 | 12 | $\overline{66}$ | 83 | $\overline{39}$ | 60 |
| 0 | 6 | 21 | 18 | | | 1 | 13 | $\overline{43}$ | 50 | $\overline{19}$ | |
| 0 | 8 | $\overline{33}$ | 37 | | | 1 | 14 | $\overline{47}$ | 44 | 10 | |
| 0 | 10 | 43 | 35 | | | 1 | 15 | 18 | 35 | 10 | |
| 0 | 12 | 8 | | | | 1 | 16 | 35 | 35 | $\overline{9}$ | |
| 0 | 14 | 39 | 51 | | | 1 | 17 | 17 | 25 | 16 | |
| 0 | 16 | 64 | 64 | | | 1 | 18 | $\overline{12}$ | | 26 | |
| 0 | 18 | 115 | 120 | | | 1 | 19 | 3 | | 19 | |
| 0 | 20 | 3 | | | | 1 | 20 | 47 | 48 | $\overline{4}$ | |
| 1 | 1 | 23 | 27 | 39 | 28 | 1 | 21 | | | $\overline{64}$ | 70 |
| 1 | 2 | 37 | 32 | 6 | | 2 | 1 | 22 | 23 | $\overline{98}$ | 133 |
| 1 | 3 | 15 | 15 | $\overline{73}$ | 60 | 2 | 2 | $\overline{17}$ | 20 | 131 | 110 |
| 1 | 4 | 40 | 39 | $\overline{4}$ | | 2 | 3 | 60 | 57 | $\overline{33}$ | 28 |

(To be continued)

TABLE 3 (continued)

| Indices | | 0. layer line $h = 0$ | | 1. layer line $h = 1$ | | Indices | | 0. layer line $h = 0$ | | 1. layer line $h = 1$ | |
|---|---|---|---|---|---|---|---|---|---|---|---|
| $k$ | $l$ | $F_{calc.}$ | $\lvert F_{obs.}\rvert$ | $F_{calc.}$ | $\lvert F_{obs.}\rvert$ | $k$ | $l$ | $F_{calc.}$ | $\lvert F_{obs.}\rvert$ | $F_{calc.}$ | $\lvert F_{obs.}\rvert$ |
| 2 | 4 | $\overline{93}$ | 87 | 25 | 18 | 4 | 2 | $\overline{52}$ | 48 | $\overline{75}$ | 75 |
| 2 | 5 | 26 | 23 | $\overline{5}$ | | 4 | 3 | $\overline{105}$ | 99 | $\overline{70}$ | 65 |
| 2 | 6 | 12 | | $\overline{37}$ | 35 | 4 | 4 | $\overline{38}$ | 39 | 23 | 28 |
| 2 | 7 | 74 | 74 | $\overline{3}$ | | 4 | 5 | $\overline{50}$ | 50 | $\overline{31}$ | 23 |
| 2 | 8 | 38 | 41 | 26 | 18 | 4 | 6 | $\overline{29}$ | 30 | $\overline{45}$ | 50 |
| 2 | 9 | $\overline{17}$ | | 27 | 20 | 4 | 7 | 44 | 43 | 29 | 33 |
| 2 | 10 | $\overline{3}$ | | $\overline{5}$ | | 4 | 8 | 41 | 55 | 48 | 55 |
| 2 | 11 | $\overline{113}$ | 102 | $\overline{24}$ | 30 | 4 | 9 | $\overline{20}$ | | $\overline{6}$ | |
| 2 | 12 | 9 | | 11 | | 4 | 10 | 30 | 34 | 48 | 43 |
| 2 | 13 | 6 | | 25 | | 4 | 11 | 21 | | $\overline{4}$ | |
| 2 | 14 | $\overline{91}$ | 101 | 52 | 68 | 4 | 12 | $\overline{59}$ | 67 | $\overline{92}$ | 90 |
| 2 | 15 | $\overline{41}$ | 35 | 21 | | 4 | 13 | 31 | | 25 | 35 |
| 2 | 16 | $\overline{4}$ | | 80 | 85 | 4 | 14 | $\overline{33}$ | 39 | $\overline{15}$ | 25 |
| 2 | 17 | 13 | | 21 | | 4 | 15 | $\overline{43}$ | 48 | 34 | 35 |
| 2 | 18 | 4 | | 38 | 40 | 4 | 16 | $\overline{41}$ | 43 | $\overline{65}$ | 73 |
| 2 | 19 | 49 | 53 | 53 | 60 | 4 | 17 | $\overline{31}$ | 34 | $\overline{15}$ | |
| 2 | 20 | $\overline{34}$ | 37 | 41 | 28 | 4 | 18 | $\overline{24}$ | 23 | $\overline{39}$ | 30 |
| 2 | 21 | | | $\overline{31}$ | 28 | 4 | 19 | $\overline{21}$ | 21 | $\overline{26}$ | 20 |
| 3 | 1 | 20 | 21 | 33 | 40 | 4 | 20 | $\overline{7}$ | | 2 | |
| 3 | 2 | $\overline{72}$ | 66 | $\overline{63}$ | 60 | 4 | 21 | | | $\overline{37}$ | 43 |
| 3 | 3 | $\overline{24}$ | 25 | $\overline{41}$ | 43 | 5 | 1 | 30 | 28 | 30 | |
| 3 | 4 | 63 | 60 | $\overline{100}$ | 95 | 5 | 2 | $\overline{89}$ | 92 | $\overline{51}$ | 58 |
| 3 | 5 | 64 | 69 | $\overline{23}$ | 20 | 5 | 3 | $\overline{24}$ | 28 | $\overline{26}$ | 25 |
| 3 | 6 | $\overline{8}$ | | 19 | | 5 | 4 | $\overline{44}$ | 46 | 75 | 63 |
| 3 | 7 | 73 | 78 | 31 | 40 | 5 | 5 | $\overline{54}$ | 55 | 42 | 43 |
| 3 | 8 | 5 | | $\overline{6}$ | | 5 | 6 | $\overline{4}$ | | $\overline{9}$ | |
| 3 | 9 | 146 | 147 | $\overline{41}$ | 40 | 5 | 7 | 19 | | 91 | 88 |
| 3 | 10 | 3 | | 32 | 48 | 5 | 8 | $\overline{12}$ | | 21 | |
| 3 | 11 | 43 | 39 | 30 | 38 | 5 | 9 | $\overline{66}$ | 71 | 85 | 80 |
| 3 | 12 | $\overline{28}$ | | 28 | 33 | 5 | 10 | 33 | 35 | $\overline{22}$ | |
| 3 | 13 | 7 | | $\overline{15}$ | | 5 | 11 | 16 | | 60 | 65 |
| 3 | 14 | $\overline{6}$ | | 44 | 78 | 5 | 12 | 21 | | $\overline{34}$ | 35 |
| 3 | 15 | $\overline{5}$ | | $\overline{38}$ | 35 | 5 | 13 | $\overline{17}$ | | $\overline{10}$ | |
| 3 | 16 | 31 | 35 | 40 | 63 | 5 | 14 | 37 | 46 | $\overline{9}$ | |
| 3 | 17 | $\overline{11}$ | | 55 | 60 | 5 | 15 | $\overline{34}$ | 39 | $\overline{29}$ | 35 |
| 3 | 18 | 3 | | $\overline{50}$ | 60 | 5 | 16 | 42 | 35 | 16 | |
| 3 | 19 | 40 | 32 | $\overline{13}$ | | 5 | 17 | 63 | 60 | 21 | |
| 3 | 20 | $\overline{36}$ | 37 | $\overline{36}$ | 43 | 5 | 18 | $\overline{39}$ | 37 | 17 | |
| 3 | 21 | | | $\overline{20}$ | | 5 | 19 | $\overline{23}$ | | 18 | |
| 4 | 1 | 38 | 34 | $\overline{3}$ | | 5 | 20 | $\overline{56}$ | 58 | $\overline{32}$ | 33 |

(To be continued)

TABLE 3 (continued)

| Indices | | 0. layer line $h = 0$ | | 1. layer line $h = 1$ | | Indices | | 0. layer line $h = 0$ | | 1. layer line $h = 1$ | |
|---|---|---|---|---|---|---|---|---|---|---|---|
| $k$ | $l$ | $F_{calc.}$ | $\lvert F_{obs.}\rvert$ | $F_{calc.}$ | $\lvert F_{obs.}\rvert$ | $k$ | $l$ | $F_{calc.}$ | $\lvert F_{obs.}\rvert$ | $F_{calc.}$ | $\lvert F_{obs.}\rvert$ |
| 5 | 21 | | | 6 | | 8 | 2 | 14 | | 35 | 33 |
| 6 | 1 | $\overline{57}$ | 60 | 47 | 60 | 8 | 3 | 4 | | 2 | |
| 6 | 2 | 91 | 85 | 22 | 28 | 8 | 4 | $\overline{14}$ | | 3 | |
| 6 | 3 | $\overline{11}$ | | 28 | 45 | 8 | 5 | 84 | 80 | $\overline{34}$ | |
| 6 | 4 | 41 | 46 | $\overline{56}$ | 55 | 8 | 6 | $\overline{14}$ | | 8 | |
| 6 | 5 | $\overline{9}$ | | 31 | 35 | 8 | 7 | 27 | | 9 | |
| 6 | 6 | $\overline{42}$ | 39 | 20 | | 8 | 8 | 27 | 25 | $\overline{14}$ | |
| 6 | 7 | 21 | 30 | 68 | 65 | 8 | 9 | $\overline{23}$ | | 11 | |
| 6 | 8 | 14 | | 41 | 53 | 8 | 10 | $\overline{10}$ | | 26 | |
| 6 | 9 | 16 | | $\overline{32}$ | 23 | 8 | 11 | $\overline{32}$ | 39 | $\overline{19}$ | |
| 6 | 10 | 15 | | 12 | 23 | 8 | 12 | $\overline{19}$ | | $\overline{7}$ | |
| 6 | 11 | $\overline{50}$ | 43 | $\overline{63}$ | 68 | 8 | 13 | $\overline{78}$ | 71 | 46 | 40 |
| 6 | 12 | $\overline{15}$ | | 1 | | 8 | 14 | $\overline{19}$ | | 27 | 20 |
| 6 | 13 | 34 | 39 | $\overline{17}$ | | 8 | 15 | $\overline{36}$ | 34 | $\overline{16}$ | 20 |
| 6 | 14 | 78 | 76 | $\overline{55}$ | 63 | 8 | 16 | $\overline{3}$ | | 60 | 68 |
| 6 | 15 | 3 | | $\overline{12}$ | | 8 | 17 | 20 | | | |
| 6 | 16 | 66 | 71 | 16 | | 9 | 1 | $\overline{18}$ | | 3 | |
| 6 | 17 | 18 | | 4 | | 9 | 2 | $\overline{8}$ | | $\overline{7}$ | |
| 6 | 18 | 43 | 37 | 1 | | 9 | 3 | $\overline{18}$ | | 27 | 25 |
| 6 | 19 | $\overline{25}$ | 35 | 53 | 48 | 9 | 4 | 0 | | $\overline{27}$ | 35 |
| 6 | 20 | 48 | 32 | $\overline{12}$ | | 9 | 5 | 40 | 35 | $\overline{82}$ | 83 |
| 7 | 1 | 36 | 37 | 34 | 30 | 9 | 6 | 14 | | $\overline{47}$ | 35 |
| 7 | 2 | $\overline{15}$ | | 4 | | 9 | 7 | 77 | 59 | 6 | |
| 7 | 3 | $\overline{65}$ | 50 | $\overline{24}$ | 30 | 9 | 8 | 58 | 55 | 6 | |
| 7 | 4 | 2 | | 40 | 53 | 9 | 9 | 47 | 43 | 14 | |
| 7 | 5 | 5 | | $\overline{58}$ | 68 | 9 | 10 | $\overline{71}$ | 59 | 29 | |
| 7 | 6 | 74 | 78 | 50 | 55 | 9 | 11 | 43 | 37 | $\overline{24}$ | |
| 7 | 7 | $\overline{69}$ | 71 | $\overline{65}$ | 75 | 9 | 12 | $\overline{15}$ | | 44 | 53 |
| 7 | 8 | 13 | | $\overline{41}$ | 43 | 9 | 13 | 16 | | $\overline{31}$ | 28 |
| 7 | 9 | $\overline{51}$ | 55 | 0 | | 9 | 14 | 27 | | 28 | 28 |
| 7 | 10 | $\overline{50}$ | 58 | 16 | | 9 | 15 | $\overline{17}$ | | 6 | |
| 7 | 11 | $\overline{22}$ | | $\overline{50}$ | 63 | 10 | 1 | $\overline{55}$ | 35 | 7 | |
| 7 | 12 | $\overline{53}$ | 58 | $\overline{50}$ | 58 | 10 | 2 | $\overline{76}$ | 60 | $\overline{47}$ | 53 |
| 7 | 13 | $\overline{14}$ | | $\overline{37}$ | 33 | 10 | 3 | $\overline{44}$ | 39 | $\overline{40}$ | 35 |
| 7 | 14 | $\overline{7}$ | | $\overline{39}$ | 33 | 10 | 4 | $\overline{1}$ | | $\overline{54}$ | 43 |
| 7 | 15 | 38 | | 19 | | 10 | 5 | 3 | | $\overline{16}$ | |
| 7 | 16 | 17 | | 41 | 35 | 10 | 6 | 12 | | 18 | |
| 7 | 17 | 15 | | 11 | | 10 | 7 | $\overline{14}$ | | $\overline{33}$ | |
| 7 | 18 | 3 | | | | 10 | 8 | $\overline{16}$ | | 15 | |
| 8 | 1 | $\overline{5}$ | | $\overline{11}$ | | 10 | 9 | 15 | | 1 | |

(To be continued)

TABLE 3 (continued)

| Indices | | 0. layer line $h = 0$ | | 1. layer line $h = 1$ | | Indices | | 0. layer line $h = 0$ | | 1. layer line $h = 1$ | |
|---|---|---|---|---|---|---|---|---|---|---|---|
| $k$ | $l$ | $F_{calc.}$ | $\lvert F_{obs.}\rvert$ | $F_{calc.}$ | $\lvert F_{obs.}\rvert$ | $k$ | $l$ | $F_{calc.}$ | $\lvert F_{obs.}\rvert$ | $F_{calc.}$ | $\lvert F_{obs.}\rvert$ |
| 10 | 10 | 13 | | 11 | | 12 | 3 | $\overline{19}$ | 20 | 67 | 63 |
| 10 | 11 | 13 | | 62 | 68 | 12 | 4 | 37 | | $\overline{36}$ | 28 |
| 10 | 12 | $\overline{29}$ | | $\overline{5}$ | | 12 | 5 | $\overline{4}$ | | 39 | 28 |
| 10 | 13 | 0 | | $\overline{11}$ | | 12 | 6 | 31 | 32 | $\overline{3}$ | |
| 10 | 14 | 14 | | $\overline{73}$ | 60 | 12 | 7 | 5 | | $\overline{28}$ | |
| 11 | 1 | $\overline{19}$ | | 4 | | 12 | 8 | $\overline{37}$ | 35 | | |
| 11 | 2 | $\overline{23}$ | 25 | 35 | | 12 | 9 | 7 | | | |
| 11 | 3 | 32 | 23 | $\overline{2}$ | | 0 | 1 | | | 0 | |
| 11 | 4 | $\overline{82}$ | 67 | $\overline{4}$ | | 0 | 3 | | | $\overline{14}$ | |
| 11 | 5 | $\overline{11}$ | | 33 | 23 | 0 | 5 | | | 130 | 150 |
| 11 | 6 | 22 | | 8 | | 0 | 7 | | | 31 | 35 |
| 11 | 7 | $\overline{16}$ | | 37 | 35 | 0 | 9 | | | $\overline{35}$ | 43 |
| 11 | 8 | 0 | | 11 | | 0 | 11 | | | $\overline{28}$ | 38 |
| 11 | 9 | $\overline{8}$ | | 115 | 85 | 0 | 13 | | | $\overline{112}$ | 115 |
| 11 | 10 | 10 | | $\overline{18}$ | | 0 | 15 | | | 52 | 63 |
| 11 | 11 | $\overline{20}$ | | 16 | | 0 | 17 | | | 26 | 35 |
| 12 | 1 | $\overline{32}$ | 20 | $\overline{19}$ | | 0 | 19 | | | $\overline{9}$ | |
| 12 | 2 | 51 | 47 | $\overline{10}$ | | 0 | 21 | | | 51 | 63 |

## Atomic arrangement

The final atomic parameters obtained for the yellow $CsPbI_3$ are reproduced in Table 4.

Interatomic distances between atoms with parameters $(x_1\ y_1\ z_1)$ and $(x_2\ y_2\ z_2)$ have been calculated from

$$d = \{(x_1 - x_2)^2 a^2 + (y_1 - y_2)^2 b^2 + (z_1 - z_2)^2 c^2\}^{1/2}$$

with $a = 4.797$ Å, $b = 10.46_2$ Å, $c = 17.78_8$ Å, and are given in Table 5. They are presumably accurate to $\pm 0.05$ Å.

Now that the structure has been resolved it turns out to be quite similar to that of $NH_4CdCl_3$ and $RbCdCl_3$ investigated long ago[14, 15] only with different interatomic distances. Each Pb-atom is surrounded by six I-atoms which form a distorted octahedron and five of these I-atoms are shared by

[14] C. H. MACGILLAVRY, H. NIJVELD, S. DIERDORP, and J. KARSTEN, *Rec. trav. chim.* **58**, 193 (1939).

[15] H. BRASSEUR and L. PAULING, *J. Am. Chem. Soc.* **60**, 288 (1938).

TABLE 4. Atomic parameters in yellow $CsPbI_3$

All the atoms are in the special positions:

$$\frac{1}{4}\,y\,z;\quad \frac{3}{4}\,\bar{y}\,\bar{z};\quad \frac{3}{4}\;\frac{1}{2}-y\;\;\frac{1}{2}+z;\quad \frac{1}{4}\;\frac{1}{2}+y\;\;\frac{1}{2}-z;$$

and for

| | | | |
|---|---|---|---|
| Cs | $x=\frac{1}{4}$ | $y=0.081$ | $z=0.328$ |
| Pb | $x=\frac{\bar{1}}{4}$ | $y=0.162$ | $z=0.062$ |
| I′ | $x=\frac{1}{4}$ | $y=0.339$ | $z=\overline{0.001}$ |
| I″ | $x=\frac{\bar{1}}{4}$ | $y=0.031$ | $z=\overline{0.114}$ |
| I‴ | $x=\frac{\bar{1}}{4}$ | $y=0.298$ | $z=0.211$ |

two or even three octahedra so that they form bridges between the Pb-atoms. Thus the result is extended chains of Pb-I-octahedra parallel to the $a$-axis of the crystal. The bonding in such a polynuclear ion $(PbI_3^-)_n$ can be pictured in the following way.

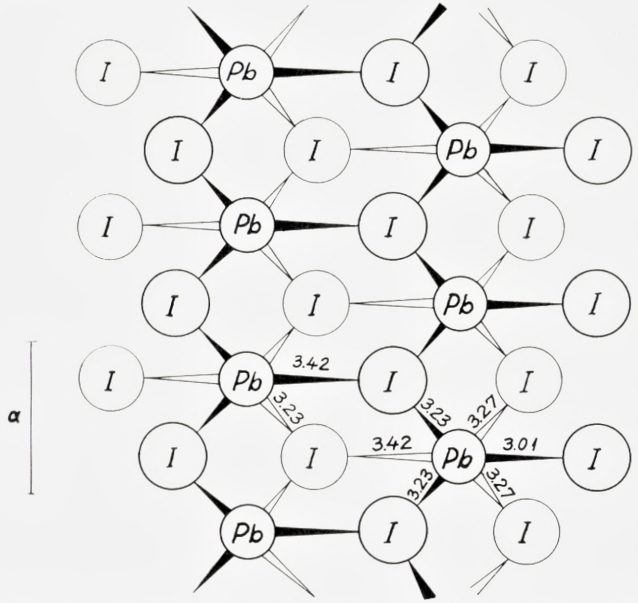


Fig. 3. $(PbI_3^-)_n$. Black, solid "bonds" point forward, light ones backward.

TABLE 5. Comparison of measured and calculated interatomic distances in yellow $CsPbI_3$

| Distance | From this investigation | From Pauling's ionic radii | From Goldschmidt's radii |
|---|---|---|---|
| $Pb^1—I^1$ ..... | 3.23 Å | 3.37 Å | 3.52 Å |
| $Pb^1—I^2$ ..... | 3.42 - | 3.37 - | 3.52 - |
| $Pb^1—I^3$ ..... | 3.27 - | 3 37 - | 3.52 - |
| $Pb^1—I^4$ ..... | 3.01 - | 3.37 - | 3.52 - |
| $Pb^1—Pb^2$ ... | 4 70 - | | |
| Pb—Cs ..... | 5.37 - | | |
| $Cs^1—I^5$ ..... | 3.96 - | 3.85 - | 3.85 - |
| $Cs^1—I^1$ ..... | 3.99 - | 3.85 - | 3.85 - |
| $Cs^1—I^6$ ..... | 3.98 - | 3.85 - | 3.85 - |
| $Cs^1—I^3$ ..... | 4 19 - | 3.85 - | 3.85 - |
| $Cs^1—I^4$ ..... | 3.90 - | 3.85 - | 3.85 - |
| $Cs^1—I^7$ ..... | 3.87 - | 3.85 - | 3.85 - |
| $I^1—I^1$ ..... | $4.79_5$ - | 4.32 - | 4.40 - |
| $I^1—I^2$ ..... | 4.49 - | 4.32 - | 4.40 - |
| $I^1—I^3$ ..... | 4.38 - | 4.32 - | 4.40 - |
| $I^1—I^4$ ..... | 4.49 - | 4.32 - | 4.40 - |

The Cs-ions are distributed between these chains of polynuclear complexes in such a way that each Cs-ion is at the centre of an almost equilateral triangle formed by three I-atoms in the planes $x = \frac{1}{4}$ or $x = -\frac{1}{4}$; six other I-atoms form two almost equilateral triangles below and above the one which is co-planar with Cs, and rotated 60° with respect to this so that Cs obtains a coordination number 9.

It would appear interesting to compare the observed interatomic distances with those obtained from the sum of the ionic radii. However, as there are two rather different empirical values for $r_{Pb^{++}}$, namely 1.21 Å (Pauling) and 1.32 Å (Goldschmidt) this comparison has been made for both Pauling and Goldschmidt ionic radii.[16]

For the Cs-I distances both sets of ionic radii give calculated distances only slightly smaller than the observed ones. The Pb-I distances calculated from the Goldschmidt ionic radii are considerably longer than those observed and would thus indicate some "covalency" or strong polarization of the Pb-I-bond. The Pauling radii here give expected distances closer to the observed ones, but also in this case the calculated distance between

[16] LANDOLT BÖRNSTEIN. I. Band, 4. Teil, p. 523. Springer Verlag 1955.

Pb-atoms and the I-atoms which are not bridging the Pb-atoms is considerably longer than the measured value. This again points to strong polarization of the I-ions and it is likely that the colour of these crystals can be explained in terms hereof. That one of the Pb-I-distances is larger than expected from the Pauling radii may be explained as being due to mutual repulsion between neighbouring Pb-ions sharing I-ions.

In the earlier work on compounds of the type $MCdCl_3$ referred to above it seemed difficult to draw any definite conclusion as to whether the differences found for the Cd-Cl-distances were significant or not. Although they did show the same trend as observed here for the Pb-I-distances the differences themselves were not much larger than the uncertainty of the measurements. From the present work it can be definitely stated that the Pb-I-distances are not equal and by analogy it may be concluded that the observed differences in the Cd-Cl distances are real.

## Conclusion

The result of the present investigations can be summarized by saying that divalent lead in yellow $CsPbI_3$ shows a great similarity to divalent Cd in similar compounds. Both form one-dimensional polynuclear complex ions where these metal ions have a coordination number 6 and where halogen bridging between the divalent metal ions is a characteristic feature. This type of complex ions indicates that the electrostatic attraction between the divalent ions and the halide ions is strongly modified by polarization, and it would be expected that somewhat similar complex polynuclear ions should exist also in aqueous solutions in equilibrium with these crystals.

## Acknowledgments

I wish to thank the Director of the Laboratory, Professor A. Tovborg Jensen, Ph. D., for his interest in this work and Mr. Børge Petersen for assisting in the lengthy calculations.

Indleveret til selskabet den 30. april 1959.
Færdig fra trykkeriet den 21. september 1959.

Matematisk-fysiske Meddelelser
udgivet af
Det Kongelige Danske Videnskabernes Selskab
Bind **32**, nr. 2

Mat. Fys. Medd. Dan. Vid. Selsk. **32**, no. 2 (1959)

# THE STRUCTURE OF PEROVSKITE-LIKE CÆSIUM PLUMBO TRIHALIDES

BY

CHRISTIAN KN. MØLLER

København 1959
i kommission hos Ejnar Munksgaard

## Synopsis

Crystalline compounds of composition $CsPbX_3$, where X = Cl or Br, may be prepared either from aqueous solutions or by fusing CsX and $PbX_2$. The pale yellow $CsPbCl_3$ has cubic perovskite structure above 47° C. (a = 5.605 Å), the orange-coloured $CsPbBr_3$ above 130° C. (a = 5.874 Å). Below these temperatures the structures are slightly distorted, but apparently without changes of volume at the transition points. $CsPbBr_3$ below 130° C. (and possibly also $CsPbCl_3$ below 47° C.) exhibits a superstructure, but not above this temperature. Application of Fourier methods shows that above as well as below the transition points, both the halogen atoms and the Cs-atoms are a little displaced from those positions expected for an ideal perovskite structure. Structure factors have been calculated on the assumption that each halogen atom occupies one of four, each Cs-atom one of six close-lying potential-minima at random; they show excellent agreement with the observed structure factors. It is suggested that such a delocalization of certain atoms may be a common feature in cubic perovskite structures where the tolerance factor $t \neq 1$. The PbCl-distances are 2.86 Å and the PbBr-distances 2.99 Å, i.e. considerably shorter than the sum of the corresponding ionic radii.



Printed in Denmark
Bianco Lunos Bogtrykkeri A-S

## Introduction

It has been demonstrated in a previous paper[1] that $CsPbI_3$ can exist in a black perovskite-like modification besides the yellow, orthorhombic form stable under ordinary conditions. It will be shown in the present study that $CsPbCl_3$ and $CsPbBr_3$ also form perovskite-like structures which in this case are the stable modifications. $CsPbF_3$ has already been found by O. SCHMITZ-DUMONT and G. BERGERHOFF to belong to this structure type[2] with the unit cell edge $a = 4.80\ kX$.

Ideally, crystals with perovskite structure are cubic with one molecule in the unit cell,[3] but very often small deviations from cubic symmetry are found. However, in such cases there usually is a transition temperature above which the structure is strictly cubic.[4] With only one molecule $ABX_3$ in a cubic unit cell one would expect that all the atomic positions were fixed by symmetry. This argument has been widely used, but may not always be applicable for the following reasons. It is known that alloys exist which exhibit a cubic structure, but where the cubic symmetry is of a statistical nature so that the distribution of atoms within only one unit cell at definite lattice sites need not at all conform to the observed "average symmetry".[5]

Secondly, it is generally agreed that crystals with perovskite structure belong to the so-called defect structures,[3] and as far as the author is aware, the nature of the defects in this case is not yet understood.

If we imagine the ions to be solid spheres with definite ionic radii $r_A$, $r_B$, and $r_X$ the following relation can easily be demonstrated for the ideal perovskite structure:

[1] C. K. MØLLER, The Structure of $CsPbI_3$, Mat. Fys. Medd. Dan. Vid. Selsk. **32**, No. 1 (1959).

[2] O. SCHMITZ-DUMONT und GÜNTHER BERGERHOFF, Z. anorg. u. allgem. Chem. **283**, 314—329 (1956).

[3] See e.g. (a). R. C. EVANS, Crystal Chemistry p. 204—214, Cambridge 1939. (b) A. F. WELLS, Structural Inorganic Chemistry p. 112, p. 330, Oxford 1945.

[4] H. D. MEGAW, Ferroelectricity in crystals, Chapters 4 and 5. Methuen, London 1957.

[5] See e.g. Ref. 3a p. 109.

$$\frac{r_A + r_X}{r_B + r_X} = \sqrt{2} \cdot t, \qquad (1)$$

where $t = 1$. However, for many crystals with perovskite structure $t$ will be found to be different from 1 — usually in the range $0.8 < t < 1$ when we insert the generally accepted ionic radii.[1]

We can interpret this either as an observable effect of the defect nature of these crystals, or as an indication that the ions are not solid spheres with fixed ionic radii. In fact, it has been proposed to use special ionic radii for ions when they form crystals of this type,[2] but from the observations to be described in what follows this procedure does not seem to be recommendable. It is presumably true that the bonding between the atoms in perovskite structures is mainly ionic and may be modified by polarization so that the interatomic distances will be shorter than calculated from the ordinary ionic radii, but this can scarcely justify the use of separate "perovskite ionic radii".

In order to clarify some of the problems connected with the perovskite structure a detailed investigation has been made of $CsPbCl_3$ and $CsPbBr_3$, as will now be described.

## Preparation and general properties

As has been shown by H. L. Wells[3] and coworkers crystals with the compositions $CsPbCl_3$ and $CsPbBr_3$ can be prepared by dissolving $PbCl_2$, resp. $PbBr_2$, in a hot aqueous solution of CsCl, resp. CsBr, of suitable concentration and then left to cooling. Besides this method of preparation we have found that compounds of the type $CsPbX_3$, where $X$ = Cl, Br, or I can also be obtained by fusing CsX and $PbX_2$ in the correct stoichiometric proportion. The identity of the crystalline compounds prepared by either method was proved by the identity of their $X$-ray powder diagrams and transition temperatures (see below).

The crystals grown in solution are quadratic or rectangular in shape, those of $CsPbCl_3$ pale yellow and those of $CsPbBr_3$ orange coloured. Their refractive indices are high, above 1.74.

Although the crystals are decomposed by water it was possible to determine the density of $CsPbCl_3$-crystals by the flotation method in a Clerici's

[1] V. M. Goldschmidt, Z. tech. Phys. **8**, 256 (1927).
[2] S. Geller, Acta Cryst. **10**, 248 (1957).
[3] H. L. Wells, Z. anorg. Chem. **3**, 195 (1893).

solution[1] of known density: $d = 4.21$ g/cm$^3$. With a rather coarse powder of $CsPbCl_3$ a pycnometer method gave $d = 4.24$ g/cm$^3$ in reasonable agreement with the first result.

## Examination with the polarizing microscope, transition temperatures

Under the polarizing microscope the coloured crystals of $CsPbCl_3$ and $CsPbBr_3$ appear birefringent and both show parallel extinction. By use of the quartz-wedge strong evidence was found from observation on a single crystal of $CsPbCl_3$, where the directions and the lengths of the axes had been determined by *X*-ray methods, that this crystal was (uniaxial) positive. Between crossed nicols very often thin twin lamellae can be observed, which form angles of 45° with the external edges. Twin formation with (110) as composition plane can easily be observed on thin crystals which between crossed nicols show first order grey as interference colour: On insertion of the gypsum plate (parallel to the extinction direction) one side of the composition plane gives yellow, the other side blue as the resulting interference colour. When these crystals of $CsPbCl_3$ or $CsPbBr_3$ are heated under the polarizing microscope with crossed nicols, the interference colours change continually, first slowly and then faster and faster, till they finally disappear at 46.9°C. or 130°C., respectively. This shows that the crystals become optically isotropic above these temperatures and attain cubic symmetry. Qualitatively one gets an impression that the interference colours, which for the same crystal is a measure of its birefringence, depend on the temperature in much the same way as the axial ratio in fig. 1. On cooling, the interference colours reappear at the same temperatures, so that the changes are completely reversible. (Temperature calibration was made by determining the known melting points for substances such as urea, benzoic acid, etc.).

## *X*-ray investigations. Unit cell dimensions

Powder diagrams of $CsPbCl_3$ and $CsPbBr_3$ have been obtained in a Guinier type focussing camera with $CuK_\alpha$-radiation. Whenever accurate $\sin^2\vartheta$-values had to be determined, the powders were mixed with NaCl (Kahlbaum, geschmolzen) which served as a standard calibration substance—due regard been paid to the dependence of its lattice constant on the temperature.[2]

[1] H.E. Vassar, Am. Mineral. **10**, 123 (1925).
[2] H.v. Bergen, Ann. Phys. **39**, 553—72 (1941).

In order to obtain diagrams of the powders at elevated temperatures the sample was fixed with the smallest possible amount of Canada balsam on a thin cover glass. This was squeezed into position between the circular metal holder and a piece of perforated mica with 6–7 turns of a 0.2 mm thick Ni-Cr-wire which could be electrically heated. It was found that the hot wire did not seriously affect the *X*-ray diagrams when it was kept perpendicular to the cylinder axis of the curved quartz-monochromator, and hence the samples were kept stationary, not rotated as is usual during the exposures. The temperatures were estimated from measurements of the resistance of the hot wire during operation, the transition temperatures determined by the optical investigation above being used as fix points.

Indices could be assigned to the "reflections" on the powder diagrams by application of the general formula

$$\sin^2\vartheta = \frac{\lambda^2}{4}\left\{\frac{1}{a^2\sin^2\gamma}h^2 + \frac{1}{b^2\sin^2\gamma}k^2 + \frac{1}{c^2}l^2 - \frac{2\cos\gamma}{ab\sin^2\gamma}hk\right\}, \qquad (2)$$

where in our case $\gamma$ was either 90° or very close to 90° and $a = b \simeq c$. The lattice constants for the crystals at different temperatures were finally evaluated from the coefficients to $h^2$, $l^2$ and $hk$ in (2) giving best agreement between observed and calculated $\sin^2\vartheta$-values. They are reproduced together with indices, estimated intensities, and $\sin^2\vartheta$-values in Tables 1 and 2 ($\lambda$ ($CuK_\alpha$) = 1.5418 Å).

A few diffuse lines on the Guinier-diagrams of $CsPbBr_3$ below the transition temperature (130°C.) cannot be accounted for with the indexing in Table 2 unless the unit cell axes are doubled. However, in order to maintain the connection with the cubic unit cell, instead of doubling the axes we have chosen to use fractional indices for these reflections. It is characteristic of these lines that they decrease in intensity as the crystalline powder is heated above room temperature, and practically disappear when the unit cell axes become of equal length at 130°C., only very faint diffuse bands being left in their place on the diagrams taken of the cubic form. From this behaviour one would infer that the lines mentioned are due to a superstructure which "melts" in the crystal at 130°C., only leaving some degree of "local order" reminiscent of the superstructure.

Also $CsPbCl_3$ in the tetragonal form shows a few lines of this type, but it is difficult to decide whether they really disappear at 47°C., and besides there are some rather sharp, very weak lines as well, which completely persist above 47°C. However, it has turned out that the latter originate from

the compound $Cs_4PbCl_6$ which then apparently is present as an impurity in $CsPbCl_3$ prepared both from aqueous solution and by fusing CsCl and $PbCl_2$.

From the density, unit cell dimensions, and molecular weight of $CsPbCl_3$ we calculate that there is one molecule in the small cubic unit cell above 47° C. By analogy and from the similarity of the compounds and their unit

TABLE 1. Comparison of observed and calculated $\sin^2\vartheta$-values for $CsPbCl_3$ at room temperature and at about 50° C.

| Indices $h\ k\ l$ | Room temperature | | | Temp. about 50° C. | | |
|---|---|---|---|---|---|---|
| | Intensity estimated | $10^4 \cdot \sin^2\vartheta_{obs.}$ | $10^4 \cdot \sin^2\vartheta_{calc.}$ | Intensity estimated | $10^4 \cdot \sin^2\vartheta_{obs.}$ | $10^4 \cdot \sin^2\vartheta_{calc.}$ |
| 001 | w | 0187 | 0188 | m | 0190 | 0190 |
| 100 | m | 0191 | 0190 | | | |
| $Cs_4PbCl_6$ | vw? | 0330 | (0330) | | | |
| 011 | (v)s | 0378 | 0378 | vs | 0379 | 0379 |
| 110 | s-m | 0381 | 0380 | | | |
| $Cs_4PbCl_6$ | vw | 0409 | (0411) | vw | 0409 | (0411) |
| $\frac{1}{2}\ 0\ \frac{3}{2}$ | vw | 0474 | 0474 | | | |
| $\frac{3}{2}\ 0\ \frac{1}{2}$ | | | 0475 | | | |
| $\frac{1}{2}\ \frac{3}{2}\ \frac{1}{2}$ | ? | 0526 | 0522 | | | |
| $Cs_4PbCl_6$ | | | (0526) | | | |
| $0\ 1\ \frac{3}{2}$ | vw | 0613 | 0612 | | | |
| $0\ \frac{3}{2}\ 1$ | | | 0614 | | | |
| $Cs_4PbCl_6$ | | | (0614) | | | |
| $\frac{1}{2}\ \frac{3}{2}\ 1$ | vw | 0663 | 0662 | | | |
| $\frac{1}{2}\ 1\ \frac{3}{2}$ | | | 0664 | | | |
| $Cs_4PbCl_6$ | | | (0662) | | | |
| 002 | (v)w | 0752 | 0750 | m | 0758 | 0758 |
| 020 | m | 0761 | 0761 | | | |
| 012 | (v)w | 0940 | 0940 | | | |
| 021 | w | 0950 | 0949 | w | 0947 | 0948 |
| 210 | | | 0951 | | | |
| 112 | w-(m) | 1130 | 1130 | m-s | 1138 | 1138 |
| 121 | m-s | 1139 | 1139 | | | |
| 202 | w-m | 1513 | 1511 | w-m | 1518 | 1516 |
| 220 | w | 1523 | 1522 | | | |
| 003 | — | — | — | vw | 1704 | 1706 |
| 122 | — | — | — | | | |
| 013 | — | — | — | w | 1897 | 1896 |
| 222 | — | — | — | vw | 2274 | 2274 |
| 123 | w | 2639 | 2639 | (v)w | 2656 | 2654 |
| 132 | w | 2651 | 2652 | | | |
| 231 | w | 2660 | 2661 | | | |
| 033 | — | — | — | vw | 3410 | 3412 |
| 114 | — | — | — | | | |
| Unit cell | $a = b = 5.590$ Å, $c = 5.630$ Å<br>$\alpha = \beta = \gamma = 90°$<br>Volume: 175.9 Å$^3$ | | | $a = b = c = 5.605$ Å<br>$\alpha = \beta = \gamma = 90°$<br>Volume: 176.1 Å$^3$ | | |

TABLE 2. Comparison of observed and calcula

| Indices $h\ k\ l$ | Room temperature | | | Temp. about 120° C. | | |
|---|---|---|---|---|---|---|
| | Intensity estimated | $10^4 \cdot \sin^2\vartheta_{obs.}$ | $10^4 \cdot \sin^2\vartheta_{calc.}$ | Intensity estimated | $10^4 \cdot \sin^2\vartheta_{obs.}$ | $10^4 \cdot \sin^2\vartheta_{calc}$ |
| 001 | m | 0172 | 0172 | m | 0172 | 0171 |
| 100 | (m-)s | 0175 | 0175 | m | 0173 | 0173 |
| 011 | vs | 0347 | 0347 | s | 0345 | 0344 |
| 110 | | | 0348 | | | 0346 |
| $1\bar{1}0$ | w | 0352 | 0352 | | | |
| $\frac{1}{2}\ \frac{3}{2}\ 0$ | w | 0437 | 0436 | vw | 0433 | 0433 |
| $\frac{1}{2}\ \frac{3}{2}\ \frac{1}{2}$ | vw | 0474 | $0476._5$ | — | — | — |
| $(\frac{1}{2}\ \frac{3}{2}\ \frac{1}{2})$ | | | $(0479._5)$ | — | — | — |
| $11\bar{1}$ | w | 0520 | 0520 | w | 0518 | 0517 |
| $1\bar{1}1$ | vw | 0524 | 0524 | | | |
| $\frac{1}{2}\ \frac{3}{2}\ 1$ | w | 0610 | 0609 | vw | 0604 | 0604 |
| $00\bar{2}$ | (m-)s | 0687 | 0687 | m | 0683 | 0684 |
| 200 | s | 0700 | 0700 | m-s | 0693 | 0693 |
| 012 | w | 0862 | 0862 | vw | 0857 | 0857 |
| 021 | m-w | 0871 | 0869 | w | 0864 | 0864 |
| 120 | | | 0871 | | | 0866 |
| $1\bar{2}0$ | vw | 0880 | 0879 | | | |
| $1\bar{1}2$ | m | 1038 | 1039 | w | 1029 | 1030 |
| 211 | m | 1043 | 1043 | w-m | 1038 | 1037 |
| $2\bar{1}1$ | m | 1053 | 1051 | | | |
| 022 | m-s | 1386 | 1387 | m | 1377 | 1377 |
| 220 | vw? | 1409 | 1408 | vw | 1385 | 1386 |
| $2\bar{1}2$ | vw | 1565 | 1566 | (v)w | 1550 | 1550 |
| 130 | vw | 1744 | 1744 | vw | 1731 | 1732 |
| 013 | vw | 1721 | 1721 | — | — | — |
| 222 | — | — | — | vw | 2068 | 2070 |
| 123 | — | — | — | — | — | — |
| Unit cell. | $a = b = 5.827$ Å $c = 5.891$ Å<br>$\alpha = \beta = 90°$ $\gamma = 89°65$<br>Volume: 200.0 Å³ | | | $a = b = 5.859$ Å $c = 5.895$ Å<br>$\alpha = \beta = \gamma = 90°$<br>Volume: 202.3 Å³ | | |

cell dimensions it may be concluded that $CsPbBr_3$ also has only one molecule in the cubic unit cell. Perovskite structure is then very likely for these compounds, but, as will be shown below, intensities calculated on the basis of the atomic parameters required by the appropriate symmetry only in a rough qualitative way agree with the observed ones. The "tolerance factor" $t$ from equation (1) is about 0.8.

## Temperature dependence of the axes

Powder diagrams of $CsPbBr_3$ taken at four different temperatures have been indexed and the results together with the lattice constants deduced from them are reproduced in Table 2. It is seen that as the crystals are cooled

$\vartheta$-values for $CsPbBr_3$ at different temperatures.

| Temp. about 125° C. | | | Temp. about 135° C. | | | Indices |
|---|---|---|---|---|---|---|
| ıtensity timated | $10^4 \cdot \sin^2 \vartheta_{obs.}$ | $10^4 \cdot \sin^2 \vartheta_{calc.}$ | Intensity estimated | $10^4 \cdot \sin^2 \vartheta_{obs.}$ | $10^4 \cdot \sin^2 \vartheta_{calc.}$ | $h\ k\ l$ |
| m-s | 0172 | 0172 | m | 0172 | 0172 | 001<br>100 |
| s | 0344 | 0345<br>0346 | s | 0345 | 0344 | 011<br>110<br>1$\bar{1}$0 |
| — | — | — | | | | $\frac{1}{2}\ \frac{3}{2}\ 0$ |
| — | — | — | | | | $\frac{1}{2}\ \frac{3}{2}\ \frac{1}{2}$ |
| — | — | — | | | | $(\frac{1}{2}\ \frac{3}{2}\ \frac{1}{2})$ |
| m-w | 0516 | 0517 | w | 0516 | 0516 | 1$\bar{1}$1<br>11$\bar{1}$ |
| — | — | — | | | | $\frac{1}{2}\ \frac{3}{2}\ 1$ |
| m | 0688 | 0687 | s | 0689 | 0689 | 002 |
| m-s | 0692 | 0691 | | | | 200 |
| (v)w | 0861 | 0860 | m | 0862 | 0861 | 012<br>021 |
| w | 0865 | 0864 | | | | 120<br>1$\bar{2}$0 |
| m-s | 1036 | (1033)<br>1036 | m-s | 1035 | 1035 | 1$\bar{1}$2<br>211<br>2$\bar{1}$1 |
| m-s | 1379 | 1378<br>1382 | m-s | 1379 | 1378 | 022<br>220 |
| vw | 1551 | 1551 | w-m | 1546 | 1550 | 2$\bar{1}$2 |
| vw | 1725 | 1728 | vw | 1721 | 1722 | 130 |
| — | — | — | | | | 013 |
| vw | 2069 | 2067 | vw | 2065 | 2066 | 222 |
| vw | c. 2400 | 2408 | vw | 2411 | 2411 | 123 |
| $= b = 5.864$ Å $c = 5.881$ Å<br>$= \beta = \gamma = 90°$<br>lume: 202.2 Å$^3$ | | | $a = b = c = 5.874$ Å<br>$\alpha = \beta = \gamma = 90°$<br>Volume: 202.7 Å$^3$ | | | Unit cell. |

from temperatures above 130° C. the unit cell changes from cubic through tetragonal to monoclinic symmetry at room temperature. Although the changes of the axes are easily demonstrated, the change of volume of the (pseudo-)unit cell when the transition point at 130° C. is passed, presumably is not significant.

Instead of making a similar investigation on powders of $CsPbCl_3$ at several different temperatures, which would be rather time-consuming, it was chosen to measure the changes of the axes of a single crystal. The crystal was carefully adjusted on a Weissenberg goniometer and a series of 3° oscillation photographs were taken of the reflections 071 and 017, which have $2\vartheta = 155°$ for $CuK_\alpha$-radiation. The layer-line screen was used to separate the zeroth layer line, and the film cylinder (diameter 57.3 mm) was kept

stationary for each pair of exposures: 071 at the "top" and the "bottom" of the film. Then the film cylinder was displaced 3.0 mm (the width of the slot in the layer-line screen) and the oscillation regions of the crystal changed so that now two similar exposures could be taken of 017 at the same temperature. After that the temperature was changed, the film cylinder displaced 3.0 mm, and a set of four exposures taken at the new temperature, and so on. Exposure times were about 10 minutes.

The crystal could be heated by a controlled stream of $N_2$ from a cylinder, passing a flowmeter and a very small, electrically heated "oven", which was placed immediately in front of the crystal. Temperature control was afforded by a copper-constantan thermocouple in connection with a millivoltmeter. The oven-current could be read on an ammeter. Calibration was made in the following way. Two small polaroids were placed on either side of the crystal, "crossed", but with maximum light passing through the crystal when it was illuminated with a beam of light through the pin-hole system of the goniometer, and the crystal was watched through the microscope attached to the goniometer. With constant $N_2$-flow the oven-current was slowly increased till the crystal just became dark (optically isotropic). The temperature must then be 47°C. For the same rate of flow of $N_2$ and nearly constant room temperature it was then assumed that there was linear dependence between the thermoelectric power of the thermocouple and the temperature of the crystal for not too wide a range of temperatures.

The relation between the changes in glancing angles $\vartheta$ measured on the film and the changes in axial lengths is obtained from (2) by differentiation. For 071 and 017 and with $\Delta c \simeq -2\,\Delta a$ it approximates to

$$\Delta a = -1.06\, a\, \cot\vartheta \cdot \Delta\vartheta \text{ and } \Delta c = -1.03\, a\, \cot\vartheta \cdot \Delta\vartheta, \tag{3}$$

where, with sufficient accuracy, $a \simeq c \simeq 5.60$ Å, as the total uncertainty on $\Delta a$ and $\Delta c$ is of the order of 10 per cent.

Similarly the change of the axial ratio is given by

$$\Delta\left(\frac{c}{a}\right) = \frac{1}{a}(\Delta c - \Delta a). \tag{4}$$

The results obtained are shown in the graphs figs. 1 and 2, where the values of the axes at room temperature and at 50°C. have been adjusted so as to coincide with the values from the Guinier diagrams mentioned above. It appears that neither for $CsPbCl_3$ is there any discernible change of the volume, V, at the transition point from the tetragonal to cubic struc-

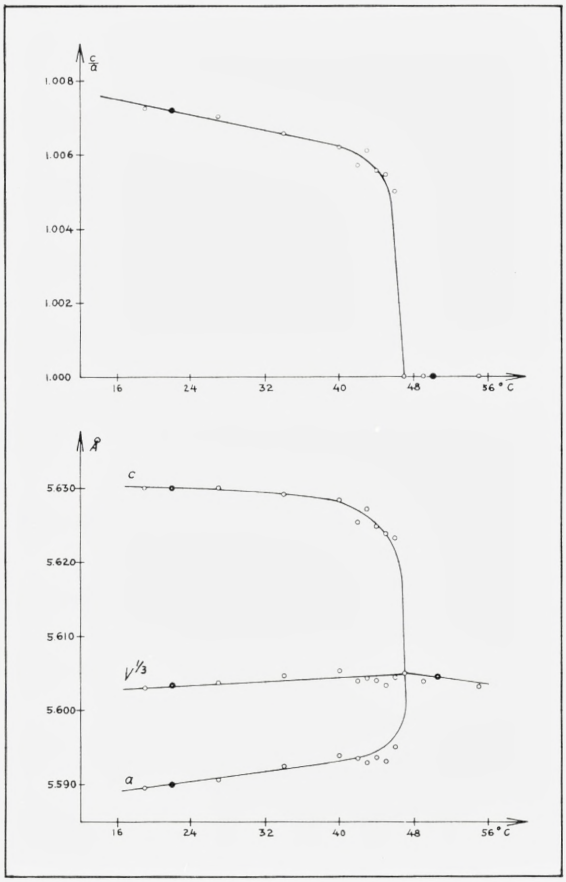


Figs. 1 and 2. Axial ratio and unit cell dimensions as functions of temperature for $CsPbCl_3$; solid circles refer to measurements from Guinier-diagrams.

ture. On the other hand it does look as if $V^{1/3}$ plotted as a function of temperature changes abruptly at the transition point, which would imply that the coefficient of thermal expansion has a discontinuity there. Unfortunately our measurements are not accurate enough to make a definite statement.

A similar temperature dependence has been found for the axes of $BaTiO_3$,[1] but here more recent experiments[2] have revealed that the curves near the transition point at 120° C. from tetragonal to cubic structure have

[1] H. D. Megaw, Proc. Roy. Soc. A. London **189**, 261 (1947).
[2] H. F. Kay and P. Vousden, Phil. Mag. Series 7, **40**, 1019 (1949).

discontinuities and also that thermal hysteresis plays a rôle. It is possible that a more refined technique will disclose similar irregularities also in the case of $CsPbCl_3$.

## Intensity measurements

In order to study the atomic arrangement in more detail, intensity measurements of the *X*-ray reflections on Weissenberg diagrams have been made on single crystals of $CsPbCl_3$ and $CsPbBr_3$, by means of $CuK_\alpha$-radiation. The reflections were photographed on sets of multiple films and relative intensities were visually estimated by comparison with an intensity scale prepared by taking a series of photographs of a particular reflection, each time increasing the exposure time by about 30 per cent. The intensities of these spots were then assumed to be proportional to their exposure times. Care was taken that *X*-ray intensity, temperature, speed of the Weissenberg motor, developer, fixer, and film material were kept as constant as possible. A new intensity scale was made for each crystal.

In order to check the reliability of this method two independent sets of measurements were made of the 0. and 1. layer lines of two different crystals of $CsPbCl_3$ at room temperature. One had the dimensions $100 \times 50 \times 40\,\mu$ and the other $100 \times 40 \times 30\,\mu$. The longest edge was the rotation axis. The agreement was found to be good, only in one case of 45 reflections measured was the deviation above 30 per cent, on an average it was about 12 per cent. of the measured intensity.

The reflections from a single crystal of $CsPbCl_3$ (and similarly of $CsPbBr_3$) were photographed with $CuK_\alpha$-radiation both at room temperature (20° C.) and at 7—10 centigrades above the transition point on the same set of multiple films. This was achieved by displacing the film cylinder 3.0 mm in its carriage between the two exposures. In this way intensity changes which might be observed of the reflections, should be influenced least possible by film material and development. Heating and temperature control was performed as explained above. The "high-temperature" reflections gave small, well-defined spots on the film, with a uniform blackening. But on the room-temperature exposures of $CsPbBr_3$, these spots had broken up into 3—4 smaller spots lying close together, so that it was necessary to add up the intensities of the separate spots belonging to the same reflection. On heating the crystal to temperatures above 130° C. these spots again coalesced, showing that it is a reversible phenomenon. The reason for its occurrence is that when the crystals are cooled from temperatures where the unit cell is strictly cubic to room temperature the unit cell is slightly

modified by expansion of, say, the original $a$-axis and shrinkage of its two other axes. However, in other parts of the "single crystal" the expansion may be along the original $b$ or $c$-axis (and shrinkage along the two others) and thus the result is a repeated twinning and microheterogeneity.[1] A similar effect could be observed on some of the diagrams of $CsPbCl_3$, but was there much less pronounced. For the particular crystal used it could also be inferred from the fact that on heating from room temperature to about 55°C. the reflections of type $0k0$ were always displaced towards smaller, those of type $00l$ towards higher $\vartheta$-values, that twinning could not be of major importance here.

The atomic scattering factors depend on the wavelength of the $X$-ray radiation used (dispersion), as do also the absorption corrections, and so it is conceivable that a more shortwaved radiation would give results different from those obtained with $CuK_\alpha$-radiation. Therefore photographs were also taken of $CsPbBr_3$ at 140°C. with $MoK_\alpha$-radiation for intensity measurements.

Correction of the directly measured intensities for the Lorentz-polarization factors was made graphically as described by Cochran.[2] It was previously found that the absorption of $X$-radiation in $CsPbI_3$ was compensated for by the temperature factor and could be included in the latter.[3] As this result presumably will also be valid here, we have made no direct corrections for the absorption. We thus finally obtain relative $|F(hkl)|^2$-values of which the uncertainty is assumed not to exceed 20—30 per cent.

As no piezoelectric effect has been detected in these crystals, neither with a dynamical[4] nor with a static method, it seems reasonable to conclude that they have centres of symmetry and consequently $F(hkl) = \pm |F(hkl)|$.

## Application of Fourier methods

With only one molecule $CsPbX_3$ in a cubic unit cell the atomic positions should be determined by symmetry. Thus we may have:

$$\text{Pb in } (0,0,0);\ \text{Cs in } \left(\frac{1}{2},\frac{1}{2},\frac{1}{2}\right);\ X \text{ in } \left(\frac{1}{2},0,0\right);\ \left(0,\frac{1}{2},0\right);\ \left(0,0,\frac{1}{2}\right) \quad \text{(a)}$$

$$\text{or Pb in } (0,0,0);\ \text{Cs in } \left(\frac{1}{2},\frac{1}{2},\frac{1}{2}\right);\ X \text{ in } \left(0,\frac{1}{2},\frac{1}{2}\right);\ \left(\frac{1}{2},0,\frac{1}{2}\right);\ \left(\frac{1}{2},\frac{1}{2},0\right). \quad \text{(b)}$$

[1] Compare V. K. Semenchenko, J. Cryst. U.S.S.R. **2**, 145 (1957).
[2] W. Cochran, J. Sci. Instr. **25**, No. 7 (1948).
[3] C. K. Møller, loc. cit. p. 11.
[4] V. Frank, Unpublished work.

Structure factors calculated on the basis of (a) with atomic scattering factors corrected for dispersion[1] do not give a very good agreement with the experimentally determined structure factors (Tables 3 and 4; Column 2 to be compared with Columns 4 and 5; see also figs. 8 and 9). The second possibility, (b), which is also equivalent to an interchange of Cs and Pb in (a), is even less satisfactory, and, furthermore, Pb would here acquire a coordination number 12, which seems rather unlikely.

Let us assume that Pb is correctly placed in (0, 0, 0), which is a centre of symmetry. As the atomic scattering factor of lead for the reflections of type $0kl$ exceeds the sum of the atomic scattering factors of Cs and $3X$, the structure factors $F(0kl)$ must be positive. Hence we can calculate the electron projection on the *bc*-plane directly from the observed $|F(0kl)|$. This has been done for both $CsPbCl_3$ and $CsPbBr_3$ above their transition temperatures, i.e. *in their cubic form*, and the result is shown in figs. 3 and 5.

It is seen that the electron clouds surrounding the halogen atoms are drawn out at right angles to the unit cell edges. As for the Cs-atoms, their peak heights come out much too low as compared with the peak height of the Pb-atoms, and on the projection of $CsPbCl_3$ their electron clouds seem to have "spikes" towards the Cl-atoms.

To estimate the contribution of diffraction effects to these somewhat unexpected results another projection on the *bc*-plane was calculated for $CsPbCl_3$, but now using the structure factors *calculated* for this compound with the atoms in position (a), instead of the observed $F(0kl)$ as coefficients in the Fourier series.

This "theoretical" projection faithfully reproduces the atoms in the expected positions, and with reasonable peak heights. It is also seen that there is a definite correlation of the "diffraction errors" in figs. 3 and 4, and it seems evident that they cannot be made responsible for the peculiar features of the "experimental" projections.

An electron projection of $CsPbBr_3$ calculated from structure factors obtained with $MoK_\alpha$-radiation gives mainly the same result as that based upon $CuK_\alpha$-radiation. It is thus unlikely that the latter kind of projection should be seriously distorted by dispersion and absorption. This conclusion gets further support from the fact that in the earlier work on $CsPbI_3$[2] the interpretation of the electron projections derived from intensities with $CuK_\alpha$-radiation was in no way obscured by any of the effects mentioned above, although they would be expected to be of greater importance in this case.

[1] Atomic scattering factors were taken from W. H. Bragg and W. L. Bragg, The Crystalline State. Vol. I p. 330—333 (London 1949), corrections for dispersion from C. H. Dauben and D. H. Templeton, Acta Cryst. **8**, 841 (1955).

[2] C. K. Møller, loc. cit.

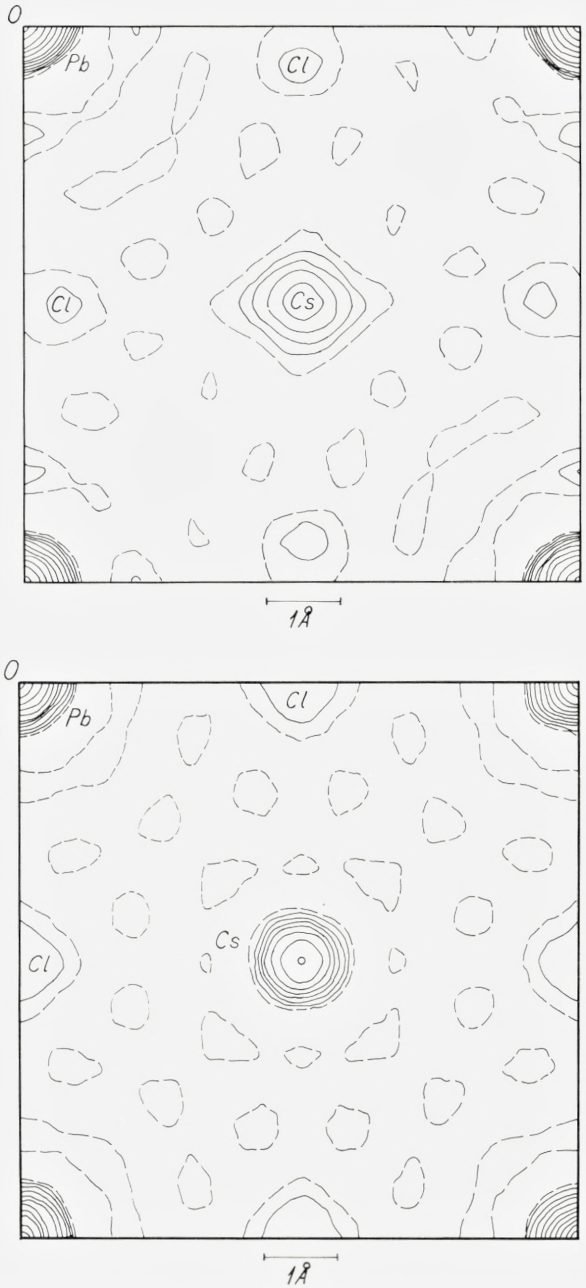


Figs. 3 and 4. Electron projections on (100) of cubic $CsPbCl_3$ based on observed $F(0kl)$ (top), and on $F(0kl)$ calculated for ideal perovskite structure (bottom). The same relative scale has been used for the electron densities and contour lines have been drawn at the levels 0 (broken lines) 15, 30, 50, 75, 100, 150, 200, 250, 300, 350, and 400.

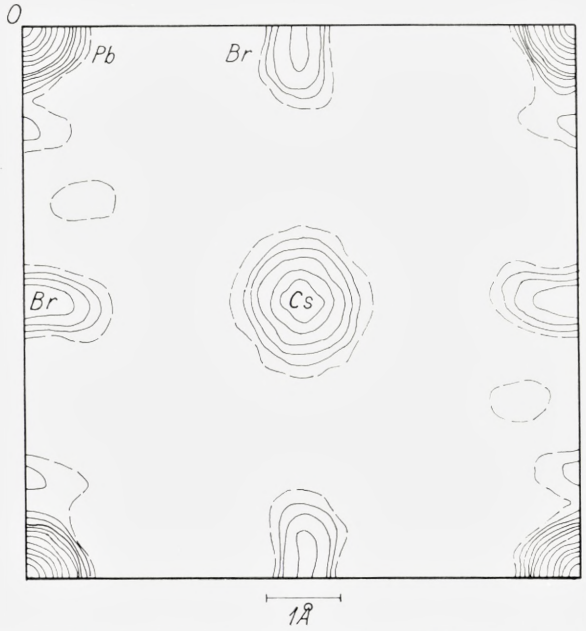


Fig. 5. Electron projection on (100) of cubic $CsPbBr_3$. Relative, arbitrary scale for electron density. Contour lines drawn as in figs. 3 and 4.

Finally a projection of tetragonal $CsPbCl_3$ has been calculated from its observed $|F(0kl)|$. The result is almost indistinguishable from that of the cubic form. Difference synthesis with the Fourier-coefficients $F(0kl)_{\text{tetr.}} - F(0kl)_{\text{cub.}}$ obtained from the experimentally determined intensities for the cubic and tetragonal modifications of both $CsPbCl_3$ and $CsPbBr_3$ also show near identity of the two forms; in fact, the only observable changes in the electron distributions on going from the tetragonal to the cubic structures seem to be a reduction in peak height of the Cs-atoms and a small displacement of the halogen atoms towards the unit cell edges (about 0.05 Å in $CsPbCl_3$).

For the interpretation of the above results it should be remembered that an electron projection derived from experimental data represents a superposition of the electron distributions in a huge number of unit cells. We have so far been referring structures to the small unit cells given in Tables 1 and 2. The existence of a superstructure below the transition temperatures shows that this cannot be correct for the tetragonal form, but above the transition points both optical and *X*-ray evidence compel us to accept the

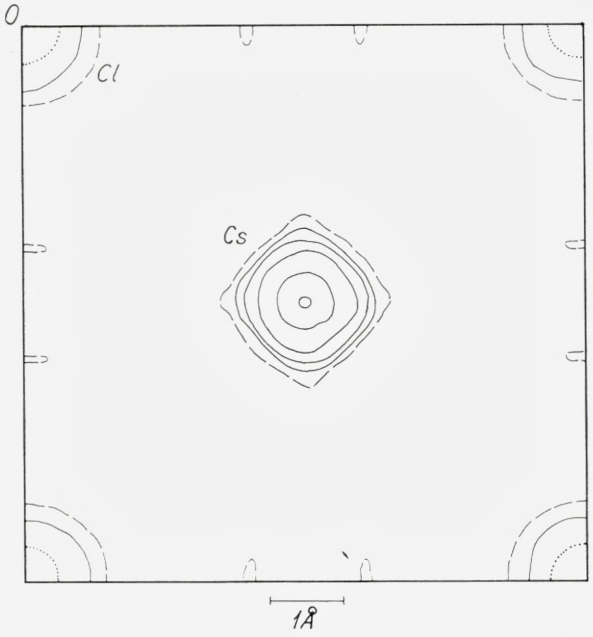


Fig. 6. Experimental electron density in the plane $x = \frac{1}{2}$ of cubic $CsPbCl_3$. Contour lines are drawn at the levels 5 (broken line), 10, 15, 30, 60, and 90 e/Å$^3$. The dotted lines near the corners indicate the maximum electron density in the Cl-regions (nearly 15 e/Å$^3$).

small unit cell combined with cubic symmetry. That the halogen peaks do not appear in the expected ideal positions (a) in projections of the latter may then either be explained as a result of the thermal movements, or we may assume that the true potential minima for Cs and the halogen atoms do not coincide with the ideal sites given in (a). Due to the limitations in resolution we cannot see the Cs- or Br-atoms in these subsidiary minima as separated peaks on the projections. Nor will it be possible to distinguish between the two mentioned possibilities from *X*-ray work alone.

To be more specific we shall assume that each Cl-(or Br-)atom in the unit cell has the choice between four potential minima lying along diagonals in sections perpendicular to the unit cell edges, about 0.5 Å away from the "ideal positions", and similarly that Cs can "choose" between 6 (or 12) minima displaced about 0.5 Å from the centre of the unit cell. Above the transition temperatures the kinetic energy of these atoms is higher than their mutual interaction energy, and there will be a constant diffusion of a halogen atom or a Cs-atom from one of its "private" potential minima

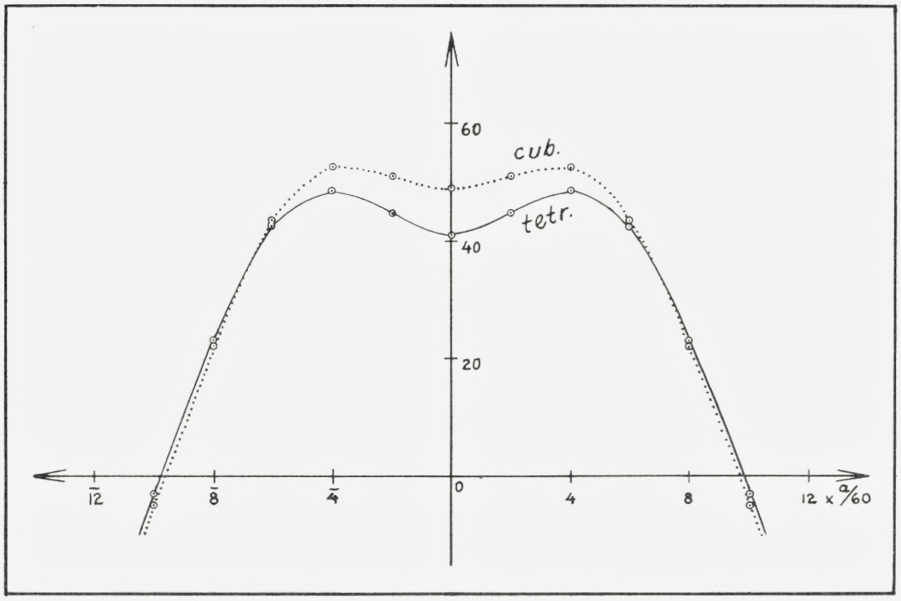


Fig. 7. Variation of the electron density along a radius vector from O in the plane $x = \frac{1}{2}$ of $CsPbCl_3$. (Unit for the electron density four times that in fig. 6).

to another, thus simulating free rotation around the unit cell axes. Below the transition points, on the other hand, their kinetic energies are too small to prevent their being locked up in a particular configuration.

On these assumptions structure factors have been calculated for both $CsPbCl_3$ and $CsPbBr_3$ (see next section) and their signs have been transferred to the experimentally determined $|F(hkl)|$. Fourier syntheses of the electron distributions in the planes $x = 0$ and $x = \frac{1}{2}$ have been made with these coefficients for $CsPbCl_3$. The section through $x = \frac{1}{2}$ is reproduced in fig. 6, where the dotted curves represent the maximum electron density in the Cl-atoms. Fig. 7 represents a plot of the electron density along a radius vector from the unit cell corner in this section and illustrates how small the differences are between the tetragonal and the cubic form in this respect.

Three-dimensional difference syntheses in these planes have also been calculated, but apart from confirming the above observations they show nothing new.

### Comparison of calculated and observed structure factors

Further evidence that the assumption of random distribution of the Cs- and the halogen atoms on certain selected sites is compatible with the *X*-ray work comes from a comparison of calculated and observed structure factors.

These calculations have been made on the basis of the formula

$$F(hkl) = \sum_i f_i(hkl) \cdot \cos 2\pi (hx_i + ky_i + lz_i), \qquad (5)$$

where $x_i$, $y_i$, $z_i$ are the atomic parameters, $f_i$ the atomic scattering factors, and the summation is over all the atoms "$i$" in the unit cell. The $f_i(hkl)$ have been obtained for the different reflections $hkl$ by a graphical method and this may give rise to small errors of the order of a few per cent of the $F(hkl)$, which, however, is small as compared with the experimental uncertainty.

Nearly all the structure factors corresponding to reflections within the limiting sphere for $CuK_\alpha$-radiation have been calculated for both $CsPbCl_3$ and $CsPbBr_3$ with the atoms in the "ideal positions" (a) and isotropic atomic scattering factors, i.e. $f(hkl) = f(\vartheta)$. It is evident from Tables 3 and 4 that the structure factors calculated in this way are not in very good agreement with the experimental ones and in several places there are real discrepancies. The differences between weak and strong reflections are much less accentuated in the latter than in the former. Plots of $\log \left| \frac{F^{id.}_{calc.}}{F_{obs.}} \right|$ against $h^2 + k^2 + l^2$ should theoretically approach a straight line,[1] but this is not very obvious as seen from the example of $CsPbBr_3$ in figs. 8 and 9.

Next we have calculated the structure factors on the assumption that the Cs- and halogen atoms are randomly displaced from their ideal positions. For the *X*-ray analysis it makes no difference whether the small displacements of the atoms are of a stationary character or whether they are caused by thermal vibrations of the lattice. This allows the two possibilities to be treated exactly alike and we can take over the whole treatment of the influence of thermal vibrations on the *X*-ray intensities.[2]

The result of these considerations is that if the displacement amplitude for the atoms of species "$i$" is given by the vector $\boldsymbol{u} = u_x \boldsymbol{a} + u_y \boldsymbol{b} + u_z \boldsymbol{c}$, their atomic scattering factor appropriate for the reflection $hkl$ with *X*-ray radia-

[1] See e.g. H. Lipson and W. Cochran, Determination of Crystal Structures, p. 61. London 1953.

[2] See e.g. R.W. James, The Optical Principles of the Diffraction of *X*-Rays. Chapters I and V. London 1948.

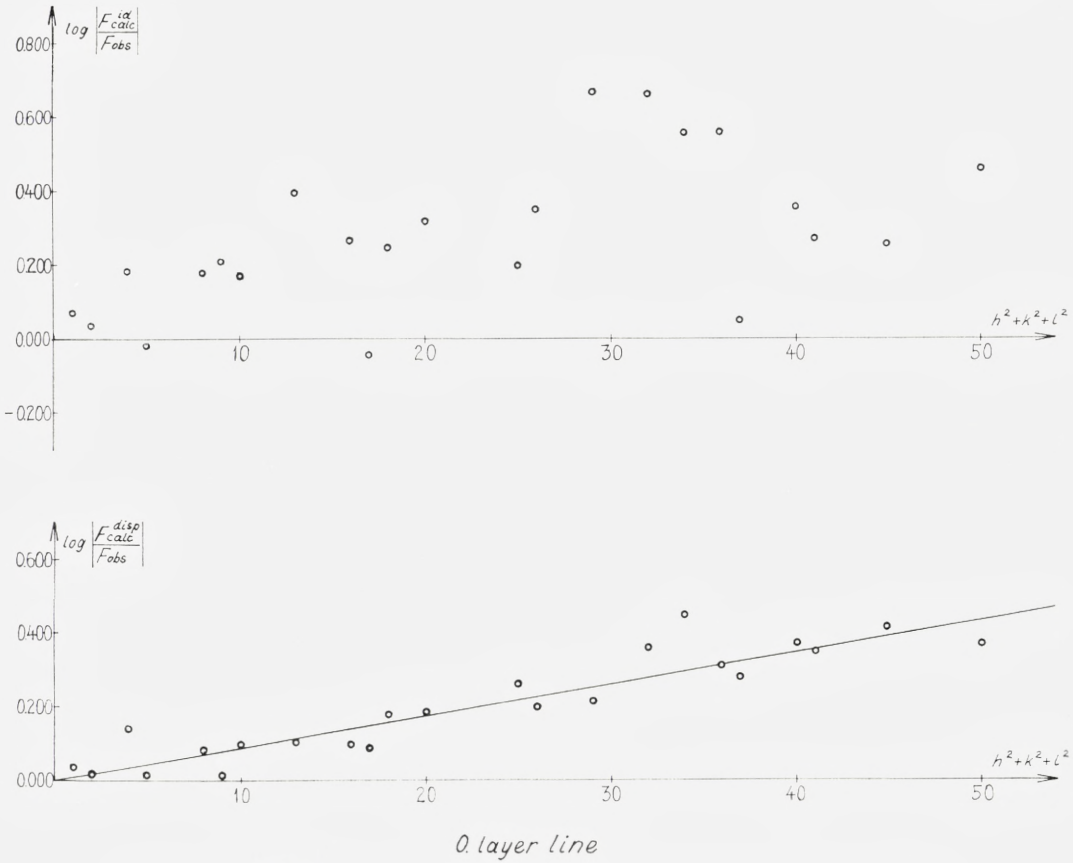


Fig. 8. $\log_{10}\left|\frac{F_{\text{calc}}}{F_{\text{obs}}}\right|$ versus $h^2+k^2+l^2$ for the zeroth layer line of cubic $CsPbBr_3$.

tion of wavelength $\lambda$ should be multiplied by $\exp\left\{-2\,\pi^2\,\overline{(\boldsymbol{S}\cdot\boldsymbol{u})^2}\right\}$, where $\overline{(\boldsymbol{S}\cdot\boldsymbol{u})^2}$ is $\left(\frac{2\sin\vartheta}{\lambda}\right)^2$ times the mean-square displacement parallel to the reciprocal vector $\boldsymbol{S}=h\,\boldsymbol{a}^*+k\,\boldsymbol{b}^*+l\,\boldsymbol{c}^*$.

For each halogen atom we have assumed four displaced positions as explained above. Hence, e. g. for the atom displaced $u\sqrt{2}$ from the ideal position $\left(\frac{1}{2},0,0\right)$ along the diagonals in the plane $x=\frac{1}{2}$, the "effective" atomic scattering factor becomes $f(\vartheta)\,\exp\left\{-2\,\pi^2u^2\,(k^2+l^2)\right\}$, and analogously for the two other halogen atoms by cyclic replacement. For the Cs-atoms we have assumed that there are six possible displacements $\boldsymbol{U}$, viz. towards the

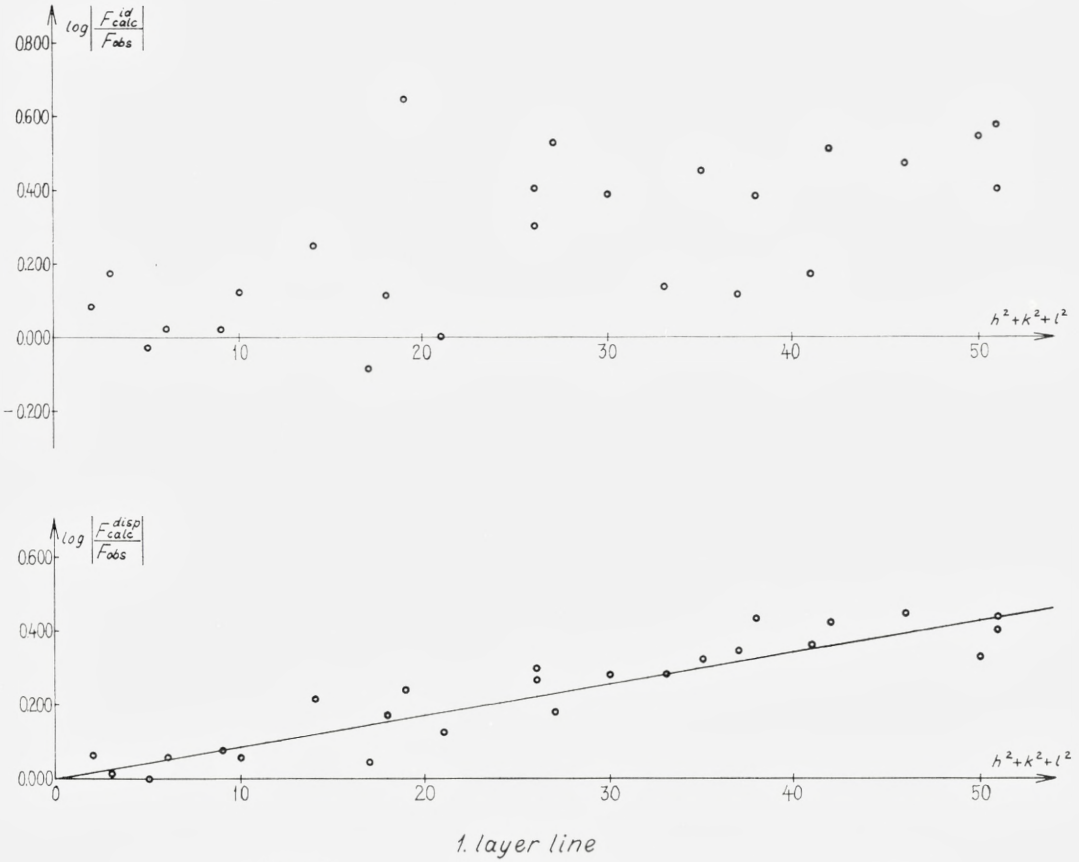


Fig. 9. $\log_{10}\left|\frac{F_{\text{calc}}}{F_{\text{obs}}}\right|$ versus $h^2+k^2+l^2$ for the first layer line of cubic $CsPbBr_3$.

centres of the unit-cell faces, but there might equally well be twelve such displacements towards the unit-cell edges. Formally this only changes the interpretation of $U$. Altogether the expression for the structure factor is then given by:

$$\left.\begin{aligned} F(hkl) = f(\vartheta)_{\text{Pb}} + f(\vartheta)_{\text{Cs}} \cdot \exp\left\{-\frac{2\pi^2 U^2}{3}(h^2+k^2+l^2)\right\} \cdot \cos\pi(h+k+l) \\ + f(\vartheta)_X [\exp\{-2\pi^2 u^2 (k^2+l^2)\} \cdot \cos\pi h + \exp\{-2\pi^2 u^2 (h^2+l^2)\} \cdot \cos\pi k \\ + \exp\{-2\pi^2 u^2 (h^2+k^2)\} \cdot \cos\pi l]; \end{aligned}\right\} \quad (6)$$

With this formula calculations of structure factors have been made for a certain range of values of $u$ and $U$. The best agreement with the experi-

TABLE 3. Comparison of observed and calculated $F$-values for $CsPbCl_3$. (0., 1., 2., and 3. layer line)

| Indices | Calculated $F$-values | | Observed $F$-values: Cubic structure | | Observed $F$-values: Tetragonal structure | |
|---|---|---|---|---|---|---|
| $h\ k\ l$ | Ideal perovskite | Displaced perovskite | $F_{obs.}$ at about 54° C. | $F_{obs.}$ temp. corr. | $F_{obs.}$ at about 20° C. | $F_{obs.}$ temp. corr. |
| 010 | 38 | 37 | 37 | 37 | 36 | 36 |
| 020 | 148 | 133 | 117 | 117 | 118 | 118 |
| 030 | 29 | 29 | 34 | 35 | 33 | 34 |
| 040 | 112 | 83 | 77 | 84 | 81 | 86 |
| 050 | 23 | 27 | 25 | 29 | 24 | 26 |
| 060 | 89 | 55 | 46 | 56 | 49 | 57 |
| 070 | 18 | 27 | 24 | 31 | 26 | 32 |
| 110 | 103 | 100 | 91 | 91 | 89 | 89 |
| 120 | 32 | 38 | 38 | 38 | 39 | 40 |
| 130 | 85 | 74 | 65 | 68 | 67 | 70 |
| 140 | 26 | 40 | 42 | 46 | 39 | 42 |
| 150 | 66 | 49 | 53 | 62 | 48 | 53 |
| 160 | 20 | 40 | 35 | 42 | 33 | 39 |
| 170 | 56 | 35 | 28 | 37 | 33 | 41 |
| 220 | 130 | 107 | 93 | 96 | 94 | 97 |
| 230 | 27 | 32 | 31 | 33 | 31 | 32 |
| 240 | 104 | 72 | 62 | 69 | 61 | 67 |
| 250 | 22 | 29 | 25 | 30 | 21 | 23 |
| 260 | 86 | 50 | 39 | 49 | 42 | 49 |
| 330 | 74 | 61 | 49 | 54 | 53 | 57 |
| 340 | 22 | 35 | 28 | 32 | 33 | 37 |
| 350 | 62 | 46 | 37 | 44 | 42 | 48 |
| 360 | 19 | 36 | 25 | 32 | 25 | 30 |
| 440 | 92 | 54 | 39 | 47 | 44 | 50 |
| 450 | 19 | 32 | 25 | 32 | 29 | 34 |
| 550 | 56 | 40 | 34 | 44 | 39 | 48 |
| 011 | 103 | 100 | 91 | 91 | 89 | 89 |
| 021 | 32 | 38 | 40 | 41 | 36 | 37 |
| 031 | 86 | 75 | 72 | 73 | 74 | 75 |
| 041 | 26 | 40 | 43 | 47 | 41 | 44 |
| 051 | 66 | 49 | 49 | 57 | 51 | 56 |
| 061 | 20 | 39 | 39 | 47 | 42 | 49 |
| 071 | 56 | 35 | 31 | 41 | 37 | 46 |
| 111 | $\overline{18}$ | $\overline{6}$ | — | — | — | — |
| 121 | 93 | 91 | 77 | 79 | 70 | 72 |
| 131 | $\overline{10}$ | 16 | — | — | — | — |
| 141 | 74 | 70 | 66 | 73 | 68 | 73 |
| 151 | $\overline{8}$ | 25 | — | — | — | — |
| 161 | 60 | 52 | 43 | 52 | 46 | 54 |
| 171 | $\overline{7}$ | 28 | — | — | — | — |
| 221 | 29 | 38 | 40 | 42 | 34 | 35 |
| 231 | 79 | 69 | 61 | 66 | 63 | 66 |
| 241 | 24 | 38 | 33 | 37 | 34 | 37 |
| 251 | 64 | 48 | 43 | 50 | 45 | 51 |
| 260 | 19 | 38 | 26 | 33 | 31 | 36 |
| 331 | $\overline{8}$ | 25 | — | — | — | — |
| 341 | 66 | 56 | 46 | 54 | 51 | 56 |
| 351 | $\overline{8}$ | 30 | — | — | — | — |
| 361 | 57 | 44 | 36 | 46 | 34 | 41 |
| 441 | 20 | 35 | 25 | 30 | 29 | 33 |
| 451 | 58 | 43 | 34 | 43 | 37 | 44 |
| 551 | $\overline{7}$ | 32 | 24 | 31 | 24 | 29 |
| 012 | 32 | 38 | 32 | 33 | 33 | 34 |
| 022 | 130 | 108 | 96 | 100 | 92 | 95 |
| 032 | 27 | 32 | 33 | 36 | 36 | 38 |
| 042 | 104 | 72 | 69 | 77 | 70 | 75 |
| 052 | 22 | 29 | 28 | 33 | 28 | 32 |
| 062 | 86 | 50 | 41 | 51 | 45 | 53 |
| 112 | 93 | 91 | 81 | 83 | 84 | 86 |
| 122 | 29 | 38 | 39 | 40 | 41 | 42 |
| 132 | 79 | 69 | 64 | 69 | 66 | 69 |
| 142 | 24 | 38 | 38 | 42 | 39 | 42 |
| 152 | 64 | 47 | 41 | 48 | 44 | 50 |
| 162 | 19 | 37 | 30 | 37 | 31 | 36 |
| 222 | 119 | 91 | 85 | 90 | 80 | 85 |
| 232 | 25 | 34 | 33 | 36 | 30 | 32 |
| 242 | 99 | 64 | 54 | 62 | 58 | 64 |
| 252 | 21 | 31 | 25 | 30 | 28 | 32 |
| 262 | 84 | 47 | 38 | 47 | 40 | 48 |
| 332 | 70 | 57 | 48 | 54 | 50 | 54 |
| 342 | 22 | 35 | 29 | 34 | 29 | 33 |
| 352 | 60 | 44 | 34 | 42 | 41 | 47 |
| 362 | 18 | 34 | 25 | 33 | 28 | 34 |
| 442 | 89 | 50 | 39 | 48 | 38 | 44 |
| 452 | 18 | 32 | 28 | 36 | 28 | 33 |
| 013 | 85 | 74 | 57 | 60 | 60 | 63 |
| 023 | 27 | 32 | 34 | 37 | 34 | 36 |
| 033 | 74 | 61 | 60 | 65 | 63 | 68 |
| 043 | 23 | 35 | 34 | 39 | 35 | 39 |
| 053 | 61 | 45 | 37 | 44 | 35 | 41 |
| 063 | 19 | 36 | 29 | 37 | 31 | 37 |
| 113 | $\overline{10}$ | 16 | 18 | 19 | 22 | 23 |
| 123 | 79 | 69 | 61 | 66 | 62 | 66 |
| 133 | $\overline{8}$ | 25 | 27 | 30 | 29 | 31 |
| 143 | 66 | 57 | 53 | 61 | 52 | 58 |
| 153 | $\overline{8}$ | 29 | 26 | 32 | 26 | 30 |
| 163 | 57 | 44 | 35 | 45 | 38 | 46 |
| 223 | 25 | 33 | 34 | 37 | 33 | 36 |
| 233 | 70 | 57 | 49 | 55 | 48 | 52 |
| 243 | 22 | 35 | 30 | 35 | 32 | 37 |
| 253 | 60 | 44 | 34 | 42 | 39 | 45 |
| 263 | 18 | 34 | 25 | 33 | 28 | 34 |
| 333 | $\overline{8}$ | 29 | 25 | 28 | 26 | 29 |
| 343 | 61 | 49 | 39 | 46 | 40 | 46 |
| 353 | $\overline{8}$ | 31 | 25 | 32 | 24 | 29 |
| 443 | 19 | 34 | 28 | 35 | 26 | 31 |
| 453 | 56 | 40 | 33 | 43 | 35 | 43 |

TABLE 4. Comparison of observed and calculated $F$-values for $CsPbBr_3$. (0. and 1. layer line)

| Indices | Calculated $F$-values | | Observed $F$-values: Cubic structure | | Observed $F$-values: Monoclinic structure | | Indices | Calculated $F$-values | | Observed $F$-values: Cubic structure | | Observed $F$-values: Monoclinic structure | |
|---|---|---|---|---|---|---|---|---|---|---|---|---|---|
| $h\,k\,l$ | Ideal perovskite | Displaced perovskite | $F_{obs.}$ at about 140° C. | $F_{obs}$ temp. corr. | $F_{obs.}$ at about 20° C. | $F_{obs.}$ temp. corr. | $h\,k\,l$ | Ideal perovskite | Displaced perovskite | $F_{obs.}$ at about 140° C. | $F_{obs}$ temp. corr. | $F_{obs.}$ at about 20° C. | $F_{obs.}$ temp. corr. |
| 010 | 54 | 50 | 46 | 47 | 48 | 49 | 011 | 86 | 82 | 71 | 74 | 76 | 78 |
| 020 | 192 | 170 | 126 | 136 | 128 | 137 | 021 | 47 | 50 | 50 | 55 | 51 | 55 |
| 030 | 42 | 27 | 26 | 31 | 23 | 26 | 031 | 74 | 63 | 56 | 68 | 52 | 60 |
| 040 | 145 | 100 | 79 | 109 | 96 | 124 | 041 | 37 | 50 | 45 | 64 | 46 | 59 |
| 050 | 33 | 19 | — | — | — | — | 051 | 58 | 43 | 23 | 39 | 31 | 45 |
| 060 | 116 | 65 | 32 | 67 | 47 | 81 | 061 | 28 | 48 | 22 | 46 | 18 | 32 |
| 070 | 26 | 20 | — | — | — | — | 071 | 49 | 29 | 14 | 37 | — | — |
| 110 | 88 | 84 | 81 | 84 | 95 | 97 | 111 | $\overline{64}$ | $\overline{44}$ | 43 | 46 | 46 | 48 |
| 120 | 47 | 50 | 49 | 54 | 53 | 57 | 121 | 79 | 86 | 75 | 85 | 79 | 86 |
| 130 | 74 | 63 | 50 | 62 | 59 | 69 | 131 | $\overline{38}$ | $\overline{3}$ | — | — | — | — |
| 140 | 37 | 51 | 41 | 58 | 49 | 64 | 141 | 65 | 75 | 50 | 73 | 65 | 85 |
| 150 | 58 | 41 | 26 | 44 | 32 | 47 | 151 | $\overline{36}$ | 17 | 11 | 20 | — | — |
| 160 | 28 | 48 | 25 | 53 | 31 | 54 | 161 | 53 | 59 | 22 | 47 | 40 | 70 |
| 170 | 49 | 29 | 14 | (37) | 21 | 46 | 171 | $\overline{30}$ | 22 | 8 | 22 | — | — |
| 220 | 172 | 133 | 110 | 130 | 126 | 142 | 221 | 43 | 48 | 41 | 49 | 50 | 57 |
| 230 | 39 | 33 | 26 | 34 | 24 | 30 | 231 | 69 | 65 | 39 | 51 | 55 | 68 |
| 240 | 137 | 84 | 55 | 83 | 58 | 79 | 241 | 34 | 46 | 34 | 52 | 46 | 63 |
| 250 | 31 | 25 | 15 | 28 | 15 | 23 | 251 | 56 | 43 | 23 | 42 | 38 | 60 |
| 260 | 112 | 57 | 24 | 55 | 27 | 51 | 261 | 28 | 43 | 19 | 43 | — | — |
| 330 | 65 | 55 | 37 | 53 | 37 | 48 | 331 | 40 | 16 | 9 | 13 | — | — |
| 340 | 33 | 39 | 21 | 36 | 24 | 34 | 341 | 58 | 58 | 29 | 50 | 41 | 60 |
| 350 | 54 | 42 | 15 | 30 | 23 | 38 | 351 | $\overline{34}$ | 25 | 12 | 24 | — | — |
| 360 | 27 | 40 | 15 | 38 | 19 | 37 | 361 | 50 | 48 | 17 | 44 | 24 | 48 |
| 440 | 120 | 59 | 26 | 50 | 24 | 39 | 441 | 30 | 39 | 22 | 42 | 49 | 80 |
| 450 | 26 | 30 | 14 | 32 | 13 | 25 | 451 | 52 | 43 | 16 | 38 | — | — |
| 550 | 49 | 39 | 17 | 46 | 18 | 40 | 551 | $\overline{30}$ | 31 | 12 | 35 | — | — |

mental $|F(hkl)|$ is obtained with $U = 0.075$ and $u = 0.070$; the latter is also derived directly from the electron projection of $CsPbCl_3$. The corresponding displacements in Å-units are for $CsPbCl_3$: 0.42 Å and 0.39 Å; and for $CsPbBr_3$ $0.43_5$ Å and $0.40_5$ Å, respectively.

Plots of $\log \left| \frac{F^{disp.}_{calc.}}{F_{obs.}} \right|$ against $h^2 + k^2 + l^2$ now show rather good approximations to straight lines of the type

$$\log_{10} \left| \frac{F_{\text{calc.}}}{F_{\text{obs.}}} \right| = \log_{10} A + B \cdot (h^2 + k^2 + l^2), \tag{7}$$

where $A$ and $B$ are constants which can easily be evaluated from the graphs. The experimentally determined relative $|F(hkl)|$-values have then been brought on absolute scales corresponding to $F(000) = 186$ for $CsPbCl_3$ and $F(000) = 234$ for $CsPbBr_3$ by multiplication with the factors A. They are

given in Tables 3 and 4 in the 4th and 6th column. The last term in (7) is due to the isotropic thermal movements of the atoms but also includes the absorption correction. In order to eliminate its influence on the experimental $F(hkl)$ they have finally been multiplied by the factor $10^{B_{\text{cub}}\,(h^2+k^2+l^2)}$. This final version of the observed structure factors, which is reproduced in Columns 5 and 7 of Table 3 and 4 shows almost perfect agreement with the structure factors calculated from (6), thus proving our assumptions to be appropriate.

Similar conversions and corrections have been applied to the structure factors measured for the tetragonal or monoclinic form of these crystals and the constants, $B_{\text{tetr.}}$ have also been determined. As pointed out above, the intensities here are more difficult to measure, and hence there is a greater uncertainty on the $F_{\text{exp.}}$. However, the $B_{\text{tetr.}}$-values determined for different layer lines of the same crystal at constant temperature are identical within the accuracy of the measurements.

Although the $B$-values do include a term contributed form the absorption, the differences $B_{\text{tetr.}} - B_{\text{cub.}}$ by our method of comparing the intensities depend only on the temperatures and the possible changes of the atomic arrangement. If we could be sure that only the changes in thermal movements of the atoms were of importance the following relation should be approximately true:[1]

$$\Delta B = 0.4343 \cdot \frac{3h^2 \cdot N}{2k\Theta_D^2} \frac{1}{Ma^2} \cdot \Delta T, \tag{8}$$

where $\Theta_D$ is the "characteristic" or Debye-temperature. Inserting $h = 6.623 \cdot 10^{-27}$, $k = 1.380 \cdot 10^{-16}$, $N = 6.025 \cdot 10^{23}$, and rearranging we get with $a$, the unit-cell edge, in Å units:

$$\Theta_D = 35.32 \frac{1}{a} \left( \frac{1}{M} \cdot \frac{\Delta T}{\Delta B} \right)^{1/2} \tag{9}$$

In this formula $M$ is the molecular weight of the vibrating particle; in our case we may presumably insert the molecular weight of the unit-cell contents, i.e. $CsPbX_3$, thus asking for a lower limit of $\Theta_D$ and considering the influence of the acoustic waves only.

Neglecting the existence of the superstructure we can then calculate the $\Theta_D$ compatible with the decrease in intensity of the $X$-ray reflections

[1] Cf. R.W. James, loc. cit. p. 219–38.

on heating the crystals from room temperature to above their transition points, the results being

$$\Theta_D = 72^\circ K \text{ for } CsPbCl_3 \text{ and } \Theta_D = 60^\circ K \text{ for } CsPbBr_3.$$

As the characteristic temperatures obtained in this way do not seem unreasonable these calculations indicate that very little happens to the atoms at the transition from cubic to tetragonal structure apart from their preferred occupation of one particular set of their possible potential minima.

On the same assumption we may also estimate an average value for the root-mean-square displacements of the atoms, due to thermal movements, from the approximate formula:

$$\sqrt{\overline{u^2}} \simeq \frac{a}{\pi} \sqrt{\frac{3}{0.8686} \cdot \frac{\Delta B}{\Delta T} \cdot T} \qquad (10)$$

We find for $CsPbCl_3$ $\sqrt{\overline{u^2}} \simeq 0.25$ Å, and for $CsPbBr_3$ $\sqrt{\overline{u^2}} \simeq 0.28$ Å – values which seem quite reasonable.

## Discussion

One of the aims of the present investigations was to determine the configuration of the lead-halogen complexes, and at first sight it seemed that a very good argument could be given for the regular octahedron from the existence of perovskite-like structures with one molecule $CsPbX_3$ in the unit cell. However, the *X*-ray analysis shows that this cannot be true, and if we accept the interpretation given above, it seems doubtful whether it is at all possible to speak of a fixed configuration of a particular $PbX_6$-unit, — or indeed of such units, in the cubic crystals.

In the tetragonal crystals, on the other hand, it appears that there is a fixed configuration, but this is not that of a regular octahedron although it is closely related to it. It is interesting that distorted $PbX_6$-octahedra are also found in the yellow, orthorhombic $CsPbI_3$ and in the compounds $Cs_4PbX_6$.[1]

Although the displacements of the atoms from their ideal positions in the cubic crystals could have been described in terms of thermal movements we have here preferred to assume the existence of several possible potential minima for the Cs and X-toms, because the vibrational amplitudes in the

[1] C. K. Moller. To be published in this series.

former description become rather large. Nor can we exclude the possibility of free rotations of these atoms in the cubic crystals, but whenever this has been assumed to explain certain transition phenomena in crystals, it has been shown that they may equally well, if not better, be explained by order-disorder transformations.[1]

It is tried to get a decision of this question from measurement of the entropy change at the transformation $(CsPbCl_3)_{tetr.} \rightleftarrows (CsPbCl_3)_{cub.}$.

On the above assumption there cannot be one single characteristic Cs-*X* distance in the cubic crystals, but rather a certain range of discrete values. The Pb-*X* distances on the other hand are well-defined, but they are considerably shorter than the distances to be expected from the sum of ionic radii.[2] (See Table 5).

This has also been observed for other crystals which contain lead and halogen atoms, and it may mean either that the ionic radius for Pb needs a revision or (more likely) that polarization ("covalency") is of importance in these compounds. The colour of the crystals also strongly suggests the latter explanation.

On the whole the perovskite-like crystals of the type $CsPbX_3$ show so many analogies to the crystals of mixed oxides of the $BaTiO_3$-type that it is tempting to apply also to the latter the interpretation given here of the transformation from tetragonal to cubic structure. In this way there would be a close analogy of dielectric phenomena in solids to those in gases: The situation at temperatures above the transition to cubic structure where "free" diffusion of anions and some cations among selected potential minima creates a structure with maximum disorder of the kind described above, corresponds to a polar gas at very high temperatures in a very weak electric field (no orientation). Below the transition temperature the preferred occupation of certain potential minima (also present in the cubic state) may result in a multiple cell with no dipole moment, in which case we have an antiferroelectric phase. This corresponds to a non-polar gas of associated dipolar molecules (internal compensation). — Or the result of the transformation may be a unit cell with a dipole moment, whose electric field will help to create a preferred configuration all through the crystal, thus giving a ferroelectric. The analogy here, of course, is a gas of polar molecules in an electric field and at not too high temperatures.

Based on ideas of this kind MASON and MATTHIAS[3] have developed a

[1] J. FRENKEL, Kinetic Theory of Liquids. Chapter II. Oxford 1948. See also J. P. MATHIEU, Yearbook. Phys. Soc. G.B., 23—29 (1956).

[2] LANDOLT-BÖRNSTEIN, I. Band, 4. Teil p. 523.

[3] W. P. MASON and B. T. MATHIAS, Phys. Rev. **74**, 1622 (1948).

TABLE 5. Some interatomic distances in the perovskite-like crystals of $CsPbCl_3$ and $CsPbBr_3$

| | | Pb-$X$ | Cs-$X_{max.}$ | Cs-$X_{prob.}$ | Cs-$X_{min.}$ |
|---|---|---|---|---|---|
| $CsPbCl_3$ | From the present work | 2.86 Å | 3.76 Å | 3.68 Å | 3.13 Å |
| | From Pauling's ionic radii | 3.02 - | | 3.50 - | |
| | From Goldschmidt's ionic radii | 3.13 - | | 3.48 - | |
| $CsPbBr_3$ | From the present work | 2.99 - | 3.94 - | 3.85 - | 3.28 - |
| | From Pauling's ionic radii | 3.16 - | | 3.64 - | |
| | From Goldschmidt's ionic radii | 3.28 - | | 3.63 - | |

theory for ferroelectricity in $BaTiO_3$ which, however, has been severely criticized by JAYNES[1] mainly for the following reason. An order-disorder transition involving 6 close-lying Ti-positions (as assumed by MASON and MATTHIAS) will require an entropy change $R\log 6 \simeq 3.6$ cal $mol^{-1}deg^{-1}$, but the measured value is only about 0.1 cal $mol^{-1}deg^{-1}$. However, it does not seem quite obvious how the entropy measurements should be interpreted, nor whether the simple calculation of the entropy is strictly valid. It is hoped that measurement of the corresponding entropy change in $CsPbCl_3$ may help to clarify some of these problems, and it is also suggested that it might be interesting to make a thorough neutron or $X$-ray investigation of $BaTiO_3$ at temperatures above 120°C.

## Acknowledgements

I wish to thank Professor A. TOVBORG JENSEN, Ph. D., for his interest in this work and Mr. PETER COLDING JØRGENSEN for carrying out many of the calculations and measurements.

[1] For a survey and references see H. D. MEGAW, Ferroelectricity in crystals, Chapter 10. Methuen, London 1957.

Indleveret til selskabet den 11. juni 1959.
Færdig fra trykkeriet den 31. december 1959.

Matematisk-fysiske Meddelelser
udgivet af
Det Kongelige Danske Videnskabernes Selskab
Bind **32**, nr. 3

Mat. Fys. Medd. Dan. Vid. Selsk. **32**, no. 3 (1960)

# ON THE STRUCTURE OF CÆSIUM HEXAHALOGENO-PLUMBATES (II)

BY

CHRISTIAN KN. MØLLER

København 1960
i kommission hos Ejnar Munksgaard

## Synopsis

Crystalline compounds of composition $Cs_4PbX_6$, in which X = Cl, Br, or I may be prepared either from aqueous solutions or by fusing CsX and $PbX_2$ together. *X*-ray investigations show that the crystals are rhombohedral and belong to space group No. 167 $R\bar{3}c$. The hexagonal unit cells have dimensions $a = 13.18_7$ Å, $c = 16.64_1$ Å for $Cs_4PbCl_6$; $a = 13.73_2$ Å, $c = 17.32_4$ Å for $Cs_4PbBr_6$; $a = 14.52_8$ Å, $c = 18.31_3$ Å for $Cs_4PbI_6$, and contain six "molecules". The molar volumes of $Cs_4PbX_6$ are larger than the sum of the molar volumes of CsX and $PbX_2$ by c. 6 cc. per gram-atom halogen. — Atomic parameters can be obtained from fairly well resolved Patterson- and electron-projections on $(1\bar{2}10)$. The Pb- and X-atoms form isolated, slightly distorted $PbX_6$-octahedra; the PbCl-distances are 2.93 Å and the PbBr-distances are 3.12 Å, i. e. in both cases a little longer than in the $CsPbX_3$-compound, but shorter than the sum of the ionic radii. The agreement between calculated and observed structure factors is not so good as wanted. This may in part be due to a small delocalization around their average positions of the Cs-atoms having an irregular 8-coordination.



Printed in Denmark
Bianco Lunos Bogtrykkeri A-S

## Introduction

In the course of a systematic study of the structure of the plumbo-halogen complex ions it became of interest also to examine the crystalline compounds with the general formula $Cs_4PbX_6$. The interpretation of the Guinier diagram of $CsPbCl_3$ had already made it necessary to investigate the powder diagram of $Cs_4PbCl_6$[1] and from this start we have continued work on structures of this type. When it had progressed so far that most of the facts mentioned in the present article could materialize it was understood from a footnote in a paper by G. BERGERHOF and O. SCHMITZ-DUMONT[2] that these authors had also been engaged on the same problem. However, they have not, apparently, published any results of their investigations, and we have therefore taken the opportunity to give an account of our own work on these compounds as they are closely related to the previously investigated structure of type $CsPbX_3$.

## Preparation and some general properties

The crystalline compounds $Cs_4PbCl_6$ and $Cs_4PbBr_6$ can be made in two ways: (1) By dissolving $PbX_2$ in a boiling aqueous solution which is almost saturated with CsX at room temperature, filtering while still hot and then leave to slow cooling.[3] (2) By fusing CsX and $PbX_2$ together in the correct stoichiometric proportion. — As for $Cs_4PbI_6$ this compound had not been prepared before; it was obtained (unintentionally) by boiling $PbBr_2$ in an aqueous solution nearly saturated with a fifty—fifty mixture of CsBr and CsI. It does not seem possible to obtain it in a pure state by melting $PbI_2$ and CsI together in the stoichiometric proportion: The powder diagrams of such products besides lines of $Cs_4PbI_6$ invariably also show the presence of

[1] C. K. MØLLER, The Structure of Perovskite-like Cæsium Plumbo Trihalides. Mat. Fys. Medd. Dan. Vid. Selsk. **32**, No. 2 (1959).

[2] G. BERGERHOF u. O. SCHMITZ-DUMONT. *Z. anorg. u. allgem. Chem.* **284**, 10 (1956).

[3] H. L. WELLS. *Z. anorg. Chem.* **3**, 195 (1893).

CsI-lines. Apart from this the identity of compounds obtained in the different ways was shown from their *X*-ray powder diagrams.

The crystals grown from solutions were colourless and their most prominent faces were parallelogram-shaped with angles 72°—60° and 108°—120°. Under the polarizing microscope the Cl- and Br-compounds showed diagonal extinction with $\alpha'$ bisecting the acute angles. The refractive indices were high, but the birefringence low. On the assumption that the crystals were hexagonal (proved from the *X*-ray work) it could be inferred from conoscopic examination that they were uniaxially positive in all three cases.

The density was determined on single crystals of $Cs_4PbCl_6$ by flotation in Clerici solutions of different densities to be $3.70 \pm 0.07$ g/cm³.

No changes of the crystals could be observed on heating them to about 320° C.

## Space group and unit cell dimensions

*X*-ray investigations on powders of $Cs_4PbCl_6$, $Cs_4PbBr_6$, and $Cs_4PbI_6$, and on single crystals of the first two were made along the same lines as in the previous paper (1).

The Weissenberg diagrams taken about twofold axes of the single crystals could be indexed on a hexagonal lattice. Reflections of type *hkil* were only observed for $-h+k+l = 3n$, and $h\bar{h}0l$ only for $l = 2n$, so that the space group can be either No. 167 $R\bar{3}c$ or No. 161 $R3c$, but as no piezoelectric effect could be detected by a dynamical method,[4] the former seems most likely. The Guinier diagrams could be indexed by application of the general quadratic form:

$$\sin^2\vartheta = \frac{\lambda^2}{3a^2}(h^2 + k^2 + hk) + \frac{\lambda^2}{4c^2}l^2 = \frac{a^{*2}}{4} \cdot s + \frac{c^{*2}}{4}l^2 \qquad (1)$$

The result of this together with the unit cell dimensions derived from the coefficients to $s$ and $l^2$ are given in Table 1 ($\lambda = 1.5418$ Å).

The number of molecules per hexagonal unit cell of $Cs_4PbCl_6$ is found from the unit cell volume, density of the crystals and molecular weight to be 5.9, i. e. 6. As it is beyond doubt that $Cs_4PbBr_6$ and $Cs_4PbI_6$ are both isomorphous with $Cs_4PbCl_6$, it is concluded that they also have 6 molecules per hexagonal unit cell (or 2 molecules per rhombohedral unit cell).

[4] W. Frank, Unpublished work.

TABLE 1. Comparison of observed and calculated $\sin^2\vartheta$-values for $Cs_4PbCl_6$, $Cs_4PbBr_6$ and $Cs_4PbI_6$

| Indices *hkil* | $Cs_4PbCl_6$ | | | $Cs_4PbBr_6$ | | | $Cs_4PbI_6$ | | |
|---|---|---|---|---|---|---|---|---|---|
| | Intensity estimated | $10^4 \cdot \sin^2\vartheta_{obs.}$ | $10^4 \cdot \sin^2\vartheta_{calc.}$ | Intensity estimated | $10^4 \cdot \sin^2\vartheta_{obs.}$ | $10^4 \cdot \sin^2\vartheta_{calc.}$ | Intensity estimated | $10^4 \cdot \sin^2\vartheta_{obs.}$ | $10^4 \cdot \sin^2\vartheta_{calc.}$ |
| $\bar{1}012$ | m-s | 0132 | 0132 | m | 0120 | 0121 | m | 0109 | 0109 |
| $11\bar{2}0$ | m-s | 0137 | 0137 | m-(w) | 0126 | 0126 | m-w | 0113 | 0113 |
| $11\bar{2}3$ | s | 0330 | 0330 | m | 0304 | 0304 | vw? | $027_0$ | 0273 |
| $21\bar{3}1$ | (v)w | 0341 | 0340 | .. | .. | .. | .. | .. | .. |
| $\bar{2}\bar{1}32$ | .. | .. | .. | vw | 0373 | 0373 | (v)w | 0335 | 0334 |
| $10\bar{1}4$ | w-m | 0389 | 0388 | .. | .. | .. | .. | .. | .. |
| $30\bar{3}0$ | (v)s | 0411 | 0410 | (m)-s | 0378 | 0378 | m(-w) | 0339 | 0338 |
| $\bar{2}024$ | m-s | 0526 | 0525 | m-s | 0485 | 0485 | m | 0435 | 0434 |
| $22\bar{4}0$ | vw | 0547 | 0547 | .. | .. | .. | .. | .. | .. |
| $\bar{3}\bar{1}41$ | m | 0614 | 0614 | m-s | 0566 | 0566 | m-(s) | 0506 | 0506 |
| $30\bar{3}3$ | .. | .. | .. | .. | .. | .. | vw? | 0496 | 0498 |
| $21\bar{3}4$ | (m)-s | 0662 | 0662 | s | 0611 | 0611 | m-s | 0547 | 0547 |
| $31\bar{4}2$ | (w)-m | 0679 | 0678 | w-m | 0626 | 0625 | m | 0560 | 0560 |
| $22\bar{4}3$ | (m)-s | 0740 | 0740 | s | 0683 | 0682 | (m)s | 0610 | 0610 |
| 0006 | w | 0772 | 0772 | w-m | 0712 | 0713 | w | 0639 | 0639 |
| $\bar{4}042$ | vw | 0815 | 0815 | .. | .. | .. | .. | .. | .. |
| $\bar{2}\bar{1}35$ | w | 0856 | 0856 | vw | 0789 | 0789 | vw | 0706 | 0707 |
| $32\bar{5}1$ | vw? | 0888 | 0888 | .. | .. | .. | .. | .. | .. |
| $11\bar{2}6$ | w-m | 0909 | 0910 | w-m | 0838 | 0839 | .. | .. | .. |
| $\bar{3}\bar{1}44$ | w-m | 0936 | 0935 | w | 0862 | 0863 | vw | 0772 | 0772 |
| $41\bar{5}0$ | w-m | 0957 | 0957 | m-w | 0882 | 0882 | w | 0788 | 0789 |
| $40\bar{4}4$ | w | 1072 | 1072 | vw | 0989 | 0989 | vw? | 0885 | 0886 |
| $31\bar{4}5$ | w-(m) | 1130 | 1128 | w | 1042 | 1041 | w | 0932 | 0932 |
| $41\bar{5}3$ | w-m | 1150 | 1150 | v-w | 1061 | 1060 | .. | .. | .. |
| $30\bar{3}6$ | w | 1183 | 1182 | .. | .. | .. | .. | .. | .. |
| $32\bar{5}4$ | s-m | 1209 | 1209 | m-s | 1116 | 1115 | m | 0996 | 0997 |
| $33\bar{6}0$ | m | 1229 | 1230 | w | 1135 | $1134._5$ | (v)w | 1012 | $1013._5$ |
| $\bar{4}\bar{2}61$ | w | 1298 | 1298 | .. | .. | .. | .. | .. | .. |
| $22\bar{4}6$ | w-m | 1319 | 1320 | w | 1216 | 1217 | w | 1090 | 1089 |
| $42\bar{6}2$ | w | 1362 | 1362 | .. | .. | .. | .. | .. | .. |
| $\bar{1}018$ | w | 1419 | 1418 | w | 1310 | 1309 | w | 1173 | 1174 |
| $51\bar{6}1$ | w | 1434 | 1434 | (v)w | 1323 | 1323 | w | 1179 | 1182 |
| $\bar{5}054$ | w | 1481 | 1482 | vw | 1366 | 1367 | .. | .. | .. |
| $20\bar{2}8$ | w | 1556 | 1555 | vw? | 1433 | 1435 | vw? | c. 1284 | 1286 |
| $\bar{4}\bar{2}64$ | w | 1621 | 1619 | .. | .. | .. | .. | .. | .. |
| $\bar{3}\bar{1}47$ | w-m | 1645 | 1644 | .. | .. | .. | .. | .. | .. |
| $60\bar{6}0$ | .. | .. | .. | w | 1512 | 1513 | m-w | 1353 | 1351 |
| $\bar{2}\bar{1}38$ | w | 1692 | 1692 | vw | 1562 | 1561 | vw | 1399 | 1399 |
| $41\bar{5}6$ | w | 1729 | 1730 | .. | .. | .. | .. | .. | .. |

(to be continued)

TABLE 1 (continued).

| Indices *hkil* | $Cs_4PbCl_6$ Intensity estimated | $10^4 \cdot \sin^2\vartheta_{obs.}$ | $10^4 \cdot \sin^2\vartheta_{calc.}$ | $Cs_4PbBr_6$ Intensity estimated | $10^4 \cdot \sin^2\vartheta_{obs.}$ | $10^4 \cdot \sin^2\vartheta_{calc.}$ | $Cs_4PbI_6$ Intensity estimated | $10^4 \cdot \sin^2\vartheta_{obs.}$ | $10^4 \cdot \sin^2\vartheta_{calc.}$ |
|---|---|---|---|---|---|---|---|---|---|
| $51\bar{6}4$ | v-w | 1755 | 1756 | .. | .. | .. | .. | .. | .. |
| $52\bar{7}0$ | w | 1776 | 1777 | vw | 1638 | 1639 | vw | 1460 | 1464 |
| $\bar{4}\bar{3}72$ | | | 1772 | .. | .. | .. | | | 1460 |
| $42\bar{6}5$ | vw? | $181_4$ | 1812 | .. | .. | .. | s | 1495 | 1494 |
| $11\bar{2}9$ | (v)-w | 1875 | 1875 | .. | .. | .. | .. | .. | .. |
| $\bar{5}1\bar{6}5$ | vw | $194_9$ | 1950 | vw | 1796 | 1798 | vw | $160_6$ | 1608 |
| $\bar{6}1\bar{7}1$ | (v)-w | 1985 | 1981 | .. | .. | .. | vw | $163_1$ | 1632 |
| $61\bar{7}2$ | (v)-w | 2044 | 2046 | vw | 1880 | 1886 | .. | .. | .. |
| $43\bar{7}4$ | v-w | 2028 | 2029 | | | 1872 | .. | .. | .. |
| $\bar{4}048$ | vw | 2102 | 2102 | .. | .. | .. | .. | .. | .. |
| $10\bar{1}10$ | vw | 2193 | 2192 | .. | .. | .. | vw? | 181- | 1813 |
| $\bar{5}057$ | | | 2190 | .. | .. | .. | | | 1807 |
| $\bar{3}\bar{2}58$ | m | 2241 | 2239 | vw | 2067 | 2065 | vw | 1848 | 1849 |
| $22\bar{4}9$ | w | 2283 | 2285 | vw | 2111 | 2108 | vw? | 1887 | 1888 |
| $61\bar{7}5$ | .. | .. | .. | m-s | 2298 | 2302 | .. | .. | .. |
| $50\bar{5}8$ | .. | .. | .. | vw? | 2318 | 2317 | vw | 2075 | $2072._5$ |
| $\bar{5}\bar{3}84$ | .. | .. | .. | .. | .. | .. | w-m | 2122 | $2122._5$ |
| $70\bar{7}4$ | .. | .. | .. | .. | .. | .. | | | |
| Unit cell: | $a = 13.18_7$ Å; $c = 16.64_1$ Å Vol: 2506 Å$^3$ | | | $a = 13.73_2$ Å; $c = 17.32_4$ Å Vol: 2829 Å$^3$ | | | $a = 14.52_8$ Å; $c = 18.31_3$ Å Vol: 3447 Å$^3$ | | |

## Volume increments

It would seem interesting to compare the molar volumes of the compounds $Cs_4PbX_6$ and $CsPbX_3$ obtained from *X*-ray analysis with the (crystal) molar volumes of CsX and $PbX_2$. The latter have been calculated from the molecular weights and the densities of the simple, crystalline compounds, but practically the same values are obtained from *X*-ray determination of the unit cell dimensions.[5] Table 3 shows the result of this comparison. The "calculated" molar volumes are those to be expected from the molar volumes of CsX and $PbX_2$ if the rule about additivity of molar volumes were valid.

In all cases of formation of these compounds from simpler ones there is thus seen to be an increase in volume. It amounts to roughly 6 cc per

[5] G. WAGNER u. L. LIPPERT. *Z. phys. Chem. B.* **31**, 263, (1936). R. W. G. WYCKOFF: *Crystal Structures* Vol. I Chapter IV. New York 1948.

TABLE 2. Molar volumes and volume increments per gr.-atom halogen

| Compound | | X = Cl | X = Br | X = J | |
|---|---|---|---|---|---|
| CsX | | 42.4 cc | 48.0 cc | 57.6 cc | |
| $PbX_2$ | | 47.6 - | 55.0 - | 74.8 - | |
| $CsPbX_3$ | Calculated | 90.0 - | 103.0 - | 132.4 - | |
| | Observed | 106.0 - | 120.5 - | 141.9 cc (perovskite) | 134.1 cc (orthorh.) |
| | Increment per X | 5.3 - | 5.8 - | 3.2 cc | 0.6 cc |
| $Cs_4PbX_6$ | Calculated | 217.2 - | 247.0 - | 305.2 cc | |
| | Observed | 251.5 - | 283.9 - | 346.0 - | |
| | Increment per X | 5.7 - | 6.2 - | 6.8 - | |

gramatom of halogen except for $CsPbI_3$ in which it is practically negligible for the orthorhombic form.

As the structure of the latter compound—and also the structures of $PbX_2$—strongly indicate polarization of the halogen ions by the Pb-ions it seems reasonable to guess that the volume increments are connected with a change of the Pb-X-bonding—presumably an increase of ionic character —. In the perovskite-like structures of $CsPbX_3$ the less economic packing of the ions makes it possible for the cæsium and the halogen ions to "choose" among several close-lying potential minima (1).

If this is the case also in crystals of the $Cs_4PbX_6$-compounds, one might expect difficulties in localizing the Cs- and X-atoms accurately by *X*-ray methods.

## Atomic arrangements

With six molecules $Cs_4PbCl_6$ in a unit cell belonging to space group No. 167 most of the atomic positions should be fixed by symmetry and only four parameters have to be determined.[6]

Patterson projections on the plane $(1\bar{2}10)$ were calculated for both $Cs_4PbCl_6$ and $Cs_4PbBr_6$ from Weissenberg diagrams taken about a twofold axis (crystal dimensions were about 75 $\mu$). The results are shown in figs. 1 and 2. The maxima at $\left(0, \frac{1}{4}\right)$ are required by space group No. 167 if 6 Cs′ are placed in the special positions "*a*" and 6 Pb in the special positions "*b*" (see Ref. 6 p. 275). The remaining 18 Cs″-atoms are then likely to be in special positions "*e*", and on this assumption the peaks marked Cs-Cs

[6] International Tables for *X*-Ray Crystallography. Volume I. London 1952.

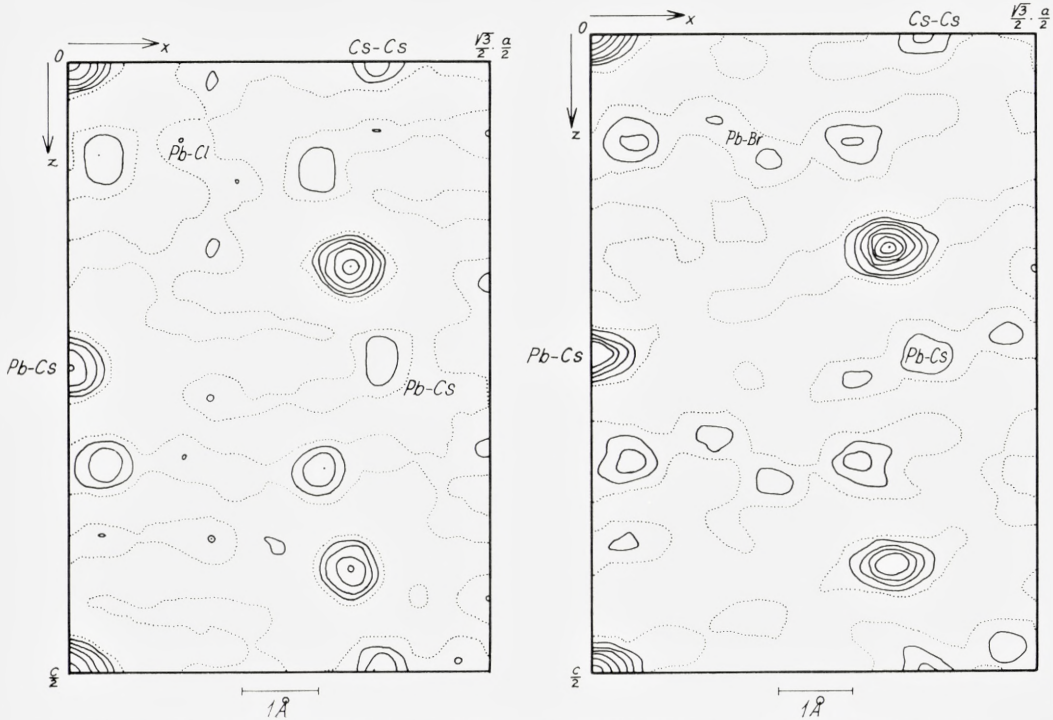


Fig. 1 and 2. Patterson projections on $(1\bar{2}\bar{1}0)$ of $Cs_4PbCl_6$ (left) and $Cs_4PbBr_6$ (right). Contour lines have been drawn at the (relative) levels: 0 (broken line) 50, 100, 150, 200, 300, 350.

and Pb-Cs provide the only missing Cs-parameter: $x = 0.37$. Having fixed the Pb- and Cs-atoms we are able to determine the signs for most of the structure factors $F(h0\bar{h}l)$ of $Cs_4PbCl_6$, and an electron projection on $(1\bar{2}10)$ was calculated. This is fairly well resolved (fig. 3). It is possible to locate the Cl-atoms with some certainty and thus to determine the still remaining three Cl-parameters. Structure factors calculated from the atomic parameters obtained in this way and from atomic scattering factors corrected for dispersion effects (1) show a fair agreement with the observed ones. However, attempts to refine the structures either by trial and error or from difference synthesis of $\varrho_{obs.} - \varrho_{calc.}$ were not successful (even less so for $Cs_4PbBr_6$!). The differences between strong and weak reflections obtained experimentally are much less pronounced than indicated by the calculated structure factors. This might be due to extinction, which is almost certain to be of importance in these crystals. Although no immediate absorption effects can be seen on the Weissenberg diagrams such ones may also be responsible for the lack of

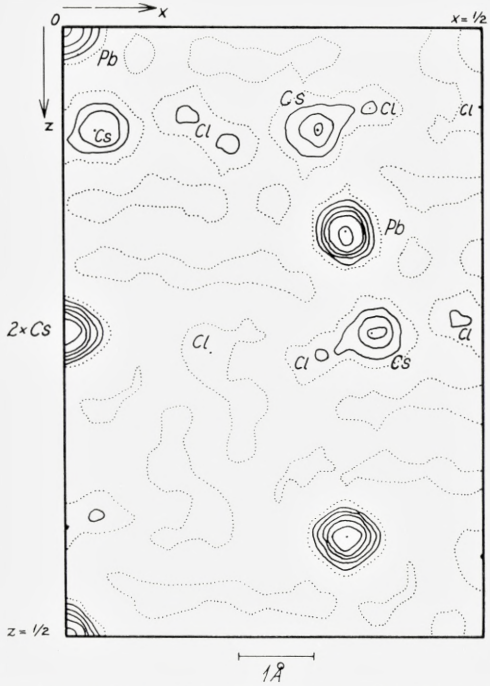


Fig. 3. Electron projection on $(1\bar{2}10)$ of $Cs_4PbCl_6$. Contour lines have been drawn as in figs. 1 and 2.

agreement: The shape of the crystals did not even approximate to something having cylindrical symmetry. (It would have been desirable to use much smaller crystals, but it was found very difficult to mount them along a body diagonal without using a micromanipulator).

However, the difference syntheses indicate that a better agreement between observed and calculated structure factors presumably could be obtained by reducing the atomic scattering factors for the $Cs''$-atoms in one way or another. This means formally introduction of a special, anisotropic temperature factor for these atoms, and physically a small delocalization of them around the average positions. In fact, it is possible in this way to get a somewhat better agreement in certain regions, but, as will be understood from the above, our measured intensities do not seem accurate enough and the whole procedure has been left out here. It is interesting that considerations of this kind achieved a definite improvement in the case of the perovskite-like structures of $CsPbX_3$ (1).

Although a completely satisfactory solution of the problem has not been

TABLE 3. Comparison of calculated and observed F-values for $Cs_4PbCl_6$

| Indices *hkl* | $F_{calc.}$ | $\lvert F_{obs.} \rvert$ | Indices *hkl* | $F_{calc.}$ | $\lvert F_{obs.} \rvert$ | Indices *hkl* | $F_{calc.}$ | $\lvert F_{obs.} \rvert$ |
|---|---|---|---|---|---|---|---|---|
| 006 | — 180 | 118 | $70\bar{1}4$ | 19 | | 211 | 24 | |
| 0012 | 220 | 182 | $70\bar{8}$ | 80 | 112 | 214 | 102 | 104 |
| 0018 | — 80 | 115 | $70\bar{2}$ | 17 | 54 | 217 | — 11 | |
| $10\bar{2}0$ | 74 | 108 | 704 | 88 | 65 | 2110 | 29 | |
| $10\bar{1}4$ | 12 | | 7010 | 22 | | 2113 | 4 | |
| $10\bar{8}$ | 91 | 87 | 7016 | 52 | | 2116 | 60 | 79 |
| $10\bar{2}$ | 58 | 65 | $80\bar{1}6$ | 164 | 126 | 2119 | — 1 | |
| 104 | 66 | 52 | $80\bar{1}0$ | — 72 | 71 | 312 | 78 | 83 |
| 1010 | 64 | 71 | $80\bar{4}$ | 170 | 160 | 315 | — 66 | 58 |
| 1016 | 35 | | 802 | — 51 | 60 | 318 | 43 | 52 |
| $20\bar{1}6$ | 104 | 180 | 808 | 126 | 123 | 3111 | 42 | |
| $20\bar{1}0$ | — 16 | | 8014 | — 25 | | 3114 | 58 | |
| $20\bar{4}$ | 147 | 125 | $90\bar{1}2$ | 39 | | 3117 | — 26 | |
| 202 | — 2 | | $90\bar{6}$ | 42 | 65 | 3120 | 27 | 52 |
| 208 | 117 | 121 | 900 | 63 | 72 | 410 | 82 | 86 |
| 2014 | 3 | | 906 | 18 | | 413 | 61 | 52 |
| 2020 | 75 | 97 | 9012 | 78 | 86 | 416 | 44 | 45 |
| $30\bar{1}8$ | — 36 | | $100\bar{1}4$ | 10 | | 419 | — 41 | |
| $30\bar{1}2$ | 142 | 166 | $100\bar{8}$ | 74 | 93 | 4112 | 55 | 63 |
| $30\bar{6}$ | — 53 | 58 | $100\bar{2}$ | 7 | | 4115 | 29 | |
| 300 | 208 | 132 | 1004 | 86 | 108 | 4118 | 37 | |
| 306 | — 79 | 71 | 10010 | 2 | | 511 | 79 | 70 |
| 3012 | 172 | 186 | $110\bar{1}0$ | — 76 | | 514 | 73 | 63 |
| 3018 | — 70 | 46 | $110\bar{4}$ | 172 | 123 | 517 | — 64 | 43 |
| $40\bar{2}0$ | 48 | 76 | 1102 | — 91 | | 5110 | 38 | |
| $40\bar{1}4$ | 28 | | 1108 | 166 | 134 | 5113 | 44 | |
| $40\bar{8}$ | 74 | 97 | $120\bar{1}2$ | 36 | | 5116 | 50 | 58 |
| $40\bar{2}$ | 46 | 67 | $120\bar{6}$ | 46 | | 5119 | — 28 | |
| 404 | 72 | 82 | 1200 | 31 | 39 | 612 | 50 | 81 |
| 4010 | 53 | 44 | 1206 | 50 | | 615 | — 97 | 88 |
| 4016 | 35 | | 12012 | 28 | | 618 | 41 | 54 |
| $50\bar{1}6$ | 104 | 110 | | | | 6111 | 85 | 88 |
| $50\bar{1}0$ | — 28 | | | | | 6114 | 48 | |
| $50\bar{4}$ | 163 | 152 | 012 | 58 | 36 | 710 | 52 | 58 |
| 502 | — 58 | 80 | 018 | 92 | 86 | 713 | 15 | |
| 508 | 169 | 152 | 0114 | 11 | | 716 | 40 | |
| 5014 | — 63 | 60 | 0120 | 73 | 86 | 719 | — 12 | |
| 5020 | 134 | 97 | 110 | 54 | 63 | 7112 | 61 | 50 |
| $60\bar{1}8$ | — 26 | | 113 | 90 | 65 | 7115 | 10 | |
| $60\bar{1}2$ | 129 | 125 | 116 | 82 | 71 | 811 | 28 | |
| $60\bar{6}$ | — 54 | 50 | 119 | — 80 | 65 | 814 | 72 | 81 |
| 600 | 179 | 177 | 1112 | 37 | | 817 | — 26 | |
| 606 | — 54 | 50 | 1115 | 66 | 63 | 8110 | 30 | |
| 6012 | 130 | 126 | 1118 | 51 | | 8113 | 24 | |
| 6018 | — 28 | | 1121 | — 61 | 52 | 8116 | 41 | 56 |

TABLE 4. Comparison of calculated and observed F-values for $Cs_4PbBr_6$

| Indices *hkl* | $F_{calc.}$ | $\lvert F_{obs.} \rvert$ | Indices *hkl* | $F_{calc.}$ | $\lvert F_{obs.} \rvert$ | Indices *hkl* | $F_{calc.}$ | $\lvert F_{obs.} \rvert$ |
|---|---|---|---|---|---|---|---|---|
| 006 | −251 | 126 | $40\bar{1}4$ | 11 | | $80\bar{1}6$ | 219 | 184 |
| 0012 | 246 | 210 | $40\bar{8}$ | 97 | 117 | $80\bar{1}0$ | −120 | 93 |
| 0018 | −52 | | $40\bar{2}$ | 37 | 42 | $80\bar{4}$ | 172 | 153 |
| $10\bar{2}0$ | 106 | 130 | 404 | 62 | 82 | 802 | −10 | |
| $10\bar{1}4$ | −22 | 33 | 4010 | 77 | 81 | 808 | 72 | 61 |
| $10\bar{8}$ | 113 | 88 | 4016 | 12 | 20 | 8014 | 16 | |
| $10\bar{2}$ | 70 | 81 | $50\bar{1}6$ | 79 | 92 | $90\bar{1}2$ | 10 | |
| 104 | 22 | | $50\bar{1}0$ | 20 | 32 | $90\bar{6}$ | 76 | 100 |
| 1010 | 109 | 122 | $50\bar{4}$ | 118 | 139 | 900 | 47 | |
| 1016 | 10 | 42 | 502 | −46 | 55 | 906 | 36 | 19 |
| 1022 | 46 | 46 | 508 | 200 | 178 | 9012 | 101 | 94 |
| $20\bar{1}6$ | 126 | 161 | 5014 | −49 | 83 | $100\bar{1}4$ | 4 | |
| $20\bar{1}0$ | −37 | 30 | 5020 | 201 | 169 | $100\bar{8}$ | 76 | 93 |
| $20\bar{4}$ | 154 | 158 | $60\bar{1}8$ | −9 | 20 | $100\bar{2}$ | 12 | |
| 202 | 10 | | $60\bar{1}2$ | 129 | 127 | 1004 | 85 | 78 |
| 208 | 98 | 176 | $60\bar{6}$ | −72 | 90 | 10010 | −1 | |
| 2014 | 17 | | 600 | 214 | 189 | $110\bar{1}0$ | −63 | |
| 2020 | 73 | 101 | 606 | −72 | 59 | $110\bar{4}$ | 172 | 107 |
| $30\bar{1}8$ | −25 | | 6012 | 140 | 116 | 1102 | −98 | 36 |
| $30\bar{1}2$ | 110 | 111 | 6018 | 25 | | 1108 | 174 | 101 |
| $30\bar{6}$ | −9 | 19 | $70\bar{1}4$ | −2 | | 11014 | −74 | |
| 300 | 179 | 188 | $70\bar{8}$ | 115 | 118 | $120\bar{1}2$ | 17 | 49 |
| 306 | −78 | 55 | $70\bar{2}$ | −73 | | $120\bar{6}$ | 70 | |
| 3012 | 197 | 251 | 704 | 127 | 85 | 1200 | 15 | 24 |
| 3018 | −98 | 72 | 7010 | 12 | 39 | 1206 | 54 | 35 |
| $40\bar{2}0$ | 59 | 69 | 7016 | 61 | 33 | 12012 | 42 | 14 |

obtained, it seems unlikely that the atomic positions can be very wrong. They are listed in Table 5 and interatomic distances calculated on the basis of this in Table 6. The latter compare quite reasonably with values obtained from the structures of $CsPbCl_3$ and $CsPbBr_3$, and, as there, the Pb-atoms are surrounded by 6 halogen atoms, which form a nearly regular octahedron (symmetry: $4\bar{3}m$). In the present structures the octahedron is compressed along a trigonal axis—viz. the one parallel to the c-axis of the crystals—so that the symmetry becomes $\bar{3}m$ only. The XPbX-angle, where the two X-atoms have the same z-coordinate, is also given in Table 6.

From what has been said above, it is clear that these results must be taken with a certain reservation, and the uncertainty as to the obtained interatomic distances may easily be 0.10 Å, thus making the deviation of these angles from 90° illusory.

Six X-atoms belonging to two different $PbX_6$-octahedra form trigonal prisms (symmetry $32m$) with the Cs′-atoms as centres, the Cs′-X distances

TABLE 5. Atomic positions in $Cs_4PbX_6$

| | | | | |
|---|---|---|---|---|
| | $(0, 0, 0)$; | $\left(\frac{1}{3}, \frac{2}{3}, \frac{2}{3}\right)$; | $\left(\frac{2}{3}, \frac{1}{3}, \frac{1}{3}\right)$ + | |
| 6 Pb in $\bar{3}$: | $(0, 0, 0)$; | $\left(0, 0, \frac{1}{2}\right)$ | | |
| 6 Cs′ in 32: | $\left(0, 0, \frac{1}{4}\right)$; | $\left(0, 0, \frac{3}{4}\right)$ | | |
| 18 Cs″ in 2: | $\left(x, 0, \frac{1}{4}\right)$; | $\left(0, x, \frac{1}{4}\right)$; | $\left(\bar{x}, \bar{x}, \frac{1}{4}\right)$; | $\left(\bar{x}, 0, \frac{3}{4}\right)$; $\left(0, \bar{x}\, \frac{3}{4}\right)$; $\left(x, x, \frac{3}{4}\right)$ |
| | For $Cs_4PbCl_6$ $x = 0.370$ and for $Cs_4PbBr_6$ $x = 0.372$ | | | |
| 36 X in 1: | $(x, y, z)$; $(\bar{y}, x\text{-}y, z)$; $(y\text{-}x, \bar{x}, z)$; $\left(\bar{y}, \bar{x}, \frac{1}{2} + z\right)$; $\left(x, x\text{-}y, \frac{1}{2} + z\right)$; $\left(y\text{-}x, y, \frac{1}{2} + z\right)$; + inverse positions. | | | |
| | For Cl in $Cs_4PbCl_6$: $x = 0.040$ $y = 0.164$ $z = 0.095$ | | | |
| | For Br in $Cs_4PbBr_6$: $x = 0.035$ $y = 0.170$ $z = 0.099$ | | | |

TABLE 6. Interatomic distances between nearest neighbours in $Cs_4PbX_6$

| Distance (frequency) | From this study | From PAULING's ionic radii | From GOLDSCHMIDT's ionic radii | From $CsPbX_3$ in Ref. 1. |
|---|---|---|---|---|
| Pb-Cl (6) | 2.93 Å | 3.02 Å | 3.13 Å | 2.86 Å |
| Cs′-Cl (6) | 3.57 - | 3.50 - | 3.48 - | (3.68)- |
| Cs″-Cl (2) | 3.59 - | | | |
| Cs″-Cl (2) | 3.85 - | | | |
| Cs″-Cl (2) | 3.43 - | | | |
| Cs″-Cl (2) | 3.43 - | | | |
| Cl-Cl | 4.01—4.28 Å | | | |
| ∢ ClPbCl | 93.6° | | | |
| Pb-Br (6) | 3.12 Å | 3.16 Å | 3.28 Å | 2.99 Å |
| Cs′-Br (6) | 3.69 - | 3.64 - | 3.63 - | (3.85)- |
| Cs″-Br (2) | 3.67 - | | | |
| Cs″-Br (2) | 3.93 - | | | |
| Cs″-Br (2) | 3.65 - | | | |
| Cs″-Br (2) | 3.60 - | | | |
| Br-Br | 4.31–4.52 Å | | | |
| ∢ BrPbBr | 92.8° | | | |

not being very different from the values expected from ionic radii.[7] – The remaining 18 Cs″-atoms in positions of rather low symmetry are each

[7] LANDOLT-BÖRNSTEIN. I. Band, 4. Teil, p. 523. Springer Verlag 1955.

surrounded by 8 X-atoms, 2 × 3 from two $PbX_6$-octahedra and 2 × 1 from two others, but here the $Cs''$-X-distances vary considerably, and it is conceivable that a disordered structure may result.

The crystals of $Cs_4PbX_6$ thus contain isolated $PbX_6^{----}$-octahedra linked together by the positive $Cs^+$-ions.

## Discussion

Apart from the supposition about disorder our conclusions concerning the structures of the $Cs_4PbX_6$-compounds are in complete agreement with the findings of G. BERGERHOF and O. SCHMITZ-DUMONT in the isomorphous $K_4CdCl_6$-crystals. This again illustrates the similarity between divalent $Pb^{++}$ and $Cd^{++}$ previously demonstrated in the case of the $CsPbI_3$ and $MeCdCl_3$ compounds.[8] It is interesting that the compounds $Cs_4PbX_6$ with isolated $PbX_6$-octahedra are precipitated from concentrated solutions of CsX, whereas from less concentrated solutions crystals are obtained in which such octahedra share X-atoms, e. g. in the perovskite-like structures of $CsPbX_3$, or in the one-dimensional polynuclear complex ion $(PbI_3^-)_n$ in $CsPbI_3$ (8). It thus seems likely that the concentrated solutions mainly contain isolated highly symmetrical $PbX_6^{----}$-ions, while in less concentrated ones bi-, tri- — — or polynuclear complex ions built up from such units may be prevailing. This may add to our understanding of the problem why in concentrated salt solutions the behaviour of some electrolytes approaches to that of electrolytes in extremely dilute solutions.

## Acknowledgements

I am very much indebted to Professor, dr. phil. A. TOVBORG JENSEN for his interest in this work and for his encouragement at critical points of the investigations. Thanks are also due to Mr. F. AMMENTORP-SCHMIDT for carrying out most of the calculations—also those which were not successful.

[8] C. K. MØLLER. The Structure of $CsPbI_3$, Mat. Fys. Medd. Dan. Vid. Selsk. **32**, No. 1 (1959).

Indleveret til selskabet 25. juli 1959.
Færdig fra trykkeriet 19. april 1960.

Matematisk-fysiske Meddelelser
udgivet af
Det Kongelige Danske Videnskabernes Selskab
Bind **32**, nr. 4

Mat. Fys. Medd. Dan. Vid. Selsk. **32**, no. 4 (1960)

# ON THE SCHRÖDINGER EIGENVALUE PROBLEM

BY

OLAVI HELLMAN

København 1960
i kommission hos Ejnar Munksgaard

## CONTENTS


1. Introduction ..... 3
2. Case I. The Schrödinger Equation with $l = 0$ ..... 5
3. Procedures for Forming the Matrizant $\Omega_0^r(A_I)$ ..... 9
4. Case II. The Schrödinger Equation with $l \neq 0$ ..... 14
5. The Solution of the Matrix Differential Equation $\frac{dX}{ds} - \left(\frac{P_{-1}}{s} + P\right) X = 0$ .. 17


---

## Synopsis


The Schrödinger eigenvalue problem is treated by a matrix method. A procedure for obtaining eigenvalues is developed for the following rather general cases: 1) $l = 0$, and the potential function is assumed to be integrable in the Lebesgue sense over a finite interval $(0, L)$, vanishing elsewhere; 2) $l \neq 0$, and the potential is assumed to be of the form $\frac{a}{r^2} - \frac{b}{r} + V_0(r)$, $V_0(r)$ possessing a power-series expansion within the interval $(0, L)$ and vanishing elsewhere (this expansion will not, however, be needed in the calculations). The eigenvalues appear as roots of a rapidly converging power series. The eigenfunctions are expressed directly in terms of the functions obtained in the process of forming the above power series.



Printed in Denmark
Bianco Lunos Bogtrykkeri A-S

## 1. Introduction

In the present paper we are going to consider the SCHRÖDINGER eigenvalue problem

$$\left.\begin{aligned} &\frac{d^2R}{dr^2}+\frac{2}{r}\frac{dR}{dr}-\frac{l(l+1)}{r^2}R+k(\lambda-V(r))R=0 \\ &R(0)<\infty \quad \text{and} \quad R(r)\to 0, \quad \text{as} \quad r\to\infty \end{aligned}\right\} \tag{1.1}$$

in the following two—fairly general—cases:

*CASE I*: $l=0$, and the potential $V(r)$ differs from zero only within a finite interval $[0, L]$. Besides that, we only assume that $V(r)$ is integrable in the LEBESGUE sense over the interval $[0, L]$. By doing this we believe to have included all potential functions of practical interest with the sole restriction that the possible singularities of the potential function for some $r'\varepsilon[0, L]$ must be of the order $(r-r')^{-\alpha}$, where $\alpha<1$.

*CASE II*: $l\neq 0$, and the potential is of the form

$$V(r)=\frac{a}{r^2}-\frac{b}{r}-V_0(r), \tag{1.1a}$$

where necessarily $a\neq 0$ (more precisely: $\sqrt{(2l+1)^2+4ka}$ must not be an integer). Furthermore, $V_0(r)$ is assumed to be different from zero only within the interval $[0, L]$, possessing there an absolutely convergent power-series expansion. This expansion will not, however, be needed in the calculations.

The basic idea of our considerations is the following: we throw the differential equation (1.1) into the matrix form

$$\frac{d}{dr}\begin{pmatrix}R'\\R\end{pmatrix}-\begin{pmatrix}-\frac{2}{r}\frac{l(l+1)}{r^2}+k(\lambda-V(r)) & \\ 1 & 0\end{pmatrix}\begin{pmatrix}R'\\R\end{pmatrix}=0 \tag{1.2}$$

and are thus led to consider a matrix differential equation of the first order, to which many useful mathematical relations apply.

Let us write (1.2) more briefly as

$$\frac{dz}{dr} - B(r)\, z = 0, \tag{1.2a}$$

where $z$ and $B(r)$ are clear from (1.2).

In *CASE I* it is easy to find a matrix $D(r)$ such that the transformation $z = D\eta$ leads to a matrix differential equation

$$\frac{d\eta}{dr} - A(r)\, \eta = 0 \tag{1.2b}$$

in which the elements of $B(r)$ are functions integrable in the Lebesgue sense over the interval $[0, L]$. If we now require that $\eta(0) = \eta_0$, then the unique solution of (1.2b) will be the well-known matrix series

$$\eta = \left( I + \int_0^r A dr + \int_0^r A dr_1 \int_0^{r_1} A dr_2 + \ldots \right) \eta_0 = \Omega_0^r(A)\, \eta_0, \tag{1.3}$$

where $I$ denotes the unit matrix. The matrix $\Omega_0^r(A)$ is usually called a matrizant. The properties of the matrizant will be discussed in section 2.

The conditions which were imposed upon $R(r)$ are now written into matrix form, and finally—as will be shown in section 2—the formula

$$\det \left\{ \Omega_0^L(A) \begin{pmatrix} 1 \\ 0 \end{pmatrix}, \begin{matrix} -\sqrt{k\,|\lambda|} \\ 1 \end{matrix} \right\} = 0 \tag{1.4}$$

for the eigenvalues is obtained.

As we see from (1.4), the matrizant $\Omega_0^L(A)$ is the core of our eigenvalue problem.

The forming of $\Omega_0^r(A)$ is possible, but highly unpractical to carry out by means of the definition (1.3). In section 3 a procedure is developed which, avoiding the direct use of (1.3), gives the matrizant $\Omega_0^r(A)$ as a power series in $\lambda$. This procedure is very little sensitive to the form of the potential function; only the above-mentioned Lebesgue integrability is needed to assure the convergence of the series obtained. The procedure is particularly well suited for handling eigenvalue problems where the potential is given in tabular form. The left-hand side of (1.4) becomes an

infinite convergent power series in $\sqrt{k|\lambda|}$ whose real zero points—when such points exist—are the discrete eigenvalues of our problem. As an application, the case of a square well is considered in section 3.

In *CASE II*, where $l \neq 0$ and where the potential function is of the form (1.1 a), it is impossible to find a matrix $D(r)$ such that the transformation $z = D(r)\eta$ leads from the differential equation (1.2 a) to a differential equation (1.2 b) in which the elements of $A(r)$ are functions integrable in the Lebesgue sense. The simplest form which one may obtain from (1.2 a) in this manner turns out to be

$$\frac{d\eta}{dr} - \left(\frac{C}{r} + G(r)\right)\eta = 0, \tag{1.5}$$

where $C$ is a constant matrix and where $G(r)$ has the same properties as $A(r)$ in (1.2 a). As is well known, the matrizant (1.3) does not exist for the matrix $\frac{C}{r} + G(r)$. It is possible, however, to obtain—by application of well-known theorems from the matrix calculus—a matrizant-like solution of (1.5), as is shown in section 5. Also a procedure of giving this modified matrizant as a power series in $\lambda$ is developed there.

The eigenvalue equation for *CASE II* is derived in section 4. The formula obtained is very similar to the formula (1.4). It contains, besides the modified matrizant, Whittaker functions. The eigenvalue problem of *CASE II* is somewhat more complicated than that of *CASE I*. There is, however, no essential difference in the handling of the two cases.

In both the above cases the functions we obtain when forming the matrizant yield the eigenfunctions without further calculations.

## 2. *Case I*

We shall consider the eigenvalue problem

$$\left.\begin{aligned} &\frac{d^2R}{dr^2} + \frac{2}{r}\frac{dR}{dr} - k(|\lambda| + V(r))\,R = 0 \\ &R(0) < \infty \quad \text{and} \quad R(r) \to 0, \quad \text{as} \quad r \to \infty \end{aligned}\right\} \tag{2.1}$$

arising from (1.1) when we put $l = 0$. Here $|\lambda|$ denotes the absolute value of the negative eigenvalue $\lambda$. The potential function $V(r)$ has the properties given on page 3.

The substitution

$$R = \frac{w}{r} \tag{2.2}$$

brings (2.1) into the form

$$\left.\begin{aligned} &\frac{d^2 w}{dr^2} - k(|\lambda| + V(r))\, w = 0 \\ &w(r) = 0(r^v),\ v \geqslant 1, \text{ as } r \to 0, \text{ and } w(r) \to 0, \text{ as } r \to \infty. \end{aligned}\right\} \tag{2.3}$$

We now throw the eigenvalue problem (2.3) into matrix form as follows:

$$\left.\begin{aligned} &\frac{d}{dr}\begin{pmatrix} \dfrac{dw}{dr} \\ w \end{pmatrix} - \begin{pmatrix} 0 & k(|\lambda| + V(r)) \\ 1 & 0 \end{pmatrix}\begin{pmatrix} \dfrac{dw}{dr} \\ w \end{pmatrix} = 0 \\ &\begin{pmatrix} \dfrac{dw}{dr} \\ w \end{pmatrix}_{r=0} = C_1 \begin{pmatrix} 1 \\ 0 \end{pmatrix} \quad \text{and} \quad \begin{pmatrix} \dfrac{dw}{dr} \\ w \end{pmatrix} \to \begin{pmatrix} 0 \\ 0 \end{pmatrix}, \text{ as } r \to \infty, \end{aligned}\right\} \tag{2.4}$$

where $C_1$ is a real constant. At $r = 0$, the above is a necessary condition for $w(r) = 0(r^v)$, $v \geqslant 1$. It is, however, also sufficient, as will be seen later (cf. (2.15)).

The differential equation in (2.4) is of the form

$$\frac{dz}{dr} - Az = 0, \tag{2.5}$$

where, in our case,

$$z = \begin{pmatrix} \dfrac{dw}{dr} \\ w \end{pmatrix} \quad \text{and} \quad A = \begin{pmatrix} 0 & k(|\lambda| + V_0(r)) \\ 1 & 0 \end{pmatrix}.$$

If it is required that $z(0) = z_0$ (= const.), the unique solution of (2.5) will be, according to what was said in section 1, the series

$$z(r) = \left(I + \int_0^r A\, d\tau_1 + \int_0^r A\, d\tau_1 \int_0^{\tau_1} A\, d\tau_2 + \dots\right) z_0 = \Omega_0^r(A)\, z_0, \tag{2.6}$$

where $I$ is the unit matrix.

For our present purpose we mention the following facts about the matrizant (1):

Let the elements $A_{ij}(r)$ of $A$ be functions integrable in the Lebesgue sense in the finite interval $[0, L]$. Then

1° the series (2.6) converges absolutely and uniformly in $[0, L]$,
2° the inverse of $\Omega_0^r(A)$ exists for every $r \varepsilon [0, L]$,
3° $\Omega_0^r(A+B) = \Omega_0^r(A)\,\Omega_0^r\{[\Omega_0^r(A)]^{-1} B\,\Omega_0^r(A)\}$,
4° for a constant matrix $A$ we shall have $\Omega_0^r(A) = \exp(Ar)$,
5° $\det \Omega_0^r(A) = \exp\left(\int_0^r Tr\,A\,d\tau\right)$.

We now return to the eigenvalue problem (2.4). Let us write

$$A_I = \begin{pmatrix} 0 & k(|\lambda| + V(r)) \\ 1 & 0 \end{pmatrix}$$

$$A_{II} = \begin{pmatrix} 0 & k|\lambda| \\ 1 & 0 \end{pmatrix}$$

$$w(r) = \begin{cases} w_I(r) & \text{for } r \varepsilon [0, L] \\ w_{II}(r) & \text{for } r \varepsilon [L, \infty]. \end{cases}$$

Then, according to what was said above,

$$\begin{pmatrix} \dfrac{dw_I}{dr} \\ w_I \end{pmatrix} = \Omega_0^r(A_I) \begin{pmatrix} C_1 \\ 0 \end{pmatrix} \tag{2.7}$$

and

$$\begin{pmatrix} \dfrac{dw_{II}}{dr} \\ w_{II} \end{pmatrix} = \Omega_0^r(A_{II})\, z_{II}, \tag{2.8}$$

where $z_{II}$ is a constant vector. Since $A_{II}$ is a constant matrix, we have (according to the property 4° of the matrizant)

$$\Omega_0^r(A_{II}) = \exp\left[\begin{pmatrix} 0 & k|\lambda| \\ 1 & 0 \end{pmatrix} r\right]. \tag{2.9}$$

This may be rewritten by the aid of the Sylvester expansion as follows:

$$\exp\left[\begin{pmatrix} 0 & k\,|\lambda| \\ 1 & 0 \end{pmatrix} r\right] = \exp\left(\sqrt{k\,|\lambda|}\, r\right) \mathfrak{Q}_1 + \exp\left(-\sqrt{k\,|\lambda|}\, r\right) \mathfrak{Q}_2, \tag{2.9a}$$

where

$$\mathfrak{Q}_1 = \frac{1}{2}\begin{pmatrix} 1 & \sqrt{k\,|\lambda|} \\ \dfrac{1}{\sqrt{k\,|\lambda|}} & 1 \end{pmatrix} \tag{2.10}$$

and

$$\mathfrak{Q}_2 = \frac{1}{2}\begin{pmatrix} 1 & -\sqrt{k\,|\lambda|} \\ -\dfrac{1}{\sqrt{k\,|\lambda|}} & 1 \end{pmatrix}. \tag{2.11}$$

Since we require in (2.4) that

$$\begin{pmatrix} \dfrac{dw_{II}}{dr} \\ w_{II} \end{pmatrix} \to \begin{pmatrix} 0 \\ 0 \end{pmatrix}, \text{ as } r \to \infty,$$

the vector $z_{II}$ in (2.8) must be chosen so that $\mathfrak{Q}_1 z_{II} = 0$, i. e.,

$$z_{II} = \begin{pmatrix} -\sqrt{k\,|\lambda|} \\ 1 \end{pmatrix} C_2, \tag{2.12}$$

$C_2$ being a real constant. We then have

$$\begin{pmatrix} \dfrac{dw_{II}}{dr} \\ w_{II} \end{pmatrix} = e^{-\sqrt{k\,|\lambda|}\, r} \begin{pmatrix} -\sqrt{k\,|\lambda|} \\ 1 \end{pmatrix} C_2. \tag{2.8a}$$

It is now required that the vectors $\begin{pmatrix} \dfrac{dw_I}{dr} \\ w_I \end{pmatrix}$ and $\begin{pmatrix} \dfrac{dw_{II}}{dr} \\ w_{II} \end{pmatrix}$ become equal at $r = L$:

$$\Omega_0^L(A_I)\begin{pmatrix} 1 \\ 0 \end{pmatrix} C_1 = e^{-\sqrt{k\,|\lambda|}\, L} \begin{pmatrix} -\sqrt{k\,|\lambda|} \\ 1 \end{pmatrix} C_2. \tag{2.13}$$

Since $C_1 \neq 0$ and $C_2 \neq 0$, we must have

$$\det\left\{ \Omega_0^L(A_I)\begin{pmatrix} 1 \\ 0 \end{pmatrix}, \quad \begin{matrix} -\sqrt{k\,|\lambda|} \\ 1 \end{matrix} \right\} = 0. \tag{2.14}$$

This is the equation which must be satisfied by the discrete eigenvalues of the eigenvalue problem (2.1). The problem of determining the discrete part of the spectrum of (2.1) is thus reduced to the problem of forming the matrizant $\Omega_0^L(A_I)$. In general, the left-hand side of (2.14) will appear as an absolutely convergent power series in $\sqrt{k|\lambda|}$.

The eigenfunction of (2.1), which belongs to the eigenvalue obtained from (2.14), will be, according to (2.2), (2.7) and (2.8a),

$$R(r) = \begin{cases} \dfrac{1}{r}\left\{(0,\ 1)\,\Omega_0^r(A_I)\begin{pmatrix}1\\0\end{pmatrix}\right\}_{\lambda=\lambda_i} C_1 \quad \text{for} \quad r\,\varepsilon\,[0,\ L] \\ \dfrac{1}{r}\,e^{\sqrt{k|\lambda_i|}\,r}\,\varkappa(|\lambda_i|)\,C_1 \quad \text{for} \quad r\,\varepsilon\,[L,\infty]. \end{cases} \tag{2.15}$$

The factor $\varkappa(|\lambda_i|)$ is obtained from (2.13) and the constant $C_1$ determined from a normalizing condition. As is seen from (3.1c) below, $R(r)$ behaves at the origin as was required in (2.1).

## 3. Procedures for Forming the Matrizant $\Omega_0^r(A_I)$

Because of the special form of $A_I$ the matrizant $\Omega_0^r(A_I)$ may be formed rather easily [2] [3]:

$$\left.\begin{aligned} \left\{\Omega_0^r(A_I)\right\}_{11} &= 1 - k\int_0^r (|\lambda| + V(r_1))\,dr_1 \int_0^{r_1} dr_2 \\ &+ k^2 \int_0^r (|\lambda| + V(r_1))\,dr_1 \int_0^{r_1} dr_2 \int_0^{r_2} (|\lambda| + V(r_3))\,dr_3 \int_0^{r_3} dr_4 + \ldots \end{aligned}\right\} \tag{3.1a}$$

$$\left.\begin{aligned} \left\{\Omega_0^r(A_I)\right\}_{12} &= -k\int_0^r (|\lambda| + V(r_1))\,dr_1 \\ &+ k^2 \int_0^r (|\lambda| + V(r_1))\,dr_1 \int_0^{r_1} dr_2 \int_0^{r_2} (|\lambda| + V(r_3))\,dr_3 + \ldots . \end{aligned}\right\} \tag{3.1b}$$

$$\left\{\Omega_0^r(A_I)\right\}_{21} = r - k\int_0^r dr_1 \int_0^{r_1} (|\lambda| + V(r_2))\,dr_2 \int_0^{r_2} dr_3 + \ldots . \tag{3.1c}$$

$$\left.\begin{aligned} \left\{\Omega_0^r(A_I)\right\}_{22} &= 1 - k\int_0^r dr_1 \int_0^{r_1} (|\lambda| + V(r_2))\,dr_2 \\ &+ k^2 \int_0^r dr_1 \int_0^{r_1} (|\lambda| + V(r_2))\,dr_2 \int_0^{r_2} dr_3 \int_0^{r_3} (|\lambda| + V(r_4))\,dr_4 + \ldots . \end{aligned}\right\} \tag{3.1d}$$

It remains, however, to rearrange these into a power series in $|\lambda|$.

In the following we shall introduce a procedure which yields more directly the matrizant as a power series in $\lambda$. First, however, we write the potential function $V(r)$ into the more convenient form

$$V(r) = -V_0 + V_0 w\left(\frac{r}{L}\right),$$

where $-V_0 = \min V(r)$ and where $w(\xi)$ is a function integrable in the Lebesgue sense over the interval $[0, 1]$ such that $w\left(\frac{r}{L}\right) = 1$ for $r \varepsilon (L, \infty]$. Then we rewrite the matrix $A_I$ as follows:

$$\left.\begin{aligned} A_I &= \begin{pmatrix} 0 & k\left(|\lambda| - V_0 + V_0 w\left(\frac{r}{L}\right)\right) \\ 1 & 0 \end{pmatrix} \\ &= \begin{pmatrix} 0 & \frac{1}{L^2}\lambda_0^2 w\left(\frac{r}{L}\right) \\ 1 & 0 \end{pmatrix} + \frac{1}{L^2}(\lambda^2 - \lambda_0^2)\begin{pmatrix} 0 & 1 \\ 0 & 0 \end{pmatrix} \\ &= A_{I_0} + \frac{1}{L^2}(\lambda^2 - \lambda_0^2)\, A_I, \end{aligned}\right\} \qquad (3.2)$$

where we introduce the dimensionless quantities $\lambda^2 = k|\lambda|L^2$ and $\lambda_0^2 = kV_0L^2$. By applying the property 3° of the matrizant we obtain

$$\Omega_0^r(A_I) = \Omega_0^r(A_{I_0})\, \Omega_0^r\left\{[\Omega_0^r(A_{I_0})]^{-1} A_{I_1} \Omega_0^r(A_{I_0}) \frac{\lambda^2 - \lambda_0^2}{L^2}\right\}. \qquad (3.3)$$

The second term on the right-hand side now appears as a power series in $|\lambda|$. The convergence of this series for all $r \varepsilon [0, L]$ and, as a matter of fact, the existence of such a power series, follow directly from the properties of the matrizant.

We see that the forming of the matrizant $\Omega_0^r(A_I)$ will take place by the following four steps:

1° The forming of $\Omega_0^r(A_{I_0})$.
2° The forming of $[\Omega_0^r(A_{I_0})]^{-1}$.
3° The forming of the matrix $S = [\Omega_0^r(A_{I_0})]^{-1} A_{I_0} \Omega_0^r(A_{I_0})$.
4° The forming of the matrizant $\Omega_0^r\left(\frac{\lambda^2 - \lambda_0^2}{L^2} S\right)$.

*Step* 1°: The matrizant $\Omega_0^r(A_{I_0})$ is formed most conveniently by means of the following relationship [4]:

$$\Omega_0^r\begin{pmatrix} 0 & \frac{1}{L^2}\lambda_0^2 w\left(\frac{r}{L}\right) \\ 1 & 0 \end{pmatrix} = \begin{pmatrix} \Omega_{11}(\xi) & \frac{1}{L}\lambda_0^2 \int_0^{\xi} w(\xi_1)\,\Omega_{22}(\xi_1)\,d\xi_1 \\ L\int_0^{\xi}\Omega_{11}(\xi_1)\,d\xi_1 & \Omega_{22}(\xi) \end{pmatrix} \tag{3.4}$$

with

$$\left.\begin{aligned} \xi &= \frac{r}{L} \\ \Omega_{11}(r) &= \sum_{n=0}^{\infty}\lambda_0^{2n}\,a_{2n}^{(1)}(\xi) \\ \Omega_{22}(r) &= \sum_{n=0}^{\infty}\lambda_0^{2n}\,a_{2n}^{(2)}(\xi) \\ a_{2n}^{(1)} &= \int_0^{\xi} w(\xi_1)\,d\xi_1\int_0^{\xi_1} d\xi_2\int_0^{\xi_2} w(\xi_3)\,d\xi_3\ldots\int_0^{\xi_{2n-2}} w(\xi_{2n-1})\,d\xi_{2n-1}\int_0^{\xi_{2n-1}} d\xi_{2n} \\ a_{2n}^{(2)} &= \int_0^{\xi} d\xi_1\int_0^{\xi_1} w(\xi_2)\,d\xi_2\int_0^{\xi_2} d\xi_3\ldots\int_0^{\xi_{2n-2}} d\xi_{2n-1}\int_0^{\xi_{2n-1}} w(\xi_{2n})\,d\xi_{2n} \\ a_0^{(1)} &= 1 \\ a_0^{(2)} &= 1\,. \end{aligned}\right\} \tag{3.5}$$

*Step* 2°: The inversion of $\Omega_0^r(A_{I_0})$ is particularly easy to carry out:

$$[\Omega_0^r(A_{I_0})]^{-1} = \begin{pmatrix}\Omega_{11} & \Omega_{12}\\ \Omega_{21} & \Omega_{22}\end{pmatrix}^{-1} = [\det\Omega_0^r(A_{I_0})]^{-1}\begin{pmatrix}\Omega_{22} & -\Omega_{12}\\ -\Omega_{21} & \Omega_{11}\end{pmatrix}.$$

But according to the property 5° of the matrizant, since $Tr\,A_{I_0} = 0$, we have $\det\Omega_0^r(A_{I_0}) = 1$.
Hence

$$[\Omega_0^r(A_{I_0})]^{-1} = \begin{pmatrix}\Omega_{22} & -\Omega_{12}\\ -\Omega_{21} & \Omega_{11}\end{pmatrix}. \tag{3.6}$$

*Step* 3°: Both $\Omega_0^r(A_{I_0})$ and $[\Omega_0^r(A_{I_0})]^{-1}$ converge absolutely for all $r\,\varepsilon\,[0, L]$. Consequently we may form the product

$$[\Omega_0^r(A_{I_0})]^{-1}A_{I_1}\Omega_0^r(A_{I_0}),$$

which will also be an absolutely convergent series for all $r \varepsilon [0, L]$. By using (3.4), (3.5) and (3.6) we obtain

$$[\Omega_0^r(A_{I_0})]^{-1}\begin{pmatrix}0 & 1\\ 0 & 0\end{pmatrix}\Omega_0^r(A_{I_0}) = \sum_{q=0}^{\infty} \lambda_0^{2q} A_{2q} \tag{3.7}$$

with

$$A_{2q} = \sum_{m=0}^{q}\begin{pmatrix} La_{2m}^{(2)}(\xi)\left(\int_0^{\xi} a_{2(q-m)}^{(1)}(\xi_1)\, d\xi_1\right) & a_{2m}^{(2)}(\xi)\, a_{2(q-m)}^{(2)}(\xi) \\ -L^2\left(\int_0^{\xi} a_{2m}^{(1)}(\xi_1)\, d\xi_1\right)\left(\int_0^{\xi} a_{2(q-m)}^{(1)}(\xi_1)\, d\xi_1\right) & -L\left(\int_0^{\xi} a_{2m}^{(1)}(\xi_1)\, d\xi_1\right) a_{2(q-m)}^{(2)}(\xi). \end{pmatrix} \tag{3.8}$$

*Step* 4°: By using (3.7) we now obtain

$$\begin{aligned}
&\Omega_0^r\left\{[\Omega_0^r(A_{I_0})]^{-1}\begin{pmatrix}0 & 1\\ 0 & 0\end{pmatrix}\Omega_0^r(A_{I_0})\frac{\lambda^2-\lambda_0^2}{L^2}\right\} \\
&= \sum_{n=0}^{\infty}(\lambda^2-\lambda_0^2)^n\left\{\sum_{i_n=0}^{\infty}\lambda_0^{2i_n}\left[\sum_{i_{n-1}=0}^{i_n}\sum_{i_{n-2}=0}^{i_{n-1}}\cdots\right.\right. \\
&\quad\cdots\sum_{i_2=0}^{i_3}\sum_{i_1=0}^{i_2}\int_0^{\frac{r}{L}} A_{2i_1}(\xi_1)\, d\xi_1\int_0^{\xi_1} A_{2(i_2-i_1)}(\xi_2)\, d\xi_2\cdots \\
&\quad\left.\left.\cdots\int_0^{\xi_{i_{n-2}}} A_{2(i_{n-1}-i_{n-2})}(\xi_{i_{n-1}})\, d\xi_{i_{n-1}}\int_0^{\xi_{i_{n-1}}} A_{2(i_n-i_{n-1})}(\xi_{i_n})\, d\xi_{i_n}\right]\right\} \\
&= I+(\lambda^2-\lambda_0^2)\left\{\sum_{i_1=0}^{\infty}\lambda_0^{2i_1}\int_0^{\frac{r}{L}} A_{2i_1}(\xi_1)\, d\xi_1\right\} \\
&\quad+(\lambda^2-\lambda_0^2)^2\left\{\sum_{i_2=0}^{\infty}\lambda_0^{2i_2}\left[\sum_{i_1=0}^{i_2}\int_0^{\frac{r}{L}} A_{2i_1}(\xi_1)\, d\xi_1\int_0^{\xi_1} A_{2(i_2-i_1)}(\xi_2)\, d\xi_2\right]\right\} \\
&\quad+(\lambda^2-\lambda_0^2)^3\left\{\sum_{i_3=0}^{\infty}\lambda_0^{2i_3}\right. \\
&\quad\left.\times\left[\sum_{i_2=0}^{i_3}\sum_{i_1=0}^{i_2}\int_0^{\frac{r}{L}} A_{2i_1}(\xi_1)\, d\xi_1\int_0^{\xi_1} A_{2(i_2-i_1)}(\xi_2)\, d\xi_2\int_0^{\xi_2} A_{2(i_3-i_2)}(\xi_3)\, d\xi_3\right]\right\} \\
&\quad+\ldots.
\end{aligned} \tag{3.9}$$

The absolute convergence of the above series follows from the absolute convergence of the matrizant and of the series (3.7).

In practical applications one would use, instead of (3.9), an approximate expression consisting of a finite number of terms. The accuracy of the approximation is easy to control when the formula (3.9) is applied.

We shall now consider the simplest eigenvalue problem of *CASE I*, i. e. the square well, applying to it the formulae (3.4) and (3.9)[1].

It is clear from these formulae that the treatment of a more general case would be essentially the same.

Now we have

$$A_I = A_{I_0} + \frac{1}{L^2}(\lambda^2 - \lambda_0^2)\, A_{I_1}$$

$$= \begin{pmatrix} 0 & 0 \\ 1 & 0 \end{pmatrix} + \frac{1}{L^2}(\lambda^2 - \lambda_0^2) \begin{pmatrix} 0 & 1 \\ 0 & 0 \end{pmatrix},$$

from which it follows that

$$\Omega_0^r(A_{I_0}) = \begin{pmatrix} 1 & 0 \\ L\xi & 1 \end{pmatrix} \tag{3.11}$$

and

$$[\Omega_0^r(A_{I_0})]^{-1} \begin{pmatrix} 0 & 1 \\ 0 & 0 \end{pmatrix} \Omega_0^r(A_{I_0}) = \begin{pmatrix} L\xi & 1 \\ -L^2\xi^2 & -L\xi \end{pmatrix}.$$

Hence

$$A_0 = \begin{pmatrix} L\xi & 1 \\ -L^2\xi^2 & -L\xi \end{pmatrix}, \text{ but } A_{2q} = 0, \text{ as } q > 0.$$

We then obtain from (2.14), (3.9) and (3.11)

[1] Actually the matrizant method yields the well-known transcendental equation

$$\cot \sqrt{\lambda_0^2 - \lambda^2} = \sqrt{\frac{\lambda^2}{\lambda_0^2 - \lambda^2}} \tag{3.10}$$

for the discrete eigenvalues in the case of a square well. If we make use of the fact that $A_I$ is now a constant matrix, we first obtain (3)

$$\Omega_0^r(A_I) = \exp(A_I r) = \begin{pmatrix} \cos\sqrt{\lambda_0^2 - \lambda^2}\,\xi & \frac{1}{L}\sqrt{\lambda_0^2 - \lambda^2}\sin\sqrt{\lambda_0^2 - \lambda^2}\,\xi \\ \frac{L}{\sqrt{\lambda_0^2 - \lambda^2}}\sin\sqrt{\lambda_0^2 - \lambda^2}\,\xi & \cos\sqrt{\lambda_0^2 - \lambda^2}\,\xi \end{pmatrix},$$

after which the above formula is easily derived from (2.14).

$$\lambda = \frac{1 - \frac{1}{2}(\lambda_0^2 - \lambda^2) + \frac{1}{24}(\lambda_0^2 - \lambda^2)^2 - \frac{1}{720}(\lambda_0^2 - \lambda^2)^3 + \ldots}{1 - \frac{1}{6}(\lambda_0^2 - \lambda^2) + \frac{1}{120}(\lambda_0^2 - \lambda^2)^2 - \frac{1}{5040}(\lambda_0^2 - \lambda^2)^3 + \ldots}.$$

Let us choose $\lambda_0^2 = 4$, in which case there will be only one discrete eigenvalue. Our formula gives $\lambda^2 = 0.4102$, and the exact formula (3.10) gives $\lambda^2 = 0.407118$. The error thus amounts only to about 0.74 per cent.

## 4. *Case II*

We now have $l \neq 0$, $a \neq 0$, and $b \neq 0$ in (1.1) and (1.2):

$$\left.\begin{aligned} &\frac{d^2R}{dr^2} + \frac{2}{r}\frac{dR}{dr} - \left[k|\lambda| + \frac{l(l+1)+ka}{r^2} - \frac{kb}{r} - kV_0\right]R = 0 \\ &R(0) < \infty \text{ and } R(r) \to 0, \text{ as } r \to \infty, \end{aligned}\right\} \quad (4.1)$$

where $|\lambda|$ is again the absolute value of the negative discrete eigenvalue. It is convenient to replace $r$ by the dimensionless parameter $s = \frac{r}{\sigma}$, $\sigma$ being a length suitable for the problem considered:

$$\left.\begin{aligned} &\frac{d^2R}{ds^2} + \frac{2}{s}\frac{dR}{ds} - \left(\Lambda + \frac{l(l+1)+A}{s^2} - \frac{G}{s} - V_1(s)\right)R = 0 \\ &R(0) < \infty \text{ and } R(s) \to 0, \text{ as } s \to \infty, \end{aligned}\right\} \quad (4.2)$$

where we have written

$$\Lambda = k\sigma^2|\lambda|, \quad A = ka, \quad G = k\sigma b, \text{ and } V_1(s) = k\sigma^2 V_0(\sigma s).$$

We must again find the solution of (4.2) separately for $s \varepsilon \left[0, \frac{L}{\sigma}\right]$, where $V_1(s) \neq 0$, and for $s \varepsilon \left[\frac{L}{\sigma}, \infty\right]$, where $V_1(s) \equiv 0$. The equation for the eigenvalues is then obtained, as in section 2, from the condition that these solutions must be equal for $s = \frac{L}{\sigma}$.

We substitute

$$R = s^p w(s), \quad (4.3)$$

where $p = \sqrt{\left(l + \frac{1}{2}\right)^2 + A} - \frac{1}{2}$, in (4.2) and find by a straightforward calculation

$$\left.\begin{aligned} &\frac{d}{ds}\begin{pmatrix}\frac{dw}{ds}\\ w\end{pmatrix}-\left\{\frac{1}{s}\begin{pmatrix}-2(p+1) & -G\\ 0 & 0\end{pmatrix}+\begin{pmatrix}0 & \Lambda-V_1(s)\\ 1 & 0\end{pmatrix}\right\}\begin{pmatrix}\frac{dw}{ds}\\ w\end{pmatrix}=0\\ &\begin{pmatrix}\frac{dw}{ds}\\ w\end{pmatrix}_{s=0}<\infty \text{ and } \begin{pmatrix}\frac{d}{ds}(s^p w)\\ s^p w\end{pmatrix}\to 0, \text{ as } s\to\infty. \end{aligned}\right\} \quad (4.4)$$

The matrix differential equation (4.4) is of the form

$$\frac{dz}{ds}-\left(\frac{P_{-1}}{s}+P\right)z=0 \quad (4.5)$$

with

$$z=\begin{pmatrix}\frac{dw}{ds}\\ w\end{pmatrix}, \quad P_{-1}=\begin{pmatrix}-2(p+1) & -G\\ 0 & 0\end{pmatrix} \text{ and } P=\begin{pmatrix}0 & \Lambda-V_1(s)\\ 1 & 0\end{pmatrix}.$$

The solution of (4.5) is not the matrizant $\Omega_0^s\left(\frac{P_{-1}}{s}+P\right)$, because the elements of the matrix $\frac{P_{-1}}{s}+P$ are not all integrable over $\left[0,\frac{L}{\sigma}\right]$. We shall use temporarily the expression

$$\begin{pmatrix}\frac{dR}{ds}\\ R\end{pmatrix}=\Phi(s)\begin{pmatrix}0\\ 1\end{pmatrix}C_1 \quad (4.6)$$

for $s\varepsilon\left[0,\frac{L}{\sigma}\right]$ and postpone the determination of this form to the next section (the matrix $\Phi(s)$ is given there by (5.17)).

We now want to find a solution of (4.4) for $s\varepsilon\left(\frac{L}{\sigma},\infty\right)$ (where $V_1(s)\equiv 0$) such that

$$\begin{pmatrix}\frac{dR}{ds}\\ R\end{pmatrix}\to\begin{pmatrix}0\\ 0\end{pmatrix}, \text{ as } s\to\infty.$$

It will be convenient to start from the equation (4.2). By substituting

$$R(s)=\frac{w(x)}{x}, \quad x=2\sqrt{\Lambda s} \quad (4.7)$$

we arrive at the Whittaker differential equation [7]

$$\frac{d^2w}{dx^2} + \left( -\frac{1}{4} + \frac{k}{x} + \frac{\frac{1}{4} - m^2}{x^2} \right) w = 0, \tag{4.8}$$

where $k = \dfrac{G}{2\sqrt{A}}$ and $m = \sqrt{\left(l + \dfrac{1}{2}\right)^2 + A}$.

The general solution of (4.8) is, according to ref. (7),

$$w(x) = h_1 W_{k,m}(x) + h_2 W_{-k,m}(-x), \tag{4.9}$$

where

$$W_{k,m}(x) = \frac{e^{-\frac{x}{2}} x^k}{\Gamma\left(\frac{1}{2} - k + m\right)} \int_0^\infty t^{-k-\frac{1}{2}+m} \left(1 + \frac{t}{x}\right)^{k-\frac{1}{2}+m} e^{-t}\, dt \tag{4.10}$$

and where $h_1$ and $h_2$ are arbitrary constants. Since $W_{k,m}(x) \to 0$ but $W_{-k,m}(-x) \to \infty$, as $x \to \infty$, we must set $h_2 = 0$. The solution of (4.2) is thus given by

$$R(s) = \frac{h_1}{s} W_{k,m}\left(2\sqrt{A}\, s\right). \tag{4.11}$$

By making use of the identity (cf. ref. (7))

$$\frac{dW_{k,m}(x)}{dx} = \frac{k - \frac{1}{2}x}{x} W_{k,m}(x) - \frac{m^2 - \left(k - \frac{1}{2}\right)^2}{x} W_{k-1,m}(x) \tag{4.12}$$

we obtain

$$\begin{pmatrix} \frac{dR}{ds} \\ R \end{pmatrix} = \frac{h_1}{s^2} \begin{pmatrix} \left[k - \left(1 + \sqrt{A}\, s\right)\right] W_{k,m}\left(2\sqrt{A}\, s\right) - \left[m^2 - \left(k - \frac{1}{2}\right)^2\right] W_{k-1,m}\left(2\sqrt{A}\, s\right) \\ s W_{k,m}\left(2\sqrt{A}\, s\right) \end{pmatrix}. \tag{4.13}$$

The solutions of (4.2) which are valid in the intervals $\left[0, \dfrac{L}{\sigma}\right]$ and $\left[\dfrac{L}{\sigma}, \infty\right]$ are given by (4.6) and (4.13) respectively. At the point $s = \dfrac{L}{\sigma}$ they must become equal:

$$\left.\begin{array}{c} \Phi\left(\frac{L}{\sigma}\right)\begin{pmatrix}0\\1\end{pmatrix} C_1 \\ = \frac{h_1}{\left(\frac{L}{\sigma}\right)^2}\begin{pmatrix}\left[k-\left(1+\sqrt{\Lambda}\frac{L}{\sigma}\right)\right] W_{k,m}\left(2\sqrt{\Lambda}\frac{L}{\sigma}\right)-\left[m^2-\left(k-\frac{1}{2}\right)^2\right] W_{k-1,m}\left(2\sqrt{\Lambda}\frac{L}{\sigma}\right) \\ \frac{L}{\sigma} W_{k,m}\left(2\sqrt{\Lambda}\frac{L}{\sigma}\right)\end{pmatrix}. \end{array}\right\} \quad (4.14)$$

In the same way as (2.14) was obtained from (2.13), we have from (4.14)

$$\det\left\{\Phi\left(\frac{L}{\sigma}\right)\begin{pmatrix}0\\1\end{pmatrix}, \begin{matrix}\left[k-\left(1+\sqrt{\Lambda}\frac{L}{\sigma}\right)\right] W_{k,m}\left(2\sqrt{\Lambda}\frac{L}{\sigma}\right)-\left[m^2-\left(k-\frac{1}{2}\right)^2\right] W_{k-1,m}\left(2\sqrt{\Lambda}\frac{L}{\sigma}\right) \\ \frac{L}{\sigma} W_{k,m}\left(2\sqrt{\Lambda}\frac{L}{\sigma}\right)\end{matrix}\right\} = 0. \quad (4.15)$$

The equation (4.15) is now the equation for the discrete eigenvalues of (4.1). The solution of the eigenvalue problem (4.3) is thus reduced—if we consider the Whittaker function $W_{k,m}(x)$ as a standard function—to the forming of the matrix $\Phi\left(\frac{L}{\sigma}\right)$, a task which we shall undertake in the next section.

The eigenfunction $R_i(s)$ which corresponds to the eigenvalue $\Lambda_i$ is obtained from (4.6), (4.11) and (4.15):

$$R_i(s) = \begin{cases} (0,\ 1)\ [\Phi(s)]_{\Lambda=\Lambda_i}\begin{pmatrix}0\\1\end{pmatrix} C_1 \text{ for } s\varepsilon\left[0,\ \frac{L}{\sigma}\right] \\ \frac{1}{s} W_{k,m}\left(2\sqrt{\Lambda_i}\, s\right)\varkappa(\Lambda_i)\, C_1 \text{ for } s\varepsilon\left[\frac{L}{\sigma},\ \infty\right], \end{cases} \quad (4.16)$$

where the factor $\varkappa(\Lambda_i)$ is defined by (4.14). The constant is obtained from a normalizing condition.

## 5. The Solution of the Matrix Differential Equation

$$\frac{dX}{ds} - \left(\frac{P_{-1}}{s} + P\right) X = 0$$

An excellent account of the properties of matrix differential equations of the form

$$\frac{dX}{ds} - \left(\frac{P_{-1}}{s} + P(s)\right) X = 0$$

may be found in the book by GANTMACHER [1].

The following theorem, a special case of a more general theorem by GAMTMACHER [1], holds true:

*Theorem*: If (1°) the power series of

$$P(s) = \frac{P_{-1}}{s} + \sum_{m=0}^{\infty} P_m s^m$$

is convergent for $s \varepsilon \left[0, \frac{L}{\sigma}\right]$, and if (2°) no two eigenvalues of $P_{-1}$ differ by an integer, then the solution of the matrix differential equation

$$\frac{dX}{ds} - P(s)\, X = 0 \tag{5.1}$$

will be of the form

$$X = A(s) \exp(P_{-1} \ln s) = A(s)\, s^{P_{-1}}, \tag{5.2}$$

where the matrix function $A(s)$ is regular at $s = 0$ and where $A(0) = I$.

Our matrix differential equation (4.5) satisfied the conditions 1° and 2° of the theorem. Indeed, according to what was said on page 3, the matrix $P(s)$ may be expressed as a power series

$$P(s) = \sum_{m=0}^{\infty} P_m s^m$$

absolutely convergent for $s \varepsilon \left[0, \frac{L}{\sigma}\right]$. Furthermore, the eigenvalues of $P_{-1}$ are zero and $-2(p+1) = -\left[\sqrt{(2l+1)^2 + 4ak} + 1\right]$, where, according to our assumption about $l$ and $a$, the eigenvalue $-2(p+1)$ is not an integer.

Our problem is now to form $A(s)$. This we could do (cf. refs. (1) and (6)) by forming and solving an infinite set of equations for the matrices $A_n$ of

$$A(s) = \sum_{n=0}^{\infty} A_n s^n.$$

But this would be nothing else than solving (4.1) by the power series substitution

$$R(s) = s^p \sum_{n=0}^{\infty} a_n s^n,$$

a procedure which would not be very efficient. In the following we shall develop a procedure which is very similar to that employed in section 3.

It will be convenient to replace the matrix $X$ of (5.1) by the new unknown matrix $Y$ defined as follows [1]:

$$Y = TXT^{-1}, \tag{5.3}$$

where

$$T = \begin{pmatrix} 1 & \dfrac{G}{2(p+1)} \\ 0 & 1 \end{pmatrix}.$$

We then obtain from (4.4) the following differential equation for $Y$:

$$\frac{dY}{ds} - \left(\frac{\theta}{s} + \gamma(s)\right) Y = 0, \tag{5.4}$$

where

$$\theta = \begin{pmatrix} -2(p+1) & 0 \\ 0 & 0 \end{pmatrix} \tag{5.4a}$$

and

$$\gamma(s) = \begin{pmatrix} \beta & -\beta^2 + \Lambda - V_1(s) \\ 1 & -\beta \end{pmatrix}, \quad \beta = \frac{G}{2(p+1)}.$$

According to the theorem on page 18 the solution of (5.4) will be of the form

$$Y = A(s)\, s^{\theta}, \tag{5.5}$$

where $A(s)$ is regular in $\left[0, \dfrac{L}{\sigma}\right]$. The substitution of (5.5) in (5.4) yields the following equation for $A(s)$:

$$\frac{dA}{ds} + \frac{1}{s}(A\theta - \theta A) - \gamma A = 0. \tag{5.6}$$

We substitute here, as Erougin does in a different connection [5],

$$A = s^{\theta}\, C(s)\, s^{-\theta} \tag{5.7}$$

and obtain the following differential equation for $C(s)$:

$$\frac{dC}{ds} - B(s)\, C = 0, \tag{5.8}$$

where

$$\left.\begin{aligned} B(s) = s^{-\theta}\,\gamma s^{\theta} &= \begin{pmatrix} \beta & [-\beta^2 + A - V_1(s)]\, s^{\alpha} \\ s^{-\alpha} & -\beta \end{pmatrix}, \\ \alpha = 2(p+1) \text{ and } \beta &= \frac{G}{\alpha}. \end{aligned}\right\} \tag{5.9}$$

The equation (5.8) is satisfied for $s\varepsilon\left(s_0, \frac{L}{\sigma}\right]$, $s_0 > 0$, by the matrix series

$$\Omega(B) = I + \int_{\bullet}^{s} B\,ds_1 + \int_{\bullet}^{s} B\,ds_1 \int_{\bullet}^{s_1} B\,ds_2 + \ldots, \tag{5.10}$$

where, in carrying out the integrations, we put constants of integration equal to zero in all terms. The uniform and absolute convergence of (5.10) for $s\varepsilon\left(s_0, \frac{L}{\sigma}\right]$, $s_0 > 0$, is easy to verify. Consequently

$$A(s) = I + s^{\theta}\left(\int_{\bullet}^{s} B\,ds_1\right)s^{-\theta} + s^{\theta}\left(\int_{\bullet}^{s} B\,ds_1 \int_{\bullet}^{s_1} B\,ds_2\right)s^{-\theta} + \ldots. \tag{5.11}$$

is an absolutely and uniformly convergent series for $s\varepsilon\left(s_0, \frac{L}{\sigma}\right]$. But the series (5.11) converges in an arbitrary neighbourhood of the origin.

Indeed, if

$$\eta_0 = \max\{\beta,\ 1 - \beta^2 + A - V_1(s),\ -\beta,\ 1\},$$

we have

$$\int_{\bullet}^{s} B\,ds_1 \leqslant \eta_0\, s \begin{pmatrix} 1 & s^{\alpha} \\ s^{-\alpha} & 1 \end{pmatrix}$$

$$\int_{\bullet}^{s} B\,ds_1 \int_{\bullet}^{s_1} B\,ds_2 \leqslant 2\,\eta_0^2\, s^2 \begin{pmatrix} 1 & s^{\alpha} \\ s^{-\alpha} & 1 \end{pmatrix}$$

$$\vdots$$

$$\int_{\bullet}^{s} B\,ds_1 \int_{\bullet}^{s_1} \ldots \int_{\bullet}^{s_n} B\,ds_{n+1} \leqslant 2^{n-1}\,\eta_0^n\, s^n \begin{pmatrix} 1 & s^{\alpha} \\ s^{-\alpha} & 1 \end{pmatrix},$$

as is easily shown by induction. Here use has been made also of the fact that $\alpha \geqslant 2$. Hence

$$s^{\theta} \int_{\bullet}^{s} B\,ds_1 \int_{\bullet}^{s_1} B\,ds_2 \ldots \int_{\bullet}^{s_n} B\,ds_{n+1}\, s^{-\theta} \leqslant 2^{n-1}\,\eta_0^n\, s^n \begin{pmatrix} 1 & 1 \\ 1 & 1 \end{pmatrix}.$$

The series (5.11) thus converges absolutely and uniformly for $s \varepsilon \left[0, \frac{1}{2\,\eta_0}\right)$, $0 < \eta_0 < \infty$. It follows that the matrix series $s^\theta\, \tilde{\Omega}(B)\, s^{-\theta}$ converges absolutely and uniformly and satisfies the differential equation (5.4) in the whole interval $\left[0, \frac{L}{\sigma}\right]$. Since $V_1(s)$ in (5.9) is an absolutely convergent power series in $s$, it follows—as would be easy to show—that all terms of (5.11) have power series in $s$ as elements. Besides, $s^\theta\, \tilde{\Omega}(B)\, s^{-\theta} \to I$, as $s \to 0$. From the theorem on page 18 we conclude that

$$Y = \left\{ s^\theta\, \tilde{\Omega}(B)\, s^{-\theta} \right\} s^\theta \tag{5.12}$$

is a solution of (5.4) (we do not write $Y = s^\theta\, \tilde{\Omega}(B)$ since we want our solution to appear in the form suggested by the theorem). From (5.3) it follows that the general solution of (4.5) is given by

$$z = T^{-1} \left\{ s^\theta\, \tilde{\Omega}(B)\, s^{-\theta} \right\} s^\theta\, T z_0, \tag{5.13}$$

where $z_0$ is an arbitrary vector. From (4.3) and (5.13) it is then seen that

$$\begin{pmatrix} \frac{dR}{ds} \\ R \end{pmatrix} = s^{p-1} \begin{pmatrix} s & p \\ o & s \end{pmatrix} T^{-1} \left\{ s^\theta\, \tilde{\Omega}(B)\, s^{-\theta} \right\} s^\theta\, T z_0. \tag{5.14}$$

The vector $z_0$ must be chosen so that the condition $R(0) < \infty$ (cf. (4.2)) is fulfilled. Now

$$s^\theta\, T z_0 = \begin{pmatrix} s^{-2(p+1)} & 0 \\ 0 & 1 \end{pmatrix} \begin{pmatrix} 1 & \frac{G}{2(p+1)} \\ 0 & 1 \end{pmatrix} z_0 = \begin{pmatrix} s^{-2(p+1)} & s^{-2(p+1)} \frac{G}{2(p+1)} \\ 0 & 1 \end{pmatrix} z_0. \tag{5.15}$$

From (5.14) and (5.15) it is clear that we must set

$$z_0 = \begin{pmatrix} -\frac{G}{2(p+1)} \\ 1 \end{pmatrix} C_1,$$

$C_1$ being a constant. Finally we obtain

$$\begin{pmatrix} \frac{dR}{ds} \\ R \end{pmatrix} = s^{p-1} \begin{pmatrix} s & p - \frac{G}{2(p+1)} s \\ 0 & s \end{pmatrix} \left\{ s^\theta\, \tilde{\Omega}(B)\, s^{-\theta} \right\} \begin{pmatrix} 0 \\ 1 \end{pmatrix} C_1. \tag{5.16}$$

The $\Phi(s)$-matrix of (4.6), (4.14), (4.15), and (4.16) is thus

$$\Phi(s) = s^{p-1} \begin{pmatrix} s & p - \dfrac{G}{2(p+1)} s \\ 0 & s \end{pmatrix} \{ s^{\theta} \tilde{\Omega}(s^{-\theta} \gamma s^{\theta}) s^{-\theta} \}, \tag{5.17}$$

the matrix $\gamma$ having been defined in (5.4a).

The eigenvalue $\Lambda$ is contained in $\gamma$. In practical applications one prefers, however, to have the matrix $\Phi(s)$ in the form of a power series in $\Lambda$. In order to achieve this, we first rewrite $\gamma$ as follows:

$$\gamma = \gamma_1 + \Lambda \gamma_2,$$

where

$$\gamma_1 = \begin{pmatrix} \beta & -\beta^2 - V_1(s) \\ 1 & -\beta \end{pmatrix} \text{ and } \gamma_2 = \begin{pmatrix} 0 & 1 \\ 0 & 0 \end{pmatrix}.$$

The differential equation (5.6) will then appear in the form

$$\frac{dA}{ds} + \frac{1}{s}(A\theta - \theta A) - (\gamma_1 + \Lambda \gamma_2) A = 0. \tag{5.18}$$

We substitute

$$A = A_1 D, \tag{5.19}$$

with

$$A_1 = s^{\theta} \tilde{\Omega}(s^{-\theta} \gamma_1 s^{\theta}) s^{-\theta},$$

in (5.18). As is seen at once, $A_1$ is the solution of

$$\left.\begin{aligned} &\frac{dA_1}{ds} + \frac{1}{s}(A_1\theta - \theta A_1) - \gamma_1 A_1 = 0 \\ &A_1(0) = I. \end{aligned}\right\} \tag{5.20}$$

Remembering that the inverse of $A_1$ exists for every $s \varepsilon \left[0, \dfrac{L}{\sigma}\right]$ (cf. ref. (6)), we obtain the differential equation

$$\frac{dD}{ds} + \frac{1}{s}(D\theta - \theta D) - \Lambda (A_1^{-1} \gamma_2 A_1) D = 0 \tag{5.21}$$

for $D$. Since $A(0) = A_1(0) = I$, we require that $D(0) = I$. Before we are able to write down the solution of (5.21), we have to consider the matrix $A_1^{-1} \gamma_1 A_1$ a little more closely. Instead of directly inverting the matrix $A_1$, we may proceed as follows: It is easy to verify that $A_1^{-1}$ satisfies the differential equation

$$\frac{dY}{ds}+\frac{1}{s}\,(Y\theta-\theta Y)+Y\gamma_1=0 \tag{5.22}$$

and furthermore, when we require $Y(0)=I$, that

$$Y=s^{\theta}\,\tilde{\psi}\,(-s^{-\theta}\,\gamma_1\,s^{\theta})\,s^{-\theta} \tag{5.23}$$

for $s\varepsilon\left[0,\frac{L}{\sigma}\right]$, where

$$\tilde{\psi}\,(-F)=I-\int_{\bullet}^{s}F\,ds_1+\int_{\bullet}^{s}ds_1\left(\int_{\bullet}^{s_1}F\,ds_2\right)F(s_1)-\ldots. \tag{5.24}$$

($F$ standing for $s^{-\theta}\gamma_1 s^{\theta}$). The matrix $s^{\theta}\,\tilde{\psi}(s^{-\theta}\gamma_1 s^{\theta})\,s^{-\theta}$ is an absolutely and uniformly convergent power series in $s$, as is easy to show by a procedure practically identical with the one used in connection with (5.11). It follows that the matrix $\Lambda\,A_1^{-1}\gamma_2 A_1$ is an absolutely and uniformly convergent power series in $s$. We conclude from this that the solution of (5.21) satisfying the condition $D(0)=I$ is given by the matrix

$$D=s^{\theta}\,\tilde{\Omega}\left\{\Lambda\,s^{-\theta}\,[s^{\theta}\,\tilde{\psi}\,(-s^{-\theta}\,\gamma_1\,s^{\theta})\,s^{-\theta}]\,\gamma_2\,[s^{\theta}\,\tilde{\Omega}\,(s^{-\theta}\,\gamma_1\,s^{\theta})\,s^{-\theta}]\,s^{\theta}\right\}s^{-\theta}. \tag{5.25}$$

Finally we obtain from (5.17), (5.19) and (5.25)

$$\left.\begin{aligned}\Phi(s)=s^{p-1}\begin{pmatrix}s & p-\dfrac{G}{2\,(p+1)}\,s\\ 0 & s\end{pmatrix}s^{\theta}\,\tilde{\Omega}\,(s^{-\theta}\,\gamma_1\,s^{\theta})\,s^{-\theta}\\ s^{\theta}\,\tilde{\Omega}\left\{\Lambda\,s^{-\theta}\,[s^{\theta}\,\tilde{\psi}\,(-s^{-\theta}\,\gamma_1\,s^{\theta})\,s^{-\theta}]\,\gamma_2\,[s^{\theta}\,\tilde{\Omega}\,(s^{-\theta}\,\gamma_1\,s^{\theta})\,s^{-\theta}]\,s^{\theta}\right\}s^{-\theta},\end{aligned}\right\} \tag{5.26}$$

which is clearly a power series in $\Lambda$. In (5.25) and (5.26) we have maintained the forms $s^{\theta}\,\Omega\,s^{-\theta}$ and $s^{\theta}\,\tilde{\psi}\,s^{-\theta}$ since they are matrices with power series in $s$ as elements. Everything that was said in section 3 in connection with (3.3) will hold for (5.26).

## Acknowledgements

I want to express my deep gratitude to Professor Niels Bohr for excellent working conditions at the Institute for Theoretical Physics in Copenhagen.

Further I want to thank Professor L. Rosenfeld and Professor C. Møller for their suggestion to add an example to section 3, which led to a revision of the whole section.

I am greatly indebted to NORDITA for the research fellowship granted me by that institute.

*NORDITA – Nordisk Institut for Teoretisk Atomfysik*
*Copenhagen, Denmark*

## References


(1) Ф. Р. Гантмахер, Теория Матриц (Гостехиздат, Москва, 1953).

(2) O. Hellman, Die Anwendung des Matrizanten bei Eigenwertaufgaben. Z. angew. Math. Mech. **35** (1955).

(3) O. Hellman, On the Solution of the One Dimensional Schrödinger Equation in Case of a Potential Well. Ann. Acad. Sci. Fennicae, Physica **6**, no. 11 (1958).

(4) O. Hellman, Ein Verfahren zur Bildung von Matrizanten. Z. angew. Math. Mech. **37** (1957).

(5) Н. П. Еругин, Приводимые системы. Труды математического инст. Стеклова XIII.

(6) E. A. Coddington and N. Levinson, Theory of Ordinary Differential Equations (McGraw-Hill, New York, 1955).

(7) E. T. Whittaker, An Expression of Certain Known Functions as Generalized Hypergeometric Functions. Bull. Am. Math. Soc. **10** (1904) 125.



Indleveret til selskabet den 12. august 1959.
Færdig fra trykkeriet den 12. februar 1960.

Matematisk-fysiske Meddelelser
udgivet af
Det Kongelige Danske Videnskabernes Selskab
Bind **32,** nr. 5

Mat. Fys. Medd. Dan. Vid. Selsk. **32,** no. 5 (1960)

# ON THE ANGULAR DISTRIBUTION OF THE SCATTERED PARTICLES IN COULOMB EXCITATION

BY

JENS BANG

København 1960
i kommission hos Ejnar Munksgaard

## CONTENTS


| | | Page |
|---|---|---|
| I. | Introduction | 3 |
| II. | Numerical Calculations of the Angular Distribution | 4 |
| III. | Errors Involved in the Calculation | 7 |
| IV. | The Cross Section for Vanishing Deflection Angle | 10 |
| V. | Concluding Remarks | 12 |
| Appendix | | 14 |
| References | | 16 |



## Synopsis

The angular distribution of scattered particles in Coulomb excitation is calculated for the case of electric quadrupole excitation and vanishing energy transfer; numerical values are given for a number of scattering angles and incident energies. Furthermore, an expression for the cross section at a deflection angle equal to zero is derived, valid also for finite energy transfer.



Printed in Denmark
Bianco Lunos Bogtrykkeri A-S

## I. Introduction

The detection of the inelastically scattered particles in Coulomb excitation has recently been used in the investigation of low-lying nuclear states.

This method has certain advantages over the one consisting in detection of the subsequently emitted gamma rays or conversion electrons. Particularly, it is profitable in that it gives information about excitation energies and cross sections which does not depend on any knowledge of the decay scheme and the conversion coefficients.

On the other hand, determination of the cross sections by this method requires either measurements at several deflection angles of the scattered particle or knowledge of the theoretical angular distribution. This angular distribution is essentially independent of the nuclear structure and, when the multipole character of the excitation is given, is calculable from electrodynamics alone. In fact, such calculations have been made by ALDER and WINTHER and the result expressed in terms of the function $\frac{df(\vartheta, \eta, \xi)}{d\Omega}$ (ref. 1, II B. 34), where $\vartheta$ is the deflection angle of the scattered particle, and $\eta$ is defined by

$$\eta = \frac{Z_1 Z_2 e^2}{\hbar v}, \tag{1}$$

where $Z_1$ and $Z_2$ are the charge numbers of the projectile and the nucleus, and $v$ their relative velocity. $\xi$ is defined by

$$\xi = \eta_i - \eta_f, \tag{2}$$

where the indices $i$ and $f$ refer to the initial and the final state respectively.

In the case of electric dipole excitation, an explicit expression for $\frac{df_{E1}(\vartheta, \eta, \xi)}{d\Omega}$ in terms of hypergeometric functions was found, but for the other excitation types calculations were only made in the limit of $\eta \to \infty$,

where the motion of the projectile can be described by a classical path, and in the limit of $\eta \to 0$, where the Born approximation applies. In the most important case, namely that of electric quadrupole excitation, the total $f$-function (integrated over $\vartheta$) was also calculated for intermediate $\eta$-values. It was found that the classical approximation was good to 5% down to $\eta$-values of the order 4. However, the angular distribution of de-excitation $\gamma$-rays, expressed in terms of the $a$-coefficients (ref. 1, II C. 26), showed a considerable deviation from the classical limit, even for rather high values of $\eta$ (ref. 1, fig. II. 8). Accordingly, it was thought to be questionable whether the classically calculated differential $f$-functions could be used in the regions of energies and charges where the experiments are actually made, and a further investigation of $\frac{df}{d\Omega}$ for intermediate values of $\eta$ was considered desirable.

In the present work, $\frac{df_{E2}(\vartheta, \eta, \xi = 0)}{d\Omega}$ has been calculated (by means of an electronic computor) for ten different angles and six different values of $\eta$. The case of $\xi = 0$ was chosen in order to simplify the calculations. Besides, an exact expression for $\frac{df_{E2}(\vartheta = 0, \eta, \xi)}{d\Omega}$ (in terms of hypergeometric functions) is given.

## II. Numerical Calculations of the Angular Distribution

The calculations reported here were made from the non-relativistic expressions II B. 34 and II B. 45 of ref. 1:

$$df_{E\lambda}(\vartheta, \eta, \xi) = \frac{4\, k_i k_f a^{2\lambda-2}}{\lambda^2 (2\lambda+1)^3} \sum_{\mu} |\langle \vec{k}_f | r_p^{-\lambda-1} Y_{\lambda\mu}(\vartheta_p, \Phi_p) | \vec{k}_i \rangle|^2 \, d\Omega \tag{3}$$

with

$$\left.\begin{aligned} \langle \vec{k}_f | r_p^{-\lambda-1} Y_{\lambda\mu}(\vartheta_p, \Phi_p) | \vec{k}_i \rangle &= (4\pi)^{\frac{3}{2}} \sum_{l_i l_f m_i m_f} i^{l_i - l_f} (-1)^{\mu} \exp(i\sigma_i + i\sigma_f) \\ \times [(2l_i+1)(2l_f+1)(2\lambda+1)]^{\frac{1}{2}} &\begin{pmatrix} l_i & l_f & \lambda \\ 0 & 0 & 0 \end{pmatrix} \begin{pmatrix} l_i & l_f & \lambda \\ m_i & -m_f & \mu \end{pmatrix} Y_{l_i, -m_i}(\vec{k}_i)\, Y_{l_f, m_f}(\vec{k}_f)\, M_{l_i, l_f}^{-\lambda-1}. \end{aligned}\right\} \tag{4}$$

Here, $a$ is half the distance of closest approach, $a = \frac{Z_1 Z_2 e^2}{m_0 v_i v_f}$ (the reduced mass of the target nucleus and projectile being $m_0$). The multipole order of the excitation is $\lambda$, the expressions in the long brackets are the Clebsch-

TABLE I

$\frac{df_{E2}(\vartheta)}{d\Omega}$

| $\vartheta$ \ $\eta$ | 0.5 | 1.0 | 1.5 | 2.0 | 4.0 |
|---|---|---|---|---|---|
| 0° | 0.1580 (−3) | 0.1267 (−4) | 0.3425 (−4) | 0.5857 (−4) | 0.2065 (−3) |
| 20° | 0.3014 (−1) | 0.6867 (−1) | 0.9909 (−1) | 0.1039 | 0.1027 |
| 40° | 0.2781 (−1) | 0.5826 (−1) | 0.7614 (−1) | 0.8455 (−1) | 0.9059 (−1) |
| 60° | 0.2624 (−1) | 0.5362 (−1) | 0.6565 (−1) | 0.7302 (−1) | 0.7698 (−1) |
| 80° | 0.2553 (−1) | 0.4972 (−1) | 0.5985 (−1) | 0.6527 (−1) | 0.6890 (−1) |
| 100° | 0.2512 (−1) | 0.4699 (−1) | 0.5616 (−1) | 0.5988 (−1) | 0.6315 (−1) |
| 120° | 0.2475 (−1) | 0.4531 (−1) | 0.5342 (−1) | 0.5800 (−1) | 0.5965 (−1) |
| 140° | 0.2448 (−1) | 0.4420 (−1) | 0.5164 (−1) | 0.5453 (−1) | 0.5752 (−1) |
| 160° | 0.2432 (−1) | 0.4344 (−1) | 0.5043 (−1) | 0.5321 (−1) | 0.5603 (−1) |
| 180° | 0.2429 (−1) | 0.4304 (−1) | 0.4987 (−1) | 0.5250 (−1) | 0.5522 (−1) |

TABLE II

| $\vartheta$ \ $\lim\left(\frac{df_{E2}(\vartheta)}{d\Omega}\cdot\eta^{-2}\right)_{\eta\to 0}$ |
|---|
| 0° 0.5585 (−1) |
| 20° 0.2189 |
| 40° 0.2220 |
| 60° 0.2241 |
| 80° 0.2238 |
| 100° 0.2231 |
| 120° 0.2231 |
| 140° 0.2235 |
| 160° 0.2232 |
| 180° 0.2232 |

TABLE III

$\eta = \infty$

| $\vartheta$ | $\frac{df_{E2}(\vartheta)}{d\Omega}$ |
|---|---|
| 0° | 1.676 (−1) |
| 10° | 1.385 (−1) |
| 20° | 1.178 (−1) |
| 30° | 1.027 (−1) |
| 40° | 0.916 (−1) |
| 50° | 0.832 (−1) |
| 60° | 0.768 (−1) |
| 70° | 0.719 (−1) |
| 80° | 0.680 (−1) |
| 90° | 0.650 (−1) |
| 100° | 0.627 (−1) |
| 110° | 0.608 (−1) |
| 120° | 0.593 (−1) |
| 130° | 0.582 (−1) |
| 140° | 0.573 (−1) |
| 150° | 0.566 (−1) |
| 160° | 0.562 (−1) |
| 170° | 0.559 (−1) |
| 180° | 0.558 (−1) |

Gordan coefficients in Wigner's notation (see II A. 1 and II A. 6 of ref. 1), the $Y_{em}$ are the normalized spherical harmonics, the $\sigma$'s are the Coulomb phase shifts, $\sigma_e = \arg \Gamma(l + 1 + i\eta)$, the $M$'s are the radial matrix elements for Coulomb excitation defined in ref. 1, II B. 46, and the wave vector of the projectile is denoted by $\vec{k}$.

If $\lambda = 2$ and $\xi = 0$ ($\eta_i = \eta_f = \eta$), and if furthermore the direction of $\vec{k}_i$ is used for the $z$-axis, this expression may be written as

$$\frac{df}{d\Omega} = \frac{4\,\eta^2}{5^3} \sum_{\mu} | \langle \vec{k}_f | r^{-3} Y_{2,\mu} | \vec{k}_i \rangle |^2 \tag{5}$$

with

$$\left.\begin{aligned} &\langle \vec{k}_f | r^{-3} Y_{2\mu} | \vec{k}_i \rangle \\ &= 5^{\frac{1}{2}} (4\pi)^{\frac{1}{2}} \sum_{l_i,\, l_f = l_i - 2,\, l_i,\, l_i + 2} i^{l_i - l_f} (-1)^{\mu} e^{i(\sigma_i + \sigma_f)} (2 l_i + 1)(2 l_f + 1) \begin{pmatrix} l_i & l_f & 2 \\ 0 & 0 & 0 \end{pmatrix} \begin{pmatrix} l_i & l_f & 2 \\ 0 & -\mu & \mu \end{pmatrix} \\ &\times \left( \frac{(l_f - \mu)!}{(l_f + \mu)!} \right)^{\frac{1}{2}} M_{l_i l_f}^{-3} P_{l_f}^{\mu}(\cos\vartheta)\, e^{i\mu\varphi} \end{aligned}\right\} \tag{6}$$

and

$$M_{l,\,l+2}^{-3} = M_{l+2,\,l}^{-3} = (6 \,|\, l + 1 + i\eta \,|\, |\, l + 2 + i\eta \,|)^{-1} \tag{7a}$$

$$M_{l,\,l}^{-3} = (2\,l\,(l + 1)\,(2\,l + 1))^{-1} (2\,l + 1 - \pi\eta + 2\,\eta\, \mathrm{Im}\,(\psi(l + 1 + i\eta))). \tag{7b}$$

Here $P_l^m(\cos\vartheta)$ denotes the associate Legendre polynomials with the usual normalization.

The procedure of the calculation was to perform the summation for $0 \leqslant l_i \leqslant 64$. The phases and matrix elements were evaluated by means of recursion formulae, and so were the Legendre polynomials. A fixed maximum value for $l_i$ was considered convenient for computational reasons, and 64 was chosen to ensure a reasonable accuracy in the regions where experiments were made. The result of the calculations is shown in table I and fig. 1. For $\eta \to 0$ the value of $\dfrac{df(\vartheta,\eta)}{d\Omega}$ tends to zero. Table II shows the function $\lim \left[ \eta^{-2} \dfrac{df(\vartheta,\eta)}{d\Omega} \right]_{\eta \to 0}$ calculated in the same way. This function is a step function, having a value for $\vartheta = 0$ equal to $^1/_4$ of its value for $\vartheta \neq 0$ (see below). For comparison, $\dfrac{df(\vartheta, \eta = \infty, \xi)}{d\Omega}$ with $\xi = 0$ calculated by ALDER and WINTHER by the semi-classical method (ref. 1, table II) is shown in table III and fig. 1.

## III. Errors Involved in the Calculation

The errors involved in the present calculation are of two kinds: 1) the systematic errors introduced by stopping the summation at $l_{\max} = 64$; 2) the more accidental errors arising from the numerical methods employed.

The errors of the first kind behave quite differently for small and for large deflection angles $\vartheta$. This is due to the fact that the signs of the Legendre polynomials $P_l^m(\cos\vartheta)$ are changed when $l$ is increased by an amount of approximately $\frac{\pi}{\vartheta}$. Thus, for $\vartheta \approx \pi$ the series are alternating apart from the slowly varying phases of the $M$'s and the $\sigma$'s. The omitted rest is then smaller than the first omitted term, which, compared with the whole series, is of the order of magnitude $(\eta/l_{\max})^2$. A comparison between

$$\frac{df(\vartheta=\pi,\,\eta=4,\,\xi=0)}{d\Omega} \quad \text{and} \quad \frac{df(\vartheta=\pi,\,\eta=\infty,\,\xi=0)}{d\Omega}$$

seems to indicate that the actual error is even smaller.

For small deflection angles, the error may be estimated in another way. The expression

$$M_{l_i,\,l_f}^{-\lambda-1} \approx \frac{k^{\lambda-2}}{4\,\eta^{\lambda}} \frac{2\,\pi}{\Gamma\left(\frac{\lambda+1-\mu}{2}\right)} e^{-(l/\eta+\pi/2)\,\xi}\,\xi^{(\lambda-\mu-1)/2}\,(2\,l/\eta)^{-(\lambda+\mu+1)/2} \tag{8}$$

(ref. 1, II E. 83),
valid for $l_i \gg 1$, shows that, owing to the exponential function in $M$, terms with $l > \frac{\eta}{\xi}$ contribute but a negligible amount to $\frac{df}{d\Omega}$. A break-off of the summation at $l_{\max} > \frac{\eta}{\xi}$ therefore has a minor influence on the cross sections. Apart from the exponential, the $M$'s and the phases are smoothly varying functions of $\xi$ in the neighbourhood of zero. Thus, a calculation for $\xi = 0$ where the summation over $l$ is stopped at a large $l = l_{\max}$, yields a result that does not differ very much from the cross section for $\xi = \eta/l_{\max}$. The effect of the break-off is then that the differential cross section for small angles calculated here corresponds to the case of $\xi = \frac{\eta}{64}$ rather than to that of $\xi = 0$. By comparison with the classical calculations for $\xi \neq 0$ (cf. ref. 1, table II.8 and fig. II.7) one must thus expect to find that the result of the present calculation is much smaller than the true value of $\frac{df}{d\Omega}$ for $\vartheta < \frac{\eta}{64}$.

The second kind of error arises from the numerical calculating procedure. Since each step in the calculations was made with the relative error $10^{-12}$, the accuracy of the result rests mainly on the numerical stability of the recurrence formulae used. The matrix elements $M$ and the phase factors were calculated in a straightforward manner from the formulae, and it is easily seen that a relative error $\Delta_l$ in the $l^{\text{th}}$ term leads to the same relative error in all subsequent terms, which means that no serious error is introduced in this way.

The error introduced by employment of the recurrence formula for the Legendre functions may be estimated as follows. Let the fractional error of the Legendre function at a certain step, $n$, be $\Delta_n(x)$, i. e., the exact value $P_n^m(x)$ is replaced by $P_n^m(x)\,(1+\Delta_n(x))$. This may also be written

$$P_n^m(x)\,(1+\Delta_n(x)) = P_n^m(x)\,(1+\Delta_n^P(x)) + Q_n^m(x)\,\Delta_n^Q(x), \tag{9}$$

where the $\Delta_n^P(x)$ and $\Delta_n^Q(x)$ are chosen so that, when the fractional error at the nearest preceding step is $\Delta_{n-1}(x)$, one has

$$P_{n-1}^m(x)\,(1+\Delta_{n-1}(x)) = P_{n-1}^m(x)\,(1+\Delta_n^P(x)) + Q_{n-1}^m(x)\,\Delta_n^Q(x). \tag{9a}$$

Here $Q_n^m(x)$ is an associated Legendre function of the second kind. As such functions obey the same recursion relations as the $P$'s, the computed value at any later step, $l$, derived from $n-1$ and $n$, is

$$P_l^m(x)\,(1+\Delta_n^P(x)) + Q_l^m(x)\,\Delta_n^Q(x), \tag{10}$$

which indicates a fractional error

$$\left.\begin{aligned} &\Delta_n^P + \frac{Q_l^m}{P_l^m}\,\Delta_n^Q \\ &= \frac{P_n^m Q_{n-1}^m \Delta_n - P_{n-1}^m Q_n^m \Delta_{n-1} + (Q_l^m/P_l^m)\,(\Delta_{n-1}-\Delta_n)\,P_n^m P_{n-1}^m}{P_n^m Q_{n-1}^m - P_{n-1}^m Q_n^m} \\ &= \Delta_n - (\Delta_n - \Delta_{n-1})\left\{\frac{Q_l^m}{P_l^m}\,P_n^m P_{n-1}^m - P_{n-1}^m Q_n^m\right\} \\ &\quad \times (-1)^m \frac{\Gamma\left(1+\frac{n-m}{2}\right)\Gamma\left(\frac{1+n-m}{2}\right)}{2^{2m+1}\,\Gamma\left(\frac{n+m}{2}\right)\Gamma\left(\frac{1+n+m}{2}\right)}. \end{aligned}\right\} \tag{11}$$

This might lead to large errors at the points where $Q_l^m$ or $Q_n^m$ tend towards infinity or $P_l^m$ towards zero. Christoffel's formula (ref. 5, 3.6 (26))

$$Q_p(x) = Q_0(x)\,P_p(x) - W_{p-1}(x) \tag{12}$$

($W_{p-1}$ being a polynomial in $x$) together with corresponding formulae for the associated functions, obtained by differentiation of (12), shows, however, that the singularities of the $Q$'s play no part here.

As for the zeros of $P_l^m$, the asymptotic formula for large $l$ (ref. 5, 3.5 (5))

$$\left.\begin{aligned} &\Gamma\left(l+\frac{3}{2}\right) P_l^m(\cos\vartheta) = 2^{\frac{1}{2}}\,(\pi\sin\theta)^{-\frac{1}{2}}\,\Gamma(l+m+1) \\ &\times \sum_{s=0}^{\infty} (-1)^s \frac{\left(\frac{1}{2}+m\right)_s \left(\frac{1}{2}-m\right)_s}{s!\,(\sin\vartheta)^s \left(l+\frac{s}{2}\right)_s} \sin\left(\left(l+\frac{1}{2}\right)\vartheta + \left(\frac{m}{2}+\frac{1}{4}\right)\pi + \frac{s}{2}\pi\right) \end{aligned}\right\} \tag{13}$$

may be applied. The method of TRICOMI [6] then leads to the expression

$$\vartheta_r^0 = \frac{r - \frac{m}{2} - \frac{1}{4}}{l+\frac{1}{2}}\,\pi + o\,(l^{-2}) \tag{14}$$

for these zeros ($r$ integer).

The distance of the zeros from any of the points for which calculations are made is of the order of magnitude $l^{-1}$, and, as the functions vary rapidly near the zeros, the ratio $\dfrac{Q_l^m}{P_l^m}$ is at most of the order of magnitude $l$. For $m = 0$ it would still seem that (11) could give a relative error of the order of magnitude $n \cdot l(\Delta_n - \Delta_{n-1}) \approx l^2 \Delta_n$ for $n \approx l$. However, the formula

$$\frac{Q_n}{P_n} - \frac{Q_l}{P_l} = \sum_{i=n+1}^{l} \frac{1}{iP_i\,P_{l-i}} \tag{11 a}$$

shows that in this case the error is rather of the order of magnitude $l\,(l-n)$ $(\Delta_n - \Delta_{n-1})$.

As regards the error in the final result caused by $\Delta_{n-1}$ and $\Delta_n$ it must furthermore be remembered that the coefficients $M$ etc. decrease with increasing $l$. In conclusion it may be stated that the errors introduced by the employment of the numerical methods are negligible compared with that which is committed by breaking off the summation at $l = 64$.

## IV. The Cross Section for Vanishing Deflection Angle

In the preceding section it was shown that the decrease for small $\vartheta$ of the $\frac{df(\vartheta)}{d\Omega}$ obtained in this calculation is due to the introduction of a finite $l_{\max}$. As the expansion on associate Legendre polynomials is a Fourier analysis, this effect seems to indicate that the cross section (5) for $\xi = 0$ as

TABLE IV

| $\eta$ | $\frac{df_{E2}}{d\Omega}(\vartheta = 0)$ |
|---|---|
| $^1/_2$ | 0.171 (−3) |
| 1 | 0.328 (−5) |
| $1^1/_2$ | 0.203 (−7) |
| 2 | 0.143 (−9) |
| 4 | 0.252 (−19) |

a function of $\vartheta$ is a step function at $\vartheta = 0$. This is supported by the fact that the classical cross section is a step function with the value 0 for $\vartheta = 0$ when one defines it by the limiting procedure $\xi \to 0$. Also in the Born-approximation limit the function $\lim\left(\eta^{-2}\frac{df(\vartheta,\eta)}{d\Omega}\right)_{\eta\to 0}$ turns out to be a step function. In this case, the summation in (6) is easily carried out for $\vartheta = 0$, the result being just one fourth of the value for $\vartheta \neq 0$.

It would seem to be of little importance to calculate the true value of $\frac{df(\vartheta,\eta,\xi=0)}{d\Omega}$ for $\vartheta = 0$. However, it is possible to give a closed expression for this function, even in the regions of $\xi \neq 0$, $\eta \neq 0$, where the cross section shows a smooth behaviour in the neighbourhood of $\vartheta = 0$.

Starting from the expression

$$df_{E2} = \frac{4\,k_i\,k_f}{5^3}\,a^2 \sum_{\mu} |\langle \vec{k}_f | r_p^{-3} Y_{2\mu}(\theta_p, \Phi_p) | \vec{k}_i \rangle|^2 \, d\Omega \tag{15}$$

with

$$\left.\begin{aligned} |\vec{k}_i\rangle &= e^{-\frac{\pi}{2}\eta_i}\,\Gamma(1+i\eta_i)\,e^{ik_i r\cos\vartheta}\,\Phi(-i\eta_i, 1; ik_i r(1-\cos\vartheta)) \\ |\vec{k}_f\rangle &= e^{-\frac{\pi}{2}\eta_f}\,\Gamma(1-i\eta_f)\,e^{ik_f r\cos\vartheta}\,\Phi(i\eta_f, 1; -ik_f r(1+\cos\vartheta)) \end{aligned}\right\} \tag{16}$$

($\Phi$ being the confluent hypergeometric function (see ref. 5)), where the common direction of $\vec{k}_i$ and $\vec{k}_f$ is chosen as $z$-axis (ref. 1, II B, eqs. 34, 40, 41), one arrives, as sketched in the appendix, at the formula

$$\frac{df_{E2}(\vartheta=0,\eta,\xi)}{d\Omega}=\frac{4\eta^2}{5^3}\left|\sqrt{5\pi}\exp(-\pi\eta)\,\Gamma(1+i\eta(1-\delta))\,\Gamma(1+i\eta(1+\delta))\right.$$
$$\times\left(\div\frac{2}{3}+\frac{i\eta}{1-2i\eta}\left\{\div 1+(i\eta(1-\delta^2))^{-1}+\frac{2(i\eta(1-\delta^2))-1}{i\eta(1-\delta^2)}\right.\right.$$
$$\times(-\delta)^{-i\eta(1-\delta)}(\delta)^{-i\eta(1+\delta)}-\delta\left[\frac{\Gamma(1+2i\eta)\,\Gamma(-i\eta(1+\delta))}{2\,\Gamma(1+i\eta(1\div\delta))}\right. \tag{17}$$
$$\times(\div 2\delta(1+\delta)^{-1})^{-2i\eta}((1-\delta)/(1+\delta))^{i\eta(1\div\delta)}$$
$$+(-1)^{i\eta(1+\delta)}(2i\eta(1+\delta))^{-1}(-\delta)^{-2i\eta}\times F\left(-2i\eta,1,1-i\eta(1+\delta);\frac{1+\delta}{2}\right)$$
$$\left.\left.\left.+\delta(1+2i\eta)^{-1}(1+\delta)^{-1}F(1,1+i\eta(1+\delta),2+2i\eta;2\delta(1+\delta)^{-1})\right]\right\}\right)\Bigg|^2,$$

where

$$\eta\equiv\frac{\eta_i+\eta_f}{2}$$

$$\delta\equiv\frac{\xi}{2\eta}=\frac{\eta_f-\eta_i}{\eta_f+\eta_i}$$

and the $F$'s are Gauss' hypergeometric functions. To zeroth order in $\delta$ the result is

$$\frac{4\eta^2}{5^3}\left|\sqrt{5\pi}\exp(-\pi\eta)\,(\Gamma(1+i\eta))^2\left(\frac{1+i\eta}{3(1-2i\eta)}\div(-\delta)^{-2i\eta}\right)\right|^2. \tag{18}$$

This expression is at first indeterminate, but one may make it finite by multiplying $\eta$ by $1+i\varepsilon$ and letting $\varepsilon$ tend towards zero.

The results of the calculation of $\frac{df(\vartheta=0,\eta,\xi=0)}{d\Omega}$ from (18) are shown in table IV. The deviation of that table from the column with $\vartheta=0$ in table I seems to be due to the errors in the calculation of the latter. In the limit of $\eta\to 0$ there is an ambiguity in the calculation of $\eta^{-2}\frac{df(0,0,0)}{d\Omega}$ from (18). If the limit of $\eta\to 0$ is used first, and then $\xi\to 0$, the result is $\frac{16\pi}{225}$; if the procedure is reversed, the result becomes $\frac{4\pi}{225}$. This seems to reflect the ambiguity in the calculation of $\lim\left(\eta^{-2}\frac{df(\vartheta=0)}{d\Omega}\right)_{\text{Born}}$ mentioned above.

## V. Concluding Remarks

Since the calculation of nuclear matrix elements of Coulomb excitation from measurements of the scattered particles has hitherto been based on the classical calculations, which have been made for a number of $\xi$ values between 0 and 4, the most important result of the present calculation seems to be the fact that it shows a very good agreement with the classical ones. For $\eta = 4$, the deviation of $\frac{df(\eta = 4, \xi = 0)}{d\Omega}$ from $\frac{df(\eta = \infty, \xi = 0)}{d\Omega}$ is less than $2\%$ in the whole angular region where the present calculations are valid ($\vartheta > 20°$). When $\eta$ is smaller, $\frac{df(\xi = 0)}{d\Omega}$ lies somewhere between the value from the classical calculations and that from the Born approximation.

In fig. 1 the curves are tentatively continued into the region of small angles in the way suggested by the above discussion. The uncertainties which still exist in the evaluation of the $\frac{df}{d\Omega}$ functions for small $\vartheta$ are not very serious, judging by the fact that this is a region where the sources of experimental errors are very considerable, and at the same time a region which contributes but a negligible amount to the total cross section.

Also the calculation of $\frac{df(\vartheta = 0)}{d\Omega}$ shows good agreement with the classical calculation. Furthermore it shows that for $\xi \neq 0$ the cross sections must decrease considerably in the forward direction, even for rather small $\eta$ values.

At present only one set of measurements of the angular dependence of the Coulomb cross section seems to be available. The experiment concerned was made by Elbek and Bockelman [2], who used 6-MeV protons on gold and detected the scattered particles from excitation of the levels at 545 and 279 keV, at angles 60°, 95°, 110°, and 130° with the incident beam. In these cases $\eta = 5.0$ and $\xi = 0.25$ and 0.12, and thus the classical theory is expected to be quite accurate. The experimental results certainly agree with the theory, but the test is not very critical owing to the rather large experimental uncertainties.

Fig. 1. The calculated values of $\frac{df_{E2}(\vartheta)}{d\Omega}$ plotted as functions of $\vartheta$.

As a consequence of the finite number of angular momenta involved in the calculations, the latter are only valid for angles $\vartheta > \frac{\eta}{64}$ (see section III). In the region of smaller angles the curves are tentatively extrapolated (the dashed part of the lines) in a way suggested by the classical curve ($\eta = \infty$) (also dashed) and the isotropy of the Born-approximation angular distribution ($\eta = 0$).

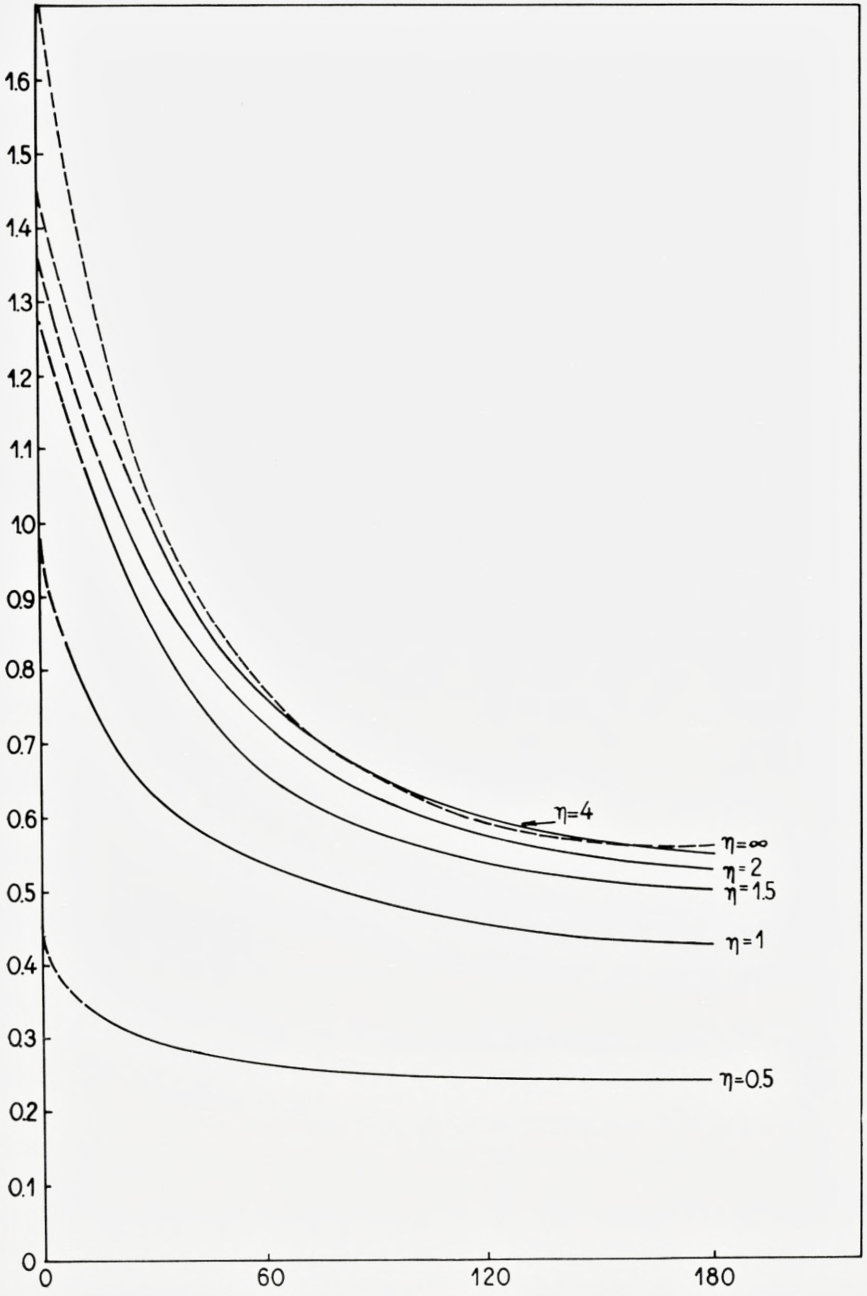
1.6
1.5
1.4
1.3
1.2
1.1
1.0
0.9
0.8
0.7
0.6
0.5
0.4
0.3
0.2
0.1
0
0
60
120
180
η=4
η=∞
η=2
η=1.5
η=1
η=0.5

## Acknowledgements

The author wishes to thank Professor Aage Bohr, Dr. S. Rakavy, Per Asisoff, M. Sc., and, particularly, Aage Winther, M. Sc., for valuable suggestions during the present work. Further he wants to express his gratitude to CERN (European Organization for Nuclear Research) and NORDITA for granting him fellowships, and to the board of the Swedish electronic computor BESK for free use of the machine during a period.

*NORDITA – Nordisk Institut for Teoretisk Atomfysik*
*Copenhagen, Denmark*

## Appendix

The integration in the matrix element (15) may be performed in the following way: the $\varphi$-integration is first carried out, leading to 0 for $m \neq 0$ and to $2\pi$ for $m = 0$. The wave functions are transformed by means of

$$\Phi(\alpha, \gamma, z) = \exp(z)\, \Phi(\gamma - \alpha, \gamma, -z) \tag{A. 1}$$

(ref. 5, 6.3 (7)) and

$$\Phi(\alpha, 1, z) = \alpha \Phi(\alpha + 1, 2, z) - (\alpha - 1)\, \Phi(\alpha, 2, z) \tag{A. 2}$$

(ref. 5, 6.4 (4)),
and the $Y_{20}$-function is expressed as a Legendre polynomial $P_2(x)$ $(x = \cos\vartheta)$; the $\vartheta$-integration then becomes

$$\left.\begin{aligned} \mathrm{I} = & -\frac{3}{2}\int_{-1}^{+1} dx\,(1-x)(1+x) \\ & \times [\beta \Phi(\beta+1, 2; -ik_i r(1-x)) - (\beta-1)\, \Phi(\beta, 2; -ik_i r(1-x))] \\ & \times [\beta' \Phi(\beta'+1, 2; -ik_f r(1+x)) - (\beta'-1)\, \Phi(\beta', 2; -ik_f r(1+x))] \\ & + \int_{-1}^{+1} dx\, \Phi(\beta, 1; -ik_i r(1-x))\, \Phi(\beta', 1; -ik_f r(1+x)), \end{aligned}\right\} \tag{A. 3}$$

where $\beta \equiv 1 + i\eta_i$, $\beta' \equiv 1 + i\eta_f$.
This integration may be carried out by means of the theorem

$$\left.\begin{aligned} & \int_0^t \frac{u^{\gamma-1}}{\Gamma(\gamma)}\, \Phi(\beta, \gamma; \lambda u)\, \frac{(t-u)^{\gamma'-1}}{\Gamma(\gamma')}\, \Phi(\beta', \gamma', \lambda'(t-u))\, du \\ & \qquad = \frac{t^{\gamma+\gamma'-1}}{\Gamma(\gamma+\gamma')}\, \Phi_2(\beta, \beta', \gamma+\gamma', \lambda t, \lambda' t), \end{aligned}\right\} \tag{A. 4}$$

which can be proved from ref. 7, 5.4 (9). Here $\Phi_2$ is a confluent hypergeometric function of two variables, defined in 5.7 (21) of ref. 5. By means of the recursion formulae

$$\Phi_2(\gamma+1)\,x = \gamma\,(\Phi_2 - \Phi_2(\beta-1)) \tag{A. 5}$$

and

$$\gamma(\gamma-1)\,\Phi_2(\gamma-1) = \gamma(\gamma-1)\,\Phi_2 + \beta x\,\Phi_2(\gamma+1,\,\beta+1) + \beta' y\,\Phi_2(\gamma+1,\,\beta'+1) \tag{A. 6}$$

the result may be transformed into I =

$$\left.\begin{aligned}
&-\frac{\beta\beta'}{2}\,y,\,\Phi_2(\beta+1,\,\beta'+1,\,5,\,x_1;\,y_1)\\
&+\beta'\left(\frac{\beta}{2}-\frac{1}{3}\right)y_1\,\Phi_2(\beta,\,\beta'+1,\,5;\,x_1,\,y_1)\\
&-\frac{\beta}{3}\,x_1\,\Phi_2(\beta+1,\,\beta',\,5;\,x_1,\,y_1)\\
&+\frac{\beta}{3}\,x_1\,\Phi_2(\beta+1,\,\beta',\,4;\,x_1,\,y_1)\\
&+\frac{\beta'}{3}\,y_1\,\Phi_2(\beta,\,\beta'+1,\,4;\,x_1\,y_1),
\end{aligned}\right\} \tag{A. 7}$$

where $x_1 \equiv -2\,ik_i\,r$, $y_1 \equiv -2\,ik_f\,r$.
If a small imaginary number is added to $k_f$, the $r$-integration may be carried out by means of the Laplace integration formula

$$\int_0^\infty dt\,e^{-pt}\,t^{\alpha-1}\,\Phi_2(\beta,\,\beta',\,\gamma,\,xt,\,yt) = \Gamma(\alpha)\,p^{-\alpha}\,F_1\left(\alpha,\,\beta,\,\beta',\,\gamma,\,\frac{x}{p},\,\frac{y}{p}\right)$$

(ref. 7, 4.24 (4)),
where $F_1$ is a hypergeometric function of two variables, defined in 5.7 (6) of ref. 5.

The result may be contracted considerably by the aid of the recursion formula on pp. 20—21 of ref. 8 and the fact that the variables in the $F_1$-function become $x = \dfrac{2\,k_i}{k_i+k_f}$ and $y = \dfrac{2\,k_f}{k_i+k_f}$, obeying the relations $x+y=2$,

$$x(\beta-1) = y(\beta'-1) = i\eta\left(1-\left(\frac{\xi}{2\,\eta}\right)^2\right)\left(\eta \equiv \frac{\eta_i+\eta_f}{2}\right).$$

In this way we get

$$\left.\begin{aligned}
\int \mathrm{I}\,e^{i(k_f+k_i)\,r}\,r^{-1}\,dr = -\frac{2}{3} + \frac{i\eta}{1-2\,i\eta}\Bigg\{\left(\frac{\xi}{2\,\eta}\right)^2\Bigg(&F_1(1,\beta,\beta',2;x,y)\\
&+F_1(1,\beta,\beta',1;x,y)\times\frac{1-2x(\beta-1)}{x(\beta-1)}\Bigg)+\frac{1}{ix(\beta-1)}-1\Bigg\}.
\end{aligned}\right\} \tag{A. 8}$$

According to ref. 5, 5.11 (1),

$$F_1(\gamma = 1) = (1-x)^{-\beta}(1-y)^{-\beta'}, \tag{A. 9}$$

whereas, according to the formulae 5.11 (2), 5.11 (10), 5.11 (11), and 5.10 (2) of ref. 5, the function $F_1$ ($\gamma = 2$) may be expressed as

$$(1-x)^{-1}(-1)^{\beta'}\left\{\frac{(-1)^{-\beta'}}{1-\beta-\beta'}\left(\frac{1-x}{x}\right)F\left(1,\beta',\beta+\beta';\frac{2(x-1)}{x}\right)\right.$$
$$+\frac{1}{\beta'-1}\left(\frac{1-x}{x}\right)^{2-\beta-\beta'}(-2)^{-1}x^{2-\beta-\beta'}F\left(2-\beta-\beta',1,2-\beta';\frac{x}{2}\right)$$
$$\left.+\frac{\Gamma(\beta+\beta'-1)\,\Gamma(1-\beta')}{\Gamma(\beta)}\left(\frac{1-x}{x}\right)^{2-\beta-\beta'}(-2)^{-\beta'}x^{-\beta+1}F\left(1-\beta,\beta',\beta';\frac{x}{2}\right)\right\},$$

where $F$ is the ordinary Gaussian hypergeometric function; here again, according to 2.8 (4) of ref. 5, $F\left(1-\beta,\beta',\beta';\frac{x}{2}\right)=\left(1-\frac{x}{2}\right)^{\beta+1}$, and, to zeroth order in $\left(\frac{\xi}{2\eta}\right)$, $F\left(2-\beta-\beta',1,2-\beta';\frac{x}{2}\right)=\frac{\Gamma(2-\beta)\,\Gamma(\frac{1}{2})}{\Gamma(\frac{3}{2}-\beta)}$ (ref. 5, 2.8 (50)).

This immediately leads to the expression (17)—(18).

## References


1) K. Alder, A. Bohr, T. Huus, B. R. Mottelson, and A. Winther, Revs. Mod. Phys. **28** (1956) 432.
2) B. Elbek and C. K. Bockelman, Phys. Rev. **105** (1957) 657.
3) B. Elbek, K. O. Nielsen and M. C. Olesen, Phys. Rev. **108** (1957) 406.
4) V. Ramšak, M. C. Olesen and B. Elbek, Nuclear Physics **6** (1958) 451.
5) A. Erdélyi, W. Magnus, F. Oberhettinger, and F. G. Tricomi, Higher Transcendental Functions (McGraw-Hill, New York, 1953) vol. I.
6) F. G. Tricomi, Ann. Mat. Pura Appl. (4) **26** (1947) 283.
7) A. Erdélyi, W. Magnus, F. Oberhettinger, and F. G. Tricomi, Tables of Integral Transforms (McGraw-Hill, New York, 1954) vol. I.
8) P. Appell and J. Kampé de Fériet, Fonctions Hypergéométriques et Hypersphériques (Gauthiers Villars, Paris, 1926).


Indleveret til selskabet den 24. september 1959.
Færdig fra trykkeriet den 14. maj 1960.

Matematisk-fysiske Meddelelser
udgivet af
Det Kongelige Danske Videnskabernes Selskab
Bind **32,** nr. 6

Mat. Fys. Medd. Dan. Vid. Selsk. **32,** no. 6 (1960)

# FURTHER PROPERTIES OF THE ENERGY-MOMENTUM COMPLEX IN GENERAL RELATIVITY

BY

M. MAGNUSSON


København 1960
i kommission hos Ejnar Munksgaard

CONTENTS

1. Introduction ..... 3
2. Conservation Laws and Transformation Properties ..... 5
3. Spatially Covariant Expressions Containing First-Order Derivatives of the Metric Tensor ..... 8
4. The Uniqueness of the Superpotential $\chi_i^{kl}$ ..... 10
5. The Energy-Momentum Complex of the Gravitational Field ..... 13

Appendix ..... 17

References ..... 22

## Synopsis

It is shown that the energy-momentum complex $\mathcal{T}_i^k$ introduced by MØLLER into the theory of general relativity is uniquely determined, when taken as a function of the metric tensor and its derivatives of the first and second orders, by two transformation requirements: 1) $\mathcal{T}_i^k$ is an affine tensor density (of weight one) so that the total energy and momentum of a closed system are transformed as a vector in linear (affine) transformations, just like the energy and momentum of a free particle; 2) $\mathcal{T}_4^4$ is a scalar density in arbitrary spatial transformations so that the total energy in a volume of space is independent of the system of spatial coordinates used. Further it is shown that in empty space it is possible, in accordance with the principle of equivalence, to introduce coordinates along a geodesic such that the gravitational energy-momentum complex vanishes along the geodesic.

Printed in Denmark
Bianco Lunos Bogtrykkeri A-S

## 1. Introduction

When EINSTEIN introduced the law of conservation of energy and momentum into the theory of general relativity[1], several objections were raised against it. These arose from the fact that the energy-momentum components $t_i^k$ of the gravitational field did not form a tensor, whereas the components $T_i^k$ of matter did. It was, e. g., shown by BAUER that for an inertial system in which no matter was present, i. e. no gravitational field, the introduction of polar instead of Cartesian space coordinates into the metric of special relativity led to components $t_i^k$ different from zero. In particular, the total energy turned out to be infinite. LEVI-CIVITA and LORENTZ proposed an alternative expression for the energy-momentum components of the gravitational field, viz. the tensor $\frac{1}{\varkappa} G_i^k$, where $G_i^k = R_i^k - \frac{1}{2}\delta_i^k R$. This proposal was rejected by EINSTEIN on the grounds that, since $T_i^k + \frac{1}{\varkappa} G_i^k = 0$ always and everywhere, according to the field equations, the total energy of a system is zero from the start, and therefore this law of conservation does not require the continued existence of the system. A material system can disintegrate into nothing without leaving any trace[2].

Finally EINSTEIN[3] showed that his formulation of the law of conservation of energy and momentum led to an unambiguous and satisfactory definition of the total energy and momentum of a closed system, independent of the choice of coordinates inside a surface surrounding the system. However, no unambiguous definition could be given of the energy or momentum of a part of a closed system. Therefore it was generally accepted that the localization of energy and momentum had no meaning in the theory of general relativity.

In recent papers, MØLLER[4, 5, 6] has derived and discussed extensively a new energy-momentum complex in general relativity. (The term "complex" is used, as by LORENTZ, to denote a quantity which is not transformed as a tensor in arbitrary space-time transformations.) In the first paper, "On the Localization of the Energy of a Physical System in the

General Theory of Relativity", it was pointed out that the 44-component of Einstein's energy-momentum complex was not transformed as a scalar density even in purely spatial transformations. It was therefore not suitable for defining an energy density. This was the reason for the above-mentioned absurd result derived by BAUER. Using the fact that the energy-momentum complex is not uniquely determined by the requirement that its ordinary divergence vanishes, MØLLER succeeded in deriving a complex $\mathcal{T}_i^k$ having all the satisfactory features of Einstein's energy-momentum complex, but such that $\mathcal{T}_4^4$ and $\mathcal{T}_4^\varkappa$ ($\varkappa = 1, 2, 3$) behaved like scalar and 3-vector densities, respectively, in arbitrary spatial transformations. With this new expression for $\mathcal{T}_i^k$, the energy of a part of a closed system is invariant in spatial transformations.

As was shown by MØLLER[6, 7], $\mathcal{T}_i^k$ can be derived from a variational principle, where the quantity to be varied is the curvature scalar density $\mathfrak{R} = \sqrt{-g}\,R$. However, it is possible to define in the theory of general relativity, as in any generally covariant theory where the field equations can be derived from a variational principle, an infinite number of quantities which satisfy conservation laws[8]. It is desirable to select among these a unique, physically significant quantity describing the energy and momentum of the field. The question of the uniqueness of Møller's energy-momentum complex $\mathcal{T}_i^k$ has been considered by himself in another paper[5], where he shows that $\mathcal{T}_i^k$ is determined uniquely by the following three conditions:

1) $\mathcal{T}_i^k$ is an affine tensor density.
2) $\mathcal{T}_4^4$, $\mathcal{T}_4^\varkappa$ ($\varkappa = 1, 2, 3$) are scalar and 3-vector densities in arbitrary spatial transformations.
3) The superpotential $\chi_i^{kl}$ from which $\mathcal{T}_i^k$ is derived, $\mathcal{T}_i^k = \chi_{i,l}^{kl}{}^*$, depends on first-order derivatives of the metric tensor up to the second degree, and does not contain higher derivatives.

$\mathcal{T}_i^k$ may be separated into a matter part, $\sqrt{-g}\,T_i^k$, and a gravitational part, $\sqrt{-g}\,t_i^k$. According to the principle of equivalence it should be possible to eliminate the gravitational field, and thus make $t_i^k$ vanish, at any point by a suitable choice of coordinate systems. Since $t_i^k$ depends on the second derivatives of the metric tensor, it will not vanish in all coordinate systems which are geodesic, i. e. in which $g_{ik,l} = 0$. MØLLER has shown, however, that $t_i^k$ can be made to vanish at any point where no matter is present, in a wide class of geodesic coordinate systems, viz. those which are "locally normal" at the point[6].

* A comma denotes partial and a semicolon covariant differentiation.

The present paper falls into two main parts. The first part deals with the uniqueness of Møller's energy-momentum complex. After considering conservation laws and the transformation properties of the energy-momentum complex we show that the complex $\mathcal{T}_i^k$, satisfying a conservation law and depending on the metric tensor and its derivatives of the first and second orders, is uniquely determined by conditions 1) and 2) above, i. e. that $\mathcal{T}_i^k$ is an affine tensor density and $\mathcal{T}_4^4$, $\mathcal{T}_4^\varkappa$ are scalar and vector densities in spatial transformations. The restriction on the degree of the first-order derivatives of $g_{ik}$ in $\chi_i^{kl}$ can be dropped. Derivatives of $g_{ik}$ higher than the second are excluded from $\mathcal{T}_i^k$, and therefore derivatives higher than the first from $\chi_i^{kl}$, since the field equations themselves are restricted to the second order. It is also easily seen that it is impossible to form a quantity $\mathcal{T}^{ik}$ such that $\mathcal{T}^{44}$ is a scalar density in spatial transformations.

In the second part it is shown that along a geodesic one can introduce coordinate systems such that, with no matter present, the gravitational energy-momentum complex $t_i^k$ vanishes along the geodesic. This is an extension of Møller's result for a point where no matter is present. It shows that an observer falling freely in a gravitational field can introduce a system of coordinates such that the effects of the gravitational field are eliminated.

## 2. Conservation Laws and Transformation Properties

The conservation laws of energy and momentum are originally integral laws. For a closed system they state that a certain well-defined space integral over the system at a certain time, called its energy or momentum, remains constant in time:

$$\frac{d}{dt}\int \mathcal{T}\, dx^1\, dx^2\, dx^3 = 0\,. \tag{1}$$

For a part of a closed system the conservation laws state that the rate of decrease of, say, the energy in a space volume V at a certain time is equal to the flux of energy through the boundary surface $S$ of $V$:

$$-\frac{d}{dt}\int_V \mathcal{T}\, dx^1\, dx^2\, dx^3 = \int_S \mathfrak{T}^\varkappa\, dS_\varkappa\,. \tag{2}$$

It is, however, more convenient to have the conservation laws in differential form. The differential conservation law equivalent to (2) is, by Gauss' theorem,

$$\frac{\partial \mathfrak{T}}{\partial t} + \frac{\partial \mathfrak{F}^{\varkappa}}{\partial x^{\varkappa}} = 0 . \tag{3}$$

In special relativity the differential conservation laws for energy and momentum are

$$\frac{\partial T_i^k}{\partial x^k} = T_{i,\,k}^{k} = 0 , \tag{4}$$

where $T_i^k$ is the energy-momentum tensor of matter. The natural generalization of (4) in general relativity is obtained by equating the covariant divergence of the tensor $T_i^k$ to zero:

$$T_{i;\,k}^{k} = \frac{1}{\sqrt{-g}} \frac{\partial}{\partial x^k} (\sqrt{-g}\, T_i^k) - \frac{1}{2} \frac{\partial g_{kl}}{\partial x^i} T^{kl} = 0 . \tag{5}$$

As is well known, this equation does not lead to integral conservation laws of the form (1) or (2), i. e., there is no conservation law for matter alone. Only an equation of the form (4) is equivalent to integral conservation laws. It is possible, however, to bring (5) into the required form by means of the field equations. One then obtains the conservation laws for matter and gravitational field in a differential form:

$$\frac{\partial \mathcal{T}_i^k}{\partial x^k} = \mathcal{T}_{i,\,k}^{k} = 0 , \tag{6}$$

where

$$\mathcal{T}_i^k = \sqrt{-g}\, (T_i^k + t_i^k) . \tag{7}$$

Here $T_i^k$ is the energy-momentum tensor of matter, and $t_i^k$ refers to the gravitational field. Of course $\mathcal{T}_i^k$, and therefore $t_i^k$, are not uniquely determined in this way, for a quantity with a vanishing divergence can be added to $\mathcal{T}_i^k$. By means of the field equations the matter variables can be eliminated and $\mathcal{T}_i^k$ expressed solely in terms of the metric tensor and its derivatives. As noted in section 1, it is natural to exclude derivatives higher than the second from $\mathcal{T}_i^k$, but there is still a wide choice of expressions for $\mathcal{T}_i^k$, which it is desirable to restrict.

The principle of general relativity requires the validity of equation (6) in all systems of coordinates. This puts restrictions on the transformation properties of $\mathcal{T}_i^k$. It is clear, e. g. from eq. (5), that $\mathcal{T}_i^k$ cannot be a tensor density (of weight one) in arbitrary space-time transformations, but only in linear (affine) space-time transformations, i. e. it can be an affine ten-

sor density. Further it can be shown that in arbitrary spatial transformations, $x'^{\iota} = f^{\iota}(x^{\varkappa})$, $x'^{4} = x^{4}$, $(\iota, \varkappa = 1, 2, 3)$, $\mathcal{T}_4^4$ and $\mathcal{T}_4^{\varkappa}$ can be scalar and tensor densities, whereas $\mathcal{T}_i^4$ and $\mathcal{T}_i^{\varkappa}$ cannot be vector and tensor densities.

Turning now to the question of determining physically reasonable transformation properties of $\mathcal{T}_i^k$, we first consider the total energy and momentum of a closed system

$$P_i = \frac{1}{c}\int \mathcal{T}_i^4 \, dx^1 dx^2 dx^3. \tag{8}$$

It is natural to require that this is transformed like the energy and momentum of a free particle, i. e. as a vector, in linear transformations. This means that $\mathcal{T}_i^k$ must be an affine tensor density (of weight one).

Now consider the gravitational energy in a small, or infinitesimal, region. It is clear that this energy will depend on the coordinate system used. According to the principle of equivalence it is possible to introduce a coordinate system in which the gravitational field vanishes. In such a system all the components of the gravitational energy-momentum complex, in particular the energy density, should vanish. The elimination of the gravitational field requires the introduction of an accelerated (freely falling) frame of reference, and hence the energy-momentum complex cannot be a tensor density in transformations to such a frame. The transformations involve time, but not linearly; so they are not affine. Thus it follows from the principle of equivalence that $\mathcal{T}_i^k$ cannot be a tensor density in arbitrary space-time transformations, whereas it can be an affine tensor density.

Within a given frame of reference, an arbitrary change in the spatial coordinates only will not eliminate or affect the gravitational field. It is then natural to require that the gravitational energy in a spatial region be invariant in arbitrary spatial transformations $x'^{\iota} = f^{\iota}(x^{\varkappa})$, $x'^{4} = x^{4}$, $(\iota, \varkappa = 1, 2, 3)$, which simply amount to a renaming of the points of reference (points with constant spatial coordinates) without any change of the rate or setting of the coordinate clocks. This is the case if $\mathcal{T}_4^4$ behaves like a scalar density in such transformations. Further, if $\mathcal{T}_4^{\varkappa}$ is a 3-vector density, the integrals in (2) with $\mathcal{T} = \mathcal{T}_4^4$ and $\mathfrak{F}^{\varkappa} = c\mathcal{T}_4^{\varkappa}$ are invariant in spatial transformations. In that case one may talk of conservation of energy in any region of space within a given frame of reference, regardless of the system of spatial coordinates used.

The situation is different as regards the momentum. $\mathcal{T}_i^4$, $\mathcal{T}_i^{\varkappa}$ cannot be vector and tensor densities in spatial transformations. Even if they were,

the corresponding integrals in equation (2) would not have simple transformation properties in such transformations (see reference 4, § 4).

Thus it is possible, within any given frame of reference, to give an unambiguous interpretation, i. e. one independent of the choice of spatial coordinates, of the conservation of the energy in any region of space, provided $\mathcal{T}_4^4$ and $\mathcal{T}_4^\varkappa$ have the above-mentioned properties, but not of the conservation of the momentum.

On the basis of these considerations we may set up the following transformation requirements for $\mathcal{T}_i^k$, consistent with eq. (6) being valid in all coordinate systems:

1) $\mathcal{T}_i^k$ must be an affine tensor density;
2) $\mathcal{T}_4^4$, $\mathcal{T}_4^\varkappa$ must be scalar and vector densities in spatial transformations $x'^\iota = f^\iota(x^\varkappa)$, $x'^4 = x^4$, $(\iota, \varkappa = 1, 2, 3)$.

Now, equation (6) is satisfied identically in all coordinate systems if one writes

$$\mathcal{T}_i^k = \chi_{i,\,l}^{kl}, \tag{9}$$

where

$$\chi_i^{kl} = -\chi_i^{lk}. \tag{10}$$

With $\mathcal{T}_i^k$ restricted to second derivatives, $\chi_i^{kl}$ must be restricted to first-order derivatives of the metric tensor.

Then $\mathcal{T}_i^k$ will have the required transformation properties if

1) $\chi_i^{kl}$ is an affine tensor density,
2) $\chi_4^{4\lambda}$, $\chi_4^{\varkappa\lambda}$ are vector and tensor densities in spatial transformations $(\varkappa, \lambda = 1, 2, 3)$.

We shall now show that the superpotential $\chi_i^{kl}$ formed from the metric tensor and its first-order derivatives is uniquely determined by these transformation requirements. Hence $\mathcal{T}_i^k$ is uniquely determined by the corresponding requirements.

## 3. Spatially Covariant Expressions Containing First-Order Derivatives of the Metric Tensor

Consider the problem of forming a rational integral function of the metric tensor and its first-order derivatives which is covariant in the spatial transformation

$$x'^\iota = f^\iota(x^\varkappa), \quad x'^4 = x^4, \quad (\iota, \varkappa = 1, 2, 3). \tag{11}$$

The transformation coefficients for (11) are

$$\left.\begin{aligned} \alpha_k^i &= \frac{\partial x'^i}{\partial x^k} : \alpha_\varkappa^\iota = \frac{\partial x'^\iota}{\partial x^\varkappa}, \ \alpha_4^\iota = \alpha_\iota^4 = 0, \ \alpha_4^4 = 1, \\ \breve{\alpha}_k^i &= \frac{\partial x^i}{\partial x'^k} : \breve{\alpha}_\varkappa^\iota = \frac{\partial x^\iota}{\partial x'^\varkappa}, \ \breve{\alpha}_4^\iota = \breve{\alpha}_\iota^4 = 0, \ \breve{\alpha}_4^4 = 1. \end{aligned}\right\} \tag{12}$$

The first-order derivatives of the metric tensor can be written in terms of the Christoffel symbols of the second kind and the metric tensor as follows:

$$\left.\begin{aligned} g_{ij,k} &= g_{im}\Gamma_{jk}^m + g_{jm}\Gamma_{ik}^m \\ g^{ij}{}_{,k} &= -g^{im}\Gamma_{mk}^j - g^{jm}\Gamma_{mk}^i. \end{aligned}\right\} \tag{13}$$

Any expression containing the first-order derivatives can therefore be written in terms of the Christoffel symbols and the metric tensor. The problem is then to form a spatially covariant expression in terms of $g_{ik}$, $g^{ik}$ and $\Gamma_{kl}^i$.

For an arbitrary space-time transformation the transformation law for $\Gamma_{kl}^i$ is[9]

$$\Gamma_{kl}'^i = \alpha_r^i \breve{\alpha}_k^s \breve{\alpha}_l^t \Gamma_{st}^r + \alpha_r^i \breve{\alpha}_{k,l}^r. \tag{14}$$

Thus $\Gamma_{kl}^i$ is not a tensor in general, because of the second term on the right-hand side. This term vanishes when the transformations are linear, i. e. $\Gamma_{kl}^i$ is an affine tensor. For the spatial transformation (11) it is easily seen that the extra term vanishes if one of the indices $i, k, l$ is equal to 4. Therefore

$$\Gamma_{kl}^4, \quad \Gamma_{4l}^i = \Gamma_{l4}^i \tag{15}$$

are tensors in spatial transformations. Any expression containing only these symbols (and the metric tensor) will be spatially covariant. This is not the case with a general expression in $\Gamma_{kl}^i$, but it is possible that some particular combination of $\Gamma_{kl}^i$ will be spatially covariant. For that to occur the extra non-tensor terms in the transformation law for the expression, arising from the extra term in (13), must somehow be cancelled. We shall now show that this is impossible.

Consider first an expression linear in $\Gamma_{kl}^i$, e. g. with a term of the type

$$\Gamma_{kl}^i g^{mn} g_{rs}, \tag{16}$$

where $i, k, l \neq 4$. The transformation law for this term is

$$\left.\begin{aligned} \Gamma'^{i}_{kl}\, g'^{mn}\, g'_{rs} = {} & \alpha^{i}_{t}\, \breve{\alpha}^{u}_{k}\, \breve{\alpha}^{v}_{l}\, \alpha^{m}_{w}\, \alpha^{n}_{x}\, \breve{\alpha}^{y}_{r}\, \breve{\alpha}^{z}_{s}\, \Gamma^{t}_{uv}\, g^{wx}\, g_{yz} \\ & + \alpha^{i}_{t}\, \breve{\alpha}^{t}_{k,l}\, \alpha^{m}_{w}\, \alpha^{n}_{x}\, \breve{\alpha}^{y}_{r}\, \breve{\alpha}^{z}_{s}\, g^{wx}\, g_{yz}. \end{aligned}\right\} \tag{17}$$

All the terms are symmetric in the same pairs of indices, $(k, l)$, $(m, n)$ and $(r, s)$, and in no others. The only nontrivial way to cancel the extra term is to subtract a corresponding expression where the indices in which the term is symmetric are interchanged. Since all the terms of (17) are symmetric in the same pairs of indices, they would all be cancelled by such a subtraction, and nothing would remain.

For an expression containing products of $\Gamma^{i}_{kl}$ the extra, non-tensor term in (14) would lead to several extra terms in the transformation law, similar to that in (17). Since, however, all the terms would be symmetric in the same pairs of indices, and in those only, it would be impossible to cancel the extra non-tensor terms without cancelling all the others as well.

The only way to obtain a covariant expression is to make the extra term in (14) vanish. For an arbitrary spatial transformation (11) this means that only the Christoffel symbols given in (15) can occur in the expression.

## 4. The Uniqueness of the Superpotential $\chi^{kl}_{i}$

The considerations in section 2 led to the following requirements for the transformation properties of the superpotential $\chi^{kl}_{i}$, depending on the metric tensor and its first-order derivatives:

1) $\chi^{kl}_{i}$ must be an affine tensor density;
2) $\chi^{4\lambda}_{4}$, $\chi^{\varkappa\lambda}_{4}$ must be vector and tensor densities in arbitrary spatial transformations.

Since $\chi^{kl}_{i}$ is to be a density (of weight one), it can be written

$$\chi^{kl}_{i} = \sqrt{-g}\, X^{kl}_{i}, \tag{18}$$

where $X^{kl}_{i}$ is an affine tensor and $X^{4\lambda}_{4}$ a vector in spatial transformations. Being an affine tensor, $X^{kl}_{i}$ must be a rational integral function of the metric tensor and its first-order derivatives.

In a spatially covariant expression for $X^{4l}_{4}$ there can only be one upper and one lower index equal to 4 since $X^{4l}_{4}$ is associated with an affine tensor of rank three, $X^{kl}_{i}$.

A spatially covariant expression for $X^{4l}_{4}$, antisymmetric in 4 and $l$, must be formed of the following quantities, and these only:

$$\Gamma^4_{mn},\ \Gamma^n_{4m},\ \Gamma^4_{4m},\ \Gamma^l_{4m},\ g_{mn},\ g_{4n},\ g^{mn},\ g^{4n},\ g^{ln},\ \delta^4_4,\ \delta^l_4, \tag{19}$$

$m$ and $n$ representing dummy indices. $g^{4l}$ cannot occur since the expression is to be antisymmetric in 4 and $l$, and $\delta^n_m$, $\delta^4_m$, $\delta^n_4$ would simply mean replacing a dummy index by 4 or another dummy index.

It is not possible to form $X^{4l}_4$ from $g_{ik}$, $g^{ik}$, $\delta^k_i$ alone, for a quantity formed from these would always have the same number of upper and lower indices. Every term must therefore have one or more $\Gamma^i_{kl}$. Terms of the third or a higher degree in $\Gamma^i_{kl}$ cannot occur as they would have three or more indices equal to 4. This excludes, according to section 3, terms of the third and higher degrees in the first-order derivatives. Terms of the second degree in $\Gamma^i_{kl}$ cannot occur since it is impossible to form from a product of two $\Gamma^i_{kl}$, the metric tensor, and the Kronecker symbol, a quantity with one more index on top than at bottom. This excludes terms of the second degree in the first-order derivatives. The only remaining possibility is to have terms linear in the $\Gamma^i_{kl}$, i. e. terms of the first degree in the first-order derivatives.

To form the quantity

$$X^{4l}_4 = -X^{l4}_4 \tag{20}$$

from the quantities in (19) and so that it is linear in the $\Gamma^i_{kl}$, consider first the use of $\Gamma^4_{mn}$ with $m$, $n$ dummy indices. Interchange of 4 and $l$ in accordance with (20) would give $\Gamma^l_{mn}$, which is not covariant. Hence the only $\Gamma$'s which can occur are $\Gamma^n_{4m}$, $\Gamma^4_{4m}$ and $\Gamma^l_{4m}$. This, however, excludes $g_{4n}$, $\delta^4_4$ and $\delta^l_4$ since there can be only one lower index equal to 4. The quantities left to form $X^{4l}_4$ are then

$$\Gamma^n_{4m},\ \Gamma^4_{4m},\ \Gamma^l_{4m},\ g_{mn},\ g^{mn},\ g^{4n},\ g^{ln}. \tag{21}$$

The possible positions for 4 and $l$ as upper indices are given by

$$\Gamma^n_{4m}\, g^{4r}\, g^{ls},\ \Gamma^4_{4m}\, g^{ls},\ \Gamma^l_{4m}\, g^{4r}. \tag{22}$$

Matching the dummy indices $m$, $n$, $r$, $s$ in all possible ways, one finds three expressions:

$$\Gamma^4_{4m}\, g^{lm},\ \Gamma^l_{4m}\, g^{4m},\ \Gamma^m_{4m}\, g^{4l}. \tag{23}$$

The last one is symmetric in 4 and $l$ and therefore cannot occur in $X^{4l}_4$. From the other two one can form only one antisymmetric quantity

$$X^{4l}_4 = a\,(\Gamma^l_{4m}\, g^{4m} - \Gamma^4_{4m}\, g^{lm}), \tag{24}$$

which is thus uniquely determined, apart from an arbitrary constant.

It is clear that the quantity

$$X_4^{\varkappa\lambda} = a\,(\Gamma_{4\,m}^{\lambda}\, g^{\varkappa m} - \Gamma_{4\,m}^{\varkappa}\, g^{\lambda m}) \tag{25}$$

is spatially covariant, as required.

Expressing the Christoffel symbols in terms of first-order derivatives of the metric tensor, one finds

$$X_4^{4\,l} = a\,(g_{4\,n,\,m} - g_{4\,m,\,n})\, g^{4\,m}\, g^{ln}. \tag{26}$$

The superpotential $\chi_i^{kl}$ is then given by

$$\chi_i^{kl} = a\sqrt{-g}\,(\Gamma_{im}^{l}\, g^{km} - \Gamma_{im}^{k}\, g^{lm}) \tag{27 a}$$

or

$$\chi_i^{kl} = a\sqrt{-g}\,(g_{in,\,m} - g_{im,\,n})\, g^{km}\, g^{ln}. \tag{27 b}$$

This is just the expression derived by MØLLER, and it is thus seen to be uniquely determined by the two transformation properties given at the beginning of this section. It follows from Møller's work that the constant $a$ is given by

$$a = 1/\varkappa = c^4/8\,\pi k, \tag{28}$$

where $k$ is the Newtonian gravitational constant.

It is now easily seen that it is impossible to form an energy-momentum complex $\mathcal{T}^{ik}$ such that $\mathcal{T}^{44}$ is a scalar density in spatial transformations. To do so one would put $\mathcal{T}^{ik} = \chi^{ikl}_{\ ,\,l}$, where $\chi^{ikl} = -\chi^{ilk}$ and $\chi^{44l}$ must be a vector density in spatial transformations. To form this latter quantity one would have to use

$$\Gamma_{mn}^{4},\ g_{mn},\ g^{mn},\ g^{4m},\ g^{ln},\ g^{4l}. \tag{29}$$

It is not possible to form it from $g_{mn}$ and $g^{mn}$ alone, nor from products of two $\Gamma_{kl}^{i}$ since there must be three free upper indices. Products of three or more $\Gamma_{kl}^{i}$ would give too many 4's, so only a linear expression in $\Gamma_{kl}^{i}$ remains. Matching indices in

$$\Gamma_{mn}^{4}\, g^{4r}\, g^{ls}, \quad \Gamma_{mn}^{4}\, g^{4l}, \tag{30}$$

one finds the following expressions:

$$\Gamma_{mn}^{4}\, g^{4l}\, g^{mn}, \quad \Gamma_{mn}^{4}\, g^{4m}\, g^{ln}. \tag{31}$$

The index 4 in $\Gamma_{mn}^{4}$ cannot be replaced by $l$ in the process of forming

$\chi^{414} = -\chi^{441}$ since $\Gamma^l_{mn}$ is not spatially covariant. The expressions in (31) are symmetric in the remaining 4 and $l$ so that an expression antisymmetric in 4 and $l$ cannot be formed from them. Thus it is impossible to form the required quantity $\chi^{441}$.

## 5. The Energy-Momentum Complex of the Gravitational Field

The energy-momentum complex of matter and gravitational field, $\mathcal{T}^k_i$, can be expressed solely in terms of the metric tensor and its first- and second-order derivatives. By means of equations (9), (27) and (28) $\mathcal{T}^k_i$ may be written

$$\mathcal{T}^k_i = \left\{ \frac{\sqrt{-g}}{\varkappa} \left( \Gamma^l_{im} g^{km} - \Gamma^k_{im} g^{lm} \right) \right\}_{, l} \tag{32a}$$

or

$$\mathcal{T}^k_i = \left\{ \frac{\sqrt{-g}}{\varkappa} \left( g_{in, m} - g_{im, n} \right) g^{km} g^{ln} \right\}_{, l} . \tag{32b}$$

$\mathcal{T}^k_i$ can be split up into a matter part, $\sqrt{-g}\, T^k_i$, and a gravitational part, $\sqrt{-g}\, t^k_i$, as in equation (7),

$$\mathcal{T}^k_i = \sqrt{-g}\, (T^k_i + t^k_i) . \tag{7}$$

This is, however, rather artificial and arbitrary since $\mathcal{T}^k_i$ can be expressed in terms of the metric tensor and its derivatives alone, the matter variables being eliminated entirely from the expression. Further, $T^k_i$ and $t^k_i$ are not conserved separately in a general coordinate system; only their sum is conserved. In general one has from (6), (7) and (5)

$$(\sqrt{-g}\, t^k_i)_{, k} = -(\sqrt{-g}\, T^k_i)_{, k} = -\frac{\sqrt{-g}}{2}\, g_{kl, i} T^{kl} . \tag{33}$$

It is possible to introduce at any given point a geodesic coordinate system such that $g_{ik, l} = 0$ and therefore also $\Gamma^i_{kl} = 0$ at the point. As was first shown by Fermi, it is also possible, for any open curve in space-time, to introduce coordinate systems such that $g_{ik, l} = 0$ at every point of the curve. At points where $g_{ik, l} = 0$, it is reasonable to talk of a matter part and a gravitational part of $\mathcal{T}^k_i$ since these are conserved separately at such points, i. e.

$$(\sqrt{-g}\, t^k_i)_{, k} = (\sqrt{-g}\, T^k_i)_{, k} = 0 . \tag{34}$$

MØLLER has shown[6] that $t^k_i$ can be written

$$t_i^k = -\frac{1}{2\varkappa} R\delta_i^k + \hat{t}_i^k \tag{35}$$

where

$$\varkappa \hat{t}_i^k = (\Gamma_{il}^l)^{,\,k} - (\Gamma_{il}^k)^{,\,l} - \Gamma_{il}^k (g_{,\,m}^{lm} + g^{lm}\Gamma_{mn}^n) - \Gamma_{in}^m \Gamma_{lm}^k g^{ln} \tag{36}$$

with

$$(\Gamma_{kl}^i)^{,\,m} = (\Gamma_{kl}^i)_{,\,n}\, g^{nm}. \tag{37}$$

At the origin of a geodesic coordinate system, (36) is reduced to

$$\varkappa \hat{t}_i^k = (\Gamma_{il}^l)^{,\,k} - (\Gamma_{il}^k)^{,\,l}. \tag{38}$$

By means of (37) and the relation

$$\Gamma_{kl}^i = g^{ir}\,\Gamma_{r,\,kl} \tag{39}$$

(38) may be written

$$\varkappa \hat{t}_i^k = [(\Gamma_{n,\,il})_{,\,m} - (\Gamma_{m,\,il})_{,\,n}]\, g^{km}\, g^{ln}. \tag{40}$$

Since this expression depends on second-order derivatives of the metric tensor, $t_i^k$ will in general not vanish at the origin of a geodesic system of coordinates.

According to the principle of equivalence it should be possible, however, to eliminate the effects of the gravitational field at a point by a suitable choice of coordinates. MØLLER has shown[6] that where no matter is present, i. e. where $R = 0$, $t_i^k$ does vanish at the origin in a large class of geodesic coordinate systems, the so-called normal or Riemannian systems. The physical significance of normal coordinates has also been discussed by other authors, who point out their correspondence to Minkowskian coordinates of special relativity[10].

MØLLER suggested that it would be possible to introduce coordinates along a geodesic such that $\hat{t}_i^k = 0$ along it, i. e. $t_i^k = 0$ where no matter is present. This is physically reasonable, for it means that an observer falling freely in a gravitational field can introduce coordinates such that the effects of the gravitational field are approximately eliminated in his neighbourhood. It actually turns out to be possible.

In the appendix it is shown that for a geodesic in Riemannian space, $V_4$, there exist coordinate systems such that for every point of the geodesic

$$\Gamma_{kl}^i = 0\,, \quad i, k, l = 1, 2, 3, 4, \tag{41}$$

$$\underset{(\varkappa\lambda\mu)}{S}(\Gamma_{\varkappa\lambda}^i)_{,\,\mu} = \frac{1}{3}(\Gamma_{\varkappa\lambda,\,\mu}^i + \Gamma_{\mu\varkappa,\,\lambda}^i + \Gamma_{\lambda\mu,\,\varkappa}^i) = 0\,, \quad \varkappa, \lambda, \mu = 1, 2, 3. \tag{42}$$

The coordinates are called Fermi coordinates for a geodesic. The spatial coordinates $x^1, x^2, x^3$ are just Riemannian or normal coordinates in the hypersurface orthogonal to the geodesic since (see A16)

$$x^\mu = z t^\mu, \quad \mu = 1, 2, 3, \tag{43}$$

where $t^\mu$ is a vector at the geodesic in this surface and $z$ is the arc length along a geodesic in the surface whose direction is specified by $t^\mu$. The fourth coordinate $x^4$ is proportional to the arc length along the geodesic. For a time-like geodesic it can be taken as $c$ times the proper time. This coordinate system is clearly time-orthogonal, and with the above choice of the fourth coordinate one finds that $g_{44} = -1$. Thus

$$g_{4\mu} = 0, \quad g_{44} = -1 \tag{44}$$

so that the metric is

$$ds^2 = g_{\mu\nu}\, dx^\mu\, dx^\nu - (dx^4)^2. \tag{45}$$

The Fermi coordinates are a special case of geodesic coordinates. From (41) it is seen that

$$g_{ik,\,l} = 0, \quad g^{ik}_{,\,l} = 0. \tag{46}$$

Equation (40) therefore holds in this system of coordinates. Since (41) and (46) hold at every point of the geodesic, it follows that

$$(\Gamma^i_{kl}),_4 = (\Gamma_{i,\,kl}),_4 = 0, \; g_{ik,\,l,\,4} = g^{ik}_{,\,l,\,4} = 0 \tag{47}$$

because $x^4$ is proportional to the arc length along the geodesic. From (44) one has

$$g^{4\mu} = 0 \;\text{ and }\; g^{44} = -1. \tag{48}$$

Using (44), (47) and (48), one finds from (40) that

$$\hat{t}^4_4 = \hat{t}^\varkappa_4 = \hat{t}^4_\iota = 0 \tag{49}$$

and

$$\varkappa \hat{t}^\varkappa_\iota = [(\Gamma_{\nu,\,\iota\lambda}),_\mu - (\Gamma_{\mu,\,\iota\lambda}),_\nu]\, g^{\varkappa\mu} g^{\lambda\nu}. \tag{50}$$

From the condition (42), satisfied by Fermi coordinates, it follows that

$$3 \underset{(\varkappa\lambda\mu)}{S} (\Gamma_{i,\,\varkappa\lambda}),_\mu = (\Gamma_{i,\,\varkappa\lambda}),_\mu + (\Gamma_{i,\,\mu\varkappa}),_\lambda + (\Gamma_{i,\,\lambda\mu}),_\varkappa = 0. \tag{51}$$

Putting $i = \iota$, one has

$$(\Gamma_{\iota,\,\varkappa\lambda}),_\mu + (\Gamma_{\iota,\,\mu\varkappa}),_\lambda + (\Gamma_{\iota,\,\lambda\mu}),_\varkappa = 0. \tag{52}$$

From (41) it is seen that

$$\Gamma_{\iota,\,\varkappa\lambda} = 0\,. \tag{53}$$

Equations (53) and (52) are the very equations satisfied by Riemannian coordinates in 3-space. From these it can be shown (see reference 6, appendix B) that

$$(\Gamma_{\iota,\,\varkappa\lambda})_{,\,\mu} = (\Gamma_{\mu,\,\varkappa\lambda})_{,\,\iota}\,. \tag{54}$$

Hence, from (50) and (54) one has

$$\hat{t}_{\iota}^{\varkappa} = 0\,.$$

Thus all the components of the complex $\hat{t}_i^k$ vanish along the geodesic.

Where $R = 0$, i. e. where no matter is present, or only an electromagnetic field, it is therefore possible to introduce along a geodesic coordinates such that the energy-momentum complex of the gravitational field vanishes on the geodesic.

## Acknowledgements

It is a pleasure for me to thank Professor C. Møller for suggesting the problems discussed in this paper and for many helpful discussions.

Moreover I want to express my gratitude to NORDITA for the fellowship granted me by that institute.

*NORDITA – Nordisk Institut for Teoretisk Atomfysik*
*Copenhagen*

## Appendix

In this appendix it will be shown that for a geodesic in an affinely connected space $A_N$ it is possible to introduce coordinate systems such that

$$\left.\begin{aligned} &\Gamma^i_{kl} = 0 && i, k, l = 1, 2, \ldots, N \\ &3\underset{(\varkappa\lambda\mu)}{S}\Gamma^i_{\varkappa\lambda,\,\mu} = \Gamma^i_{\varkappa\lambda,\,\mu} + \Gamma^i_{\mu\varkappa,\,\lambda} + \Gamma^i_{\lambda\mu,\,\varkappa} = 0, && \varkappa, \lambda, \mu = 1, 2, \ldots, N-1 \\ &\text{etc.} \end{aligned}\right\} \quad \text{(A 1)}$$

at every point of the curve. A complete proof for a general curve in $A_N$ has been given by SCHOUTEN[11]. The present proof is a simplified version of his. Of course the results hold *a fortiori* for a Riemannian space $V_N$.

Let the equation of the geodesic be given by

$$\xi^i = f^i(t), \quad \xi^i_0 = f^i(0). \tag{A 2}$$

Consider the hypersurface orthogonal to the geodesic at the point $P_0$ with coordinates $\xi^i_0$. For a neighbouring point $Q_0$ in this surface, with coordinates $\xi^i$, there is a unique geodesic passing through $P_0$ and $Q_0$. Its direction at $P_0$ is given by the vector

$$t^i_0 = \left(\frac{d\xi^i}{dz}\right)_0, \tag{A 3}$$

where $z$ is an affine parameter on the geodesic. In a Riemannian space, $z$ can always be taken as the arc length along the (non-null) geodesic.

The equation of the geodesic through $P_0$ and $Q_0$ is

$$\frac{d^2\xi^i}{dz^2} + \Gamma^i_{kl}\frac{d\xi^k}{dz}\frac{d\xi^l}{dz} = 0. \tag{A 4}$$

One may expand the coordinates $\xi^i$ of $Q_0$ in a series as follows, putting $z = 0$ at $P_0$:

$$\xi^i = \xi_0^i + \left(\frac{d\xi^i}{dz}\right)_0 z + \frac{1}{2!}\left(\frac{d^2\xi^i}{dz^2}\right)_0 z^2 + \frac{1}{3!}\left(\frac{d^3\xi^i}{dz^3}\right)_0 z^3 + \cdots . \tag{A 5}$$

Differentiation of (A 4) gives

$$\left.\begin{aligned} \frac{d^3\xi^i}{dz^3} &= -\left[(\Gamma^i_{kl})_{,\,m}\frac{d\xi^k}{dz}\frac{d\xi^l}{dz}\frac{d\xi^m}{dz} + 2\,\Gamma^i_{kl}\frac{d^2\xi^k}{dz^2}\frac{d\xi^l}{dz}\right] \\ &= -\left[(\Gamma^i_{kl})_{,\,m} - 2\,\Gamma^r_{kl}\Gamma^i_{mr}\right]\frac{d\xi^k}{dz}\frac{d\xi^l}{dz}\frac{d\xi^m}{dz} \\ &= -\,\Gamma^i_{klm}\frac{d\xi^k}{dz}\frac{d\xi^l}{dz}\frac{d\xi^m}{dz}, \end{aligned}\right\} \tag{A 6}$$

where

$$\Gamma^i_{klm} = \underset{(klm)}{S}\left[(\Gamma^i_{kl})_{,\,m} - 2\,\Gamma^r_{kl}\Gamma^i_{mr}\right]. \tag{A 7}$$

$S$ is a symmetrizing operator defined by

$$\underset{(klm)}{S}\,P_{klm} = \frac{1}{3!}\left(P_{klm} + P_{mkl} + P_{lmk} + P_{mlk} + P_{kml} + P_{lkm}\right). \tag{A 8}$$

In general, $\underset{(n_1 n_2 \ldots n_p)}{S}\,P_{n_1 n_2 \ldots n_p}$ is the sum of all $p!$ quantities $P_{n_1 n_2 \ldots n_p}$ with all permutations of $n_1 n_2 \ldots n_p$, divided by $p!$.

Then one finds that

$$\frac{d^p\xi^i}{dz^p} = -\,\Gamma^i_{k_1 k_2 \ldots k_p}\frac{d\xi^{k_1}}{dz}\frac{d\xi^{k_2}}{dz}\cdots\frac{d\xi^{k_p}}{dz}, \tag{A 9}$$

where

$$\Gamma^i_{k_1 k_2 \ldots k_p} = \underset{(k_1 k_2 \ldots k_p)}{S}\left[(\Gamma^i_{k_1 k_2 \ldots k_{p-1}})_{,\,k_p} - (p-1)\,\Gamma^r_{k_1 k_2}\Gamma^i_{k_3 \ldots k_p r}\right]. \tag{A 10}$$

The coordinates $\xi^i$ of any point $Q_0$ in the neighbourhood of the geodesic can then, by (A 5), (A 9) and (A 3), be expressed by the equation

$$\left.\begin{aligned} \xi^i = \xi_0^i + t_0^i z - \frac{1}{2!}\Gamma^i_{kl}(\xi_0^i)\,t_0^k t_0^l z^2 - \frac{1}{3!}\Gamma^i_{klm}(\xi_0^i)\,t_0^k t_0^l t_0^m z^3 \\ - \frac{1}{4!}\Gamma^i_{klmn}(\xi_0^i)\,t_0^k t_0^l t_0^m t_0^n z^4 - \cdots . \end{aligned}\right\} \tag{A 11}$$

For every point $Q_0$ there is one vector $t_0^i$ orthogonal to the geodesic. If one makes a parallel displacement along the geodesic from $P_0$ to a general point $P$, with coordinates $\xi^i = f^i(t)$, the vectors $t_0^i$ at $P_0$ go over into vectors $t^i$ at $P$ orthogonal to the geodesic. The vector $t^i$ will depend on the parameter $t$ of the geodesic and the parameters specifying the vector $t_0^i$. To every

neighbouring point $Q$ in the orthogonal hypersurface at $P$ corresponds one vector $t^i$ giving the direction at $P$ of the geodesic from $P$ to $Q$. The coordinates $\xi^i$ of the point $Q$ can then be expressed by an equation corresponding to (A11):

$$\left.\begin{aligned}\xi^i = f^i(t) + t^i z - \frac{1}{2!}\,\Gamma^i_{kl}\{f^i(t)\}\,t^k t^l z^2 - \frac{1}{3!}\,\Gamma^i_{klm}\{f^i(t)\}\,t^k t^l t^m z^3 \\ - \frac{1}{4!}\,\Gamma^i_{klmn}\{f^i(t)\}\,t^k t^l t^m t^n z^4 - \cdots\cdots\end{aligned}\right\} \quad \text{(A12)}$$

Now at $P_0$ introduce $N$ linearly independent vectors $e^{0\,i}_1, e^{0\,i}_2, \ldots, e^{0\,i}_N$ such that $e^{0\,i}_N$ is tangential to the geodesic and $e^{0\,i}_\mu$, $\mu = 1, 2, \ldots, N-1$ are orthogonal to it. The vectors $e^{0\,i}_\mu$ span the orthogonal hypersurface at $P_0$ so that the vectors $t^i_0$ can be expressed in terms of them:

$$t^i_0 = t^\mu e^{0\,i}_\mu, \quad \mu = 1, 2, \ldots, N-1. \qquad \text{(A13)}$$

The $t^\mu$ will depend on the parameters specifying the vector $t^i_0$. If one makes a parallel displacement along the geodesic from $P_0$ to $P$, the vectors $e^{0\,i}_\mu$, $e^{0\,i}_N$ go over into $N$ linearly independent vectors $e^i_\mu$, $e^i_N$ such that $e^i_N$ is tangential to the geodesic and the $e^i_\mu$ orthogonal to it. Thus the $e^i_\mu$ span the orthogonal hypersurface at $P$, and the $t^i$ can be expressed in terms of them:

$$t^i = t^\mu e^i_\mu. \qquad \text{(A14)}$$

Unlike the vectors $e^i_\mu$, the $t^\mu$ are independent of $t$, depending only on the parameters specifying the original $t^i_0$. This is due to the fact that the covariant derivatives of $t^i$ and $e^i_\mu$ vanish along the curve.

The coordinates of a point in the neighbourhood of the geodesic may then be expressed by the equation

$$\left.\begin{aligned}\xi^i = f^i(t) + z t^\mu e^i_\mu(t) - \frac{1}{2!}\,\Gamma^i_{kl}\{t\}\,z^2 t^\mu t^\nu e^k_\mu(t)\,e^l_\nu(t) \\ - \frac{1}{3!}\,\Gamma^i_{klm}\{t\}\,z^3 t^\mu t^\nu t^\varrho\, e^k_\mu(t)\,e^l_\nu(t)\,e^m_\varrho(t) \\ - \frac{1}{4!}\,\Gamma^i_{klmn}\{t\}\,z^4 t^\mu t^\nu t^\varrho t^\sigma e^k_\mu(t)\,e^l_\nu(t)\,e^m_\varrho(t)\,e^n_\sigma(t) - \cdots\cdots\end{aligned}\right\} \quad \text{(A15)}$$

The $\xi^i$ can thus be given in terms of the $N$ independent variables $zt^\mu$, $t$. The $e^i_\mu$ are known functions of $t$, depending on the initial choice of $e^{0\,i}_\mu$. Along the curve the $\Gamma^i_{kl}$ are functions of $t$ only.

Introducing a new coordinate system, defined by

$$\left.\begin{aligned} \eta^{\mu} &= z t^{\mu}, \quad \mu = 1, 2, \ldots, N-1, \\ \eta^{N} &= t, \end{aligned}\right\} \tag{A 16}$$

we shall now show that the basis vectors of this system on the geodesic, i. e. the vectors along the coordinate curves or parametric lines, are the very vectors $e^i_\mu$, $e^i_N$ already defined at every point of the curve. The coordinate system $(\eta)$ is then defined at every point of the geodesic.

Substituting from (A 16) in (A 15), one has

$$\left.\begin{aligned} \xi^i = f^i(\eta^N) + \eta^\mu e^i_\mu(\eta^N) - \frac{1}{2!} \Gamma^i_{kl}\{\eta^N\}\, \eta^\mu \eta^\nu e^k_\mu(\eta^N) e^l_\nu(\eta^N) \\ - \frac{1}{3!} \Gamma^i_{klm}\{\eta^N\}\, \eta^\mu \eta^\nu \eta^\varrho e^k_\mu(\eta^N) e^l_\nu(\eta^N) e^m_\varrho(\eta^N) \\ - \frac{1}{4!} \Gamma^i_{klmn}\{\eta^N\}\, \eta^\mu \eta^\nu \eta^\varrho \eta^\sigma e^k_\mu(\eta^N) e^l_\nu(\eta^N) e^m_\varrho(\eta^N) e^n_\sigma(\eta^N) - \cdots . \end{aligned}\right\} \tag{A 17}$$

The equation of the geodesic in the new coordinate system is

$$\eta^\mu = 0, \quad \mu = 1, 2, \ldots, N-1. \tag{A 18}$$

The $k^{th}$ basis vector of the new system, i. e. the vector along the $k^{th}$ coordinate curve $\eta^i = \text{const.}$, $i \neq k$, is $\dfrac{\partial \xi^i}{\partial \eta^k}$ in the old coordinate system since $d\xi^i = \dfrac{\partial \xi^i}{\partial \eta^k} d\eta^k$. On the geodesic one finds from (A 17)

$$\left(\frac{\partial \xi^i}{\partial \eta^\mu}\right)_{\eta^\mu = 0} = e^i_\mu(\eta^N), \quad \left(\frac{\partial \xi^i}{\partial \eta^N}\right)_{\eta^\mu = 0} = \frac{df^i}{dt} = e^i_N, \tag{A 19}$$

which was to be shown.

Equation (A 17) expresses the general coordinates $\xi^i$ in terms of the particular coordinates $\eta^k$. This equation holds for any coordinates $\xi^i$, in particular for $\xi^i = \eta^i$. In that case one has $e^i_k = \dfrac{\partial \eta^i}{\partial \eta^k} = \delta^i_k$ so that equation (A 17) becomes

$$\left.\begin{aligned} \eta^i = f^i(\eta^N) + \eta^\mu \delta^i_\mu - \frac{1}{2!} \Gamma^i_{\mu\nu}\{\eta^N\}\, \eta^\mu \eta^\nu \\ - \frac{1}{3!} \Gamma^i_{\mu\nu\varrho}\{\eta^N\}\, \eta^\mu \eta^\nu \eta^\varrho - \frac{1}{4!} \Gamma^i_{\mu\nu\varrho\sigma}\{\eta^N\}\, \eta^\mu \eta^\nu \eta^\varrho \eta^\sigma - \cdots \end{aligned}\right\} \tag{A 20}$$

Differentiating this equation with respect to $(\eta^\mu, \eta^\nu)$, $(\eta^\mu, \eta^\nu, \eta^\varrho)$, $(\eta^\mu, \eta^\nu, \eta^\varrho, \eta^\sigma)$, etc., and putting $\eta^\mu = 0$, one finds that on the geodesic

$$\left.\begin{aligned} \Gamma^i_{\mu\nu}\left\{\eta^N\right\} &= 0 \\ \Gamma^i_{\mu\nu\varrho}\left\{\eta^N\right\} &= 0 \\ \Gamma^i_{\mu\nu\varrho\sigma}\left\{\eta^N\right\} &= 0, \\ &\text{etc.} \end{aligned}\right\} \tag{A 21}$$

Along the curve $\xi^i = f^i(t)$ the covariant derivatives of the vectors $e^i_k$ vanish ($k = \mu$, $N$ is not a vector index, but a label for the different vectors), by definition, i. e.

$$\frac{de^i_k}{dt} + \Gamma^i_{rs}\left\{t\right\} e^r_k \frac{df^s}{dt} = 0 \tag{A 22}$$

or, by equation (A 19),

$$\frac{de^i_k}{dt} + \Gamma^i_{rs}\left\{t\right\} e^r_k e^s_N = 0. \tag{A 23}$$

In the coordinate system $(\eta)$ one has $e^i_k = \delta^i_k$. Therefore, in that system (A 23) shows that on the curve

$$\Gamma^i_{kN}\left\{\eta^N\right\} = 0, \quad k = 1, 2, \ldots, N. \tag{A 24}$$

Now, since $\Gamma^i_{\mu\nu} = 0$, one has

$$\Gamma^i_{\mu\nu\varrho} = \underset{(\mu\nu\varrho)}{S}\left[\Gamma^i_{\mu\nu,\varrho} - 2\,\Gamma^r_{\mu\nu}\,\Gamma^i_{\varrho r}\right] = \underset{(\mu\nu\varrho)}{S}\,\Gamma^i_{\mu\nu,\varrho} \tag{A 25}$$

and

$$\Gamma^i_{\mu\nu\varrho\sigma} = \underset{(\mu\nu\varrho\sigma)}{S}\left[\Gamma^i_{\mu\nu\varrho,\sigma} - 3\,\Gamma^r_{\mu\nu}\,\Gamma^i_{\varrho\sigma r}\right] = \underset{(\mu\nu\varrho\sigma)}{S}\,\Gamma^i_{\mu\nu\varrho,\sigma} = \underset{(\mu\nu\varrho\sigma)}{S}\,\Gamma^i_{\mu\nu,\varrho,\sigma}. \tag{A 26}$$

From (A 21) and (A 24) — (A 26) it is then found that

$$\left.\begin{aligned} \Gamma^i_{kl} &= 0 \qquad i, k, l = 1, 2, .., N \\ \underset{(\mu\nu\varrho)}{S}\;\Gamma^i_{\mu\nu,\varrho} &= 0 \qquad \mu, \nu, .. = 1, 2, \ldots, N-1 \\ \underset{(\mu\nu\varrho\sigma)}{S}\;\Gamma^i_{\mu\nu,\varrho,\sigma} &= 0, \\ &\text{etc.} \end{aligned}\right\} \tag{A 27}$$

at all points of the curve. The coordinates for which the equations (A 27) hold are called Fermi coordinates by SCHOUTEN, for Fermi was the first to show that coordinates can be chosen along any curve in Riemannian space $V_N$ so that $\Gamma^i_{kl} = 0$ at every point of the curve.

## References


(1) A. Einstein, Ann. Phys. **49** (1916) 769.

(2) See W. Pauli, Relativitätstheorie, § 61, in Encyklopädie der Mathematischen Wissenschaften V. 2 (B. G. Teubner, Leipzig, 1921), where references are given.

(3) A. Einstein, S. B. preuss. Akad. Wiss. (1918) 448.

(4) C. Møller, Annals of Physics **4** (1958) 347.

(5) C. Møller, Max-Planck-Festschrift (Deutscher Verlag der Wissenschaften, Berlin, 1958) Artikel 9.

(6) C. Møller, Mat. Fys. Medd. Dan. Vid. Selsk. **31**, no. 14 (1959).

(7) B. Laurent, Nuovo Cimento **9** (1959) 740.

(8) J. N. Goldberg, Phys. Rev. **111** (1958) 315.
P. G. Bergmann, Phys. Rev. **112** (1958) 287.

(9) C. Møller, The Theory of Relativity (Oxford University Press, London and New York, 1952) eq. (IX, 53).

(10) F. A. E. Pirani, Phys. Rev. **105** (1957) 1089, § 4.
T. Y. Thomas, Phil. Mag. **48** (1924) 1056.
G. D. Birkhoff, Relativity and Modern Physics (Harvard University Press, Cambridge, Mass., 1923).

(11) J. A. Schouten, Ricci-Calculus, second edition (Springer-Verlag, Berlin and London, 1954) pp. 166 ff.



Indleveret til Selskabet den 24. september 1959.
Færdig fra trykkeriet den 27. maj 1960.

Matematisk-fysiske Meddelelser
udgivet af
Det Kongelige Danske Videnskabernes Selskab
Bind **32,** nr. 7

Mat. Fys. Medd. Dan. Vid. Selsk. **32,** no. 7 (1960)

# NOTES ON SOME LOWER CAMBRIAN FOSSILS FROM FRENCH WEST AFRICA

BY

CHR. POULSEN


København 1960
i kommission hos Ejnar Munksgaard

## CONTENTS


| | Page |
|---|---|
| Preface | 3 |
| Notes on the Geology of the Zemmour Region | 3 |
| Description and Discussion of the Fossils | 6 |
| *Neobolus* cf. *warthi* WAAGEN | 6 |
| *Lingulella* cf. *fuchsi* REDLICH | 7 |
| *Botsfordia paucigranulata* n. sp. | 8 |
| *Acrothele sougyi* n. sp. | 9 |
| *Acrothele spinulosa* n. sp. | 9 |
| *Redlichia*? sp. | 10 |
| Conclusive Remarks | 11 |
| Plates | 13 |


## Synopsis


In 1955 two occurrences of fossiliferous Lower Cambrian were discovered in the Zemmour region of Mauritania (French West Africa). The fossil fauna consists of six species, three of which are established as new, and it appears to be related to that of the *Neobolus* Beds at Fort Kusak in the Salt Range (Pakistan). In the writer's opinion the material at hand is significant as additional evidence of the existence of a Tethys already in early Cambrian time.



Printed in Denmark
Bianco Lunos Bogtrykkeri A-S

## Preface

The material described and discussed in the present paper was collected in the Zemmour region of northern Mauritania, partly by Dr. J. Sougy of the Direction Fédérale des Mines et de la Géologie de l'Afrique Occidentale Française, partly by J. Borocco and R. Nyssen. At the request of Dr. Sougy the writer undertook the examination of the material, and the results are presented in the following pages. Geological information and several photographs were placed at the writer's disposal; thanks for this aid are expressed. The figures in the plates are photographs partly furnished by Dr. Sougy, partly taken by the writer. Several prints were made with great care and ability by Mr. C. Halkier.

# NOTES ON THE GEOLOGY OF THE ZEMMOUR REGION

The fossils, almost exclusively brachiopods, originate from Aghachan el Akhdhar and Gara Bouya Ali, marked on the map (fig. 1) as 1 and 2, respectively, and the geological position of these occurrences appears partly from the map (fig. 1), partly from the stratigraphic table (p. 5), made by Dr. Sougy and kindly placed at the writer's disposal.

In addition to the geological map and the stratigraphic table Dr. Sougy has kindly sent the following brief information concerning the series of strata:

"La Série d'El Thlethyate a livré des Stromatolithes et la Série de Garat el Hamoueïd des empreintes indéterminables de Camarotoechiidae. Deux niveaux de la Série de l'Oumat el Ham *sensu stricto* ont livré des empreint de Brachiopodes Inarticulés: les Argiles vertes micacées d'Aghachan el Akhdhar (niveau local 6) et les Minerais de fer de Gara Bouya Ali.

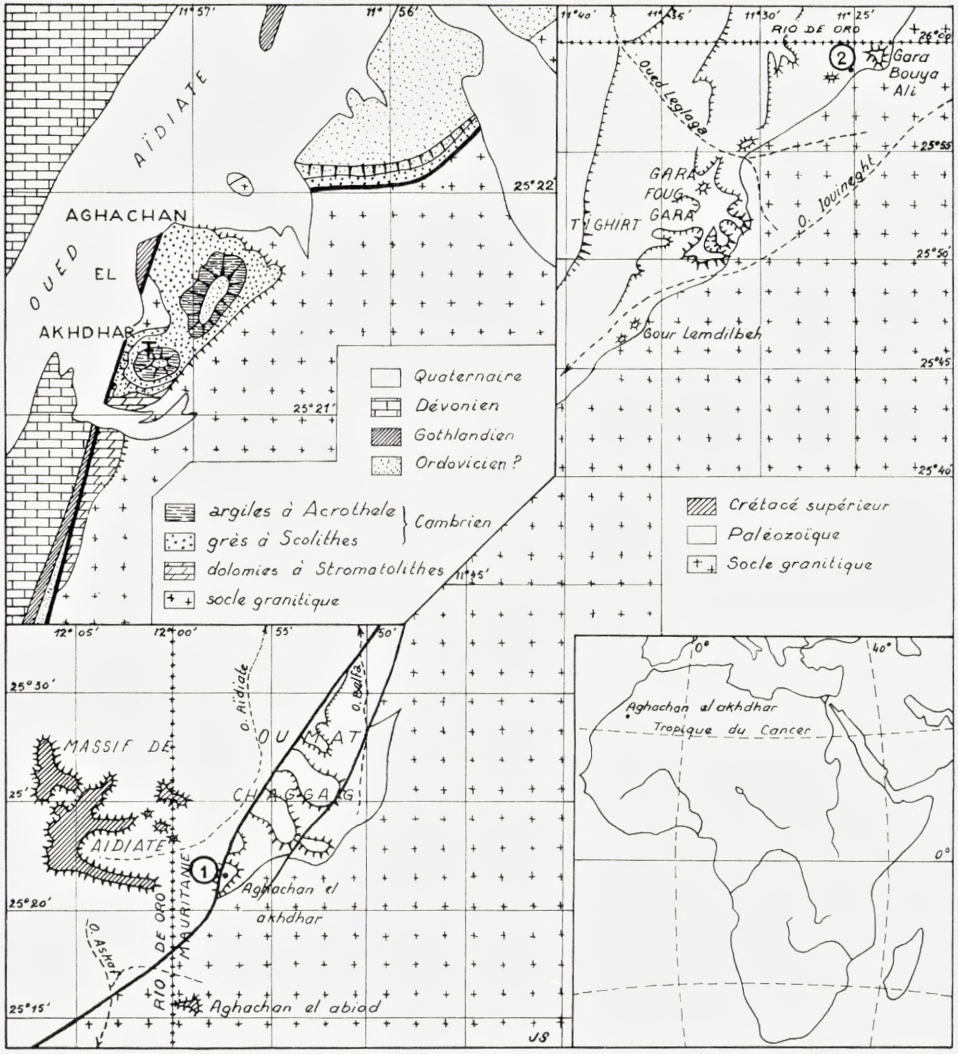


Fig. 1. Position des deux gisements de Brachiopodes inarticulés du Cambrien du Zemmour. 1. Aghachan el Akhdhar. 2. Gara Bouya Ali.

La série stratigraphique du Paléozoique inférieur du Zemmour, définie dans deux notes de J. Sougy (1956 et 1957) peut se résumer dans le tableau suivant:

| Ages | | Puissances | Echelle locale | Niveaux |
|---|---|---|---|---|
| GOTLANDIEN | | 6 à 50 m | 16 | Schistes à *Monograptus triangulatus* |
| ORDOVICIEN? | Serie de Garat el Hamouid | 15 à 150 m | 15 | Grès-quartzites massifs |
| | | | 14 | Conglomérat de base remaniant les pélites du niveau 8 et à nodules phosphatés |
| | | | 13 | Zone d'altération de la paléosurface d'érosion |
| Lacune | | | | Discordance de ravinement |
| CAMBRIEN | Serie de l'Oumat el Ham sensu stricto | 6 m | 12 | Grès schisteux de l'Oued Ezrayeb |
| | | 5 m | 11 | Grès à *Scolithus linearis* supérieurs |
| | | 0.30 m | 10 | Grès et conglomérat à nodules phosphatés |
| | | 1 m? | 9 | Argiles supérieures |
| | | 120 m | 8 | Pélites et siltstones micacés à glauconie, à micro-débris de Lingulidés |
| | | 0 à 15 m | 7 | Niveau ferrugineux de Gara Bouya Ali à empreintes de Brachiopodes Inarticulés |
| | | 0 à 6 m | 6 | Argiles micacées vertes d'Aghachan el Akhdhar, à *Acrothele* |
| | | 0 à 40 m | 5 | Grès à *Scolithus linearis* inférieurs |
| | | 0 à 12 m | 4 | Grès feldspathiques grossiers roses |
| | | 0 à 1 m | 3 | Conglomérat de base transgressif |
| Lacune probable | | | | |
| INFRA-CAMBRIEN | Serie d'el Thlethyate | 0 à 600 m | 2 | Dolomies à *Conophyton* |
| | | | 1 | Base mal connue de la formation |
| Lacune | | | | Discordance angulaire |
| PRECAMBRIEN | | | | Socle granitique |

(a) Les Argiles à *Acrothele* d'Aghachan el Akhdhar:

Cette formation repose directement sur les Grès à *Scolithus* inférieurs. Ce sont des argiles illitiques très micacées de 6 mètres de puissance, qui comportent des passées plus grossières et passent insensiblement vers le haut à la puissante série de pélites micacées à glauconie.

Les empreintes ont été découvertes par J. Sougy le 31 mars 1955 à Aghachan el Akhdhar. Le gisement, dont la position est précisée par la figure 1, a les coordonnées suivantes:

Latitude: 25°21′15″ N.
Longitude: 11°57′12″ W.

Il se trouve dans un petit rû descendant du piton sud de la colline, et qui a mis à jour les argiles. Ces argiles appartiennent à la base de la Série de l'Oumat et Ham *sensu stricto* définie en 1957.

(b) Les Minerais de fer de Gara Bouya Ali:

Les minerais de fer de Gara Bouya Ali sont un faciès latéral des pélites à glauconie qui se développe vers la base de cellesci dans le Nord du Zemmour, au NE de la Gara Foug Gara. Ces minerais proviennent de l'altération de niveaux particulièrement riches en glauconie. Ce sont des minerais siliceux à 33 % de fer métal.

La position approximative des empreintes est la suivante:

Latitude: 25°58′30″ N.
Longitude: 11°25′ W.

Les empreintes ont été découvertes par J. Borocco et R. Nyssen le 10 mars 1955. L'affleurement est très étendu et les empreintes se trouvent sur les débris de roches qui jonchent le sol.

La position stratigraphique des Minerais de Gara Bouya Ali est très légèrement supérieure à celle des Argiles d'Aghachan el Akhdhar."

## DESCRIPTIONS AND DISCUSSIONS OF THE FOSSILS

### BRACHIOPODA

Order **ATREMATA** Beecher

Superfamily **OBOLACEA** Schuchert

Family **OBOLIDAE** King

Subfamily **Neobolinae** Waagen

Genus Neobolus Waagen

*Neobolus* cf. *warthi* Waagen, 1885.

Pl. 1, figs. 1—4.

For synonyms see Schindewolf & Seilacher 1955, pp. 325—326.

Material: Two ventral valves and six dorsal valves, all of them more or less fragmentary.

Locality: Aghachan el Akhdhar.

Remarks: The specimens agree fairly well with those from Salt Range (Pakistan) as described by SCHINDEWOLF (1955) with regard to the outline of the valves, which may vary from subcircular to transversely subelliptic. Some of the specimens show the same somewhat coarse surface markings as those figured by SCHINDEWOLF & SEILACHER, but most of them have less coarse and more regular surface markings and are in this respect intermediate between SCHINDEWOLF & SEILACHER's specimens and those figured by WALCOTT (1912, pl. 1, figs. 4—5; pl. 81, figs. 2, 2a—d). One of the African specimens, a natural cast of the interior of a dorsal valve, shows impression of apical plate and median septum; the former is poorly defined when compared with specimens figured by WALCOTT and by SCHINDEWOLF & SEILACHER; it is well-known, however, that in inarticulate brachiopods internal characters of one and the same species may vary to a considerable extent. It deserves notice that the African specimens are much smaller than those from Salt Range; the maximum diameter of the Salt Range specimens is about 10 mm, whereas that of the African specimens hardly exceeds 2 mm; in view of this fact and the poor state of preservation the specific determination is given with reservation.

## Subfamily **Lingulellinae** SCHUCHERT

### Genus Lingulella SALTER

### *Lingulella* cf. *fuchsi* REDLICH, 1899.

Pl. 1, figs. 5—9.

1899. *Lingulella fuchsi* REDLICH, p. 7, Pl. 1, figs. 10a–e.
1905. *Obolus* (*Lingulella*) *fuchsi* WALCOTT, p. 332.
1912. *Lingulella fuchsi* WALCOTT, p. 502, Pl. 39, figs. 2, 2a–c, 3.
1955. *Lingulella fuchsi* SCHINDEWOLF in SCHINDEWOLF & SEILACHER, p. 307, Pl. 8, figs. 21–28.

Material: Twenty-three more or less fragmentary specimens most of which appear to be dorsal valves.

Locality: Aghachan el Akhdhar.

Remarks: It appears from SCHINDEWOLF's figures that *Lingulella fuchsi* shows great variation with regard to the outline of the valves so that in many cases it is impossible to distinguish ventral valves from dorsal ones by means of this character only, and the situation is the same as far as the African material is concerned. The specimens having the same almost perfectly oval outline as those figured by WALCOTT 1912 as Pl. 39, figs. 2b—c are supposed

to be dorsal valves, whereas those having acute posterior ends are supposed to be ventral valves. Judging from figures of the holotype (Redlich 1899, Pl. 1, fig. 10c; Walcott 1912, Pl. 39, fig. 3) the external surface may have longitudinal striae radiating from the apex; in the African material such striae are indistinctly shown by the specimen represented in Pl. 1, fig. 8, whereas the other specimens, like those figured by Schindewolf, fail to show this character; the same specimen also shows indications of the papillae described by Schindewolf (p. 307) and shown in one of his figures (Pl. 8, fig. 26).

Most of the African specimens are within the variation limits shown by the several specimens from Salt Range as figured by Schindewolf, although some of the former are larger, measuring up to 6 mm in length, but it deserves notice that ventral valves with very acute posterior ends as shown in Redlich's Pl. 1, fig. 10c, and Schindewolf's Pl. 8, figs. 25–26, have not been met with, and in view of this fact and the fragmentary state of preservation the specific determination is given with some hesitation.

## Order **NEOTREMATA** Beecher

## Superfamily **BOTSFORDIACEA** Schindewolf

## Family **BOTSFORDIIDAE** Schindewolf

### Genus Botsfordia Matthew

### *Botsfordia paucigranulata* n. sp.

Pl. 2, figs. 1–3.

Material: A dorsal valve and casts of the external surface of two specimens, one of which is a ventral valve, the other possibly a dorsal valve.

Locality: Gara Bouya Ali.

Description: General form subcircular with posterior end of ventral valve very obtusely angular. Ventral valve slightly convex, with overhanging apex situated at a level very close to that of the commissure of the valves and maximum elevation very close to the apex. External surface marked by very few concentric lines of growth and a system of fine, more or less inosculating ridges upon which there are minute rounded to oblong granules that have no extended systematic arrangement; in some places the granules are arranged in diagonal rows that cross each other. Internal characters of the ventral valve unknown. Dorsal valve more perfectly circular than the ventral one, almost flat, and with surface markings similar to that of the

ventral valve, the interior of the dorsal valve shows a low, relatively thick median septum extending to the central part of the valve and becoming increasingly low towards the centre. Main vascular sinuses evenly curved, forming parts of one and the same circle, originating from points remote from the median septum, and terminating at the posterior third line. The length of the specimens represented in Pl. 2, figs. 1—3, is about 3, 2.2, and 2.8 mm, respectively.

Remarks: This species is readily distinguished from the hitherto known members of the genus *Botsfordia* by its more spaced surface granulae and by the short, evenly curved main vascular sinuses.

Superfamily **ACROTRETACEA** Schuchert

Family **ACROTRETIDAE** Schuchert

Subfamily **Acrothelinae** Walcott & Schuchert

Genus Acrothele Linnarsson

*Acrothele sougyi* n. sp.

Pl. 2, figs. 4—7; 8—9?

Material: Eleven ventral valves.

Locality: Aghachan el Akhdhar.

Description: Ventral valve subcircular in outline, low, subconical with the apex a very short distance behind the centre. A pseudo-interarea is very indistinctly defined. An elongate foraminal aperture occurs just behind and beneath the apex. External surface marked by concentric, more or less undulating, partly inosculating ridges; the breadth of the interspaces is equal to that of the ridges; in the central part of the valve the concentric ridges are delicate, more regular, and crossed by numerous extremely fine radiating striae; one specimen (Pl. 2, fig. 7) shows a tendency to formation of coarse radiating ribs at some distance from the apex. Diameter of the valves rarely exceeding 3 mm.

Remarks: The almost central apex and the rather coarse, irregular, partly inosculating concentric ridges are characters which serve to distinguish this species from the hitherto described ones.

*Acrothele spinulosa* n. sp.

Pl. 3, figs. 1—6.

Material: Twenty-one specimens, mainly ventral valves.

Locality: Aghachan el Akhdhar.

Description: General form subcircular, frequently with a slight triangular or quadrangular tendency, and with numerous slender, closely set spines radiating from the margin. Ventral valve low, subconical, with the apex some distance behind the centre. A pseudo-interarea is very indistinctly defined. An oval foraminal aperture occurs just behind and beneath the apex. Surface markings consisting of concentric ridges, which are delicate, regular, and closely set in the central part of the valve, whereas in the peripheral part they are very coarse, irregularly undulating, and partly inosculating; in the peripheral part of the valve the breadth of the interspaces exceeds that of the ridges; in the central part the concentric ridges are crossed by numerous, delicate, closely set, radiating ribs so as to form a fine reticulate pattern. Dorsal valve perfectly flat, with a pair of tubercles at the marginal apex; marginal spines and surface markings as in the ventral valve. Nothing is known of the interior of the valves. Diameter of the valves rarely exceeding 3.3 mm.

Remarks: *Acrothele spinulosa* appears to be closely related to the preceding species, from which it differs by having a more posteriorly located ventral apex, more spaced concentric ridges, and marginal spines; as far as is known, marginal spines have not been observed in other species of the genus *Acrothele*.

## TRILOBITA

Order **REDLICHIIDA** Richter

Suborder **Redlichiina** Harrington

Superfamily **REDLICHIACEA** Poulsen

Family **REDLICHIIDAE** Poulsen

Subfamily **Redlichiinae** Poulsen?

Genus Redlichia Cossmann?

*Redlichia?* sp.

Pl. 1, fig. 10.

The specimen figured is the only representative of the trilobites in the material at hand. Unfortunately, the fragmentary state of preservation prevents a safe reference to subfamily, genus, and species. The specimen in question may be regarded as a fragment of the librigena of an early meraspid individual, showing the genal angle and the proximal part of the genal

spine, and it may be compared with the genal angle region of *Redlichia* as figured by KOBAYASHI & KATO (1957).

Locality: Aghachan el Akhdhar.

## CONCLUSIVE REMARKS

The Lower Cambrian age of the material is indicated by the occurrence of sandstone with *Scolithus linearis* below and above the levels from which the above-described fossils originate. This age of the faunule is further corroborated by the fact that the genus *Neobolus* is only known from Lower Cambrian strata.

The faunule is related to that of the *Neobolus* Beds at Fort Kusak in the Salt Range (Pakistan) described by SCHINDEWOLF (1955); this appears from the fact that two species from Aghachan el Akhdhar seem to be identical with or at any rate very closely related to *Neobolus warthi* WAAGEN and *Lingulella fuchsi* REDLICH from the mentioned *Neobolus* Beds, and the affinity is further emphasized by the occurrence of species of *Botsfordia* in both regions. Accordingly, the genera of brachiopods in the *Neobolus* Beds of Salt Range are not "local genera" as maintained by NEAVERSON (1955).

In the writer's opinion the above-described faunule is significant in a palaeographical respect as additional evidence of the existence of a Tethys already in early Cambrian time.

## References


Anonyme (1957): Carte géologique de l'A.O.F. au 2000000. Notice explicative de la feuille no. 7: Mauritanie.

Furon, R. (1956). Lexique Stratigraphique International, vol. 4, Afrique, fasc. 2: Afrique occidentale et Sahara, p. 31 et p. 47.

Kobayashi, T. & Kato, F. (1951): "On the Ontogeny and the ventral Morphology of *Redlichia chinensis* with description of *Alutella nakamurai* n. gen. and sp.". — Journ. Faculty Sci. Univ. Tokyo, Sect. 2, vol. 8, Pt. 3.

Neaverson, E. (1955): "Stratigraphical Palaeontology".

Redlich, K. A. (1899): "The Cambrian Fauna of eastern Salt Range". — Mem. Geol. Surv. India, "Palaeontologia indica", N. Ser., 1, No. 1.

Schindewolf, O. H. & Seilacher, A. (1955): "Beiträge zur Kenntnis des Kambriums in der Salt Range (Pakistan)". — Akad. d. Wissenschaften und der Literatur, Abh. d. math.-naturwiss. Klasse, Jahrg. 1955, No. 10.

Sougy, J. (1955): "Nouvelles observations de terrain sur la géologie du Zemmour noir". — Rapp. inéd. Dir. Féd. Min. Géol., 61 p., 43 fig., 6 cartes.

Sougy, J. (1956): "Nouvelles observations sur le "Cambro-Ordovicien" du Zemmour (Sahara occidental)". — Bull. Soc. Géol. France, pp. 99—113.

Sougy, J. (1957): "Division en deux séries distinctes de la Série de l'Oumat el Ham (Mauritanie septentrional). — C. R. somm., Soc. Géol. France, no. 10, pp. 180—181.

Waagen, W. (1885): "Salt Range Fossils". — Mem. Geol. Surv. India, "Palaeontologia indica", 13th Ser., vol. 1, Pt. 4.

Walcott, C. D. (1905): "Cambrian Brachiopoda, with descriptions of new genera and species". — Proc. U. S. Nat. Mus., vol. 28.

Walcott, C. D. (1912): "Cambrian Brachiopoda". — Monogr. U. S. Geol. Surv., vol. 51.



Indleveret til selskabet den 20. november 1959.
Færdig fra trykkeriet den 7. april 1960.

# PLATES

PLATE 1.

Page

Fig. 1—4. *Neobolus* cf. *warthi* WAAGEN ..... 6
- 1—2. Dorsal valves, × 10.
- 3. Dorsal valve, × 20.
- 4. Ventral valve?, × 10.
- 5—9. *Lingulella* cf. *fuchsi* REDLICH ..... 7
- 5. Ventral valve?, × 10.
- 6. External cast of the same, × 10.
- 7. Dorsal valve?, × 10.
- 8. Ventral valve?, × 10, with partly preserved surface markings.
- 9. Dorsal valve, × 10.
- 10. *Redlichia*? sp., genal angle with proximal part of genal spine, × 10..... 10

5

1

6

2

7

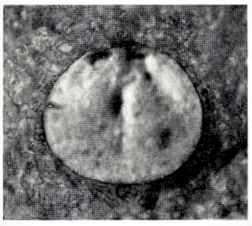

3

8

4

9

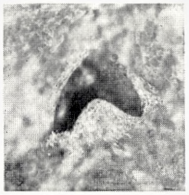

10

## Plate 2.

Page

Fig. 1—3. *Botsfordia paucigranulata* n. sp. . . . . 8

- 1. Ventral valve, cast , × 10.
- 2. Dorsal valve?, cast, × 10.
- 3. Dorsal valve (holotype), × 10; shell partly removed to show natural cast of median septum and main vascular sinuses.

- 4—7. *Acrothele sougyi* n. sp. . . . . 9

- 4. Ventral valve, × 10.
- 5. Ventral valve (holotype), × 10.
- 6. External cast of the same, × 10.
- 8. *Acrothele* cf. *sougyi* n. sp., ventral valve, × 10.
- 9. Lateral view of the same, × 10.

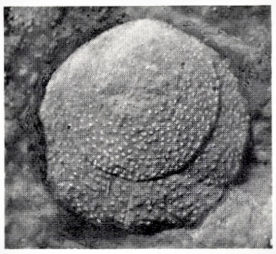

1

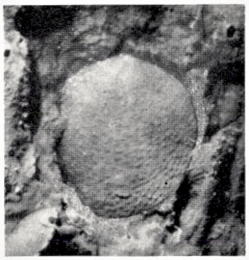

2

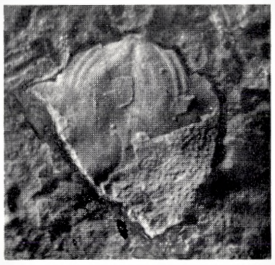

3

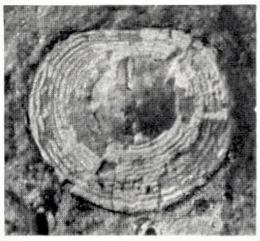

4

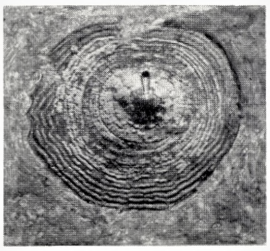

5

6

7

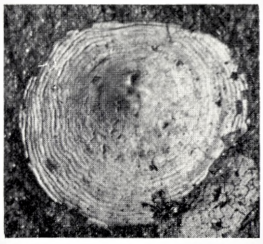

8

9

## Plate 3.

Page

Fig. 1—6. *Acrothele spinulosa* n. sp. . . . . 9

- 1—4. Ventral valves, × 10; the specimen represented by fig. 2 is the holotype.
- 5. Dorsal valve, × 10.
- 6. Fragment of ventral valve, × 10, showing unusually delicate surface markings.

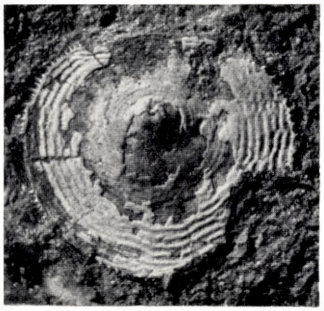

1

2

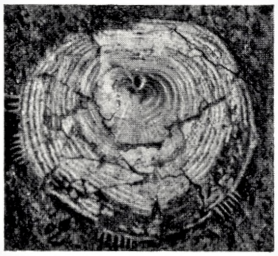

3

5

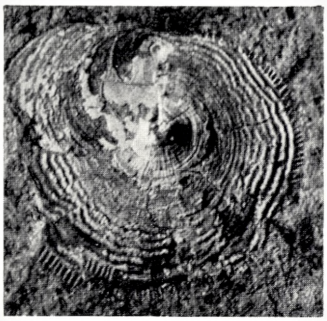

4

6

Matematisk-fysiske Meddelelser
udgivet af
Det Kongelige Danske Videnskabernes Selskab
Bind **32**, nr. 8

Mat. Fys. Medd. Dan. Vid. Selsk. **32**, no. 8 (1960)

# ON THE THEORY OF MULTIPLE COULOMB EXCITATION WITH HEAVY IONS

BY

KURT ALDER AND AAGE WINTHER

København 1960
i kommission hos Ejnar Munksgaard

# CONTENTS


| | Page |
|---|---|
| 1. Introduction | 3 |
| 2. Characteristic Parameters | 4 |
| 3. General Theory | 8 |
| A. Expansion Methods | 8 |
| B. Choice of Coordinate System | 11 |
| C. Dependence on Deflection Angle | 14 |
| 4. Diagonalization Method | 17 |
| A. Sudden Approximation | 17 |
| B. Examples | 20 |
| C. First Order Expansion in $\xi$ | 26 |
| 5. Excitation of Rotational States | 29 |
| A. Sudden Approximation | 29 |
| B. First Order Correction in $\xi$ | 42 |
| C. Numerical Results | 47 |
| D. Classical Treatment | 56 |
| 6. Excitation of Vibrational States | 59 |
| 7. Excitation of Coupled Rotational Bands | 66 |
| 8. Conclusion | 70 |
| References | 72 |


## Synopsis


The present paper contains formulae and tables for the evaluation of multiple Coulomb excitation cross sections of rotational and vibrational states. For other cases, general calculational procedures have been developed and these are illustrated through examples. For the larger part of the work, the collision time is assumed to be short compared to the nuclear period. The investigation is furthermore simplified by an approximate treatment of the dependence of the cross section on the deflection angle of the projectile. The accuracy of the approximations is also discussed.



Printed in Denmark
Bianco Lunos Bogtrykkeri A/S

## 1. Introduction

In the last few years, the Coulomb excitation process has become a valuable tool for the investigation of low lying nuclear states. Several review articles on the experimental and theoretical aspects of Coulomb excitation have appeared, [1], [2], [3], [4] which contain bibliographies of the earlier work on this subject*.

The Coulomb excitation process has certain advantages over other nuclear reactions. The fact that the forces responsible for the process are well understood, and the theory is well developed, allows one from a careful analysis of the reaction to determine a number of quantities characteristic of the nuclear states. The main approximation in the existing calculations is the use of perturbation theory which is valid if the probability for nuclear excitation in a single encounter is small. If protons or $\alpha$-particles are used as projectiles, and if the bombarding energy is kept so low that no nuclear reactions take place, this criterion will always be fulfilled. In these cases there is, however, a strong limitation on the number of states which can be investigated. The limitation lies, firstly, in the selection rules for the low multipole interactions which are important for the excitation process. Secondly, only low lying states are accessible, since the reaction for higher excitation energies soon becomes adiabatic. A way to overcome these difficulties is to use heavier ions as projectiles. The electric field exerted on the nucleus then becomes so large that higher order processes occur. While, e. g., a state with spin $4^+$ in first-order perturbation treatment can only be reached from a ground state of spin $0^+$ through an $E4$ interaction, it might already in second order be excited through a state of spin $2^+$ by means of quadrupole interactions. In many cases, one might still use the perturbation expansion to calculate the excitation probabilities (see ref. 1, Chapt. II D, and ref. 2). If, however, the interaction becomes so strong that many levels are actively involved in the excitation process, one has to solve directly the set of coupled

* In the following, the notation of ref. 1 will always be used.

equations which describes the population of the nuclear states during the collision.

The feasibility of such multiple excitations with heavy ions has recently been proved and, from these experiments as well as from the following calculations, it seems that a number of new possibilities are opened for the investigation of nuclear states[5], [6].

In the following we shall consider such multiple excitations. In Section 2, a discussion is given of the parameters which are important for the process. Section 3 contains the general formalism, while the following sections are concerned with special models and numerical tables.

## 2. Characteristic Parameters

The Coulomb excitation process is characterized by a number of parameters. These quantities describe the kind of approximations which are appropriate for the process in question.

A parameter which describes the motion of the projectile in the Coulomb field of the nucleus is $\eta$ defined by

$$\eta = \frac{Z_1 Z_2 e^2}{\hbar v}, \tag{2.1}$$

where $Z_1$ and $Z_2$ are the charge numbers of the projectile and the target nucleus, respectively, while $v$ is the relative velocity of the incident particle and the nucleus. While for protons this parameter may be as small as two, it is, for the heavy ions which are being considered in the following, always much larger than one. Since, furthermore, the projectile in a collision loses only a small part of its energy, one may to a very good approximation use a classical description for its path. The hyperbolic orbit of the particle will be described by the deflection angle $\vartheta$ (see Fig. 1).

The Coulomb interaction between the projectile and the nucleus is given by (see ref. 1, Eqs. (II A. 8) to (II A. 11))

$$\mathfrak{H}_E(t) = Z_1 e \int \varrho(\vec{r}) \frac{d\tau}{|\vec{r} - \vec{r}_p(t)|}, \tag{2.2}$$

where $\varrho(\vec{r})$ is the charge density operator at the position $r$ of the nucleus and $\vec{r}_p(t)$ is the position vector of the projectile, which for a given hyperbolic orbit is a known function of time. The interaction can be expanded in multipole components

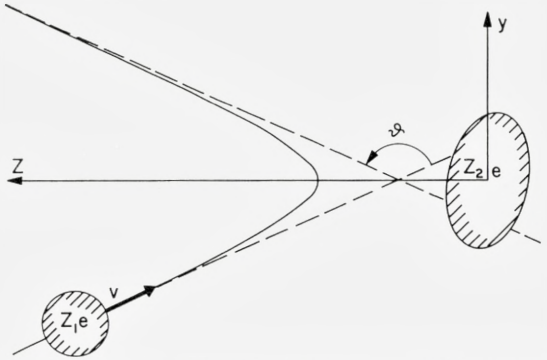


Fig. 1. Classical picture of the projectile orbit in the Coulomb field of the nucleus. The hyperbolic orbit of the projectile is shown in the frame of reference where the nucleus is at rest. The coordinate system which is employed in the present paper, with the $z$-axis along the axis of symmetry, is indicated. The charges of nucleus and projectile are denoted by $Z_2 e$ and $Z_1 e$, respectively, $v$ is the initial relative velocity, and $\vartheta$ is the deflection angle.

$$\mathfrak{H}_E(t) = 4\pi Z_1 e \sum_{\lambda=1}^{\infty} \sum_{\mu=-\lambda}^{+\lambda} \frac{1}{2\lambda+1} r_p^{-\lambda-1} Y_{\lambda\mu}(\vartheta_p, \varphi_p)\, \mathfrak{M}^*(E\lambda, \mu), \tag{2.3}$$

where $\mathfrak{M}(E\lambda, \mu)$ is the electric multipole moment of order $\lambda$ of the nucleus defined by

$$\mathfrak{M}(E\lambda, \mu) = \int r^{\lambda} Y_{\lambda\mu}(\vartheta, \varphi)\, \varrho(\vec{r})\, d\tau. \tag{2.4}$$

In first order perturbation treatment, one finds the following expression for the total probability $P$ for the transition from the nuclear state 1 to the state 2 in a given collision with deflection angle $\vartheta$ (see ref. 1, Eqs. (II A. 4), (II A. 28), and (II A. 29)):

$$P_{1\to 2} = \frac{Z_1^2 \cdot e^2}{\hbar^2 v^2} \sum_{\lambda=1}^{\infty} \frac{16\pi^2}{(2\lambda+1)^3} \cdot \frac{1}{a^{2\lambda}} \cdot B(E\lambda) \sum_{\mu=-\lambda}^{+\lambda} \left| Y_{\lambda\mu}\left(\frac{\pi}{2}, 0\right) \right|^2 \cdot |I_{\lambda\mu}(\vartheta, \xi)|^2. \tag{2.5}$$

Here, $a$ is half the distance of closest approach in a head-on collision

$$a = \frac{Z_1 Z_2 e^2}{m v^2}, \tag{2.6}$$

where $m$ is the reduced mass of the projectile and the target nucleus. The reduced transition probability $B(E\lambda, I_1 \to I_2)$ is defined by

$$\left.\begin{aligned} B(E\lambda, I_1 \to I_2) &= \sum_{\mu M_2} |\langle I_1 M_1 | \mathfrak{M}(E\lambda, \mu) | I_2 M_2 \rangle|^2 \\ &= \frac{1}{2 I_1 + 1} |\langle I_1 || \mathfrak{M}(E\lambda) || I_2 \rangle|^2. \end{aligned}\right\} \quad (2.7)$$

For two states with spins $I_1$ and $I_2$, practically only one value of $\lambda$ will give a contribution to the sum in (2.5).

The orbital integrals[7] $I_{\lambda\mu}(\vartheta, \xi)$ depend on the deflection angle and on the parameter $\xi$ which is defined by

$$\xi_{1\to 2} = \eta_f - \eta_i \simeq \frac{Z_1 Z_2 e^2}{\hbar v} \frac{E_2 - E_1}{2E}. \quad (2.8)$$

The quantities $\eta_i$ and $\eta_f$ are given by (2.1), substituting for the velocity the initial and final velocities, respectively. Similarly, $E_1$ and $E_2$ denote the energies of the nucleus in the states 1 and 2, while $E$ is the energy of the projectile. The parameter $\xi$ measures the suddenness of a head-on collission. In general, the suddenness is measured by the quantity

$$\xi(\vartheta) = \frac{\xi}{\sin \frac{\vartheta}{2}}. \quad (2.9)$$

If $\xi(\vartheta)$ is large, the process is essentially adiabatic and the excitation probability small. If $\xi(\vartheta)$ is small, the process has the character of a sudden impact and one may use a sudden approximation.

In the case of multiple Coulomb excitation, the parameter $\xi$ is no more a characteristic of a nuclear state. A definite nuclear state can in this case be populated in different ways. The $\xi$ which is important for the excitation of the state in question need not be the one corresponding to the excitation from the ground state, but is rather a set of $\xi$'s corresponding to the transitions through which it is populated.

The validity of the perturbation treatment which leads to the result (2.5) is guaranteed if $P$ is small compared to one. We may introduce the square root of the contribution to $P$ from a definite multipole order as a measure of the strength with which the state 2 is coupled to the state 1 through the interaction with the projectile

$$\chi^{(\lambda)}_{1\to 2}(\vartheta, \xi) = \pm \sqrt{P^{(\lambda)}_{1\to 2}(\vartheta, \xi)}. \quad (2.10)$$

The sign is to be the same as the sign of the reduced matrix element $\langle I_1 || \mathfrak{M}(E\lambda) || I_2 \rangle$.

If all the parameters $\chi$ which connect the states of the nucleus are small compared to unity, one may use a first order perturbation treatment. This will practically always be the case when protons are used as projectiles. For $\alpha$-particles and heavier ions, the $\chi$'s will also mostly be smaller than one if the matrix elements are of the order of the single-particle value (see ref. 1, Chapt. II A). One may, in such cases, still use the perturbation treatment, when necessary, to second or third order (see ref. 1, Chapt. II D). If, however, the nucleus possesses excited states of collective type[8] with strongly enhanced $B(E\,2)$ transition probabilities, $\chi^{(2)}$ might be as large as 5. Then, one has to use an approach which avoids the perturbation expansion. On the other hand, states with large quadrupole transition probabilities have usually small excitation energies, and one may use an expansion appropriate for small $\xi$.

The parameter $\chi\ (\vartheta, \xi)$ attains its largest value for $\xi = 0$ and $\vartheta = \pi$. It will be useful to introduce this value as the fundamental parameter, in the same way as $\xi$ is used instead of $\xi(\vartheta)$. We thus define (see ref. 1, Chapt. II E. 4)

$$\chi_{1\to 2}^{(\lambda)} = \sqrt{16\,\pi}\,\frac{(\lambda-1)!}{(2\lambda+1)!!}\cdot\frac{Z_1 e}{\hbar v}\cdot\frac{\langle I_1 \,||\, \mathfrak{M}(E\lambda) \,||\, I_2\rangle}{a^{\lambda}\sqrt{2\,I_1+1}}. \tag{2.11}$$

It will also be convenient sometimes to introducc the value of $\chi(\vartheta, \xi)$ for $\xi = 0$, but arbitrary $\vartheta$ as a parameter. We call this $\chi(\vartheta)$ and, according to (2.5), (2.10), and (2.11), it is defined by

TABLE 1

A survey of different limiting cases of the characteristic parameters $\eta$, $\xi$, and $\chi$. In the table is indicated the kind of approximation which is appropriate for the different cases and the values of $\lambda$ for which computations have been performed. The calculations mentioned under the heading "$\xi$ arbitrary" are quoted in ref. 1. The computations for arbitrary $\eta$ and $\xi \ll 1$ are given in ref. 11, while those mentioned in the last entry refer to the present work.

| | $\eta$ arbitrary | $\eta \gg 1$ semiclassical |
|---|---|---|
| $\xi$ arbitrary | $\chi \ll 1$<br>1. order perturbation<br>$\lambda = 1, 2$ | $\chi < 1$<br>1. and 2. order perturbation<br>$\lambda = 1, 2, 3, 4$ |
| $\xi \ll 1$<br>sudden<br>approximation | $\chi \ll 1$<br>1. order perturbation<br>$\lambda = 3, 4$ | $\chi$ arbitrary<br>multiple excitation<br>$\lambda = 2$ |

$$\chi^{(\lambda)}_{1\to 2}(\vartheta) = \chi^{(\lambda)}_{1\to 2}\frac{(2\lambda-1)!!}{(\lambda-1)!}\left[\frac{\pi}{(2\lambda+1)}\sum_{\mu}{}^{\prime}\left|Y_{\lambda\mu}\left(\frac{\pi}{2},0\right)I_{\lambda\mu}(\vartheta,0)\right|^2\right]^{\frac{1}{2}}. \qquad (2.12)$$

In Table I, a survey is given of the different limiting cases for which computations on Coulomb excitation have until now been made, including the present work. In the following, we shall limit ourselves mainly to the case of quadrupole excitations ($\lambda = 2$).

## 3. General Theory

In this section, we investigate the equations which determine the multiple Coulomb excitation and discuss some general approximation methods. It will be shown that the special solution for $\xi = 0$ and $\vartheta = \pi$ is a convenient basic solution by means of which the excitation probability for small values of $\xi$ and arbitrary angles may be expressed.

### A. Expansion Methods

The Schrödinger equation for the nuclear state vector $|\psi\rangle$ is

$$i\hbar\frac{\partial}{\partial t}|\psi\rangle = [\mathfrak{H}_0 + \mathfrak{H}_E(t)]\,|\psi\rangle, \qquad (3.1)$$

where $\mathfrak{H}_0$ is the Hamiltonian of the free nucleus and $\mathfrak{H}_E(t)$ the interaction energy given by (2.2), (2.3), and (2.4). It will be useful to introduce a new state vector $|\Phi\rangle$ defined by

$$|\psi\rangle = e^{-\frac{i}{\hbar}\mathfrak{H}_0 t}\,|\Phi\rangle. \qquad (3.2)$$

Before and after the collision this state vector is time-independent and it satisfies the equation

$$i\hbar\frac{\partial}{\partial t}|\Phi\rangle = \tilde{\mathfrak{H}}(t)\,|\Phi\rangle, \qquad (3.3)$$

where

$$\tilde{\mathfrak{H}}(t) = e^{\frac{i}{\hbar}\mathfrak{H}_0 t}\cdot\mathfrak{H}_E(t)\,e^{-\frac{i}{\hbar}\mathfrak{H}_0 t}. \qquad (3.4)$$

The equation (3.3) may also be formulated as a set of coupled differential equations for the amplitudes on the nuclear eigenstates. If we thus define

$$a_n(t) = \langle n\,|\,\Phi\rangle, \qquad (3.5)$$

where $|n\rangle$ is the time-independent eigenstate belonging to the eigenvalue $E_n$ of $\mathfrak{H}_0$,

$$\mathfrak{H}_0 \mid n \rangle = E_n \mid n \rangle, \tag{3.6}$$

we obtain

$$i\hbar \dot{a}_n = \sum_m \langle n \mid \mathfrak{H}_E(t) \mid m \rangle e^{\frac{i}{\hbar}(E_n - E_m)t} a_m(t). \tag{3.7}$$

The solution of (3.3) and (3.7) can often conveniently be expressed as a series in powers of $\mathfrak{H}_E(t)$. This is the usual perturbation expansion which can be obtained by an iteration procedure. It can be written in a closed form due to Dyson

$$\mid \Phi(t) \rangle = T e^{-\frac{i}{\hbar}\int_{-\infty}^{t} \tilde{\mathfrak{H}}(t)\, dt} \mid \Phi(t = -\infty) \rangle, \tag{3.8}$$

where the symbol $T$ stands for the time ordered product, i. e.,

$$\left.\begin{aligned} T e^{-\frac{i}{\hbar}\int_{-\infty}^{t} \tilde{\mathfrak{H}}(t')\, dt'} &= 1 - \frac{i}{\hbar}\int_{-\infty}^{t} \tilde{\mathfrak{H}}(t')\, dt' \\ &+ \left(\frac{-i}{\hbar}\right)^2 \int_{-\infty}^{t} \tilde{\mathfrak{H}}(t')\, dt' \int_{-\infty}^{t'} \tilde{\mathfrak{H}}(t'')\, dt'' + \left(\frac{-i}{\hbar}\right)^3 \int_{-\infty}^{t} \tilde{\mathfrak{H}}(t')\, dt' \int_{-\infty}^{t'} \tilde{\mathfrak{H}}(t'')\, dt'' \int_{-\infty}^{t''} \tilde{\mathfrak{H}}(t''')\, dt'''. \end{aligned}\right\} \tag{3.9}$$

If the nucleus before the collision is in the ground state $\mid 0 \rangle$, the solution (3.8) leads to the following expression for the amplitudes on the different excited states after the collision:

$$a_n(+\infty) = \langle n \mid T e^{-\frac{i}{\hbar}\int_{-\infty}^{+\infty} \tilde{\mathfrak{H}}(t)\, dt} \mid 0 \rangle. \tag{3.10}$$

When one inserts the series (3.9), one obtains exactly the usual perturbation expansion for the excitation amplitudes.

As has been mentioned above, the case where $\xi = 0$ for all states involved is of special importance for the problem of multiple Coulomb excitations. In this case, one has $E_n = E_m$ and $\tilde{\mathfrak{H}} = \mathfrak{H}$, and one can then leave out the time ordering in (3.8). The expression (3.10) now takes the simple form

$$a_n(+\infty) = \langle n \mid e^{-\frac{i}{\hbar}\int_{-\infty}^{\infty} \mathfrak{H}(t)\, dt} \mid 0 \rangle \tag{3.11}$$

characteristic of the sudden approximation. This formula is also applicable in cases where $\int_{-\infty}^{\infty} \mathfrak{H}(t)\, dt \gg \hbar$ since, for the evaluation, it is not necessary to perform a series expansion of the exponential function.

By means of formula (3.11) one may thus avoid the perturbation expansion. On the other hand, the effect of the motion of the nucleus during

the collision has been neglected. The sudden approximation, however, forms a convenient starting point for a series expansion in powers of $\mathfrak{H}_0$. Such a series expansion is generated by the following substitution:

$$| \Phi \rangle = e^{-\frac{i}{\hbar}\int_{-\infty}^{t} \mathfrak{H}_E(t)\,dt} | \varphi \rangle . \tag{3.12}$$

The Schrödinger equation (3.3) then takes the form

$$i\hbar \frac{\partial | \varphi \rangle}{\partial t} = e^{\frac{i}{\hbar}\int_{-\infty}^{t} \mathfrak{H}_E(t)\,dt} [\tilde{\mathfrak{H}}(t) - \mathfrak{H}_E(t)]\, e^{-\frac{i}{\hbar}\int_{-\infty}^{t} \mathfrak{H}_E(t)\,dt} . \tag{3.13}$$

In this expression, one can expand $\tilde{\mathfrak{H}}(t)$ in powers of $\mathfrak{H}_0$ in the following way:

$$\tilde{\mathfrak{H}}(t) = \mathfrak{H}_E(t) + \frac{i}{\hbar} t\, [\mathfrak{H}_0, \mathfrak{H}_E(t)] + \frac{1}{2}\left(\frac{i}{\hbar} t\right)^2 [\mathfrak{H}_0 [\mathfrak{H}_0, \mathfrak{H}_E(t)]] + \cdots \tag{3.14}$$

and (3.13) takes the form

$$i\hbar \frac{\partial | \varphi \rangle}{\partial t} = \left\{ \frac{i}{\hbar} t\, [\overline{\mathfrak{H}}_0, \mathfrak{H}_E(t)] + \frac{1}{2}\left(\frac{i}{\hbar} t\right)^2 [\overline{\mathfrak{H}}_0 [\overline{\mathfrak{H}}_0, \mathfrak{H}_E(t)]] + \cdots \right\} | \varphi \rangle , \tag{3.15}$$

where

$$\overline{\mathfrak{H}}_0 = e^{\frac{i}{\hbar}\int_{-\infty}^{t} \mathfrak{H}_E(t)\,dt}\, \mathfrak{H}_0\, e^{-\frac{i}{\hbar}\int_{-\infty}^{t} \mathfrak{H}_E(t)\,dt} . \tag{3.16}$$

The expression on the right-hand side of (3.15) is a series in powers of nuclear energy differences times the collision time, i. e., it is a series in powers of the $\xi$'s involved. If we express the solution in a similar way,

$$| \varphi \rangle = | \varphi_0 \rangle + | \varphi_1 \rangle + | \varphi_2 \rangle + \cdots , \tag{3.17}$$

where $| \varphi_1 \rangle$ is of the order $\xi$ times $| \varphi_0 \rangle$, $| \varphi_2 \rangle$ of the order $\xi^2$ times $| \varphi_0 \rangle$, etc., we obtain the following set of differential equations for these $| \varphi_n \rangle$'s:

$$\left.\begin{aligned}
& i\hbar \frac{\partial | \varphi_0 \rangle}{\partial t} = 0 \\
& i\hbar \frac{\partial | \varphi_1 \rangle}{\partial t} = \frac{i}{\hbar} t\, [\overline{\mathfrak{H}}_0, \mathfrak{H}_E(t)] \, | \varphi_0 \rangle \\
& i\hbar \frac{\partial | \varphi_2 \rangle}{\partial t} = \frac{i}{\hbar} t\, [\overline{\mathfrak{H}}_0, \mathfrak{H}_E(t)] \, | \varphi_1 \rangle + \frac{1}{2}\left(\frac{i}{\hbar} t\right)^2 [\overline{\mathfrak{H}}_0 [\overline{\mathfrak{H}}_0, \mathfrak{H}_E(t)]] \, | \varphi_0 \rangle \\
& \cdots\cdots\cdots\cdots\cdots\cdots
\end{aligned}\right\} \tag{3.18}$$

The initial condition determines $|\varphi_0\rangle$ to be

$$|\varphi_0\rangle = |0\rangle. \tag{3.19}$$

From $|\varphi_0\rangle$ one may determine $|\varphi_1\rangle, |\varphi_2\rangle$, etc. by means of quadratures

$$\left.\begin{aligned} |\varphi_1\rangle &= \frac{1}{\hbar^2}\int_{-\infty}^{t} dt'\, t'\, [\bar{\mathfrak{H}}_0(t'), \mathfrak{H}_E(t')]\,|0\rangle \\ |\varphi_2\rangle &= \frac{1}{\hbar^4}\int_{-\infty}^{t} dt'\, t'\, [\bar{\mathfrak{H}}_0(t'), \mathfrak{H}_E(t')]\int_{-\infty}^{t'} dt''\, t''\, [\bar{\mathfrak{H}}_0(t''), \mathfrak{H}_E(t'')]\,|0\rangle \\ &\quad + \frac{1}{2}\frac{i}{\hbar^3}\int_{-\infty}^{t} dt'\, t'^2\, [\bar{\mathfrak{H}}_0(t'), [\bar{\mathfrak{H}}_0(t'), \mathfrak{H}_E(t')]]\,|0\rangle. \end{aligned}\right\} \tag{3.20}$$

If the interaction energy $\mathfrak{H}_E(t)$ tends to zero sufficiently rapidly, all integrals converge, and (3.20) offers a systematic expansion in powers of the $\xi$'s. In the case of quadrupole Coulomb excitation, however, $\mathfrak{H}_E(t)$ is of the order of $|t|^{-3}$ for large times, and already the second term in $|\varphi_2\rangle$ diverges. This difficulty is also encountered if one tries to expand the orbital integrals $I_{2,\mu}(\vartheta, \xi)$ in powers of $\xi$. The exact expression for these quantities in terms of confluent hypergeometric functions (see ref. 1, Eq. (II E. 50)) shows that the correct expansion is of the form

$$I_{2,\mu}(\vartheta, \xi) \approx a + b\,\xi + c\,\xi^2 + d\,\xi^2 \log \xi + \cdots. \tag{3.21}$$

In the following, we shall calculate only the first order terms of (3.20). For the evaluation of the higher terms a cut-off procedure might be used.

### B. Choice of Coordinate System

In earlier calculations of Coulomb excitation, the orbital integrals were evaluated in the so-called focal system. In this coordinate system the $z$-axis is perpendicular to the plane of the orbit, and the $x$-axis is along the symmetry axis of the hyperbola. In this paper, another system will be used, where the $z$-axis is along the symmetry axis (see Fig. 1). This system is of special convenience for head-on collisions ($\vartheta = \pi$), where the invariance of the entire Hamiltonian for rotations around the $z$-axis ensures the conservation of the magnetic quantum number during the excitation process.

The time-dependence of the interaction energy (2.3) is, for $\lambda = 2$, given by the collision functions

$$\bar{S}_{2,\mu}(t) = r_p^{-3}(t)\, Y_{2,\mu}[\vartheta_p(t), \varphi_p(t)]. \tag{3.22}$$

In the new coordinate system these collision functions are explicitly given by

$$\left.\begin{aligned}
\bar{S}_{2,2}(t) = \bar{S}_{2,-2}(t) &= -\sqrt{\frac{15}{32\pi}}\frac{1}{r_p(t)^3}\cdot\frac{y_p(t)^2}{r_p(t)^2} \\
\bar{S}_{2,1}(t) = \bar{S}_{2,-1}(t) &= -i\sqrt{\frac{15}{8\pi}}\frac{1}{r_p(t)^3}\cdot\frac{z_p(t)\cdot y_p(t)}{r_p(t)^2} \\
\bar{S}_{2,0}(t) &= \sqrt{\frac{5}{16\pi}}\frac{1}{r_p(t)^3}\cdot\frac{3\,z_p(t)^2 - r_p(t)^2}{r_p(t)^2}
\end{aligned}\right\} \tag{3.23}$$

For the perturbation treatment, the important quantities are the orbital integrals defined by

$$S_{E2,\mu}(\vartheta, \xi) = \int_{-\infty}^{+\infty} \bar{S}_{2,\mu}(t)\, e^{i\xi\frac{v}{a}t}\, dt. \tag{3.24}$$

In the old focal system these orbital integrals were expressed by means of the tabulated functions $I_{2,\mu}$ (see ref. 7) in the following way:

$$S^{\text{old}}_{E2,\mu} = \frac{1}{va^2}\, Y_{2,\mu}\left(\frac{\pi}{2}, 0\right) I_{2,\mu}(\vartheta, \xi). \tag{3.25}$$

In the new coordinate system one can again express the orbital integrals in terms of the $I_{2,\mu}$.

$$\left.\begin{aligned}
S_{E2,0}(\vartheta, \xi) &= \frac{1}{va^2}\sqrt{\frac{5}{16\pi}}\left\{\frac{1}{2} I_{2,0}(\vartheta, \xi) + \frac{3}{4} I_{2,2}(\vartheta, \xi) + \frac{3}{4} I_{2,-2}(\vartheta, \xi)\right\} \\
S_{E2,\pm1}(\vartheta, \xi) &= \frac{1}{va^2}\sqrt{\frac{15}{32\pi}}\left\{\frac{1}{2} I_{2,-2}(\vartheta, \xi) - \frac{1}{2} I_{2,2}(\vartheta, \xi)\right\} \\
S_{E2,\pm2}(\vartheta, \xi) &= \frac{-1}{va^2}\sqrt{\frac{15}{32\pi}}\left\{\frac{1}{2} I_{2,0}(\vartheta, \xi) - \frac{1}{4} I_{2,2}(\vartheta, \xi) - \frac{1}{4} I_{2,-2}(\vartheta, \xi)\right\}
\end{aligned}\right\} \tag{3.26}$$

Since $\bar{S}_{2,\pm1}(t)$ is an odd function of time, one sees that $S_{2,\pm1}$ vanishes for $\xi = 0$. The two remaining orbital integrals can be expressed in a way similar to (3.25):

$$S_{E2,\mu}(\vartheta, \xi = 0) = -\frac{1}{va^2}\, Y_{2,\mu}\left(\frac{\pi}{2} 0\right) J_{2,\mu}(\vartheta), \tag{3.27}$$

where

$$\left.\begin{aligned} J_{2,\pm 2}(\vartheta) &= \frac{1}{2}\left[I_{2,0}(\vartheta,0) - I_{2,2}(\vartheta,0)\right] \\ J_{2,0}(\vartheta) &= \frac{3}{2} I_{2,2}(\vartheta,0) + \frac{1}{2} I_{2,0}(\vartheta,0). \end{aligned}\right\} \quad (3.28)$$

These quantities can be expressed by elementary functions, since (see ref. 1, Eq. (II E. 71))

$$\left.\begin{aligned} I_{2,\pm 2}(\vartheta,0) &= \frac{2}{3}\sin^2\frac{\vartheta}{2} \\ I_{2,0}\ (\vartheta,0) &= 2\tan^2\frac{\vartheta}{2}\left[1 - \frac{\pi-\vartheta}{2}\tan\frac{\vartheta}{2}\right] \end{aligned}\right\} \quad (3.29)$$

and they are tabulated in Table 2.

TABLE 2.

The classical orbital integrals for $\xi = 0$ in the coordinate system of Fig. 1. In the two first columns, the functions $J_{2,0}(\vartheta)$ and $J_{2,2}(\vartheta)$ (see Eq. (3.28)) are listed as functions of the deflection angle $\vartheta$. The third column shows the ratio $J_{2,2}(\vartheta)/J_{20}(\vartheta)$ which is important for the $\chi(\vartheta)$ approximation, while the last two columns contain the quantities

$$\chi_{\text{eff}}(\vartheta)/\chi = J_{2,0}(\vartheta) \,/\, J_{2,0}(\pi) \quad \text{and} \quad \chi(\vartheta) \,/\, \chi = \sqrt{(J_{20}(\vartheta))^2 + 3\,(J_{22}(\vartheta))^2} \,/\, J_{20}(\pi).$$

The entries are given in the form of a number followed (in paranthesis) by the power of ten by which it should be multiplied.

| $\vartheta$ | $J_{2,0}(\vartheta)$ | $J_{2,2}(\vartheta)$ | $J_{2,2}/J_{2,0}$ | $\chi_{\text{eff}}/\chi$ | $\chi(\vartheta)/\chi$ |
|---|---|---|---|---|---|
| 0 | 0.0000 | 0.0000 | 3.333 (—1) | 0.00000 | 0.00000 |
| 10 | 1.4257 (—2) | 4.1288 (—3) | 2.896 (—1) | 0.01069 | 0.01196 |
| 20 | 5.3589 (—2) | 1.3386 (—2) | 2.498 (—1) | 0.04019 | 0.04379 |
| 30 | 1.1360 (—1) | 2.4285 (—2) | 2.138 (—1) | 0.08520 | 0.09085 |
| 40 | 1.9054 (—1) | 3.4574 (—2) | 1.814 (—1) | 0.1429 | 0.1498 |
| 50 | 2.8102 (—1) | 4.2878 (—2) | 1.526 (—1) | 0.2108 | 0.2180 |
| 60 | 3.8180 (—1) | 4.8467 (—2) | 1.269 (—1) | 0.2864 | 0.2932 |
| 70 | 4.8973 (—1) | 5.1078 (—2) | 1.043 (—1) | 0.3673 | 0.3732 |
| 80 | 6.0169 (—1) | 5.0792 (—2) | 8.442 (—2) | 0.4513 | 0.4561 |
| 90 | 7.1460 (—1) | 4.7935 (—2) | 6.708 (—2) | 0.5360 | 0.5396 |
| 100 | 8.2543 (—1) | 4.2997 (—2) | 5.209 (—2) | 0.6191 | 0.6216 |
| 110 | 9.3125 (—1) | 3.6570 (—2) | 3.927 (—2) | 0.6984 | 0.7000 |
| 120 | 1.0293 | 2.9301 (—2) | 2.847 (—2) | 0.7720 | 0.7729 |
| 130 | 1.1170 | 2.1831 (—2) | 1.954 (—2) | 0.8378 | 0.8382 |
| 140 | 1.1921 | 1.4772 (—2) | 1.239 (—2) | 0.8941 | 0.8943 |
| 150 | 1.2527 | 8.6659 (—3) | 6.918 (—3) | 0.9395 | 0.9396 |
| 160 | 1.2971 | 3.9600 (—3) | 3.053 (—3) | 0.9728 | 0.9728 |
| 170 | 1.3242 | 1.0393 (—3) | 7.848 (—4) | 0.9932 | 0.9932 |
| 180 | 1.3333 | 0.0000 | 0.000 | 1.0000 | 1.0000 |

For the special case $\vartheta = \pi$, one has $y_p = 0$, and the only non-vanishing collision function is $\bar{S}_{2,0}(t)$. In this case, $J_{2,\mu}(\pi) = 4/3\,\delta_{\mu,0}$. The special simplification for backward scattering is connected with the symmetry of the problem around the $z$-axis.

Also for $\vartheta \neq \pi$ one can obtain some general rules by symmetry considerations. The Hamiltonian is thus always invariant under a reflection in the plane of the orbit. This reflection brings a state vector $|I, M\rangle$ with spin $I$ and magnetic quantum number $M$ into a state $|I, -M\rangle$. One finds

$$|I, M\rangle \rightarrow (-1)^{p+M+I}\,|I, -M\rangle, \tag{3.30}$$

where $p$ is the parity of the state. This rule implies that the excitation probabilities of states with magnetic quantum numbers $M$ and $-M$ are equal, if the initial state is unoriented. The equality of $\bar{S}_{2,\mu}$ and $\bar{S}_{2,-\mu}$ follows also from this symmetry.

For $\xi = 0$, one has the additional symmetry that the Hamiltonian is invariant under a rotation of 180 degrees around the $z$-axis. This rotation gives rise to the following transformation:

$$|I, M\rangle \rightarrow e^{i\pi M}\,|I, M\rangle, \tag{3.31}$$

which implies

$$(-1)^{M_f - M_i} = 1\,, \tag{3.32}$$

where $M_f$ and $M_i$ are the magnetic quantum numbers in the final and initial states, respectively. The disappearance of $S_{1,\pm 1}$ for $\xi = 0$ is also a consequence of this symmetry.

### C. Dependence on Deflection Angle

In the sudden approximation, the interaction energy $\mathfrak{H}_E(t)$ only enters through the expression (see Eqs. (2.3), (3.22), and (3.27))

$$\frac{1}{\hbar}\int_{-\infty}^{+\infty} \mathfrak{H}_E(t)\,dt = -\frac{4\pi Z_1 e}{5\,\hbar\,v a^2} \sum_{\mu}{}' Y_{2,\mu}\left(\frac{\pi}{2}, 0\right) J_{2,\mu}(\vartheta)\,\mathfrak{M}^*(E2, \mu). \tag{3.33}$$

In this expression it will be convenient to collect the dependence on $Z_1$, $v$, and $a$ in the parameter $\chi$, which corresponds to the excitation from the ground state with spin $I_0$ to one of the excited states with spin $I_1$.

$$\chi_{0\rightarrow 1} = \frac{\sqrt{16\pi}}{15}\,\frac{Z_1 e}{\hbar\,v a^2} \cdot \frac{\langle I_0 \| \mathfrak{M}(E2) \| I_1 \rangle}{\sqrt{2\,I_0 + 1}}. \tag{3.34}$$

The expression (3.33) then takes the form

$$\frac{1}{\hbar}\int_{-\infty}^{+\infty}\mathfrak{H}_E(t)\,dt = -\chi_{0\to 1}\sqrt{9\pi}\sum_{\mu} Y_{2,\mu}\left(\frac{\pi}{2},\,0\right) J_{2,\mu}(\vartheta)\,\frac{\mathfrak{M}^*(E\,2,\mu)\sqrt{2\,I_0+1}}{\langle I_0\|\mathfrak{M}(E\,2)\|I_1\rangle}. \quad (3.35)$$

The relative order of magnitude of the terms with $|\mu| = 2$ and $\mu = 0$ is given by the ratio $J_{2,2}(\vartheta)\,/\,J_{2,0}(\vartheta)$. This ratio, which vanishes for $\vartheta = \pi$, is given numerically in Table 2 and it is seen that it is very small for most angles.

This observation gives rise to the convenient approximation of neglecting the terms with $|\mu| = 2$. In this approximation, (3.35) has the same form for all angles and one may write it as follows:

$$\frac{1}{\hbar}\int_{-\infty}^{+\infty}\mathfrak{H}_E(t)\,dt = -\chi_{\mathrm{eff}}(\vartheta)\sqrt{9\pi}\,Y_{2,0}\left(\frac{\pi}{2},\,0\right) J_{2,0}(\pi)\,\frac{\mathfrak{M}^*(E\,2{,}0)\sqrt{2\,I_0+1}}{\langle I_0\|\mathfrak{M}(E\,2)\|I_1\rangle}, \quad (3.36)$$

where

$$\chi_{\mathrm{eff}}(\vartheta) = \chi_{0\to 1}\frac{J_{2,0}(\vartheta)}{J_{2,0}(\pi)} = \frac{3}{4}J_{2,0}(\vartheta)\,\chi_{0\to 1}. \quad (3.37)$$

If one uses the approximate interaction Hamiltonian (3.36), the final state vector for arbitrary deflection angles $|\Phi(\vartheta,\chi)\rangle$ is simply related to the state vector for backward scattering, i. e.,

$$|\Phi(\vartheta,\chi)\rangle \approx |\Phi(\pi,\chi_{\mathrm{eff}}(\vartheta))\rangle. \quad (3.38)$$

The accuracy of this approximation can easily be estimated by writing the state vector $|\Phi(\vartheta,\chi)\rangle$ in the form

$$|\Phi(\vartheta,\chi)\rangle = e^{i\chi_{\mathrm{eff}}(\vartheta)\sqrt{\frac{15}{2}}\frac{J_{22}(\vartheta)}{J_{20}(\vartheta)}\frac{\sqrt{2\,I_0+1}}{\langle I_0\|\mathfrak{M}(E\,2)\|I_1\rangle}\sum_{\mu=\pm 2}\mathfrak{M}^*(E\,2,\mu)}\,|\Phi(\pi,\chi_{\mathrm{eff}}(\vartheta))\rangle, \quad (3.39)$$

which follows from (3.11) and (3.35). In this expression, a series development of the exponential function may be performed, and one is thus led to the following expansion which contains (3.38) as the first term:

$$\left.\begin{aligned}
&|\Phi(\vartheta,\chi)\rangle = |\Phi(\pi,\chi_{\mathrm{eff}}(\vartheta))\rangle\\
&+i\chi_{\mathrm{eff}}(\vartheta)\sqrt{\frac{15}{2}}\frac{J_{22}(\vartheta)}{J_{20}(\vartheta)}\frac{\sqrt{2\,I_0+1}}{\langle I_0\|\mathfrak{M}(E\,2)\|I_1\rangle}\sum_{\mu=\pm 2}\mathfrak{M}^*(E\,2,\mu)\,|\Phi(\pi,\chi_{\mathrm{eff}}(\vartheta))\rangle\\
&(\chi_{\mathrm{eff}}(\vartheta))^2\frac{15}{4}\left(\frac{J_{22}(\vartheta)}{J_{20}(\vartheta)}\right)^2\frac{2\,I_0+1}{|\langle I_0\|\mathfrak{M}(E\,2)\|I_1\rangle|^2}\sum_{\mu\mu'}\mathfrak{M}^*(E\,2,\mu)\mathfrak{M}^*(E\,2,\mu')\,|\Phi(\pi,\chi_{\mathrm{eff}}(\vartheta))\rangle\\
&+\cdots
\end{aligned}\right\} \quad (3.40)$$

An indication of the accuracy of the approximation (3.36) can be obtained by applying it to the old perturbation calculation. For $\xi = 0$ one thus finds, by considering only the term with $\mu = 0$, a total cross section which only differs 5 per cent from the correct one, even though the forward angles, where the approximation is worst, here play a rather important role.

In the following, we shall apply the approximation (3.38) and in a number of cases also investigate the accuracy by calculating the correction terms in (3.40).

We have earlier, in Section 2, introduced a quantity $\chi(\vartheta)$ (see Eq. (2.12)) which is not very different from $\chi_{\text{eff}}(\vartheta)$; the connection between them is given by

$$\left.\begin{aligned} \chi(\vartheta) &= \chi \frac{3}{4} \sqrt{(J_{20}(\vartheta))^2 + 3\,(J_{22}(\vartheta))^2} \\ &\approx \chi_{\text{eff}}(\vartheta) \left\{ 1 + \frac{3}{2} \left( \frac{J_{22}(\vartheta)}{J_{20}(\vartheta)} \right)^2 + \cdots \right\}. \end{aligned}\right\} \tag{3.41}$$

As can be seen from Table 2, the two quantities $\chi(\vartheta)$ and $\chi_{\text{eff}}(\vartheta)$ differ at the most by 15 per cent, but for most angles the difference is much smaller. For foreward angles where the difference is largest, the excitation process can essentially be treated by the first order perturbation theory, where the excitation probability is $|\chi(\vartheta)|^2$. If we thus substitute $\chi(\vartheta)$ for $\chi_{\text{eff}}(\vartheta)$ in the approximation (3.38), we have made a change only of the order of $(J_{2,2}(\vartheta)/J_{2,0}(\vartheta))^2$, but on the other hand obtained an expression which leads to the correct result for the excitation probability for foreward angles.

In the more general case where the sudden approximation is not applicable, the interaction energy $\mathfrak{H}_E(t)$ enters in a more complicated way into the problem. For $\vartheta = \pi$, again only the term with $\mu = 0$ will appear. For other angles, however, the order of magnitude of the terms with $\mu \neq 0$ depends directly on the collision functions (see Eq. (3.23)). These, especially $\bar{S}_{2,1}(t)$, are in general not very small compared to $\bar{S}_{2,0}(t)$, and the approximation is thus only valid in the neighbourhood of $\vartheta = \pi$. One may here investigate the angular dependence by considering the terms with $\mu \neq 0$ in $\mathfrak{H}_E(t)$ as a perturbation in the Hamiltonian. In the sudden approximation, this method would just lead to the result (3.40).

For the sake of completeness it should be mentioned that, once the final amplitudes $a_{I,M}(\infty)$ on the states with spin $I$ and magnetic quantum number $M$ are known, one may easily obtain all the quantities which are important for the experiments. Thus, the total excitation probability of a level of spin $I_f$ is given by

$$P_{I_f I_i} = \frac{1}{2\,I_i + 1} \sum_{M_i,\, M_f} | a_{I_f M_f} |^2. \tag{3.42}$$

The differential cross section $d\sigma$ is obtained by multiplying $P$ with the Rutherford cross section, i. e.,

$$\left.\begin{aligned} d\sigma &= P_{I_f I_i}\, d\sigma_R \\ &= \frac{a^2}{4} P_{I_f I_i} \sin^{-4}\left(\frac{\vartheta}{2}\right) d\Omega. \end{aligned}\right\} \tag{3.43}$$

The angular distribution of $\gamma$-quanta emitted after the excitation is also calculable from the amplitudes. One must here take into account that a level which emits the $\gamma$-quantum under consideration may be populated not only through an excitation, but also through the deexcitation by cascade $\gamma$'s from higher excited states.

## 4. Diagonalization Method

In this section, we shall discuss a method of evaluating the multiple Coulomb excitation which does not use any specific nuclear model. We shall thus consider the properties of the nuclear states, i. e., energies and transition matrix elements as empirically determined quantities. Since, in this case, we have a very large number of parameters in the problem, it is not practically possible to give a systematic numerical tabulation of cross sections, etc., and we shall therefore confine ourselves to a few numerical examples which illustrate some important aspects of the problem.

### A. Sudden Approximation

In the sudden approximation (3.11), we have the following expression for the final amplitude $a_n$ on the state $| n \rangle$:

$$a_n = \langle n \,|\, e^{-\frac{i}{\hbar}\int_{-\infty}^{\infty} \mathfrak{H}_E(t)\, dt} \,|\, 0 \rangle, \tag{4.1}$$

where the exponent is given by (3.33) or (3.35). If the wave functions of the nuclear states are known, the problem is reduced to calculate matrix elements of a known operator. Usually one will be interested, however, in calculating the cross sections from a knowledge of the matrix elements of

the multipole operators themselves. These matrix elements enter in other processes also and are often determined from nuclear spectroscopy.

In order to perform this calculation, we introduce a unitary transformation $U$ which diagonalizes the hermitian operator (3.33) and which is thus defined by the equations

$$U^\dagger U = UU^\dagger = 1 \tag{4.2}$$

and

$$\left.\begin{aligned} \langle n \mid U^\dagger \frac{1}{\hbar} \int_{-\infty}^{+\infty} \mathfrak{H}_E(t)\, dt\, U \mid q \rangle &= \delta_{nq} \cdot \lambda_q \\ = \sum_{m,\,p} \langle n \mid U^\dagger \mid m \rangle \langle m \mid \frac{1}{\hbar} \int_{-\infty}^{+\infty} \mathfrak{H}_E(t)\, dt \mid p \rangle \langle p \mid U \mid q \rangle &. \end{aligned}\right\} \tag{4.3}$$

The result (4.1) can then be expressed in terms of $U$ and the eigenvalues $\lambda_q$ in the following way:

$$\left.\begin{aligned} a_n &= \langle n \mid UU^\dagger e^{-\frac{i}{\hbar}\int_{-\infty}^{+\infty} \mathfrak{H}_E(t)\, dt} UU^\dagger \mid 0 \rangle \\ &= \sum_m \langle n \mid U \mid m \rangle e^{-i\lambda_m} \langle m \mid U^\dagger \mid 0 \rangle \\ &= \sum_m \langle n \mid U \mid m \rangle \langle 0 \mid U \mid m \rangle^* e^{-i\lambda_m}. \end{aligned}\right\} \tag{4.4}$$

The determination of $U$ requires the knowledge of the matrix elements of the operator (3.33). If we specify the nuclear states by means of the spin $I_n$ and magnetic quantum number $M_n$, these matrix elements are expressible by the reduced multipole matrix elements* [9] defined by

$$\langle I_m \| \mathfrak{M}(E2) \| I_n \rangle = (-1)^{I_m - M_m} \begin{pmatrix} I_m & 2 & I_n \\ -M_m & \mu & M_n \end{pmatrix}^{-1} \langle I_m M_m \mid \mathfrak{M}(E2, \mu) \mid I_n M_n \rangle. \tag{4.5}$$

For the diagonalization it will be convenient to apply the $\chi(\vartheta)$ approximation. In this approximation, the operator $\int_{-\infty}^{\infty} \mathfrak{H}_E(t)\, dt$ (see Eq. (3.36)) is diagonal in $M$, and one may write the matrix elements in the form

$$\langle I_m M \mid \frac{1}{\hbar} \int_{-\infty}^{+\infty} \mathfrak{H}_E(t)\, dt \mid I_n M' \rangle \approx \chi_{\text{eff}}(\vartheta)\, \varrho_{mn}^M \delta_{MM'}, \tag{4.6}$$

where the (symmetric) matrix $\varrho_{mn}^M$ is defined by

* For the angular momentum algebra we use throughout this paper the notation of ref. 9.

$$\varrho^{M}_{mn} = (-1)^{I_m - M} \sqrt{5\,(2\,I_0 + 1)} \begin{pmatrix} I_m & 2 & I_n \\ -M & 0 & M \end{pmatrix} \frac{\langle I_m \,||\, \mathfrak{M}(E2) \,||\, I_n \rangle}{\langle I_0 \,||\, \mathfrak{M}(E2) \,||\, I_1 \rangle}. \tag{4.7}$$

The number of states which have to be included in the matrix (4.6) by the diagonalization depends of course on the $\chi$'s. Only those states which are mutually connected with large (collective) matrix elements must be taken into account. One may furthermore classify these in different groups where states within a group are strongly coupled, while states from two different groups are weakly coupled. A group consists, e. g., of the states in a rotational band, and the different groups are the bands belonging to different single-particle states. For each group one must perform the diagonalization and must here take into account a number of those states which are most directly coupled to the ground state. This number will depend on the $\chi$'s and must be determined so that the inclusion of still more states would not change the result. The weak interplay between the groups can be treated by a perturbation calculation.

Since the energy of the projectile and the deflection angle enter only through the common factor $\chi_{\mathrm{eff}}(\vartheta)$, the diagonalization can be used for all energies and all $\vartheta$'s.

The deviation from the $\chi_{\mathrm{eff}}(\vartheta)$ approximation is given by the expression (3.40) which we may write explicitly in the form

$$\left.\begin{aligned} a_{I_f M_f} &= a^{(0)}_{I_f M_f}(\chi_{\mathrm{eff}}(\vartheta))\,\delta_{M_i M_f} \\ &+ i\chi_{\mathrm{eff}}(\vartheta)\frac{J_{22}(\vartheta)}{J_{20}(\vartheta)} \sum_{z\,\mu=\pm 2} \sqrt{\frac{3}{2}} \begin{pmatrix} I_z & 2 & I_f \\ -M_i & \mu & M_f \end{pmatrix} \begin{pmatrix} I_z & 2 & I_f \\ -M_i & 0 & M_i \end{pmatrix}^{-1} \varrho^{M_i}_{zf}\, a^{(0)}_{I_z M_i}(\chi_{\mathrm{eff}}(\vartheta)) \\ &- \left(\chi_{\mathrm{eff}}(\vartheta)\frac{J_{22}(\vartheta)}{J_{20}(\vartheta)}\right)^2 \sum_{zz'\,\mu\mu'=\pm 2} \frac{3}{4} \begin{pmatrix} I_z & 2 & I'_z \\ -M_i & \mu & M'_z \end{pmatrix} \begin{pmatrix} I_z & 2 & I'_z \\ -M_i & 0 & M_i \end{pmatrix}^{-1} \varrho^{M_i}_{zz'} \\ &\quad \times \begin{pmatrix} I'_z & 2 & I_f \\ -M'_z & \mu & M_f \end{pmatrix} \begin{pmatrix} I'_z & 2 & I_f \\ -M_i & 0 & M_i \end{pmatrix}^{-1} \varrho^{M_i}_{z'f}\, a^{(0)}_{I_z M_i}(\chi_{\mathrm{eff}}(\vartheta)) \\ &+ \cdots, \end{aligned}\right\} \tag{4.8}$$

where $a^{(0)}$ indicates the amplitude in the $\chi_{\mathrm{eff}}(\vartheta)$ approximation. Since, in this approximation, $M_i = M_f$, it is seen that, while the first term only contributes to this substate, the second term proportional to $J_{22}(\vartheta) / J_{20}(\vartheta)$ only contributes to the states with $M_f = M_i \pm 2$. The third term proportional to $(J_{22}(\vartheta) / J_{20}(\vartheta))^2$ contributes to both $M_f = M_i$ and $M_f = M_i \pm 4$. The excitation probability will thus contain no terms linear in $J_{22}(\vartheta) / J_{20}(\vartheta)$. The

terms quadratic in this quantity will arise partly from the square of the second term, and partly from an interference between the first and third term.

One may also avoid the $\chi(\vartheta)$ approximation and the expansion (4.8) by directly diagonalizing the matrix of the complete Hamiltonian (3.35). This matrix is no more diagonal in the magnetic quantum number $M$ and is essentially different for different angles so that the diagonalization will have to be performed for all angles.

For not too large values of $\chi(\vartheta)$ it may be advantageous to use the perturbation expansion to higher order instead of the diagonalization method. The power series expansion of (3.11) leads to the following expression for the excitation amplitude:

$$\left.\begin{aligned} a_n &= \langle I_n M \mid e^{-\frac{i}{\hbar}\int_{-\infty}^{\infty} \mathfrak{H}_E(t)\,dt} \mid I_0 M \rangle \\ &= \delta_{no} - i\chi(\vartheta)\varrho^M_{no} - \frac{1}{2!}\chi(\vartheta)^2 \sum_r \varrho^M_{nr}\varrho^M_{ro} \\ &\quad + \frac{i}{3!}\chi(\vartheta)^3 \sum_{rs} \varrho^M_{nr}\varrho^M_{rs}\varrho^M_{so} + \cdots . \end{aligned}\right\} \tag{4.9}$$

This expansion can also be useful for the discussion of small changes in the matrix elements, e. g., from a rotational model.

### B. Examples

In this section, we shall consider some examples of the methods discussed above. They will mainly be given in order to illustrate how many levels one has to take into account in the diagonalization method, and secondly to illustrate the accuracy of the perturbation expansion and the $\chi(\vartheta)$ approximation. For the sake of comparison with the exact treatment (see Section 5), we shall use the matrix elements characteristic of a rotational band.

For a pure rotational band, one may express the reduced matrix elements entering in (4.7) by means of the constant intrinsic quadrupole moment $Q_0$. One finds

$$\left.\begin{aligned} \langle I_m \,||\, \mathfrak{M}(E2) \,||\, I_n \rangle = \sqrt{\frac{5}{16\pi}}(-1)^{I_m - K}(2I_m+1)^{1/2}(2I_n+1)^{1/2} \\ \begin{pmatrix} I_m & 2 & I_n \\ -K & 0 & K \end{pmatrix} e\,Q_0 , \end{aligned}\right\} \tag{4.10}$$

where $K$ is the (constant) projection of the total angular momentum on the nuclear symmetry axis. We shall consider only the case of an even-even nucleus with ground state spin $I_0 = K = 0$. In this case, the matrix $\varrho_{mn}$ (see Eq. (4.7)) takes the form

$$\varrho_{mn} = \sqrt{5}\,(2\,I_m + 1)^{1/2}\,(2\,I_n + 1)^{1/2} \begin{pmatrix} I_m & 2 & I_n \\ 0 & 0 & 0 \end{pmatrix}^2 . \tag{4.11}$$

We shall now successively take more and more states into account. If we include only the ground state and the first excited state $I_1 = 2$, we have to diagonalize the matrix

$$\varrho_{mn} = \begin{Vmatrix} 0 & 1 \\ 1 & \dfrac{2\sqrt{5}}{7} \end{Vmatrix} . \tag{4.12}$$

The eigenvalues of this matrix are

$$\lambda_0 = \frac{\sqrt{5} - 3\sqrt{6}}{7} \quad \text{and} \quad \lambda_1 = \frac{\sqrt{5} - 3\sqrt{6}}{7} . \tag{4.13}$$

The unitary matrix which diagonalizes (4.12) is then found to be

$$\langle m \mid U \mid n \rangle = \begin{Vmatrix} \dfrac{\sqrt{18 + \sqrt{30}}}{6} & \dfrac{\sqrt{18 - \sqrt{30}}}{6} \\ -\dfrac{\sqrt{18 - \sqrt{30}}}{6} & \dfrac{\sqrt{18 + \sqrt{30}}}{6} \end{Vmatrix} . \tag{4.14}$$

According to (4.4) we thus obtain the result

$$\left.\begin{aligned} a_0 &= \frac{18 + \sqrt{30}}{36}\, e^{-i\chi(\vartheta)\frac{\sqrt{5}-3\sqrt{6}}{7}} + \frac{18 - \sqrt{30}}{36}\, e^{-i\chi(\vartheta)\frac{\sqrt{5}+3\sqrt{6}}{7}} \\ &= e^{-i\frac{\sqrt{5}}{7}\chi(\vartheta)} \left[\cos\frac{3\sqrt{6}}{7}\,\chi(\vartheta) + i\sqrt{\frac{5}{54}}\sin\frac{3\sqrt{6}}{7}\,\chi(\vartheta)\right] \\ a_1 &= -\frac{7\sqrt{6}}{36}\, e^{-i\chi(\vartheta)\frac{\sqrt{5}-3\sqrt{6}}{7}} + \frac{7\sqrt{6}}{36}\, e^{-i\chi(\vartheta)\frac{\sqrt{5}+3\sqrt{6}}{7}} \\ &= i\frac{7\sqrt{6}}{18}\, e^{-i\frac{\sqrt{5}}{7}\chi(\vartheta)} \sin\frac{3\sqrt{6}}{7}\,\chi(\vartheta) . \end{aligned}\right\} \tag{4.15}$$

The excitation probability $P_2 = |a_1|^2$ is then

$$P_2 = \frac{49}{54} \sin^2 \frac{3\sqrt{6}}{7} \chi(\vartheta). \tag{4.16}$$

This quantity and the probability that the nucleus is left in the ground state $P_0 = |a_0|^2 = 1 - P_2$ are illustrated in Fig. 2 as a function of $\chi(\vartheta)$.

In Fig. 3 and Fig. 4 are shown the extensions of the above calculation to include two and four excited states in the rotational band. The matrix $\varrho_{mn}$, in the latter case, is explicitly given by

$$\varrho_{mn} = \left\{ \begin{array}{ccccc} 0 & 1.0000 & 0 & 0 & 0 \\ 1.0000 & 0.6389 & 0.8571 & 0 & 0 \\ 0 & 0.8571 & 0.5808 & 0.8457 & 0 \\ 0 & 0 & 0.8457 & 0.5692 & 0.8423 \\ 0 & 0 & 0 & 0.8423 & 0.5649 \end{array} \right\} \tag{4.17}$$

In the case that one includes only two of the excited states, one finds the eigenvalues

$$\lambda_0 = -0.9270, \quad \lambda_1 = 0.3484 \quad \text{and} \quad \lambda = 1.7984 \tag{4.18}$$

and the matrix $U$ is then

$$\langle m | U | n \rangle = \left\{ \begin{array}{ccc} 0.6840 & -0.6006 & 0.4139 \\ -0.6341 & -0.2093 & 0.7444 \\ 0.3605 & 0.7717 & 0.5240 \end{array} \right\} \tag{4.19}$$

The final amplitudes on the three states are thus, according to (4.4),

$$\left. \begin{array}{l} a_0 = \quad 0.4679\, e^{i0.9270\chi} + 0.3608\, e^{-i0.3484\chi} + 0.1713\, e^{-i1.7984\chi} \\ a_1 = -0.4338\, e^{i0.9270\chi} + 0.1257\, e^{-i0.3484\chi} + 0.3081\, e^{-i1.7984\chi} \\ a_2 = \quad 0.2466\, e^{i0.9270\chi} - 0.4635\, e^{-i0.3484\chi} + 0.2169\, e^{-i1.7984\chi} \end{array} \right\} \tag{4.20}$$

Similarly, one finds for the complete matrix (4.17) the eigenvalues

$$\left. \begin{array}{l} \lambda_0 = -1.0437 \\ \lambda_1 = -0.4880 \\ \lambda_2 = \quad 0.4302 \\ \lambda_3 = \quad 1.3920 \\ \lambda_4 = \quad 2.0633 \end{array} \right\} \tag{4.21}$$

and the matrix U

$$\langle m \mid U \mid n \rangle = \left\{ \begin{array}{rrrrr} 0.5436 & -0.5189 & 0.4681 & -0.3866 & 0.2582 \\ -0.5674 & 0.2532 & 0.2014 & -0.5381 & 0.5328 \\ 0.4795 & 0.2725 & -0.5951 & -0.0218 & 0.5841 \\ -0.3461 & -0.6010 & -0.0981 & 0.5245 & 0.4840 \\ 0.1812 & 0.4808 & 0.6137 & 0.5342 & 0.2721 \end{array} \right\} \quad (4.22)$$

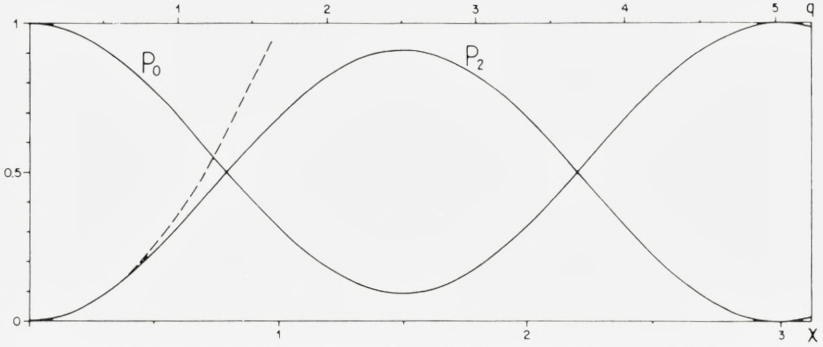


Fig. 2. The result of the two-state calculation for a rotational band on a $0^+$ ground state. The probability for the excitation in the $2^+$ state, $P_2$, and the probability for no excitation, $P_0$, are given as functions of $\chi_{0\to 2}(\vartheta)$ and as a function of the parameter $q(\vartheta)$ characteristic of the rotational model (see Eq. (5.11)). The broken curve shows the result of the first order perturbation calculation.

Figs. 2, 3, and 4 show a very general feature of the multiple excitation process. The excitation probability for a definite state has a maximum as a function of $\chi$. Where this maximum is reached depends on how directly the state is connected with the ground state. The more intermediate states that have to be passed, the higher is the value of $\chi$ for which the maximum is attained. For the rotational band on the $0^+$ ground state, the $2^+$ state is maximally excited for $\chi \simeq 1$, the $4^+$ for $\chi \simeq 2$, the $6^+$ for $\chi \simeq 3$, etc. The heights of the maxima decrease as one passes to higher excited states, partly because a small tail is left in the excitation probability of the lower states. If the band is broken off as in the above calculation, the maximum in the excitation of the last state is much higher than that of any of the others.

A comparison of the curves shows that the deletion of higher states practically does not change the excitation probability of the lower states. This is true at least as long as the last state included is not strongly excited. In Fig. 2, the curve for $P_0$ is thus essentially correct until $\chi = 0.8$. In Fig. 3, the curves for $P_0$ and $P_2$ are similarly correct until $\chi = 1.5$ and, in Fig. 4, one expects $P_0$, $P_2$, $P_4$, and $P_6$ to be correct until $\chi = 3$.

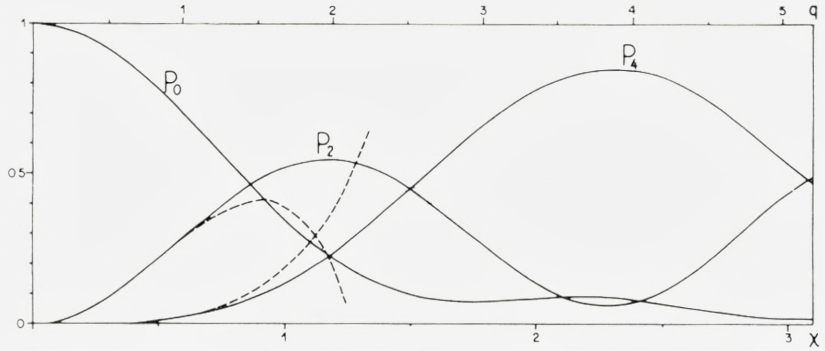


Fig. 3. The result of the three-state calculation for a rotational band on a $0^+$ ground state. The excitation probability in the $2^+$ and $4^+$ states, $P_2$ and $P_4$, and the probability for no excitation, $P_0$, are given as a function of $\chi_{0\to 2}(\vartheta)$ and as a function of the parameter $q(\vartheta)$ characteristic of a rotational model (see Eq. (5.11)). The broken curves show the result of the second order perturbation calculation.

It is interesting to compare the above results with the perturbation calculation. According to the equation (4.9) one finds

$$\left.\begin{aligned} a_0 &= 1 \qquad -0.5000\,\chi(\vartheta)^2 + i\,0.1065\,\chi(\vartheta)^3 + 0.0893\,\chi(\vartheta)^4 - i\,0.0242\,\chi(\vartheta)^5 \\ &\qquad -0.0092\,\chi(\vartheta)^6 \\ a_1 &= -i\,\chi(\vartheta) - 0.3195\,\chi(\vartheta)^2 + i\,0.3571\,\chi(\vartheta)^3 + 0.1210\,\chi(\vartheta)^4 - i\,0.0551\,\chi(\vartheta)^5 \\ a_2 &= \qquad -0.4286\,\chi(\vartheta)^2 + i\,0.1742\,\chi(\vartheta)^3 + 0.1274\,\chi(\vartheta)^4 \\ a_3 &= \qquad\qquad + i\,0.1208\,\chi(\vartheta)^3 \end{aligned}\right\} \quad (4.23)$$

The power expansion in $\chi$ of the excitation probabilities contains (since $\xi = 0$) only even powers of $\chi$. It is noted that, e. g., a third order perturbation calculation leads to the correct answer for $P_6$ to terms of the order of $\chi^6$, while $P_2$ and $P_4$ are correct only to terms of the order of $\chi^4$, and $P_0$ only to terms of the order of $\chi^2$.

In the comparison of the perturbation expansion with the more exact treatment given above, we have calculated the excitation probabilities to second, fourth, and sixth order. In Fig. 2 is shown the calculation to second order (first order perturbation). This gives a good approximation only up to $\chi \simeq 0.4$. In Fig. 3 is shown the calculation to fourth order in $\chi$. This is good up to $\chi \simeq 0.7$. Similarly, the calculation to sixth order in $\chi$ shown on Fig. 4 is seen to be correct only up to $\chi \simeq 1.0$. It thus seems that the perturbation expansion only offers a poor approximation for large values of $\chi$.

The accuracy of the $\chi(\vartheta)$ approximation which we have used can be

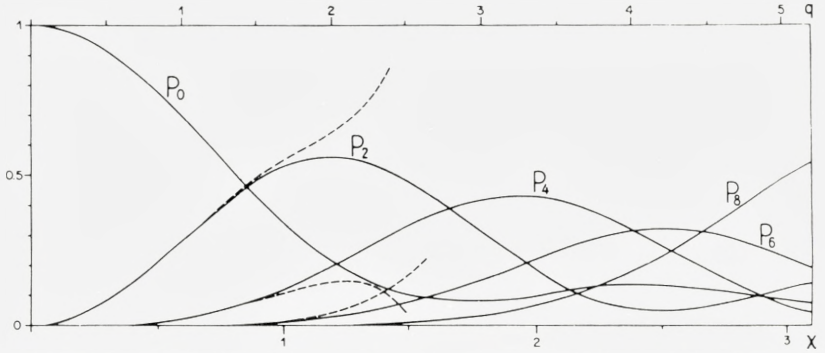


Fig. 4. The result of the five-state calculation for a rotational band on a $0^+$ ground state. The excitation probabilities for the $2^+$, $4^+$, $6^+$ and $8^+$ states $P_2$, $P_4$, $P_6$ and $P_8$, and the probability for no excitation, $P_0$, are given as a function of $\chi_{0\to 2}(\vartheta)$ and as a function of the parameter $q(\vartheta)$ characteristic of a rotational model (see Eq. (5.11)). The broken curves show the result of the third order perturbation calculation.

evaluated by means of Eq. (4.8). We shall only do the explicit calculation in the case of the two-state model (4.12) to (4.16). One finds directly from (4.8) the following expressions to second order in $J_{22}(\vartheta) / J_{20}(\vartheta)$:

$$
\left.
\begin{aligned}
{}'_{22} &= i\chi_{\mathrm{eff}}(\vartheta)\frac{J_{22}(\vartheta)}{J_{20}(\vartheta)}\, e^{-i\frac{\sqrt{5}}{7}\chi_{\mathrm{eff}}(\vartheta)}\left[\sqrt{\frac{3}{2}}\cos\frac{3\sqrt{6}}{7}\chi_{\mathrm{eff}}(\vartheta)+i\frac{\sqrt{5}}{2}\sin\frac{3\sqrt{6}}{7}\chi_{\mathrm{eff}}(\vartheta)\right]\\
{}'_{20} &= a_1^{(0)}-\left(\chi_{\mathrm{eff}}(\vartheta)\frac{J_{22}(\vartheta)}{J_{20}(\vartheta)}\right)^2 e^{-i\frac{\sqrt{5}}{7}\chi_{\mathrm{eff}}(\vartheta)}\left[-\frac{3\sqrt{5}}{7}\cos\frac{3\sqrt{6}}{7}\chi_{\mathrm{eff}}(\vartheta)-i\frac{5\sqrt{6}}{14}\sin\frac{3\sqrt{6}}{7}\chi_{\mathrm{eff}}(\vartheta)\right]\\
{}'_{00} &= a_0^{(0)}-\left(\chi_{\mathrm{eff}}(\vartheta)\frac{J_{22}(\vartheta)}{J_{20}(\vartheta)}\right)^2 e^{-i\frac{\sqrt{5}}{7}\chi_{\mathrm{eff}}(\vartheta)}\left[\frac{3}{2}\cos\frac{3\sqrt{6}}{7}\chi_{\mathrm{eff}}(\vartheta)+i\frac{\sqrt{30}}{4}\sin\frac{3\sqrt{6}}{7}\chi_{\mathrm{eff}}(\vartheta)\right].
\end{aligned}
\right\} \quad (4.24)
$$

In these expressions, $a^{(0)}$ are the amplitudes in the $\chi_{\mathrm{eff}}(\vartheta)$ approximation (4.15).

From (4.24) one obtains the excitation probability

$$
P_2(\vartheta,\chi)=\frac{49}{54}\sin^2\frac{3\sqrt{6}}{7}\chi_{\mathrm{eff}}(\vartheta)+\left(\chi_{\mathrm{eff}}(\vartheta)\frac{J_{22}(\vartheta)}{J_{20}(\vartheta)}\right)^2\left[\frac{5}{6}+\frac{13}{6}\cos^2\frac{3\sqrt{6}}{7}\chi_{\mathrm{eff}}(\vartheta)\right]. \quad (4.25)
$$

One observes that the correction term is an oscillating function of $\chi_{\mathrm{eff}}(\vartheta)$ which has its maxima where $P_2^{(0)}$ shows its minima. The tendency of the correction is thus to fill out the minima of the excitation probability.

To illustrate the magnitude of the correction we have evaluated (4.25)

TABLE 3.

Comparison between the correct excitation probability $P_2(\vartheta, \chi)$ and the $\chi(\vartheta)$ approximation in the two-state model for $\chi = 3$. The quantity $\chi_{\text{eff}}(\vartheta)$ and the probability in the $\chi_{\text{eff}}(\vartheta)$ approximation $P_2(\chi_{\text{eff}}(\vartheta))$ as well as $\chi(\vartheta)$ and the corresponding probability $P_2(\chi(\vartheta))$ are listed for different angles together with $P_2(\vartheta, \chi)$.

| | 180° | 150° | 120° | 90° | 60° | 30° |
|---|---|---|---|---|---|---|
| $P_2(\vartheta, \chi)$ | 0.000 | 0.031 | 0.396 | 0.880 | 0.578 | 0.072 |
| $\chi_{\text{eff}}(\vartheta)$ | 3.000 | 2.820 | 2.315 | 1.698 | 0.859 | 0.256 |
| $P_2(\chi_{\text{eff}}(\vartheta))$ | 0.000 | 0.030 | 0.387 | 0.868 | 0.558 | 0.064 |
| $\chi(\vartheta)$ | 3.000 | 2.820 | 2.318 | 1.709 | 0.880 | 0.272 |
| $P_2(\chi(\vartheta))$ | 0.000 | 0.030 | 0.384 | 0.863 | 0.578 | 0.072 |

numerically in the case of $\chi = 3$, and the result is given in Table 3. One observes here that the maximum correction ($\sim 0.020$) appears for angles between 60 and 90 degrees. This is connected with the fact that $J_{22}(\vartheta)$ is maximal in this range. In the two last rows we have made a comparison with the approximation where $\chi(\vartheta)$ is used instead of $\chi_{\text{eff}}(\vartheta)$. It is seen that this approximation reproduces the correct excitation probability for small angles until the angle which gives the maximum probability. On the other side of the maximum, the $\chi(\vartheta)$ approximation is no improvement over the $\chi_{\text{eff}}(\vartheta)$ approximation.

### C. First Order Expansion in $\xi$

In this paragraph, we shall consider the first order corrections in $\xi$ to the results which were derived earlier in this section.

In Section 3A, we obtained the following expression for the amplitude to first order in $\xi$:

$$\left.\begin{aligned} a_n &= a_n(\xi = 0) \\ &+ \frac{1}{\hbar^2} \langle n \mid e^{-\frac{i}{\hbar}\int_{-\infty}^{\infty} \mathfrak{H}_E(t)\,dt} \int_{-\infty}^{\infty} dt\, t\, e^{\frac{i}{\hbar}\int_{-\infty}^{t} \mathfrak{H}_E(t')\,dt'} [\mathfrak{H}_0, \mathfrak{H}_E(t)]\, e^{-\frac{i}{\hbar}\int_{-\infty}^{t} \mathfrak{H}_E(t')\,dt'} \mid 0 \rangle. \end{aligned}\right\} \quad (4.26)$$

We shall here make the simplifying assumption that $\vartheta = \pi$. One may use the result which we shall obtain, for other angles also, by the usual substitution $\chi \to \chi_{\text{eff}}(\vartheta)$. As was discussed earlier, the approximation is here less accurate than it was in the case of the sudden approximation.

The simplification by considering only terms with $\mu = 0$ in $\mathfrak{H}_E(t)$ is that

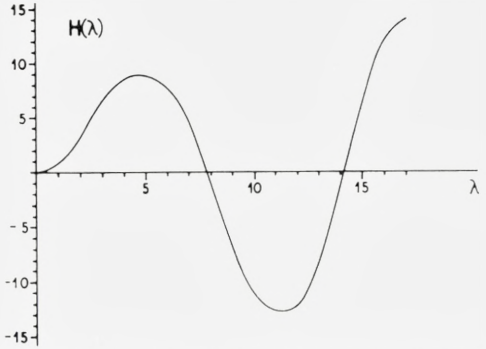


Fig. 5. The function $H(\lambda)$. This function is of importance for the evaluation of the deviation from the sudden approximation in the diagonalization method (see Eq. (4.31)).

the unitary matrix $U$ (see Eqs. (4.2) and (4.3)) diagonalizes not only $\int_{-\infty}^{\infty} \mathfrak{H}_E(t)\,dt$, but also $\int_{-\infty}^{t} \mathfrak{H}_E(t)\,dt$ and $\mathfrak{H}_E(t)$. We thus have

$$\langle n \mid U^\dagger \frac{1}{\hbar} \int_{-\infty}^{t} \mathfrak{H}_E(t)\,dt\, U \mid q \rangle = \lambda_q\, \delta_{qn} \left( \frac{1}{2} + h(t) \right) \tag{4.27}$$

and

$$\langle n \mid U^\dagger \frac{1}{\hbar} \mathfrak{H}_E(t)\, U \mid q \rangle = \lambda_q\, \delta_{qn}\, g(t), \tag{4.28}$$

where

$$h(t) = (S_{E\,2,0}(\vartheta, 0))^{-1} \int_0^t \bar{S}_{20}(t)\,dt \tag{4.29}$$

and

$$g(t) = (S_{E\,2,0}(\vartheta, 0))^{-1}\, \bar{S}_{20}(t). \tag{4.30}$$

The functions $S_{E\,2,0}$ and $\bar{S}_{2,0}$ are defined in Eqs. (3.23) and (3.24), and one sees that $h(t)$ is an odd function while $g(t)$ is an even function of $t$.

By introducing an appropriate number of factors $UU^\dagger$ in (4.26) one may write it in the form

$$\left.\begin{aligned} a_n &= a_n(\xi = 0) \\ &- i \sum_{lm} \langle n \mid U \mid l \rangle\, e^{-i\frac{1}{2}(\lambda_l + \lambda_m)}\, H(\lambda_l - \lambda_m)\, \Xi_{lm} \langle m \mid U^\dagger \mid 0 \rangle, \end{aligned}\right\} \tag{4.31}$$

where the $\Xi$ matrix is the transformed energy matrix

$$\left.\begin{aligned} \Xi_{lm} &= \frac{a}{\hbar v} (U^\dagger \mathfrak{H}_0\, U)_{lm} \\ &= \sum_p \langle l \mid U^\dagger \mid p \rangle \frac{a E_p}{\hbar v} \langle p \mid U \mid m \rangle. \end{aligned}\right\} \tag{4.32}$$


Fig. 6. The excitation probability $P_2\ (\pi, \lambda)$ for backward scattering in the two-state model is shown as a function of $\chi$ for $\xi = 0$ and $\xi = 0.05$.

Since a constant energy will give no contribution, one may replace the energies in (4.32) by the $\xi$'s corresponding to the excitation of the $p$'s state from the ground state, i. e.,

$$\xi_p = \frac{a\,(E_p - E_0)}{\hbar v}\,. \tag{4.33}$$

One thus finds

$$\Xi_{lm} = \sum_p \xi_p \langle p \mid U \mid l \rangle^* \langle p \mid U \mid m \rangle. \tag{4.34}$$

The function $H\,(\lambda)$ which appears in (4.32) is defined by

$$H\,(\lambda) = \frac{v}{a}\,\lambda \int_{-\infty}^{\infty} dt\, t\, g\,(t) \sin\,(\lambda h\,(t)). \tag{4.35}$$

One observes that $H\,(\lambda)$ is a symmetric function of $\lambda$, i.e.,

$$H\,(-\lambda) = H\,(\lambda) \tag{4.36}$$

and that the $\Xi$ matrix is symmetric also in the indices $l$ and $m$.

The function $H\,(\lambda)$ has been evaluated numerically and is given in Fig. 5. For small values of $\lambda$ it is quadratic in $\lambda$, as may be seen from (4.35), and one finds

$$H\,(\lambda) \approx 0.9172\,\lambda^2 \qquad (\lambda \ll 1). \tag{4.37}$$

For larger values of $\lambda$, $H\,(\lambda)$ is an oscillating function whose amplitude increases slowly. From formula (4.31) one may thus draw the general conclusion that the first order correction in $\xi$ is only a slowly increasing (and oscillating) function of $\chi$.

As an illustration we shall apply the result (4.31) to the two-state model.

Using the Eqs. (4.12) to (4.16) one finds the following expression for the excitation probability to first order in $\xi$:

$$P_2 = \frac{49}{54} \sin^2 \frac{3\sqrt{6}}{7} \chi - \xi \frac{49\sqrt{30}}{972} \sin\left(\frac{3\sqrt{6}}{7} \chi\right) H\left(\frac{6\sqrt{6}}{7} \chi\right). \tag{4.38}$$

This result is illustrated in Fig. 6, where the excitation probability for $\xi = 0.05$ is compared to the earlier calculated excitation probability for $\xi = 0$.

## 5. Excitation of Rotational States

In this section we shall treat the excitation of a rotational band. It will be shown that, in the sudden approximation, one can obtain a closed expression for the cross section including all (infinitely many) states in the band. The problem is analogous to the classical problem of a charged ellipsoid which is set in motion by a fast projectile. At the end of the section we shall make some comments on this classical treatment.

### A. Sudden Approximation

We shall assume that we have a pure rotational band and that only this band is involved in the excitation process. The Schrödinger equation (3.1) for the rotational motion may then be written in the form

$$i\hbar \frac{\partial \bar{\psi}}{\partial t} = H_0 \bar{\psi} + H'(t) \bar{\psi}, \tag{5.1}$$

where $\bar{\psi}$ only depends on the Eulerian angles $\alpha$ and $\beta$ describing the orientation of the nuclear symmetry axis. The complete wave function $\psi$ is connected with $\bar{\psi}$ through the equation

$$\psi = e^{-\frac{i}{\hbar} E_{\text{intr}} t} \bar{\psi}(\alpha, \beta, t) \chi(x'), \tag{5.2}$$

where $\chi(x')$ is the intrinsic wave function and $E_{\text{intr}}$ is the intrinsic energy. The free Hamiltonian for the rotation $H_0$ is given by

$$H_0 = -\frac{\hbar^2}{2\Im} \left\{ \frac{\partial^2}{\partial \beta^2} + \cot \beta \frac{\partial}{\partial \beta} + \frac{1}{\sin^2 \beta} \frac{\partial^2}{\partial \alpha^2} \right\}, \tag{5.3}$$

where $\Im$ is the moment of inertia. Since the quadrupole operator can be expressed in terms of the intrinsic quadrupole moment $Q_0$ in the following way:

$$\mathfrak{M}(E2, \mu) = \frac{1}{2} Q_0 Y_{2\mu}(\beta, \alpha), \tag{5.4}$$

the interaction Hamiltonian $H'(t)$ is given by

$$H'(t) = \frac{2\pi Z_1 e^2}{5} Q_0 \sum_{\mu} \bar{S}_{2\mu}(t) Y^*_{2\mu}(\beta, \alpha). \tag{5.5}$$

The evaluation of the excitation amplitudes in the sudden approximation has now been reduced to the calculation of matrix elements of a known operator. We shall specify the eigenstates of $H_0$ by means of the spin $I$, the magnetic quantum number $M$, and the (constant) projection $K$ of the total angular momentum on the nuclear symmetry axis. The wave function may then be written

$$\bar{\psi}_{IMK} = \sqrt{\frac{2I+1}{4\pi}} D^I_{MK}(\alpha, \beta, 0), \tag{5.6}$$

where $D^I_{MK}$ is the rotation matrix. The excitation amplitude on the state specified by $I_f$, $M_f$, and $K$ is then, according to (3.11), (3.24), and (3.27),

$$\left.\begin{aligned} a_{I_f M_f} = \sqrt{\frac{(2I_i+1)(2I_f+1)}{(4\pi)^2}} \int_0^{2\pi} d\alpha \int_0^{\pi} d\beta \sin\beta \, (D^{I_f}_{M_f K}(\alpha, \beta, 0))^* \\ \times D^{I_i}_{M_i K}(\alpha, \beta, 0) \exp\left\{ i \frac{2\pi Z_1 e Q_0}{5 \hbar v a^2} \sum_{\mu}{}' Y_{2\mu}\left(\frac{\pi}{2}, 0\right) J_{2\mu}(\vartheta) Y^*_{2\mu}(\beta, \alpha) \right\}. \end{aligned}\right\} \tag{5.7}$$

We shall now first show that the excitation of any rotational band with ground state spin $I_i$ and final state spin $I_f$ can be expressed by means of the amplitudes for the excitation of a band with ground state spin 0. This follows from (5.7) by expanding the product of the two $D$-functions on $D$-functions. The amplitude (5.7) may then be expressed in the following way:

$$\left.\begin{aligned} a_{I_f M_f} = \sum_I (2I_i+1)^{1/2} (2I_f+1)^{1/2} (2I+1) (-1)^{M_i - K} \\ \times \begin{pmatrix} I_f & I_i & I \\ -M_f & M_i & M_f - M_i \end{pmatrix} \begin{pmatrix} I_f & I_i & I \\ -K & K & 0 \end{pmatrix} A_{I, M_f - M_i}(\vartheta, q), \end{aligned}\right\} \tag{5.8}$$

where we have introduced the functions

$$A_{IM}(\vartheta, q) = [4\pi(2I+1)]^{-1/2} \times \int_0^{2\pi} d\alpha \int_0^{\pi} d\beta \sin\beta\, Y_{IM}(\beta, \alpha)\, e^{i\frac{8\pi}{5} q \sum_{\mu} Y_{2\mu}\left(\frac{\pi}{2}, 0\right) J_{2\mu}(\vartheta)\, Y^*_{2\mu}(\beta, \alpha)} . \tag{5.9}$$

One observes that these functions are proportional to the amplitudes on the state $I, M$ in a rotational band with ground state spin 0, i. e.,

$$A_{IM}(\vartheta, q) = \frac{1}{\sqrt{2I+1}} a_{IM}(I_i = M_i = 0). \tag{5.10}$$

The quantity $q$ is defined by

$$q = \frac{Z_1 e Q_0}{4\hbar v a^2}. \tag{5.11}$$

This quantity is independent of the spins in the rotational band and plays the role of a common $\chi$. It is connected with the $\chi$ corresponding to the first excitation in an even-even nucleus with the same intrinsic quadrupole moment by the relation

$$q = \sqrt{\frac{45}{16}}\, \chi_{0\to 2}. \tag{5.12}$$

The calculation of the excitation cross sections of any rotational band is then reduced to the determination of the functions $A_{I,M}(\vartheta, q)$. From Eq. (5.8) one obtains, e. g., according to (3.42), the following formula for the excitation probability of the state of spin $I_f$:

$$P_{I_f I_i} = (2I_f+1) \sum_{IM} (2I+1) \begin{pmatrix} I_f & I_i & I \\ -K & K & 0 \end{pmatrix}^2 |A_{IM}(\vartheta, q)|^2. \tag{5.13}$$

The functions $A_{I,M}$ can most easily be evaluated in the $\chi(\vartheta)$ approximation where the terms with $|\mu| = 2$ in the exponential function are neglected. The integration over $\alpha$ in (5.9) shows then that $A_{I,M}$ vanishes except for $M = 0$, where one finds

$$A_{I0}(\vartheta, q) \approx A_{I0}(\pi, q_{\text{eff}}(\vartheta)) = e^{i\frac{2}{3} q_{\text{eff}}(\vartheta)} \int_0^1 dx\, P_I(x)\, e^{-2i q_{\text{eff}}(\vartheta) x^2}. \tag{5.14}$$

We have here introduced a quantity

$$q_{\text{eff}}(\vartheta) = \frac{3}{4} J_{20}(\vartheta)\, q \tag{5.15}$$

which corresponds to the $\chi_{\text{eff}}(\vartheta)$ introduced in paragraph 3C. The function

$P_I(x)$ is the Legendre polynomial of order $I$. The integral (5.14) can be expressed in terms of a confluent hypergeometric function ${}_1F_1$ with the following result (see ref. 10, Vol. I, p. 171):

$$A_{I0}(\pi, q) = \frac{\Gamma\left(\frac{I+1}{2}\right)}{2\,\Gamma\left(\frac{2I+3}{2}\right)} e^{-i\frac{4}{3}q} (-2iq)^{\frac{I}{2}} {}_1F_1\left(\frac{I+2}{2}, \frac{2I+3}{2}, 2iq\right). \tag{5.16}$$

The confluent hypergeometric function which appears here can always be expressed by means of Fresnel integrals. For $I = 0$,the expression (5.16) thus takes the simple form (see ref. 10, Vol. I, p. 266)

$$A_{00}(\pi, q) = \sqrt{\frac{\pi}{4q}}\, e^{i\frac{2}{3}q} [C(2q) - iS(2q)], \tag{5.17}$$

where $C(x)$ and $S(x)$ are the Fresnel integrals which are tabulated in refs. 12 and 13.

The functions $A_{I0}$ for higher values of $I$ are most easily obtained by means of recursion formulae. The existence of such relations is guaranteed by the theorem that three confluent hypergeometric functions with parameters differing only by integer numbers are linear dependent. Accordingly, one finds the following recursion formula for the functions $A_{I0}$:

$$\left.\begin{aligned}(I+2)(2I-1)\,A_{I+2,0}(\pi, q) = &\left[\frac{(2I-1)(2I+1)(2I+3)}{4iq} + 2I + 1\right] A_{I0}(\pi, q) \\ &+ (I-1)(2I+3)\,A_{I-2,0}(\pi, q).\end{aligned}\right\} \tag{5.18}$$

For the application of this formula one needs two consecutive $A$'s. Instead of $A_{2,0}$ it is practical to use the non-physical function $A_{-2,0}$ which, according to (5.16), is a simple exponential function

$$A_{-2,0}(\pi, q) = -\frac{1}{4iq} e^{-i\frac{4}{3}q}. \tag{5.19}$$

The functions $A_{I,0}(\pi, q)$ have been computed numerically in this way. The result is given in Table 4.

The excitation probabilities in a rotational band with ground state spin 0 are easily found from these numbers. They are tabulated in Table 5 and the result is shown in Fig. 7.

TABLE 4.

The functions $A_{I,0}(\pi, q)$ for backward scattering. The real part, Re $A_{I,0}$, and the imaginary part, Im $A_{I,0}$, are tabulated as functions of the parameter $q$ for spin values up to 22.

| $q$ | Re $A_{0,0}$ | Im $A_{0,0}$ | Re $A_{2,0}$ | Im $A_{2,0}$ | Re $A_{4,0}$ | Im $A_{4,0}$ |
|---|---|---|---|---|---|---|
| 0.0 | 1.00000 | 0.00000 | 0.00000 | 0.00000 | 0.00000 | 0.00000 |
| 0.5 | 0.95625 | 0.00276 | —0.01228 | —0.12916 | —0.01236 | 0.00150 |
| 1.0 | 0.83311 | 0.02081 | —0.04427 | —0.23461 | —0.04567 | 0.01123 |
| 1.5 | 0.65268 | 0.06336 | —0.08317 | —0.29888 | —0.08980 | 0.03372 |
| 2.0 | 0.44537 | 0.12960 | —0.11265 | —0.31506 | —0.13173 | 0.06754 |
| 2.5 | 0.24234 | 0.20825 | —0.11852 | —0.28773 | —0.15978 | 0.10530 |
| 3.0 | 0.06838 | 0.28073 | —0.09370 | —0.23062 | —0.16731 | 0.13599 |
| 3.5 | —0.06252 | 0.32687 | —0.04075 | —0.16163 | —0.15447 | 0.14879 |
| 4.0 | —0.14819 | 0.33131 | 0.02890 | —0.09722 | —0.12756 | 0.13695 |
| 4.5 | —0.19556 | 0.28834 | 0.09852 | —0.04786 | —0.09629 | 0.10036 |
| 5.0 | —0.21596 | 0.20372 | 0.15132 | —0.01611 | —0.06998 | 0.04592 |
| 5.5 | —0.22000 | 0.09300 | 0.17549 | —0.00242 | —0.05425 | —0.01454 |
| 6.0 | —0.21388 | —0.02302 | 0.16734 | —0.01578 | —0.04929 | —0.06786 |
| 6.5 | —0.19840 | —0.12396 | 0.13171 | 0.03154 | —0.05024 | —0.10350 |
| 7.0 | —0.17046 | —0.19497 | 0.07968 | 0.05327 | —0.04959 | —0.11644 |
| 7.5 | —0.12642 | —0.22953 | 0.02453 | 0.07913 | —0.04044 | —0.10807 |
| 8.0 | —0.06545 | —0.22954 | —0.02240 | 0.10270 | —0.01943 | —0.08498 |
| 8.5 | 0.00816 | —0.20297 | —0.05466 | 0.11574 | 0.01177 | —0.05610 |
| 9.0 | 0.08504 | —0.16012 | —0.07155 | 0.11168 | 0.04694 | —0.02948 |
| 9.5 | 0.15274 | —0.11018 | —0.07677 | 0.08834 | 0.07745 | —0.00979 |
| 10.0 | 0.19925 | —0.05912 | —0.07582 | 0.04909 | 0.09538 | 0.00255 |

(to be continued)

It is interesting to compare these curves with the excitation probabilities which were obtained for the same situation by means of the diagonalization method. It is seen that the excitation curves for the five-state model (see Fig. 4) are in good agreement with the exact calculation for $\chi$ values up to 3. It is interesting that also the secondary maxima of the excitation curves are present in the calculation with infinitely many levels. These secondary maxima which for $P_2$ appear for $q = 5.5$ and $q = 9$ must be understood as rudiments of the secondary maxima in the calculation with a finite number of states. In the two-state calculation the secondary maxima of $P_2$ appear at $q = 7.5$, 12.5, etc. When more states are introduced, these maxima are decreased (and shifted) due to the possibility of exciting the higher states which are introduced. One must expect that the secondary maxima are rather characteristic of the multiple Coulomb excitation of a pure rotational

TABLE 4 (continued).

| $q$ | Re $A_{6,0}$ | Im $A_{6,0}$ | Re $A_{8,0}$ | Im $A_{8,0}$ | Re $A_{10,0}$ | Im $A_{10,0}$ |
|---|---|---|---|---|---|---|
| 0.0 | 0.00000 | 0.00000 | 0.00000 | 0.00000 | 0.00000 | 0.00000 |
| 0.5 | 0.00012 | 0.00087 | 0.00006 | —0.00003 | | |
| 1.0 | 0.00176 | 0.00647 | 0.00074 | —0.00020 | | |
| 1.5 | 0.00813 | 0.01934 | 0.00324 | —0.00143 | —0.00014 | —0.00045 |
| 2.0 | 0.02255 | 0.03862 | 0.00872 | —0.00546 | —0.00104 | —0.00160 |
| 2.5 | 0.04638 | 0.06013 | 0.01724 | —0.01443 | —0.00352 | —0.00400 |
| 3.0 | 0.07751 | 0.07799 | 0.02728 | —0.03002 | —0.00899 | —0.00767 |
| 3.5 | 0.11025 | 0.08694 | 0.03601 | —0.05229 | —0.01881 | —0.01192 |
| 4.0 | 0.13660 | 0.08451 | 0.04021 | —0.07890 | —0.03361 | —0.01518 |
| 4.5 | 0.14878 | 0.07217 | 0.03764 | —0.10527 | —0.05272 | —0.01549 |
| 5.0 | 0.14179 | 0.05491 | 0.02823 | —0.12555 | —0.07385 | —0.01113 |
| 5.5 | 0.11535 | 0.03947 | 0.01454 | —0.13437 | —0.09335 | —0.00157 |
| 6.0 | 0.07426 | 0.03174 | 0.00120 | —0.12857 | —0.10705 | 0.01195 |
| 6.5 | 0.02704 | 0.03448 | —0.00650 | —0.10847 | —0.11151 | 0.02635 |
| 7.0 | —0.01664 | 0.04613 | —0.00457 | —0.07794 | —0.10518 | 0.03733 |
| 7.5 | —0.04883 | 0.06126 | 0.00809 | —0.04338 | —0.08909 | 0.04069 |
| 8.0 | —0.06558 | 0.07250 | 0.02898 | —0.01177 | —0.06674 | 0.03370 |
| 8.5 | —0.06765 | 0.07320 | 0.05252 | 0.01150 | —0.04311 | —0.01632 |
| 9.0 | —0.05967 | 0.05992 | 0.07176 | 0.02413 | —0.02313 | —0.00852 |
| 9.5 | —0.04797 | 0.03368 | 0.08053 | 0.02740 | —0.01011 | —0.03548 |
| 10.0 | —0.03808 | —0.00022 | 0.07552 | 0.02535 | —0.00474 | —0.05831 |

(to be continued)

band, and sensitive to any deviation. The maxima are also, as we shall see, less pronounced for finite $\xi$, and the deviation from the $q(\vartheta)$ approximation will also tend to wash out the oscillations.

The deviation from the $q(\vartheta)$ approximation can be treated by means of the expansion discussed in paragraph 3C. From (3.40), (3.34), (5.4), and (5.12) one finds the amplitude $a_{IM}$ to second order in $J_{22}(\vartheta)/J_{20}(\vartheta)$

$$\left.\begin{aligned} a_{IM} &= a_{IM}^{(0)} \\ &+ i\sqrt{\frac{32\pi}{15}}\, q_{\mathrm{eff}}(\vartheta)\frac{J_{22}(\vartheta)}{J_{20}(\vartheta)} \sum_{I_z M_z \mu=\pm 2}' \langle IM \mid Y_{2\mu}^{*}(\beta,\alpha) \mid I_z M_z \rangle a_{I_z M_z}^{(0)} \\ &- \frac{16\pi}{15}\left(q_{\mathrm{eff}}(\vartheta)\frac{J_{22}(\vartheta)}{J_{20}(\vartheta)}\right)^2 \sum_{I_z M_z \mu,\, \mu'=\pm 2}' \langle IM \mid Y_{2\mu}^{*}(\beta,\alpha)\, Y_{2\mu'}^{*}(\beta,\alpha) \mid I_z M_z \rangle a_{I_z M_z}^{(0)} \end{aligned}\right\} \quad (5.20)$$

where $a^{(0)}$ are the amplitudes in the $q_{\mathrm{eff}}(\vartheta)$ approximation.

The formula (5.20) for the special case of $I_i = M_i = 0$ may, according

TABLE 4 (continued).

| $q$ | Re $A_{12,0}$ | Im $A_{12,0}$ | Re $A_{14,0}$ | Im $A_{14,0}$ | Re $A_{16,0}$ | Im $A_{16,0}$ |
|---|---|---|---|---|---|---|
| 0.0 | | | | | | |
| 0.5 | | | | | | |
| 1.0 | | | | | | |
| 1.5 | | | | | | |
| 2.0 | —0.00025 | 0.00013 | | | | |
| 2.5 | —0.00074 | 0.00072 | | | | |
| 3.0 | —0.00180 | 0.00220 | 0.00040 | 0.00032 | | |
| 3.5 | —0.00330 | 0.00551 | 0.00137 | 0.00079 | 0.00018 | 0.00031 |
| 4.0 | —0.00478 | 0.01151 | 0.00331 | 0.00130 | 0.00033 | —0.00080 |
| 4.5 | —0.00531 | 0.02089 | 0.00691 | 0.00157 | 0.00041 | —0.00197 |
| 5.0 | —0.00358 | 0.03361 | 0.01263 | 0.00096 | 0.00022 | —0.00406 |
| 5.5 | 0.00172 | 0.04865 | 0.02065 | —0.00145 | —0.00071 | —0.00746 |
| 6.0 | 0.01128 | 0.06390 | 0.03052 | —0.00667 | —0.00305 | —0.01228 |
| 6.5 | 0.02462 | 0.07658 | 0.04106 | —0.01541 | —0.00758 | —0.01833 |
| 7.0 | 0.03983 | 0.08387 | 0.05050 | —0.02764 | —0.01492 | —0.02496 |
| 7.5 | 0.05373 | 0.08389 | 0.05682 | —0.04231 | —0.02530 | —0.03100 |
| 8.0 | 0.06255 | 0.07637 | 0.05836 | —0.05723 | —0.03822 | —0.03508 |
| 8.5 | 0.06303 | 0.06298 | 0.05444 | —0.06944 | —0.05230 | —0.03587 |
| 9.0 | 0.05349 | 0.04698 | 0.04574 | —0.07585 | —0.06541 | —0.03266 |
| 9.5 | 0.03460 | 0.03232 | 0.03437 | —0.07411 | —0.07500 | —0.02564 |
| 10.0 | 0.00945 | 0.02241 | 0.02338 | —0.06344 | —0.07872 | —0.01619 |

(to be continued)

to (5.10), be interpreted as an expansion of the function $A_{I,M}$. The specialization $I_i = M_i = 0$ may thus be done without any loss of generality, since the amplitudes for other ground state spins can be computed by means of (5.8). Introducing this simplification we obtain

$$\left.\begin{aligned} A_{I0}(\vartheta, q) = A_{I0}(\pi, q_{\text{eff}}(\vartheta)) - \frac{8}{3}\left(q_{\text{eff}}(\vartheta)\frac{J_{22}(\vartheta)}{J_{20}(\vartheta)}\right)^2 \sum_{I_z I_z'}{}' (2I_z+1)(2I_z'+1) \\ \times \begin{pmatrix} I & 2 & I_z' \\ 0 & 0 & 0 \end{pmatrix}\begin{pmatrix} I & 2 & I_z' \\ 0 & -2 & 2 \end{pmatrix}\begin{pmatrix} I_z' & 2 & I_z \\ 0 & 0 & 0 \end{pmatrix}\begin{pmatrix} I_z' & 2 & I_z \\ -2 & 2 & 0 \end{pmatrix} A_{I_z 0}(\pi, q_{\text{eff}}(\vartheta)) \end{aligned}\right\} \quad (5.21)$$

$$\left.\begin{aligned} A_{I,\pm 2}(\vartheta, q) = i\sqrt{\frac{8}{3}}\, q_{\text{eff}}(\vartheta)\frac{J_{22}(\vartheta)}{J_{20}(\vartheta)} \sum_{I_z}{}' (2I_z+1) \\ \begin{pmatrix} I_z & 2 & I \\ 0 & 0 & 0 \end{pmatrix}\begin{pmatrix} I_z & 2 & I \\ 0 & -2 & 2 \end{pmatrix} A_{I_z 0}(\pi, q_{\text{eff}}(\vartheta)) \end{aligned}\right\} \quad (5.22)$$

TABLE 4 (continued).

| $q$ | Re $A_{18,0}$ | Im $A_{18,0}$ | Re $A_{20,0}$ | Im $A_{20,0}$ | Re $A_{22,0}$ | Im $A_{22,0}$ |
|---|---|---|---|---|---|---|
| 0.0 | | | | | | |
| 0.5 | | | | | | |
| 1.0 | | | | | | |
| 1.5 | | | | | | |
| 2.0 | | | | | | |
| 2.5 | | | | | | |
| 3.0 | | | | | | |
| 3.5 | | | | | | |
| 4.0 | | | | | | |
| 4.5 | −0.00051 | −0.00009 | | | | |
| 5.0 | −0.00114 | −0.00004 | 0.00000 | 0.00027 | | |
| 5.5 | −0.00236 | 0.00027 | 0.00009 | 0.00069 | | |
| 6.0 | −0.00429 | 0.00116 | 0.00037 | 0.00133 | | |
| 6.5 | −0.00706 | 0.00312 | 0.00111 | 0.00240 | 0.00071 | −0.00034 |
| 7.0 | −0.01056 | 0.00672 | 0.00261 | 0.00392 | 0.00130 | −0.00090 |
| 7.5 | −0.01435 | 0.01248 | 0.00530 | 0.00580 | 0.00209 | −0.00199 |
| 8.0 | −0.01768 | 0.02072 | 0.00958 | 0.00774 | 0.00301 | −0.00389 |
| 8.5 | −0.01958 | 0.03125 | 0.01575 | 0.00922 | 0.00384 | −0.00692 |
| 9.0 | −0.01904 | 0.04330 | 0.02382 | 0.00952 | 0.00420 | −0.01133 |
| 9.5 | −0.01540 | 0.05540 | 0.03334 | 0.00788 | 0.00354 | −0.01718 |
| 10.0 | −0.00863 | 0.06564 | 0.04338 | 0.00371 | 0.00128 | −0.02423 |

and

$$\left.\begin{aligned} A_{I,\pm 4}(\vartheta, q) = -\frac{4}{3}\left(q_{\mathrm{eff}}(\vartheta)\frac{J_{22}(\vartheta)}{J_{20}(\vartheta)}\right)^2 \sum_{I_z I_z'}{}' (2I_z+1)(2I_z'+1) \\ \times \begin{pmatrix} I & 2 & I_z' \\ 0 & 0 & 0 \end{pmatrix}\begin{pmatrix} I & 2 & I_z' \\ 4 & -2 & -2 \end{pmatrix}\begin{pmatrix} I_z' & 2 & I_z \\ 0 & 0 & 0 \end{pmatrix}\begin{pmatrix} I_z' & 2 & I_z \\ 2 & -2 & 0 \end{pmatrix} A_{I_z 0}(\pi, q_{\mathrm{eff}}(\vartheta)). \end{aligned}\right\} \quad (5.23)$$

In the excitation probabilities (see Eq. (5.13)) only the squares of the $A_{I,M}$ appear and to second order in $J_{22}(\vartheta)/J_{20}(\vartheta)$ only $A_{I,0}$ and $A_{I,2}$ contribute. The seamplitudes have been calculated numerically for $I = 0,2$, and 4 by means of the known functions $A_{I,0}(\pi, q_{\mathrm{eff}}(\vartheta))$. The probability for the excitation of the states in an even-even nucleus can be written

$$P_I = P_I^{(0)}(q_{\mathrm{eff}}(\vartheta)) + \left(\frac{J_{22}(\vartheta)}{J_{20}(\vartheta)}\right)^2 \Delta_I(q_{\mathrm{eff}}(\vartheta)), \quad (5.24)$$

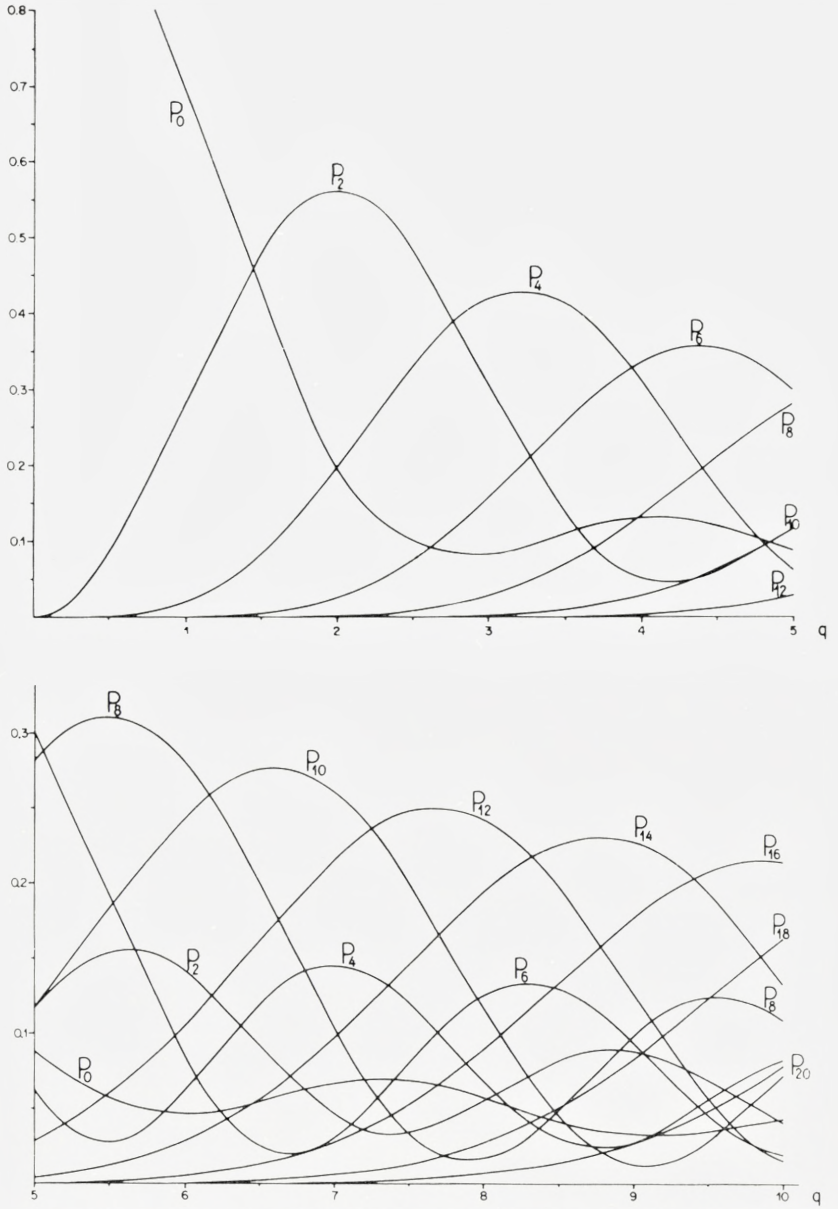


Fig. 7. The multiple Coulomb excitation of a pure rotational band in an even-even nucleus. The excitation probability $P_I$ of the state with spin $I$ is given as a function of the parameter $q$ for backward scattering. The excitation probabilities for other deflection angles and other ground state spins can also be inferred from these curves (see Sect. 5).

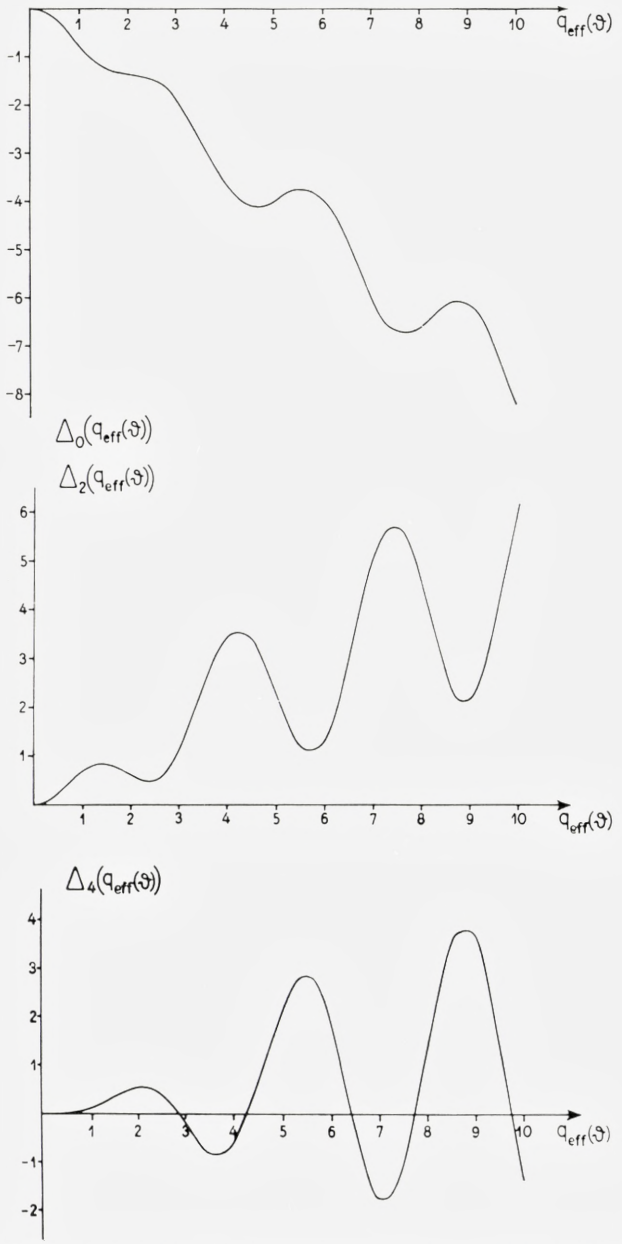


Fig. 8. The coefficients $\Delta_I$ for the correction of the excitation probabilities in the $q_{\text{eff}}(\vartheta)$ approximation. The coefficients $\Delta_I$ (which are defined in Eq. (5.24)) are plotted as functions of $q_{\text{eff}}(\vartheta)$ for the three lowest states $I = 0$, 2, and 4 in a rotational band in an even-even nucleus.

where $P_I^{(0)}$ are the probabilities given in Fig. 7. The coefficients $\Delta_I$ receive a contribution, partly from $A_{I,0}$ partly from $A_{I,2}$. The numerical result for $\Delta_I$ in the cases of $I = 0,2$, and 4 are given in Table 6 and are illustrated in Fig. 8.

It is seen that $\Delta_I$ is an oscillating function of $q_{\text{eff}}(\vartheta)$, and a rough estimate shows that the correction may amount to about 0.1, but usually it will be much smaller. If one compares the curves for $\Delta_I$ and $P_I$, one sees that the tendency of the correction is to fill out the minima of $P_I$. The relative error at the minima of $P_I$ might be rather considerable, as is shown on Fig. 9. The relative error in $P_2$ is here plotted as a function of $q_{\text{eff}}(\vartheta)$ for different angles. The curves end at the value of $q_{\text{eff}}(\vartheta)$ where $q$ reaches the value 10. The maxima on the curves appear as expected at the points where $P_2^{(0)}$ is minimal.

One sees also that for small angles the relative error is rather considerable in the whole range of $q$. This discrepancy can, as was discussed in paragraph 3C, be removed by applying $q(\vartheta)$ defined by

$$q(\vartheta) = q\frac{3}{4}\left[(J_{20}(\vartheta))^2 + 3\,(J_{22}(\vartheta))^2\right]^{1/2} \tag{5.25}$$

instead of $q_{\text{eff}}(\vartheta)$. This approximation will lead to the correct result for angles where the perturbation calculation is applicable. In Fig. 10 we have plotted the relative error of this latter approximation. It is seen that for $q(\vartheta)$ less than 2 one obtains a considerable improvement over the $q_{\text{eff}}(\vartheta)$ approximation (compare Fig. 9). For $q(\vartheta)$ larger than 2, the error is mostly larger than the error of the $q_{\text{eff}}(\vartheta)$ approximation, but it is here not very different from this. As a net result the $q(\vartheta)$ approximation is preferable.

In the case of a pure rotational band, one may calculate the excitation amplitude for arbitrary angles directly from (5.8). This can be done in the following way. We write the exponent in (5.9) explicitly in the form

$$\left.\begin{aligned} &\frac{8\pi}{5}\,q\sum_{\mu}{}' Y_{2\mu}\left(\frac{\pi}{2}, 0\right) J_{2\mu}(\vartheta)\, Y_{2\mu}^{*}(\beta, \alpha) \\ &= q\left[\frac{1}{2}J_{20}(\vartheta)\,(1 - 3\cos^2\beta) + \frac{3}{2}J_{22}(\vartheta)\sin^2\beta\cos 2\alpha\right]. \end{aligned}\right\} \tag{5.26}$$

For the spherical harmonics we use the definition

$$Y_{IM}(\beta, \alpha) = (-1)^M\left[\frac{(2I+1)\,(I-M)!}{4\pi\,(I+M)!}\right]^{\frac{1}{2}} P_I^M(\cos\beta)\, e^{iM\alpha}. \tag{5.27}$$

The integration over $\alpha$ may then be expressed by means of a Bessel function $J_{M/2}$ of order $M/2$ with the following result[10]:

$$\left.\begin{aligned} A_{IM}(\vartheta, q) &= i^{M}\left[\frac{(I-M)!}{(I+M)!}\right]^{\frac{1}{2}} e^{i\frac{1}{2}qJ_{20}(\vartheta)} \\ &\times \int_0^1 dx P_I^M(x) J_{\frac{M}{2}}\left(\frac{3}{2}qJ_{22}(\vartheta)(1-x^2)\right) e^{-i\frac{3}{2}qJ_{20}(\vartheta)x^2}. \end{aligned}\right\} \quad (5.28)$$

This formula applies to $I$ and $M$ even. For $I$ or $M$ odd, $A_{I,M}$ vanishes. One observes furthermore the symmetry relation

$$A_{I,-M}(\vartheta, q) = A_{I,M}(\vartheta, q). \quad (5.29)$$

One may then proceed by using the following integral representation of the Bessel function (see ref. 10, Vol. II, p. 81)

$$J_n(y) = \frac{(y/2)^n}{\Gamma\left(n+\frac{1}{2}\right)\sqrt{\pi}} \int_{-1}^{1} dt\, e^{iyt}(1-t^2)^{n-\frac{1}{2}}. \quad (5.30)$$

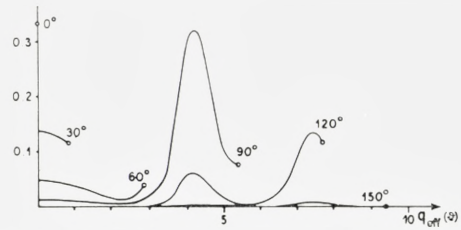


Fig. 9. The relative error of the $q_{\text{eff}}(\vartheta)$ approximation for the excitation of the $2^+$ rotational state in an even-even nucleus. The error $[P_2(\vartheta, q) - P_2(\pi, q_{\text{eff}}(\vartheta))]/P_2(\pi, q_{\text{eff}}(\vartheta))$ is plotted as a function of $q_{\text{eff}}(\vartheta)$ for different angles. The curves end at a value of $q_{\text{eff}}(\vartheta)$ where $q$ reaches the value 10.

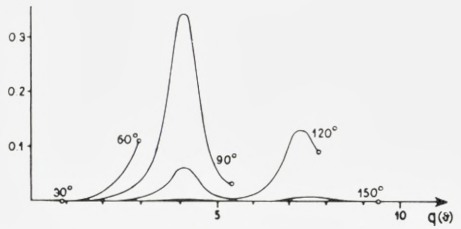


Fig. 10. The relative error of the $q(\vartheta)$ approximation for the excitation of the $2^+$ rotational state in an even-even nucleus. The error $[P_2(\vartheta, q) - P_2(\pi, q(\vartheta))]/P_2(\pi, q(\vartheta))$ is plotted as a function of $q(\vartheta)$ for different angles. The curves end at a value of $q(\vartheta)$ where $q$ reaches the value 10.

The integration over $x$ can be done by expanding the exponential function in power series in $q\,[J_{2,0}(\vartheta)+tJ_{2,2}(\vartheta)]$ (see ref. 10, Vol. I, p. 172). The integration over $t$ can finally be done when the powers of this quantity are expanded according to the binomial formula. The result is a double series

$$\left.\begin{aligned} A_{IM}(\vartheta, q) = {} & \left[\frac{(I+M)!}{(I-M)!}\right]^{\frac{1}{2}} \frac{\Gamma\left(\frac{I-M+1}{2}\right)(-1)^{\frac{I-M}{2}}}{2^{M+1}\,\Gamma\left(\frac{2I+3}{2}\right)\Gamma\left(\frac{M+2}{2}\right)}\, e^{-i\frac{4}{3}q_{\mathrm{eff}}(\vartheta)} \\ & \times \sum_{m,\,n}{}' \frac{\left(\frac{I+M+2}{2}\right)_m \left(-\frac{I-M}{2}-m\right)_{2n}}{\left(\frac{2I+3}{2}\right)_m \left(\frac{M+2}{2}\right)_n} \frac{(2\,iq_{\mathrm{eff}}(\vartheta))^{m+\frac{I}{2}}}{m!}\, \frac{b^{2n+\frac{M}{2}}}{n!}, \end{aligned}\right\} \tag{5.31}$$

where

$$b = \frac{J_{22}(\vartheta)}{2\,J_{20}(\vartheta)}. \tag{5.32}$$

We have furthermore used the notation

$$\alpha_m = \alpha(\alpha+1)\,.\,.\,.\,.\,(\alpha+m-1). \tag{5.33}$$

The formula (5.31) holds for $M \geqslant 0$. The functions $A_{I,M}$ for negative $M$ are determined by means of (5.29).

It is useful to perform the summation over $M$ whereby (5.31) may be written in the form

$$\left.\begin{aligned} A_{IM}(\vartheta, q) = {} & \left[\frac{(I+M)!}{(I-M)!}\right]^{\frac{1}{2}} \frac{\Gamma\left(\frac{I-M+1}{2}\right)}{2^{M+1}\,\Gamma\left(\frac{2I+3}{2}\right)\Gamma\left(\frac{M+2}{2}\right)}\, e^{-i\frac{4}{3}q_{\mathrm{eff}}(\vartheta)} \\ & \times (-2\,iq_{\mathrm{eff}}(\vartheta))^{\frac{I}{2}} (-b)^{\frac{M}{2}} \sum_{n}{}' \frac{b^{2n}}{\left(\frac{M+2}{2}\right)^n n!} (q_{\mathrm{eff}}(\vartheta))^{2n-\frac{I-M}{2}} \\ & \times \frac{d^{2n}}{(dq_{\mathrm{eff}}(\vartheta))^{2n}} \left[(q_{\mathrm{eff}}(\vartheta))^{\frac{I-M}{2}}\, {}_1F_1\left(\frac{I+M+2}{2}, \frac{2I+3}{2}, 2\,iq_{\mathrm{eff}}(\vartheta)\right)\right]. \end{aligned}\right\} \tag{5.34}$$

If one sets $b = 0$ the expressions (5.31) and (5.34) reduce to the simple result (5.16). The expression (5.34) is, similar to (5.20), a systematic expansion in powers of $J_{22}(\vartheta)/J_{20}(\vartheta)$.

### B. First Order Correction in $\xi$

In paragraph 3 A it was outlined how one may calculate the deviation of the excitation amplitudes from the sudden approximation. The result was expressed in a power series in the $\xi$'s which enter into the excitation process. For rotational bands, one may define a common $\xi$ in terms of the moment of inertia in a similar way as, for such spectra, we defined a common $\chi$ in terms of the intrinsic quadrupole moment. We shall use the notation

$$\xi = \frac{3\,\hbar a}{v\Im}, \tag{5.35}$$

where $\Im$ is the moment of inertia entering in (5.3). The quantity (5.35) is identical to the $\xi$ corresponding to the excitation of the lowest rotational state in an even-even nucleus.

The excitation amplitudes which were evaluated in the previous paragraph are essentially complex numbers. The first order corrections must also be expected to be complex, and it follows therefore that the excitation probabilities have linear terms in $\xi$. This is in contrast to the first order perturbation theory which is independent of $\xi$ to first order in this quantity.

To first order, the excitation amplitude $a_n$ may be written in the form

$$a_n = a_n^{(0)} + a_n^{(1)}, \tag{5.36}$$

where $a_n^{(0)}$ is the amplitude (5.7) in the sudden approximation. The first order correction $a_n^{(1)}$ is, according to (3.20), given by

$$\left.\begin{aligned} a_n^{(1)} &= \langle\, n \,|\, e^{-\frac{i}{\hbar}\int_{-\infty}^{\infty} H'(t)\,dt} \,|\, \varphi_1 \,\rangle \\ &= \frac{\xi v}{6\,\hbar a} \langle\, n \,|\, e^{-\frac{i}{\hbar}\int_{-\infty}^{\infty} H'(t)\,dt} \int_{-\infty}^{\infty} e^{\frac{i}{\hbar}\int_{-\infty}^{t} H'(t')\,dt'} t\,[L^2, H'(t)] e^{-\frac{i}{\hbar}\int_{-\infty}^{t} H'(t')\,dt'} dt \,|\, 0 \,\rangle. \end{aligned}\right\} \tag{5.37}$$

In this equation, $H'(t)$ is given by (5.5) and (5.11)

$$H'(t) = \frac{8\pi\hbar v a^2}{5} q \sum_{\mu} \bar{S}_{2\mu}(t)\, Y_{2\mu}^{*}(\beta, \alpha), \tag{5.38}$$

while $H_0$ (see Eq. (5.3)) has been expressed by means of $\xi$ and the angular momentum operator $L$ through

$$H_0 = \frac{\hbar v}{6\,a} \xi L^2. \tag{5.39}$$

For the evaluation of (5.37) we shall proceed in the following way: Firstly, the differentiations of the operator $L^2$ are performed. Hereby the two exponential functions in $|\varphi_1\rangle$ will cancel. The expression for $|\varphi_1\rangle$ will then be suitable for an expansion in terms of the eigenfunctions $|m\rangle$ of $H_0$, and the problem is reduced to the already performed calculation of matrix elements in the sudden approximation.

The result of the first step in this program can be written in the form

$$\left.\begin{aligned} |\varphi_1\rangle = &-i\frac{8\pi}{5} q\xi \sum_\mu f_\mu Y^*_{2\mu}(\beta,\alpha)\,|0\rangle \\ &-\frac{8\pi}{15} q\xi \sum_\mu f_\mu \left(\frac{\partial Y^*_{2\mu}}{\partial\beta}\cdot\frac{\partial}{\partial\beta}+\frac{1}{\sin^2\beta}\frac{\partial Y^*_{2\mu}}{\partial\alpha}\frac{\partial}{\partial\alpha}\right)|0\rangle \\ &+i\frac{61\pi^2}{75} q^2\xi \sum_{\mu\mu'} f_{\mu\mu'}\left(\frac{\partial Y^*_{2\mu}}{\partial\beta}\frac{\partial Y^*_{2\mu'}}{\partial\beta}+\frac{1}{\sin^2\beta}\frac{\partial Y^*_{2\mu}}{\partial\alpha}\frac{\partial Y^*_{2\mu'}}{\partial\alpha}\right)|0\rangle, \end{aligned}\right\} \quad (5.40)$$

where the coefficients $f_\mu$ and $f_{\mu\mu'}$ are defined by

$$f_\mu = iv^2 a\int_{-\infty}^{\infty} t\,\bar{S}_{2\mu}(t)\,dt \quad (5.41)$$

and

$$f_{\mu\mu'} = v^3 a^3 \int_{-\infty}^{\infty} \bar{S}_{2\mu}(t)\, t \int_{-\infty}^{t} \bar{S}_{2\mu'}(t')\,dt'\,dt. \quad (5.42)$$

From the symmetries of the $\bar{S}_{2,\mu}(t)$ (see Eq. (3.23)) one sees immediately that $f_1 = f_{-1}$ is the only non-vanishing $f_\mu$. The first two terms of (5.40) also appear in the first order perturbation treatment while the third, which is proportional to $q^2$, is characteristic of higher order excitations. The second term arises from the initial motion of the rotator, and it disappears for the ground-state spin $I = 0$.

For the evaluation of (5.40) one has to use the properties of the eigenfunctions $|0\rangle$ which are given in terms of the $D$-function in (5.6). We note the following formula

$$\left.\begin{aligned} &2\left[\frac{\partial D^I}{\partial\beta}\frac{\partial D^{I'}}{\partial\beta}+\frac{1}{\sin^2\beta}\frac{\partial D^I}{\partial\alpha}\frac{\partial D^{I'}}{\partial\alpha}\right] \\ &= D_I L^2(D^{I'}) + D^{I'} L^2(D^I) - L^2(D^I D^{I'}) \\ &= (I(I+1)+I'(I'+1)-L^2)\,D^I D^{I'}, \end{aligned}\right\} \quad (5.43)$$

where we have suppressed the lower indices $M$ and $K$ on the $D$ functions. By means of this formula the problem of expanding $|\varphi_1\rangle$ in terms of $|m\rangle$ is reduced to the problem of expanding a product of $D$ functions in terms of $D$ functions.

The result can be expressed by means of the functions $A_{IM}$ defined in (5.9) in the following way:

$$\left.\begin{aligned} a^{(1)}_{I_f M_f} = &-\sqrt{\frac{16\pi}{5}}\, q\, \xi \sum_{II'M\mu=\pm 1} f_\mu(\vartheta)\left[1+\frac{1}{6}I_i(I_i+1)-\frac{1}{6}I'(I'+1)+i\right] \\ &\times (2I_i+1)^{\frac{1}{2}}(2I_f+1)^{\frac{1}{2}}(2I+1)(2I'+1) \\ &\times \begin{pmatrix} 2 & I_i & I' \\ -\mu & M_i & \mu - M_i \end{pmatrix}\begin{pmatrix} 2 & I_i & I' \\ 0 & K & -K \end{pmatrix}\begin{pmatrix} I_f & I' & I \\ -M_f & \mu - M_i & M \end{pmatrix}\begin{pmatrix} I_f & I' & I \\ -K & K & 0 \end{pmatrix} A_{IM}(\vartheta, q) \\ &+ i\frac{8\pi}{15}\, q^2\, \xi \sum_{II'Mlm} (-1)^m f^l_m(\vartheta)(2I_i+1)^{\frac{1}{2}}(2I_f+1)^{\frac{1}{2}}(2I+1)(2I'+1) \\ &\times \begin{pmatrix} l & I_i & I' \\ -m & M_i & m - M_i \end{pmatrix}\begin{pmatrix} l & I_i & I' \\ 0 & K & -K \end{pmatrix}\begin{pmatrix} I_f & I' & I \\ -M_f & m - M_i & M \end{pmatrix}\begin{pmatrix} I_i & I' & I \\ -K & K & 0 \end{pmatrix} A_{IM}(\vartheta, q) \end{aligned}\right\} \quad (5.44)$$

We have here introduced the notation

$$f^l_m(\vartheta) = (2l+1)\begin{pmatrix} 2 & 2 & l \\ 0 & 0 & 0 \end{pmatrix}[12 - l(l+1)] \sum_{\mu\mu'} \begin{pmatrix} 2 & 2 & l \\ \mu & \mu' & m \end{pmatrix} f_{\mu\mu'} \quad (5.45)$$

for the tensors of rank 0,2, and 4 which can be built up of the $f_{\mu\mu'}$, given by (5.42).

The coefficients $f_\mu(\vartheta)$ and $f^l_m(\vartheta)$ which are necessary for the evaluation of $a^{(1)}$ have been computed for a few angles and the result is given in Table 7. We note the following property of the $f^l_m$ functions:

$$f^l_{-m}(\vartheta) = f^l_m(\vartheta). \quad (5.46)$$

The $f^l_m$ functions for odd values of $m$ may be expressed by means of $f_1$ and the functions $J_{2,\mu}(\vartheta)$ defined by (3.27):

$$f^2_1(\vartheta) = \quad i\frac{3\sqrt{5}}{28\sqrt{\pi}} f_1[3J_{22}(\vartheta) + J_{20}(\vartheta)] \quad (5.47)$$

$$f^4_1(\vartheta) = -i\frac{3\sqrt{3}}{7\sqrt{2\pi}} f_1[2J_{20}(\vartheta) - J_{22}(\vartheta)] \quad (5.48)$$

$$f^4_3(\vartheta) = \quad i\frac{3\sqrt{3}}{\sqrt{14\pi}} f_1 J_{22}(\vartheta). \quad (5.49)$$

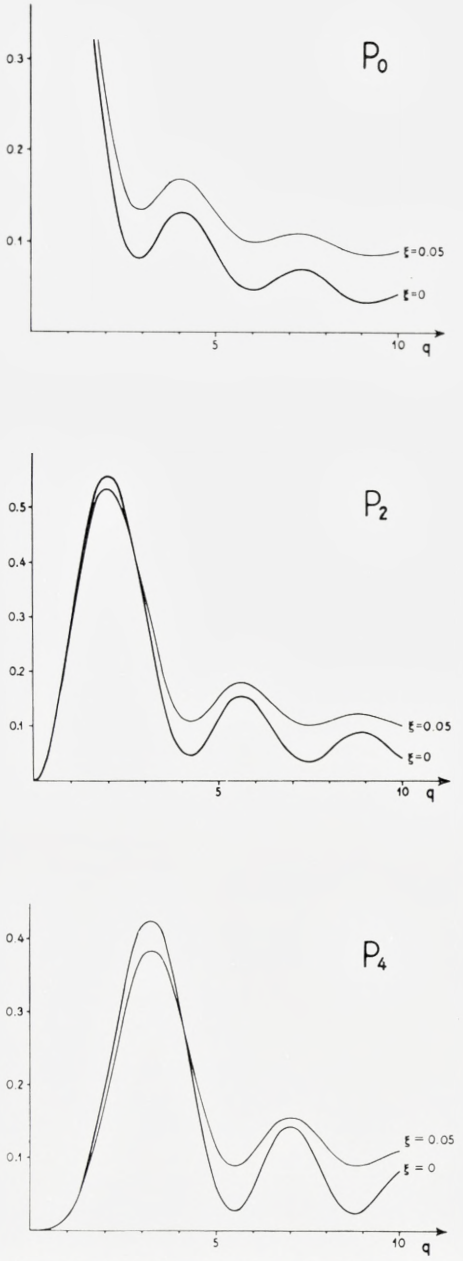


Fig. 11. The first order correction in $\xi$ for the excitation of a rotational band in an even-even nucleus. The curves show the excitation probabilities of the states of spin 2 ($P_2$) and of spin 4 ($P_4$) and the probability that the nucleus stays in its ground state ($P_0$). The probabilities are given as functions of $q$ for backward scattering and for the cases $\xi = 0$ and $\xi = 0.05$.

For backward scattering the only non-vanishing $f$-functions are $f_0^0$, $f_0^2$, and $f_0^4$. This is a consequence of the fact that all $f_\mu$ and $f_{\mu\mu'}$ of Eqs. (5.41) and (5.42) vanish, except $f_{00}$.

We shall here illustrate the first order correction in $\xi$ by considering the special case of backward scattering on an even-even nucleus. In this case, the only non-vanishing amplitude $a^{(1)}$ is

$$\left.\begin{aligned} a_{I_f 0}^{(1)} &= i\frac{8\pi}{15} q^2 \xi (2I_f+1)^{\frac{1}{2}} f_0^0(\pi) \sum_I (2I+1) \\ &\times \left\{ \begin{pmatrix} 0 & I_f & I \\ 0 & 0 & 0 \end{pmatrix}^2 + \begin{pmatrix} 2 & I_j & I \\ 0 & 0 & 0 \end{pmatrix}^2 + \begin{pmatrix} 4 & I_f & I \\ 0 & 0 & 0 \end{pmatrix}^2 \right\} A_{I0}(\pi, q). \end{aligned}\right\} \quad (5.50)$$

We have here used that $f_0^2(\pi) = 5/7\, f_0^0(\pi)$ and $f_0^4(\pi) = -12/7\, f_0^0(\pi)$ which follows from the definition (5.45). The excitation probabilities to first order in $\xi$ may be written in the form

$$P_I(\pi, q) = P_I(\xi = 0) + \Lambda_I(q)\, \xi. \quad (5.51)$$

The coefficient $\Lambda_I(q)$ has been evaluated numerically and is given in Table 8. It is seen that $\Lambda_I$ is an oscillating function of $q$ which is of the order of magnitude 1. The corrections for $\xi \neq 0$ are thus not dominated by the factor $q^2$ in (5.50). The oscillations in $\Lambda_I$ follow the oscillations of $P_I(\xi = 0)$ in such a way that the first maximum of $P_I$ is cut down, while the excitation probability for larger values of $q$ is increased. This increment is largest at the minima of $P_I$ and the effect of $\xi \neq 0$ is thus essentially to smooth out the whole excitation curve. This is clearly seen on Fig. 11 where the excitation probabilities for $I = 0$, 2, and 4 and $\xi = 0.05$ are compared with the excitation probabilities for $\xi = 0$.

For other deflection angles one may use the $q_{\text{eff}}(\vartheta)$ approximation. One must here substitute only the $q$ in $A_{I0}(\pi, q)$ with $q_{\text{eff}}(\vartheta)$. Furthermore, the $f_0^0(\pi)$ should be replaced by $f_0^0(\vartheta)$. As was discussed earlier, this approximation is much less accurate here than in the sudden approximation. An indication of the accuracy can be obtained by comparing the limiting case of (5.50) for $q \ll 1$ with the second order perturbation calculation performed in ref. 14. This comparison shows that the approximation should not be applied for angles less than 90 degrees.

The failure of the $q_{\text{eff}}(\vartheta)$ approximation for $\xi \neq 0$ is due to the fact that the relative importance of the different coefficients $f_m^l(\vartheta)$ in (5.44) for angles smaller than 90 degrees is completely different from the relative importance

in the neighbourhood of 180 degrees where only $f_{00}$ is different from zero. This means that one has to take into account also the amplitudes on the states with magnetic quantum number $M \neq 0$.

For $\xi \neq 0$, one observes from (5.44) that also the states with magnetic quantum numbers which differ by an odd integer from the magnetic quantum number of the ground state are populated. The amplitude on these states will be proportional to $\xi f_1(\vartheta)$ and the excitation probability will thus only receive a contribution of the order $\xi^2$ from such terms.

### C. Numerical Results

In this paragraph we shall collect the numerical results which have been obtained for the excitation of rotational states together with some formulae which facilitate the application of these results to the experiments.

It is thus convenient to write the important parameters directly as functions of the energy of the incident projectile in the laboratory system (see ref. 1, Chapter II C). We shall here quote the expression for half the distance of closest approach in a head-on collision

$$a = 0.07199\left(1+\frac{A_1}{A_2}\right)\frac{Z_1 Z_2}{E_{\mathrm{MeV}}}\times 10^{-12}\,\mathrm{cm}. \tag{5.52}$$

Here, $A_1, Z_1$ and $A_2, Z_2$ are the mass numbers and charges of projectile and target nucleus, respectively. The quantity $E_{\mathrm{MeV}}$ is the bombarding energy expressed in MeV.

The parameter $\xi$ is similarly given by

$$\xi_{1\to 2} = \frac{Z_1 Z_2 A_1^{\frac{1}{2}} \Delta E'_{\mathrm{MeV}}}{12.65\left(E_{\mathrm{MeV}}-\frac{1}{2}\Delta E'_{\mathrm{MeV}}\right)^{3/2}}, \tag{5.53}$$

where $\Delta E'$ is connected with the energy difference $E_2 - E_1$ by the relation

$$\Delta E' = \left(1+\frac{A_1}{A_2}\right)(E_2 - E_1). \tag{5.54}$$

An expression for the parameter $\chi$ (in the case $\lambda = 2$) is found by inserting (5.52) in (2.11), i. e.,

$$\chi_{1\to 2} = 14.52 \frac{A_1^{\frac{1}{2}} [B(E2, I_1 \to I_2)]^{1/2}}{(1 + A_1/A_2)^2 Z_1 Z_2^2} E_{\mathrm{MeV}}^{3/2}. \tag{5.55}$$

The reduced transition probability $B(E2)$ is here measured in units of $e^2 \cdot 10^{-48}\,\mathrm{cm}^4$.

For the excitation of rotational states we have introduced two parameters which are related to $\chi_{1\to 2}$ and $\xi_{1\to 2}$ and are defined in terms of the nuclear moments, so that they are independent of the spin sequence in the rotational bands. We have thus (see Eq. (5.35)) defined a common $\xi$ in terms of the moment of inertia $\Im$ by means of (5.53) where

$$\Delta E' = \left(1 + \frac{A_1}{A_2}\right)\left(\frac{3\,\hbar}{\Im}\right)_{\mathrm{MeV}}. \tag{5.56}$$

For an even-even nucleus this $\xi$ is identical with the $\xi_{0\to 2}$ for the excitation of the lowest rotational state.

We have furthermore defined a quantity $q$ by means of the intrinsic quadrupole moment $Q_0$ in the following way (see Eq. (5.11)):

$$q = 7.6241 \frac{A_1^{\frac{1}{2}} Q_0}{(1 + A_1/A_2)^2 Z_1 Z_2^2} E_{\mathrm{MeV}}^{3/2}, \tag{5.57}$$

where $Q_0$ is measured in units of $e \cdot 10^{-24}\,\mathrm{cm}^2$. The quantity $q$ is related to the $\chi$ for the excitation of the lowest state in an even-even nucleus by Eq. (5.12).

The differential Coulomb excitation cross section is given by (3.43) through the excitation probability $P_{I_f,\, I_i}(\vartheta, q, \xi)$ which is the probability that the nucleus is excited from the ground state with spin $I_i$ into the state with spin $I_f$ when the projectile moves in an orbit with deflection angle $\vartheta$ in the center of mass system.

The probabilities $P$ as well as other quantities interesting for the experiments can be obtained from the excitation amplitudes (see Eq. (3.42)). For $\xi \ll 1$ the amplitudes $a_{I_f,\, M_f}(\vartheta, q, \xi)$ are easily obtainable from the functions $A_{IM}(\vartheta, q)$ (see Eq. (5.8)). These functions can in turn be expressed by the functions $A_{I0}(\pi, q)$ which are related to the amplitudes for the excitation of rotational states in an even-even nucleus for $\vartheta = \pi$ and $\xi = 0$ by means of (5.10). These fundamental quantities have been calculated according to the formulae given in paragraph 5 A, and the result is given in Table 4.

For other deflection angles, the functions $A_{IM}(\vartheta, q)$ can be obtained to a good approximation from those tabulated by means of Eqs. (5.21) to (5.23) which we shall quote here for the cases $M = 0$ and $M = \pm 2$:

$$\begin{aligned} A_{I0} = A_{I0}(\pi, q_{\text{eff}}) - \left(q_{\text{eff}} \frac{J_{22}(\vartheta)}{J_{20}(\vartheta)}\right)^2 \Bigg\{ & \frac{(I-3)(I-2)(I-1)I}{(2I-5)(2I-3)(2I-1)(2I+1)} A_{I-4,0}(\pi, q_{\text{eff}}) \\ & - \frac{4(I-1)I[(I-1)I-4]}{(2I-5)(2I-1)(2I+1)(2I+3)} A_{I-2,0}(\pi, q_{\text{eff}}) \\ & + \frac{2[3I^2(I+1)^2 - 14I(I+1)+12]}{(2I-3)(2I-1)(2I+3)(2I+5)} A_{I,0}(\pi, q_{\text{eff}}) \\ & - \frac{4(I+1)(I+2)[(I+1)(I+2)-4]}{(2I-1)(2I+1)(2I+3)(2I+7)} A_{I+2,0}(\pi, q_{\text{eff}}) \\ & + \frac{(I+1)(I+2)(I+3)(I+4)}{(2I+1)(2I+3)(2I+5)(2I+7)} A_{I+4,0}(\pi, q_{\text{eff}}) \Bigg\} \end{aligned} \tag{5.58}$$

and

$$\begin{aligned} A_{I,\pm 2} = iq_{\text{eff}} \frac{J_{22}(\vartheta)}{J_{20}(\vartheta)} [(I-1)I(I+1)(I+2)]^{\frac{1}{2}} \Bigg\{ & \frac{1}{(2I-1)(2I+1)} A_{I-2,0}(\pi, q_{\text{eff}}) \\ & - \frac{2}{(2I-1)(2I+3)} A_{I,0}(\pi, q_{\text{eff}}) + \frac{1}{(2I+1)(2I+3)} A_{I+2,0}(\pi, q_{\text{eff}}) \Bigg\}. \end{aligned} \tag{5.59}$$

In these equations, $q_{\text{eff}}(\vartheta)$ is given by (5.15). The ratio $q_{\text{eff}}(\vartheta)/q$ is shown in Table 2 where also the ratio $J_{22}(\vartheta)/J_{20}(\vartheta)$ has been tabulated.

The excitation amplitudes for arbitrary spin sequence in the rotational band is given by Eq. (5.8). The first order correction in the amplitude for $\xi \neq 0$ is expressed by means of the $A_{I,M}(\vartheta, q)$ in Eq. (5.44). We shall in this paragraph only consider the application of $A_{I,M}(\vartheta, q)$ for the evaluation of the excitation probability $P_{I_f, I_i}(\vartheta, q, \xi)$.

In the simplest case of the excitation of a rotational band in an even-even nucleus for $\xi = 0$ and $\vartheta = \pi$, the excitation probabilities $P_I(q) = P_{I,0}(\pi, q, 0)$ are given by

$$P_I(q) = (2I+1) \mid A_{I,0}(\pi, q) \mid^2. \tag{5.60}$$

These probabilities have been evaluated in Table 5, and they are plotted in Fig. 7.

For other deflection angles the probability can be obtained from (5.58) and (5.59). To second order in $J_{22}(\vartheta)/J_{20}(\vartheta)$ it may be written

$$P_{I,0}(\vartheta, q, 0) = P_I(q_{\text{eff}}(\vartheta)) + \left(\frac{J_{22}(\vartheta)}{J_{20}(\vartheta)}\right)^2 \Delta_I(q_{\text{eff}}(\vartheta)). \tag{5.61}$$

TABLE 5.

The probabilities for excitation of the rotational states in an even-even nucleus. The result which is given for backward scattering and $\xi = 0$ is tabulated as a function of $q$ and of the spin of the excited state. The excitation probability for other deflection angles and other spins can easily be inferred from these numbers.

| $q$ | $P_0$ | $P_2$ | $P_4$ | $P_6$ | $P_8$ | $P_{10}$ | $P_{12}$ |
|---|---|---|---|---|---|---|---|
| 0.0 | 1.0000 | 0.0000 | 0.0000 | 0.0000 | 0.0000 | 0.0000 | 0.0000 |
| 0.5 | 0.9144 | 0.0842 | 0.0014 | | | | |
| 1.0 | 0.6945 | 0.2850 | 0.0199 | 0.0006 | | | |
| 1.5 | 0.4300 | 0.4812 | 0.0828 | 0.0057 | 0.0002 | | |
| 2.0 | 0.2152 | 0.5597 | 0.1972 | 0.0260 | 0.0018 | 0.0001 | |
| 2.5 | 0.1021 | 0.4842 | 0.3296 | 0.0750 | 0.0086 | 0.0006 | |
| 3.0 | 0.0835 | 0.3098 | 0.4184 | 0.1572 | 0.0280 | 0.0029 | 0.0002 |
| 3.5 | 0.1108 | 0.1389 | 0.4140 | 0.2563 | 0.0685 | 0.0104 | 0.0010 |
| 4.0 | 0.1317 | 0.0514 | 0.3152 | 0.3354 | 0.1333 | 0.0286 | 0.0039 |
| 4.5 | 0.1214 | 0.0600 | 0.1741 | 0.3555 | 0.2125 | 0.0634 | 0.0116 |
| 5.0 | 0.0881 | 0.1158 | 0.0630 | 0.3006 | 0.2815 | 0.1171 | 0.0285 |
| 5.5 | 0.0571 | 0.1540 | 0.0284 | 0.1932 | 0.3105 | 0.1831 | 0.0593 |
| 6.0 | 0.0463 | 0.1412 | 0.0633 | 0.0848 | 0.2810 | 0.2436 | 0.1053 |
| 6.5 | 0.0547 | 0.0917 | 0.1191 | 0.0250 | 0.2007 | 0.2757 | 0.1618 |
| 7.0 | 0.0671 | 0.0459 | 0.1442 | 0.0312 | 0.1036 | 0.2616 | 0.2155 |
| 7.5 | 0.0687 | 0.0343 | 0.1198 | 0.0798 | 0.0331 | 0.2014 | 0.2481 |
| 8.0 | 0.0570 | 0.0552 | 0.0684 | 0.1242 | 0.0166 | 0.1174 | 0.2436 |
| 8.5 | 0.0413 | 0.0819 | 0.0296 | 0.1292 | 0.0491 | 0.0446 | 0.1985 |
| 9.0 | 0.0329 | 0.0879 | 0.0276 | 0.0930 | 0.0974 | 0.0128 | 0.1267 |
| 9.5 | 0.0355 | 0.0685 | 0.0549 | 0.0447 | 0.1230 | 0.0286 | 0.0560 |
| 10.0 | 0.0432 | 0.0408 | 0.0819 | 0.0189 | 0.1079 | 0.0719 | 0.0148 |

(to be continued)

The coefficient $\Delta_I(\vartheta)$ has been evaluated numerically for $I = 0,2$, and 4 and the result is given in Table 6 and Fig. 8.

In many cases a simpler approximation for $P_{I,0}(\vartheta, q, 0)$ will be quite adequate, namely the $q(\vartheta)$ approximation. In this approximation the excitation probability is given by

$$P_{I,0}(\vartheta, q, 0) \approx P_I(q(\vartheta)), \tag{5.62}$$

where the quantity $q(\vartheta)$ is defined by (5.25). The ratio $q(\vartheta) / q$ is given in Table 2. The accuracy of the approximation (5.62) is illustrated in Fig. 10.

As an illustration of the application of (5.62) the differential and total cross sections have been evaluated for the case $q = 3$, and the result is given in Fig. 12. While the cross sections for all higher states tend towards zero for small deflection angles, the excitation of the $I = 2$ state reaches a finite

TABLE 5 (continued).

| $q$ | $P_{14}$ | $P_{16}$ | $P_{18}$ | $P_{20}$ | $P_{22}$ | $P_{24}$ | $P_{26}$ |
|---|---|---|---|---|---|---|---|
| 0.0 | 0.0000 | 0.0000 | 0.0000 | 0.0000 | 0.0000 | 0.0000 | 0.0000 |
| 0.5 | 0.0000 | | | | | | |
| 1.0 | 0.0000 | | | | | | |
| 1.5 | 0.0000 | | | | | | |
| 2.0 | 0.0000 | | | | | | |
| 2.5 | 0.0000 | | | | | | |
| 3.0 | 0.0000 | | | | | | |
| 3.5 | 0.0001 | | | | | | |
| 4.0 | 0.0004 | | | | | | |
| 4.5 | 0.0014 | 0.0001 | | | | | |
| 5.0 | 0.0046 | 0.0007 | | | | | |
| 5.5 | 0.0124 | 0.0018 | 0.0002 | | | | |
| 6.0 | 0.0283 | 0.0053 | 0.0007 | 0.0001 | | | |
| 6.5 | 0.0558 | 0.0130 | 0.0022 | 0.0003 | | | |
| 7.0 | 0.0961 | 0.0279 | 0.0058 | 0.0009 | 0.0001 | | |
| 7.5 | 0.1455 | 0.0529 | 0.0134 | 0.0025 | 0.0004 | | |
| 8.0 | 0.1938 | 0.0888 | 0.0274 | 0.0062 | 0.0011 | 0.0002 | |
| 8.5 | 0.2258 | 0.1327 | 0.0503 | 0.0136 | 0.0028 | 0.0004 | 0.0001 |
| 9.0 | 0.2275 | 0.1764 | 0.0828 | 0.0270 | 0.0066 | 0.0013 | 0.0002 |
| 9.5 | 0.1935 | 0.2073 | 0.1223 | 0.0481 | 0.0138 | 0.0031 | 0.0005 |
| 10.0 | 0.1326 | 0.2132 | 0.1622 | 0.0777 | 0.0265 | 0.0069 | 0.0014 |

TABLE 6.

The coefficient $\Delta_I(q)$ for the correction of the $q_{\text{eff}}(\vartheta)$ approximation (see Eq. (5.61)), in the case of a rotational band in an even-even nucleus for $\xi = 0$. The result is given for the states of spin $I = 0$, 2, and 4 as a function of $q$.

| $q$ | $\Delta_0$ | $\Delta_2$ | $\Delta_4$ | $q$ | $\Delta_0$ | $\Delta_2$ | $\Delta_4$ |
|---|---|---|---|---|---|---|---|
| 0.0 | 0.000 | 0.000 | 0.000 | 5.5 | —3.756 | 1.178 | 2.844 |
| 0.5 | —0.247 | 0.239 | 0.008 | 6.0 | —3.960 | 1.387 | 1.766 |
| 1.0 | —0.787 | 0.678 | 0.103 | 6.5 | —4.841 | 3.078 | —0.349 |
| 1.5 | —1.225 | 0.821 | 0.347 | 7.0 | —5.993 | 5.048 | —1.746 |
| 2.0 | —1.381 | 0.585 | 0.561 | 7.5 | —6.712 | 5.700 | —1.046 |
| 2.5 | —1.477 | 0.490 | 0.404 | 8.0 | —6.654 | 4.538 | 1.409 |
| 3.0 | —1.887 | 1.120 | —0.206 | 8.5 | —6.195 | 2.733 | 3.639 |
| 3.5 | —2.712 | 2.390 | —0.796 | 9.0 | —6.120 | 2.156 | 3.664 |
| 4.0 | —3.608 | 3.441 | —0.610 | 9.5 | —6.898 | 3.655 | 1.329 |
| 4.5 | —4.084 | 3.787 | 0.630 | 10.0 | —8.213 | 6.188 | —1.379 |
| 5.0 | —4.000 | 2.263 | 2.214 | | | | |

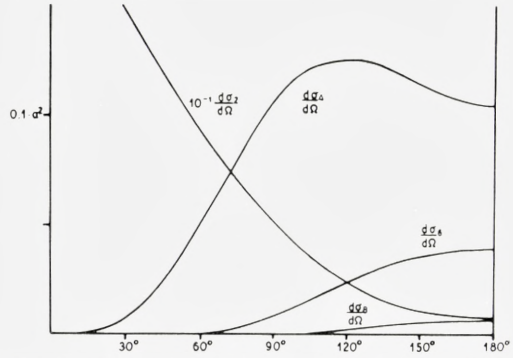


Fig. 12. The differential cross sections for multiple Coulomb excitation of a rotational band in an even-even nucleus for $q = 3$. The curves show the cross sections $d\sigma_I/d\Omega$ for the excitation of the state with spin $I$ in the sudden approximation in units of $a^2$. The curve for the first excited state has been scaled down by a factor 10.

value for $\vartheta = 0°$. This is seen from the perturbation expression which is valid in this region. One thus finds

$$\left(\frac{d\sigma_2}{d\Omega}\right)_{\vartheta=0} = \frac{4}{15} q^2 a^2. \tag{5.63}$$

From the differential cross sections the following values for the total cross sections have been obtained

$$\left.\begin{aligned} \sigma_{I=2} &= 7.93 \quad a^2 \\ \sigma_{I=4} &= 1.06 \quad a^2 \\ \sigma_{I=6} &= 0.160\, a^2 \\ \sigma_{I=8} &= 0.016\, a^2. \end{aligned}\right\} \tag{5.64}$$

For other ground state spins the excitation probabilities of the rotational band can be obtained by means of (5.13). Since $K = I_i$ this equation may be written

$$\left.\begin{aligned} P_{I_f I_i}(\vartheta, q, 0) &= (2I_f+1) \sum_I \begin{pmatrix} I_f & I_i & I \\ -I_i & I_i & 0 \end{pmatrix}^2 P_{I,0}(\vartheta, q, 0) \\ &= \frac{(2I_f+1)!\,(2I_i)!\,(I_i+I_f)!}{(I_f-I_i)!} \sum_I \frac{(I_f-I_i+I)!\, P_{I,0}(\vartheta, q, 0)}{(I_i+I_f+I+1)!\,(I_i-I_f+I)!\,(I_i+I_f-I)!} \end{aligned}\right\} \tag{5.65}$$

As an illustration, the case of $I_i = 5/2$ is shown in Fig. 13 for $\vartheta = 180°$.

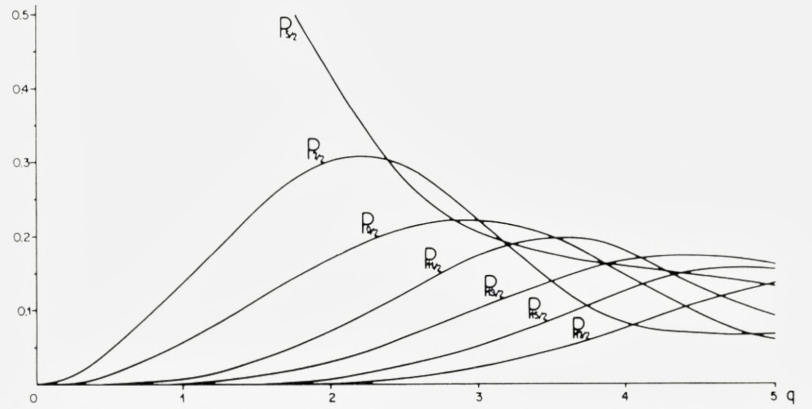


Fig. 13. The multiple Coulomb excitation of a pure rotational band in an odd $A$ nucleus with ground state spin 5/2. The excitation probability $P_I$ of the state with spin $I$ is given as a function of the parameter $q$ for backward scattering.

TABLE 7.

The coefficients $f_1(\vartheta)$ and $f_m^l(\vartheta)$ for the first order corrections in $\xi$ to the excitation of rotational states (see Eq. (5.44)). The coefficients are given as functions of the deflection angle $\vartheta$ (in degrees) for even values of $m$. For odd values of $m$ the $f_m^l(\vartheta)$ are easily obtained from $f_1(\vartheta)$ and the functions $J_{2,\mu}(\vartheta)$ given in Table 2 by means of the Eqs. (5.47) to (5.49). The entries are given in the form of a number followed by the power of ten by which it should be multiplied.

| $\theta$ | $f_1$ | $f_0^0$ | $f_0^2$ | $f_2^2$ |
|---|---|---|---|---|
| 180 | 0.000 | 3.893 (—1) | 2.781 (—1) | 0.000 |
| 150 | 1.917 (—1) | 3.423 (—1) | 2.423 (—1) | 9.405 (—3) |
| 120 | 3.242 (—1) | 2.188 (—1) | 1.495 (—1) | 2.672 (—2) |
| 90 | 3.586 (—1) | 9.615 (—2) | 5.915 (—2) | 3.181 (—2) |
| 60 | 2.904 (—1) | 2.370 (—2) | 9.662 (—3) | 1.920 (—2) |
| 30 | 1.513 (—1) | 1.442 (—3) | —1.047 (—3) | 4.078 (—3) |

| $\theta$ | $f_0^4$ | $f_2^4$ | $f_4^4$ |
|---|---|---|---|
| 180 | —6.673 (—1) | 0.000 | 0.000 |
| 150 | —5.935 (—1) | 1.015 (—3) | —4.062 (—5) |
| 120 | —3.942 (—1) | 4.773 (—3) | —4.713 (—4) |
| 90 | —1.880 (—1) | 8.893 (—3) | —1.373 (—3) |
| 60 | —5.511 (—2) | 8.255 (—3) | —1.654 (—3) |
| 30 | —5.787 (—3) | 2.628 (—3) | —6.296 (—4) |

TABLE 8.

The coefficients $A_l(q)$ for the first order correction in $\xi$ to the excitation probability of even-even nuclei. The coefficient which is defined in Eq. (5.51) is given for backward scattering on even-even nuclei. An approximate expression for other deflection angles can be obtained from the table by means of Eq. (5.67).

| $q$ | $A_0$ | $A_2$ | $A_4$ | $A_6$ | $A_8$ | $A_{10}$ |
|---|---|---|---|---|---|---|
| 0.0 | 0.000 | 0.000 | 0.000 | 0.000 | 0.000 | 0.000 |
| 0.5 | 0.030 | —0.029 | —0.001 | | | |
| 1.0 | 0.204 | —0.186 | —0.017 | | | |
| 1.5 | 0.537 | —0.422 | —0.106 | —0.008 | | |
| 2.0 | 0.890 | —0.512 | —0.325 | —0.050 | —0.004 | |
| 2.5 | 1.084 | —0.250 | —0.636 | —0.175 | —0.022 | —0.002 |
| 3.0 | 1.044 | 0.337 | —0.861 | —0.427 | —0.083 | —0.009 |
| 3.5 | 0.861 | 0.963 | —0.773 | —0.775 | —0.234 | —0.038 |
| 4.0 | 0.714 | 1.282 | —0.278 | —1.073 | —0.509 | —0.117 |
| 4.5 | 0.728 | 1.159 | 0.451 | —1.107 | —0.880 | —0.288 |
| 5.0 | 0.880 | 0.783 | 1.053 | —0.735 | —1.224 | —0.578 |
| 5.5 | 1.033 | 0.510 | 1.216 | —0.025 | —1.344 | —0.966 |
| 6.0 | 1.061 | 0.580 | 0.919 | 0.721 | —1.080 | —1.341 |
| 6.5 | 0.955 | 0.930 | 0.465 | 1.136 | —0.433 | —1.526 |
| 7.0 | 0.821 | 1.266 | 0.249 | 1.039 | 0.370 | —1.351 |
| 7.5 | 0.780 | 1.321 | 0.456 | 0.579 | 0.969 | —0.779 |
| 8.0 | 0.865 | 1.082 | 0.922 | 0.148 | 1.087 | 0.031 |
| 8.5 | 0.995 | 0.785 | 1.278 | 0.099 | 0.728 | 0.751 |
| 9.0 | 1.055 | 0.701 | 1.259 | 0.480 | 0.199 | 1.063 |
| 9.5 | 0.996 | 0.901 | 0.920 | 1.006 | 0.089 | 0.855 |
| 10.0 | 0.880 | 1.204 | 0.580 | 1.282 | —0.094 | 0.322 |

(to be continued)

The first order corrections for $\xi \neq 0$ must be calculated by means of Eq. (5.44) from the quantities $A_{IM}(\vartheta, q)$ and from the functions $f_m^l(\vartheta)$ and $f_1(\vartheta)$. The latter have been evaluated numerically for some angles and the result is given in Table 7.

The excitation probability may be written in the form (5.51)

$$P_{I_f I_i}(\vartheta, q, \xi) \approx P_{I_f I_i}(\vartheta, q, 0) + A_{I_f I_i}(\vartheta, q)\, \xi. \tag{5.66}$$

The functions $A$ have been calculated for the special case of $\vartheta = \pi$ and $I_i = 0$, and the result is given in Table 8. The effect of the correction in the excitation probability is illustrated in Fig. 11. The result (5.66) may be applied for angles in the neighbourhood of 180 degrees by the following substitution:

TABLE 8 (continued).

| $q$ | $A_{12}$ | $A_{14}$ | $A_{16}$ | $A_{18}$ | $A_{20}$ |
|---|---|---|---|---|---|
| 0.0 | 0.000 | 0.000 | 0.000 | 0.000 | 0.000 |
| 0.5 | | | | | |
| 1.0 | | | | | |
| 1.5 | | | | | |
| 2.0 | | | | | |
| 2.5 | | | | | |
| 3.0 | —0.001 | | | | |
| 3.5 | —0.004 | | | | |
| 4.0 | —0.017 | —0.001 | | | |
| 4.5 | —0.055 | —0.007 | | | |
| 5.0 | —0.149 | —0.025 | —0.003 | | |
| 5.5 | —0.336 | —0.073 | —0.016 | | |
| 6.0 | —0.640 | —0.180 | —0.034 | —0.005 | |
| 6.5 | —1.038 | —0.380 | —0.092 | —0.016 | —0.001 |
| 7.0 | —1.436 | —0.694 | —0.210 | —0.044 | —0.007 |
| 7.5 | —1.669 | —1.101 | —0.421 | —0.110 | —0.021 |
| 8.0 | —1.571 | —1.516 | —0.744 | —0.238 | —0.055 |
| 8.5 | —1.072 | —1.788 | —1.163 | —0.459 | —0.128 |
| 9.0 | —0.284 | —1.753 | —1.586 | —0.789 | —0.266 |
| 9.5 | 0.511 | —1.324 | —1.888 | —1.210 | —0.495 |
| 10.0 | 0.981 | —0.571 | —1.907 | —1.648 | —0.832 |

$$A_{I_f 0}(\vartheta, q) \approx \frac{q^2 f_0^0(\vartheta)}{(q_{\text{eff}}(\vartheta))^2 f_0^0(\pi)} A_{I_f 0}(\pi, q_{\text{eff}}(\vartheta)). \tag{5.67}$$

This equation only holds as long as $f_0^0$, $f_0^2$, and $f_0^4$ dominate over the coefficients $f_2^2$, $f_2^4$, and $f_4^4$.

The collision between the target nucleus and the projectile may also lead to an excitation of the projectile. The results which we have obtained for target excitation can also be used for projectile excitations, since we have worked in a relative coordinate system. The parameter $\xi$ (see Eq. (2.8)) is thus given by the Eqs. (5.53) and (5.54) where one must insert for $E_2 - E_1$ the excitation energy of the projectile. Similarly the expression for $\chi$ (see Eq. (2.11)) is given by

$$\chi_{1\to 2}^{\text{proj}} = 14.52 \frac{A_1^{1/2} [B(E2, I_1 \to I_2)]^{1/2}}{(1 + A_1/A_2)^2 Z_2 Z_1^2} E_{\text{MeV}}^{3/2}, \tag{5.68}$$

where $B(E2)$ now refers to the projectile. The formula for $q^{\text{proj}}$ has the same relation to $q$ in (5.57) as $\chi^{\text{proj}}$ has to $\chi$ in (5.55).

### D. Classical Treatment

We shall make a few comments about the classical limit of the excitation of rotational states, which can be used for large angular momenta and large $q$. The classical problem of a collision between a charged particle and a charged symmetric top leads to a non-linear equation of motion which, like in the quantum mechanical problem, can only be solved in closed form in the limit where the collision time is short compared to the time of rotation of the top.

The classical Hamiltonian can be written in the form

$$H = \frac{v}{6\,a\hbar}\,\xi\left[p_\beta^2 + \frac{1}{\sin^2\beta}\,p_\alpha^2\right] + \frac{8\,\pi}{5}\,\hbar\,v\,a^2\,q\sum_{\mu}\bar{S}_{2\,\mu}(t)\,Y_{2\,\mu}^{*}(\beta,\,\alpha), \tag{5.69}$$

where $p_\beta$ and $p_\alpha$ are the momenta which are conjugate to the Eulerian angles $\beta$ and $\alpha$, describing the orientation of the axis of the top.

We shall here consider only the case where one may neglect the terms with $\mu \neq 0$, i.e., we limit ourselves to the case of backward scattering or the $q\,(\vartheta)$ approximation. In this case the angle $\alpha$ is a cyclic variable. For the angle $\beta$ one obtains from (5.69) the following equation of motion:

$$\ddot{\beta} = \sqrt{\frac{4\,\pi}{5}}\,q\,\xi\,a v^2\,\bar{S}_{20}(t)\sin 2\beta\,. \tag{5.70}$$

In the sudden approximation one assumes $\beta$ on the right-hand side to be unchanged (equal to $\beta_0$) during the collision, and the final angular velocity $\dot{\beta}_f$ is thus given by

$$\dot{\beta}_f = \dot{\beta}_i + \frac{2\,v}{3\,a}\,q_{\mathrm{eff}}(\vartheta)\,\xi\,\sin 2\beta_0. \tag{5.71}$$

We have here used Eqs. (5.15), (3.24), and (3.27), and have denoted the angular velocity $\dot{\beta}$ before the collision by $\dot{\beta}_i$.

From (5.71) we obtain the following simple expression for the transfer of angular momentum $\Delta L_\perp$ perpendicular to the symmetry axis of the orbit.

$$\Delta L_\perp = 2\,q_{\mathrm{eff}}(\vartheta)\,\hbar\,\sin 2\beta_0, \tag{5.72}$$

while the component of $L$ parallel to the axis is unchanged.

In the classical treatment one thus finds that the angular momentum transfer depends on the initial orientation of the top and one sees that the projectile can transfer at most (for $\beta_i = \pi/4$) an angular momentum of magnitude

$$\Delta L_{\max} = 2\,q_{\mathrm{eff}}(\vartheta)\,\hbar\,. \tag{5.73}$$

If one considers all initial orientations of the top to be equal probable, one may evaluate the classical energy distribution of the top after the collision. In the simplest case where the nucleus is at rest before the collision, one finds corresponding to (5.73) also a maximum energy transfer $E_{\max} = 2(q_{\text{eff}}(\vartheta))^2 \hbar^2/\Im$. In this case, the energy distribution can be written in the form

$$P(E)\,dE = \frac{d\varepsilon}{4\sqrt{\varepsilon}\sqrt{1-\sqrt{\varepsilon}}}, \tag{5.74}$$

where

$$\varepsilon = \frac{E}{E_{\max}} = \frac{\Im}{2(q_{\text{eff}}(\vartheta))^2 \hbar^2} E. \tag{5.75}$$

This energy distribution (5.74) is illustrated in Fig. 14.

The classical treatment gives a qualitative understanding of the result of the quantum mechanical calculations of Fig. 7. In the classical limit, the excitation probability of a state of spin $I$ is zero until $q$ reaches the value $I/2$. As a function of $q$ the excitation probability thereafter goes through a maximum and finally decreases slowly. The quantum mechanical energy distribution is a function of both $q$ and the discrete excitation energies. For a fixed value of $q$ the points corresponding to the different energies oscillate around the classical curve. On Fig. 14 we have illustrated the case of $q = 10$, and we have here, for illustrative purposes, connected the points (indicated by circles) by a smooth curve. It is seen that the result is still far from the classical limit.

Like in the quantum mechanical treatment, the case of $\xi \neq 0$ can be solved for small values of $\xi$. One must then take into account that the nucleus is moving during the collision time. In first order one may consider the change in the right-hand side of (5.70) to be linear in $\beta$. One is thereby led to a hypergeometric differential equation which can be solved explicitly.

The result for the angular momentum transfer perpendicular to the $z$ axis can be written in the form

$$\Delta L_{\perp} = 2\, q_{\text{eff}}(\vartheta)\, \hbar \sin 2\beta_0\, F(q\,\xi \cos 2\beta_0), \tag{5.76}$$

where the correction factor $F$ to the result for $\xi = 0$ is given by

$$F(x) = \frac{3\cos\left(\pi\sqrt{\frac{9}{4} - 4x}\right)}{4\pi x(2x-1)} \approx 1 + \frac{22}{9}x \quad \text{for} \quad x \ll 1. \tag{5.77}$$

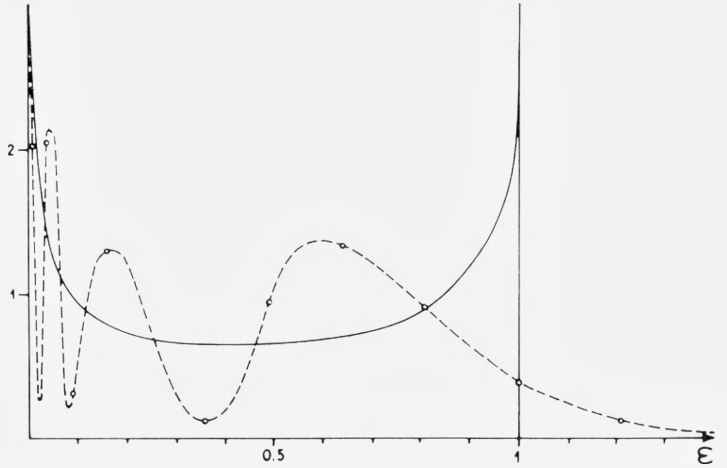


Fig. 14. The classical energy distribution of a charged symmetric top after a head-on impact of a charged particle (full drawn curve). The top is assumed to be at rest before the collision and the impact is assumed to be sudden. The scale of the abscissa is the ratio between the energy of the top $E$ and the maximum energy $E_{\max}$ which can be transferred. The circles, which are connected by a broken curve, show the corresponding quantum mechanical result for $q = 10$.

It is illustrative to evaluate the average excitation energy of the nucleus after the collision. If we assume an isotropic distribution for the orientation of the nucleus before the collision, we find from (5.76) to first order in $\xi$ (and backward scattering)

$$\langle E \rangle = \frac{16}{15} \frac{q^2 \hbar^2}{\Im} \left(1 - \frac{44}{63} q \xi\right). \tag{5.78}$$

This result must be correct also in the quantum mechanical treatment. In the limit of $q \ll 1$ where only the lowest state in a rotational band in even-even nuclei is excited, one may use it to calculate the excitation probability. Since the energy of the state of spin 2 is $E_2 = 3\hbar^2/\Im$, one finds

$$P_2 = \frac{16}{45} q^2 \left(1 - \frac{44}{63} q \xi\right). \tag{5.79}$$

If one compares this result with the result (5.51) in the limit of $q \ll 1$, one finds

$$f_0^0(\pi) = \frac{11}{9\pi} = \frac{7}{5} f_0^2(\pi) = -\frac{7}{12} f_0^4(\pi) \tag{5.80}$$

in agreement with Table 7.

## 6. Excitation of Vibrational States

Another important kind of collective excitations in nuclei is that connected with the vibrational degree of freedom. In even-even nuclei a number of low-lying states have been identified as vibrational levels but, in general, the spectra are not as well understood as the corresponding rotational states in deformed nuclei. A survey of the experimental and theoretical status is given in ref. 1, Chapt. V C.

The excitation of pure vibrational states can be solved exactly not only in the sudden approximation, but also for arbitrary $\vartheta$, $\xi$, and $\chi$. The problem is analogous to the classical problem of a forced vibration which can also be solved in an explicit form.

For a pure quadrupole vibration, the Hamiltonian of the free nucleus is given by

$$H_0 = \frac{1}{2} B \sum_{\mu} |\dot{\alpha}_{2\mu}|^2 + \frac{1}{2} C \sum_{\mu} |\alpha_{2\mu}|^2, \tag{6.1}$$

where $B$ is the inertial parameter and $C$ the restoring force. The parameters $\alpha_{2,\mu}$, where $\mu = -2, -1, 0, 1, 2$ describe the shape of the nuclear surface. In the idealized case where the surface is sharply defined and where the nuclear density is constant, the nuclear shape is given by

$$R(\vartheta, \varphi) = R_0 \left[1 + \sum_{\mu} \alpha_{2\mu} Y_{2\mu}(\vartheta, \varphi)\right]. \tag{6.2}$$

The eigenstates of the Hamiltonian (6.1) can be classified according to the five vibrational quantum numbers $n_\mu$, where $n_\mu = 0, 1, 2 \ldots$. The energy of a state $|\, n_\mu \rangle$ can thus be written in the form

$$E = \hbar\omega \sum_{\mu} \left(n_\mu + \frac{1}{2}\right) = \hbar\omega \left(N + \frac{5}{2}\right). \tag{6.3}$$

Here, the frequency $\omega$ is given by

$$\omega = \sqrt{\frac{C}{B}}, \tag{6.4}$$

while the principal quantum number $N$ is defined by

$$N = \sum_{\mu} n_\mu. \tag{6.5}$$

The degenerate nuclear states can also be labelled by this principal quantum number together with the total angular momentum $I$ and the mag-

netic quantum number $M$. For $N \leqslant 3$ these numbers are sufficient to specify the state completely, while for $N > 3$ one needs additional quantum numbers[17]. The connection between the two labellings $n_\mu$ and $N, I, M$ is given in refs. 15 and 16 for a number of cases.

In the following, it will be convenient to introduce a dimensionless coordinate $x_\mu$ defined by the equation

$$\alpha_{2\mu} = \sqrt{\frac{\hbar}{\sqrt{BC}}}\, x_\mu \tag{6.6}$$

instead of $\alpha_{2,\mu}$. If we introduce furthermore $\xi$ by means of the equation

$$\xi = \omega \frac{a}{v}, \tag{6.7}$$

we may write $H_0$ in the form

$$H_0 = \frac{\hbar v \xi}{2a} \sum_\mu [\, | p_\mu/\hbar |^2 + | x_\mu |^2 \,], \tag{6.8}$$

where the momenta $p_\mu$ are defined by

$$p_\mu = -B \dot{\alpha}^*_{2\mu} = -\sqrt{\hbar \sqrt{\frac{B}{C}}}\, \dot{x}^*_\mu. \tag{6.9}$$

The nuclear multipole moments $\mathfrak{M}(E2, \mu)$ are related to the deformation parameters $\alpha_{2,\mu}$ by the following expression (see ref. 1, Eq. (V. 24)),

$$\mathfrak{M}(E2, \mu) = \frac{3}{4\pi} Z_1 e R_0^2 \alpha^*_{2\mu}. \tag{6.10}$$

By evaluating the reduced matrix element of (6.10) between the ground state and the first excited state one finds the following expression for the parameter $\chi$ (see Eq. (2.12)):

$$\chi = \frac{Z_1 Z_2 e^2 R_0^2}{v a^2 \sqrt{10\pi\hbar\sqrt{BC}}} \tag{6.11}$$

and one may therefore write the interaction Hamiltonian (2.3) in the following form:

$$H'(t) = \sqrt{\frac{18\pi}{5}}\, \hbar v a^2 \chi \sum_\mu \bar{S}_{2\mu}(t)\, x_\mu, \tag{6.12}$$

where $\bar{S}_{2\mu}(t)$ is given by (3.23).

The eigenstates of the free Hamiltonian $H_0$ are given in terms of the Hermite polynomials $H_n(x)$, i.e.,

$$\left.\begin{aligned}\psi_{n_{-2}\, n_{-1}\, n_0\, n_1\, n_2}(x) &= \prod_\mu \psi_{n_\mu}(x_\mu) \\ &= \prod_\mu \frac{1}{\sqrt{\sqrt{\pi}\, 2^{n_\mu}\, n_\mu!}}\, e^{-\frac{1}{2}x_\mu^2}\, H_{n_\mu}(x_\mu).\end{aligned}\right\} \quad (6.13)$$

The excitation amplitude in the sudden approximation (3.11) is now very easily found.

The result for the distribution on the different energy levels ($N$) turns out to be a Poisson distribution, where the mean excitation energy is the same as that one would find in the perturbation calculation (see Eq. (6.27) below). This result can be understood by noting that the excitation of an harmonic oscillator can always be interpreted as the collective motion of a large number of mutually uncoupled harmonic oscillators which are, each of them, only weakly excited. The weak excitation of these oscillators can be treated by a perturbation calculation and, since they are mutually uncoupled, the resulting total energy distribution must be a Poisson distribution.

Since the above argument is independent of the sudden approximation, we shall in the following give the details of the calculation in the more general case of $\xi \neq 0$.

The first step in the program will be to introduce a number of auxiliary variables $x^{(i)}$, where $i = 1, 2, \ldots\ldots \mathfrak{N}$ and where $x_\mu^{(1)} = x_\mu$. The $5\,(\mathfrak{N}-1)$ new degrees of freedom are supposed to be coordinates for free vibrations which have the same frequency $\omega$ as the $x_\mu$ oscillators. Furthermore, we take them to be coupled, neither to each other nor to the old $x_\mu$. Under these circumstances they will be left undisturbed in the Coulomb excitation process and will only change the problem in a trivial way. The total Hamiltonian will thus be

$$H = \frac{\hbar v \xi}{2a} \sum_{\mu,\, i} \left[ \left| \frac{p_\mu^{(i)}}{\hbar} \right|^2 + |\, x_\mu^{(i)}\, |^2 \right] + \sqrt{\frac{18\pi}{5}}\, \hbar v a^2 \chi \sum_\mu \bar{S}_{2\mu}(t)\, x_\mu^{(1)}, \quad (6.14)$$

while the eigenstates which are of physical interest will be

$$\psi(x) = \psi_{n_{-2},\, n_{-1},\, n_0, n_1,\, n_2}(x^{(1)}) \prod_{\substack{\mu \\ i \neq 1}} \psi_0(x_\mu^{(i)}) \quad (6.15)$$

where $\psi_0$ is the ground state wave function (6.13) with $n_\mu^{(i)} = 0$.

We perform now a linear transformation on the coordinates $x_\mu^{(i)}$ and introduce hereby new coordinates $Q_\mu^{(i)}$ and new momenta $P_\mu^{(i)}$. The transformation matrix $U$ is supposed to be unitary, i. e.

$$UU^\dagger = 1 \tag{6.16}$$

and is assumed to be diagonal in $\mu$, i. e.,

$$Q_\mu^{(i)} = \sum_j U_{ij}^{(\mu)} x_\mu^{(j)}. \tag{6.17}$$

Furthermore, we prescribe the first row of $U^{(\mu)}$ for all values of $\mu$ to be given by

$$U_{1,j}^{(\mu)} = \frac{1}{\sqrt{\mathfrak{N}}}. \tag{6.18}$$

The new Hamiltonian in the variables $Q_\mu^{(i)}$ and $P_\mu^{(i)}$ is found from (6.14) (6.16), and (6.18) to be

$$H = \frac{\hbar v \xi}{2a} \sum_{\mu i} [\,|\, P_\mu^{(i)}/\hbar \,|^2 + |\, Q_\mu^{(i)} \,|^2] + \sqrt{\frac{18\pi}{5}}\, \hbar v a^2 \frac{\chi}{\sqrt{\mathfrak{N}}} \sum_\mu \bar{S}_{2\mu}(t) \sum_i Q_\mu^{(i)}. \tag{6.19}$$

The Schrödinger equation for the variables $Q_\mu^{(i)}$ is again separable and the eigenstates of the free Hamiltonian are

$$\varphi_n(Q) = \prod_{i\mu} \psi_{n_\mu^{(i)}}(Q_\mu^{(i)}), \tag{6.20}$$

where all $n_\mu^{(i)}$ can take the values $n_\mu^{(i)} = 0, 1, 2 \ldots\ldots$

In the new Hamiltonian, however, the interaction term can be made very small for all values of $\mu$ and $i$ by choosing $\mathfrak{N}$ to be a large number. In the new variables, the excitation process can therefore be treated by a perturbation calculation, and one obtains for each of the oscillators $(\mu, j)$ only a very small probability that the oscillator is excited. In the perturbation treatment one finds, for each oscillator the following excitation amplitude on the first excited state:

$$a_\mu^{(j)} = \frac{1}{i\hbar} \langle 1 \,|\, \int_{-\infty}^{+\infty} \sqrt{\frac{18\pi}{5}}\, \hbar v a^2 \frac{\chi}{\sqrt{\mathfrak{N}}} \bar{S}_{2\mu}(t)\, Q_\mu^{(j)}\, e^{i\omega t}\, dt \,|\, 0 \rangle. \tag{6.21}$$

Since the matrix element of $Q_\mu^{(j)}$ between the states of one phonon $|\,1\,\rangle$ and the ground state $|\,0\,\rangle$ is given by

$$\langle 1 \mid Q_\mu^{(j)} \mid 0 \rangle = \frac{(-1)^\mu}{\sqrt{2}}, \tag{6.22}$$

one may write (6.21) in the form

$$a_\mu^{(j)} = -\frac{i}{\sqrt{\mathfrak{N}}} \chi_\mu(\vartheta, \xi), \tag{6.23}$$

where (see also Eq. (3.24))

$$\chi_\mu(\vartheta, \xi) = \sqrt{\frac{9\pi}{5}} v a^2 (-1)^\mu S_{E2,\mu}(\vartheta, \xi). \tag{6.24}$$

We can now easily determine the total excitation probability. We ask first for the probability that any one of the five oscillators belonging to a definite value of $j$ is excited. This probability is

$$P_{(j)} = \sum_\mu \mid a_\mu^{(j)} \mid^2 = \frac{1}{\mathfrak{N}} \mid \chi(\vartheta, \xi) \mid^2, \tag{6.25}$$

where $\chi(\vartheta, \xi)$ is given by Eq. (2.12), i. e.,

$$\chi(\vartheta, \xi) = \chi \frac{9\pi}{5} \sum_\mu \mid Y_{2\mu}\left(\frac{\pi}{2}, 0\right) I_{2\mu}(\vartheta, \xi) \mid^2. \tag{6.26}$$

We can then calculate the probability that all the $\mathfrak{N}$ groups of five oscillators have together the total excitation energy $N\hbar\omega$. Since all groups have the same probability (6.25) of having the energy $\hbar\omega$, we obtain in the limit of $\mathfrak{N} \to \infty$ a Poisson distribution for this probability $P_N$

$$P_N = \frac{1}{N!} e^{-[\chi(\vartheta, \xi)]^2} [\chi(\vartheta, \xi)]^{2N}. \tag{6.27}$$

In the old variables $x_\mu^{(i)}$, this result must be interpreted as the total excitation probability of the vibrational state with principal quantum number $N$.

We shall be interested also in the amplitudes on the eigenstates (6.13). We shall evaluate these by calculating the amplitudes $\langle \varphi_n(Q) \mid \Phi(Q) \rangle$ of the final wave function, $\Phi$, on the eigenstates (6.20) as well as the amplitudes $\langle \psi(x(Q)) \mid \varphi_n(Q) \rangle$ of (6.13) on these eigenstates.

From (6.23) one finds directly the amplitude on the states (6.20)

$$\langle \varphi_n(Q) \mid \Phi(Q) \rangle = \prod_{\mu, i} [a_\mu^{(i)}]^{n_\mu^{(i)}} [1 - \mid a_\mu^{(i)} \mid^2]^{(1 - n_\mu^{(i)})/2}, \tag{6.28}$$

where the quantum numbers $n_\mu^{(i)}$ are all 0 or 1.

The amplitude of (6.13) on (6.20) follows from the expansion of a Hermite polynomial of a linear function of $Q_\mu^{(i)}$ in terms of a product of Hermite polynomials of $Q_\mu^{(i)}$. One finds from ref. 10 (Vol. 2, p. 196)

$$\langle \psi(x(Q)) \mid \varphi_n(Q) \rangle = \prod_\mu \sqrt{\frac{n_\mu!}{\mathfrak{N}^{n_\mu}(n_\mu^{(1)})!\,(n_\mu^{(2)})!\cdots(n_\mu^{(\mathfrak{N})})!}}. \tag{6.29}$$

According to (6.28) and (6.29), the expression for the excitation amplitude is

$$\left.\begin{aligned} a_{n_{-2}\,n_{-1}\,n_0\,n_1\,n_2} &= \sum_n \langle \psi(x(Q)) \mid \varphi_n(Q) \rangle \langle \varphi_n(Q) \mid \Phi(Q) \rangle \\ &= \prod_\mu \sqrt{\frac{(n_\mu)!}{\mathfrak{N}^{n_\mu}}} \left(\frac{-i\chi_\mu(\vartheta,\xi)}{\sqrt{\mathfrak{N}}}\right)^{n_\mu} \left(1 - \frac{(\chi_\mu(\vartheta,\xi))^2}{\mathfrak{N}}\right)^{\frac{\mathfrak{N}}{2} - \frac{n_\mu}{2}} \binom{\mathfrak{N}}{n_\mu}. \end{aligned}\right\} \tag{6.30}$$

We have here utilized that $n_\mu^{(i)} = 0$ or 1 and have performed the summation over $n_\mu^{(i)}$ with the restriction $\Sigma\, n_\mu^{(i)} = n_\mu$ by multiplying with the number of ways in which $n_\mu$ objects may be chosen among $\mathfrak{N}$ objects. When we let $\mathfrak{N} \to \infty$ the expression (6.30) takes the form

$$a_{n_{-2}\,n_{-1}\,n_0\,n_1\,n_2} = \prod_\mu \frac{(-i)^{n_\mu}}{\sqrt{(n_\mu)!}} (\chi_\mu(\vartheta,\xi))^{n_\mu} e^{-\frac{1}{2}(\chi_\mu(\vartheta,\xi))^2}. \tag{6.31}$$

This equation offers the complete solution of the excitation of pure vibrational states.

It is interesting to observe that the total excitation probability (6.27) depends on $\vartheta$ and $\xi$ only through the quantity $\chi(\vartheta, \xi)$. This means that the excitation probability for arbitrary $\vartheta$ and $\xi$ can be obtained from the probabilities for $\vartheta = \pi$ and $\xi = 0$ by substituting $\chi(\vartheta, \xi)$ for $\chi$, i. e.,

$$P_N(\vartheta, \xi, \chi) = P_N(\pi, 0, \chi(\vartheta, \xi)). \tag{6.32}$$

In the special case of $\xi = 0$ this equation shows that the $\chi(\vartheta)$ approximation (see Eq. (5.62)) in the case of vibrational states is exactly fulfilled.

The function $P_N(\pi, 0, \chi)$ is illustrated on Fig. 15, as a function of $\chi$. It is interesting to compare this result with the corresponding result for the excitation of a rotational band which is illustrated on Fig. 7. The maximum excitation probabilities are larger for rotational states than for vibrational states. However, in the latter case, higher lying states are reached for a definite value of $\chi$.

The ground state and the first excited state have the definite angular momenta 0 and 2. The second excited state, however, is a triplet with spins 0, 2 and 4. Since the vibrational states in nuclei are not pure, the degeneracy

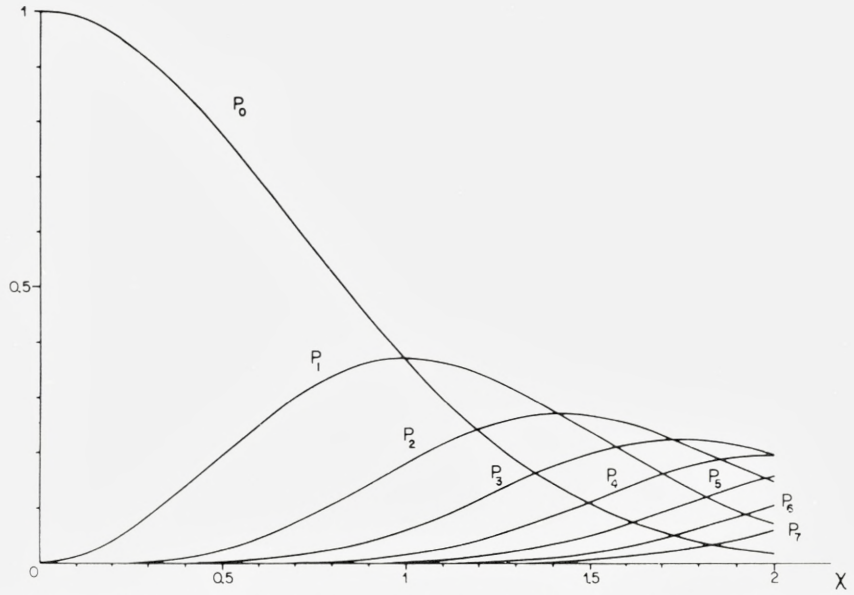


Fig. 15. The multiple Coulomb excitation of a pure vibrational band in an even-even nucleus. The excitation probability $P_N$ of the state with principal quantum number $N$ is given as a function of the parameter $\chi(\vartheta, \xi)$.

is in actual cases removed, and it is thus interesting to find how the total excitation probability (6.27) is distributed on each of the substates.

To perform this calculation one needs the expression (6.31) for the amplitudes on the states specified by $n_{-2}, n_{-1}, \ldots . n_2$. Furthermore, one needs the coefficients for the transformation between the $n_\mu$ and the $N, I, M$ labelling (see refs. 15 and 16).

One finds in the case of $N = 2$ the following result

$$\left.\begin{aligned} P_{2,\,I=0} &= 1/5 \quad P_2 \\ P_{2,\,I=2} &= 2/7 \quad P_2 \\ P_{2,\,I=4} &= 18/35\, P_2 \end{aligned}\right\} \qquad (6.33)$$

where $P_2$ is given by (6.27) for $N = 2$. In this case the rule (6.32) thus also holds for the excitation of the substates with $I = 0, 2$ and 4. This is, however, not true any more for the excitation of the substates of the state with principal quantum number $N = 3$.

## 7. Excitation of Coupled Rotational Bands

In the two preceding sections, we have treated the multiple Coulomb excitation of a pure rotational band and of a pure vibrational band, and we assumed there that only the rotational or vibrational degrees of freedom were involved in the excitation process. In actual cases several different degrees of freedom can be excited. One might have cases, such as in most deformed nuclei, where both rotational and vibrational degrees of freedom are involved, or one might have to consider the excitation of the intrinsic degrees of freedom.

In this section, we shall consider a situation where the low energy nuclear spectrum consists of a number of rotational bands which differ in internal (or vibrational) structure. The excitation of these bands can be treated rigorously in the sudden approximation, in some cases when only a finite number of bands have to be taken into account.

In most cases, however, one will find that the parameter $\chi$ (see Eq. (2.12)) which describes the transition between the bands is small, and one may then simplify the calculation by a perturbation expansion for the transition from one band to the others. The transitions within any one of the bands must in any case be treated rigorously.

We shall assume that the nuclear states are described by state vectors of the form

$$|\psi\rangle = |n, K\rangle |I, K, M\rangle, \tag{7.1}$$

where $|I, K, M\rangle$ stands for a rotational wave function of the form (5.6) which only depends on the Eulerian angles describing the orientation of the nuclear axis, while $|n, K\rangle$ describes a state of the intrinsic and vibrational degrees of freedom, which has a component of angular momentum $K$ along the nuclear symmetry axis. The state vector $|n, K\rangle$ depends only on relative coordinates measured with respect to a coordinate system which has its $z$-axis along the nuclear axis.

In actual cases, the nuclear state vector will be a linear combination of state vectors of the form (7.1). Firstly, it will always contain a term identical with (7.1), except for a change of sign on $K$. Secondly, it may often contain admixtures from other bands with different values of $K$ and $n$. The actual excitation probabilities can, however, easily be evaluated once the excitation probabilities for states of the simple type (7.1) are known.

It is convenient to transform the interaction energy to the rotating coordinate system which has its $z$-axis along the nuclear axis.

For the multipole operator (2.4) one finds

$$\mathfrak{M}(E2,\mu) = \sum_{\nu} D^{2}_{\mu,\nu}(\alpha,\beta,0)\,\mathfrak{M}_{\mathrm{int}}(E2,\nu), \tag{7.2}$$

where the intrinsic multipole operator $\mathfrak{M}_{\mathrm{int}}(E2,\nu)$ is independent of the Eulerian angles $\alpha$ and $\beta$.

If we adopt the $\chi(\vartheta)$ approximation, the excitation amplitude in the sudden approximation (3.11) may be written

$$a^{(f)}_{I_f M_f K_f} = \langle I_f K_f M_f \,|\, \langle f K_f \,|\, e^{-i\sqrt{\frac{64\pi}{45}}\sum_{\nu}\mathfrak{q}_{\nu}(\vartheta)\,Y^{*}_{2\nu}(\beta,0)} \,|\, i K_i \rangle \,|\, I_i K_i M_i \rangle \tag{7.3}$$

where the operator $\mathfrak{q}_{\nu}(\vartheta)$ is defined by

$$\mathfrak{q}_{\nu}(\vartheta) = \sqrt{\frac{\pi}{5}}\,\frac{Z_1 e^2 \mathfrak{M}^{*}_{\mathrm{int}}(E2,\nu)}{\hbar\nu a^2}\,\frac{3}{4}\,J_{2,0}(\vartheta). \tag{7.4}$$

The expectation value of $\mathfrak{q}_{\nu}$ for states within a band is exactly the earlier defined quantity of $q_{\mathrm{eff}}(\vartheta)$ for this band (see Eq. (5.15)),viz.,

$$\langle nK \,|\, \mathfrak{q}_{\nu}(\vartheta) \,|\, nK \rangle = q^{(n)}_{\mathrm{eff}}(\vartheta)\,\delta_{\nu 0} \approx q^{(n)}(\vartheta)\,\delta_{\nu 0}. \tag{7.5}$$

If the matrix elements of $\mathfrak{q}_{\nu}$ between the bands are small, and if the expectation value of $\mathfrak{q}_{\nu}$ or the intrinsic quadrupole moment is not very different in the initial and final band, one may use a perturbation expansion to evaluate (7.3). We may write the amplitude (7.3) in the form

$$\left.\begin{aligned} a^{(f)}_{I_f K_f M_f} &= \langle I_f K_f M_f \,|\, e^{-i\sqrt{\frac{64\pi}{45}}\,q(\vartheta)\,Y_{2,0}(\beta,0)} \\ \times \langle f K_f \,|\, e^{-i\sqrt{\frac{64\pi}{45}}\sum_{\nu}[\mathfrak{q}_{\nu}(\vartheta)-\delta_{\nu 0}\,q(\vartheta)]\,Y^{*}_{2\nu}(\beta,0)} \,|\, i K_i \rangle \,|\, I_i K_i M_i \rangle, \end{aligned}\right\} \tag{7.6}$$

where $q(\vartheta)$ is the $q$ for the initial band. We then perform a series expansion of the second exponential whereby we obtain the following expression for the excitation amplitude for a band different from the ground state band:

$$\left.\begin{aligned} a^{(f)}_{I_f K_f M_i} &\approx -i\sqrt{\frac{64\pi}{45}}\,\langle f K_f \,|\, \mathfrak{q}_{K_f - K_i}(\vartheta) \,|\, i K_i \rangle \\ \times \langle I_f K_f M_f \,|\, Y^{*}_{2,\,K_i - K_f}(\beta,0)\, e^{-i\sqrt{\frac{64\pi}{45}}\,q(\vartheta)\,Y_{2,0}(\beta,0)} \,|\, I_i K_i M_i \rangle. \end{aligned}\right\} \tag{7.7}$$

The excitation probability in the perturbation treatment can thus be written in the form

$$P^{(f)}_{I_f} = r^{2}_{if} N^{(f)}_{I_f K_f}(q(\vartheta)) \tag{7.8}$$

where we have introduced the notation

$$r_{if} = \frac{\langle fK_f \mid \mathfrak{q}_{K_f - K_i}(\vartheta) \mid iK_i \rangle}{q(\vartheta)} = \frac{\langle fK_f \mid \mathfrak{M}(E2, \nu) \mid iK_i \rangle}{\langle iK_i \mid \mathfrak{M}(E2, 0) \mid iK_i \rangle}. \tag{7.9}$$

From (7.7), one observes that the total probability of exciting any member of the final band is given by the simple expression

$$P^{(f)} = \sum_I P_{I_f}^{(f)} = \frac{16}{45} r_{if}^2 [q(\vartheta)]^2. \tag{7.10}$$

This result is identical with the expression which would be obtained in the ordinary perturbation theory for $q \ll 1$, and one sees that the strong coupling within the bands give rise only to a redistribution of the single probabilities $P_{I_f}^{(f)}$.

In the perturbation treatment which we have used here one may also approximately take into account the effect of finite $\xi$. If the energy difference between the ground states of the two bands is larger than the energy of the lowest states in the bands, the $\xi$ corresponding to the possible transitions between the two bands will be approximately constant. One may then take $\xi$ into account by calculating the total transition probability (7.10) for the finite $\xi$ in the ordinary perturbation treatment and apply the same distribution $P_{I_i}^{(f)}/P^{(f)}$ as for $\xi = 0$.

The matrix element (7.7) can be expressed in terms of the functions $A_{I,M}(\pi, q)$ (see Eq. (5.9)) by expanding the product of $D$-functions in terms of $D$-functions (compare also Eq. (5.20)). The result has been evaluated in the special case of $I_i = 0$. For a band with $K_f = 2$, one finds

$$\left.\begin{aligned} a_{I,2,0}^{(f)} = -i\frac{2}{3} r_{if}\, q(\vartheta) \sqrt{6(I-1)I(I+1)(I+2)(2I+1)} \\ \times \left\{ \frac{1}{2(2I+1)(2I+3)} A_{I+2,0}(q(\vartheta)) - \frac{1}{(2I-1)(2I+3)} A_{I,0}(q(\vartheta)) \right. \\ \left. + \frac{1}{2(2I-1)(2I+1)} A_{I-2,0}(q(\vartheta)) \right\}. \end{aligned}\right\} \tag{7.11}$$

For a band with $K_f = 0$ one finds similarly

$$\left.\begin{aligned} a_{I,0,0}^{(f)} = -i\frac{2}{3} r_{if} \cdot q(\vartheta) \sqrt{2I+1} \\ \times \left\{ \frac{3(I+1)(I+2)}{(2I+1)(2I+3)} A_{I+2,0}(q(\vartheta)) + \frac{2I(I+1)}{(2I-1)(2I+3)} A_{I,0}(q(\vartheta)) \right. \\ \left. + \frac{3(I-1)I}{(2I-1)(2I+1)} A_{I-2,0}(q(\vartheta)) \right\}. \end{aligned}\right\} \tag{7.12}$$

The resulting excitation probabilities are given in Figs. 16 and 17 in terms of the coefficients $N^f_{I_f, K_f}$. This coefficient is plotted for $K_f = 0$, $I = 0, 2$ and 4 and for $K_f = 2$, $I = 2$ and 4. The states with odd spins in the $K = 2$ band are not excited in the $q(\vartheta)$ approximation.

The perturbation treatment (7.7) is only correct if the quantity $r_{if}\, q(\vartheta)$ is smaller than one (compare Fig. 2).

If the bands are strongly coupled through the interaction with the projectile one may evaluate the matrix element (7.3) by a diagonalization method. We thus introduce a unitary transformation $U$ which diagonalizes the matrix elements of the exponent in (7.3), i. e.,

$$\langle aK_a \mid U^\dagger \sum_\nu q_\nu(\vartheta)\, Y^*_{2,\nu}(\beta, 0)\, U \mid bK_b \rangle = \delta_{ab} \cdot \lambda_a . \tag{7.13}$$

The result (7.3) can then be written in the form

$$a_{I_f K_f M_f} = \sum_z \langle I_f K_f M_f \mid \langle f \mid U \mid z \rangle e^{-i \sqrt{\frac{64\pi}{45}} \lambda_z} \langle z \mid U^\dagger \mid i \rangle \mid I_i K_i M_i \rangle . \tag{7.14}$$

Since $\lambda$ and the unitary matrix $U$ in the general case depend on the Eulerian angle $\beta$ in a rather complex way, this result is of practical interest only in some special cases. We shall consider the case where only two bands are involved in the excitation process. We assume that they have the same intrinsic quadrupole moment and that $K_i = K_f$. The matrix diagonalization is then easily performed and one finds the result

$$\left.\begin{aligned} a^{(i)}_{IKM} &= \frac{1}{2}\left\{a_{IM}\left[q(1+r_{if})\right] + a_{IM}\left[q(1-r_{if})\right]\right\} \\ a^{(f)}_{IKM} &= \frac{1}{2}\left\{a_{IM}\left[q(1+r_{if})\right] - a_{IM}\left[q(1-r_{if})\right]\right\} . \end{aligned}\right\} \tag{7.15}$$

It is interesting to compare this result with the result (7.7) from the perturbation treatment. In Fig. 18 we have plotted the excitation probability for the state $\mid 2,0,0 \rangle$ as a function of $q$ for different values of $r$. It is seen that the perturbation treatment is correct if $rq \lesssim 1$, as was to be expected. This condition will in actual cases usually be fulfilled.

If $\mid K_f - K_i \mid$ is larger than 2 the transition between the bands is $K$ forbidden. A possible transition between the bands can then occur only if the wave function (7.1) contains admixtures from other bands. Such admixtures can also play an important role in $K$ allowed transitions[18].

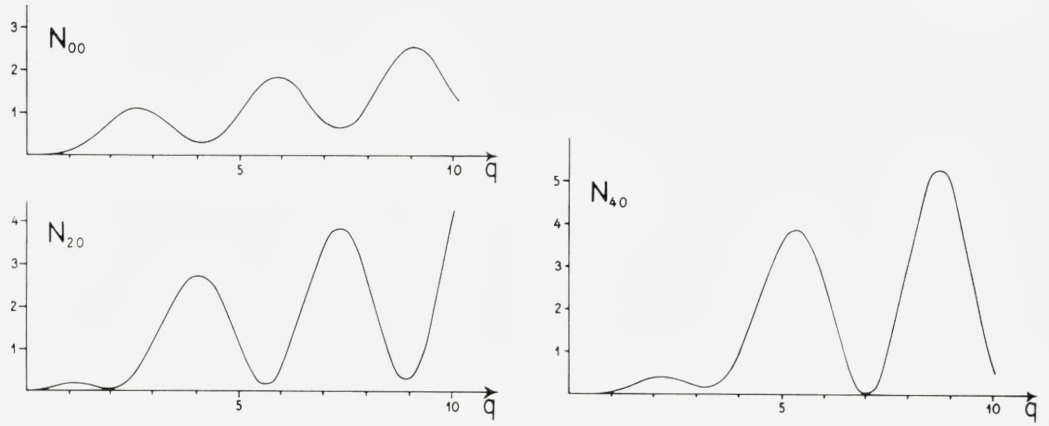


Fig. 16. The excitation probability of a weakly coupled pure rotational band with $K = 0$ in an even-even nucleus. The figure shows the coefficient $N^{(f)}_{I,0}$ in the perturbation treatment (see Eq. (7.8)) for $I = 0,2$ and 4 as a function of $q(\vartheta)$, which is assumed to be the same for the two bands.

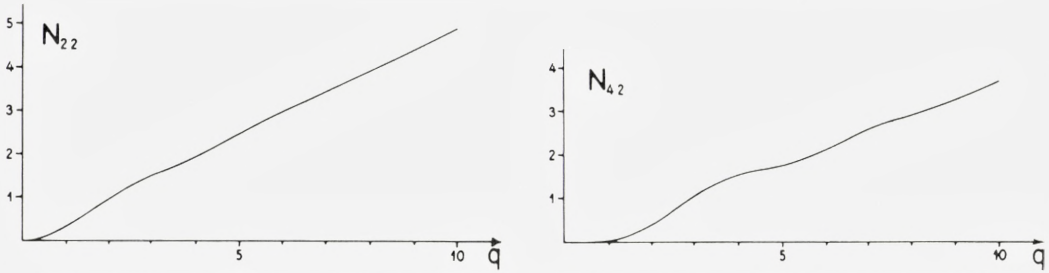


Fig. 17. The excitation probability of a weakly coupled, pure rotational band with $K = 2$ in an even-even nucleus. The figure shows the coefficient $N^{(f)}_{I,2}$ in the perturbation treatment (see Eq. (7.8)) for $I = 2$ and 4 as a function of $q(\vartheta)$ which is assumed to be the same for the two bands. In the $q(\vartheta)$ approximation, which has been used for the evaluation of $N$, the states with odd $I$ are not excited.

## 8. Conclusion

The multiple Coulomb excitation has until now been observed only in a few cases, but, from these observations (see refs. 5 and 6) as well as from the survey given in the present paper, it seems that a large number of experimental possibilities are offered. Especially it seems promising to investigate the excitation of the vibrational degrees of freedom of the nucleus, since our present knowledge on such states is rather limited. It is known that the vibrational states are mostly rather impure and for a quantitative comparison one may need some modification of the present theory. Simi-

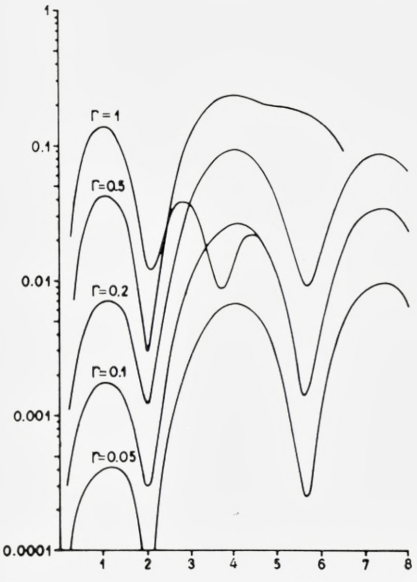


Fig. 18. The excitation probability of a strongly coupled pure rotational band with $K = 0$. The figure shows the excitation probability of the $I = 2$ state for different values of the coupling $r$ (see Eq. (7.9)). The probabilities are given as functions of $q(\vartheta)$ which is assumed to be equal in the two bands.

larly deviations from the pure rotational model have been observed. These deviations introduce a number of new parameters in the theory, and these can, in turn, be determined by a comparison of the experimental cross sections with the theory. On the other hand the increasing number of parameters make a systematic tabulation of cross sections increasingly difficult.

The larger part of the present paper was written during a stay of one of the authors (A.W.) at the Federal Institute of Technology in Zürich, Switzerland. We wish to thank Professor Paul Scherrer for making this stay possible. Sincere thanks are due Professor Aage Bohr for his continual interest in our work.

*Federal Institute of Technology, Zürich, Switzerland*
*and*
*Institute for Theoretical Physics, University of Copenhagen, Denmark.*

## References


1) K. Alder, A. Bohr, T. Huus, B. Mottelson and A. Winther, Revs. Mod. Phys. **28**, 432 (1956).
2) G. Breit and R. L. Gluckstern, Encyclopedia of Physics (Springer, Berlin, 1959) Vol. XLI/1 p. 496.
3) N. P. Heydenburg and G. M. Temmer, Annual Review of Nuclear Science (Annual Reviews Inc., Palo Alto, Calif. 1956) Vol. 6, p. 77.
4) R. Huby, Reports on Progress in Physics, (The Physical Society, London 1958) Vol. XXI p. 59.
5) J. O. Newton and F. S. Stephens, Phys. Rev. Let. **1**, 63 (1958).
6) F. S. Stephens and R. Diamont, Private communieation.
7) K. Alder and A. Winther, Mat. Fys. Medd. Dan. Vid. Selsk. **31**, no. 1 (1956).
8) A. Bohr and B. Mottelson, Mat. Fys. Medd. Dan. Vid. Selsk. **27**, no. 16 (1953).
9) A. R. Edmonds, Angular Momentum in Quantum Mechanics (Princeton University Press, Princeton, 1957).
10) A. Erdélyi et al., Higher Transcendental Functions, (Mc Graw-Hill Book Company, Inc., New York, 1953).
11) L. C. Biedenharn and R. M. Thaler, Phys. Rev. **104**, 1643 (1956).
12) G. N. Watson, A Treatise on the Theory of Bessel Functions, (Cambridge University Press, Cambridge, England, 1952).
13) E. Jahnke and F. Emde, Tables of Functions, (Dover Publications, New York, 1945).
14) G. Breit, R. L. Gluckstern and J. E. Russel, Phys. Rev. **103**, 727 (1956).
15) D. C. Choudhury, Mat. Fys. Medd. Dan. Vid. Selsk. **28**, no. 4 (1954).
16) K. W. Ford and C. Levinson, Phys. Rev. **100**, 1 (1955).
17) G. Racavy, Nucl. Phys. **4**, 289 (1957).
18) P. Gregers Hansen, O. B. Nielsen and R. K. Sheline, Nucl. Phys. **12**, 389 (1959).



Indleveret til Selskabet den 5. december 1959
Færdig fra trykkeriet den 25. juli 1960.

Matematisk-fysiske Meddelelser
udgivet af
Det Kongelige Danske Videnskabernes Selskab
Bind **32,** nr. 9

Mat. Fys. Medd. Dan. Vid. Selsk. **32,** no. 9 (1960)

# PAIRING PLUS LONG RANGE FORCE FOR SINGLE CLOSED SHELL NUCLEI

BY

L. S. KISSLINGER AND R. A. SORENSEN

København 1960
i kommission hos Ejnar Munksgaard

## Synopsis

The low energy properties of nuclei are calculated, using a model which combines certain important features of the unified nuclear model and the independent-particle model with a two-body residual interaction. The residual interaction used has two parts, a pairing force and a long range part. Calculations are done for nuclei with a major closed proton or neutron shell, $A > 48$, for various values of the two strength parameters, using single-particle levels taken from experiment. In each region, the calculated energy levels and spins agree in considerable detail with systematic experimental data. In addition, the even-odd-$A$ mass difference, the electromagnetic transition rates, and other properties are calculated and compared to experiment. The approximate $1/A$ dependence of the parameters is consistent with a volume force.

Printed in Denmark
Bianco Lunos Bogtrykkeri A/S

# CONTENTS


| | Page |
|---|---|
| I. Introduction | 5 |
| II. The Hamiltonian and Approximate Solutions | 8 |
| A. The Hamiltonian | 8 |
| B. Pairing Force | 10 |
| 1. Canonical Transformation to an Independent-Particle Hamiltonian | 10 |
| 2. Energy Spectrum | 12 |
| 3. Number of Particles | 12 |
| 4. Accuracy of the Solutions | 13 |
| C. $P^{(2)}$ Force | 14 |
| 1. Perturbation Theory | 14 |
| 2. Collective Coordinates | 16 |
| III. Energy Level Systematics | 22 |
| A. The Shell Model Particle Well | 22 |
| B. The Choice of Parameters | 23 |
| C. Energy Levels in S.C.S Nuclei | 25 |
| 1. Pb Isotopes | 26 |
| 2. Sn Isotopes | 32 |
| 3. Ni Isotopes | 36 |
| 4. $N = 82$ | 36 |
| 5. $N = 50$ | 40 |
| 6. $N = 28$ | 47 |
| IV. Total Binding Energies | 50 |
| A. Even-Odd Mass Differences | 50 |
| B. Absolute Binding Energies | 52 |
| V. Electric Quadrupole Moments | 57 |
| VI. Magnetic Dipole Moments in Odd Nuclei | 59 |
| A. Magnetic Moments with a Pairing and $P^{(2)}$ Force Model | 59 |
| B. Magnetic Moments with Configurations Admixed by a $\delta$-Function Force | 61 |
| VII. Electromagnetic Transition Rates | 63 |
| A. Odd-$A$ Nuclei | 63 |
| B. Even-$A$ Nuclei | 69 |
| 1. Single-Particle Transitions in Two Quasi-Particle States | 69 |
| 2. The $2^+ \rightarrow 0^+$ $E2$ Transitions | 73 |
| VIII. Summary | 75 |
| Acknowledgements | 77 |
| Appendix | 77 |
| References | 81 |

## I. Introduction

In the past several years, much evidence has been gathered by studying the low energy spectra of nuclei, and it has been possible to interpret many of the main observed features by the Unified Nuclear Model, i. e., in terms of the motions of individual particles in an effective nuclear potential[1] and collective excitations of rotational and vibrational character[2].

At the same time, attempts have been made to understand nuclear properties in terms of shell model particles interacting with a two-body force[3]. The detailed calculations in a single $j$ shell for lighter nuclei have shown that in many cases it is possible to calculate approximately the energy levels by using specific nuclear forces. However, these calculations with pure configurations are not valid for heavier nuclei where configuration mixing becomes very important. Still, shell model calculations with a two-body force show that it is possible to derive many of the properties of nuclei with a few particles outside of closed shells by using a two-body force between particles which move in a well taken from experiment. However, for more than two or three particles in the system such calculations become extremely involved.

More recently, progress has been made in solving the many-body problem for specific models. Such work shows that it may be possible to derive the Unified Nuclear Model from a shell model description with the inclusion of a two-body interaction[4]. The first step was made by ELLIOTT who showed how the collective deformation and the associated rotational spectra can be obtained for particles in a harmonic oscillator potential interacting with a specific two-body force having angular dependence given by $P^{(2)}(\cos\theta)$, with $\theta$ representing the angle between the particles[5]. Later work[6] provided evidence that this is a general characteristic of the coupling scheme arising from interactions with a slow angular dependence, such as that of $P^{(2)}(\cos\theta)$. Since the low multipoles of the force are associated with the relatively long range part of the interaction, it therefore appears that this part of the nuclear interaction may be treated in terms of a deformed field acting

upon the individual nucleons, and is responsible for the associated collective nuclear properties.

The observed nuclear spectra clearly reveal, however, that there are important additional interaction effects which cannot be incorporated into the nuclear field. These residual interactions are responsible, for instance, for the shift of the intrinsic observed levels from the independent-particle prediction, for the collapse of the deformation with the approach to the closed shell regions, and for the energy gap observed in the intrinsic nuclear spectra. These two-body interactions should arise from the relatively short range part of the two-body interaction. A crucial problem has therefore been to develop methods to treat the effect of the short range part of the nuclear force in many-particle configurations.

A new approach to this problem was suggested by the recent development in the theory of superconductivity[7]. Methods have become available for treating the effects of a simplified interaction, the "pairing force", by which we mean a force which has constant matrix elements in a $(jm)$, $(j-m)$ representation. I.e., the matrix elements of the pairing force between states of two particles in a $j$-level and two particles in a $j'$-level are proportional to $\sqrt{[(2j+1)/2]\,[(2j'+1)/2]}$ if the total angular momentum in both states is zero, and vanishes otherwise. Such a force appears to represent many of the characteristic features of a short range interaction[8),9]. It is hoped that specific differences between a short range force and the pairing force interaction can be calculated for individual properties when such differences are important.

The pairing force is a generalization of an interaction operator earlier introduced by RACAH, which characterizes the seniority coupling scheme for $(j)^n$ configurations. The new method therefore also leads to a generalization of the seniority concept in terms of the "quasi-particles". States of different seniority are separated by relatively large energies, and the gap in the nuclear excitation spectrum is thereby introduced, in analogy to that of the superconducting metals.

A nuclear model in which the interaction is represented by two simple components, the pairing force plus the long range part, usually represented by a quadrupole force, has been studied in some detail by BELYAEV[10] who showed that it contains the main qualitative features of the observed spectra. In particular, it accounts for the gradual transition from the closed shell regions to the regions of deformed nuclei with the associated vibrational and rotational modes of excitation.

Calculations with the model have so far, however, been based on a

greatly simplified single-particle level spectrum; especially the case of particles in a single degenerate level, such as a major shell in an oscillator field, have been treated[11]. A quantitative comparison with experimental data has therefore not been possible. To this purpose it is essential to introduce the proper succession and separation of the low lying single-particle levels available to the particles outside of closed shells.

In the present investigation we have attempted to perform such more realistic calculations, with a pairing force plus a $P^{(2)}$ force, based on available information about the single-particle level spectrum of the shell model, and to make a comparison with experimental data on the low energy nuclear properties.

For simplicity, we have restricted ourselves to nuclei in which either the neutrons or the protons are in a major closed shell. We shall refer to these as s.c.s. (single closed shell) nuclei. For this reason, we do not have to deal with the difficult problem of the short range interaction between neutrons and protons. These isotopes do not seem to possess a static equilibrium deformation and we can therefore use the spherical wave functions as a basis from which to start the calculation. The single-particle levels, when known, are taken from experiments on isotopes with one particle or hole outside of a double closed shell. In other cases, their positions are estimated from other experimental results and from theoretical calculations of the nuclear well.

Since the s.c.s. nuclei have a spherical equilibrium shape, the pairing force must in some sense be stronger than the $P^{(2)}$ force. For this reason, we first calculate the excitation energies of the s.c.s. nuclei with only the pairing force acting between shell model particles. We do this approximately, using the Bardeen solutions. Subsequently, the effect of the $P^{(2)}$ force is determined by the deformed field method. Of course, with such a simple force we cannot expect to derive the detailed quantitative properties of these nuclei, but rather attempt to find the main systematic features and to identify the main parts of the nuclear wave functions. We do expect that certain of the specific nuclear properties which are not given correctly by our wave functions might be derived from them by perturbation theory.

In Chapter II, the canonical transformation of the pairing Hamiltonian to the quasi-particle system is reviewed and the results are given which are important for the present calculation. We also describe the transformation to the collective coordinates to obtain the collective states. As an example of a possible interaction between quasi-particles, the perturbation theory results for the $P^{(2)}$ force are derived.

In Chapter III, the results for the energy levels of odd-$A$ and even-$A$ nuclei are presented for the various nuclear regions treated, along with discussions of the single-particle wells and the strength of the pairing and $P^{(2)}$ force in each case. In Chapter IV, the gap which results from our solutions is compared to that measured by the even-odd mass differences. In Chapter V, the expressions for the quadrupole moments are derived with our wave functions, and our theoretical predictions are compared to experiment. In Chapter VI, our calculated magnetic moments are compared to experiment and the additional shifts in the magnetic moments which are produced by a short range force differing from the pairing force are considered. In Chapter VII, the alterations of the electromagnetic transition rates caused by the pairing force and the $P^{(2)}$ force are investigated and the results compared to the experimental values.

## II. The Hamiltonian and Approximate Solutions

### A. The Hamiltonian

The basic assumption of this work is that, in the space of the wave functions for the low energy states of nuclei, the nuclear system can be represented as closed shells plus shell model particles which move in a well which changes only slowly as the number of particles changes, and which interact with a pairing force and a $P^{(2)}$ force.

Implicit in this assumption is the fact that the excitations of the core particles involve energies which are large compared to the excitations of the extra-core particles. To the extent that this is true we expect that the main effect of ignoring the core states as well as ignoring the states in the shells higher than the shell which we consider is to renormalize the parameters of the residual two-body interaction. Since we use a force which reproduces the low energy properties of s.c.s. nuclei, we implicitly include such contributions.

With regard to the long range part of the force, there are additional contributions from the core as are revealed by the polarization effects for one particle outside of a double closed shell, such as the enhanced $E2$ transitions in $O^{17}$ and $Pb^{207}$. These are included in the present work by using a renormalized charge and quadrupole moment for the extra-core particles. The change in the positions of the single-particle levels with $A$ is neglected within each s.c.s. region.

Letting $|0\rangle$, $|jm\rangle$, and $|j-m\rangle$ stand for the shell model particle

vacuum, and states with one shell model particle with angular momentum $j$- and $z$-component $m$ and $-m$, respectively, the other quantum numbers being suppressed, we define the particle-creation operators

$$\left.\begin{aligned} b^{\dagger}_{jm}\,|\,0\,\rangle &= |\,jm\,\rangle \\ b^{\dagger}_{j-m}\,|\,0\,\rangle &= |\,j-m\,\rangle = \tau\,|\,jm\,\rangle, \end{aligned}\right\} \tag{1}$$

where $\tau$ is the time-reversal operator*. In terms of these operators, the assumption is that the low energy states of s.c.s. nuclei are eigenstates of the Hamiltonian

$$\left.\begin{aligned} H' = \sum_{jm} \varepsilon_j\, b^{\dagger}_{jm}\, b_{jm} - \frac{1}{2}\, G \sum_{jj'mm'} b^{\dagger}_{j'm'}\, b^{\dagger}_{j'-m'}\, b_{j-m}\, b_{jm} \\ -\frac{1}{2}\,\chi \sum_{\substack{j_1 j_2 j_1' j_2' \\ m_1 m_2 m_1' m_2'}} \langle j_1' m_1' j_2' m_2' \,|\, \mathfrak{P}^{(2)} \,|\, j_2 m_2 j_1 m_1 \rangle\, b^{\dagger}_{j_1' m_1'}\, b^{\dagger}_{j_2' m_2'}\, b_{j_2 m_2}\, b_{j_1 m_1}. \end{aligned}\right\} \tag{2}$$

In (2), $\varepsilon_j$ are the single $j$ shell particle levels, $G$ is the strength parameter for the pairing force, and $\mathfrak{P}^{(2)}$ is the operator for the $P^{(2)}$ force (cf. II. C.), with a strength parameter $\chi$.

Since the solution to the pairing part of the problem is simplified by transforming to a system in which the number of particles is not conserved, an auxiliary Hamiltonian is introduced which is related to $H'$ by

$$H = H' - \lambda N = H' - \lambda \sum b^{\dagger}_{jm}\, b_{jm}, \tag{3}$$

where $\lambda$, the chemical potential, is a Lagrangian multiplier included to take into account the constraint that for the solutions $\Psi$, $(\Psi\,|\,N\,|\,\Psi) = n$, the proper number of particles. Solutions to $H$ with various values of $G$ and $\chi$ are found for each s.c.s. region and a comparison shows that the $A$ dependence of these parameters is consistent with their being a volume force.

* The states $|\,j-m\,>$ have the phases $(-1)^{j-m}\times$ the states used by A. R. Edmonds "Angular Momentum in Quantum Mechanics", Princeton University Press, Princeton, New Jersey (1957). Thus, the orbital spherical harmonics are defined as $i^l Y_{1m}$ and the spin states have an intrinsic phase of $\pi/2$ under time reversal. This choice of phases results in the same signs for the amplitudes of the $|\,jm\,>|\,j-m\,>$ states which are components of a $(j^2)_0$ state.

### B. Pairing Force

1. *Canonical Transformation to an Independent-Particle Hamiltonian*

The ground state of the independent-particle Hamiltonian without residual interactions corresponds to filling of the single-particle levels with a sharp cutoff at the Fermi energy. I.e., all of the single-particle levels below the Fermi energy are definitely occupied and all of those above the Fermi energy are definitely unoccupied in the shell model ground state configurations. In the presence of the residual interactions, some of the particles are excited from the occupied single-particle levels to the levels which were unoccupied. The ground state of the Hamiltonian with a short range residual interaction corresponds to a diffuse distribution of the particles in the single-particle levels, with a region of energy near the Fermi energy, where the product, $U^2 V^2$, of the probability of occupation of a level, $V^2$, and the probability of non-occupation of a level, $U^2$, is not zero. Based on this physical picture, the method used in the present work is to express the ground state of the Hamiltonian with a pairing force residual interaction as an admixture of shell model configurations with the admixture coefficients determined by the $U$'s and $V$'s.

The energy level of an excited state of the independent-particle Hamiltonian without residual interactions is found simply by summing the single-particle energies of the excited configuration. In the presence of short range forces, the present method of solution allows one to identify once more independent modes of excitation, so that the energy level of an excited state eigenfunction with pairing forces present can be found approximately by simply adding the elementary excitation energies. Indeed, the independent excitations in the presence of the pairing forces are usually quite different from the single-particle shell model energy differences.

A convenient approximate solution for that part of Eq. (3) not including the $P^{(2)}$ force can be found by introducing the Bogolubov-Valatin canonical transformation into "quasi-particle" creation and annihilation operators[7]

$$\left.\begin{aligned} \alpha_{jm} &= U_j b_{jm} - V_j b^{\dagger}_{j-m} \\ \beta_{jm} &= U_j b_{j-m} + V_j b^{\dagger}_{jm} \\ U_j^2 &+ V_j^2 = 1. \end{aligned}\right\} \qquad (4)$$

Thus, a quasi-particle creation operator is a linear combination of a shell model particle and a shell model hole creation operator. The physical interpretation of $U_j$ and $V_j$ will be that $V_j^2$ is the probability of the pair

$(jm, j-m)$ being found in the ground state, while $U_j^2$, of course, is the probability for non-occupancy, as can be seen from Eq. (8). Written in terms of these new Fermion operators, the Hamiltonian (in normal form) is

$$H^G = U + H_{11} + H_{20} + H_{\text{int}}, \tag{5}$$

where $H^G$ refers to the Hamiltonian (3) without the $P^{(2)}$ force. $U$ is independent of quasi-particle operators, $H_{11}$ is an operator of single quasi-particle type, i.e., each term has a factor $(\alpha^+ \alpha + \beta^+ \beta)$, and $H_{20}$ creates or annihilates two quasi-particles. $H_{\text{int}}$, which contains products of four quasi-particle creation or annihilation operators, is ignored.[7), 10)] Therefore, when $H_{20}$ is set identically equal to zero, the Hamiltonian (5) describes a system of non-interacting quasi-particles. The long range part of the two-body force will lead to an interaction between quasi-particles, as will be seen in the next section.

The result of setting $H_{20} = 0$ is the gap equation

$$\frac{G}{2} \sum_j \frac{\Omega_j}{\sqrt{(\varepsilon_j - \lambda)^2 + \Delta^2}} = 1, \tag{6}$$

where

$$\left.\begin{aligned} \Delta &= G \sum_j \Omega_j U_j V_j \\ U_j^2 &= \frac{1}{2}\left[1 + \frac{\varepsilon_j - \lambda}{\sqrt{(\varepsilon_j - \lambda)^2 + \Delta^2}}\right] \\ V_j^2 &= \frac{1}{2}\left[1 - \frac{\varepsilon_j - \lambda}{\sqrt{(\varepsilon_j - \lambda)^2 + \Delta^2}}\right], \end{aligned}\right\} \tag{7}$$

and $\Omega_j = j + 1/2$ is the pair degeneracy of the $j$ level. The essential problem in finding the solutions is determining $\lambda$ and $\Delta$, which are found by the simultaneous solution of the gap equation (6) together with the equation which results from fixing the mean number of particles (cf. (13)).

The wave functions are simply the quasi-particle creation operators operating on the quasi-particle vacuum. For an even-$A$ nucleus, the ground state is the quasi-vacuum state, i.e., a state where all shell model particles are coupled in pairs to zero angular momentum. The excited states are the two, four, etc. quasi-particle states, corresponding to two, four, etc. elementary excitations. In terms of the shell model particle states, the ground state of the even-$A$ nuclei is

$$\Psi_0 = \prod_j \prod_{m>0} (U_j + V_j b^\dagger_{jm} b^\dagger_{j-m}) |0\rangle, \tag{8}$$

where $|0>$ is the vacuum for a shell model particle, defined as $b|0> = 0$. One obtains the one, two, etc. quasi-particle states by operating on $\Psi_0$ with quasi-particle creation operators.

2. *Energy Spectrum*

The ground state energy for even-$A$ nuclei is

$$\left.\begin{aligned} (\Psi_0 | H^G | \Psi_0) + \lambda n = U + \lambda n \equiv U' \\ = \sum_j{}' \Omega_j \varepsilon_j \left[1 - \frac{\varepsilon_j - \lambda}{\sqrt{(\varepsilon_j - \lambda)^2 + \Delta^2}}\right] - \sum_j{}' \frac{\Omega_j \Delta^2}{2\sqrt{(\varepsilon_j - \lambda)^2 + \Delta^2}} \\ - \frac{G}{4} \sum_j{}' \Omega_j \left[1 - \frac{\varepsilon_j - \lambda}{\sqrt{(\varepsilon_j - \lambda)^2 + \Delta^2}}\right]^2, \end{aligned}\right\} \tag{9}$$

while the energy of a two quasi-particle state is

$$\left.\begin{aligned} (\Psi(j_1 j_2) | H^G | \Psi(j_1 j_2)) + \lambda n = U' + \sqrt{(\varepsilon_{j_1} - \lambda)^2 + \Delta^2} + \sqrt{(\varepsilon_{j_2} - \lambda)^2 + \Delta^2} \\ = U' + E_{j_1} + E_{j_2}, \end{aligned}\right\} \tag{10}$$

where the two quasi-particles have angular momenta $j_1$ and $j_2$. From Eqs. (9) and (10) it is clear that there is a gap of at least $2\Delta$ between the ground state and the two quasi-particle states of even nuclei. The ground state of odd-$A$ nuclei is a one quasi-particle state, while the excited states are one, three, etc. quasi-particle states. Usually the three quasi-particle states are quite far removed in energy. Thus the energies of the ground and low excited states in odd-$A$ nuclei are

$$(\Psi(j) | H^G | \Psi(j)) + \lambda n = U' + \sqrt{(\varepsilon_j - \lambda)^2 + \Delta^2} = U' + E_j, \tag{11}$$

where $j$ is the angular momentum of the quasi-particle. Since there are several one quasi-particle states in each odd-$A$ isotope, there is no gap like that in the even isotopes.

3. *Number of Particles*

For a state with $r$ quasi-particles, $1, \ldots, r$, the expectation value of the number operator is

$$(\Psi_1 \ldots r \,|\, N \,|\, \Psi_1 \ldots r) = \sum_j{}' \Omega_j \left[1 - \frac{\varepsilon_j - \lambda}{\sqrt{(\varepsilon_j - \lambda)^2 + \Delta^2}}\right] + \sum_{i=1}^{r}{}' \frac{\varepsilon_i - \lambda}{\sqrt{(\varepsilon_i - \lambda)^2 + \Delta^2}}. \quad (12)$$

In even-$A$ nuclei, the average number of particles in the ground state is

$$(\Psi_0 \,|\, N \,|\, \Psi_0) = n = \sum_j{}' \Omega_j \left[1 - \frac{\varepsilon_j - \lambda}{\sqrt{(\varepsilon_j - \lambda)^2 + \Delta^2}}\right]. \quad (13)$$

Given the shell model energies in a particular shell, (13) and (6) are sufficient to determine $\lambda$ and $\Delta$, for a given isotope, which in turn determine the ground state wave function and energy. The same values of $\lambda$ and $\Delta$ are used for the excited states. This insures that those states are orthogonal to the ground states, and is expected to be a good approximation for states of few quasi-particles, which are the only ones considered in the present work. One could adjust $\lambda$ and $\Delta$ for higher states. However, in this work, the average number of particles differs from the number $N$ in the ground state. For instance, in a state with two quasi-particles of angular momentum $k$, the average number of particles differs from that of the ground state by

$$(\Psi(k,k) \,|\, N \,|\, \Psi(k,k)) - (\Psi_0 \,|\, N \,|\, \Psi_0) = 2\,\frac{\varepsilon_k - \lambda}{\sqrt{(\varepsilon_k - \lambda)^2 + \Delta^2}}. \quad (14)$$

Although for the lowest quasi-particle states this quantity is small, since $\lambda \approx \varepsilon_k$ for the lowest elementary excitations, this variation in average number is sometimes nearly two for the distant two quasi-particle states. On the other hand, the error in the energy value of the state is not expected to be large since the solutions of $H^G$ are stationary with respect to a variation in $n$. Still, a basic assumption of this work is that the excited states vary smoothly and slowly from isotope to isotope.

For the odd-$A$ isotopes Eq. (13) is also used. In this case, the error in the average number of particles is small for the lowest states and unimportant in determining energy eigenvalues for the high one quasi-particle states for the same reason.

4. *Accuracy of the Solutions*

For a degenerate level, the Bardeen solutions give energies which are correct to order $\Omega^{-1}$ when compared to the exact solutions with the pairing force. In other words, the energies are good to order $G/\Delta$, since $\Delta = G\Omega$ in this case. For a system of non-degenerate levels there is an effective pairing degeneracy,

$$\Omega_{\text{eff}} \equiv \frac{\Delta}{G} = \frac{1}{2} \sum_j \frac{\Omega_j}{\sqrt{\left(\frac{\varepsilon_j - \lambda}{\Delta}\right)^2 + 1}}, \tag{15}$$

which indicates the accuracy. Therefore, even if the state near the Fermi surface has a low degeneracy, the solutions can give useful results so long as the pairing force scatters sufficiently to other states. One situation in which one might expect these solutions to be inaccurate is that in which a nuclear shell has a $j = 1/2$ subshell rather isolated from other levels. Such a situation may occur in the region of 50 neutrons. In this case, the solutions might be quite inaccurate for two or three isotopes near the point where the gap is small.

In addition to the small errors in the calculated energies which have been discussed above, the present approximation method introduces a characteristic uncertainty which arises directly from the fact that the wave functions are not eigenfunctions of the number of nuclear particles. This is the introduction of spurious states, and in particular of one spurious spin zero two quasi-particle state.[8), 9)] Many levels are involved when the gap is large, so this spurious state is then distributed over many levels; there are, nevertheless, some situations in which one state is almost entirely spurious, as is the case in $Pb^{206}$. One can usually recognize such a situation when it occurs.

### C. $P^{(2)}$ Force

1. *Perturbation Theory*

For the long range part of the shell model particle interaction we use the last term of (2) as two-body $P^{(2)}$ force:

$$\left.\begin{aligned} H_{\text{long range}} &= -5/4\,\pi \frac{1}{2} \chi \sum_{ij} F(r_i, r_j)\, P^{(2)}(\cos\theta_{ij}) \\ &= -\frac{1}{2} \chi \sum \langle j_1 m_1 j_2 m_2 | F(r_1, r_2) \sum_{\mu} (-1)^{\mu} Y^2_{\mu}(1)\, Y^2_{-\mu}(2) | j_2' m_2' j_1' m_1' \rangle \\ &\qquad b^{\dagger}_{j_1 m_1} b^{\dagger}_{j_2 m_2} b_{j_2' m_2'} b_{j_1' m_1'}, \end{aligned}\right\} \tag{16}$$

where $P^{(2)}(\cos\theta)$ is the Legendre polynomial of order two. The reason for this choice of force is that, for nuclei far from a closed shell, it can produce permanent quadrupole deformations which are experimentally observed; and for nuclei with or near closed shells, where its effect is weaker, it can provide an explanation for the observed quadrupole vibrational spectra.

Even for s.c.s. nuclei, which we consider, the long range interaction between the outside nucleons and the closed shell core plays an important role. However, we shall take the $P^{(2)}$ force acting only among the outside nucleons, and assume that the effect of the core can be included as a quadrupole force and charge renormalization for the outside particles.

For the perturbation treatment to follow, the radial dependence of the force is of less importance than the angular dependence given by $P^{(2)}(\cos\theta)$. In a $j$ shell, for example, the energy spectrum is given entirely by the angular dependence of the force. For the evaluation of the matrix elements, we use the radial dependence $r_i^2 r_j^2$, as this is simply connected with the quadrupole field description of § II. C 2. This is the force, $r_i^2 r_j^2 P^{(2)}(\cos\theta)$, which is diagonal in the $U(3)$ coupling scheme of Elliott.[5] For the evaluation of the radial matrix elements, harmonic oscillator wave functions are used.

If it is sufficiently weak, the $P^{(2)}$ force may be treated as a perturbation to the pairing force calculation. For this purpose, it is convenient to expand the force (16) in terms of creation and annihilation operators for quasi-particles:

$$H_{\text{long range}} = \frac{1}{2}\chi\left\{\mathfrak{P}_{00}{}^{(2)} + \mathfrak{P}_{20}{}^{(2)} + \mathfrak{P}_{11}{}^{(2)} + \mathfrak{P}_{40}{}^{(2)} + \mathfrak{P}_{31}{}^{(2)} + \mathfrak{P}_{22}{}^{(2)}\right\}, \qquad (17)$$

where, as in Belyaev, the subscripts refer to the number of creation and annihilation operators, respectively. The general form of the terms is given by Belyaev[10]. In first order perturbation theory, only $\mathfrak{P}_{11}{}^{(2)}$ and $\mathfrak{P}_{22}{}^{(2)}$ contribute to the relative level spacing. The effect of $\mathfrak{P}_{11}{}^{(2)}$ is to add to the energy of a quasi-particle of angular momentum $j$ an amount

$$\langle\alpha_j|\,\mathfrak{P}_{11}{}^{(2)}\,|\alpha_j^\dagger\rangle = \chi\sum_{j_1}{}' \frac{5}{4\pi}\left(C^{2\ j\ j_1}_{0\ \frac{1}{2}\ \frac{1}{2}}\right)^2\left\{U_j^2 - (U_{j_1}U_j - V_{j_1}V_j)^2\right\}\langle j\,|\,r^2\,|\,j_1\rangle^2, \qquad (18)$$

where the "$C$"-symbol is a Clebsch-Gordan coefficient.

For the perturbation to have no effect on the number of particles in the ground state, to first order in the coupling constant $\chi$, the chemical potential must be shifted simultaneously by an amount

$$\left.\begin{aligned}\Delta\lambda = \chi\sum_{jj_1}{}' \frac{5}{4\pi}\left(C^{2\ j\ j_1}_{0\ \frac{1}{2}\ \frac{1}{2}}\right)^2\left(j+\frac{1}{2}\right)E_j^{-1}\left[(2U_jV_j)^2V_{j_1}^2 - (2U_jV_j)(U_j^2-V_j^2)U_{j_1}V_{j_1}\right]\\ \langle j\,|\,r^2\,|\,j_1\rangle^2\left[\sum_{j'}{}'\left(j'+\frac{1}{2}\right)E_{j'}^{-1}(2U_{j'}V_{i'})^2\right]^{-1}.\end{aligned}\right\} \qquad (19)$$

This causes an additional shift in energy for a quasi-particle of angular momentum $j$ of an amount

$$\Delta E_j = -\Delta\lambda\,(U_j^2 - V_j^2). \tag{20}$$

If $G \ll \Delta$, the inclusion of this contribution is equivalent to the readjustment of the $U$'s and $V$'s so as to satisfy (6) and (13) with the inclusion of $P^{(2)}$ to first order in $\chi$, thus leaving the quasi-particles independent except for the interaction part of the Hamiltonian, $\mathfrak{P}_{40}{}^{(2)} + \mathfrak{P}_{31}{}^{(2)} + \mathfrak{P}_{22}{}^{(2)}$. This contribution due to $\Delta\lambda$ is unimportant except for quasi-particles far from the Fermi surface.

The term $\mathfrak{P}_{22}{}^{(2)}$ has no effect on zero or one quasi-particle states, but for two quasi-particle states it splits the energy according to the total angular momentum, $J$, to which the two quasi-particles are coupled, thus breaking the degeneracy of the pairing Hamiltonian. For two quasi-particles of angular momentum $j_1$ and $j_2$ coupled to $J$, the energy shift is

$$\begin{aligned}\frac{1}{2}\chi\langle[\alpha_{j_1}\beta_{j_2}]^J \mathfrak{P}_{22}{}^{(2)}[\beta_{j_2}^\dagger \alpha_{j_1}^\dagger]^J\rangle = -\frac{5}{4\pi}\frac{\chi}{2}\sqrt{(2j_1+1)(2j_2+1)}\\ \Big\{(-1)^{j_1+j_2-J} C_{0\,\frac{1}{2}\,\frac{1}{2}}^{2j_1 j_1} C_{0\,\frac{1}{2}\,\frac{1}{2}}^{2j_2 j_2} W(j_1 j_2 j_1 j_2; J2)\langle j_1|r^2|j_1\rangle\langle j_2|r^2|j_2\rangle (U_1^2 - V_1^2)(U_2^2 - V_2^2)\\ -(-1)^{j_1-j_2} C_{0\,\frac{1}{2}\,\frac{1}{2}}^{2j_1 j_2} C_{0\,\frac{1}{2}\,\frac{1}{2}}^{2j_2 j_1} W(j_1 j_2 j_2 j_1; J2)\langle j_1|r^2|j_2\rangle^2 (U_1 U_2 - V_1 V_2)^2\\ +\frac{1}{5}(-1)^{j_1-j_2} C_{0\,\frac{1}{2}\,\frac{1}{2}}^{2j_1 j_2} C_{0\,\frac{1}{2}\,\frac{1}{2}}^{2j_2 j_1} \delta_{J2}\langle j_1|r^2|j_2\rangle^2 (U_1 V_2 + U_2 V_1)^2\Big\}.\end{aligned} \tag{21}$$

where "$W$" is a Racah coefficient.

The first two terms on the right, which have the $J$ dependence of the direct and exchange part of two shell model particles interacting with a $P^{(2)}$ force, arise from the normal interaction of the hole and particle part of the two quasi-particles with each other, the $U$, $V$ factor expressing the fact that a hole and a particle interact with opposite sign from two particles or two holes. The third term, which only affects $J = 2$ states, arises from the mutual annihilation of the hole and particle parts of the quasi-particles and their subsequent creation through the $P^{(2)}$ force.

2. *Collective Coordinates*

It is easily seen from the experimental data on transition rates and excitation energies that this perturbation treatment of the long range force is not adequate for all states of most of the isotopes considered. First, the large

$B(E2)$ values for the deexcitation from the first excited $2^+$ state of even nuclei to the $0^+$ ground state make it impossible to explain this state as a two quasi-particle state perturbed by a $P^{(2)}$ force. The pairing correlations may introduce some enhancement of the $B(E2)$ values above a "single-particle" estimate, but in all cases they introduce less enhancement than that indicated by the collective treatment which follows. One finds, in the case of $Pb^{206}$, that the enhancement predicted by the collective treatment is 2.4 times that of the two quasi-particle $2^+$ state with the largest enhancement. For $Pb^{206}$, where the effective charge (see Eq. (34)) is known from experiments in $Pb^{207}$, the transition rate agrees better with the collective $B(E2)$ than with the quasi-particle value. Thus, even though the collective approach may be least accurate in the Pb case, it may still be more accurate than the perturbation approach. In all other cases, the collective treatment increases the enhancement over that produced by pairing correlations alone by larger factors: a factor of about six for the Sn isotopes and about four for the Ni isotopes, for example. In these cases, the effective charge is not known from experiments analogous to those on $Pb^{207}$, but the collective treatment agrees with experimental transition rates for effective charges of about the magnitude of that in $Pb^{207}$, while larger effective charges would have to be used to obtain a fast enough decay from a perturbation treatment.

Second, the lowest $2^+$ state is well below the two quasi-particle states produced by a pairing force of such strength as to be consistent with other data, this lowering also being the smallest in the case of the Pb isotopes. Since this $2^+$ state must be constructed from the quasi-particle states, and is far separated from them in energy and of a different character from them, a non-perturbation treatment is necessary for this state.

We assume with Belyaev that we can define a collective parameter, $Q$, the quadrupole field or the total nuclear quadrupole moment, and that the main effect of the long range force can be described as an interaction of each particle with that field. Then,

$$H_{\text{long range}}(Q_\mu) = -\frac{1}{2}\chi \sum_\mu Q_\mu \hat{Q}_\mu, \tag{22}$$

where $\hat{Q}_\mu$, the quadrupole moment operator, is given by

$$\left.\begin{aligned} \hat{Q} = &\sum_\nu q^\mu_{\nu\nu} 2V_\nu^2 + \sum_{\nu\nu'} q^\mu_{\nu\nu'}(U_\nu U_{\nu'} - V_\nu V_{\nu'})(\alpha^\dagger_\nu \alpha_{\nu'} + \beta^\dagger_{\nu'}\beta_\nu) \\ &+ \sum_{\nu\nu'} q^\mu_{\nu\nu'}(U_\nu V_{\nu'} + V_\nu U_{\nu'})(\alpha^\dagger_\nu \beta^\dagger_{\nu'} + \beta_\nu \alpha_{\nu'}), \end{aligned}\right\} \tag{23}$$

and

$$q^{\mu}_{\nu\nu'} = \langle \nu \,|\, r^2 Y^2_{\mu} \,|\, \nu' \rangle \quad \text{with} \quad \nu \equiv jm\,. \tag{24}$$

Using harmonic oscillator wave functions, we have the selection rules that the parity of $\nu$ is the same as of $\nu'$ and

$$|j_{\nu} - j_{\nu'}| \leqslant 2\,. \tag{25}$$

We shall also require the condition of self-consistency: that the quadrupole moment of the outside nucleons associated with the $Y^2_{\mu}$ degree of freedom be equal to $Q_{\mu}$. For this purpose we use a Lagrangian multiplier $\mu$ and the auxiliary Hamiltonian

$$H' = H - \mu \hat{Q} = H_{\text{pairing}} - \frac{1}{2}\chi Q \cdot \hat{Q} - \mu \hat{Q}\,, \tag{26}$$

where, for simplicity, we have dropped the subscript $\mu$ and consider for the moment only the contribution to the energy of the $Y^2_0$ quadrupole degree of freedom. To obtain the ground state energy of $H$ we follow a method suggested by A. Bohr which is equivalent, within the approximations used, to that of Belyaev. If the quadrupole moment is not too large, the intrinsic ground state wave functions for (26) for even-$A$ nuclei can be written in perturbation theory

$$\Psi(Q) = \Psi_0 - \left(\frac{1}{2}\chi Q + \mu\right) \sum_{\nu\nu'}{}' \frac{q_{\nu\nu'}(U_{\nu}V_{\nu'} + V_{\nu}U_{\nu'})}{E_{\nu} + E_{\nu'}}\, \alpha^{\dagger}_{\nu}\beta^{\dagger}_{\nu'}\Psi_0\,. \tag{27}$$

The Lagrangian multiplier $\mu$ is then fixed by the self-consistency condition

$$(\Psi(Q) \,|\, \hat{Q} \,|\, \Psi(Q)) = -2\left(\frac{1}{2}\chi Q + \mu\right) \sum_{\nu\nu'}{}' \frac{q^2_{\nu\nu'}(U_{\nu}V_{\nu'} + V_{\nu}U_{\nu'})^2}{E_{\nu} + E_{\nu'}} = Q\,. \tag{28}$$

The ground state energy may then be calculated as a function of $Q$ as

$$\left.\begin{aligned}(\Psi(Q) \,|\, H \,|\, \Psi(Q)) &= U' + \left\{\left[4 \sum_{\nu\nu'}{}' \frac{q^2_{\nu\nu'}(U_{\nu}V_{\nu'} + V_{\nu}U_{\nu'})^2}{E_{\nu} + E_{\nu'}}\right]^{-1} - \frac{1}{2}\chi\right\} Q^2 \\ &= U' + \frac{1}{2} C Q^2,\end{aligned}\right\} \tag{29}$$

defining the restoring force parameter $C$. The rotationally invariant collective Hamiltonian, utilizing the five quadrupole degrees of freedom $Q_{\mu}$ associated with a $Y^2_{\mu}$ deformation, is then given by

$$H_{\text{coll}} = U' + \frac{1}{2} C \sum_{\mu} Q_{\mu}^2 + \frac{1}{2} B \sum_{\mu} \dot{Q}_{\mu}^2, \tag{30}$$

where the inertial parameter $B$ is calculated in adiabatic perturbation theory to be[12)]

$$B = 2 \sum_{i} \frac{(i \mid \delta/\delta Q \mid \Psi(Q))^2}{w_i - w_0} = \frac{1}{2} \sum \frac{q_{\nu\nu'}^2 (U_\nu V_{\nu'} + V_\nu U_{\nu'})^2}{(E_\nu + E_{\nu'})^3} \left[ \sum \frac{q_{\nu\nu'}^2 (U_\nu V_{\nu'} + V_\nu U_{\nu'})^2}{E_\nu + E_{\nu'}} \right]^{-2}. \tag{31}$$

When quantized, the Hamiltonian (30) will lead to the spectrum associated with the harmonic qadrupole surface oscillations, the quanta being phonons of spin 2. With this description of the lowest $2^+$ state, its properties can easily be obtained. The energy $0^+ - 2^+$ is given by

$$\hbar\omega = \sqrt{C/B}. \tag{32}$$

The ground state energy shift due to the $P^{(2)}$ force is obtained from the zero point energy

$$\Delta E_0 = \frac{5}{2} \hbar\omega(\chi) - \frac{5}{2} \hbar\omega(\chi = 0). \tag{33}$$

Assuming the $2^+$ state to contain the entire quadrupole matrix element with the ground state, the $B(\mathrm{E2})$ value for excitation of the $2^+$ from the $0^+$ ground state is given by

$$B(E2) = \frac{5}{2} \frac{e_{\text{eff}}^2}{\sqrt{BC}}, \tag{34}$$

where $e_{\text{eff}}$ is the effective charge of the extra-core nucleons. The effective charge of a nucleon is its own charge plus an additional positive charge arising from the fact that the extra-core nucleons can polarize the proton core to some extent. Experiments indicate that the effective charge of neutrons in $Pb^{207}$ is about unity[13)]. In oxygen the proton core deformability seems to be somewhat less[14)]. For our calculations we take the effective charge of a neutron to be unity and of a proton to be two. The factor 5 occurs since the five quadrupole degrees of freedom contribute equally.

For the validity of this collective treatment of the $P^{(2)}$ force two conditions are required. First, the amplitude of the collective zero point oscillation, $Q_{\text{ave}}$, of the quadrupole moment $Q$ must be large enough compared

to the fluctuations, $\delta Q$, of the quadrupole moment of the intrinsic state for the validity of Eq. (22). Second, the amplitude of collective oscillation must be small enough that the lowest order perturbation theory expression for (27) be sufficient. For the first condition it is required that

$$\left.\begin{aligned}\left(\frac{\delta Q}{Q_{\text{ave}}}\right)^2 = \hbar\omega \sum q^2_{\nu\nu'} \frac{(U_\nu V_{\nu'} + V_\nu U_{\nu'})^2}{(E_\nu + E_{\nu'})^3} \cdot \sum q^2_{\nu\nu'} (U_\nu V_{\nu'} + V_\nu U_{\nu'})^2 \\ \left[\sum \frac{q^2_{\nu\nu'} (U_\nu V_{\nu'} + V_\nu U_{\nu'})^2}{E_\nu + E_{\nu'}}\right]^{-2} < 1 .\end{aligned}\right\} \quad (35)$$

This says roughly that the $2^+$ level must lie well below the quasi-particle excitation energies, the same condition which is required for the adiabatic perturbation calculation of the inertial parameter $B$ to be valid. In practice, this condition seems to be satisfied for the first $2^+$ level in the s.c.s. nuclei considered, but in all cases the $0^+$, $2^+$, $4^+$, second excited state lies near the top of or above the gap. Another way of stating condition (35) is that the collective state must collect a sufficient part of the total oscillator strength; i.e., that the collective $B(E2)$ be greater than the sum of the $B(E2)$'s for the various two quasi-particle $2^+$ states. The second condition is a measure of the degree to which the collective oscillation is really harmonic. Although these conditions seem quite restrictive at first sight, in certain cases, at least, they are not. For one degenerate level of degeneracy $2\Omega$, the collective oscillation has been shown to be harmonic and correctly described by the above treatment[9] as long as the coupling parameter is not so large that one is too near the transition point at which a stable equilibrium deformation occurs. Thus, in this model, the only errors in the collective treatment are of order $\Omega^{-1}$ even though the $2^+$ state lies just below or far below the quasi-particle excitations. In this work, the collective properties of s.c.s. even nuclei are described by the above method. This affects mainly the total binding energy and properties of the $2^+$ first excited state. For the other states, this effect of the $P^{(2)}$ force on the excitation energies is estimated by first order perturbation theory, using the quasi-particle states given by the pairing force. This is not expected to describe correctly the splitting of the quasi-particle levels, since there may be other equally important effects from other components of the force which are not included in this calculation.

In the case of s.c.s. odd-$A$ nuclei, one also expects that there should be collective electromagnetic transitions and that a perturbation treatment of the $P^{(2)}$ force is not adequate in all cases. Thus we use a collective treatment,

analogous to that above, for the effect of the $P^{(2)}$ force on the one quasi-particle levels of these nuclei, corresponding to the coupling of the quasi-particle to the collective oscillation. The intrinsic wave function in this case is

$$\Psi_\nu(Q) = \alpha_\nu^\dagger \Psi_0 - \left(\frac{1}{2}\chi Q + \mu\right) \sum' \frac{q_{\nu'\nu''}(U_{\nu'}V_{\nu''} + V_{\nu'}U_{\nu''})}{E_{\nu'} + E_{\nu''}} \alpha_{\nu'}^\dagger \beta_{\nu''}^\dagger \alpha_\nu^\dagger \Psi_0 . \quad (36)$$

The quadrupole moment is given by

$$\left.\begin{aligned} &(\Psi_\nu(Q) \mid \hat{Q} \mid \Psi_{\nu'}(Q)) \\ &= q_{\nu\nu'}(U_\nu U_{\nu'} - V_\nu V_{\nu'}) - 2\left(\frac{1}{2}\chi Q + \mu\right) \sum_{\substack{\nu''' \\ \nu'' \neq \nu}}' \frac{q_{\nu''\nu'''}^2 (U_{\nu''}V_{\nu'''} + V_{\nu''}U_{\nu'''})^2}{E_{\nu''} + E_{\nu'''}} \delta_{\nu\nu'} \end{aligned}\right\} \quad (37)$$

where the first term is the single-particle quadrupole moment of the quasi-particle. Ignoring the restriction on the $\nu''$ sum, we may associate the second term with the collective quadrupole moment $Q$ of the corresponding even system (cf. Eq. (28)). This approximation should be good to the extent that there are large numbers of states contributing to the sum. The Hamiltonian for the intrinsic state as a function of $Q$ contains non-diagonal as well as diagonal terms in the one quasi-particle state and may be written

$$\left.\begin{aligned} H &= U' + \frac{1}{2} CQ^2 + \sum_\nu E_\nu (\alpha_\nu^\dagger \alpha_\nu + \beta_\nu^\dagger \beta_\nu) \\ &+ \chi \sum_{\nu\nu'} q_{\nu\nu'}(U_\nu U_{\nu'} - V_\nu V_{\nu'})(\alpha_\nu^\dagger \alpha_{\nu'} + \beta_{\nu'}^\dagger \beta_\nu) Q , \end{aligned}\right\} \quad (38)$$

the two terms in addition to those of (29) being the quasi-particle energy and the cross term from $1/2\ \chi(Q + Q_{\text{s.p.}})^2$. Assuming $Q \gg Q_{\text{s.p.}}$, we have dropped the term quadratic in $Q_{\text{s.p.}}$. In the collective Hamiltonian we utilize the five quadrupole degrees of freedom $Q$ to produce the rotationally invariant expression

$$\left.\begin{aligned} H_{\text{coll}} &= U' + \frac{1}{2} C \sum_\mu Q_\mu^2 + \frac{1}{2} B \sum_\mu Q_\mu^2 + \sum_\nu E_\nu (\alpha_\nu^\dagger \alpha_\nu + \beta_\nu^\dagger \beta_\nu) \\ &+ \chi \sum_{\nu\nu'\mu} q_{\nu\nu'}^\mu (U_\nu U_{\nu'} - V_\nu V_{\nu'})(\alpha_\nu^\dagger \alpha_{\nu'} + \beta_{\nu'}^\dagger \beta_\nu) Q_\mu . \end{aligned}\right\} \quad (39)$$

$C$ and $B$ are given by (29) and (31), respectively. We thus ignore the difference in the inertial parameters for neighbouring even-even and odd-$A$ nuclei (cf. Ref. 10, (136)).

This differs from the Bohr-Mottelson collective Hamiltonian for a vibrator coupled to a single particle by the factor $(U_\nu U_{\nu'} - V_\nu V_{\nu'})$ in $H_{\text{int}}$. The effect of this factor is that quasi-particles near the Fermi surface are more weakly coupled to the oscillation, while those farther from the Fermi surface are coupled more strongly. It also differs from the Bohr-Mottelson collective Hamiltonian in that the pairing energy is included. For simplicity, and because the coupling is not too strong for the single closed shell nuclei, we have calculated the effect of the last term in (39) by second order perturbation theory. In this case, the low lying one quasi-particle states receive an energy shift

$$\Delta E_j = -\frac{\chi^2}{2C} \sum_{j'} \frac{5}{4\pi} \left( C^{2\,j\,j'}_{0\,\frac{1}{2}\,\frac{1}{2}} \right)^2 \frac{\hbar\omega}{\hbar\omega + E_{j'} - E_j} (U_j U_{j'} - V_j V_{j'})^2 \langle j \,|\, r^2 \,|\, j \rangle^2. \qquad (40)$$

The Hamiltonian (39) will also have associated collective states, but there is not yet experimental evidence for these states for s.c.s. odd-$A$ nuclei.

## III. Energy Level Systematics

### A. The Shell Model Particle Well

The energy levels of the s.c.s. nuclei, Eqs. (9), (10), and (11), are found by first calculating the quasi-particle energies, using a numerical solution of Eqs. (6) and (13). Next, the collective properties are determined as discussed in § II. C 2 and, finally, $P^{(2)}$ interactions between quasi-particles and their coupling to the vibrations are treated by the perturbation methods of § II. In order to proceed with such a calculation one must know the single-particle energies for a shell model particle moving in the effective well for one particle outside of a double closed shell, and must also know how these levels shift with $A$ as one proceeds through the nuclear region.

When the levels of the one particle outside of the closed shell are not known, there is some uncertainty added to the calculation. There are some theoretical calculations for the level positions based on effective potentials with a few parameters, from which one has some knowledge of the well.[15),16)] Also, there are experimental energy level results from nuclei other than the s.c.s. nuclei treated in this work, which can be used to determine the single-particle energy levels in a particular region. If we wish to find, say, the single neutron levels for a region with a closed proton shell, we look at the energy levels of isotopes with one neutron and even numbers of protons outside

of the closed shells. For regions with large enough proton numbers, such that the neutrons and protons are filling different orbits ($Z \geq 28$), the short range interaction between the protons and neutrons is small (it is zero for our pairing force unless the particles are in the same levels). Therefore, it is reasonable to calculate the effect of the even numbers of protons on the odd neutron as a long range force for which an intermediate coupling phonon calculation can be used. Such calculations have had some qualitative success for heavy nuclei,[17] although it is not certain that such a simple treatment of the effect of the neutrons and the protons on each other is quantitatively correct. We have made only crude use of this method, with the hope of gaining some knowledge of the single-particle levels in a particular region, working backward from the known experimental levels to try to find the values of the single-particle levels which are consistent with the experimental data. In this work, both of these methods have been used to determine the single-particle levels. However, the lack of experimental data and single-particle levels is a major uncertainty in this work.

The rate and manner in which the single-particle states shift with $A$ are difficult to establish. However, if the dependence is something like $A^{-1/3}$, then our results are very little affected by this motion in most regions. In none of our s.c.s. regions is there direct evidence that the change in the single-particle energies with $A$ affects the accuracy of our calculations, particularly in view of the uncertainty in the level positions. Still, there is a possibility that, when the number of particles changes as much as it does in, say, the Sn region, there are systematic deviations introduced. The change in the single-particle levels with $A$ does apparently play an important role in determining the levels of $N = 50$. In this work, we have not changed the energy level separation of the levels in any one region, although we have investigated the variation in the depth of the well in the binding energy calculation.

### B. The Choice of Parameters]

Once the single-particle well with its energy levels has been established for a given closed shell region, the consequences of our model are determined in terms of the two coupling parameters $G$ and $\chi$. It is well established that a short range residual nuclear force is necessary in a description of nuclei. The strength of this force, which is simulated in our calculation by the pairing force with its coupling parameter $G$, can be determined in many ways. For example, the systematic experimental odd-even mass difference

discussed in the next section is affected very little by the long range force, and can thus be used to determine $G$ to about $30\%$ in most regions. Closely related to this is the so-called energy gap of even-even nuclei.[18] In heavy highly deformed nuclei, this shows up in the fact that the first intrinsic excited state of an even-even nucleus usually lies above 1 Mev, while very low intrinsic excitations often occur in the neighbouring odd-$A$ nuclei. In the case of the spherically symmetric s.c.s. even-$A$ nuclei which we consider, there is also an energy gap in which only the collective $2^+$ level occurs. The position in energy of the two quasi-particle excited states, which lie at or above the top of the gap, depends strongly upon the strength of the coupling parameter $G$. In cases where an experimentally observed excited state can be uniquely associated with a two quasi-particle excitation, one can make an independent estimate of $G$. Such a situation occurs in the case of observed states of high spin, $J$, and odd parity. First, the two quasi-particles forming such a state must have opposite parity. In each mass region considered there is always just one single-particle state of parity opposite from the rest, and this must be the $j$-state of one of the quasi-particles. The high $J$ value of the excited state can then determine rather uniquely which is the second quasi-particle. The $9^-$ levels in $Pb^{204}$ and $Pb^{202}$ and the $7^-$ level in $Sn^{120}$ permit such a determination to be made. This leads to a value of $G$ between $23/A$ and $30/A$ for Pb and about $19/A$ for Sn. The $P^{(2)}$ force is included as a perturbation in this determination.

Once the value of $G$ has been determined, the coupling parameter $\chi$ of the long range part of the force may be determined from the quantities it most affects, namely the position of the first $2^+$ states of the even-$A$ nuclei and the $B(E2)$ value for the $(0^+ \rightarrow 2^+)$ transition. For any one isotope the experimental excitation energy can be fit with the theoretical value by an appropriate choice of $\chi$, a larger $G$ requiring a correspondingly larger $\chi$. However, we require that in any one mass region (corresponding to a particular double closed shell with one kind of particles outside) one value of $G$ and $\chi$ or rather $X$ (cf. below, Eq. (41)) be used for all the isotopes. With this requirement, one can determine the $G$ and $\chi$ which together give the best fit to the position of the first excited $2^+$ level as a function of $Z$ or $N$ in an entire mass region. Where good comparison can be made, the $G$ determined this way is in agreement with that determined by the previous methods.

Although the $B(E2)$ value depends strongly on $\chi$, it also contains a factor $e_{\text{eff}}^2$ which may vary somewhat from shell to shell. Thus, except in the case of the Pb isotopes for which $e_{\text{eff}}$ is independently determined

from $E2$ transition rates in $Pb^{207}$, one can determine $e_{\text{eff}}$ only from the $B(E2)$ values and, assuming $e_{\text{eff}}$ to be constant in one mass region, see whether the variation from isotope to isotope is consistent with experiment. The $G$ and $\chi$ determined for Pb from the $B(E2)$ value of $Pb^{206}$ are consistent with the values determined from the previous methods.

Although we did not try to determine uniquely the best values for $G$ and $\chi$, it is seen that both have a simple and smooth $A$ dependence in going from region to region. $G$ varies more or less as $A^{-1}$, the value $19A^{-1}$ Mev being better for the regions from $N = 28$ to Sn, and $G = 23A^{-1}$ being better for $N = 82$ and Pb. The corresponding value of $\chi$ in going from region to region varies more or less as $A^{-7/3}$ is expected (cf. Ref. 10, (93)). We consider instead the quantity $X$ defined by

$$X = \chi \frac{5}{4\pi} \langle j \,|\, r^2 \,|\, j \rangle_u^2 = \chi \frac{5}{4\hbar} \left( \frac{\hbar}{M\omega_0} \right)^2 \left( n + \frac{3}{2} \right)^2, \tag{41}$$

where $M$ is the nucleon mass, $\hbar\omega_0 = 41\,A^{-1/3}$ Mev, $n$ is the total number of oscillator quanta associated with most of the single-particle (harmonic oscillator wave functions) states in the region in question. That is $n = 3$ for the $N = 28$, Ni, and $N = 50$ regions; $n = 4$ for the Sn and $N = 82$ regions, and $n = 5$ for the Pb. For the calculations, $X$ was considered as a fixed constant in each region and $\hbar\omega_0$ was defined in each region in terms of a representative value of the mass number $A$. This quantity was then found to have a value of about $X = 110\,A^{-1}$ in each of the regions considered. The actual parameters used will be indicated with the theoretical results.

### C. Energy Levels in S.C.S. Nuclei

In this section and in the Appendix, we shall present figures and tables from which the reader may estimate the position of all of the calculated zero, one, and two quasi-particle states and the collective $2^+$ state, and from which he may determine the calculated wave functions. In the case of $Pb^{206}$ and $Pb^{204}$, all of the calculated levels will be explicitly shown to indicate how the two quasi-particle states labelled by their spins, $j$ and $j'$, and parity are broken up by the $P^{(2)}$ force according to the total angular momentum $J$ of the resulting state. For other even-$A$ nuclei only those excited states, aside from the collective $2^+$ state, which correspond to two identical quasi-particles will be indicated, and the breakup of the degeneracy

by $P^{(2)}$ obtainable from (18)—(21) will not be shown. From such a figure, the positions of the other excited states corresponding to two different quasi-particles can be obtained, aside from the effect of $P^{(2)}$, as the mid-point between the two excited states corresponding to pairs of quasi-particles of the two types (cf. Eq. (10)). This procedure is indicated in the figures for $Pb^{206}$ and $Pb^{204}$. For the odd-$A$ isotopes all of the one quasi-particle states are indicated. These are each non-degenerate levels aside from the $m$ degeneracy of the quasi-particle angular momentum, $J = j$.

1. *Pb Isotopes*

The energy levels in $Pb^{207}$ define the neutron hole well quite accurately. Since the experimental single-particle levels are known for the entire 82—126 neutron shell, this region should be a good one for our methods.

One also knows the positions of some of the particle levels in the next shell from $Pb^{207}$. Since these are unimportant in $Pb^{206}$, and grow even less important as the number of neutron holes in the 126 shell is increased, they serve only to renormalize $G$ in our calculation.

The one disadvantageous feature for the Pb isotopes is that the first hole level has spin 1/2. For this reason, in the two-hole calculation, $Pb^{206}$, the lowest excited state is one with two quasi-particles of angular momentum 1/2, which is simply a $0^+$ state. For reasonable magnitudes of $G$, this state seems to be almost entirely spurious, and must therefore be ignored.

In the odd-$A$ Pb isotopes the main systematic experimental feature is the position of the $i_{13/2}$ state, which has been determined by a study of the $M4$ isomeric transition to the $f_{5/2}$ state.[19] For any reasonable strength of the pairing force, $G$, we obtain the correct position for this level. It is generally true that, although the absolute energies depend on the size of $G$ in odd-$A$ nuclei, the relative positions of the one quasi-particle levels are not very sensitive to the strength of the pairing force or the $P^{(2)}$ force, but depend mainly on the positions of the single-particle levels for any $G$ which is consistent with the gap.

All of the experimental odd-$A$ Pb ground states are found within 0.1 Mev, as can be seen in Fig. 1. In $Pb^{205}$, the theoretical $(1/2)^-$ state is below the $(5/2)^-$ state by about 0.05 Mev, while experiment gives the ground state spin as $(5/2)^-$,[20]; and the $(5/2)^-$ state might rise a little fast, since it is above the $(3/2)^-$ state by about 0.1 Mev in $Pb^{197}$, while rather uncertain experimental results give $(5/2)^-$ as the ground state spin. Such small deviations can easily be explained by the uncertainties expected in the calculations, especially by the presence of other perturbations besides the $P^{(2)}$.

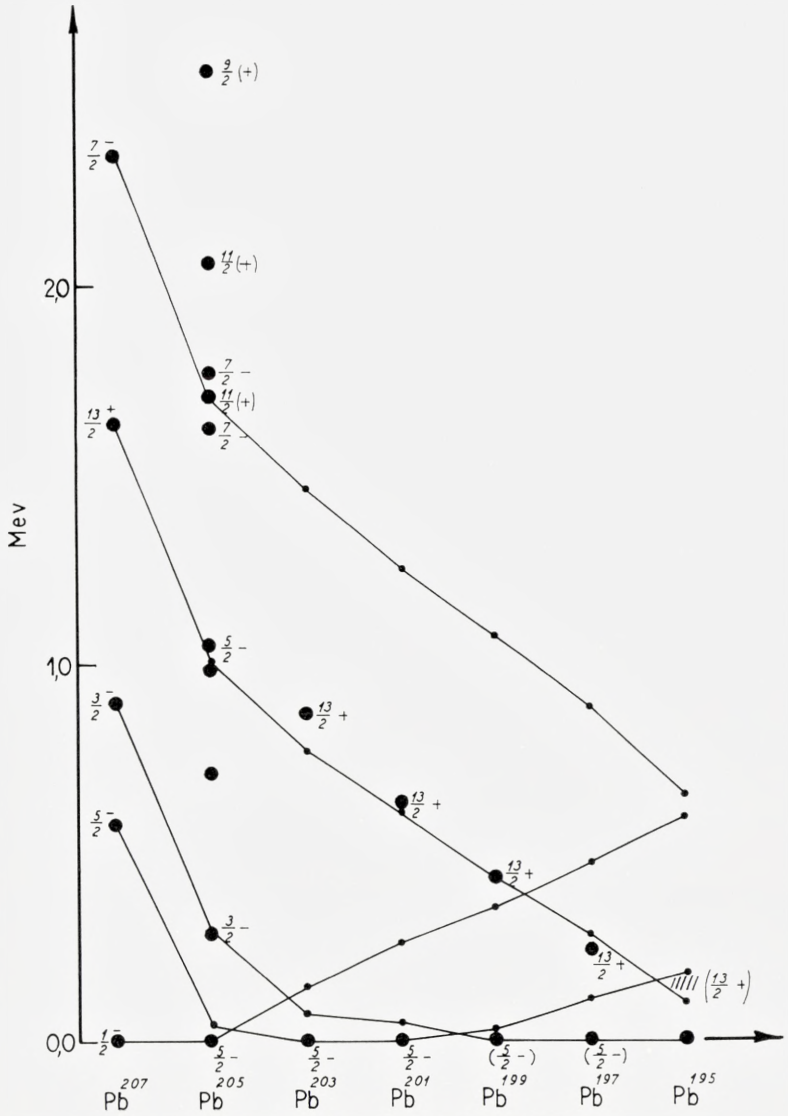


Fig. 1. *Energy levels of the odd-A* Pb *isotopes.*

The experimental points are large dots with spin and parity assignments placed on the right when known. The theoretical results are the small dots joined by solid lines giving the positions of the one quasi-particle states for $G = 23/A$ and $X = 0.4$. The effect of the coupling of the quasi-particle to the collective oscillation is included by Eq. (40) for the lowest few states. The labels on the experimental curves are the angular momenta of the one quasi-particle states. The experimental values are taken from Bergström and Andersson,[19] the table of Strominger, Hollander and Seaborg, and the work of Dželepow and Peker[21].

Above about 0.8 Mev a number of other states are arising from the phonons which have not been indicated in the figure. We seem to predict a $(3/2)^-$ ground state in $Pb^{195}$ and the presence of low lying $(3/2)^-$ and $(1/2)^-$ states in $Pb^{203}$ and $Pb^{201}$.

In the even-$A$ Pb isotopes the position of the $2^+$ level is known down to $Pb^{200}$. Using $G \approx 0.1$ Mev, this energy level is predicted quite well as the lowest two quasi-particle level which can give rise to a $2^+$ level. However, the $B(E2)$ for this state in $Pb^{206}$ is four times the single-particle value[22], suggesting that the intrinsic states lie somewhat higher and that the $2^+$ state is collective. The position of the $2^+$ level as a function of $A$ and the value of the $B(E2)$ in $Pb^{206}$ are accurately predicted. (Cf. § VII). However, of all of the s.c.s. nuclei, perhaps in Pb is the collective treatment of the $2^+$ state least well justified. The $2^+$ level and the levels corresponding to two identical quasi-particles appear together with some of the experimental levels in Fig. 2. Fig. 3 shows how the calculated levels vary as a function of $G$.

The positions of all of the zero and two-quasi-particle levels are shown in Figs. 4 and 5 for $Pb^{206}$ and $Pb^{204}$, together with the experimental values. The agreement with experiment for $Pb^{206}$ is, as expected, not as good as the results of TRUE and FORD.[13] However, all of the experimental levels with measured spins can be matched with quasi-particle levels to within a few tenths of one Mev, except for the lowest $2^+$ level for which the collective treatment gives the correct energy. It must be pointed out that our treatment, which introduces the collective $2^+$ level and retains as higher excited states all of the $J = 2$ two quasi-particle states as effected by $P^{(2)}$ in perturbation theory, contains a spurious $2^+$ two quasi-particle state analogous to the spurious $0^+$ two quasi-particle state of the Belyaev solution of the pairing Hamiltonian. Thus, in Figures 4 and 5, there is one extra $0^+$ and one extra $2^+$ state. In our case as in that of Ref. 13, the ground state of $Pb^{206}$ is mostly $(p_{1/2})^2$ $J = 0$ so that the state composed of two $p_{1/2}$ quasi-particles is mostly spurious, the other two quasi-particle spin zero states being mostly real. On the other hand, the lowest $2^+$ state of Ref. 13 and likewise our collective $2^+$ state have large contributions from $(p_{1/2}\ f_{5/2})$ and $(p_{1/2}\ p_{3/2})$ and lesser contributions from several other configurations, so that, with our method of calculating, the spurious character is spread over several of the low lying $2^+$ two quasi-particle states.

For $G = 0.128$ which is chosen so as to fit the position of the $9^-$ level in $Pb^{204}$, and which is consistent with the data for $Pb^{206}$, one predicts the energy of the $9^-$ level in $Pb^{202}$ to be 2.09 as compared with the experimental

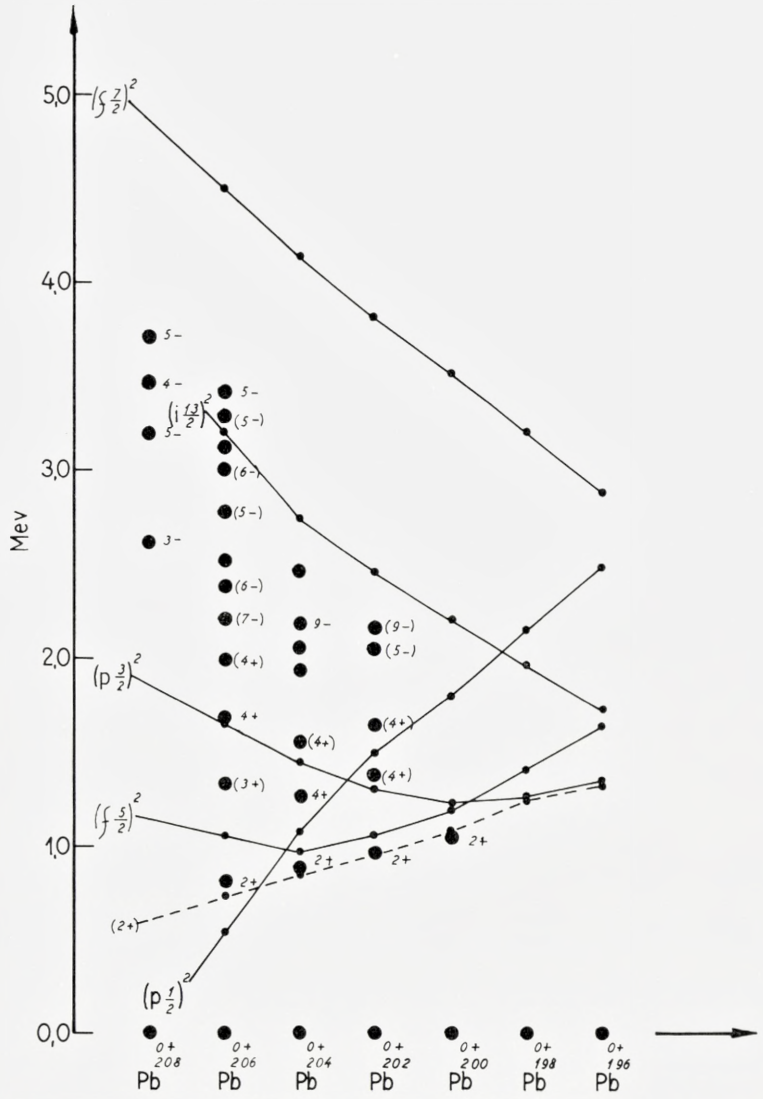


Fig. 2. *Energy levels of even-A* Pb *isotopes.*

The experimental points are large dots with spin and parity assignments placed on the right when known. The theoretical points are indicated by small dots. Those theoretical points which are joined by solid lines are the two identical quasi-particle states for $G = 23/A$ and are labelled to the left by the angular momenta of the quasi-particles. The effect of the $P^{(2)}$ force is not included for these states. The other two quasi-particle energies are found by taking the average energy between the appropriate two levels (see Figures 4 and 5). The collective $2^+$ theoretical level is shown by small dots joined by a dashed line. The experimental values are taken from the table of STROMINGER, HOLLANDER and SEABORG and the work of DŽELEPOW and PEKER[21]). $X = 0.4$.

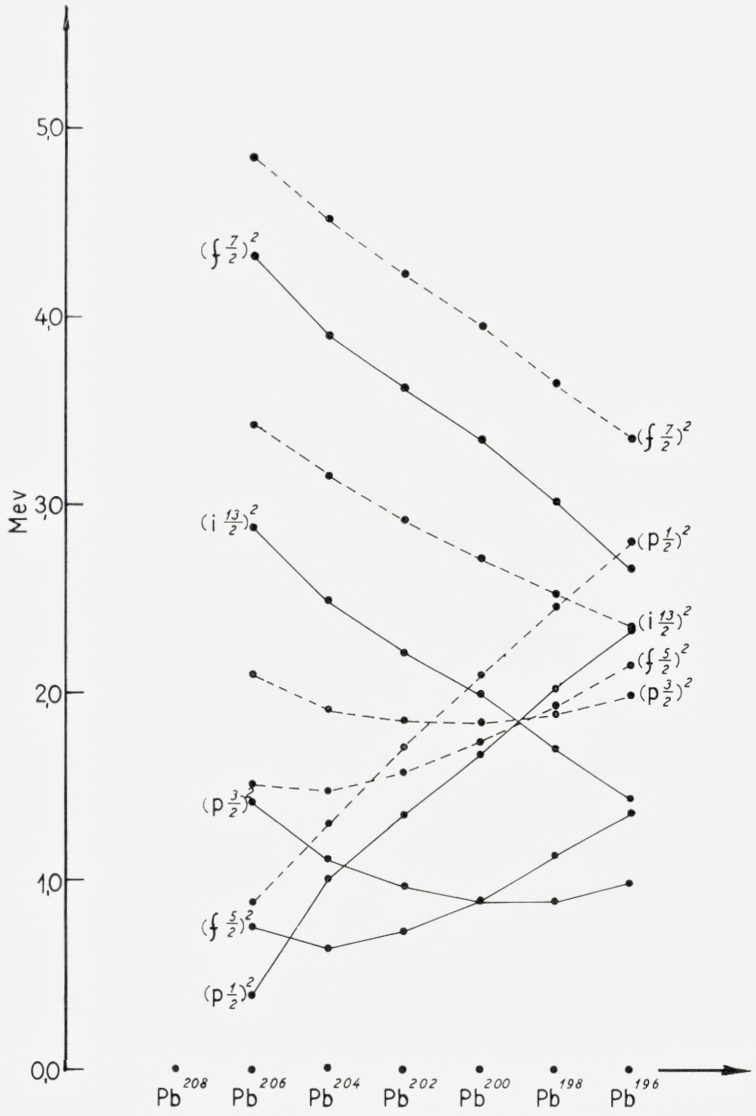


Fig. 3a.

Fig. 3. *Theoretical energy levels in even- and odd-A* Pb *isotopes as a function of G.* The notation is that of Figs. 1 and 2. Only the zero and two identical quasi-particle states are given for the even-$A$ isotopes and the one quasi-particle states for the odd-$A$ isotopes. The solid lines are for $G = 0.0911$ and the dashed line for $G = 0.145$.

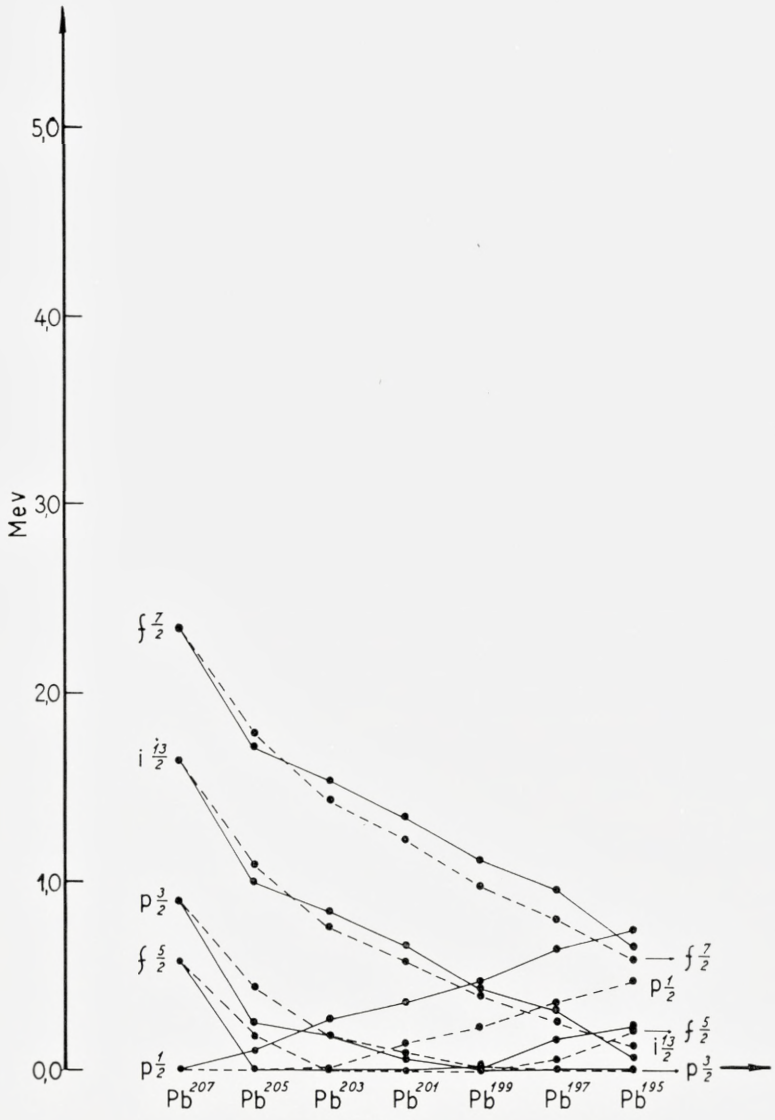


Fig. 3b.

value of 2.171. The long lifetime of this level shows that it must lie below the near lying $6^-$, $7^-$, and $8^-$ levels. The $P_{22}^{(2)}$ force puts the $9^-$ below these other states coming from $(f_{5/2}\, i_{13/2})$, but the $(p_{1/2}\, i_{13/2})$ $6^-$, $7^-$ quasi-particle states lie well below the $9^-$ in $Pb^{206}$, close in $Pb^{204}$, and above

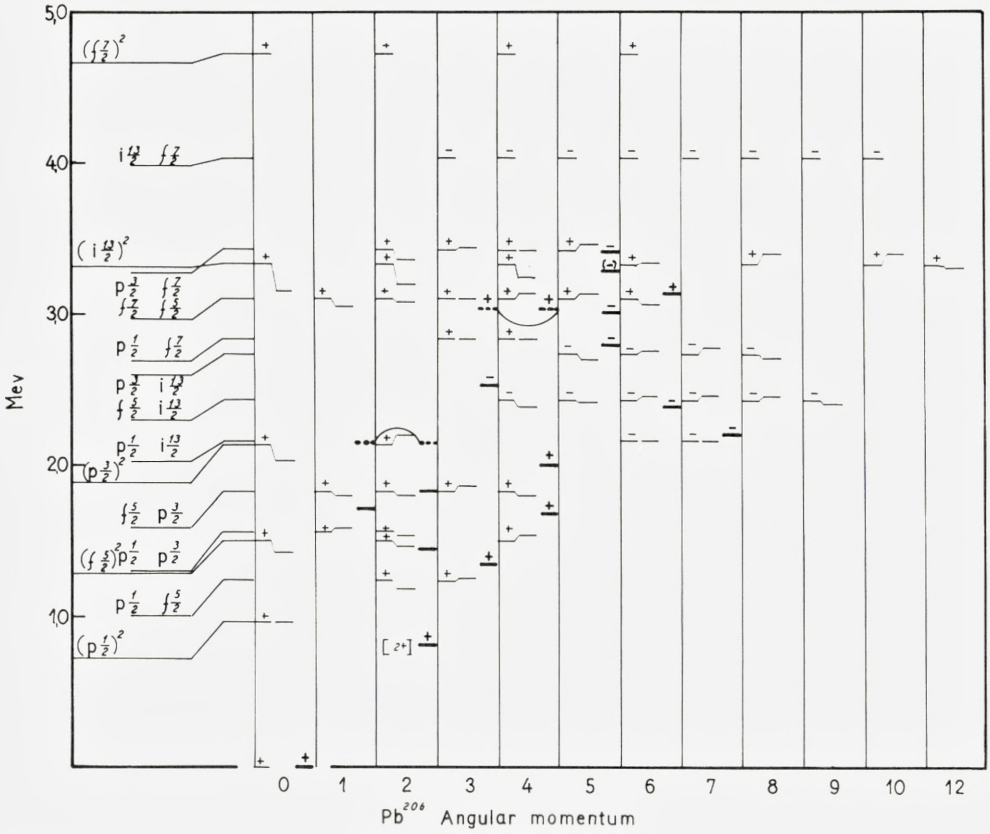


Fig. 4. *Energy levels of* $Pb^{206}$.

The experimental levels, taken from TRUE and FORD[13]), are given on the right for each spin. On the left for each spin for $G = 0.128$ is the two quasi-particle state perturbed by $\mathfrak{P}_{11}^{(2)}$ and Eq. (20) (see text), the labelled unperturbed states being given to the left of the diagram. The second column for each spin also includes the effect of $\mathfrak{P}_{22}^{(2)}$. The lowest $2^+$ level, marked $[2^+]$, is the collective level. The state $(P_{1/2})_{J=0}^2$ is mostly spurious and there is one spurious state among the low lying $2^+$ quasi-particle states. The $\mathfrak{P}_{22}^{(2)}$ effect is omitted in the highest states. $X = 0.4$.

in $Pb^{202}$. Thus, we can understand why this long-lived $9^-$ state is seen in $Pb^{202}$, and $Pb^{204}$, but not in $Pb^{206}$.

## 2. *Sn Isotopes*

In the odd-$A$ Sn isotopes nine ground states are known. In addition, systematic information about the $(11/2)^- - (3/2)^+$ separation is obtained from the isomeric $M4$ transition, and several excited states are known in $Sn^{117}$.

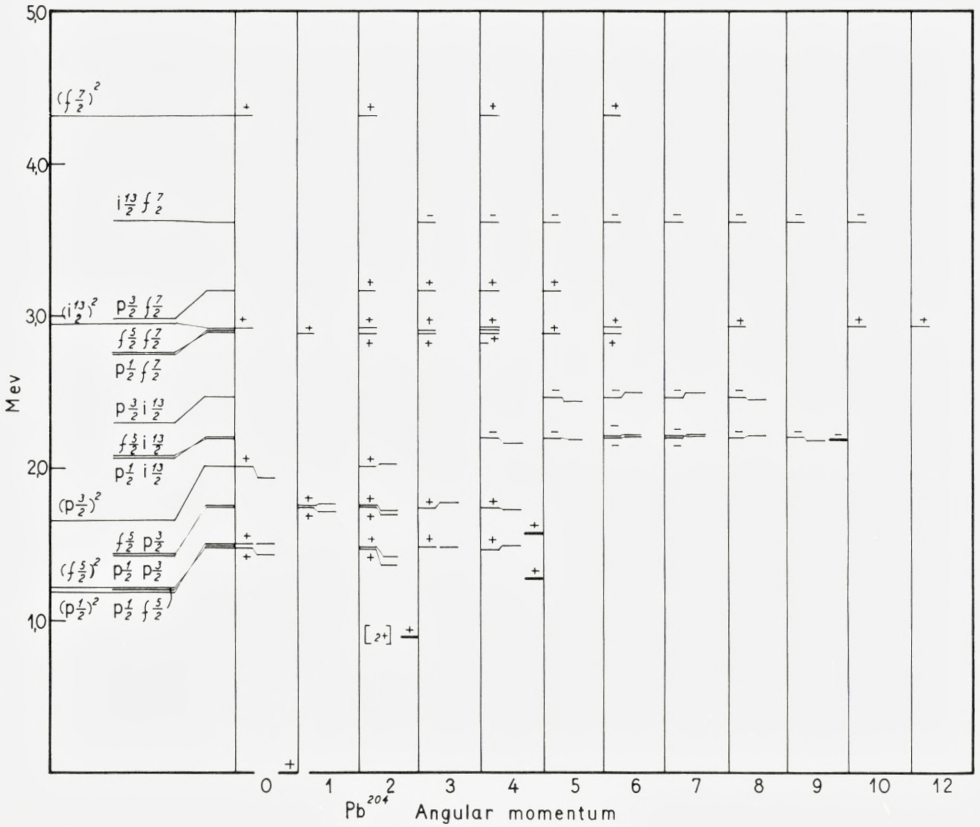


Fig. 5. *Energy levels of* $Pb^{204}$.
The notation is the same as in Fig. 4. The spurious character is spread over several of the low lying $0^+$ states in this case.

Of course, $Sn^{101}$ is far from the stability curve, so the single-particle well cannot be obtained directly from experiment. One can learn something about the $(11/2)^- - (3/2)^+$ separation from the isotopes with 81 neutrons and even numbers of protons ($^{52}Te^{133}_{81}$, $^{54}Xe^{135}_{81}$, $^{56}Ba^{137}_{81}$, and $^{58}Ce^{139}_{81}$). However, one has a hard time to place the $(1/2)^+$ state correctly with respect to these two states and the separation between the 5/2, 7/2 states and the 1/2, 3/2, 11/2 states is not known very well.

We tried calculations with several values of the single-particle energies. Although it is possible to choose a well which gives better results, the results using the well of S. G. Nilsson[11] are presented in Fig. 6. All of the important features which are known experimentally fit well (to about

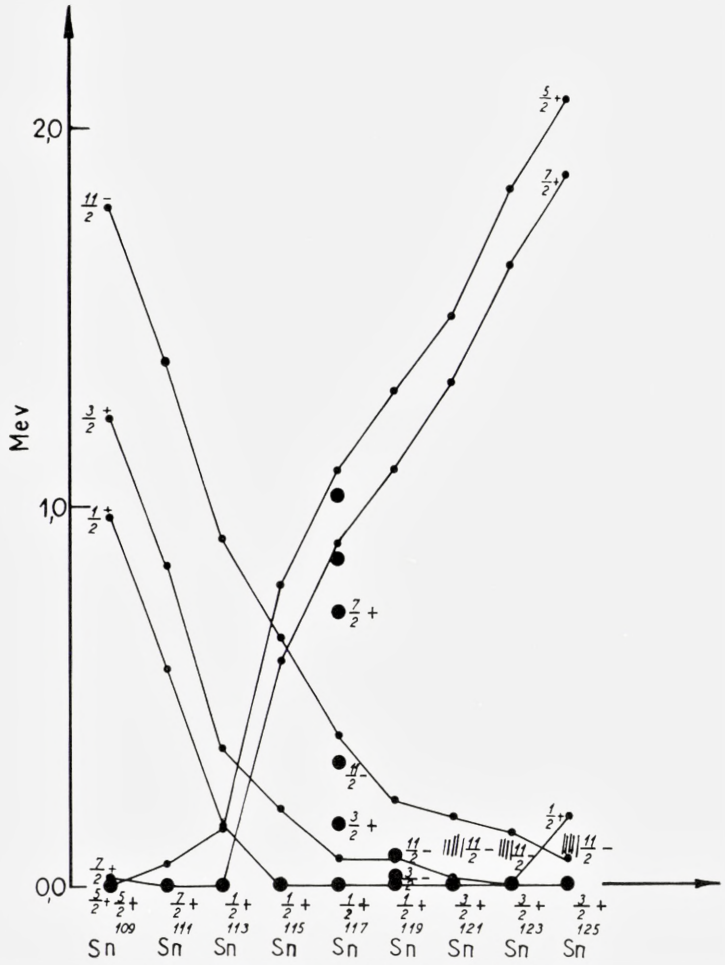


Fig. 6. *Energy levels of the odd-A Sn isotopes.*

The notation is the same as in Fig. 1, with $G = 19/A$ and $X = 1.1$. The single-particle levels are taken as

$$f_{5/2}(0);\ g_{7/2}(0.22);\ S_{1/2}(1.9);\ d_{3/2}(2.20);\ h_{11/2}(2.8\ \text{Mev}).$$

0.1 Mev). One should notice that the 1/2 state remains the ground state as $A$ changes by six. This feature depends not only upon the pairing force, but also upon the $P^{(2)}$ force. Also the $P^{(2)}$ force is important for keeping $(3/2)^+$ the ground state spin in Sn 123 and 125, for without it the $(11/2)^-$ would be the ground state, contrary to experiment.

For the even-$A$ Sn isotopes shown in Fig. 7 the $7^-$ state in $Sn^{120}$, coming almost entirely from the two-quasi-particle state with one $(11/2)^-$ and

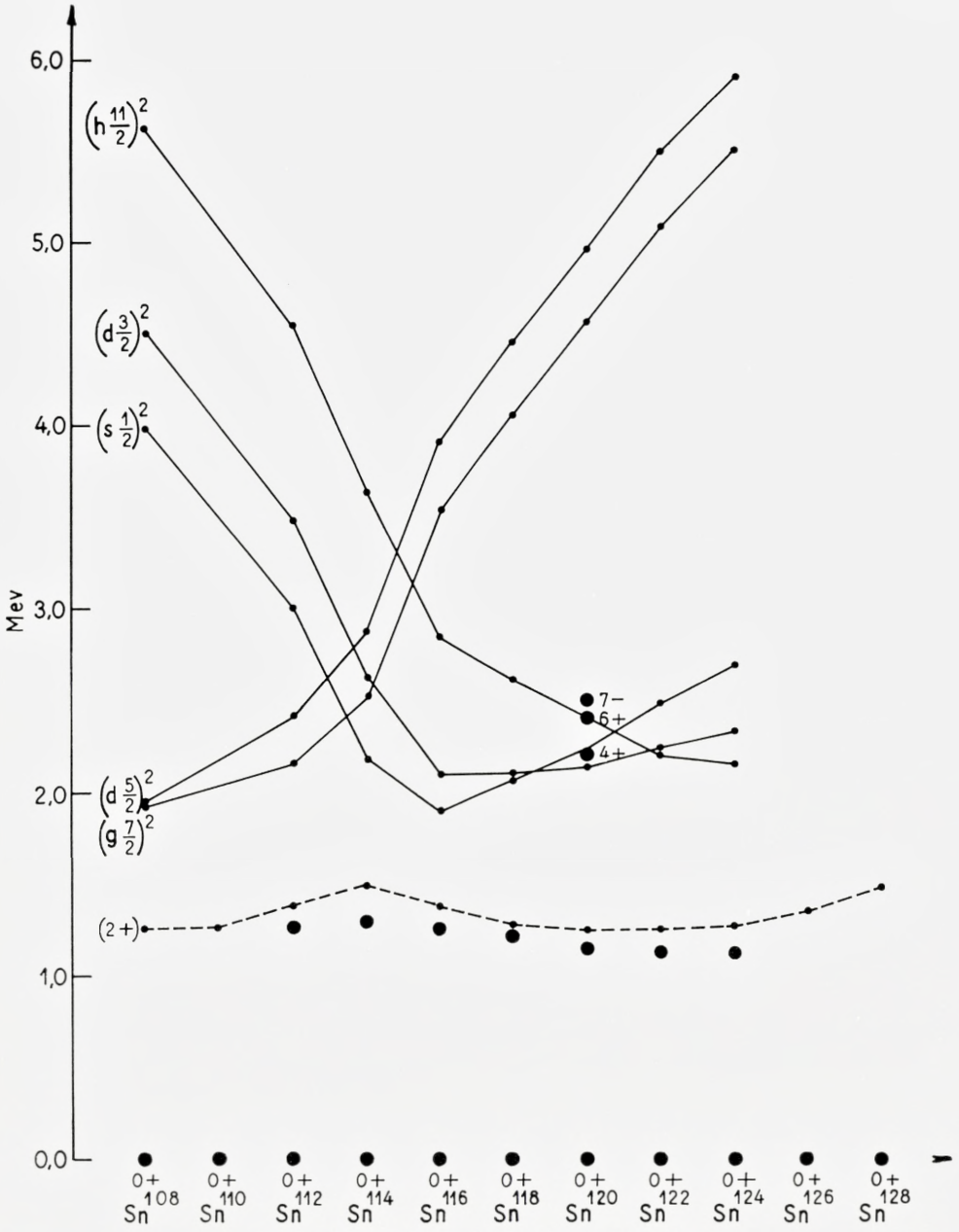


Fig. 7. *Energy levels of the even-A Sn isotopes.*
The notation is the same as in Fig. 2, with $G = 19/A$ and $X = 1.1$; and the single-particle energies are given in Fig. 6.

one $(3/2)^+$ quasi-particle, is moved little by the long range force. It is fit quite well by $G = 0.187$, corresponding to 0.0911 in Pb ($G = 19/A$). The $6^+$ state from two $(11/2)^-$ quasi-particles is also fit well, falling about 0.1 Mev below the $7^-$ level when $\mathfrak{P}_{11}^{(2)}$ and $\mathfrak{P}_{20}^{(2)}$ are included by (18), (19), and (20).

However, the important experimental results for the even-$A$ Sn isotopes are the $2^+$ states. There is a maximum in the $2^+ - 0^+$ energy separation at $Sn^{114}$.[23] This feature is fit in quite good detail by the collective state which occurs for the $G = 0.187$. In this case, the higher values of $G$ will give rise to collective $2^+$ states which will not fit the experimental values very well. Thus the combination of the $7^-$ and $6^+$ states in $Sn^{120}$ and the detailed experimental results for the $2^+$ state serve to pick the value of $G$ accurately as 19/A.

### 3. *Ni Isotopes*

Since the levels in $Ni^{57}$ are not known we must again use indirect evidence to find the well. For the neutrons moving in the 28—50 shell, the $p_{3/2} - p_{1/2}$ separation is known rather well from the magnitude of the spin orbit interaction. One needs to know, in addition, the position of the $(9/2)^+$ and the $(5/2)^-$ levels with respect to the $p$ levels.

The $(9/2)^+ - (1/2)^-$ separation can be estimated from the isotopes with 49 neutrons and even numbers of protons. The pairing-force calculation is insensitive to this, since the $(9/2)^+$ state does not play a very important role in the Ni isotopes. However, the position of the $(5/2)^-$ level is quite important. Fig. 8 shows a sample calculation of how the levels in ${}_{26}Fe_{29}^{55}$ can give some information about this level. However the well of S. G. Nilsson[16] seems adequate for these isotopes, in spite of the apparent inconsistency of the $(9/2)^+ - (1/2)^-$ separation with experimental data.

Choosing the energy levels for the neutrons from ref. 13, we carry out the pairing force plus $P^{(2)}$ calculation. The results are shown in Figs. 9 and 10. The calculated ground state spins in the odd-$A$ isotopes all agree with experiment to within 0.1 Mev. The motion of the $2^+$ first excited state in the even-$A$ Ni isotopes is best fit by the $G = 19/A$.

### 4. $N = 82$

There are experimental results for isotopes with 82 neutrons, for protons in the 50—82 shell from ${}_{52}Te^{134}$ to ${}_{64}Gd^{146}$. For all these isotopes, most of

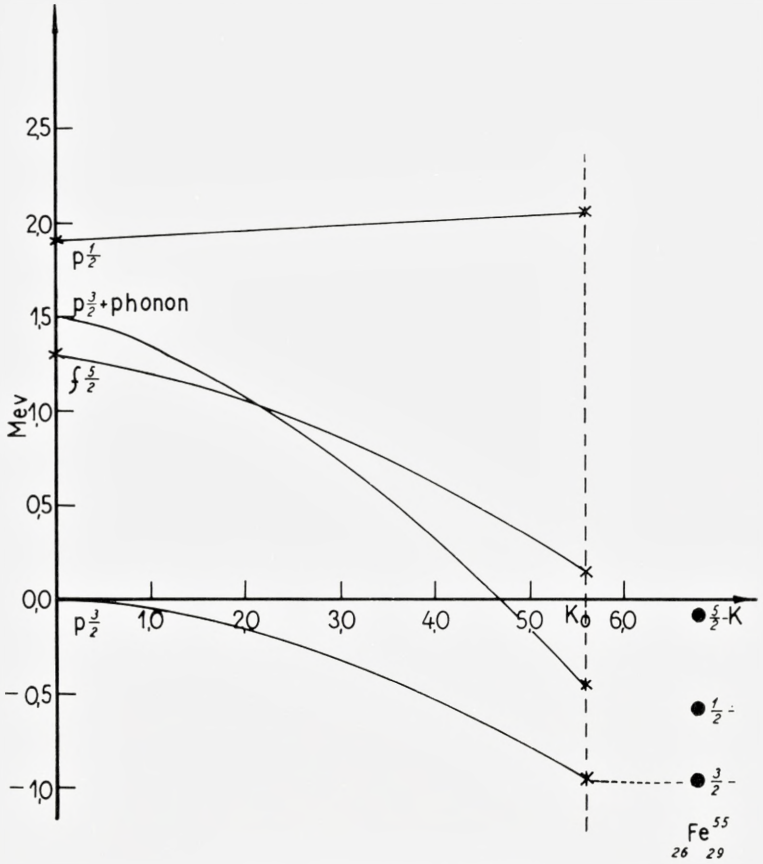


Fig. 8. *Energy levels of* $_{26}Fe^{55}_{29}$.
$K$ is the strength of the coupling of the single-neutron states to the collective proton vibration. At $K = 0$, one has the assumed single-particle levels plus a phonon at 1.5 Mev. For $K = K_0$, the value of $K$ is estimated from $_{26}Fe^{54}_{28}$, $_{26}Fe^{56}_{30}$, and $_{28}Ni^{58}_{30}$, the results are compared to the experimental values for $Fe^{55}$, which are given as large dots with energies to the right. The $p_{3/2}$ + phonon state which is given in the figure is the one with $J = 1/2$.

the extra-core protons are in the $(7/2)^+$ and $(5/2)^+$ levels. Therefore, only the separation of these levels need be known very well, especially since the 1/2, 3/2, 11/2 states are well separated from these levels. We use a separation of 1 Mev for the protons between the $(5/2)^+$ and $(7/2)^+$ states, which seems to be consistent with the levels in $_{51}Sb^{72}$ and $_{51}Sb^{74}$. The three higher states are taken as one state of pair degeneracy nine at 2.0 Mev.

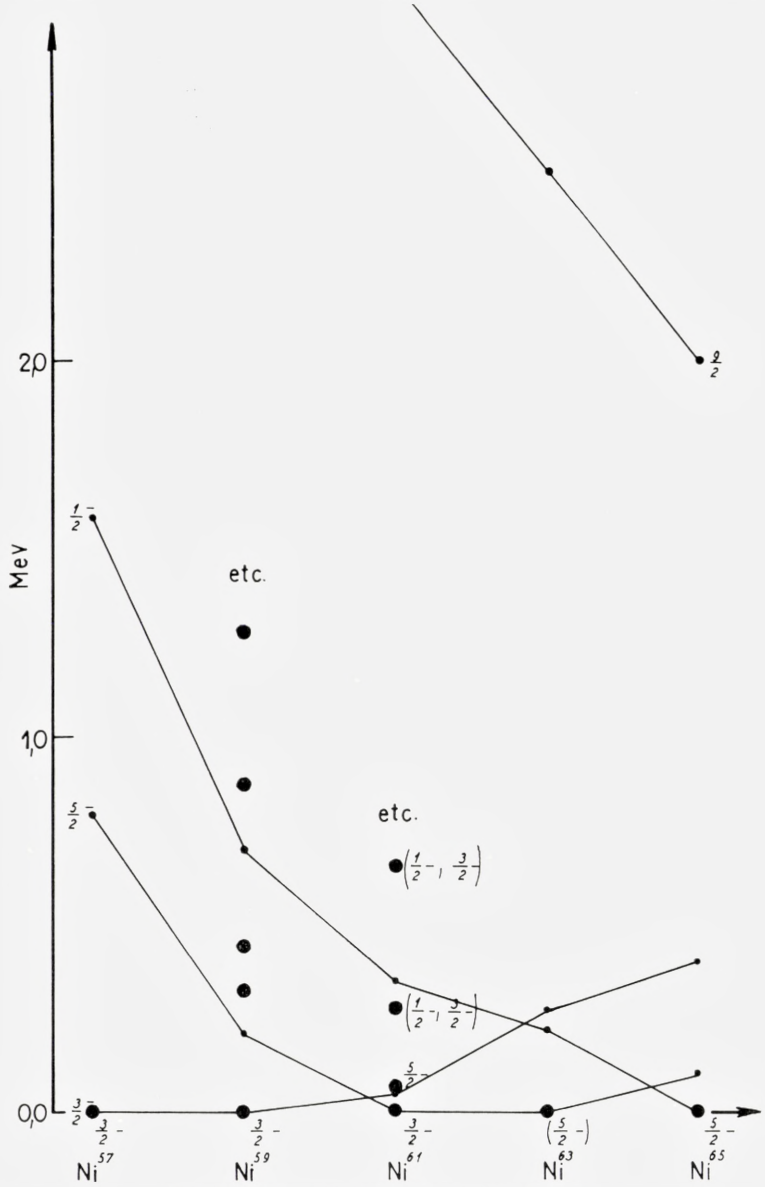


Fig. 9. *Energy levels of odd-A Ni isotopes.*

The notation is the same as in Fig. 1 with $G = 19/A$ and $X = 1.85$. The single-particle energy levels are

$p_{3/2}(0)$; $f_{5/2}(0.73)$; $p_{1/2}(1.56)$, and $g_{9/2}(4.52$ Mev).

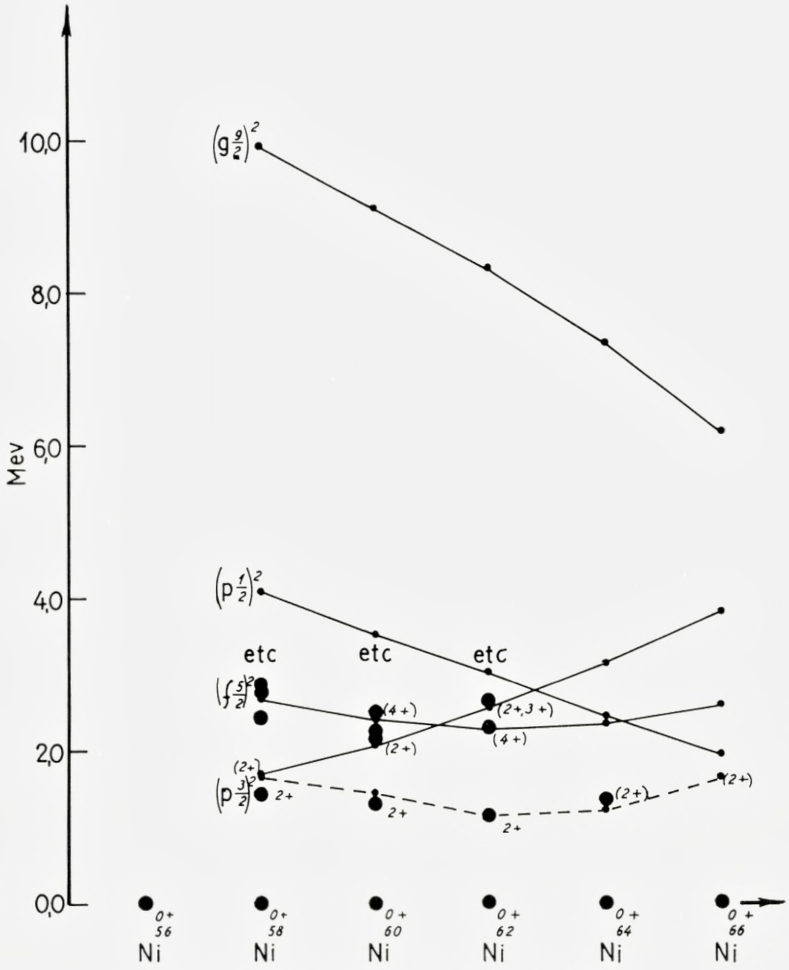


Fig. 10. *Energy levels of even-A Ni isotopes.*
The notation is the same as in Fig. 2 with $G = 19/A$, $X = 1.85$, and the single-particle levels of Fig. 9.

Figs. 11 and 12 give the result of this calculation. For the odd-$A$ nuclei the ground states are correctly determined, as are the only two excited levels whose spins are known, the 0.163 Mev, $(5/2)^+$ level in $La^{139}$ and the 0.145 Mev, $(7/2)^+$ level in $Pr^{141}$.

In the even-$A$ nuclei one finds that the $2^+$ collective levels are well determined for $G = 23/A$.

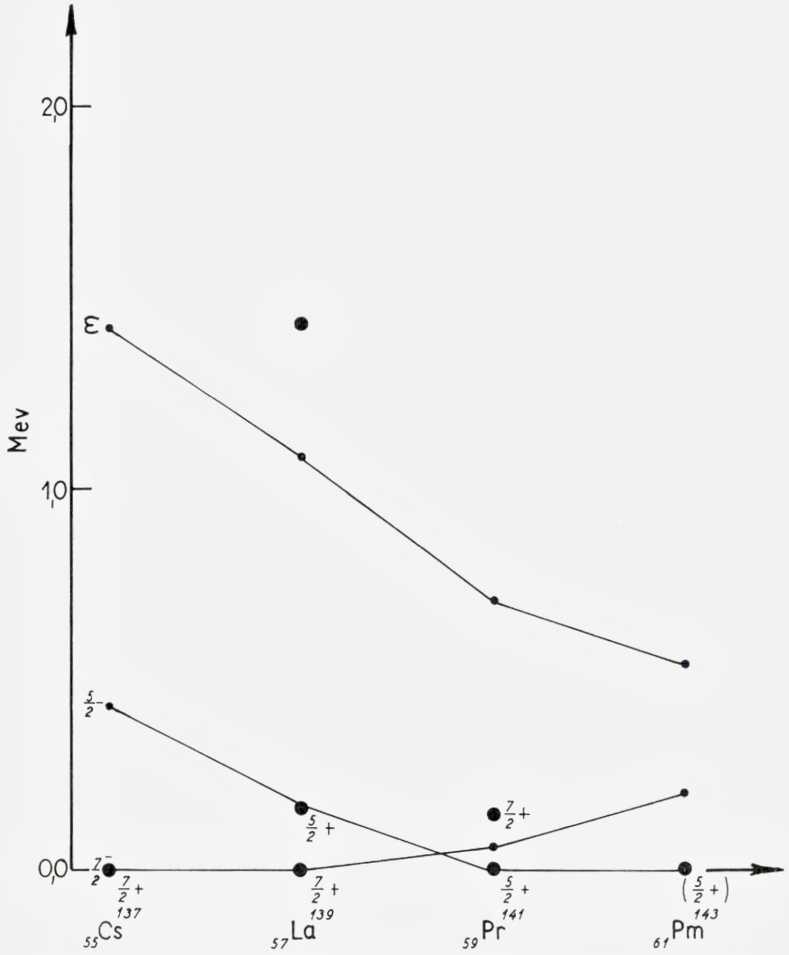


Fig. 11. *Energy levels of odd-A isotopes for* $N = 82$.
The notation is the same as in Fig. 1. See the text for the discussion of the well. $G = 23/A$ and $X = 0.975$.

5. $N = 50$

The region with a closed shell of neutrons and various numbers of protons in the 28—50 shell is a poor one for our calculation for several reasons. The first difficulty is that of finding the proper well for one proton outside of the double closed shell, i.e., ${}_{29}\mathrm{Cu}_{50}^{79}$. But just as important in this case seems to be the fact that the percentage change in $A$ is so great before one is at the isotopes for which there is empirical information that the well seems to have changed quite a bit.

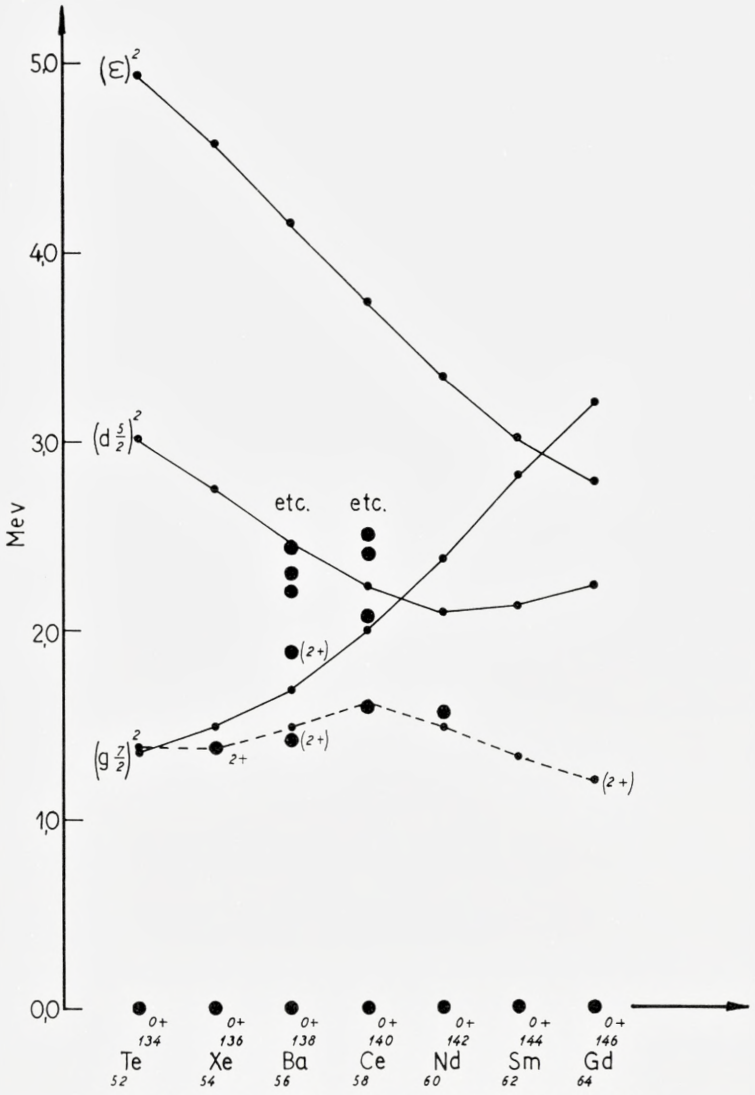


Fig. 12. *Energy levels of even-A isotopes for* $N = 82$.
The notation is the same as in Fig. 2. See the text for the discussion of the well. $G = 23/A$ and $X = 0.975$.

Another characteristic of this region is that the $Z$'s of the stable isotopes are just at the values for which the $p_{1/2}$ level is being filled. From the information we have, this level is rather separated from the other levels

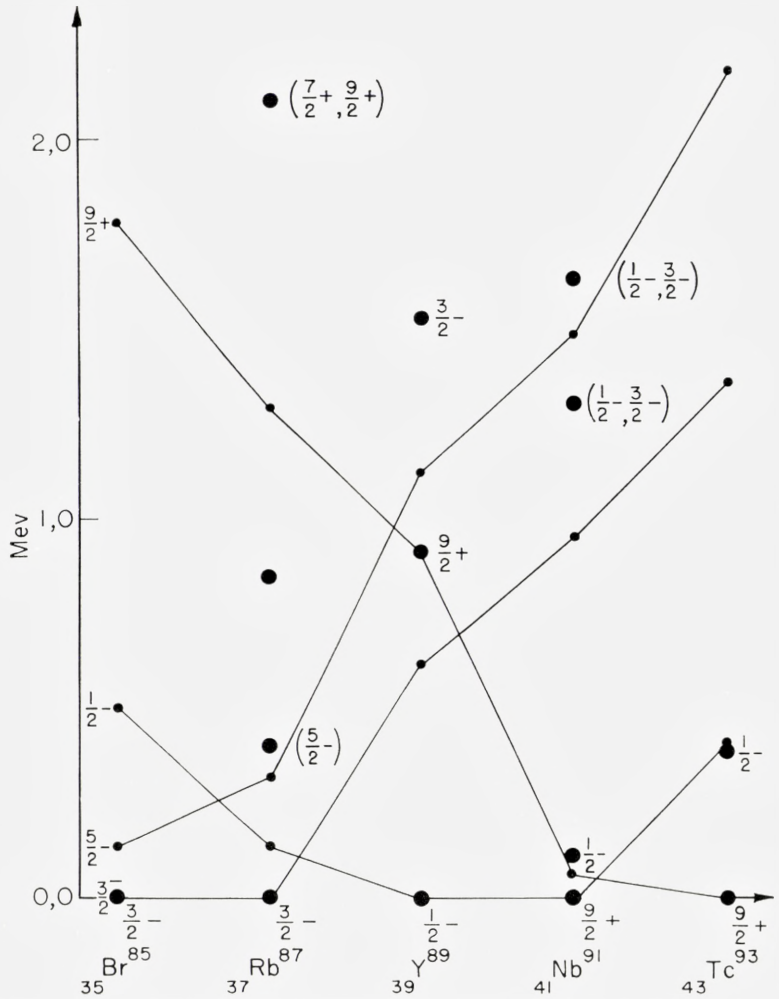


Fig. 13. *Energy levels of odd-A isotopes for* $N = 50$.
The notation is the same as in Fig. 1. $G = 26/A$, $X = 1.22$, and the single-particle energy levels are $f_{5/2}(0)$; $p_{3/2}(0.6)$; $p_{1/2}(1.8)$; $g_{9/2}(3.4$ Mev).

of the shell. As explained in § II, such a situation can result in the Bardeen solution to the pairing force being very inaccurate.

A one-phonon intermediate coupling calculation is done, using the Cu levels to find the proton well in the same way as $Fe^{55}$ is used to find the neutron well. This places the $p_{3/2}$, $f_{5/2}$, $p_{1/2}$ states in roughly the same positions for the single proton as the corresponding neutron states in the same

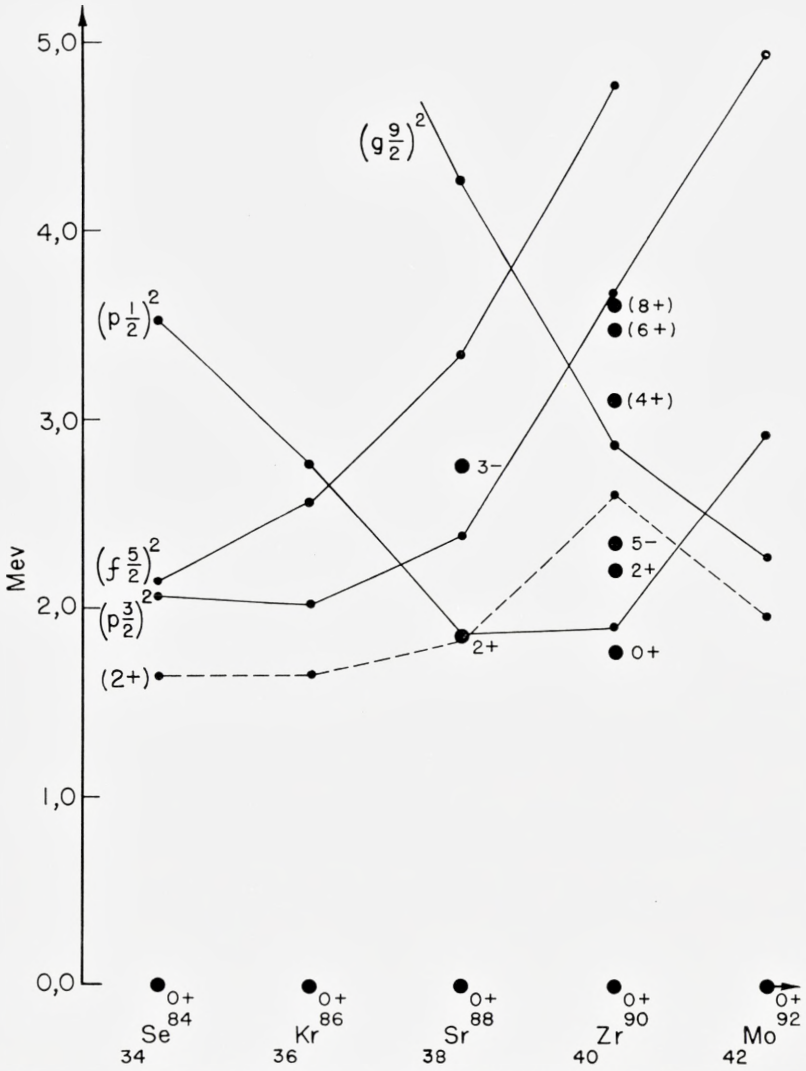


Fig. 14. *Energy levels of even-A isotopes for* $N = 50$.
The notation is the same as in Fig. 2 with $G$, $X$, and the well as in Fig. 13.

shell. One finds the $f_{5/2}$ state of the order of 1 Mev above the $p_{3/2}$ state. If this is the well for the protons, it is impossible to obtain the experimental $(3/2)^-$ ground states in $_{35}Br^{85}$ and $_{37}Rb^{87}$ with reasonable values of the $G$ and $\chi$ parameters.

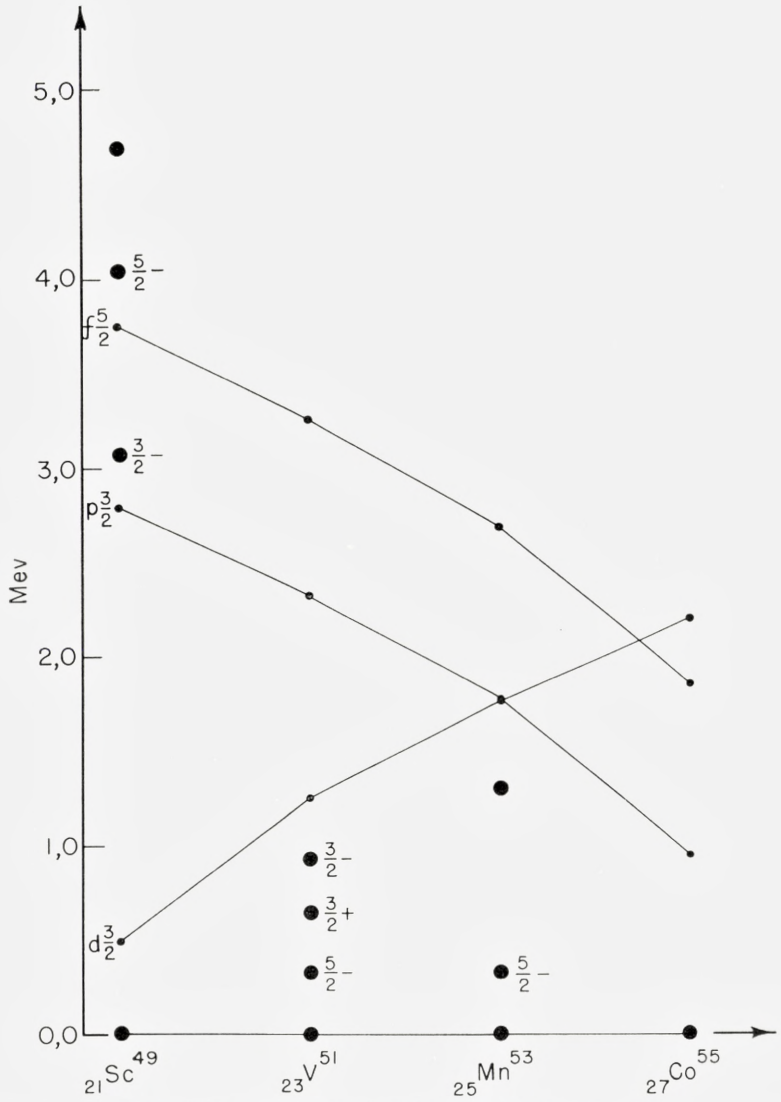


Fig. 15. *Energy levels of odd-A isotopes for* $N = 28$.
The notation is the same as in Fig. 1. $G = 19/A$, $X = 3.06$, and the single-particle levels are $d_{3/2}$, (0); $f_{7/2}$, (2.5); $p_{3/2}$, (5.57); $f_{5/2}$, (6.54 Mev).

On the other hand, it is true that for the $N = 50$ isotopes the values of $A$ are considerably larger than for the Cu isotopes used to determine the proton well. As one increases $A$, the spin orbit force decreases. It is possible

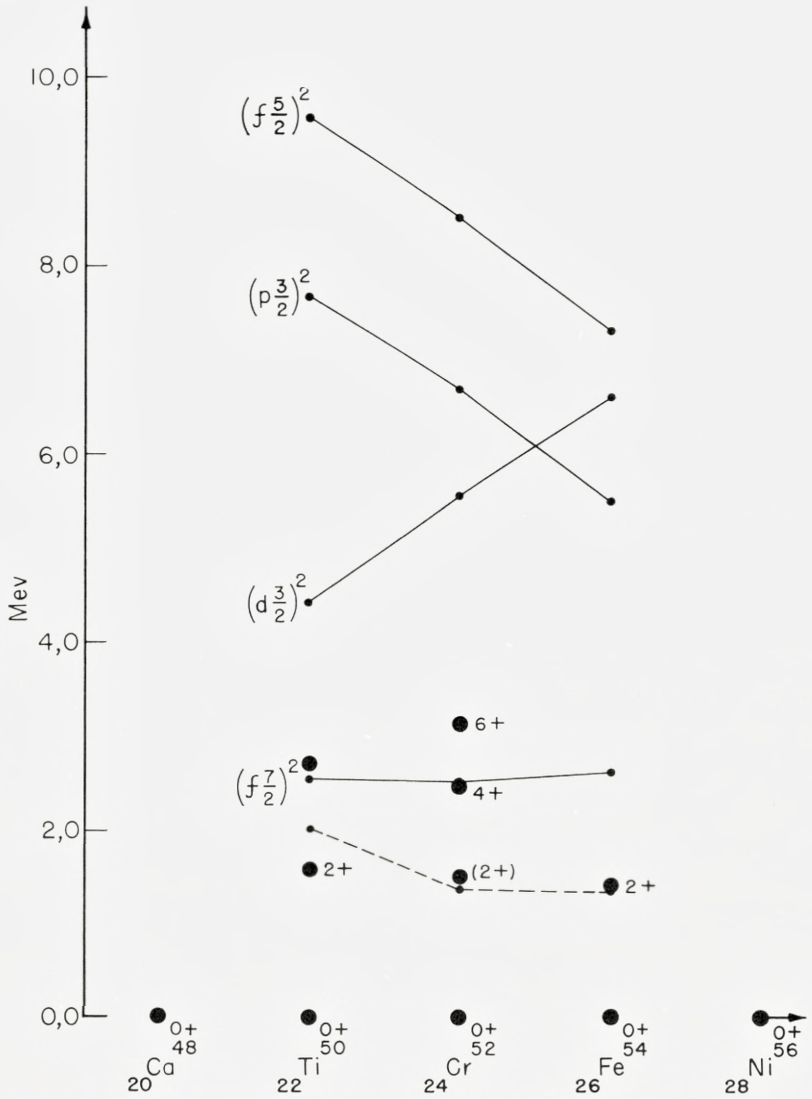


Fig. 16. *Energy levels of even-A isotopes for* $N = 28$.
The notation is the same as in Fig. 2 with $G$, $X$, and the well as in Fig. 15.

that the $f_{7/2}-f_{5/2}$ and $p_{3/2}-p_{1/2}$ separations have decreased so much as one goes from 63 to 85 that the $(5/2)^-$ state has come below the $(3/2)^-$ state. If one takes such a well, with a level ordering of $f_{5/2}$, $p_{3/2}$, $p_{1/2}$, $g_{9/2}$, it is possible to fit all of the odd-$A$ $N = 50$ ground states as well as the known

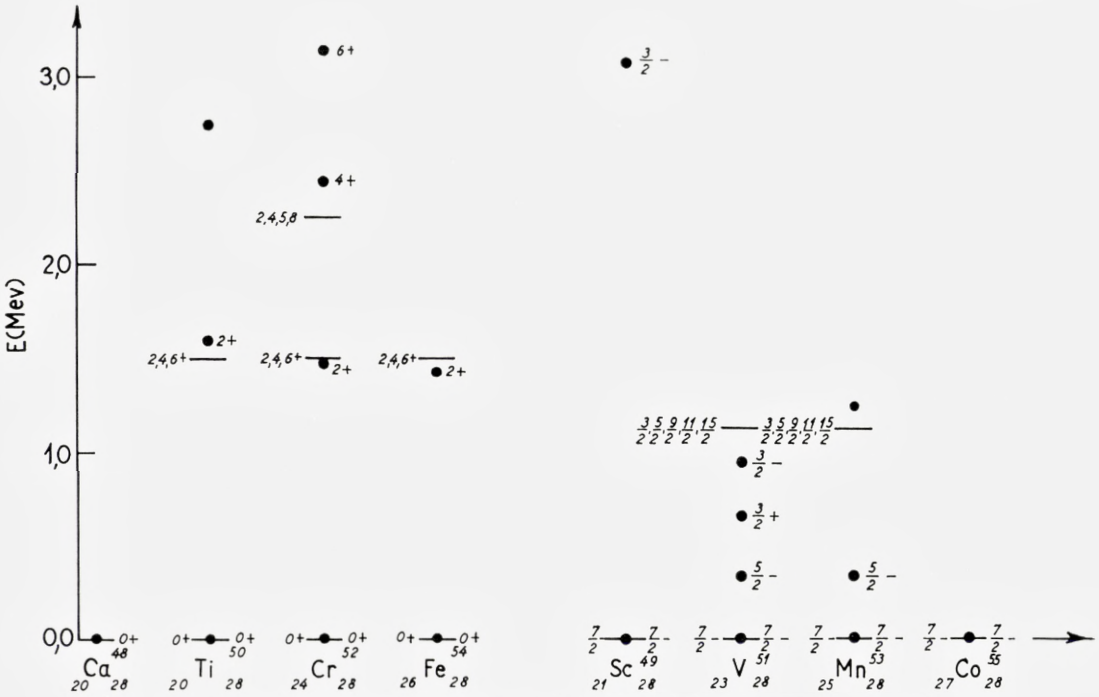


Fig. 17. *Exact diagonalization of pairing force for particles moving in a $j = 7/2$ shell compared with the experimental levels of the $N = 28$ isotopes.*

The experimental levels are indicated by dots with spin and parity assignments to the right and the theoretical levels by lines with the resultant angular momentum shown to the left of the line.

excited state information, within the accuracy of these methods, if the $(9/2)^+ - (1/2)^-$ separation is taken to be about 2.0 Mev and with $G = 26/A$. (Cf. Fig. 13).

For the even-$A$ nuclei shown in Fig. 14 the most interesting feature is the low $0^+$ excited state in ${}_{40}Zr_{50}^{90}$. From our calculation we obtain a state of two quasi-particles of spin 1/2 about at this position for $G = 23/A$. As this state must be $0^+$, this is a possible explanation for the experimental state. However, the state might be quite spurious, in which case the real lowest $0^+$ excited state would be somewhat higher in energy for the same $G$. The $(9/2)^+ - (1/2)^-$ separation is critical in determining how spurious this state is. With only the levels in $Sr^{88}$ and $Zr^{90}$ it is difficult to draw much more information from these isotopes. Incidentally, if the $0^+$ state is really associated with the two quasi-particle state, we would expect a

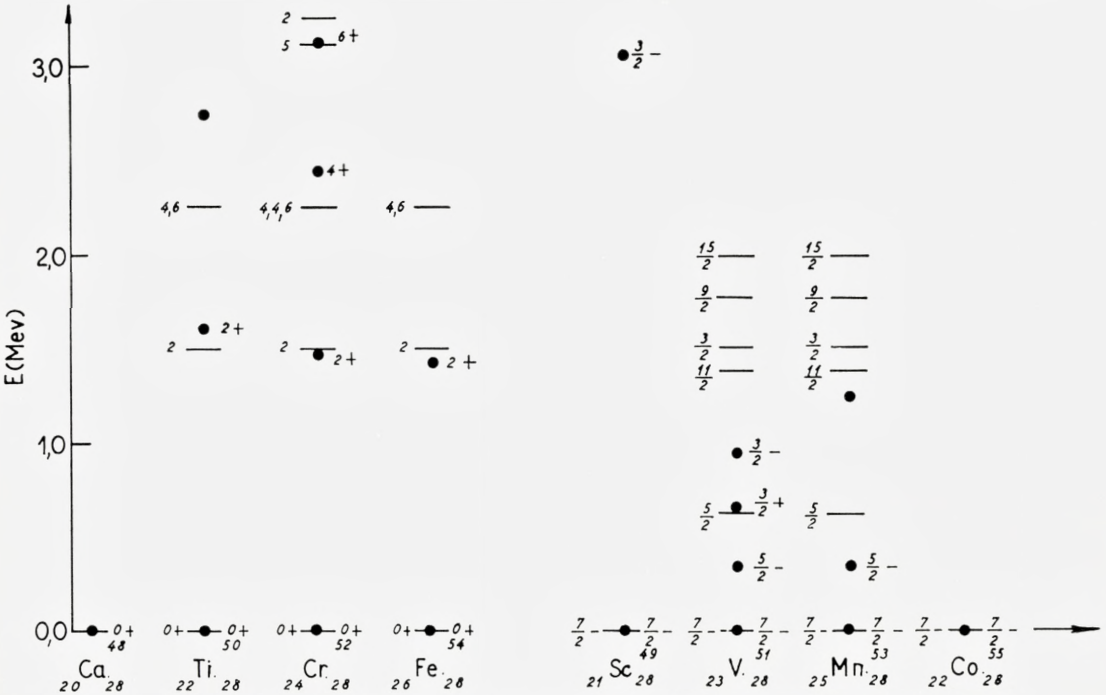


Fig. 18. Same as Fig. 17 except that in this case the force diagonalized is the sum of a pairing force plus a $P^{(2)}$ force of such relative strengths that the $0^+-2$ separation of the even isotopes is produced by the combined results of the two parts of the force, the pairing force contributing two thirds and the $P^{(2)}$ force contributing one third to the separation.

$0^+$ state to lie near the $2^+$ 1.85 Mev state in $Sr^{88}$. The most significant manner in which our $Zr^{90}$ results differ from previous detailed calculations[24] is that the $f_{5/2}$, and especially the $p_{3/2}$, configurations are admixed, and seem to contribute to the low energy spectrum.

The results for both even-$A$ and odd-$A$ isotopes are quite sensitive to the choice of the single-particle levels in this region, and the results shown in Fig. 13 have been obtained only after several calculations with rather wide freedom in the choice of the single-particle values.

6. $N = 28$

Although ${}_{21}Sc_{28}^{49}$ experiments give the proton well for neutrons in a closed shell of 28, the region is still not a good one for our calculation. The small degeneracy of the levels in this region, i.e., $\Omega_{\text{eff}} \simeq 4$, leads to poor Bardeen solutions. The results of the calculation with a $G = 19/A$

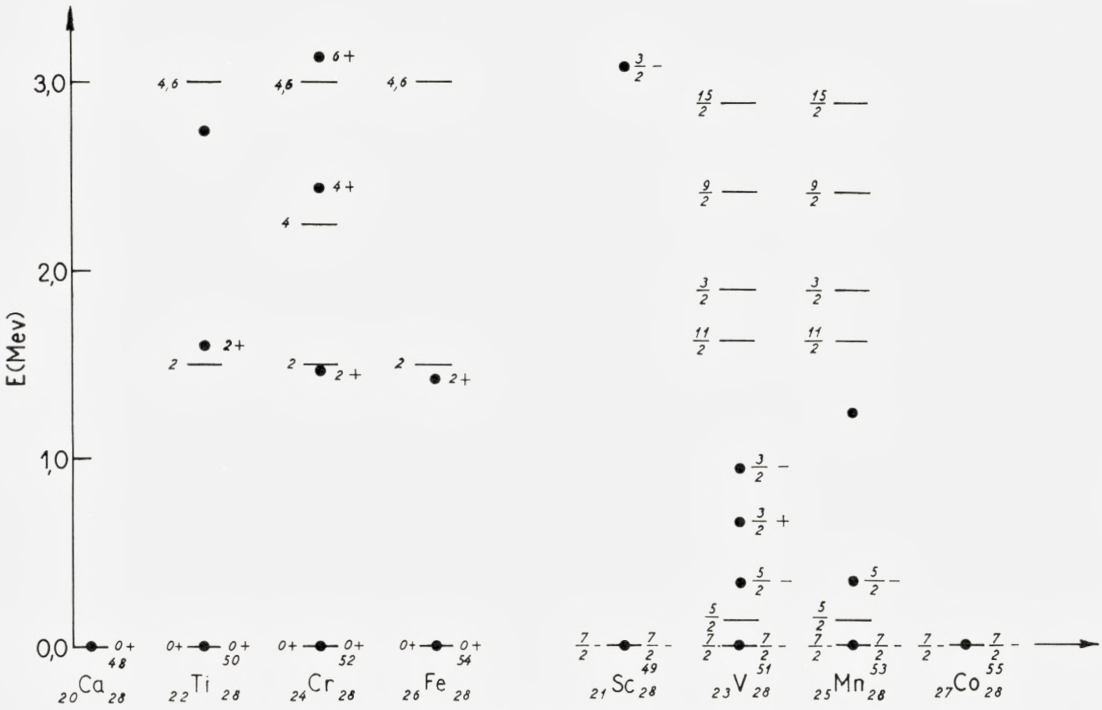


Fig. 19. Same as Figs. 16 and 17, but with a relatively stronger $P^{(2)}$ force, the pairing force only contributing one third and the $P^{(2)}$ contributing two thirds to the $0^+-2^+$ separation of the even isotopes.

and $P^{(2)}$ force are given in Figs. 15 and 16. Although the $2^+$ state is fit pretty well as a collective state, the levels in the odd-$A$ isotopes are not well fit. If the low lying odd parity excited states in $_{23}V^{51}$ and $_{25}Mn^{53}$ are to come from the single quasi-particle states corresponding to elementary excitations to levels in the next shell, such a large long range force perturbation will be needed to break down the seniority coupling scheme. Certainly, perturbation theory is inadequate for the long range force. The theoretical $(3/2)^+$ state listed in Fig. 15 is the one quasi-particle state associated with the $d_{3/2}$ level in the shell below.

We also performed an exact diagonalization of the pairing force plus $P^{(2)}$ force under the assumption of a degenerate $f_{7/2}$ level. Fig. 17, Fig. 18, and Fig. 19 give the results for three different combinations of $G$ and $P^{(2)}$, all taken to fit the mean position of the $2^+$ levels in the even-$A$ nuclei. From these figures we see that it is possible to fit the experimental data for

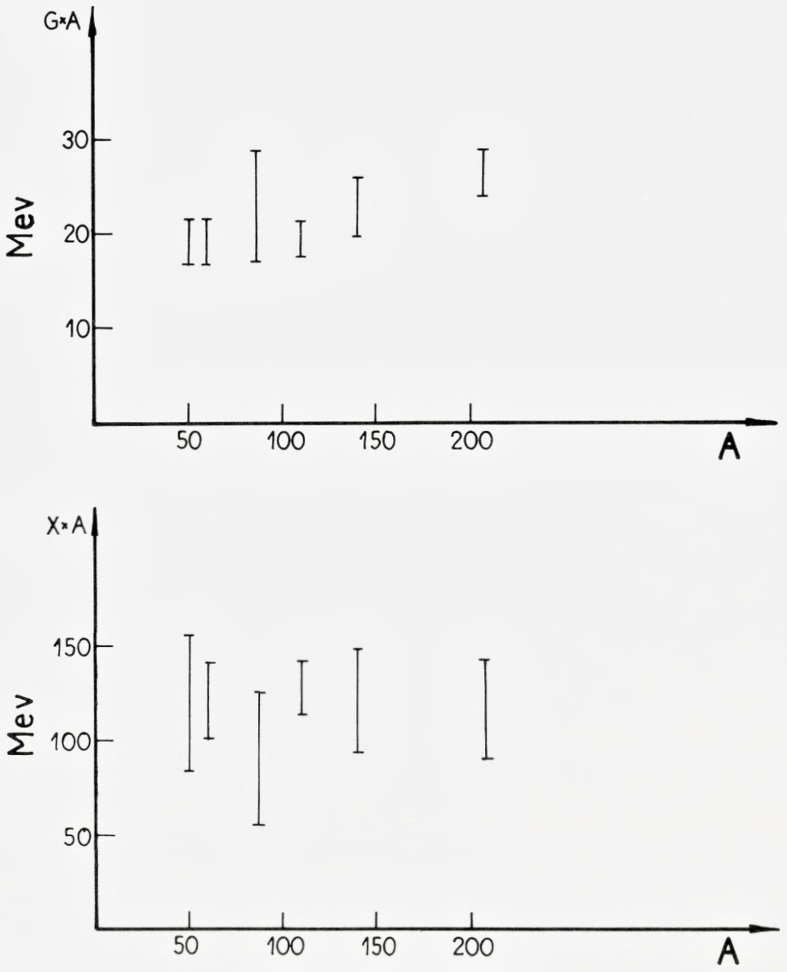


Fig. 20. *Coupling parameters.*
The coupling parameters used in each mass region are indicated. The vertical lines indicate the extent to which the magnitude of the parameters may be determined by fitting the experimental data.

the even-$A$ isotopes and the low lying $(5/2)^-$ states in the odd-$A$ isotopes with a pairing plus a $P^{(2)}$ force. The $(3/2)^+$ state in $V^{51}$ presumably is associated with excitations from the shell below. If the $f_{5/2}$, $p_{3/2}$, and $p_{1/2}$ states from the next shell were included, one would obtain somewhat different results, and in particular the $(3/2)^-$ state might be lowered.

For regions lighter than $N = 28$, one would not expect our methods

to work very well. In these regions, the protons and neutrons are filling the same levels, so that the short range interaction between protons and neutrons becomes important to the extent that the particles in the closed shell are excited into the next higher shell. For example, there is evidence that the double closed shell of $N = Z = 20$ is not strong enough for our methods to be very accurate. Moreover, the effective pair degeneracy of the well becomes rather small. In conclusion, for the s.c.s. nuclei with $A \geq 49$, we fit the energy level systematics rather well with an approximate solution to the pairing plus $P^{(2)}$ residual force. Only in the $N = 50$ case does the change in the well with $A$ in one region seem to give important effects. The two parameters, $G$ and $X$, which are obtained as likely in each region are plotted in Fig. 20. From this it is seen that their $A$ dependence is consistent with a volume force. This means that with only two parameters the low energy systematics for the intrinsic and $2^+$ collective states of nuclei with one closed shell can be derived approximately.

## IV. Total Binding Energies

### A. Even-Odd Mass Differences

Assuming that an interacting shell model picture is a good one, the binding energies of nuclei can give information about the residual interaction. A systematic difference in the binding energies of even-odd and even-even nuclei is a direct consequence of the pairing force. The $P^{(2)}$ force, on the other hand, produces a ground state energy shift which, though large, has very little even-odd structure. Thus, a comparison between the experimental odd-even mass differences of the s.c.s. nuclei which we consider and the theoretical ground state energy differences between odd- and even-$A$ nuclei can be used to help determine the magnitude of the pairing force constant $G$.

We define the quantities $P_n$ and $P_p$

$$P_n(Z, N) = E(Z, N) + E(Z, N-2) - 2E(Z, N-1), \tag{42a}$$

$$P_p(Z, N) = E(Z, N) + E(Z-2, N) - 2E(Z-1, N), \tag{42b}$$

where $E(Z, N)$ is the total binding energy of the nucleus, $(Z, N)$. We consider $P_n$ for $Z$ closed and $P_p$ for $N$ closed. From (30) and (39) we see that, aside from the small shift due to the coupling of the quasi-particle to the

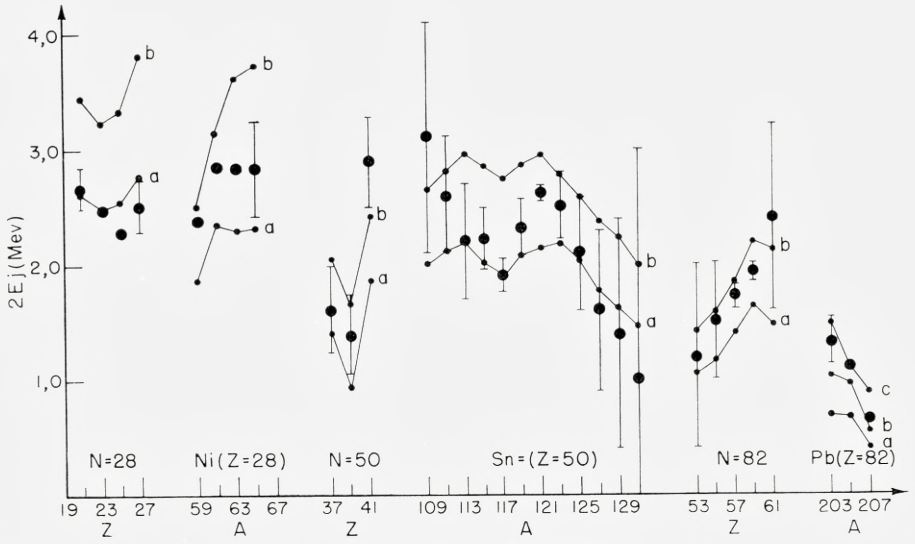


Fig. 21. *Even-odd-A mass difference.*

The $P_n\,(Z, N) = E\,(Z, N) + E\,(Z, N-2) - 2E\,(Z, N-1)$ and $P_p\,(ZN) = E\,(Z, N) + E\,(Z-2, N) - 2E\,(Z-1, N)$ are experimental quantities.[25] The theoretical curves are simply $2E_v$, twice the energy of the lowest lying quasi-particle for the odd-$A$ isotope. Curves $a$ and $b$ correspond to $G = 19/A$ and $23/A$, respectively. Curve $c$ (for lead only) corresponds to $G = 30/A$.

phonons, which we ignore, the odd-even-$A$ difference given by $P_n$ or $P_p$ should just equal twice the energy of the odd-$A$ quasi-particle, $2E_j$. In Fig. 21, the lines represent the quantity $2E_j$ for the ground state for various values of the coupling parameter $G$. The points are the experimental quantities $P_n$ or $P_p$.

In each of the six pictured mass regions, the lower curve is the calculated mass difference value for $G = 19/A$, $A$ being the representative mass number of the region. The next curve is for $G = 23/A$, and in the Pb region a third curve for $G = 30/A$ is included. The experimental points indicate that the data is consistent with the selected $G$ values, but does not very strongly choose one over the other. Perhaps in the Pb region the two stronger values of $G$ are preferred, while in the $N = 28$ region the lower value is better. This is in agreement with the energy level information discussed in the preceding section which indicates a preference for the value $G = 23/A$ in the Pb, $N = 82$, and $N = 50$ regions and the weaker $G = 19/A$ in the other regions.

### B. Absolute Binding Energies

In addition to the evidence for the gap, and therefore for the strength of the short range part of the residual shell model two-body interaction, the total binding energy data can give evidence for the absolute ground state energies of nuclei. Although the residual force employed in this work is certainly not the true force, it is hoped that in choosing a two-body interaction which gives the correct energy level spacing, one obtains the most important portions of the nuclear states. In particular, one would like to

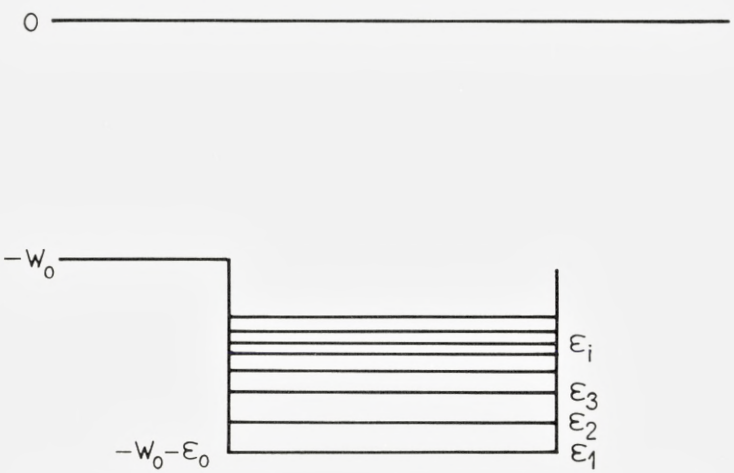


Fig. 22. *Energy diagram for non-interacting shell model particles.*

be able to calculate the total binding energy of the shell model particles outside of the closed shells.

In a particular region let us call the binding energy of the double closed shell nucleus $W_0$. Neglecting the Coulomb effect for the moment, if one adds one extra particle (or hole) it experiences an additional binding energy of $\varepsilon_0$ (cf. Fig. 22). The assumptions of this work imply that as more particles of the same type are added they fill the well defined by the isotope with one particle outside the double closed shells, so that, except for a possible gradual change with $A$ of $\varepsilon_0$ and of the energies of the well, as well as of the binding energy of the core, $W_0$, the additional binding energy due to the outside particles is determined by single-particle energies, the two-body interaction, and the Coulomb force. Including the Coulomb force, the binding energy of the isotope with one particle outside the double closed shell is

$$W(1) = W_0 + \varepsilon_0 - (E_c^{(1)} - E_c^{(0)}), \tag{43}$$

where the Coulomb energy, $E_c$, is given by the Weizsäcker mass formula[26] as

$$E_c = 0.6 \frac{Z(Z-1)}{A^{1/3}} \text{ Mev.} \tag{44}$$

The binding energy of the isotope with $n$ particles outside of the double closed shell is

$$W(n) = W_0 + \sum_{i=1}^{n} \left[\varepsilon_0 - (\varepsilon_i - \varepsilon_1)\right] - V_G(n) - V_L(n) - (E_c^{(n)} - E_c^{(0)}), \tag{45}$$

where $V_G$ is the total interaction energy of the pairing force and $V_L$ is the effect of the $P^{(2)}$ force in the ground state of the $n$ particle system.

From Eqs. (9) and (45), one finds

$$-W(n) + W_0 + n\varepsilon_0 = U'(n) + V_L(n) + E_c^{(n)} - E_c^{(0)} \tag{46}$$

for an even-$A$ nucleus, while

$$-W(n) + W_0 + n\varepsilon_0 = U'(n) + V_L(n) + E_c^{(n)} - E_c^{(0)} + \sqrt{(\varepsilon - \lambda)^2 + \Delta^2} \tag{47}$$

for an odd-$A$ nucleus. In Eq. (47) the quasi-particle energy which appears is the smallest one for the isotope. It is difficult to know a priori the $A$ dependence of $\varepsilon_0$ and $W_0$ or whether it should be the same for all regions. We make two calculations in each case, one holding $\varepsilon_0$ constant and the second giving $\varepsilon_0$ an $A^{-1/3}$ dependence. We use the average $\varepsilon_0$ as determined from adjacent nuclei.

The most favourable case to consider is that of the Pb isotopes, for here the experiments are accurate and one knows the binding energy of the double closed shell isotope, $Pb^{208}$, and the isotope with one hole in the neutron shell, $Pb^{207}$. From these one finds[27]

$$\varepsilon_0(Pb^{207}) = -7.357 \pm 0.043. \tag{48}$$

Using (48), one has accurate experimental values for $-W(n) + W_0 + n\varepsilon_0$ for $Pb^{206}$ and $Pb^{204}$. In Fig. 23 these values are compared to the theoretical ones for $G = 0$, $G = 0.111$, and $G = 0.145$. One sees that both for $\varepsilon_0$ constant and for $\varepsilon_0 \sim A^{-1/3}$ the theoretical results are consistent with the data, and

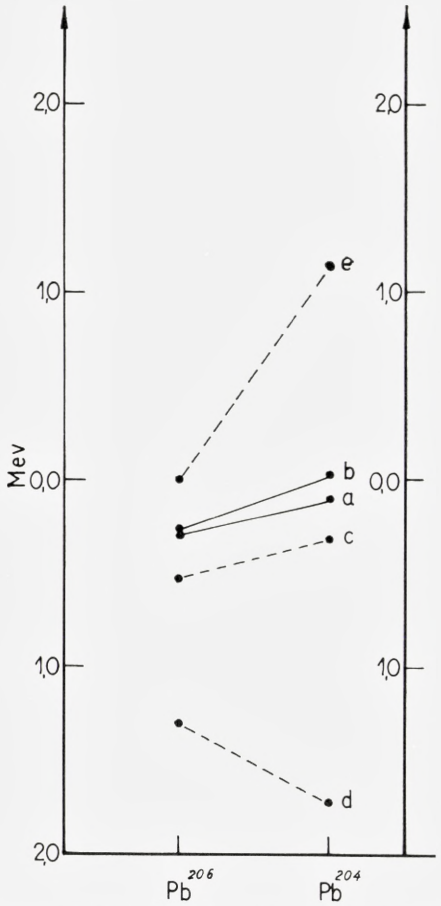


Fig. 23. *Absolute binding energies of the Pb isotopes.*
*a* and *b* are the experimental curves of $-W(n)+W_0+n\varepsilon_0$ for $\varepsilon_0$ constant and $\varepsilon_0 \sim A^{-(1/3)}$, respectively; *c*, *d*, and *e* are the theoretical curves for $U(n)+V_L(n)$ for $G = 0.111$, $G = 0.145$, and $G = 0$, respectively. $\varepsilon_0 = -7.357$ from $Pb^{208}$ and $Pb^{207}$ experimental binding energies.[27]

the value of $G =$ about $23/A$ is favoured. This is consistent with the results of the energy level calculation. However, the errors in the experimental results are large enough to make this result somewhat uncertain.

For the Ni isotopes and for the $N = 82$ region, one is at the beginning of a major shell. However, for neither of these series of isotopes is the binding energy known for the double closed shell and the double closed shell plus one nucleon isotopes. Therefore, one can merely determine if the results

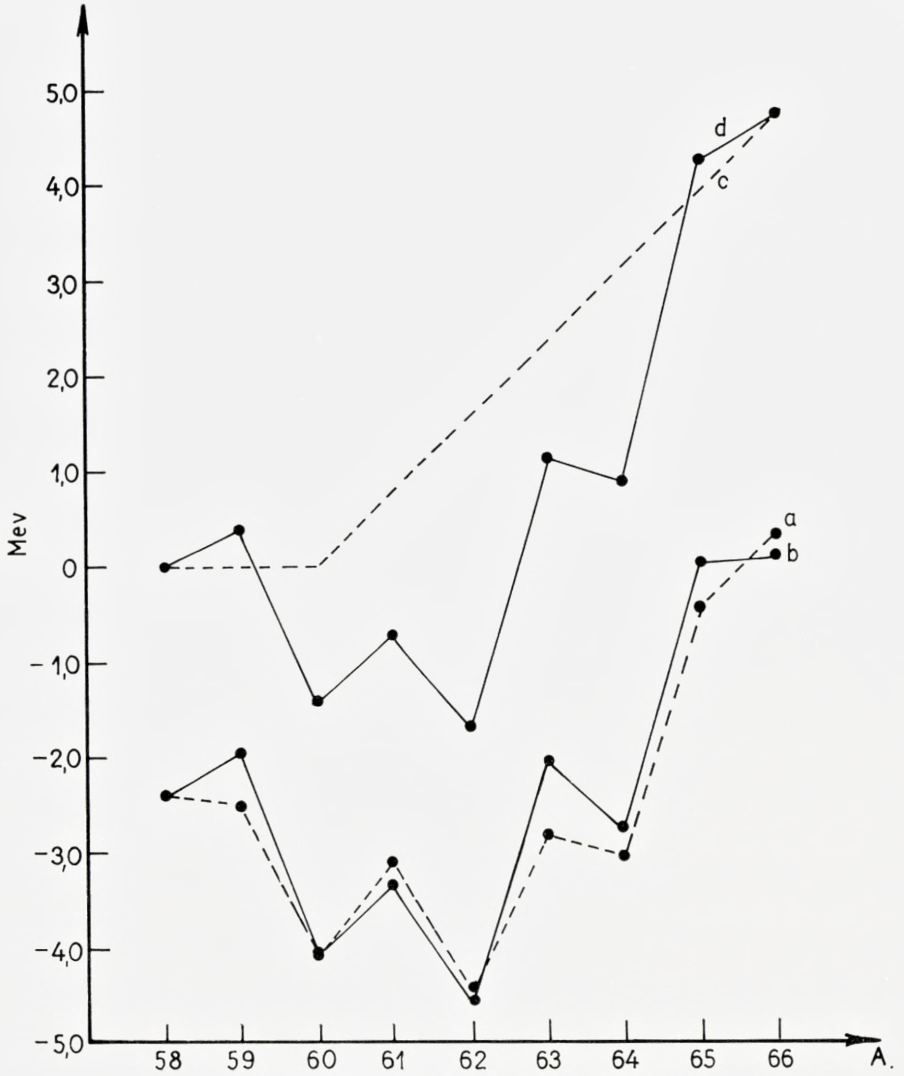


Fig. 24. *Binding energies of the Ni isotopes.*
*a* is the theoretical curve of $U'(n)+V_L(n)$ for $G = 19/A$, *b* is $-W(n)+W_0+n\varepsilon_0$ with $\varepsilon_0 \sim A^{-(1/3)}$. The curves have been fit at $Ni^{58}$. Curves *c* and *d* are analogous to *e* and *a* of Fig. 23, respectively.

of the theoretical calculation are consistent with the known experimental results, and cannot experimentally determine the total binding energy of the $n$ particles outside of the closed shells. However, the binding energy curves have considerable structure, reflecting the two-body force by a dip

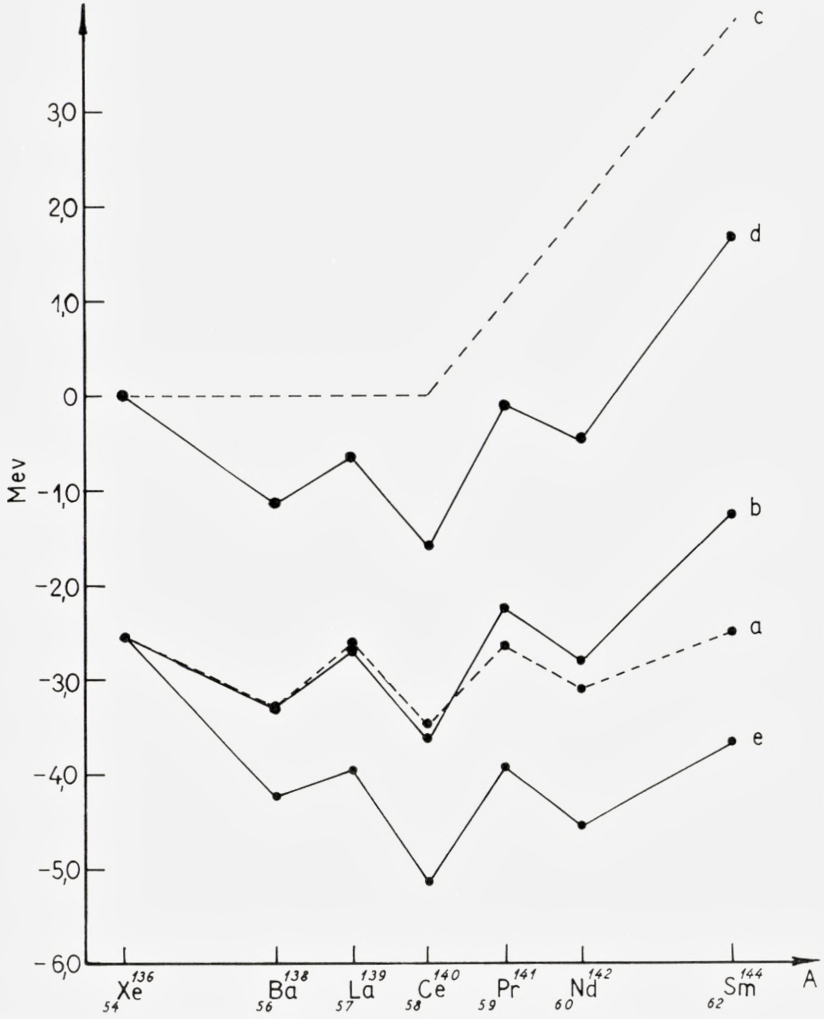


Fig. 25. *Binding energy of the $N = 82$ isotopes.*
$a$ is the theoretical curve for $U(n) + V_L(n)$, $b$ and $e$ are the values of $-W(n) + W_0 + n\varepsilon_0$ for $\varepsilon_0 \sim A^{-(1/3)}$ and $\varepsilon_0$ constant, respectively; they are fit at $_{54}X^{136}_{82}$. Curves $c$ and $d$ are analogous to $a$ and $e$, respectively, for $G = 0$.

in the $-W(n) + W_0 + n\varepsilon_0$ curve for the even-$A$ and odd-$A$ nuclei separately, as well as the even-odd mass difference (cf. Figs. 24 and 25). In both cases, after the experimental curves are normalized at the first point, the dip is quite well reproduced if $\varepsilon_0 \sim A^{-1/3}$, but the statistics do not rule out a constant $\varepsilon_0$.

The Sn isotopes are in the middle of a shell, forcing us once more to fit at one isotope; and there is very little structure to the curves except the rise of the Fermi level and the even-odd mass difference. For this reason we do not present the diagram. In this case the constant $\varepsilon_0$ seems to be favoured. Of course, these results depend upon the positions of the single-particle levels which are not too well known. The $N = 50$ region is also in the middle of a shell, so the total binding energy information is not so useful, since one must fit at one point.

In conclusion, we see that the total binding energy data is consistent with the theoretical results in every case. In addition, in the Pb region, the results can be used to help select the $G$ which is most favourable. There is an indication that the well depth changes as $A^{-1/3}$ near closed shells and that it might have a slightly different $A$ dependence in the middle of a shell than at the beginning or end. One should remember that there are rather large uncertainties in both the theoretical and emperical results which go into drawing these conclusions.

## V. Electric Quadrupole Moments

For s.c.s. odd-A nuclei described by the collective Hamiltonian (39), the total quadrupole moment operator is the sum of the single-particle and collective operators

$$Q_0^T = \sum_{\nu\nu'} q^0_{\nu\nu'} (U_\nu U_{\nu'} - V_\nu V_{\nu'}) (\alpha^\dagger_{\nu'} \alpha_{\nu'} + \beta^\dagger_{\nu'} \beta_\nu) + Q_0 . \tag{49}$$

The single-particle operator, $Q_{\text{s.p.}}$, of which we have only included the part diagonal in the number of quasi-particles, cannot change the number of collective quanta (phonons); and the collective operator changes the number of phonons by $\pm 1$, but does not affect the quasi-particles. Thus $Q_{\text{s.p.}}$ contributes to the quadrupole moment in zeroth order perturbation theory, while the contribution from $Q_0$ first appears in a term proportional to $\chi$. For a quasi-particle of angular momentum $j$, the single-particle moment is

$$\left.\begin{aligned} Q_{\text{s.p.}} &= \sqrt{\frac{16\pi}{5}} \langle j \,|\, r^2 Y^2_0 \,|\, j \rangle_{m=j} (U_j^2 - V_j^2)\, e_{\text{eff}} \\ &= + \frac{2j-1}{2(j+1)} \langle j \,|\, r^2 \,|\, j \rangle (U_j^2 - V_j^2)\, e_{\text{eff}} . \end{aligned}\right\} \tag{50}$$

For the coupled system, making the same assumptions needed to obtain (34), we obtain for the collective moment contribution

$$Q_{\text{coll}} = +\frac{2j-1}{2(j+1)}\langle j\,|\,r^2\,|\,j\rangle\,(U_j^2-V_j^2)\,\frac{\chi}{C}\,e_{\text{eff}}, \tag{51}$$

so that the total quadrupole moment is given in perturbation theory by

$$Q = +\frac{2j-1}{2(j+1)}\langle j\,|\,r^2\,|\,j\rangle\,(U_j^2-V_j^2)\,e_{\text{eff}}\left(1+\frac{\chi}{C}\right). \tag{52}$$

Quadrupole moments are known experimentally for only four of the s.c.s. odd-$A$ nuclei which we consider. The experimental and theoretical moments calculated, using $G$ and $\chi$ which best fit other data, are shown in Table I. An effective charge of two units was used in the calculation.

TABLE I

| Isotope | $j$ | $\frac{\chi}{C}$ | $(U^2-V^2)$ | $Q$ theoretical [$10^{-24}$ cm$^2$] | $Q$ experimental ($10^{-24}$ cm$^2$) |
|---|---|---|---|---|---|
| $_{57}La^{139}$ | 7/2 | 1.2 | −.25 | +.21 | +.27 |
| $_{59}Pr^{141}$ | 5/2 | 1.6 | .44 | −.36 | −.05 |
| $_{37}Rb^{87}$ | 3/2 | 1.0 | −.47 | +.15 | +.14 |
| $_{23}V^{51}$ | 7/2 | 2.2 | .25 | −.17 | +.03 |

The table compares the experimental and theoretical electric quadrupole moments of s.c.s. nuclei, based on the coupled system of quasi-particle and quadrupole vibration.

It is seen that the $La^{139}$ and $Rb^{87}$ moments agree well with experiment. The theoretical moment of $Pr^{141}$ is too large by a factor of 7, but this result could be improved considerably by the use of a different shell model well which would in turn alter particularly the quantity $(U^2-V^2)$ in (52). However, it is difficult to see how the sign of the $V^{51}$ moment could be changed within our model, for this would mean that, with only three protons beyond the twenty closed shell, the $f_{7/2}$ shell is effectively more than half filled. Including the $d_{3/2}$ levels below the shell in the calculation of the $V$'s and $U$'s does not seem to have a strong enough effect to cause this. The meager experimental data for the quadrupole moments of odd-$A$ s.c.s. nuclei do not provide a detailed test of the nuclear wave functions. Thus, the question

remains open as to whether admixed configurations to the pairing force wave function other than those produced by the quadrupole field may also contribute significantly to the quadrupole moment. Also other authors have not succeeded in explaining the $V^{51}$ moment by considering configuration mixing[28].

## VI. Magnetic Dipole Moments in Odd Nuclei

### A. Magnetic Moments with Pairing and $P^{(2)}$ Force Model

The magnetic moment operator for the coupled system of phonons and quasi-particles is the sum of the quasi-particle magnetic moment and that of the phonon. The quasi-particle magnetic moment operator is

$$\left.\begin{aligned}\hat{\mu}_{\text{s.p.}} = &\sum_{\nu\nu'} \langle \nu \,|\, \mu \,|\, \nu' \rangle \,(U_\nu U_{\nu'} + V_\nu V_{\nu'})\,(\alpha^\dagger_\nu \alpha_{\nu'} - \beta^\dagger_{\nu'} \beta_\nu) \\ &+ \sum_{\nu\nu'} \langle \nu \,|\, \mu \,|\, \nu' \rangle \,(U_\nu V_{\nu'} - V_\nu U_{\nu'})\,(\alpha^\dagger_\nu \beta^\dagger_{\nu'} - \beta_\nu \alpha_{\nu'}),\end{aligned}\right\} \tag{53}$$

where $\mu$ is the usual particle magnetic moment

$$\mu = j g_j = j\left(g_l \pm \frac{1}{2\,l+1}\,(g_s - g_l)\right); \quad j = l \pm \frac{1}{2}, \tag{54}$$

$g_j$ is the total single-particle $g$-factor, and

$$g_s = \left\{\begin{matrix} 5.585 \\ -3.826 \end{matrix}\right\} \quad \text{and} \quad g_l = \left\{\begin{matrix} 1 \\ 0 \end{matrix}\right\} \tag{55}$$

for protons and neutrons, respectively. The only non-diagonal terms in (53) are those for which $\nu$ and $\nu'$ are spin orbit partners. It is seen from (53) that quasi-particles have the same magnetic moments as particles, since $(U^2 + V^2) = 1$. This is easily understood, since particles and the corresponding holes also have the same magnetic moments. The second term in (53) plays no role since the collective Hamiltonian (29) cannot change the number of quasi-particles. Thus, with only pairing forces, the odd-$A$ nuclei will exhibit single-particle values (the Schmidt line values) for their magnetic moments.

The collective Hamiltonian (39) will lead to magnetic moments different from single-particle values by coupling the quasi-particle to a phonon and, of more importance, by admixing near lying quasi-particle states. For the

first and less important effect we must know the $g$-factor, $g_R$, for the phonon. This depends upon what part of the angular momentum of the collective $2^+$ state comes from the protons and what part from the neutrons. Our model, in which the collective motion involves the extra-core particles together with the core (included as a renormalization effect), suggests a somewhat higher $g$-factor for extra-core proton than for extra-core neutron nuclei. However, for the calculations we have taken $g_R = 0.45$. The phonon magnetic moment operator is then $g_R R$, where $R$ is the phonon angular momentum. Since neither the phonon nor quasi-particle magnetic moment operators can change the number of phonons, the shift of the magnetic moment from its single-particle value will first appear in perturbation theory in a term proportional to $\chi^2$.

In the perturbation approximation one obtains[2] from the diagonal part of (53)

$$\left.\begin{aligned}\mu = \mu_{\text{s.p.}} + \frac{5}{16\pi}\frac{1}{j}\frac{\chi^2}{\hbar\omega\, C}\sum_{j'}\{-\alpha_{jj'}(g_j - g_R) + \beta_{jj'}(g_{j'} - g_R)\} \\ \left(\frac{\hbar\omega}{\hbar\omega + E_{j'} - E_j}\right)^2 (U_j U_{j'} - V_j V_{j'})^2,\end{aligned}\right\} \quad (56)$$

where $\alpha_{jj'}$ and $\beta_{jj'}$ are tabulated by Bohr and Mottelson (Table V, Ref. 2) or can be taken as

$$\alpha_{jj'} = 2\left(C^{2\,j\,j'}_{0\,\frac{1}{2}\,\frac{1}{2}}\right)^2 j^2 \quad (57\,\text{a})$$

$$\alpha_{jj'} - \beta_{jj'} = \left(C^{2\,j\,j'}_{0\,\frac{1}{2}\,\frac{1}{2}}\right)^2 \frac{j}{j+1}\left[j(j+1) - j'(j'+1) + 6\right]. \quad (57\,\text{b})$$

If quasi-particle states $j'$, $j''$ which are spin orbit partners of each other appear in the one phonon amplitude, there is an additional contribution to $\mu$ from the non-diagonal part of (53). This additional contribution is

$$\left.\begin{aligned}\delta\mu = \frac{5}{16\pi}\frac{1}{j}\frac{\chi^2}{\hbar\omega\, C}(g_s - g_l)\, 2\, C^{2\,j\,j'}_{0\,\frac{1}{2}\,\frac{1}{2}}\, C^{2\,j\,j''}_{0\,\frac{1}{2}\,\frac{1}{2}}\frac{j}{(j+1)(2l+1)} \\ \sqrt{\left(j+l-\frac{3}{2}\right)\left(j+l+\frac{7}{2}\right)}\cdot\sqrt{\left(l-j+\frac{5}{2}\right)\left(j-l+\frac{5}{2}\right)}\frac{\hbar\omega}{\hbar\omega + E_{j'} - E_j} \\ \frac{\hbar\omega}{\hbar\omega + E_{j''} - E_j}(U_\nu U_{\nu'} - V_\nu V_{\nu'})(U_\nu U_{\nu''} - V_\nu V_{\nu''})(U_{\nu'} U_{\nu''} + V_{\nu'} V_{\nu''}),\end{aligned}\right\} \quad (58)$$

where

$$j' = l - \frac{1}{2}, \quad j'' = l + \frac{1}{2}. \tag{59}$$

For $j = j'$ or $j = j''$ this expression (without the U, V factor) is equivalent to IV. 8, Ref. 2. The other cases where these terms can contribute are when $j = j' - 1$ and $j = j'' + 1$.

Using (56) and (58) and the $G$ and $\chi$ which best fit other data, we have calculated the shift of the magnetic moment from the Schmidt line for all s.c.s. nuclei for which the magnetic moments are known experimentally. The result is that, although the shift from the single-particle moment is always in the right direction, it is always too small by a factor of from four to ten. The reason for this is the factor $(U_\nu U_{\nu'} - V_\nu V_{\nu'})$, appearing in the collective Hamiltonian (39), which greatly weakens the coupling of the ground state to the collective vibration. Thus it does not seem to be possible to understand the shift of the quasi-particle magnetic moment of s.c.s. odd-$A$ nuclei from the single-particle value on the basis of the coupling of the quasi-particle to the collective oscillations.[29]

### B. Magnetic Moments with Configurations Admixed by a $\delta$-Function Force

ARIMA and HORIE[30], and BLIN-STOYLE,[31] have pointed out that a small amount of mixing of certain kinds of configurations can produce large changes in the magnetic moments of nuclei, without changing appreciably the pure shell model configurations upon which they base their calculations.

From the results of Section A of this chapter it is clear that the configuration mixing produced by the long range part of the force is insufficient to account for deviations of the magnetic moments from the Schmidt lines. Moreover, the pairing force which we use to approximate the short range force does differ from an actual short range $\delta$-force in several ways. Although these differences do not seem to show up in calculations of the gross properties of the nuclear wave function, it is easy to see that they are extremely important in calculating magnetic moments. If we assume that an improved Hamiltonian, $H_R$, is of the form of a $\delta$-function force and a $P^{(2)}$ force,

$$H_R = \sum_j{}' \varepsilon_j + \frac{1}{2} \sum_{ij}{}' v(r_i, r_j)\, \delta(r_i - r_j) + \frac{\chi}{2} \sum_{ij}{}' P^{(2)}(ij), \tag{60}$$

then the Hamiltonian, $H$, used in this work is related to this Hamiltonian by

$$H_R = H + V, \tag{61}$$

where

$$V = \sum_{ij} v(r_i, r_j)\, \delta(r_i - r_j) - \sum_{ij} G_{ij}, \tag{62}$$

and $G_{ij}$ is the pairing force as defined in Chapter II. If we use $V$ as the perturbation in calculating the extra configuration mixing which plays a part for magnetic moments, then the calculation is quite similar to that of Ref. 30.

As these authors point out, there are only a few kinds of admixed configurations which can change the magnetic moments in first order perturbation theory on shell model states. There are two such kinds of admixtures. First, when the unperturbed state has an even number of particles in both the $j_1 = l_1 + 1/2$ and the $j_2 = l_1 - 1/2$ shells of a spin-orbit doublet, and the upper level is not filled, there are contributing configurations in which one particle in the lower level is elevated to the higher level, with a total angular momentum for particles in the two levels being unity. I.e., the original configuration $j_1^{n_1}(0) j_2^{n_2}(0)$ is changed to $\left[j_1^{n_1-1}(j_1) j_2^{n_2+1}(j_2)\right](1)$. The second type is quite similar, but in this case a particle is transferred between the states of the particles in the odd group and its spin orbit partner.

Our pairing force does not admix configurations of these types and, since the strength of the pairing force needed in our calculations gives about the same gap as the force used in Ref. 30 for configurations of identical particles, we can use the same $\delta$-force to obtain the admixed configurations instead of using $V$. As a rough check on the consistency of our wave functions with the experimental values of the magnetic moments, we carry out a configuration mixing calculation with a $\delta$-function force with the same parameters as used in Ref. 30. We use constant radial matrix elements. Our calculation differs from that of Arima and Horie only in that (i) our ground state wave functions are admixtures of many different configurations with mixture coefficients given by our pairing force calculation, the only configurations which are in our odd-$A$ ground state wave functions neglecting the phonon admixtures, being of the type $j_1^{n_1}(0) j_2^{n_2}(0) \ldots j^{P-1}(0)\, j; jm\rangle$, where $j$ is the angular momentum of the ground state quasi-particle; and (ii) our wave functions contain a spread in the number of particles.

In Table II we give the results of this calculation. The wave functions used are those parts of the one quasi-particle states which have the correct number of particles. The calculation was carried out for only one Sn isotope since the results will be similar for the other two Sn isotopes in which the

TABLE II

Magnetic moments in odd-$A$ nuclei. $\mu_{s.p.}$ is the Schmidt value for the isotope. The experimental values are taken from Ref. 32.

| Isotope | Spin | $\mu_{s.p.}$ | $\mu_{theor.}$ | $\mu_{exp}$ |
|---|---|---|---|---|
| $Ni^{61}$ | $(3/2)^-$ | −1.91 | −0.21 | 0 |
| $La^{139}$ | $(7/2)^+$ | 1.72 | 2.24 | 2.76 |
| $Pr^{141}$ | $(5/2)^+$ | 4.79 | 3.92 | 3.92 |
| $Sn^{115}$ | $(1/2)^+$ | −1.91 | −0.70 | −0.91 |

magnetic moment is known. In the $N = 28$ region our wave functions with a fixed number of particles are almost pure configurations, so there is almost no change in the results of Ref. 30.

For the most part, our results are an average of the results of configurations used in Ref. 30, although this is not always true. It would take a detailed calculation to prove that the magnetic moments of odd-$A$ nuclei can actually be determined by this method; however, one sees that perturbations of the type considered produce shifts of the magnetic moments from the Schmidt lines of the observed order of magnitude.

## VII. Electromagnetic Transition Rates

In addition to the valuable information concerning parity and spins considered in § III, electromagnetic transition rates can yield much more detailed information about the wave functions of nuclear states. We have already seen how the strong enhancement of the $E2$ transition rates in even-$A$ nuclei not only can be used to identify the collective states, but that the magnitude of the transition rates can help select the proper force strengths for our pairing and $P^{(2)}$ type of force (cf. § III. B). In this chapter, we investigate more systematically the electromagnetic transition rates from the collective $2^+$ states in the even-$A$ nuclei as well as the single-particle part of the transitions from quasi-particle states.

### A. Odd-$A$ Nuclei

Electromagnetic transitions between states in odd-$A$ nuclei will proceed by both particle and collective types of operators. The latter type will be most important for $E2$ transitions. But since there is at present no evidence

on this type of transition, we restrict ourselves to the single-particle part of the transition operator. For any single-particle operator, the matrix element for a transition from a single quasi-particle state of angular momentum $j_i$ to a single quasi-particle state of angular momentum $j_f$ is given by

$$(\Psi_{j_f m_f} | \mathfrak{O} | \Psi_{j_i m_i}) = (U_{j_f} U_{j_i} - (-1)^T V_{j_f} V_{j_i}) \langle j_f m_f | \mathfrak{O} | j_i m_i \rangle, \tag{63}$$

where $\langle j_f m_f | \mathfrak{O} | j_i m_i \rangle$ is the ordinary single-particle matrix element. In equation (63) the factor $(-1)^T$ is $\pm 1$, depending upon whether the operator is even or odd under time reversal, i.e., $\tau 0 \tau^{-1} = (-1)^T \mathfrak{O}$; or in terms of the matrix elements,

$$\langle \tau j_i m_i | \mathfrak{O} | \tau j_f m_f \rangle = (-1)^T \langle j_f m_f | \mathfrak{O} | j_i m_i \rangle. \tag{64}$$

The single-particle operators for the electric and magnetic $2^L$ pole transitions are

$$\mathfrak{M}(EL) = f_1(r) Y_M^L + i f_2(r) \boldsymbol{\sigma} \times \boldsymbol{r} \cdot \operatorname{grad} Y_M^L, \tag{65a}$$

$$\mathfrak{M}(ML) = f_3(r) \boldsymbol{L} \cdot \operatorname{grad} Y_M^L + f_4(r) \boldsymbol{\sigma} \cdot \operatorname{grad} Y_M^L, \tag{65b}$$

where the $f_i(r)$ are real functions of the scalar $r$. From these we see that

$$\langle \tau j_i m_i | \mathfrak{M}(EL) | \tau j_f m_f \rangle = \langle j_f m_f | \mathfrak{M}(EL) | j_i m_i \rangle, \tag{66a}$$

$$\langle \tau j_i m_i | \mathfrak{M}(ML) | \tau j_f m_f \rangle = -\langle j_f m_f | \mathfrak{M}(ML) | j_i m_i \rangle, \tag{66b}$$

holds for all values of $L$. Therefore, from equation (63)

$$(\Psi_{j_f m_f} | \mathfrak{M}(EL) | \Psi_{j_i m_i}) = (U_{j_f} U_{j_i} - V_{j_f} V_{j_i}) \langle j_f m_f | \mathfrak{M}(EL) | j_i m_i \rangle \tag{67a}$$

$$(\Psi_{j_f m_f} | \mathfrak{M}(ML) | \Psi_{j_i m_i}) = (U_{j_f} U_{j_i} + V_{j_f} V_{j_i}) \langle j_f m_f | \mathfrak{M}(ML) | j_i m_i \rangle. \tag{67b}$$

From equations (67a) and (67b) one can express the lifetimes for transitions between one quasi-particle states in terms of the lifetime for transitions between single-particle states with the same electrical properties, angular momenta, and energy separation. Calling the lifetime of the single-particle states $\tau^{\text{s.p.}}$ [33], the reciprocal lifetimes for the single quasi-particle transitions are

$$\frac{1}{\tau_{i \to f}} = D_{fi} \frac{1}{\tau_{i \to f}^{\text{s.p.}}}, \tag{68}$$

with

$$D_{fi}(ML) = \frac{1}{2}\left[1 + \frac{(\varepsilon_f-\lambda)(\varepsilon_i-\lambda)}{\sqrt{(\varepsilon_f-\lambda)^2+\Delta^2}\sqrt{(\varepsilon_i-\lambda)^2+\Delta^2}} + \sqrt{\left(1-\frac{(\varepsilon_f-\lambda)^2}{(\varepsilon_f-\lambda)^2+\Delta^2}\right)\left(1-\frac{(\varepsilon_i-\lambda)^2}{(\varepsilon_i-\lambda)^2+\Delta^2}\right)}\right] \tag{69a}$$

$$D_{fi}(EL) = \frac{1}{2}\left[1 + \frac{(\varepsilon_f-\lambda)(\varepsilon_i-\lambda)}{\sqrt{(\varepsilon_f-\lambda)^2+\Delta^2}\sqrt{(\varepsilon_i-\lambda)^2+\Delta^2}} - \sqrt{\left(1-\frac{(\varepsilon_f-\lambda)^2}{(\varepsilon_f-\lambda)^2+\Delta^2}\right)\left(1-\frac{(\varepsilon_i-\lambda)^2}{(\varepsilon_i-\lambda)^2+\Delta^2}\right)}\right], \tag{69b}$$

where $D(ML)$ and $D(EL)$ are the reduction factors for magnetic and electric $2^L$ pole transitions, respectively. From equation (69) one can easily see the effect of the pairing force upon the transition rates. If the states $i$ and $f$ are both far above the position of the chemical potential, so that $\frac{\varepsilon-\lambda}{\sqrt{(\varepsilon-\lambda)^2+\Delta^2}} \cong 1$, the transition rate is single-particle. This is the case when the probablility of the ground state containing a configuration with particles in these states is almost zero. As one adds particles, $\lambda$ approaches the value $\varepsilon_f$, from below, and both the electric and magnetic reduction factors diminish in size, but the reduction of the electric transitions below the single-particle value is faster than the reduction in the magnetic transitions. For example, when $\varepsilon_i - \varepsilon_f \ll \Delta$, by the time $\lambda = \varepsilon_f$, equation (69) shows $D(ML) = 1$ while $D(EL) = 0$. This is quite a different behaviour than would be predicted by a pure shell model or a shell model with a diagonal pairing energy. (By a diagonal pairing force we mean a pairing force which acts within each $j$-shell with no matrix elements between different $j$-shells). For instance, in the magnetic case, the non-diagonal matrix elements of the pairing force are very important in keeping the matrix element approximately constant while the chemical potential, $\lambda$, moves through two close lying levels. This feature depends simply on populating both of these states equally. Since one does not do this in either a non-interacting shell model or with a diagonal pairing force, the magnitude of the reduction factor will vary much more in these cases as the number of particles is changed. Generally, the result is that the magnetic transitions tend to vary rather more gradually with changes in the number of particles than the shell model result, and that the electric transitions can display strong reductions even in pure quasi-particle states. In comparing the experimental transition rates to the theoretical ones it is most significant to compare the experimental with

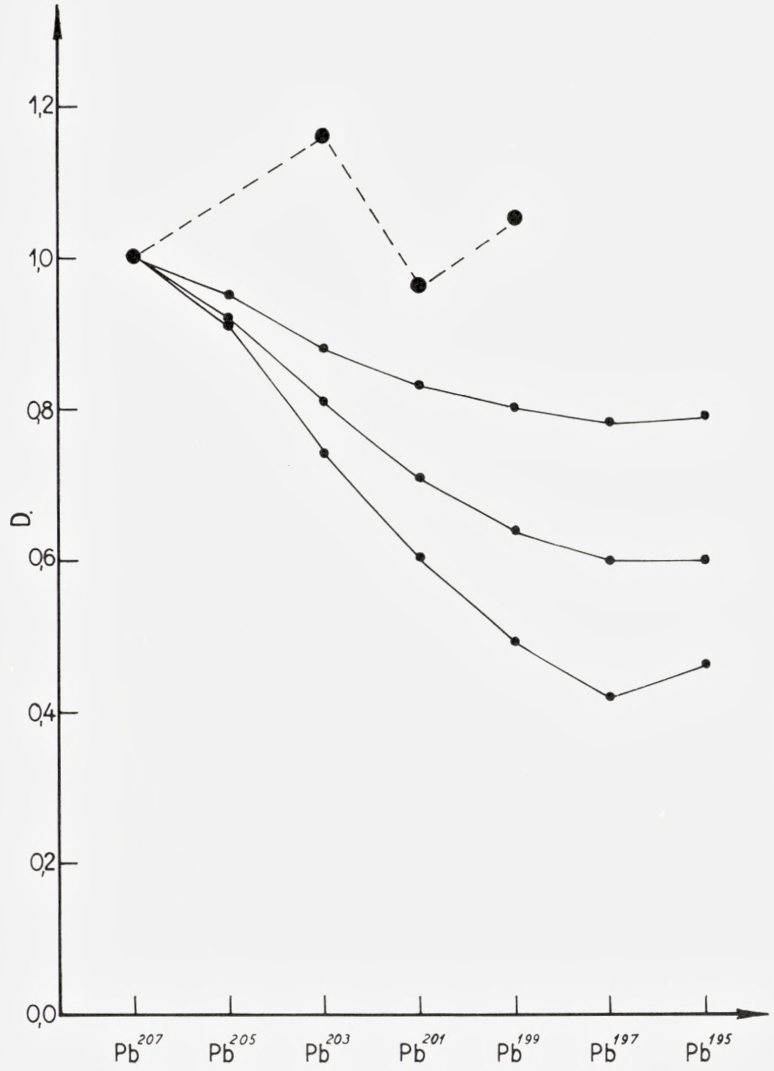


Fig. 26. *M4 transition rate in odd-A Pb isotopes.*
Curves *a*, *b*, *c* are the theoretical values of the reduction from single-particle for $G = 30/A$, $23/A$, and $19/A$. The experimental values[19] are normalized at $Pb^{222}$.

the theoretical reduction factors in order to remove the very large effects of energy differences.

In the odd-*A* s.c.s. nuclei, the only lifetimes which have been measured are those of the isomeric states. The most complete results are for the Pb

isotopes, for which the $M4$ transitions between the $i_{13/2}$ and $f_{5/2}$ states have served so well to trace the position of the $i_{13/2}$ state (cf. Chapter III). The lifetimes are measured in $Pb^{207}$, $Pb^{203}$, $Pb^{201}$, $Pb^{199}$, and $Pb^{197}$ [19]. The comparison of the experimental reduction factors with the prediction of the pairing force calculation is made in Fig. 26. The single-particle $2^L$ pole electromagnetic transition rate has an energy dependence given by $(E_i - E_f)^{2L+1}$. Using this dependence and the experimental lifetimes, energies, and conversion coefficients, one finds that the experimental reduction is almost constant for the five isotopes. These "experimental" reduction factors are based on a comparison with a single-particle estimate which neglects shell effects on the nuclear radii, an approximation which could affect the relative $M4$ reduction factors, where the nuclear radius enters in the sixth power.

The values plotted in the figure are normalized to the $Pb^{207}$ value, which is unity in our model. Because of the uncertainty in the experimental reduction factor, a detailed comparison with the theoretical curves may not be significant. It is of interest, however, that, for the values of $G$ indicated by other evidence, the $M4$ reduction factors are indeed expected to vary only little over the isotopes considered. As already mentioned, this would

TABLE III

Electromagnetic transitions in one quasi-particle states. $D_{exp} = P_{exp}/P_{s.p.}$, where $P_{s.p.}$ is a theoretical estimate of the transition when treated as single-particle.[33] $D_{theor}$ is for $G = 0.128$ in Pb, 0.187 in Sn, and 0.238 in $N = 50$. $a_0$ is the radius parameter.

| Element | Transition | Assumed Level Change | $D_{exp}$ ($a_0 = 1.2$) | $D_{exp}$ ($a_0 = 1.1$) | $D_{theor.}$ |
|---|---|---|---|---|---|
| $Pb^{207}$ ..... | 1.064 M4 | $i_{13/2} \rightarrow f_{5/2}$ | 0.25 | 0.42 | 1.00 |
| $Pb^{205}$ ..... | | $i_{13/2} \rightarrow f_{5/2}$ | | | 0.93 |
| $Pb^{203}$ ..... | 0.825 M4 | $i_{13/2} \rightarrow f_{5/2}$ | 0.30 | 0.49 | 0.85 |
| $Pb^{201}$ ..... | 0.629 M4 | $i_{13/2} \rightarrow f_{5/2}$ | 0.24 | 0.41 | 0.78 |
| $Pb^{199}$ ..... | 0.424 M4 | $i_{13/2} \rightarrow f_{5/2}$ | 0.26 | 0.44 | 0.73 |
| $Pb^{197}$ ..... | 0.235 M4 | $i_{13/2} \rightarrow f_{5/2}$ | 0.27 | 0.46 | 0.70 |
| $Pb^{195}$ ..... | | $i_{13/2} \rightarrow f_{5/2}$ | | | 0.70 |
| $Sn^{117}$ ..... | 0.159 M4 | $h_{11/2} \rightarrow d_{3/2}$ | 0.41 | 0.68 | 0.96 |
| $Sn^{119}$ ..... | 0.065 M4 | $h_{11/2} \rightarrow d_{3/2}$ | 0.57 | 0.95 | 0.94 |
| $_{39}Y^{89}_{50}$ ..... | 0.913 M4 | $g_{9/2} \rightarrow p_{1/2}$ | 0.26 | 0.43 | 0.68 |
| $_{41}Nb^{91}_{50}$ ..... | 0.105 M4 | $g_{9/2} \rightarrow p_{1/2}$ | 0.20 | 0.33 | 0.48 |
| $_{43}Tc^{93}_{50}$ ..... | 0.390 M4 | $p_{1/2} \rightarrow g_{9/2}$ | 0.35 | 0.59 | 0.65 |

not have been the case if the configuration mixing introduced by the pairing force had not been taken into account. As to the absolute values of the transition probabilities, the single-particle estimate for the expected nuclear radius is larger by a factor of two or three than the experimental value for $Pb^{207}$; however, there is considerable uncertainty in the theoretical single-particle estimate (cf. Table III, p. 67).

The lifetimes of the $h_{11/2}$ states are known in $Sn^{117}$ and $Sn^{119}$ [34]. The internal conversion coefficients, which are quite large for these transitions, have not been measured. However, the errors in the values of $D_{exp}$, the experimental reduction factor introduced by using the theoretical values of the internal conversion coefficients[35], are less than those due to the uncertainty in the single-particle estimate. The theoretical value of the $M4$ reduction factor in the pairing force calculation is almost unity, since in this case the separation between the $d_{3/2}$ and $h_{11/2}$ levels is small compared to the gap. These results would be approximately unaltered for any values of the pairing strength and of the single-particle energies which fit the spins and energy levels, as well as the $2^+ \rightarrow 0^+$ transition rates of the Sn isotopes. Table III, in which $D_{theor}$, the value of the reduction factor in the pairing calculation, is calculated with a pairing strength and single-particle energy levels used to give the results shown in Fig. 6, indicates that the experimental and theoretical results are consistent.

In the $N = 50$ region, lifetimes have been measured for three $M4$ transitions between the $p_{1/2}$ and $g_{9/2}$ states: ${}_{39}Y^{89}$, ${}_{41}Nb^{91}$, and ${}_{43}Tc^{93}$ [21]. Using the theroretical conversion coefficients, one finds that the reduction factors given by the experiments and the single-particle estimates are consistent with the pairing force results. The values of $D_{theor}$ quoted in the table are calculated from the energy levels and pairing strength which leads to the energy levels of Fig 13. The heightened reduction in the $M4$ matrix elements for ${}_{41}Nb^{91}_{50}$ apparently reflects the diminution in the gap due to the filling of the level with spin 1/2, which is far in energy from other levels, as discussed in § III. The relative values of the experimental reduction factors also show a dip for $Nb^{91}$ compared to $Y^{89}$ and $Tc^{93}$, although this might not be accurate enough to be significant.

In the $N = 82$ region the lifetimes are known for the 0.165 Mev $M1$ transition in $La^{139}$ and the 0.142 Mev $M1$ transition in $Pr^{141}$. However, both of these transitions are "$l$-forbidden", and a configuration mixing calculation of the same kind as was used for magnetic moments (§ V) would therefore be needed in order to account for these transitions[36]. The 0.024 Mev transition in $Sn^{119}$ is also $l$-forbidden.

In a similar way, perturbations must also admix other configurations to all the single quasi-particle states. The amount of admixture would presumably depend upon the unperturbed states, and thus would vary for a one quasi-particle state of a particular type as the number of particles changes. Such effects could alter some of the quantitative results, for instance, in the $M4$ reduction factors.

### B. Even-$A$ Nuclei

1. *Single-Particle Transitions in Two Quasi-Particle States*

In the same way as the result (68) was obtained for one quasi-particle states, for a transition between two states which can be described as two quasi-particle states, $\Psi_i [j_1 j_i]^J \to \Psi_f [j_1 j_f]^{J'}$, the reciprocal lifetime is given by

$$\frac{1}{\tau_{i\to f}} = D_{if} \frac{1}{\tau^{\text{s.p.}}_{i\to f}}, \tag{70}$$

where $\tau^{\text{s.p.}}$ is the single-particle lifetime* for the electromagnetic $(2)^L$ multipole transition $J \to J'$, $j_i \to j_f$.

The best experimental comparison can be made for transitions from the high angular momentum odd-parity states discussed in § III. These states may often represent rather unique quasi-particle configurations. We restrict our discussion to those cases in which the experimental lifetimes are known.

The $7^-$ to $6^+$ $E1$ transition in $Sn^{170}$ is reduced about $2.5 \times 10^{-8}$ compared to a single-particle estimate. Since there are no possible shell model configurations in this region of isotopes which would lead to $E1$ transitions, any shell model theory would lead to a transition rate of essentially zero.

The half-life of the 2.2 Mev state in $Pb^{206}$ is $1.25 \times 10^{-4}$ sec.[22),37)]. We predict that this $7^-$ state is mainly a combination of an $i_{13/2}$ quasi-particle coupled with a $p_{3/2}$ quasi-particle and an $f_{5/2}$ quasi-particle. The 2.00 and 1.68 Mev $4^+$ states to which the $7^-$ states decay by $E3$ transitions are mainly combinations of the $(f_{5/2}\, p_{3/2})_4$ and $(f_{5/2})^2_4$ two quasi-particle states. For these main parts of the wave functions the $E3$ single-

* $\tau^{\text{s.p.}}_{i\to f}$ in Eq. (70) is related to Moszkowski's $\tau^{\text{s.p.}}_{i\to f}$ in Ref. 33 by

$$\frac{1}{\tau^{\text{s.p.}}_{i\to f}} = (2J'+1)(2j_i+1)\,|W(j_f J' j_i J;\, j_1 L)|^2 \left(\frac{1}{\tau^{\text{s.p.}}_{i\to f}}\right)_{\text{Moszkowski.}}$$

particle transition is forbidden. There will also be a certain amount of the $(f_{5/2}\, f_{7/2})_4$ and $(p_{3/2}\, f_{7/2})_4$ two quasi-particle states in these $4^+$ states, which allow the $E3$ transitions; however, we expect the transition rate to be far below single-particle. In units of the single-particle estimate, the transition

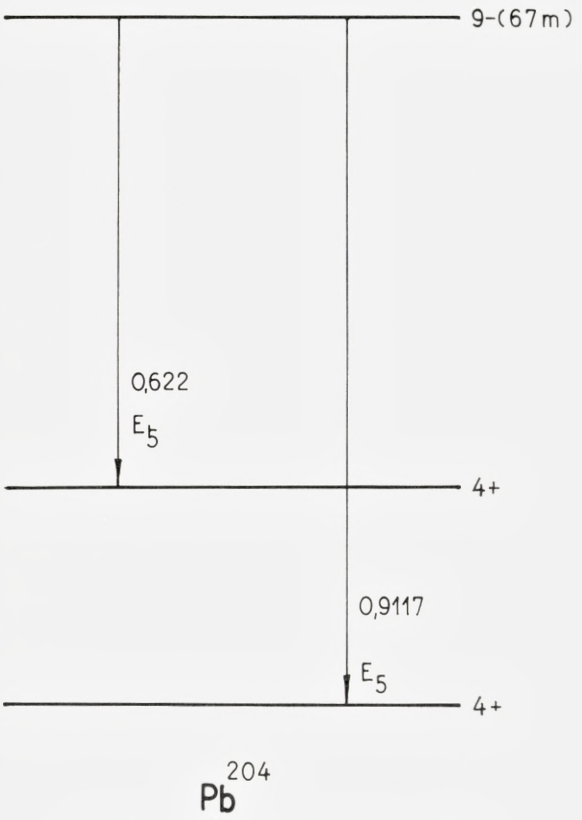


Fig. 27. *Decay of the* $9^-$ *state in* $Pb^{204}$.

strengths for the 0.202 and 0.516 Mev transitions are of the order of 0.3, which seems to be somewhat large from the considerations mentioned above. However, it is difficult to estimate the amount of mixing of quasi-particle configurations which does occur.

The half-life of the $9^-$ state in $Pb^{204}$ is measured to be $4.02 \times 10^3$ sec[38] for decay into two $4^+$ states by a 0.912 and a 0.622 Mev $E5$ transition. The $9^-$ state is mostly a state of an $i_{13/2}$ and an $f_{5/2}$ quasi-particle coupled

to their maximum spin. We find that the $4^+$ final state for the 0.912 Mev transition is mainly a state of two $f_{5/2}$ quasi-particles, while the $4^+$ state associated with the 0.662 Mev transition is mainly one with one $f_{5/2}$ and one $p_{3/2}$ quasi-particle. Of course, these states are so close in energy that

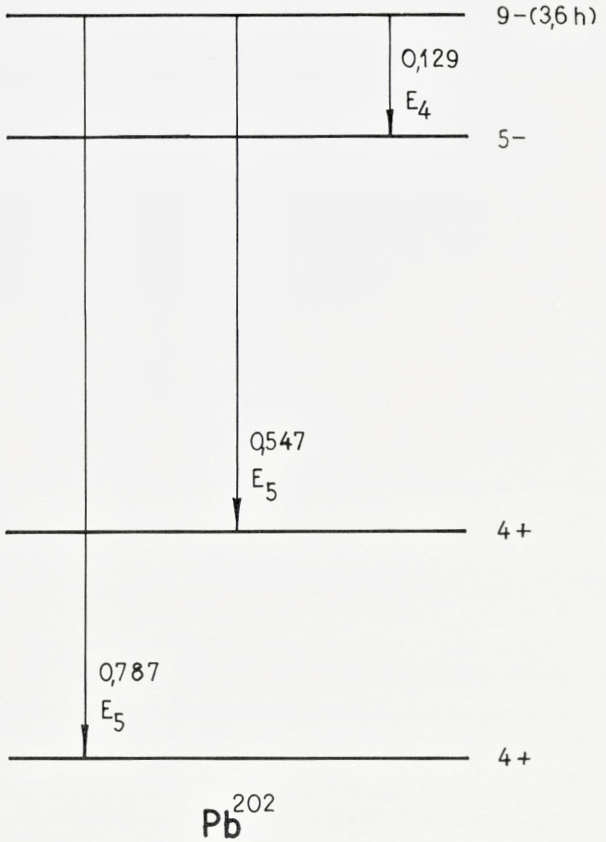


Fig. 28. *Decay of the* $9^-$ *state in* $Pb^{202}$.

one can expect an admixture of these configurations. Table IV shows that the 0.622 Mev transition is consistent with a description that it proceeds via a two quasi-particle transition between the states which are expected to dominate, the reduction factor being about 0.7. The 0.912 Mev transition, however, is enhanced compared to the theoretical value by a factor of the order of 100 if the transition proceeds via $(i_{13/2}\, f_{5/2})_9 - \rightarrow (f_{5/2})^2_4 +$.

TABLE IV

Electromagnetic transitions in two quasi-particle states. $G = 0.128$ (in Pb). The column titled "Assumed Level Change" indicates the type of the quasi-particle which changes during the transition. Where two assumptions have been made for the spin assignments, the states might be admixtures, with the first assignment having the heaviest weight. $D_{\text{exp}}$ is given in units of $(e_{\text{eff}}/e)^2$.

| Element | Transition | Assumed Level Change | $D_{\text{exp}}$ $(a_0 = 1.2)$ | $D_{\text{exp}}$ $(a_0 = 1.1)$ | $D_{\text{theor}}$ |
|---|---|---|---|---|---|
| $Pb^{206}$ ... | 0.516 E3 | $[i_{13/2}p_{3/2}]_{7-} + [i_{13/2}f_{5/2}]_{7-} \rightarrow [f_{7/2}p_{3/2}]_{4+} + [f_{7/2}f_{5/2}]_{4+}$ | 0.26 | 0.45 | $0.98 \times$ prob. of $f_{7/2}$ quasi-particle in $4^+$ state |
| | 0.202 E3 | $[i_{13/2}p_{3/2}]_{7-} + [i_{13/2}f_{5/2}]_{7-} \rightarrow f_{7/2}p_{3/2}]_{4+} + [f_{7/2}f_{5/2}]_{4+}$ | 0.18 | 0.29 | |
| $Pb^{204}$ ... | 0.912 E5 | $[f_{5/2}i_{13/2}]_{9-} \rightarrow [f_{5/2}p_{3/2}]_{4+}$ | 47 | 112 | 0.58 |
| | | $[f_{5/2}i_{13/2}]_{9-} \rightarrow [f_{5/2}p_{3/2}]_{4+}$ | 2.6 | 6.2 | 0.73 |
| | 0.622 E5 | $[f_{5/2}i_{13/2}]_{9-} \rightarrow [f_{5/2}p_{3/2}]_{4+}$ | 0.4 | 0.94 | 0.73 |
| | | $[f_{5/2}i_{13/2}]_{9-} \rightarrow [f_{5/2}]^2_{4+}$ | 7 | 17 | 0.58 |
| $Pb^{202}$ ... | 0.787 E5 | $[f_{5/2}i_{13/2}]_{9-} \rightarrow [f_{5/2}]^2_{4+}$ | 37 | 88 | 0.56 |
| | | $[f_{5/2}i_{13/2}]_{9-} \rightarrow [f_{5/2}p_{3/2}]_{4+}$ | 2.1 | 4.9 | 0.34 |
| | 0.547 E5 | $[f_{5/2}i_{13/2}]_{9-} \rightarrow [f_{5/2}p_{3/2}]_{4+}$ | 0.31 | 0.74 | 0.34 |
| | | $[f_{5/2}i_{13/2}]_{9-} \rightarrow [f_{5/2}]^2_{4+}$ | 5.6 | 13 | 0.56 |
| | 0.129 E4 | $[i_{13/2}f_{5/2}]_{9-} \rightarrow [i_{13/2}p_{3/2}]_{4-}$ | 0.29 | 0.60 | 0.15 |
| $Sn^{120}$ ... | 0.089 E1 | | $2.5 \times 10^{-8}$ | | 0 |

Even if the $4^+$ state is taken as a $(f_{5/2}p_{3/2})_4$ two quasi-particle state, this $E5$ transition is enhanced by a factor of perhaps 5.

In $Pb^{202}$ there is a situation which is almost identical to the one in $Pb^{204}$ (cf. Fig. 28)[39), 40)]: a 0.787 Mev $E5$ transition which might be expected from energy considerations to be largely between $(i_{13/2}f_{5/2})_9$ and $(f_{5/2})^2_4$ two quasi-particle states, and a 0.547 Mev $E5$ transition which might be expected to be largely $(i_{13/2}f_{5/2})_{9-} \rightarrow (f_{5/2}p_{3/2})_{4+}$, corresponding to the 0.912 Mev and 0.622 Mev transitions in $Pb^{204}$, respectively.

For the 0.547 Mev transition, a reduction factor of 0.34, which results from the pairing force calculation with the assumption of a $(i_{13/2}f_{5/2})_{9-} \rightarrow (f_{5/2}p_{3/2})_{4+}$ transition, is consistent with the experimental results. However,

the 0.787 Mev transition seems to be strongly enhanced above the theoretical value, resembling the 0.912 Mev transition in $Pb^{204}$.

The $9^-$ state in $Pb^{202}$ decays with a 37% probability into a $5^-$ state by a 0.129 Mev $E4$ transition.[39] As explained in § III, the $5^-$ state associated with the $(i_{13/2}\, f_{5/2})$ two quasi-particle states is placed above the $9^-$ state by a $P^{(2)}$ force in perturbation theory, while the $5^-$ state lies lowest in the $(i_{13/2}\, p_{3/2})$ two quasi-particle configuration. Moreover, these results are in agreement with the detailed calculations in $Pb^{206}$. [41] We thus expect the 0.129 Mev $E4$ transition in $Pb^{202}$ to correspond to a transition between the $(i_{13/2}\, f_{5/2})_{9-}$ and $(i_{13/2}\, p_{3/2})_{5-}$ two quasi-particle states. Table IV shows that a theoretical reduction factor of 0.15 is consistent with the experimental results if we use this interpretation.

2. *The* $2^+ \rightarrow 0^+$ $E2$ *Transitions*

As indicated in the discussion of the choice of parameters, the $B(E2)$ values for the lowest $2^+ \rightarrow 0^+$ transition of the collective state may be used to determine the effective charge.[42] In Table V we list the experimental $B(E2)$ values together with the theoretical values for the s.c.s. nuclei for which the $2^+$ level has been seen. The theoretical values are calculated using (34) with $e_{\text{eff}} = 1$ for the closed proton shell nuclei and $e_{\text{eff}} = 2$ for the closed neutron shell nuclei.

It is seen that the correct value of the $B(E2)$ is obtained for $Pb^{206}$ with use of the experimentally measured effective charge $e_{\text{eff}} = 1.1$[13]. The Sn $B(E2)$ values are also reasonably well accounted for by $e_{\text{eff}} = 1$. For the Ni isotopes a somewhat larger value of $e_{\text{eff}}$ seems to be required——about $e_{\text{eff}} = 1.4$. All of the closed neutron shell nuclei seem to require an effective charge well above unity to fit the few measured values, as expected. However, the value $e_{\text{eff}} = 2$ seems to be a little too high. A value $e_{\text{eff}} = 1.5$ would give a better fit to the $B(E2)$ of these nuclei.

In conclusion, the experimental values for the reduction in the $M4$ transition rates in the odd-$A$ Pb isotopes appear to be rather constant, which is consistent with the theoretical reductions for the values of $G$ used in this work. The theoretical reduction factors for $M4$ transitions in the other odd-$A$ s.c.s. nuclei are also consistent with experiment, in all cases the reduction factor being not less than 0.5 (and greater than 0.7, except in rather unusual cases). This result can be extended qualitatively to other nuclei. In every case, the pairing correlations will tend for magnetic transitions to maintain the transition rate near the single-particle value even as particles

TABLE V. *B(E2) values*

The theoretical and experimental B($E2$) $0^+ \to 2^+$ reduced transition probability is shown for s.c.s. nuclei. The value $e_{\text{eff}} = 1$ is used in computing the theoretical value for Pb, Sn, and Ni, and $e_{\text{eff}} = 2$ for $N = 82$, $N = 50$, and $N = 28$. In the fourth column the "single-particle" estimate $\text{B}(E2)_{\text{s.p.}} = 3\ 10^{-5}\ A^{4/3}\ e^2\ 10^{-48}\,\text{cm}^4$ was used; and in the last column the experimental references are given.

| Isotope | $\text{B}(E2)_{\text{exp}}$ $e^2\ 10^{-48}\,\text{cm}^4$ Theoretical | $\text{B}(E2)_{\text{exp}}$ $e^2\ 10^{-48}\,\text{cm}^4$ Experimental | $\frac{\text{B}(E2)_{\text{exp}}}{\text{B}(E2)_{\text{s.p.}}}$ | Ref. |
|---|---|---|---|---|
| $Pb^{206}$ ..... | 0.13 | 0.14 | 4 | (22) |
| $Pb^{204}$ ..... | 0.22 | | | |
| $Pb^{202}$ ..... | 0.29 | | | |
| $Pb^{200}$ ..... | 0.33 | | | |
| $Sn^{112}$ ..... | 0.25 | 0.18 | 11 | (44) |
| $Sn^{114}$ ..... | 0.20 | 0.20 | 11 | (44) |
| $Sn^{116}$ ..... | 0.26 | 0.21 | 12 | (22) |
| $Sn^{118}$ ..... | 0.29 | 0.23 | 13 | (22) |
| $Sn^{120}$ ..... | 0.28 | 0.22 | 13 | (22) |
| $Sn^{122}$ ..... | 0.25 | 0.25 | 14 | (22) |
| $Sn^{124}$ ..... | 0.20 | 0.21 | 12 | (22) |
| $Ni^{58}$ ..... | 0.020 | 0.072 | 11 | (45) |
| $Ni^{60}$ ..... | 0.046 | 0.091 | 13 | (45) |
| $Ni^{62}$ ..... | 0.071 | 0.083 | 11 | (45) |
| $Ni^{64}$ ..... | 0.068 | | | |
| $Xe^{136}$ ..... | 0.34 | | | |
| $Ba^{138}$ ..... | 0.51 | | | |
| $Ce^{140}$ ..... | 0.73 | 0.36 | 16 | (46) |
| $Nd^{142}$ ..... | 1.01 | | | |
| $Sr^{88}$ ..... | 0.180 | 0.13 | 12 | (46) |
| $Zr^{90}$ ..... | 0.113 | | | |
| $Ti^{50}$ ..... | 0.078 | | | |
| $Cr^{52}$ ..... | 0.16 | 0.085 | 14 | (46) |
| $Fe^{54}$ ..... | 0.23 | | | |

are placed in the levels involved in the transition——a result which might explain the striking constancy in the $M4$ reduction factors throughout the periodic table.[43)]

For even-$A$ nuclei, we conclude that our results for quasi-particle transition rates are consistent with experiment within the accuracy obtainable by our methods, with the possible exception of an enhancement of

certain $E5$ transitions in $Pb^{204}$ and $Pb^{202}$. For the collective states, the lifetimes can be used to determine the effective charge. In addition, in $Pb^{206}$ we can use the experimentally measured value of $e_{eff}$ to help select $G$.

As the systematic experimental data is extended, the transition rates will provide a detailed test of the wave functions obtained with this model.

## VIII. Summary

An approximate calculation of the properties of nuclei with one closed proton or neutron shell is attempted. Using the approximation methods introduced by the theory of superconductivity, we have calculated the effects of those parts of the short range part of the residual interaction which are common to the pairing force, obtaining the quasi-particle energies for several strengths, $G$, of the pairing force. The deformed field approximation is used to calculate the effect of the relatively long range part of the nuclear force, and in particular to determine the positions and $B(E2)$'s of the $2^+$ collective states in the even-$A$ isotopes.

The most important systematic experimental feature for the even-$A$ s.c.s. isotopes is the position of the first excited $2^+$ state. This state, which is of collective character, has a rather constant energy above the ground state, and is often quite a bit lower in energy than the next higher excited states, thus lying in the gap between the ground state and the intrinsic excited states.

We find a simple explanation for this $2^+$ state. This state, which in our work is always the first excited quadrupole vibrational level, is located below the first states of two quasi-particles, sometimes rather far below, as in the case of the Sn isotopes. In every case, the second excited vibrational level is among the quasi-particle states so that it becomes more difficult to explore the possibility of higher collective states.

Also in even-$A$ nuclei we find that we can approximately derive not only the positions of the $2^+$ levels, but also the positions of the levels of high angular momentum with values of the pairing and $P^{(2)}$ force which do not differ much from region to region, except for the $A$ dependence of a volume force.

For the odd-$A$ isotopes, the most significant systematic experimental feature is the gradual change in the positions of the states which correspond

to our one quasi-particle states, motions which are much smoother than those predicted by an independent shell model.

In the odd-$A$ isotopes the positions of the quasi-particle levels do not depend upon the strengths of the pairing and $P^{(2)}$ force so much as upon the separation of the single-particle energy levels, for values of the pairing force which are consistent with the data in the even-$A$ isotopes. The ground state spins are determined within the accuracy expected. In Pb, where both the single-particle well is known and systematic measurements for the position of the $i_{13/2}$ states have been made, we find that we can quite accurately and rather unambiguously predict the relative position of the $i_{13/2}$ state.

The even-odd mass data gives values for the gap which are in agreement with our results. The determination of the absolute binding energy involves questions which are beyond the scope of our methods, but the experimental data seems to be consistent with our results.

Very little data is available on quadrupole moments of s.c.s. nuclei, but our calculated values are in fair agreement with experiment when one considers the change which can occur with the inclusion of small admixtures of configurations other than those arising from a pairing plus $P^{(2)}$ interaction. The magnetic moment data is much more extensive. Although for our wave functions the calculated magnetic moments are too close to the single-particle values, the small admixture of other configurations can change these moments by amounts of the right order to agree with experiment.

The main systematic results from the theoretical study of the collective part of the electromagnetic transition rate is the theoretical value for the effective charge. The main systematic feature which we have calculated for electromagnetic transitions between quasi-particle states is the tendency for the $M4$ reduction factors to remain rather constant for the $i_{13/2} \rightarrow f_{5/2}$ $M4$ transitions in the Pb odd-$A$ isotopes, which seems to be indicated by the experiments. This feature depends essentially on the strongly mixed configurations which occur in our calculation. Qualitatively, this result would tend to lead to a rather constant reduction factor for magnetic transitions compared to electric transitions, which is a possible explanation for the striking constancy in the $M4$ reduction factors, while the $E3$ reduction factors are widely varying.

We conclude that the simple model which we have tried has been successful in deriving the observed low energy systematic features of s.c.s. nuclei, and that our results might serve as a good basis for a more detailed quantitative investigation.

## Acknowledgements

We wish to thank Professor NIELS BOHR for the hospitality of the Institute for Theoretical Physics, Copenhagen, where most of this work was done. Special thanks are due Dr. BEN MOTTELSON who acquainted the authors with many of the physical ideas and mathematical methods on which this work is based. We are grateful to Professor AAGE BOHR for his encouragement and many valuable suggestions during the course of the work and the preparation of the paper. We also wish to acknowledge the assistance of other members and guests at the Institute, and in particular their stimulation during the regular meetings in which many of the problems connected with this work were discussed. For discussions of the experimental aspects of this work we thank many members and visitors at the Institute, as well as those at Upsala and Stockholm.

One of the authors (L. S. K.) would like to acknowledge the support of the Research Corporation for a postdoctoral fellowship while in Copenhagen on leave of absence from Western Reserve University, Cleveland, Ohio. For that part of the work done at Western Reserve University, he acknowledges the support of the U. S. Air Force.

The other author (R. A. S.) would like to acknowledge the support of the National Science Foundation for a postdoctoral fellowship during his stay in Copenhagen. For that part of the work done at Columbia University, New York, he acknowledges the support of the U. S. Atomic Energy Commission.

## Appendix

In this Appendix we list the quantities needed to obtain the nuclear energy levels and wave functions for typical strengths of the pairing force parameter, $G$, and long range force parameter, $X$, which are consistent with the known energy levels. For each region, the single-particle energies, $\varepsilon_j$, are given, with the subscript giving the angular momentum of the level. Using Eqs. (9) and (10), the quasi-particle energies are determined for each isotope by $\lambda$ and $\Delta$, which is listed in the table.

The properties of the collective state are conveniently calculated from the quantities $\mathfrak{A}$ and $\mathfrak{B}$, which are included in the table for each isotope, defined by

$$\mathfrak{A} = \sum_{jj'} \frac{(U_j V_{j'} + V_j U_{j'})^2}{E_j + E_{j'}} \frac{1}{10} (2j'+1) \left( C^{2\,j'\,j}_{0\,\frac{1}{2}\,\frac{1}{2}} \right)^2 \frac{\langle j \,|\, r^2 \,|\, j' \rangle^2}{\langle j \,|\, r^2 \,|\, j \rangle_u^2}, \qquad \text{A(1)}$$

$$\mathfrak{B} = \sum_{jj'} \frac{(U_j V_{j'} + V_j U_{j'})^2}{(E_j + E_{j'})^3} \frac{1}{10} (2j'+1) \left( C^{2\,j'\,j}_{0\,\frac{1}{2}\,\frac{1}{2}} \right)^2 \frac{\langle j \,|\, r^2 \,|\, j' \rangle^2}{\langle j \,|\, r^2 \,|\, j \rangle_u^2}, \qquad \text{A(2)}$$

where $\langle j \,|\, r^2 \,|\, j \rangle_u^2$ is defined in Eq. (41). The relation of these quantities to the collective parameters B and C of Eq. (3) is given by

$$B = \frac{1}{2} \frac{\beta}{\alpha^2} \frac{1}{\frac{5}{4\pi} \langle \,|\, r^2 \,|\, \rangle_u^2} \qquad \text{A(3)}$$

$$C = \frac{1}{2\alpha} [1 - 2\alpha X] \frac{1}{\frac{5}{4\pi} \langle \,|\, r^2 \,|\, \rangle_u^2} \qquad \text{A(4)}$$

$Z = 82$, holes in the $N = 126$ shell (Pb isotopes) for $G = 0.111$ Mev.

$\varepsilon_{p_{1/2}} = 0$, $\varepsilon_{f_{5/2}} = 0.57$, $\varepsilon_{p_{3/2}} = 0.90$, $\varepsilon_{i_{13/2}} = 1.634$, $\varepsilon_{f_{7/2}} = 2.35$ Mev.

| A | $\lambda$ (Mev) | $\Delta$ (Mev) | $\mathfrak{A}$ (Mev$^{-1}$) | $\mathfrak{B}$ (Mev$^{-3}$) |
|---|---|---|---|---|
| 206 | 0.11 | 0.25 | 0.40 | 0.50 |
| 205 | 0.25 | 0.34 | | |
| 204 | 0.33 | 0.42 | 0.52 | 0.42 |
| 203 | 0.42 | 0.48 | | |
| 202 | 0.52 | 0.53 | 0.56 | 0.33 |
| 201 | 0.60 | 0.55 | | |
| 200 | 0.69 | 0.58 | 0.57 | 0.27 |
| 199 | 0.78 | 0.60 | | |
| 198 | 0.88 | 0.63 | 0.56 | 0.20 |
| 197 | 0.97 | 0.64 | | |

$Z = 50$, neutrons in 50—126 shell (Sn isotopes) for $G = 0.187$ Mev.

$$\varepsilon_{d_{5/2}} = 0,\ \varepsilon_{g_{7/2}} = 0.22,\ \varepsilon_{s_{1/2}} = 1.90,\ \varepsilon_{d_{3/2}} = 2.20,\ \varepsilon_{h_{11/2}} = 2.80 \text{ Mev}.$$

| A | $\lambda$ (Mev) | $\Delta$ (Mev) | $\mathfrak{A}$ (Mev$^{-1}$) | $\mathfrak{B}$ (Mev$^{-3}$) |
|---|---|---|---|---|
| 108 | 0.17 | 0.97 | 0.33 | 0.061 |
| 109 | 0.29 | 0.98 | | |
| 110 | 0.44 | 0.98 | 0.34 | 0.057 |
| 111 | 0.60 | 0.97 | | |
| 112 | 0.76 | 0.94 | 0.33 | 0.049 |
| 113 | 0.97 | 0.90 | | |
| 114 | 1.20 | 0.89 | 0.32 | 0.044 |
| 115 | 1.43 | 0.92 | | |
| 116 | 1.64 | 0.96 | 0.34 | 0.048 |
| 117 | 1.81 | 1.00 | | |
| 118 | 1.97 | 1.03 | 0.35 | 0.052 |
| 119 | 2.12 | 1.05 | | |
| 120 | 2.26 | 1.07 | 0.35 | 0.054 |
| 121 | 2.40 | 1.08 | | |
| 122 | 2.53 | 1.07 | 0.34 | 0.057 |
| 123 | 2.65 | 1.06 | | |
| 124 | 2.78 | 1.03 | 0.32 | 0.060 |
| 125 | 2.88 | 1.00 | | |
| 126 | 3.01 | 0.96 | 0.29 | 0.060 |
| 127 | 3.12 | 0.90 | | |
| 128 | 3.24 | 0.83 | 0.22 | 0.053 |
| 129 | 3.36 | 0.72 | | |

$Z = 28$, neutrons in 28—50 shell (Ni isotopes) for $G = 0.331$ Mev.

$$\varepsilon_{p_{3/2}} = 0,\ \varepsilon_{f_{5/2}} = 0.78,\ \varepsilon_{p_{1/2}} = 1.56,\ \varepsilon_{g_{9/2}} = 4.52 \text{ Mev}.$$

| A | $\lambda$ (Mev) | $\Delta$ (Mev) | $\mathfrak{A}$ (Mev$^{-1}$) | $\mathfrak{B}$ (Mev$^{-3}$) |
|---|---|---|---|---|
| 58 | −0.31 | 0.80 | 0.11 | 0.024 |
| 59 | −0.09 | 0.94 | | |
| 60 | 0.14 | 1.04 | 0.18 | 0.028 |
| 61 | 0.38 | 1.11 | | |
| 62 | 0.59 | 1.15 | 0.21 | 0.032 |
| 63 | 0.84 | 1.16 | | |
| 64 | 1.09 | 1.14 | 0.21 | 0.032 |
| 65 | 1.39 | 1.08 | | |
| 66 | 1.64 | 0.99 | 0.15 | 0.022 |
| 67 | 1.99 | 0.81 | | |

$N = 82$, protons in 50—82 shell for $G = 0.173$ Mev.

$\varepsilon_{g_{7/2}} = 0$, $\varepsilon_{d_{5/2}} = 1.0$, $\varepsilon = 2.0$ Mev.

| A | $\lambda$ (Mev) | $\Delta$ (Mev) | $\mathfrak{A}$ (Mev$^{-1}$) | $\mathfrak{B}$ (Mev$^{-3}$) |
|---|---|---|---|---|
| 134 | −0.41 | 0.54 | 0.13 | 0.053 |
| 135 | −0.29 | 0.65 | | |
| 136 | −0.17 | 0.73 | 0.22 | 0.065 |
| 137 | −0.05 | 0.78 | | |
| 138 | 0.09 | 0.83 | 0.26 | 0.058 |
| 139 | 0.22 | 0.88 | | |
| 140 | 0.37 | 0.92 | 0.30 | 0.048 |
| 141 | 0.52 | 0.96 | | |
| 142 | 0.66 | 0.99 | 0.34 | 0.051 |
| 143 | 0.78 | 1.02 | | |
| 144 | 0.93 | 1.06 | 0.38 | 0.055 |
| 145 | 1.05 | 1.09 | | |
| 146 | 1.15 | 1.11 | 0.41 | 0.057 |

$N = 50$, protons in 28—50 shell for $G = 0.291$ Mev.

$\varepsilon_{f_{5/2}} = 0$, $\varepsilon_{p_{3/2}} = 0.6$, $\varepsilon_{p_{1/2}} = 1.8$, $\varepsilon_{g_{9/2}} = 3.4$ Mev.

| A | $\lambda$ (Mev) | $\Delta$ (Mev) | $\mathfrak{A}$ (Mev$^{-1}$) | $\mathfrak{B}$ (Mev$^{-3}$) |
|---|---|---|---|---|
| 83 | 0.16 | 0.98 | | |
| 84 | 0.36 | 1.01 | 0.21 | 0.038 |
| 85 | 0.58 | 1.01 | | |
| 86 | 0.82 | 0.98 | 0.22 | 0.037 |
| 87 | 1.10 | 0.92 | | |
| 88 | 1.44 | 0.86 | 0.18 | 0.030 |
| 89 | 1.83 | 0.83 | | |
| 90 | 2.24 | 0.84 | 0.10 | 0.011 |
| 91 | 2.59 | 0.93 | | |
| 92 | 2.85 | 1.00 | 0.15 | 0.025 |
| 93 | 3.08 | 1.04 | | |

$N = 28$, protons in 20—28 shell for $G = 0.385$ Mev.

$\varepsilon_{d_{3/2}} = 0$, $\varepsilon_{f_{7/2}} = 2.5$, $\varepsilon_{p_{3/2}} = 5.57$, $\varepsilon_{f_{5/2}} = 6.54$ Mev.

| A | $\lambda$ (Mev) | $\Delta$ (Mev) | $\mathfrak{A}$ (Mev$^{-1}$) | $\mathfrak{B}$ (Mev$^{-3}$) |
|---|---|---|---|---|
| 50 | 1.90 | 1.12 | 0.088 | 0.010 |
| 51 | 2.19 | 1.22 | | |
| 52 | 2.48 | 1.26 | 0.13 | 0.014 |
| 53 | 2.77 | 1.25 | | |
| 54 | 3.08 | 1.18 | 0.14 | 0.013 |
| 55 | 3.45 | 1.02 | 0.13 | 0.011 |

## References


1. M. G. Mayer, Phys. Rev. **75**, 1969 (1949); **78**, 16 (1950).
   Haxel, Jensen and Suess, Phys. Rev. **75**, 1766 (1949); Z. Physik **128**, 295 (1950).
2. A. Bohr, Mat. Fys. Medd. Dan. Vid. Selsk. **26**, no. 14 (1952).
   A. Bohr and B. R. Mottelson, Mat. Fys. Medd. Dan. Vid. Selsk. **27**, no. 16 (1953).
3. See J. P. Elliott and A. M. Lane, "Handbuch der Physik" XXXIX (Springer: Berlin, 1957), p. 241, for a discussion and references.
4. See F. Villars, Annual Review of Nuclear Science, I, 185 (1957) for a discussion of the work on the derivation of the collective motions and individual references.
5. J. P. Elliott, Proc. Roy. Soc. **245** (A), 128 (1958); 562 (1958).
6. B. Bayman, Proceedings of the International Congress on Nuclear Physics, Paris (1958).
7. Bardeen, Cooper, and Schrieffer, Phys. Rev. **108**, 1175 (1957).
   N. N. Bogolubov, JETP, USSR **34**, 58; 73 (1958).
   — Nuovo Cimento **7**, 794 (1958).
   J. G. Valatin, Nuovo Cimento **7**, 843 (1958).
8. B. R. Mottelson, Notes from Cours de l'École d'Été de Physique Théorique des Houches, 283 (1958).
9. A. Bohr and B. R. Mottelson (to be published).
10. S. T. Belyaev, Mat. Fys. Medd. Dan. Vid. Selsk. **31**, no. 11 (1959).
11. D. Bés, Nucl. Phys. **10**, 373 (1959).
21. D. R. Inglis, Phys. Rev. **96**, 1059 (1954); **97**, 901 (1955).
13. W. True and K. Ford, Phys. Rev. **109**, 1675 (1958).
14. A. M. Lane, Proceedings of the International Congress on Nuclear Physics, Paris (1958).
15. Numerous theoretical calculations for the single-particle levels have been made; for earlier references, see Ref. 5.
16. S. G. Nilsson, Mat. Fys. Medd. Dan. Vid. Selsk. **29**, no. 16 (1955).
17. L. A. Silverberg (to be published).
18. A. Bohr, Mottelson, and Pines, Phys. Rev. **110**, 936 (1958).
19. I. Bergström and G. Andersson, Arkiv Fysik **12**, 415 (1957).
20. Schmorak, Stockendal, McDonell, Bergström, and Gerholm, Nucl. Phys. **2**, 193 (1956–57).
21. We use the nuclear compilations of D. Strominger, J. M. Hollander, and G. T. Seaborg, Revs. Modern Phys. **30**, 585 (1958), and B. S. Dželepow and L. K. Peker, "Decay Schemes of Radioactive Nuclei" (Academy of Sciences of the USSR Press: Moscow, 1958).
22. P. H. Stelson and P. K. McGowan, Phys. Rev. **99**, 112 (1955).
23. F. K. McGowan and P. Stelson, Phys. Rev. **110**, 489 (1958).
24. Bayman, Reiner, and Sheline, Phys. Rev. **115**, 1627 (1959).
   K. W. Ford, Phys. Rev. **98**, 1516 (1955).
25. The mass data is taken from Nuclear Data Sheets, and from Everling, König, Mattauch, and Wapstra (to be published in Nucl. Phys.).
26. J. M. Blatt and V. F. Weisskopf, "Theoretical Nuclear Physics" (John Wiley and Sons: New York, 1952).
27. Demirkhanov, Gutin, and Dorokhov, JETP, U.S.S.R., **35**, 679 (1959).

28. H. Horie and A. Arima, Phys. Rev. **99**, 778 (1955).
29. Conclusions similar to these have been drawn by K. W. Ford, Phys. Rev. **92**, 1094 (1953).
30. A. Arima and H. Horie, Prog. Theor. Phys. (Japan) **12**, 623 (1954).
31. R. J. Blin-Stoyle, Proc. Phys. Soc. A, 1158 (1953).
32. G. Laukien, "Handbuch der Physik" XXXVIII/1 (Springer: Berlin, 1957), p. 120.
33. For the numerical calculations in the odd-*A* isotopes we have used the single-particle estimate from S. A. Moszkowski's article in Siegbahn, "Gamma and Beta Spectroscopy" (Interscience: New York, 1955). See the footnote on p. 69.
34. J. M. Mihelich and R. D. Hill, Phys. Rev. **79**, 781 (1950).
35. M. E. Rose, "Internal Conversion Coefficients" (North-Holland: Amsterdam, 1958).
36. Arima, Horie, and Sano, Prog. Theor. Phys. (Japan) **17**, 567 (1957).
37. P. A. Tove, Nuclear Instruments I, 95 (1957).
38. A. A. Bartlett and G. Rebka, Bull. Am. Phys. Soc. ser. II, **3**, 64 (1958).
39. J. A. McDonell, R. Stockendall, C. J. Herrlander, and I. Bergström, Nucl. Phys. **3**, 513 (1957).
40. B. Astrom, Arkiv Fysik **12**, 237 (1957).
41. See Cpt. III and Ref. 13.
42. Alder, Bohr, Huus, Mottelson, and Winther, Revs. Modern Phys. **28**, 432 (1956).
43. M. Goldhaber and A. W. Sunyar, Phys. Rev. **83**, 906 (1951).
44. Alkhazev, Andreev, Ereldina, and Lomberg, JETP, U.S.S.R., **33**, 1040 (1958).
45. P. H. Stelson and F. K. McGowan, Bull. Am. Phys. Soc., Ser. II, **4**, 232 (1959).
46. S. Ofer and A. Schwarzschild, Phys. Rev. Letters **3**, 384 (1959).

Indleveret til Selskabet den 12. februar 1960.
Færdig fra trykkeriet den 26. august 1960.

Matematisk-fysiske Meddelelser
udgivet af
Det Kongelige Danske Videnskabernes Selskab
Bind **32,** nr. 10

Mat. Fys. Medd. Dan. Vid. Selsk. **32,** no. 10 (1960)

# ON THE SCHRÖDINGER EIGENVALUE PROBLEM II

BY

OLAVI HELLMAN

København 1960
i kommission hos Ejnar Munksgaard

# CONTENTS


Page

1. Introduction and Summary ..... 3
2. The Derivation of the Eigenvalue Equation ..... 5
3. The Form and Properties of the Matrix $\tilde{\Omega}[s^{-P-1}P(s)s^{P-1}]$ ..... 11

References ..... 15


## Synopsis


The present work is a continuation of the author's paper 'On the Schrödinger Eigenvalue Problem', Mat. Fys. Medd. Dan. Vid. Selsk. **32**, no. 4. (1960) 24 pp., in which the potential was assumed to be of the form $\frac{a}{r^2}-\frac{b}{r}-V_0(r)$, $V_0(r)$ possessing a power-series expansion within a finite interval and vanishing elsewhere. It was required that $\sqrt{(2l+1)^2+4ka}$ was not an integer, a condition which is now dropped. The eigenvalue problem is again reduced to the formation of a series whose terms are obtained by a simple process the main operation of which is the integration. The formulae contain the potential $V_0(r)$ as such. The eigenvalues appear as roots of rapidly converging power series; the eigenfunctions are expressed in terms of functions obtained in the process of forming the said power series. The method is applicable also to the case where the mass is a function of r.



Printed in Denmark
Bianco Lunos Bogtrykkeri A-S

## 1. Introduction and Summary

In this paper we shall consider the Schrödinger eigenvalue problem

$$\left.\begin{aligned} &\frac{d^2R}{dr^2}+\frac{2}{r}\frac{dR}{dr}-\frac{l(l+1)}{r^2}R+k(E-V(r))R=0 \\ &R(0)<\infty \quad \text{and} \quad R(r)\to 0 \quad \text{for} \quad r\to\infty, \end{aligned}\right\} \tag{1.1}$$

with $l = 0,1,2,\ldots$ and

$$V(r)=\frac{a}{r^2}-\frac{b}{r}-V_0(r), \tag{1.2}$$

where $V_0(r)\neq 0$ only for $r\varepsilon[0, L]$, possessing in that interval an absolutely convergent power-series expansion in $r$; $a$ and $b$ are arbitrary real constants.

In a previous paper[1] the above eigenvalue problem was considered in the special case of $l = 0$ and in the case where $\sqrt{(2l+1)^2+4ka}$ is not an integer —a condition which we shall drop here, thus including in our treatment the important case of $a = 0$.

The main result of the present paper will be the formula

$$\det\begin{pmatrix} -\frac{\varkappa}{2}A(1)+C(1) & (c-p-1-\lambda)\,W_{c,q}(2\lambda)-\left[q^2-\left(c-\frac{1}{2}\right)^2\right]W_{c-1,q}(2\lambda) \\ A(1) & W_{c,q}(2\lambda) \end{pmatrix}=0 \tag{1.3}$$

for the eigenvalue $\lambda=\sqrt{k\,|\,E\,|\,L^2}$. Here

$$\left.\begin{aligned} A(s)=e^{-\frac{\varkappa}{2}s}\Bigg\{1+\sum_{n=1}^{\infty}\int_0^s e^{\varkappa s_1}s_1^{-m}\,ds_1\int_0^{s_1}e^{-\varkappa s_2}s_2^m(\lambda^2-V(s_2))\,ds_2\int_0^{s_2}\cdots \\ \cdots\int_0^{s_{2n-1}}e^{-\varkappa s_{2n}}s_{2n}^m(\lambda^2-V(s_{2n}))\,ds_{2n}\Bigg\} \end{aligned}\right\} \tag{1.4}$$

and

$$C(s) = e^{\frac{\varkappa}{2}s} s^{-m} \int_0^s e^{-\frac{\varkappa}{2}s_1} s_1^m (\lambda^2 - V(s_1)) A(s_1)\, ds_1, \tag{1.5}$$

where $V(s) = \left(\frac{\varkappa}{2}\right)^2 + kL^2 V_0(Ls)$ and $s = \frac{r}{L}$ (see also (2.18a)). The series $A(s)$ converges absolutely for every $s \varepsilon [0, 1]$ and for every finite $\lambda$. The functions $W_{c,q}(x)$ — known as Whittaker functions—are defined by the integral formula[3]

$$W_{c,q}(x) = \frac{e^{-\frac{x}{2}} x^c}{\Gamma\left(\frac{1}{2} - c + q\right)} \int_0^\infty t^{-c-\frac{1}{2}+q} \left(1 + \frac{t}{x}\right)^{c-\frac{1}{2}+q} e^{-t}\, dt, \tag{1.6}$$

which may be used in practical calculations at least in the case where $q-c$ and $q+c$ are integers*. The constants $\varkappa$, $c$, $m$, $q$, and $p$ of the formulae (1.3)—(1.6), expressed in the notation of (1.1) and (1.2), are as follows:

$$\varkappa = \frac{2\,kbL}{2(p+1)},\ c = \frac{kbL}{2\lambda},\ m = 2(p+1),\ q = \frac{m-1}{2},\ p = \sqrt{\left(l + \frac{1}{2}\right)^2 + ka} - \frac{1}{2}. \tag{1.7}$$

The eigenfunction of (1.1), corresponding to the eigenvalue $\lambda_i$, is given by

$$R_i(s) = \begin{cases} C s^{\frac{m-2}{2}} A_i(s) & \text{for} \quad s \varepsilon [0, 1] \\ C \sigma(\lambda_i) \frac{1}{s} W_{c,q}(2\lambda_i s) & \text{for} \quad s \varepsilon (1, \infty). \end{cases} \tag{1.8}$$

Here, $A_i(s)$ is defined by (1.4) with $\lambda_i$ substituted for $\lambda$, the factor $\sigma(\lambda_i)$ is obtained from (1.3), and $C$ is the normalizing constant. As is seen, the eigenfunction is obtained as a by-product of our calculations.

In certain shell-model problems of nuclear physics the constant $k$ of (1.1) appears as a function of $r$. In the cases where $k(r)(E - V(r))$ is of the form (1.2) our method is applicable after a straightforward modification.

The eigenvalue problem (1.1) is thus on the whole reduced to the forming of the series (1.4). The terms of that series contain the potential function $V_0(r)$ as such. Consequently the power-series expansion of $V_0(r)$ is not needed in the calculations; the mere existence of such an expansion is all

* Cf. J. Blomqvist and S. Wahlborn, Arkiv för Fysik **16** (1960) 545.

that is required for our purposes. Otherwise the method is largely independent of the form of the potential function—which may very well be tabular or graphical—and the elementary character of the analysis employed makes it particularly well suited for digital computers.

In practical applications one would calculate a finite number of terms of (1.4) for (1.5).

In section 2 the solution of (1.1) is found for $r \varepsilon [0, L]$ by the aid of a general theorem from the matrix calculus. The solution of (1.1) for $r \varepsilon [L, \infty]$ is known in closed form in terms of Whittaker functions ((1.6)). Equation (1.3) is obtained from the condition that $R(r)$ and $\frac{dR(r)}{dr}$ must be continuous at $r = L$. By way of application, the case of a square well is considered. The treatment of a more general case ($V_0(r)$ as defined on page 3) would be practically the same.

The matrix calculations of section 2 are carried out in detail in section 3, where also the convergence questions are dealt with.

## 2. The Derivation of the Eigenvalue Equation

We put (1.1) into matrix form as follows:

$$\frac{dz}{ds} - \left( \frac{P_{-1}}{s} + P(s) \right) z = 0 , \tag{2.1}$$

where

$$P_1 = \begin{pmatrix} 0 & 0 \\ 0 & -2(p+1) \end{pmatrix}, \tag{2.2}$$

$$P(s) = \begin{pmatrix} -\frac{\varkappa}{2} & 1 \\ -\left(\frac{\varkappa}{2}\right)^2 + \lambda^2 - V_1(s) & \frac{\varkappa}{2} \end{pmatrix} \tag{2.3}$$

and

$$z = s^{-p} \begin{pmatrix} 0 & 1 \\ 1 & \frac{\varkappa}{2} - \frac{p}{s} \end{pmatrix} \begin{pmatrix} \frac{dR}{dr} \\ R \end{pmatrix}. \tag{2.4}$$

In the above formulae one has

$$\left.\begin{aligned} \varkappa &= \frac{2\,kbL}{2\,(p+1)} \\ p &= \sqrt{\left(l+\frac{1}{2}\right)^2 + ka} - \frac{1}{2} \\ \lambda^2 &= k\,|\,E\,|\,L^2 \\ V_1(s) &= kL^2\,V_0(Ls)\,. \end{aligned}\right\} \tag{2.5}$$

The properties of matrix differential equations of the kind (2.1) in which $P(s)$ possesses a power-series expansion in $s$ converging absolutely for every $s$ within a finite interval $[0, s_1]$ are set out in a theorem by GANTMACHER[2]. It follows from this theorem, since the matrix $P(s)$ of (2.1) possesses the required power-series expansion, that the general solution of (2.1) will be of the form

$$z = A\,(s)\,s^{P_{-1}}\,s^{U}\,z_0 \tag{2.6}$$

with $z_0$ an arbitrary vector. Here

$$U = \begin{pmatrix} 0 & \alpha \\ 0 & 0 \end{pmatrix}, \tag{2.6a}$$

where $\alpha$ is a constant that depends on $P_{-1}$ and $P(s)$, vanishing if $2\,(p+1)$ in $P_{-1}$ is not an integer. The matrix $A(s)$ is regular at $s=0$ so that $A(0)=I$. Consequently there exists a convergent power-series expansion

$$A\,(s) = I + \sum_{k=1}^{\infty} A_k s^k. \tag{2.7}$$

We shall now calculate the matrix $A\,(s)$ by a procedure, similar to that employed in ref. [1], which obviates the use of power-series expansions (cf. for instance ref.[2]).

Substitution of (2.6) in (2.1) yields for $A$ the equation

$$\frac{dA}{ds} + \frac{1}{s}\,(AP_{-1} - P_{-1}A) - P(s)\,A + s^{m-1}\,AU = 0\,, \tag{2.8}$$

where $m$ stands for $2\,(p+1)$. As is seen on direct substitution, (2.8) is satisfied for every $s\,\varepsilon\,[s_0, 1]$, $s_0 > 0$, by the matrix

$$A = s^{P_{-1}}\,\tilde{\Omega}\,[s^{-P_{-1}}\,P(s)\,s^{P_{-1}}] \begin{pmatrix} 1 & -\ln s^{\alpha} \\ 0 & 1 \end{pmatrix} s^{-P_{-1}}, \tag{2.9}$$

where $B = s^{-P-1} P(s) s^{P-1}$. The matrix $\tilde{\Omega}(B)$ is defined as follows[1]:

$$\tilde{\Omega}(B) = I + \int^{s} B ds_1 + \int^{s} B ds_1 \int^{s_1} B ds_2 + \int^{s} B ds_1 \int^{s_1} B ds_2 \int^{s_2} B ds_3 + \cdots, \tag{2.10}$$

where, in carrying out the integrations, we put the constants of integration equal to zero in all terms.

We shall prove in section 3 that $A$, as defined by (2.9), may be expanded into a power series in $s$ which converges absolutely for every $s \varepsilon [0, 1]$ and has the value $I$ for $s = 0$, i.e., we shall prove that the expression (2.9) is really the $A(s)$-matrix of the general solution of the matrix differential equation (2.1).

From (2.4) and (2.9) it now follows that

$$\begin{pmatrix} \frac{dR}{dr} \\ R \end{pmatrix} = s^{p-1} \begin{pmatrix} -\frac{\varkappa}{2} s + p & s \\ s & 0 \end{pmatrix} \left\{ \begin{pmatrix} 1 & 0 \\ 0 & s^{-m} \end{pmatrix} \begin{pmatrix} A & B \\ C & D \end{pmatrix} \begin{pmatrix} 1 & -\ln s^{\alpha} \\ 0 & 1 \end{pmatrix} \begin{pmatrix} 1 & 0 \\ 0 & s^{m} \end{pmatrix} \right\} \times \left. \times \begin{pmatrix} 1 & 0 \\ 0 & s^{-m} \end{pmatrix} \begin{pmatrix} 1 & \ln s^{\alpha} \\ 0 & 1 \end{pmatrix} z_0 , \right. \tag{2.11}$$

where we have written briefly

$$\tilde{\Omega}(s^{-P-1} P(s) s^{P-1}) = \begin{pmatrix} A & B \\ C & D \end{pmatrix}. \tag{2.12}$$

The elements $A$, $B$, $C$, and $D$ are calculated in section 3 (cf. eqs. (3.12), (3.13)). Our $\begin{pmatrix} \frac{dR}{dr} \\ R \end{pmatrix}$ is required to be regular at the origin. Now, the expression in braces has this property, and besides $p \geqslant 1$; consequently the vector

$$\begin{pmatrix} 1 & 0 \\ 0 & s^{-m} \end{pmatrix} \begin{pmatrix} 1 & \ln s^{\alpha} \\ 0 & 1 \end{pmatrix} z_0 = \begin{pmatrix} 1 & \ln s^{\alpha} \\ 0 & s^{-m} \end{pmatrix} z_0 \tag{2.13}$$

must be regular at the origin. This implies the following form for $z_0$:

$$z_0 = \begin{pmatrix} 1 \\ 0 \end{pmatrix} C_1 , \tag{2.14}$$

where $C_1$ is a constant. For $s \neq 0$ we obtain from (2.11) and (2.14)

$$\begin{pmatrix} \frac{dR}{dr} \\ R \end{pmatrix} = s^{p-1} \begin{pmatrix} s & p \\ 0 & s \end{pmatrix} \begin{pmatrix} -\frac{\varkappa}{2} A + s^{-m} C \\ A \end{pmatrix} C_1 . \tag{2.15}$$

The vector (2.15) is now the general solution of (2.1) for every $s \varepsilon [0,1]$ which is regular at the origin. As the constant $\alpha$ has disappeared, we are spared the tedious task of calculating its value.

The solution of (2.1) for $s \varepsilon (1, \infty)$ such that $\begin{pmatrix} \frac{dR}{dr} \\ R \end{pmatrix} \to 0$ for $s \to \infty$ is, according to ref.[1],

$$\begin{pmatrix} \frac{dR}{dr} \\ R \end{pmatrix} = \frac{C_2}{s^3} \begin{pmatrix} s & p \\ 0 & s \end{pmatrix} \begin{pmatrix} (c-p-1-\lambda s) W_{c,q}(2\lambda s) - \left[ q^2 - \left( c - \frac{1}{2} \right)^2 \right] W_{c-1,q}(2\lambda s) \\ s W_{c,q}(2\lambda s) \end{pmatrix}; \tag{2.16}$$

here $C_2$ is an arbitrary constant, and the function $W_{c,q}(x)$ is defined by (1.6). The constants $p$, $\varkappa$, $m$, $c$, and $q$ are given by (1.7) and (2.5). Since the vectors (2.15) and (2.16) must be equal for $s = 1$, it is necessary that

$$\det \begin{pmatrix} -\frac{\varkappa}{2} A(1) + C(1) & (c-p-1-\lambda) W_{c,q}(2\lambda) - \left[ q^2 - \left( c - \frac{1}{2} \right)^2 \right] W_{c-1,q}(2\lambda) \\ A(1) & W_{c,q}(2\lambda) \end{pmatrix} = 0, \tag{2.17}$$

where, according to (2.12), (3.8), (3.9), and (3.13),

$$A(s) = e^{-\frac{\varkappa}{2} s} \left\{ 1 + \right. \\ \left. + \sum_{n=1}^{\infty} \int_0^s e^{\varkappa s_1} s_1^{-m} ds_1 \int_0^{s_1} e^{-\varkappa s_2} s_2^m F(s_2) ds_2 \int_0^{s_2} \cdots \int_0^{s_{2n-1}} e^{-\varkappa s_{2n}} s_{2n}^m F(s_{2n}) ds_{2n} \right\} \tag{2.18}$$

and

$$C(1) = e^{\frac{\varkappa}{2}} \int_0^1 e^{-\varkappa s} s^m F(s) \left\{ 1 + \right. \\ \left. + \sum_{n=1}^{\infty} \int_0^s e^{\varkappa s_1} s_1^{-m} ds_1 \int_0^{s_1} e^{-\varkappa s_2} s_2^m F(s_2) ds_2 \int_0^{s_2} \cdots \int_0^{s_{2n-1}} e^{-\varkappa s_{2n}} s_{2n}^m F(s_{2n}) ds_{2n} \right\} ds. \tag{2.19}$$

We summarize the symbols used in (2.17)—(2.19):

$$\left.\begin{aligned} F(s) &= -\left(\frac{\varkappa}{2}\right)^2 + \lambda^2 - kL^2 V_0(Ls) \\ \varkappa &= \frac{2\,kbL}{m} \\ m &= 2(p+1) \\ c &= \frac{2\,bL}{2\,\lambda} \\ \lambda^2 &= k\,|E|\,L^2 \\ p &= \sqrt{\left(l+\frac{1}{2}\right)^2 + ka} - \frac{1}{2}. \end{aligned}\right\} \quad (2.20)$$

For practical calculations it is convenient first to expand (2.18) into a power series in $\lambda^2$. This we are allowed to do because (2.18) converges absolutely for every $s\varepsilon\,[0,1]$ (cf. section 3). As would be easy to show, we obtain

$$A(s) = 1 + \sum_{k=1}^{\infty} \sum_{r=k}^{\infty} \lambda^{2k} (-1)^{r+k} \sum (r;k) \int_0^s f ds_1 \int_0^{s_1} h ds_2 \int_0^{s_2} \cdots \int_0^{s_{2r-1}} g ds_{2r}$$

with

$$f = e^{\varkappa s} s^{-m}, \quad g = e^{-\varkappa s} s^m \left[\left(\frac{\varkappa}{2}\right)^2 + V_1(s)\right] \quad \text{and} \quad h = e^{-\varkappa s} s^m.$$

The term

$$\sum (r;k) \int_0^s f ds_1 \int_0^{s_1} h ds_2 \int_0^{s_2} \cdots \int_0^{s_{2r-1}} g ds_{2r}$$

has the following meaning: $k$ $g$'s out of the $r$ $g$'s of the integral

$$\sum (r;0) \int_0^s f ds_1 \int_0^{s_1} \cdots \int_0^{s_{2r-1}} g ds_{2r} = \int_0^s f ds_1 \int_0^{s_1} g ds_2 \int_0^{s_2} f ds_3 \int_0^{s_3} \cdots f ds_{2r-1} \int_0^{s_{2r-1}} g ds_{2r}$$

are replaced by $h$, and the summation is extended over the integrals obtained on the performance of all permutations of these $k$ $h$'s and $r-k$ $g$'s. For instance,

$$\sum (2;1) \int_0^s f ds_1 \int_0^{s_1} h ds_2 \int_0^{s_2} f ds_3 \int_0^{s_3} g ds_4$$

$$= \int_0^s f ds_1 \int_0^{s_1} g ds_2 \int_0^{s_2} f ds_3 \int_0^{s_3} h ds_4 + \int_0^s f ds_1 \int_0^{s_1} h ds_2 \int_0^{s_2} f ds_3 \int_0^{s_3} g ds_4.$$

As is clear from (2.15) and (2.16),

$$R_i(s) = \begin{cases} C_1 s^p A_i(s) & \text{for } s\varepsilon[0,1] \\ C_1 \sigma(\lambda_i) \dfrac{1}{s} W_{c,q}(2\lambda s) & \text{for } s\varepsilon(1,\infty], \end{cases} \tag{2.21}$$

the factor $\sigma(\lambda_i)$ being obtained from (2.17). The constant $C_1$ is obtained from a normalizing condition.

For an application we shall consider the simplest example, the square well. It is clear from the above formulae that the treatment of a more general case would be essentially the same. Now

$$a = b = 0$$

and

$$V_0(r) = \begin{cases} V_0 & \text{for } r\varepsilon[0, L] \\ 0 & \text{for } r\varepsilon(L, \infty]. \end{cases}$$

According to (2.20) we have

$$\varkappa = 0, \quad m = 2(l+1), \quad c = 0, \quad \text{and} \quad q = l + \frac{1}{2}.$$

We then obtain from (2.17)—(2.19)

$$\det\begin{pmatrix} \dfrac{(\lambda^2-\lambda_0^2)}{m+1} + \sum_{n=1}^{\infty} \dfrac{(\lambda^2-\lambda_0^2)^{n+1}}{2^n n!\,(m+2n+1)!!} & -(1+l+\lambda) W_{0,q}(2\lambda) - \left(q^2 - \dfrac{1}{4}\right) W_{-1,q}(2\lambda) \\ 1 + \sum_{n=1}^{\infty} \dfrac{(\lambda^2-\lambda_0^2)^n}{2^n n!\,(m+2n-1)!!} & W_{0,q}(2\lambda) \end{pmatrix} = 0, \tag{2.22}$$

where $\lambda^2 = k\,|E|\,L^2$, $\lambda_0^2 = kV_0L^2$ and $(m+2n\pm1)!! = \prod_{k=0}^{n}(m+2k\pm1)$. The functions $W_{0,l+\frac{1}{2}}(x)$ and $W_{-1,l+\frac{1}{2}}(x)$ are calculated most conveniently by application of (1.6).

In case $m = 4$, we have, as is readily seen,

$$\det\begin{pmatrix} \left(\sqrt{\lambda_0^2-\lambda^2}\right)^2 \sin\sqrt{\lambda_0^2-\lambda^2} + 3\sqrt{\lambda_0^2-\lambda^2}\cos\sqrt{\lambda_0^2-\lambda^2} - 3\sin\sqrt{\lambda_0^2-\lambda^2} & \lambda^2+3\lambda+3 \\ -\sqrt{\lambda^2-\lambda^2}\cos\sqrt{\lambda_0^2-\lambda^2} + \sin\sqrt{\lambda_0^2-\lambda^2} & -\lambda-1 \end{pmatrix} = 0. \tag{2.23}$$

By using the power-series expansions of $\sin\sqrt{\lambda_0^2-\lambda^2}$ and $\cos\sqrt{\lambda_0^2-\lambda^2}$ and the formula (1.6) it is easy to show that (2.23) and (2.22), with $m = 4$, are identical.

### 3. The Form and Properties of the Matrix $\tilde{\Omega}[s^{-P-1} P(s) s^{P-1}]$

We shall first establish a useful property of the matrices $\tilde{\Omega}$. *Lemma*: Let us assume that it is possible to write the (square) matrix $H$ defined in the interval $[0,1]$ and singular at the origin in the form $H = H_1 + H_2$ so that the elements of the matrix $H_1$ are integrable over the interval $[0,1]$ and those of $H_2$ are integrable over every interval $[s_0, 1]$ with $0 < s_0 < 1$. Then, for $s \varepsilon [s_0, 1]$,

$$\tilde{\Omega}(H_1 + H_2) = \Omega_0^s(H_1)\, \tilde{\Omega}\{[\Omega_0^s(H_1)]^{-1} H_2 \Omega_0^s(H_1)\}, \tag{3.1}$$

where

$$\Omega_0^s(H_1) = I + \int_0^s H_1\, ds_1 + \int_0^s H_1\, ds_1 \int_0^{s_1} H_1\, ds_2 + \cdots.$$

As is well known[2], the formula (3.1) holds in the case of $s_0 = 0$.

*Proof*: Since the elements of $H_1$ are integrable over the interval $[0,1]$, the matrizant $\Omega_0^s(H_1)$ exists for every $s \varepsilon [0, 1]$, and so does $[\Omega_0^s(H_1)]^{-1}$ (cf. ref.[2]). Consequently the matrix $[\Omega_0^s(H_1)]^{-1} H_2 \Omega_0^s(H_1)$ has the same properties as the matrix $H_2$. We now proceed by the same method as that applied to the case of $s_0 = 0$ in ref.[2]. Let us put

$$X = \Omega_0^s(H_1), \qquad Y = \tilde{\Omega}(H_1 + H_2)$$

and $Y = XZ$. By differentiation we obtain

$$(H_1 + H_2) Y = H_1 XZ + X \frac{dZ}{ds}$$

for every $s \varepsilon [s_0, 1]$, $0 < s_0 < 1$, from which it follows that

$$\frac{dZ}{ds} = X^{-1} H_2 XZ = [\Omega_0^s(H_1)]^{-1} H_2 \Omega_0^s(H_1)\, Z.$$

Hence

$$Z = \tilde{\Omega}\{[\Omega_0^s(H_1)]^{-1} H_2 \Omega_0^s(H_1)\}$$

for all $s \varepsilon [s_0, 1]$, $0 < s_0 < 1$, which completes the proof.

As was shown in ref.[1], the series $\tilde{\Omega}(B)$, where $B$ is a matrix singular at $s = 0$, converges absolutely for every $s \varepsilon [s_0, 1]$ when $0 < s_0 < 1$.

Remembering (2.2) and (2.3), we then obtain

$$s^{-P-1} P(s) s^{P-1} = \begin{pmatrix} -\frac{\varkappa}{2} & s^{-m} \\ F(s) s^m & \frac{\varkappa}{2} \end{pmatrix} = \begin{pmatrix} -\frac{\varkappa}{2} & 0 \\ 0 & \frac{\varkappa}{2} \end{pmatrix} + \begin{pmatrix} 0 & s^{-m} \\ F(s) s^m & 0 \end{pmatrix},$$

where $m$ stands for $2(p+1)$ and $F(s)$ for $-\left(\frac{\varkappa}{2}\right)^2+\lambda^2-V_1(s)$. We can now identify $H_1$ and $H_2$ of our lemma with

$$\begin{pmatrix} -\frac{\varkappa}{2} & 0 \\ 0 & \frac{\varkappa}{2} \end{pmatrix} \quad \text{and} \quad \begin{pmatrix} 0 & s^{-m} \\ F(s)\, s^m & 0 \end{pmatrix}$$

respectively. Then

$$\left.\begin{aligned} \Omega_0^s(H_1) &= \begin{pmatrix} e^{-\frac{\varkappa}{2}s} & 0 \\ 0 & e^{\frac{\varkappa}{2}s} \end{pmatrix}, \\ [\Omega_0^s(H_1)]^{-1} &= \begin{pmatrix} e^{\frac{\varkappa}{2}s} & 0 \\ 0 & e^{-\frac{\varkappa}{2}s} \end{pmatrix} \end{aligned}\right\} \tag{3.2}$$

and

$$[\Omega_0^s(H_1)]^{-1} H_2\, \Omega_0^s(H_1) = \begin{pmatrix} 0 & e^{\varkappa s} s^{-m} \\ e^{-\varkappa s} s^m F(s) & 0 \end{pmatrix}. \tag{3.3}$$

By an obvious modification of a formula introduced in ref.[4] we obtain for $s \varepsilon [s_0, 1]$, $0 < s_0 < 1$,

$$\tilde{\Omega}\left\{[\Omega_0^s(H_1)]^{-1} H_2\, \Omega_0^s(H_1)\right\} = \begin{pmatrix} \omega_{11}(s) & \int_{\bullet}^{s} e^{\varkappa s_1} s_1^{-m}\, \omega_{22}(s_1)\, ds_1 \\ \int_{\bullet}^{s} e^{-\varkappa s_1} s_1^m F(s_1)\, \omega_{11}(s_1)\, ds_1 & \omega_{22}(s) \end{pmatrix} \tag{3.4}$$

with

$$\omega_{ii}(s) = \sum_{n=0}^{\infty} \alpha_{2n}^{(i)}(s), \qquad i = 1,2, \tag{3.5}$$

$$\left.\begin{aligned} &\alpha_{2n}^{(1)}(s) = \\ &\int_{\bullet}^{s} e^{\varkappa s_1} s_1^{-m}\, ds_1 \int_{\bullet}^{s_1} e^{-\varkappa s_2} s_2^m F(s_2)\, ds_2 \int_{\bullet}^{s_2} \dots \int_{\bullet}^{s_{2n-1}} e^{\varkappa s_{2n-1}} s_{2n-1}^{-m}\, ds_{2n-1} \int_{\bullet}^{s_{2n-1}} e^{-\varkappa s_{2n}} s_{2n}^{-m} F(s_{2n})\, ds_{2n} \end{aligned}\right\} \tag{3.6}$$

and

$$\left.\begin{aligned} &\alpha_{2n}^{(2)}(s) = \\ &\int_{\bullet}^{s} e^{-\varkappa s_1} s_1^m F(s_1)\, ds_1 \int_{\bullet}^{s_1} e^{\varkappa s_2} s_2^{-m}\, ds_2 \int_{\bullet}^{s_2} \dots \int_{\bullet}^{s_{2n-1}} e^{-\varkappa s_{2n-1}} s_{2n-1}^m F(s_{2n-1})\, ds_{2n-1} \int_{\bullet}^{s_{2n-1}} e^{\varkappa s_{2n}} s_{2n}^{-m}\, ds_{2n}, \end{aligned}\right\} \tag{3.7}$$

where $\alpha_0^{(1)}(s) = \alpha_0^{(2)}(s) = 1$*.

* The formula (3.4) may be verified also by direct differentiation after the absolute convergence of the power series $\omega_{11}(s)$ and that of the power series $\alpha_{22}^{(1)}(s)$ contained in $\omega_{22}(s)$ (cf. (3.10)) have been proved.

The series $\omega_{11}(s)$ now converges absolutely for every $s\varepsilon[0,1]$ (i.e., not only for $s\varepsilon[s_0,1]$). Indeed, from the fact that, for $s\varepsilon[0,1]$,

$$|F(s)|<M<\infty,\quad e^{\varkappa s}\leqslant e^{\varkappa}\quad\text{and}\quad e^{-\varkappa s}\leqslant 1,$$

it follows that

$$|\alpha_{2n}^{(1)}(s)|<(e^{\varkappa}M)^n\frac{s^{2n}}{2^n n!(m+1)(m+3)\ldots(m+2n-1)}$$

for every $n=0,1,2,\ldots$ and for every $s\varepsilon[0,1]$.

As both $e^{\pm\varkappa s}$ and $F(s)$ possess a power-series expansion in $s$ absolutely convergent for every $s\varepsilon[0,1]$, the same is true of $\omega_{11}(s)$. Since it was required that $A(0)=I$, and since $\omega_{11}(s)$ is regular at $s=0$ and $\Omega_0^0(H_1)=I$, we must replace (3.6) by

$$\alpha_{2n}^{(1)}(s)=\int_0^s e^{\varkappa s_1}s_1^{-m}\,ds_1\int_0^{s_1}e^{-\varkappa s_2}s_2^m F(s_2)\,ds_2\int_0^{s_2}\ldots\int_0^{s_{2n-1}}e^{-\varkappa s_{2n}}s_{2n}^m F(s_{2n})\,ds_{2n}. \tag{3.8}$$

As $e^{-\varkappa s}s^m F(s)$ is continuous for every $s\varepsilon[0,1]$, and the series $\omega_{11}(s)$ is absolutely continuous for every $s\varepsilon[0,1]$, the integral $\int_0^s e^{-\varkappa s_1}s_1^m F(s_1)\,\omega_{11}(s_1)\,ds_1$ exists for every $s\varepsilon[0,1]$ and has the properties of $s^{m+1}\omega_{11}(s)$. In compliance with the requirement that $\omega_{21}(0)=0$, we set

$$\omega_{21}(s)=\int_0^s e^{-\varkappa s_1}s_1^m F(s_1)\,\omega_{11}(s_1)\,ds_1. \tag{3.9}$$

The series $\omega_{22}(s)$ is more complicated since the integrations will produce an $\ln s$—function in each $\alpha_{2n}^{(2)}(s)$. As may be shown by means of the absolutely convergent power-series expansions of $e^{\pm\varkappa s}$ and $F(s)$, the functions $\omega_{22}(s)$ and $\omega_{12}(s)$ have the respective forms

$$\omega_{22}(s)=\left(\sum_{k=1}^m Q_k\right)\left\{\int_0^s e^{-\varkappa s_1}s_1^m F(s_1)\,\omega_{11}(s_1)\,ds_1\right\}\cdot\ln s+\omega_{22}^{(2)}(s) \tag{3.10}$$

and

$$\omega_{12}(s)=\left(\sum_{k=1}^m Q_k\right)\omega_{11}(s)\cdot\ln s+s^{-m+1}\omega_{22}^{(1)}(s), \tag{3.11}$$

where the lower limits of the integrals have been chosen to meet the requirement $A(0)=I$. The $Q_k$ are numbers depending on $\varkappa$, $m$ and $F(s)$. The functions $\omega_{22}^{(1)}(s)$ and $\omega_{22}^{(2)}(s)$ have the properties of $\omega_{11}(s)$; in particular, $\omega_{22}^{(1)}(0)=\omega_{22}^{(2)}(0)=1$.

We now have from (3.1), (3.2) and (3.4)

$$\tilde{\Omega}(s^{-P_{-1}} P s^{P_{-1}}) = \left( \begin{array}{cc} e^{-\frac{\varkappa}{2}s}\,\omega_{11}(s) & e^{-\frac{\varkappa}{2}s}\left[\left(\sum_{k=1}^{m} Q_k - \alpha\right)\omega_{11}(s)\ln s + s^{-m+1}\omega_{22}^{(2)}(s)\right] \\ e^{\frac{\varkappa}{2}s}\int_0^s e^{-\varkappa s_1} s_1^m F(s_1)\,\omega_{11}(s_1)\,ds_1 & e^{\frac{\varkappa}{2}s}\left[\left(\sum_{k=1}^{m} Q_k - \alpha\right)\left\{\int_0^s e^{-\varkappa s_1} s_1^m F\omega_{11}\,ds_1\right\}\ln s + \omega_{22}^{(1)}(s)\right] \end{array} \right), \tag{3.12}$$

$\omega_{11}(s)$ being defined by (3.5) and (3.8). By choosing $\alpha = \sum_{k=1}^{m} Q_k$ we obtain from (2.9) and (3.12)

$$A(s) = \left( \begin{array}{cc} e^{-\frac{\varkappa}{2}s}\,\omega_{11}(s) & e^{-\frac{\varkappa}{2}s}\,s\omega_{22}^{(2)}(s) \\ e^{\frac{\varkappa}{2}s}\,s^{-m}\int_0^s e^{-\varkappa s_1} s_1^m F(s_1)\,\omega_{11}(s_1)\,ds_1 & e^{\frac{\varkappa}{2}s}\,\omega_{22}^{(1)}(s) \end{array} \right). \tag{3.13}$$

Since the functions $\omega_{22}^{(1)}(s)$ and $\omega_{22}^{(2)}(s)$ are not needed in the calculations, their forms are not given here. As was made clear above, the matrix $A(s)$ has all the required properties: $A(s)$ may be expanded into a power series in $s$ convergent in the interval $[0,1]$, and $A$ has the property $A(0) = I$. From the fact that $A(s)$ satisfies (2.8) for every $s \varepsilon [s_0, 1]$, $0 < s_0 < 1$, it now follows that $A(s)$ satisfies (2.8) for every $s \varepsilon [0, 1]$.

## Acknowledgements

I want to express my deep gratitude to Professor NIELS BOHR for excellent working conditions at the Institute for Theoretical Physics in Copenhagen.

Further I want to thank Mr. FL. STEENBUCH for his great assistance in revising my work linguistically.

I am greatly indebted to NORDITA for the research fellowship granted me by that institute.

*NORDITA – Nordisk Institut for Teoretisk Atomfysik*
*Copenhagen*

## References

(1) O. HELLMAN, On the Schrödinger Eigenvalue Problem. Mat. Fys. Medd. Dan. Vid. Selsk. **32,** no. 4 (1960).
(2) Ф. Р. Гантмахер, Теория Матриц (Гостехиздат, Москва, 1953).
(3) E. T. WHITTAKER, An Expression of Certain Known Functions as Generalized Hypergeometric Functions. Bull. Am. Math. Soc. **10** (1904) 125.
(4) O. HELLMAN, Application of the So-called Matrizant in Certain Eigenvalue Problems. Nordisk Symposium över användning av matematikmaskiner, Karlskrona, 1959.

Indleveret til selskabet den 11. marts 1960.
Færdig fra trykkeriet den 16. november 1960.

Matematisk-fysiske Meddelelser
udgivet af
Det Kongelige Danske Videnskabernes Selskab
Bind **32**, nr. 11

Mat. Fys. Medd. Dan. Vid. Selsk. **32**, no. 11 (1960)

DANISH SCIENTIFIC INVESTIGATIONS IN ARGENTINA UNDER THE AUSPICES OF FUNDACIÓN WILLIAMS, BUENOS AIRES

# FOSSILS FROM THE LATE MIDDLE CAMBRIAN BOLASPIDELLA ZONE OF MENDOZA, ARGENTINA

BY

CHR. POULSEN

København 1960
i kommission hos Ejnar Munksgaard

# CONTENTS


| | Page |
|---|---|
| Introduction | 3 |
| Remarks on the locality, Cerrillo El Solitario | 5 |
| Descriptions of genera and species | 5 |
| Brachiopoda | 5 |
| *Dicellomus?* sp. ind. | 5 |
| Mollusca? | 5 |
| *Orthotheca* sp. | 5 |
| Trilobita | 6 |
| *Agnostus exsulatus* n. sp. | 6 |
| *Baltagnostus hospitus* n. sp. | 7 |
| — *mendozensis* n. sp. | 8 |
| *Clavagnostus chipiquensis* (Rusconi) | 9 |
| *Diplagnostus jarillensis* Rusconi? | 10 |
| *Kormagnostus propinquus* n. sp. | 11 |
| *Oedorhachis australis* n. sp. | 13 |
| *Peronopsis ultima* n. sp. | 13 |
| *Phoidagnostus solitariensis* (Rusconi) | 14 |
| *Stigmagnostus canotensis* (Rusconi) | 15 |
| *Prometeoraspis canotensis* n. sp. | 17 |
| *Williamsina cortesi* n. sp. | 19 |
| — *harringtoni* n. sp. | 20 |
| — *mikkelseni* n. sp. | 21 |
| — *ornata* n. sp. | 22 |
| *Talbotinella communis* n. sp. | 24 |
| — *leanzai* n. sp. | 25 |
| — *rusconii* n. sp. | 27 |
| *Bolaspidella lucieae* n. sp. | 28 |
| *Canotaspis aliena* | 29 |
| *Goycoia tellecheai* Rusconi | 30 |
| — *brevicauda* n. sp. | 31 |
| — *pecoralis* n. sp. | 32 |
| Undetermined specimens | 32 |
| The age of the fauna | 33 |
| References | 41 |
| Plates | 43 |


## Synopsis


Twenty-five species, mainly trilobites, from the Cambrian of Cerillo El Solitario in the province of Mendoza are described and discussed, and five new genera and eighteen new species are defined. The occurrence of the North American, Pacific genus *Bolaspidella* and a considerable number of Acado-Baltic agnostid genera in the fauna shows that the strata should be correlated with the late Cambrian, Pacific *Bolaspidella* zone of North America and the *Jincella brachymetopa* zone of the Acado-Baltic *Paradoxides forchhammeri* stage, respectively.



Printed in Denmark
Bianco Lunos Bogtrykkeri A-S

# Introduction

The geological and palaeontological research carried out in Argentina October 1954 to March 1955 by VALDEMAR POULSEN, M. Sc., and the writer was made possible by means of generous financial support from the Williams Foundation, Buenos Aires. The writer is also greatly indebted to Mr. T. J. WILLIAMS, K. D., and all members of his staff for their constant efforts to make our stay in Argentina a pleasant and unforgettable experience. He likewise wishes to express his gratitude to the Carlsberg Foundation and to the Danish State Research Foundation for financial support covering expenses in connection with the voyage and the purchase of scientific equipment, respectively.

Special acknowledgements are made to Professor, Dr. ARMANDO F. LEANZA of the Geological Institute of the University of Buenos Aires for allowing the writer to study his important collections of Lower Palaeozoic fossils from Argentina.

Finally the writer is indebted to Professor CARLOS RUSCONI, Director of the Natural History Museum of Mendoza, for kind permission to study selected fossils from the Cambro-Ordovician of the San Isidro region west of the city of Mendoza.

The main task of the expedition was a study of the Cambrian sections of the San Isidro region in connection with collection of fossils for the Mineralogical-Geological Institute of the University of Copenhagen. As a result of this study and collection VALDEMAR POULSEN published a paper in 1958 under the title of "Contributions to the Middle Cambrian Paleontology and Stratigraphy of Argentina" (Matematisk-fysiske Meddelelser udgivet af Det Kongelige Danske Videnskabernes Selskab, Bd. 31, No. 8).

It was planned to continue the collection of Cambrian fossils at San Isidro to the end of our stay in Argentina, but heavy rain in the mountains resulted in swelling rivers and destruction of roads so as to prevent further activity in this region. It was therefore decided to spend the last few days

at Cerrillo El Solitario, a hill at Canota, 36 km north of the city of Mendoza, where Rusconi has discovered a rich and in several respects highly interesting Cambrian fauna, described in papers of 1950, 1951, and 1952. A fairly rich palaeontological material was collected here, containing several new genera and species and forming a considerable supplement to the material described by Rusconi. This new material, described and discussed in the present paper, is preserved in the Mineralogical-Geological Institute of the University of Copenhagen.

It should be noted that circumstances beyond the writer's control prevented direct comparison with Rusconi's material so that any comparison with his specimens and comments on generic determinations are founded on his descriptions and figures.

All figures in the plates accompanying this paper are photographs taken by the writer; the prints have been made with great care and ability by Mr. C. Halkier.

## Remarks on the Locality, Cerrillo el Solitario

Cerrillo El Solitario is a small hill in the Canota region 36 km north of the city of Mendoza. The hill is the summit of a mountain the lower part of which is completely covered by a huge alluvial cone forming the surrounding Pampa. The sections in the hill show a 50 m series of strongly sloping strata, mainly dark limestone, which form an isolated stratigraphic unit without connection with younger and older formations.

## Descriptions of Genera and Species

Phylum **MOLLUSCOIDEA**

Class **BRACHIOPODA**

Order **ATREMATA** Beecher, 1891

Superfamily **OBOLACEA** Schuchert, 1896

Family **OBOLIDAE** King, 1846

Subfamily **BICIINAE** Walcott, 1908

Genus Dicellomus Hall, 1873

*Dicellomus*? sp. ind.

Pl. 1, fig. 1

Material: Two ventral valves.

Remarks: The specimens are fairly similar to *Dicellomus appalachia* Walcott, but they are not preserved well enough for accurate comparison.

Phylum **MOLLUSCA**

Class uncertain

Order uncertain

Family **HYOLITHIDAE** Nicholson

Genus Orthotheca Novak, 1887

*Orthotheca* sp.

Pl. 1, fig. 2

Material: Eight more or less fragmentary specimens.

Description: Shell rather rapidly increasing in width, with an apical angle of 11° and a rounded triangular cross-section. Dorsal face more flat

than ventral ones, sometimes even with a shallow median depression. External surface smooth to the naked eye, but a high-power lens (× 20 or more) reveals surface markings consisting of extremely delicate, very closely set transversal striae. Operculum unknown.

Dimensions:

Length of figured specimen ..... 7.0 mm
Maximum diameter of the same .. 1.6 –

## Phylum **ARTHROPODA**

## Class **TRILOBITA**

### Order **AGNOSTIDA** Kobayashi, 1935

In his excellent monograph of 1946, "Agnostidea of the Middle Cambrian of Sweden", Westergård pointed out that opinions diverge greatly with regard to the taxonomic position of a great many genera, and that "much work remains to be done before it is possible to establish a safe phyletic foundation"; he also pointed out that in many cases the criteria or combinations of characters used by several authors fail to give a reliable answer to the question whether an individual form is referable to one or the other family or subfamily. The present writer is of opinion that Westergård's judgment deserves much consideration, and, accordingly, the following ten agnostidean genera are simply described in alphabetic order under the heading:

### Suborder **Agnostidea** Salter, 1852

#### Genus Agnostus Brongniart, 1822

##### *Agnostus exsulatus* n. sp.

Pl. 1, figs. 3—4

Material: Two cephala and two pygidia.

Description: Cephalon and pygidium of moderate convexity, a little wider than long, rounded subquadrate in outline. Axial furrows of cephalon well-defined throughout. Glabella occupying about 0.75 of cephalic length and 0.28 of width, slightly elevated above genae, parallel-sided, evenly rounded in front; anterior glabellar lobe slightly wider than long, occupying about 0.33 of glabellar length; transverse glabellar furrow well-defined

throughout; posterior glabellar lobe attaining its highest convexity in the rear, with median tubercle situated opposite anterior ends of basal lobes. Basal lobes relatively large, subequilateral, connected by very narrow band. Genae separated anteriorly by well-defined preglabellar median furrow. Cephalic border narrow, fairly prominent, defined by wide, deeply impressed border furrow.

Thorax unknown.

Axial furrows of pygidium well-defined throughout. Axis occupying about 0.8 of pygidial length and about 0.4 of width, almost parallel-sided, broadly rounded posteriorly, yet with a tendency to become slightly pointed, divided by indistinctly defined furrows into 2 axial rings and a posterior portion without indication of segmentation; second axial ring with elongate median tubercle posteriorly. Pleural fields of uniform width for the greater part of their length, separated by faintly marked posterior median furrow. Border like that of the cephalon, but with a pair of marginal spines opposite axial termination.

Judging from small, well preserved parts of pygidial exoskeleton the external surface of *Agnostus exsulatus* is smooth.

Dimensions: Cephalon (holotype) 3 mm long and 3.7 mm wide; figured pygidium 2.9 mm long and 3.5 mm wide.

Remarks: *Agnostus exsulatus* displays a close resemblance to *A. pisiformis* (Linnaeus), but it is distinct from the latter by having rounded subquadrate cephalic and pygidial outline and shorter glabella with median tubercle of posterior glabellar lobe opposite anterior ends of basal lobes.

## Genus Baltagnostus Lochman, 1944

### *Baltagnostus hospitus* n. sp.

Pl. 1, figs. 5—6

Material: Two cephala and an associated pygidium.

Description: Cephalon rounded subquadrate, slightly wider than long, moderately convex. Axial furrows well-defined throughout, wide posteriorly, narrow anteriorly. Glabella occupying about 0.6 of cephalic length and about 0.3 of width, moderately convex, practically parallel-sided, evenly rounded in front; anterior glabellar lobe low, semicircular, occupying 0.35 af glabellar length; transverse glabellar furrow narrow; posterior glabellar lobe subrectangular, with indistinctly defined, oblong median node or keel. Basal lobes small, subequilateral. Genae of uniform width throughout,

confluent, regularly convex. Cephalic border narrow, moderately convex, defined by distinctly marked, narrow border furrow.

Thorax unknown.

Pygidium slightly wider than long, rounded subquadrate, moderately convex. Axis defined by relatively wide, well impressed axial furrows, occupying about 0.85 of pygidial length and about 0.4 of width, moderately convex, with slightly expanded posterior third, broadly rounded posteriorly, touching border furrow at median line; axial segmentation almost effaced, but 2 pairs of shallow notches indicate the presence of 2 anterior axial rings, the second of them carrying an indistinctly defined median tubercle. Border furrow slightly wider than that of the cephalon. Border narrow, almost flat, with a minute, blunt marginal spine on each side opposite axial termination.

Surface of exoskeleton smooth.

Dimensions: Pygidium (holotype) 3 mm long and 3.4 mm wide; figured cephalon 2.5 mm long and 2.7 mm wide.

Remarks: Unfortunately, the holotype of the type species of *Baltagnostus* (*Proagnostus*? *centerensis* Resser, 1938) is poorly preserved, and accordingly, it is difficult to use it for comparisons with other species of the genus. Nevertheless it is evident that *Baltagnostus hospitus* must be closely related to *B. centerensis* (Resser) and that it differs from the latter in having wider cephalon with wider glabella and shorter preglabellar field, and wider pygidium with reduced or poorly developed marginal spines. Lochman (1944) referred two other species to *Baltagnostus*, viz. *B. maryvillensis* (Resser) and *B. beltensis* Lochman; *B. hospitus* differs from the former in having a wider pygidium, and it is distinct from the latter by having a wider pygidium with angular outline and narrower axis. It is possible that the associated cephala provisionally combined with the holotype pygidium may belong to *Peronopsis ultima* n. sp. (p. 13).

### *Baltagnostus mendozensis* n. sp.

Pl. 1, fig. 7

Material: Two pygidia.

Description: Pygidium fairly convex, as long as wide, rounded subquadrate in outline. Axial furrows fairly wide and deeply impressed anteriorly, narrow and shallow posteriorly. Axis occupying about 0.8—0.9 of total length and about 0.5 of total width, unfurrowed, moderately convex, with slightly expanded posterior third, broadly rounded posteriorly, touching border furrow at median line, and carrying a small, oblong median node in

place corresponding to second axial ring. Border furrow narrow, but distinctly defined. Border narrow, almost flat, with a minute, acute marginal spine on each side opposite axial termination.

Surface smooth.

Dimensions: Length and width of holotype pygidium 2.6 mm (width estimated); length and width of smaller pygidium 1.7 mm.

Remarks: The unfurrowed pygidial axis of *Baltagnostus mendozensis* serves to distinguish this species from hitherto known species except *B. beltensis* Lochman; the pygidium differs from that of the latter in having a rounded subquadrate outline, narrower border furrow, narrower border with acute marginal spines, and a smooth surface.

## Genus Clavagnostus Howell, 1937

### *Clavagnostus chipiquensis* (Rusconi, 1952)

Pl. 1, fig. 14

1952. *Culipagnostus chipiquensis* Rusconi, Rev. Mus. Hist. Nat. Mendoza, Vol. 6, p. 11.

1952. *?Triplagnostus chipiquensis* Rusconi, ibid., pl. 1, fig. 11 (same specimen as that described on page 11).

It appears from Rusconi's figure that the specimen ("Tipo No. 11250") described by him as "cranideo" of "*Culipagnostus chipiquensis* n. sp." and figured as "cranideo" of "?*Triplagnostus chipiquensis* n. sp." has no basal lobes, and, accordingly, it must be a pygidium. This view is confirmed by the fact that the present writer's material contains two pygidia, which agree in most respects with Rusconi's figure; these pygidia have the same rounded outline, the same gradually tapering axis truncated by a border furrow and furnished with a well-defined, keel-shaped median tubercle, and crossed by a wide transverse furrow; Rusconi's figure fails to show marginal spines and a pair of pits in the wide transverse depression crossing the axis; in other respects the pygidia agree so well with the figure mentioned that they are referred by the present writer to the same species; judging from the characters of the pygidia, especially those of the axis, it admits of no doubt whatever that this species belongs to the genus *Clavagnostus* Howell.

Description: Pygidium subquadrangular, with strongly curved lateral margins, a little wider than long, of low convexity. Axis of about the same width as pleural fields, gradually tapering, truncated posteriorly by border furrow, divided a short distance posterior to centre by a wide transverse depression containing a pair of almost circular pits, and bearing a keel-

shaped median node on crest of anterior half. Axial furrows wide and deeply impressed throughout. Border furrow narrow, deeply impressed. Border somewhat convex, narrow at sides, expanded posteriorly, and furnished with a pair of relatively long, slender, diverging marginal spines.

Dimensions: Holotype pygidium about 2 mm long (estimated) and about 2.4 mm wide.

Remarks: The pygidium of *Clavagnostus chipiquensis* and that of *C. repandus* (Westergård) (the type species) differ from the other hitherto known species in having the axis truncated posteriorly by border furrow, and the former differs from the latter in having strongly curved lateral margins, longer marginal spines, and almost circular axial pits.

The pygidum from Cerrillo El Solitario described and figured by Rusconi (1950 a) as "*Clavagnostus calensis* n. sp." ("Tipo 7592") disagrees with that of the type species in so many respects that it can hardly be accepted as a member of the genus *Clavagnostus*.

## Genus Diplagnostus Jaekel, 1909

### *Diplagnostus jarillensis* Rusconi, 1952?

Pl. 1, fig. 9.

Material: A cephalon.

Description: Cephalon a little wider than long, rounded subquadrate in outline, fairly convex. Axial furrows wide, deeply impressed. Glabella occupying about 0.66 of cephalic length and about 0.33 of width, with depressed anterior glabellar lobe defined by shallow transglabellar furrow, occupying about 0.25 of glabellar length; posterior part of glabella unfurrowed, parallel-sided, and highly elevated above anterior glabellar lobe and genae. Basal lobes relatively small, subequilateral. Genae separated anteriorly by wide, well-defined longitudinal preglabellar furrow extending to border furrow and continuing backwards into anterior portion of anterior glabellar lobe. Cephalic border narrow, moderately convex, defined by narrow, well impressed border furrow.

External surface smooth.

Dimensions: Cephalon about 1.6 mm long and about 1.7 mm wide.

Remarks: Two pygidia have been referred by Rusconi to the genus *Diplagnostus* viz. *D. jarillensis* Rusconi, 1952 ("Tipo 9539") from Cerrillo El Solitario ("Horizonte Villavicense") and *D. indianus* Rusconi, 1955 ("Tipo 18618") from the Middle Cambrian of the San Isidro region west of the city

of Mendoza ("Horizonte Isidrense"). In *D. indianus* the broadly rounded posterior axial termination is calculated to call the generic reference into dispute. The pygidium of *D. jarillensis* agrees tolerably well with that of the type species, *D. planicauda* (TULLBERG). The above-described cephalon is tentatively referred to *D. jarillensis*. Before 1952 the genus was known from Scandinavia and Australia only. The Cephalon of *D. jarillensis* differs from that of Scandinavian species in having much smaller basal lobes and a wide, deeply impressed longitudinal preglabellar furrow extending to the border furrow, and it is distinguished from the Australian *D. humilis* (WHITEHOUSE) by its wider longitudinal preglabellar furrow and rounded subquadrate cephalic outline.

## Genus Kormagnostus RESSER, 1938

In RESSER's diagnosis this genus is "characterized by the absence of an anterior glabellar lobe" and by having "a wide pygidial axis which expands slightly rearward and extends to the marginal furrow. Pygidial border rather wide and slightly thickened". It may be added that the pygidial axis is prominent and with faintly indicated, almost effaced segmentation, and that the pygidial border is provided with a pair of marginal spines. LOCHMAN (1940) is of opinion that "*Kormagnostus* is a clear-cut, distinctive genus", and that is correct when combined cephalic and pygidial characters are taken into consideration, but it deserves notice that the cephalon of *Kormagnostus* displays a striking resemblance to that of *Hypagnostus* JAEKEL so as to make determination of isolated cephala very problematic; accordingly, the generic reference of the isolated cephalon described in the following is open to doubt.

### *Kormagnostus? propinquus* n. sp.

Pl. 1, fig. 10

Material: A fragmentary cephalon.

Description: Cephalon fairly convex, slightly wider than long (estimated), considerably decreasing in width posteriorly. Axial furrows narrow and very shallow. Posterior glabellar lobe without traces of segmentation, occupying about 0.5 of cephalic length (estimated) and about 0.4 of width, slightly convex, somewhat tapering, abruptly truncated anteriorly by narrow, very shallow transverse furrow, with a very small, oblong median tubercle

in front of lobal centre. Basal lobes small, triangular, slightly convex. Genae strongly convex at sides, falling rather steeply to wide, shallow border furrow. Border of medium width, slightly convex.

External surface smooth.

Dimensions: Cephalon about 2.5 mm long (estimated) and about 2.7 mm wide.

Remarks: As mentioned above, the writer is of opinion that isolated cephala of *Kormagnostus* can hardly be distinguished from those of *Hypagnostus*. It is therefore necessary to compare the cephalon of *Kormagnostus? propinquus* with those referred by Rusconi to *Hypagnostus* viz. *H. andinus* Rusconi, 1955 ("Tipo 18610") from the Middle Cambrian of the San Isidro region ("Horizonte Isidrense"), *H. huilichensis* Rusconi, 1955 ("Tipo 18447") from the Upper Cambrian of the San Isidro region, and *H. mollensis* Rusconi, 1952 ("Tipo 9574") from the Cambrian of Cerrillo El Solitario. *Kormagnostus? propinquus* differs from *H. andinus* in having larger glabella and different cephalic outline, and from *H. huilichensis* in having shorter, more tapering glabella with unfurrowed posterior lobe, indistinctly defined basal lobes, and different cephalic outline; with regard to cephalic outline it agrees fairly well with *H. mollensis*, but it is clearly distinct from that species by its tapering glabella and narrower cephalic border. It is much more similar to *Kormagnostus esterius* Lochman, 1940, from the Bonneterre dolomite of southeastern Missouri and the Pilgrim formation of Montana, from which it is distinguished by its indistinctly defined basal lobes and by the lack of an indicated anterior glabellar lobe. It is impossible for the time being to decide whether one or the other of the two pygidia described and figured by Rusconi (1954) as "*Kormagnostus cuchillensis* n. sp." and "*Kormagnostus lanceolatus* n. sp.", both from Cambrian strata near San Isidro, should be combined with the cephalon of *K.? propinquus* or not.

## Genus Oedorhachis Resser, 1938

Original diagnosis: "Agnostid with a normal cranidium, which possibly lacks a median furrow in typical species. The pygidium has a long rhachis, extending almost or altogether to the marginal furrow; rear lobe greatly expanded in exfoliated specimens, but poorly impressed on the outer test."

Resser referred six new species to his new genus viz. *O. typicalis* (type species), *O. ulrichi*, *O. boltonensis*, *O. tennesseeensis*, *O. mesleri*, and *O. greendalensis*. It appears from Resser's figures that these species represent two different groups, one characterized by wide, subquadrate pygidium with the expanded posterior axial portion well-defined by deeply impressed axial

furrows, the other characterized by a more rounded pygidial outline and by having the expanded posterior axial portion indistinctly defined by more or less effaced axial furrows. The latter group of species seems to agree very well with the general conception of *Pseudagnostus* JAEKEL, 1909, and the species in question may belong to this genus; one of the species (*Oedorhachis mesleri*) has already been referred by LOCHMAN (1940) to *Pseudagnostus*. The other group, which contains *O. typicalis* and *O. ulrichi*, seems to constitute a well-founded genus.

*Oedorhachis australis* n. sp.

Pl. 1, fig. 8

Material: An exfoliated pygidium.

Description: Pygidium subquadrangular, wider than long, moderately convex. Axial furrows well-defined. Axis occupying about 0.8 of pygidial length and about 0.4 of width, broadly rounded posteriorly, extending to border furrow, divided by indistinctly defined furrows into 2 axial rings and an expanded posterior portion; second axial ring crossed by narrow, well-defined median keel extending from posterior part of first axial ring to anterior part of posterior axial lobe. Pleural fields tapering posteriorly, separated by confluent axial and border furrows. Border furrow very wide. Border narrow at sides, somewhat expanded at the rear and divided by shallow, transverse depression in front of which it is raised into a sharp ridge; marginal spines extremely small, situated opposite axial termination.

Surface markings not observed.

Dimensions: Length of pygidium 3.4 mm, width 5 mm.

Remarks: *Oedorhachis australis* seems to be very closely related to *O. typicalis* RESSER (type species) and *O. ulrichi* RESSER; it differs, however, from these species in its less abruptly expanding posterior axial lobe and in having the expanded posterior border divided by a long, transverse depression extending from one marginal spine to the other; *O. ulrichi* shows a tendency to develop a similar, but much shorter transverse depression on the expanded posterior border.

Genus Peronopsis HAWLE & CORDA, 1847

*Peronopsis ultima* n. sp.

Pl. 1, fig. 13

Material: A single pygidium.

Description: Pygidium moderately convex, slightly longer than wide,

tending to become subquadrangular, with very narrow, slightly convex border, and fairly wide, shallow border furrow. Axis occupying about 0.7 af pygidial length and about 0.3 of width, defined by fairly wide, deeply impressed axial furrows, moderately elevated above pleural fields, lanceolate, with acute posterior termination, quite effaced segmentation, and almost effaced elongate median tubercle situated a little behind axial centre. Pleural fields evenly sloping, slightly increasing in width posteriorly, separated by wide, relatively deep longitudinal furrow.

Surface smooth.

Dimensions:

| | |
|---|---|
| Length of pygidium | 2.0 mm |
| Width - – | 1.8 – |
| Length - axis | 1.3 – |
| Width - – at anterior end | 0.7 – |

Remarks: The following combination of characters serve to distinguish this species from other species of the genus *Peronopsis*: Very short axis, almost effaced median axial tubercle, wide longitudinal furrow, and extremely narrow border of almost even width throughout. It is possible that the cephala provisionally referred to *Baltagnostus hospitus* n. sp. (p. 7) may belong to *Peronopsis ultima*.

## Genus Phoidagnostus Whitehouse, 1936

### *Phoidagnostus solitariensis* (Rusconi, 1950)

Pl. 1, fig. 15

1950. *Gallagnostus solitariensis* Rusconi, Rev. Mus. Hist. Nat. Mendoza, Vol. 4, p. 72, p. 83, figs. 2 a–b.

Material: An almost complete pygidium and a fragmentary natural cast of external pygidial surface.

Description: Pygidium practically as long as wide, subcircular in outline. Axial region and pleural fields strongly convex, forming an almost hemispheric main body with a small median tubercle half-way between centre and anterior margin. Border furrow wide, extremely shallow. Border fairly wide, almost flat, horizontal.

Surface smooth.

Dimensions: Length 3.5 mm, width 3.6 mm.

Remarks: The pygidium at hand agrees very well with the specimen described and figured by Rusconi as "cranideo", and it is referred by the

present writer to the same species; there is a slight difference with regard to the location of the median tubercle, which in RUSCONI's drawing is placed a little closer to the anterior margin. The highly convex, almost hemispheric pygidial main body, the indistinctly defined border furrow, and the flat, horizontal border constitute the most conspicuous distinguishing characters of this species.

With regard to the generic reference it should be noticed that pygidia of *Phoidagnostus* are very similar to those of *Gallagnostus*; species of the latter have a sharply marked pygidial border furrow, whereas species of the former (as far as is known) have a moderately developed, less distinct border furrow. RUSCONI's species in this respect agrees better with *Phoidagnostus* than with *Gallagnostus*.

## Genus Stigmagnostus n. g.

(Type species: ?*Tomagnostus canotensis* RUSCONI, 1951)

Diagnosis: Genus displaying the general characters of *Peronopsis* HAWLE & CORDA, 1847, but distinct from it by having a coarsely pitted pygidium. *Derivatio nominis:* στιγμα = *Stigma* (brand).

Remarks: This genus is known from the Cambrian of Cerrillo El Solitario only. In RUSCONI's type specimen ("Tipo 11228"), described and figured as "cranideo", neither anterior glabellar lobe nor basal lobes are shown; accordingly, the specimen in question must be a pygidium. As far as is known, coarsely pitted pygidia have not been observed in other genera of the Agnostida. *Stigmagnostus* should probably be placed in the subfamily Peronopsinae. The type species appears to be the only known representative of this new genus.

### *Stigmagnostus canotensis* (RUSCONI, 1951)

Pl. 1, figs. 11—12

1951. ?*Tomagnostus canotensis* RUSCONI, Rev. Mus. Hist. Nat. Mendoza, Vol. 5, p. 14; p. 26, fig. 29.

Original description: "Cranideo[1] de 2.6 mm de longitud por 2.2 mm de ancho (fig. 29). Forma ellíptica. El céphalo es sumamente alargado y estrecho, y adelante hay una leve bipartición que parecería corresponder a la glabella, pero que carece del surco transversal que la divide. La concha

[1] See the above remarks in connection with the generic diagnosis.

es relativamente chata y está constituída por doble hilera de vacuidades o pozuelos algo alargados y dispuestos transversalamente. En derredor del limbo hay una pestaña o borde angosto."

Material: A somewhat fragmentary pygidium and two associated cephala.

Description: Cephalon inconsiderably wider than long, moderately convex, with almost evenly rounded antero-lateral outline. Glabella occupying about 0.7 of cephalic length and about 0.25 of width, defined by fairly wide, well impressed axial furrows; anterior glabellar lobe semicircular in outline, depressed, defined posteriorly by well impressed transverse furrow; Posterior glabellar lobe more convex than anterior lobe. Basal lobes well-defined, approximately equilateral. Genae confluent, of almost even width throughout, gently sloping anteriorly and laterally. Border furrow relatively wide, well impressed. Border narrow, fairly convex.

Pygidium of about same shape as cephalon. Axis occupying about 0.64 of pygidial length and 0.2 of width, defined by wide, deeply impressed axial furrows, lanceolate, sharply pointed posteriorly, moderately convex, inconsiderably elevated above pleural fields, and without perceptible annulation; median tubercle not observed. Pleural fields of almost uniform width throughout, gently sloping, separated posteriorly by long well-defined longitudinal furrow. Border furrow relatively wide, well impressed. Border narrow, fairly convex, without marginal spines.

Surface of genae and pleural fields coarsely pitted.

Dimensions: Figured cephalon 1.85 mm long and 1.95 mm wide. Figured pygidium 2.8 mm long (estimated) and 3 mm wide.

Remarks: Judging from Rusconi's coarse drawing the type specimen is narrower than the pygidium figured here as Pl. 1, fig. 12; this may be due to the folding of the Cambrian rocks of Cerrillo El Solitario, which has resulted in deformation of some of the fossils; both specimens, however, have very narrow, lanceolate, posteriorly pointed, unfurrowed axis, long, well-defined postaxial longitudinal furrow, narrow border, and coarsely pitted pleural fields, and, accordingly, they are regarded as conspecific.

Order **PTYCHOPARIIDA** RICHTER, 1932

Suborder **Ptychopariina** RICHTER, 1932

Superfamily **CREPICEPHALACEA** KOBAYASHI, 1935

Family **TRICREPICEPHALIDAE** PALMER, 1954

Genus Prometeoraspis n. sp.

(Type species: *Prometeoraspis canotensis* n. sp.)

The Family Tricrepicephalidae was established by PALMER (1954) to cover the genera *Tricrepicephalus* KOBAYASHI, 1935 and *Meteoraspis* RESSER, 1935. Both genera are characterized by having ptychoparoid cranidia with deep axial, occipital, and border furrows, 2 or 3 pits in border furrow, and pygidia with a pair of more or less backward-directed spines.

The material from Cerrillo El Solitario contains a single cranidium, which shows the essential characters of *Meteoraspis* with the exception of the pits in the border furrow and the excessive upturning and convexity of the anterior border. In spite of the fact that the mentioned pits are indistinctly defined in some species of *Meteoraspis*, the writer is inclined to regard the complete absence of pits in the border furrow as a character of generic value.

Diagnosis: Tricrepicephalid trilobites with cranidium like that of *Meteoraspis* but differing from it by lack of pits in the border furrow and by having moderately convex, not upturned anterior border.

*Prometeoraspis canotensis* n. sp.

Pl. 1, figs. 16—17

Material: A fragmentary, slightly deformed cranidium.

Description: Cranidium oblong in shape, considerably curved on a transverse axis. Glabella defined by deeply impressed axial furrows, occupying about 0.83 of cephalic length and about 0.3 of width, about 1.4 times as long as wide, moderately convex, moderately tapering, almost evenly rounded in front, with 3 indistinctly defined anterior pairs of lateral glabellar furrows, followed by four well impressed, symmetrically arranged pits representing a strongly oblique posterior pair. Occipital furrow very broad, deeply impressed at sides, shallow at axial line. Occipital ring fairly convex, apparently with its greatest width (sag.) at the median line of the cranidium. Anterior and palpebral areas of fixigenae very narrow, the former strongly

sloping towards the border furrow and the anterior sections of the facial suture, the latter highly convex, elevated almost to the level of the crest of the glabella; posterior areas of about the same width (trans.) as the glabella, tongue-shaped, with bluntly terminating, strongly sloping extremities, divided by the broad, shallow posterior border furrow into subequal parts. Eye-ridges obscure. Palpebral lobes slightly curved, fairly prominent, extending backwards from a point opposite the second pair of lateral glabellar furrows to terminate well beyond the posterior pair of lateral glabellar furrows. Anterior sections of facial suture slightly converging from eyes to anterior border; posterior sections running almost directly outwards for the greater part of their length, then forming even backward curves. Preglabellar field extremely short. Anterior border furrow narrow, evenly curved. Anterior border fairly wide, moderately arched in longitudinal and transverse profile. External surface smooth to the naked eye, but a very delicate granulation is revealed by magnification × 20.

Dimensions:

| | | |
|---|---|---|
| Length of cranidium (estimated) | 5.0 | mm |
| Width – – at anterior end of palpebral lobes | 3.3 | – |
| – – – – posterior border | 7.4 | – |
| Maximum distance between eyes | 4.7 | – |
| Length of glabella (exclusive of occipital ring) | 3.3 | – |
| Width – – at base | 2.7 | – |
| – – – – anterior end of palpebral lobes | 2.0 | – |

Remarks: The type species described above seems to be the only known representative of the genus *Prometeoraspis*.

Superfamily **ASAPHISCACEA** Raymond, 1924

Family **ASAPHISCIDAE** Raymond, 1924

Subfamily **ASAPHISCINAE** Raymond, 1924

Genus Williamsina n. g.

(Type species: *Williamsina cortesi* n. sp.)

Four species from Cerrillo El Solitario are referred to this new genus, which displays considerable resemblance to the genera *Blountia* Walcott, 1916, and *Blainia* Walcott, 1916, of the Asaphiscinae.

Diagnosis: Asaphiscinae with relatively large, approximately semicir-

cular, somewhat depressed palpebral lobes situated opposite the glabellar centre, and furthermore characterized by lack of a palpebral furrow and a palpebral rim. Associated pygidium short, wide, indistinctly segmented, with tapering axis of about 6 rings and flat or slightly concave border. Hypostome, thorax, and ventral parts unknown.

Remarks: *Williamsina* differs from *Blountia* in having larger, strongly curved, depressed palpebral lobes without palpebral furrow and palpebral rim and tongue-shaped lateral extremities of fixigenae, and it is distinguished from *Blainia* by the mentioned characters of its palpebral lobes and by the more diverging course of the anterior sections of its facial suture between eyes and anterior border.

*Williamsina cortesi* n. sp.

Pl. 1, figs. 19—24

Material: Thirty cranidia, five librigenae, and fourteen pygidia.

Description: Cranidium 1.4 times as wide as long, considerably arched longitudinally and transversally. Glabella well-defined by narrow axial furrows, occupying 0.54 of cranidial length and 0.4 of width, as wide as long, considerably tapering, evenly rounded in front, separated from the anterior border by a well-developed preglabellar field, fairly convex, well elevated above palpebral areas of fixigenae, with three pairs of oblique, almost completely effaced lateral glabellar furrows. Occipital furrow narrow, deeply impressed at sides, very shallow at axial line. Occipital ring narrow (sag.), slightly convex. Anterior and palpebral areas of fixigenae moderately wide; eye-ridges practically effaced; palpebral lobes relatively large, approximately semicircular, depressed, without palpebral furrow and palpebral rim, situated opposite glabellar centre; posterior areas tongue-shaped, strongly sloping, divided by fairly broad, well impressed posterior border furrow into subequal portions. Anterior sections of facial suture considerably diverging from eyes to anterior border furrow, then strongly converging to cephalic margin; posterior sections directed outward and slightly backwards, paralleling posterior cephalic margin for a considerable distance, then curving evenly backwards to cut posterior border very close to genal angles. Anterior border furrow narrow and shallow, gently curved, paralleling anterior cranidial margin for a considerable distance. Anterior border fairly wide, flat, horizontal to slightly upturned. Librigenae of medium width, moderately convex, with narrow, shallow lateral border furrow,

fairly wide, flat lateral border, and well-developed, wide, rapidly tapering genal spine in direct continuation of lateral border.

Pygidium about 1.8 times as wide as long, approximately semicircular in outline, moderately convex. Axis defined by wide, shallow axial furrows, about twice as long as wide, rapidly tapering, extending to posterior border furrow, occupying about 0.77 of pygidial length and about 0.24 of width, fairly convex, divided by almost effaced transverse furrows into about 6 axial rings and a small terminal portion. Pleural fields smooth or with extremely faint indications of segmentation. Border furrow very shallow. Border fairly wide, slightly concave, crossed by indistinctly defined postaxial ridge.

Surface of cranidium, librigenae and pygidium smooth.

Dimensions:

| | | | | | |
|---|---|---|---|---|---|
| Length | of | cranidium | (holotype) | ..... | 5.5 mm |
| Width | - | – | – | at anterior border furrow ..... | 4.5 – |
| – | - | – | – | - centre of palpebral lobes ... | 5.0 – |
| – | - | – | – | - posterior border ..... | 7.7 – |
| Length | - | glabella | – | (exclusive of occipital ring).... | 3.0 – |
| Width | - | – | – | at base..... | 3.0 – |
| – | - | – | – | - anterior end of palpebral lobes | 2.0 – |
| Length | - | figured | pygidium | ..... | 3.5 – |
| Width | - | – | – | ..... | 6.2 – |
| Length | - | pygidial | axis | ..... | 2.7 – |
| Width | - | – | – | ..... | 1.5 – |

Remarks: *Willamsina cortesi* is the dominant species in the material at hand.

*Williamsina harringtoni* n. sp.

Pl. 1, fig. 29

Material: A pygidium.

Description: Pygidium about 1.7 times as wide as long, approximately semicircular in outline, moderately convex. Axis defined by narrow, shallow axial furrows, about twice as long as wide, moderately tapering, extending a little beyond posterior border furrow, occupying about 0.9 of pygidial length and about 0.18 of width, fairly convex, divided by almost effaced transverse furrows into 5 axial rings and a small terminal portion. Segmentation of pleural fields almost completely effaced. Border furrow shallow but fairly well defined. Border narrow and flat laterally, gradually in-

creasing in width toward axis and becoming slightly concave. Surface smooth.

Dimensions:

| | | | |
|---|---|---|---|
| Length of pygidium (holotype) | ..... | 2.65 | mm |
| Width - – | ..... | 4.65 | – |
| Length - axis | ..... | 2.35 | – |
| Width - – | ..... | 1.18 | – |

Remarks: The pygidium of this species is easily distinguished from that of *Williamsina cortesi* (the type species) by its less tapering axis and the increasing width of the border towards the axis.

*Williamsina mikkelseni* n. sp.

Pl. 1, figs. 25—28

Material: A cranidium (holotype) and a pygidium.

Description: Cranidium about 1.4 times as wide as long, slightly arched longitudinally and transversally. Glabella well-defined by narrow axial furrows, occupying 0.6 of cranidial length and 0.3 of width, 1.22 times as wide as long, somewhat tapering, evenly rounded in front, separated from anterior border by well-developed preglabellar field, moderately convex, slightly elevated above palpebral areas of fixigenae, with two pairs of distinctly defined, oblique lateral glabellar furrows. Occipital ring narrow (sag.), slightly convex. Occipital furrow narrow, distinctly marked throughout. Anterior and palpebral areas of fixigenae moderately wide; eye-ridges faintly marked, fairly oblique; palpebral lobes fragmentary, probably like those of the type species (p. 19); posterior areas tongue-shaped, moderately sloping, divided by fairly broad, well impressed posterior border furrow into subequal portions. Anterior sections of facial suture strongly diverging from eyes to anterior border furrow, then strongly converging to cephalic margin; posterior sections directed outwards, paralleling posterior cephalic margin for a considerable distance, then curving evenly backwards. Anterior border furrow fairly wide, distinctly marked, paralleling anterior cranidial margin for a considerable distance. Anterior border fairly wide, almost flat.

Pygidium about twice as wide as long, approximately semicircular in outline, almost flat. Axis defined by shallow axial furrows, about twice as long as wide, moderately convex, extending to posterior border furrow, occupying about 0.8 of pygidial length and about 0.2 of width, divided by almost effaced transverse furrows into 5 (6?) axial rings and a small rounded

terminal portion followed by very short postaxial ridge. Segmentation of pleural fields almost completely effaced. Border furrow very shallow. Border fairly wide, approximately horizontal, slightly concave.

Surface of cranidium and pygidium smooth.

Dimensions:

| | |
|---|---|
| Length of cranidium | 4.5 mm |
| Width - – at anterior border furrow | 4.2 – |
| – - – - centre of palpebral lobes | 4.2 – |
| – - – - posterior border | 6.2 – |
| Length - glabella (exclusive of occipital ring) | 2.7 – |
| Width - – at base | 2.2 – |
| – - – - anterior end of palpebral lobes | 1.7 – |
| Length - pygidium | 3.7 – |
| Width - – | 7.7 – |
| Length of pygidial axis | 3.0 – |
| Width - – – | 1.5 – |

Remarks: This species differs from *Williamsina cortesi* n. sp. (the type species (p. 19)) in having a less arched cranidium with a less tapering glabella, better defined lateral glabellar furrows, almost straight posterior fixigenal margin, more diverging anterior sections of the facial suture, a more curved anterior border furrow, and a wider, almost flat pygidium with a less tapering axis and approximately horizontal border.

### *Williamsina ornata* n. sp.

Pl. 2, fig. 1; Pl. 3, fig. 1

Material: Six more or less fragmentary pygidia.

Description: Pygidium 1.54 to 1.65 times as wide as long, moderately convex, with evenly rounded postero-lateral outline. Axis defined by shallow axial furrows, 1.84 to more than twice as long as wide, moderately tapering, prominent, extending to posterior border furrow or slightly encroaching on posterior border, occupying 0.63 to about 0.8 of pygidial length and 0.21 to 0.27 of width, divided by almost effaced transverse furrows into 5—6 axial rings and a small terminal portion. Segmentation of pleural fields indicated by raised segmental edges. Border furrow shallow, indistinctly marked. Border fairly wide, slightly concave, more or less sloping, covered with more or less distinctly marked network formed by raised, inosculating lines (more distinctly marked in the holotype than in the other specimens).

Dimensions:

| | I | II | III | IV (holotype) |
|---|---|---|---|---|
| Length of pygidium .... | 3.1 | 3.2 | 4.6 | 5.3 mm |
| Width - ..... | 4.8 | 5.3 | 7.4 | 8.4 – |
| Length - axis ..... | 2.4 | 2.5 | 3.9 | 4.3 – |
| Width - – ..... | 1.3 | 1.3 | 1.6 | 2.3 – |

Remarks: The raised segmental edges of the pleural fields and the surface markings of the pygidial border serve to distinguish *Williamsina ornata* from other species.

## Superfamily **SOLENOPLEURACEA** Angelin, 1854

## Family **LONCHOCEPHALIDAE** Hupé, 1953

### Genus Talbotinella n. g.

(Type species: *Talbotinella communis* n. sp.)

Diagnosis: Lonchocephalidae with relatively short, strongly tapering glabella, four pairs of strongly oblique lateral glabellar furrows; first pair developed as shallow pits remote from axial furrows; second pair broad and shallow, almost in contact with axial furrows; third pair better defined, bifurcating distally so as to circumscribe an extraordinary, usually somewhat swollen lateral lobe; fourth pair almost in contact with axial furrows, indistinctly defined in some specimens or even effaced. Occipital furrow broad, deeply impressed at sides. Occipital ring narrow (sag.) and slightly convex (sag.), with well developed occipital spine in typical species. Glabella usually separated from anterior border by fairly ample preglabellar field. Anterior and palpebral areas of fixigenae narrow; posterior areas slightly narrower than base of glabella, with broad deeply impressed posterior border furrow; posterior border convex; eye-ridges more or less indistinctly defined, oblique; palpebral lobes small strongly curved, situated moderately in advance of glabellar centre. Anterior sections of facial suture subparallel or slightly diverging from eyes to anterior border; posterior sections extending obliquely backwards to cross posterior border very close to genal angles. Anterior border furrow narrow, well impressed. Anterior border relatively narrow, moderately convex. Librigenae moderately wide, evenly arched, with flat lateral border and well developed, slender, obliquely backward-directed genal spine almost in continuation of lateral border.

Hypostome and other ventral parts unknown.

Thorax unknown.

Pygidium of type species short, very wide, subelliptic in outline, moderately convex, with prominent, slightly tapering axis consisting of three rings and a rounded terminal portion extending to indistinctly defined, concave border; pleural fields and border with well marked pleural furrows and interpleural grooves.

External surface of cranidium and librigenae densely covered with minute granulae, distinctly marked on glabella and occipital ring and indistinct or even effaced on palpebral and posterior areas of fixigenae and on librigenae; preglabellar field, anterior areas of fixigenae, and librigenae further marked by extremely delicate, raised, inosculating lines radiating from glabella, eye-ridges, and eyes.

Remarks: *Talbotinella* recalls the genus *Talbotina* Lochman, especially when compared with *Talbotina jeweli* Lochman (Lochman & Duncan, 1944, p. 130, pl. 12, figs. 6—12). The genera have several features in common, such as outline, convexity, and surface markings of cranidium, shape of pygidial axis, pleural fields and border of pygidium with well marked pleural furrows and interpleural grooves. *Talbotinella*, however, differs from *Talbotina* in having more tapering glabella, a pair of extraordinary lateral glabellar lobes defined by distal bifurcation of third pair of lateral glabellar furrows, occipital ring narrower (trans.) than base of glabella, ampler preglabellar field, less convex anterior cranidial border, smaller, strongly curved palpebral lobes, and shorter and wider pygidium.

### *Talbotinella communis* n. sp.

Pl. 2, figs. 2—8; Pl. 3, fig. 2

Material: Eight cranidia, a librigena, and two associated pygidia.

Description: Cranidium 1.3 times as wide as long exclusive of occipital spine; its anterior part moderately arched longitudinally and transversally, posterior part considerably arched transversally. Glabella well defined by narrow axial furrows, occupying 0.56 of cranidial length and 0.45 of width, almost as wide as long, strongly tapering, subtriangular in outline, evenly and narrowly rounded in front, separated from anterior border by well-developed preglabellar field, moderately convex, yet well elevated above palpebral areas of fixigenae (for description of lateral glabellar furrows see generic diagnosis p. 23). Occipital furrow very broad, deeply impressed at sides, shallow at axial line. Occipital ring narrow (sag.), much narrower (trans.) than base of glabella, with well-developed occipital

spine of unknown length. Anterior and palpebral areas of fixigenae relatively narrow; posterior areas moderately wide, subtriangular, strongly sloping; palpebral lobes very small, strongly curved, situated moderately in advance of glabellar centre; eye-ridges faintly marked, oblique; posterior border furrow broad, deeply impressed; posterior border convex, extending obliquely backwards from axial furrows. Anterior border furrow narrow, well impressed, gently curved. Anterior border relatively narrow, moderately convex. Anterior sections of facial suture slightly diverging from eyes to anterior border; posterior sections curving gently outwards and backwards to cross posterior border very close to genal angles. Librigenae of medium width, evenly arched, with narrow, flat lateral border slightly increasing in width posteriorly; genal spines well-developed, slender, obliquely backward-directed, practically in continuation of lateral border.

For pygidium and surface markings see generic diagnosis p. 24.

Dimensions:

| | I (holotype) | II |
|---|---|---|
| Length of cranidium (exclusive of occipital spine) | 10.2 ... | ? mm |
| Width - – at anterior border furrow | 7.7 ... | 8.7 – |
| – - – - centre of palpebral lobes | 8.7 ... | 9.7 – |
| – - – - posterior border | 13.2 ... | 14.2 – |
| Length of glabella (exclusive of occipital ring) | 6.0 ... | 6.3 – |
| Width - – at base | 5.7 ... | 6.0 – |
| – - – - anterior end of palpebral lobes | 3.7 ... | 4.0 – |
| Length - figured pygidium | 3.1 mm | |
| Width - – – | 6.2 – | |
| Length - pygidial axis | 2.6 – | |
| Width - – – | 2.2 – | |

Remarks: *Talbotinella communis* is distinguished from other species of this new genus by the narrowly rounded front of its glabella and the strongly oblique backward course of the posterior cranidial margin from the axial furrows to the facial suture.

*Talbotinella leanzai* n. sp.

Pl. 2, figs. 9—12

Material: A cranidium and a librigena.

Description: Cranidium about 1.7 times as wide as long exclusive of occipital spine; its anterior part moderately arched longitudinally and transversally, posterior part considerably arched transversally. Glabella

defined by narrow, well impressed axial furrows, occupying about 0.7 of cranidial length and 0.38 of width, a little wider than long, strongly tapering, subtriangular in outline, evenly and broadly rounded in front, separated from anterior border by well-developed preglabellar field, moderately convex, yet well elevated above palpebral areas of fixigenae, (for description of lateral glabellar furrows see generic diagnosis p. 23). Occipital furrow broad, very deeply impressed at sides. Occipital ring narrow (sag.), a little narrower (trans.) than base of glabella. Anterior and palpebral areas of fixigenae relatively narrow; posterior areas of medium width, subtriangular, strongly sloping; eye-ridges very indistinctly defined, oblique; palpebral lobes small, strongly curved, situated moderately in advance of glabellar centre; posterior border furrow broad, deeply impressed; posterior border convex, extending almost directly outwards from axial furrows. Anterior border furrow narrow, well impressed, gently curved. Anterior border narrow, moderately convex. Anterior sections of facial suture almost parallel between eyes and anterior border; posterior sections extending outwards and backwards to cross posterior border at genal angles. Librigenae of medium width, evenly arched, with flat lateral border; genal spines well-developed, slender, obliquely backward-directed, not quite in continuation of lateral border.

For description of surface markings see generic diagnosis p. 24.

Dimensions of cranidium (holotype):

| | | |
|---|---|---|
| Length of cranidium (exclusive of occipital spine) | 6.3 | mm |
| Width - – at anterior border furrow | 4.8 | – |
| – - – - centre of palpebral lobes | 5.7 | – |
| – - – - posterior border | 10.0 | – |
| Length - glabella (exclusive of occipital ring) | 3.7 | – |
| Width - – at base | 3.8 | – |
| – - – - anterior end of palpebral lobes | 2.3 | – |

Remarks: *Talbotinella leanzai* appears to be very closely related to *T. communis* (the type species); the former differs from the latter in having a wider glabella with broadly rounded front, narrower, more convex anterior border, subparallel course of anterior sections of facial suture between eyes and anterior border, posterior sections crossing posterior border at genal angles, and posterior cephalic border almost perpendicular to cephalic median line. The associated librigena differs from that of the type species in having a slightly wider lateral border, and the genal spine not quite in continuation of the lateral border.

*Talbotinella rusconii* n. sp.

Pl. 2, figs. 13—15

Material: A somewhat fragmentary cranidium.

Description: Cranidium of unknown width (postero-lateral extremities not preserved); its anterior part considerably arched longitudinally and moderately arched transversally. Glabella defined by narrow, well impressed axial furrows, occupying about 0.7 of cranidial length, a little longer than wide, moderately tapering, evenly rounded in front, separated from anterior border by short preglabellar field, moderately convex, yet well elevated above palpebral areas of fixigenae (for description of lateral glabellar furrows see generic diagnosis p. 23). Occipital furrow broad, very deeply impressed at sides, shallow at axial line. Occipital ring narrow (sag.), much narrower (trans.) than base of glabella, provided with small median node. Anterior and palpebral areas of fixigenae relatively narrow; eye-ridges well-defined, oblique; palpebral lobes small, moderately curved, situated a little in front of glabellar centre. Anterior border furrow narrow and shallow, rectilinear. Anterior border relatively narrow, almost flat. Anterior sections of facial suture subparallel between eyes and anterior border.

For description of surface markings see generic diagnosis p. 24.

Dimensions:

| | | |
|---|---|---|
| Length of cranidium | 9.3 | mm |
| Width - – at anterior border furrow | 7.7 | – |
| – - – - centre of palpebral lobes | 9.0 | – |
| – - – - posterior border | ? | – |
| Length - glabella (exclusive of occipital ring) | 6.3 | – |
| Width - – at base | 5.5 | – |
| – - – - anterior end of palpebral lobes | 3.3 | – |

Remarks: *Talbotinella rusconii* is easily distinguished from the two preceding species by its narrower, less tapering glabella, short preglabellar field, well marked eye-ridges, moderately curved palpebral lobes, rectilinear anterior border furrow, almost perfectly flat anterior border, and lack of occipital spine.

Superfamily **NORWOODIACEA** Walcott, 1916

Family **MENOMONIIDAE** Walcott, 1916

Genus Bolaspidella Resser, 1937

*Bolaspidella lucieae* n. sp.

Pl. 2, figs. 16—17

Material: Five cranidia and a librigena.

Description: Cranidium almost twice as wide as long. Glabella well defined by deeply impressed axial furrows, occupying about 0.5 of cranidial length and 0.2 of width, 1.3 times as long as wide, moderately tapering, somewhat truncated in front, separated from anterior border by well-developed preglabellar field, fairly convex, with three pairs of very shallow, indistinctly defined marginal impressions representing lateral glabellar furrows. Occipital furrow well impressed, narrow at axial line, broad at sides. Occipital ring wide at axial line, strongly tapering at sides, with a small median node. Anterior and palpebral areas of fixigenae moderately wide, the latter elevated above crest of glabella and sloping off rather steeply towards axial furrows; posterior areas very wide, with strongly sloping lateral extremities; eye-ridges indistinctly defined, perpendicular to axis; palpebral lobes small, situated well in advance of glabellar centre; posterior border furrow broad, deeply impressed; posterior border convex, slightly backward-directed near posterior termination of facial suture. Anterior border furrow fairly broad, well impressed, gently curved. Anterior border of medium width, convex. Anterior sections of facial suture parallel or nearly so between eyes and anterior border; posterior sections curving outwards from eyes, then backwards to cross posterior border very close to genal angles. Librigenae wide, with moderately and evenly arched proximal area, well impressed lateral border furrow, and convex lateral border becoming almost flat and increasingly wide near genal angles; genal spines well-developed, flat, backward-directed, in continuation of the lateral border, rapidly tapering.

External surface of cranidium and librigenae marked by a relatively small number of scattered tubercles and more numerous, irregularly spaced granules.

Dimensions af cranidium (holotype):

| | | |
|---|---|---|
| Length of cranidium | 1.8 | mm |
| Width - – at anterior border furrow | 1.47 | – |
| – - – - centre of palpebral lobes (estimated) | 1.67 | – |

| | | | | |
|---|---|---|---|---|
| Width of cranidium at posterior border | | | 3.35 | mm |
| Length - glabella (exclusive of occipital ring) | | | 0.9 | – |
| Width - – at base | | | 0.66 | – |
| – - – - anterior end of palpebral lobes | | | 0.53 | – |

Remarks: This species is readily distinguished from the hitherto known species of the genus *Bolaspidella* by the following combination of characters: Almost parallel-sided glabella, very shallow, indistinctly defined lateral glabellar furrows, and broad, curved anterior border furrow. The librigena figured by Howell (1937, pl. 5, fig. 34) as *Champlainia rectimargo* shows striking resemblance to that of *Bolaspidella lucieae*; accordingly, the present writer is of opinion that the librigena mentioned should be referred to the genus *Bolaspidella*.

## Incertae Sedis

### Genus Canotaspis n. g.

(Type species: *Canotaspis aliena* n. sp.)

This genus is known from the cranidium alone.

Diagnosis: Cranidium approximately semicircular in outline, almost evenly arched longitudinally and transversally, with unfurrowed, slightly tapering, anteriorly truncated glabella, narrow (sag.) occipital ring, short preglabellar field, wide fixigenae, small palpebral lobes situated well in front of the glabellar centre, evenly curved anterior border furrow, narrow, flat anterior border, and smooth external surface.

Remarks: The affinities of this trilobite are obscure. The general shape is much the same as in *Aposolenopleura? brevifrons* Rasetti (1944, p. 239, pl. 36, fig. 46), which is "not quite typical of the genus"; *Canotaspis aliena*, however, differs from Rasetti's species in having wider fixigenae and a curved anterior border furrow.

### *Canotaspis aliena* n. sp.

Pl. 2, figs. 21—22

Material: An almost complete cranidium.

Description: Cranidium approximately semicircular in outline, almost evenly arched longitudinally and transversally, about 1.8 times as wide as long. Glabella well-defined by narrow, moderately impressed axial furrows, occupying about 0.7 of cranidial length and 0.33 of width, almost

as wide as long, slightly tapering, truncated in front, unfurrowed, separated from anterior border by a short preglabellar field, moderately convex, somewhat elevated above level of the fixigenae. Occipital furrow narrow, well impressed. Occipital ring narrow (sag.). Anterior and palpebral areas of fixigenae relatively wide; posterior areas of medium width; eye-ridges effaced; palpebral lobes small, situated well in front of the glabellar centre; posterior border furrow narrow and deeply impressed near axial furrows, becoming gradually wide and shallow towards the facial suture; posterior border narrow, convex. Anterior border furrow narrow and shallow, gently curved. Anterior border narrow and flat. Facial suture almost evenly curved from anterior to posterior cephalic margin.

External surface smooth.

Dimensions:

| | | |
|---|---|---|
| Length of cranidium | 13.0 | mm |
| Width - – at anterior border furrow | 15.0 | – |
| – - – - centre of palpebral lobes | 19.0 | – |
| – - – - posterior border | 24.0 | – |
| Length - glabella (exclusive of occipital ring) | 9.0 | – |
| Width - – at base | 8.0 | – |
| – - – - anterior end of palpebral lobes | 5.5 | – |

## Genus Goycoia Rusconi, 1950.

This genus was proposed by Rusconi to include pygidia of two species from the Cambrian of Cerrillo El Solitario, viz. *Goycoia tellecheai* Rusconi and *G. limpida* Rusconi; in 1952 the same writer added *G. cerrillensis* Rusconi from the same locality. No type species was chosen. These pygidia are of a generalized type, which shows considerable resemblance to Asaphiscidae such as *Asaphiscus* Meek, 1873 and *Blountia* (*Homodictya*) Raymond, 1937, and, in the present writer's opinion the validity and position of *Goycoia* must be regarded as problematic until appertinent cephalic parts have been found. Taking the possible validity of *Goycoia* into consideration, *Goycoia tellecheai* Rusconi, 1950 is here chosen as type species.

### *Goycoia tellecheai* Rusconi, 1950

Pl. 2, fig. 24

1950. *Goycoia tellecheai* Rusconi, Rev. Mus. Hist. Nat. Mendoza, Vol. 4, Entregas 3 a–4 a, p. 76, fig. 8.

Material: Three more or less complete pygidia.

Original description: "Pigidio, de 10 mm de longitud por 14.8 mm

de ancho (fig. 8). El pigaxis es estrecho con un ancho casi igual en toda su longitud. Hay 7 levísimos anillos que se los ve únicamente cuando la pieza es colocada en posición perpendicular. De estos bosquejos de anillos los dos primeros son algo más aparentes y los posteriores no están definidos en la parte medial y superior. También en esa posición perpendicular se alcanzan a ver en el ejemplar tipo, pequeñas manchas alargadas u ovales, dispuestas obliquamente de adentro hacia afuera y adelante.

En la mitad de la concha hay un surco semicircular y entre éste y el borde externo existe una franja ancha y levemente excavata. En cambio, dentro de la periferia determinada por el surco semicircular se advierten 6 levísimas pigopleuras, siendo algo más visibles las anteriores, mientras que las posteriores se alcanzan a ver con dificultad cuando la pieza es colocada perpendicularmente. De esta especie conozco muchos ejemplares con los detalles indicados. Además, la concha de estos pigidios son relativamente chatas, y tanto su ornamentación como los otros trilobitas de Mendoza, motivos por el qual creo que se trata de un nuevo genero tal vez vinculado al grupo Opisthoparia."

The specimens at hand agree well with Rusconi's description and figure although the latter shows a more strongly rounded antero-lateral outline, which may probably be due to partly sediment-covered articulating facets. It may be added to Rusconi's description that the axial furrows are narrow and extremely shallow, that the border is crossed by a postaxial ridge, and that the external surface is smooth.

Dimensions of figured pygidium:

| | |
|---|---|
| Length | 14.0 mm |
| Width | 21.0 – |
| Length of axis | 10.0 – |
| Width - – anteriorly | 4.0 – |
| – - – posteriorly | 3.0 – |

*Goycoia brevicauda* n. sp.

Pl. 2, fig. 23

Material: Three more or less complete pygidia.

Description: Pygidium 1.7 times as wide as long, semielliptic in outline, moderately convex. Axis defined by narrow, extremely shallow axial furrows, about 1.8 times as long as wide, moderately tapering, extending to border furrow, occupying about 0.7 of pygidial length and about 0.2 of width, moderately convex, divided by almost effaced transverse furrows into

six hardly visible axial rings and a small, rounded terminal portion. Pleural fields small, showing five faintly indicated segments. Border furrow wide and shallow. Border wide, slightly concave, crossed by faintly indicated postaxial ridge.

External surface smooth.

| Dimensions: | I | II (holotype) |
|---|---|---|
| Length | 6.0 | 8.0 mm |
| Width | 10.0 | 14.0 – |
| Length of axis | 4.0 | 5.5 – |
| Width - – anteriorly | 2.2 | 3.0 – |
| – - – posteriorly | 1.3 | 1.8 – |

Remarks: This species is closely related to *Goycoia tellecheai* Rusconi (the type species), but differs in having shorter pygidium; it is easily distinguished from *G. cerrillensis* Rusconi by its shorter pygidium and more tapering axis.

*Goycoia pecoralis* n. sp.

Pl. 2, fig. 25

Material: A pygidium (natural cast of the interior).

Description: Pygidium about 1.3 times as wide as long, semielliptic in outline, moderately convex. Axis defined by moderately broad, very shallow axial furrows, about 2.5 times as long as wide, moderately tapering, extending to border furrow, occupying about 0.7 of pygidial length and 0.2 of width, moderately convex, divided by faintly indicated transverse furrows into seven flat axial rings and a short, rounded terminal portion. Pleural fields small, showing six faintly indicated segments. Border furrow apparently shallow. Border wide, concave.

Dimensions:

| | |
|---|---|
| Length | 11.0 mm |
| Width | 15.0 – |
| Length of axis | 7.5 – |
| Width - – anteriorly | 3.0 – |
| – - – posteriorly | 2.0 – |

Remarks: *Goycoia pecoralis* differs from other species of the same genus in having a longer pygidium with narrower, less tapering axis and wider border.

## Undetermined specimens

A librigena (Pl. 1, fig. 18) and a fragment of a pygidium (Pl. 2, fig. 26) fail to show sufficient diagnostic characters, and, accordingly, these speci-

mens must remain undetermined until more complete material has been found.

A pygidium (Pl. 2, figs. 18—19) is considered too fragmentary to be safely determined; it shows the general characters of *Coosella*, but it differs from the hitherto known species in its greater width and more strongly sloping border; the lack of *Coosella* cranidia in the material should be noticed in this connection.

A librigena (Pl. 2, fig. 20) is in several respects similar to that of *Coosia*; the hesitation in generic reference is due to the lack of associated *Coosia* cranidia and to the fact that here we have to do with a somewhat generalized type of librigena, which may occur in several different genera.

## The Age of the Fauna

In papers of 1950, 1951, and 1952 Rusconi has published descriptions of a good number of species of trilobites from Cerrillo El Solitario which were referred to the following genera:

| | | |
|---|---|---|
| *Amphoton?* | *Gallagnostus* | *Notocoryphe* |
| *Asaphellus* | *Geragnostus* | *Ogyginus?* |
| *Bathyurus?* | *Goycoia* | *Olenoides* |
| *Briscoia?* | *Homagnostus* | *Parabriscoia* |
| *Canotagnostus* | *Huarpagnostus* | *Phalacroma* |
| *Canotiana* | *Hypagnostus* | *Prosaukia?* |
| *Clavagnostus* | *Hystricurus?* | *Pseudagnostus* |
| *Cotalagnostus* | *Keithiella* | *Pseudolevinia* |
| *Culipagnostus* | *Levinia* | *Spinagnostus?* |
| *Diplagnostus* | *Mendodiscus* | *Tomagnostus?* |

Nine of these thirty genera, *Canotagnostus*, *Canotiana*, *Culipagnostus*, *Goycoia*, *Huarpagnostus*, *Levinia*, *Mendodiscus*, *Notocoryphe*, and *Pseudolevinia* were published as new genera, and, accordingly, they could not contribute essentially to stratigraphic correlations. Furthermore, these new genera, with the exception of *Canotagnostus*, *Culipagnostus*, *Goycoia*, and *Huarpagnostus*, were placed by contributors to the trilobite volume of the "Treatise of Invertebrate Paleontology" (Lochman and Rasetti 1959) under the heading "Unrecognizable genera".

The stratigraphic range of the other genera (as far as is known) is given in the following table (p. 34) (M.C. = Middle Cambrian, U.C. = Upper Cambrian, L.O. = Lower Ordovician, M.O. = Middle Ordovician).

It appears from this table that eight genera are Middle Cambrian, six genera are Upper Cambrian, four genera are Lower Ordovician, and one genus is Middle Ordovician, whereas one genus is known from Middle and Upper Cambrian and another from Middle Cambrian and Lower Ordovician.

| | M.C. | U.C. | L.O. | M.O. |
|---|---|---|---|---|
| *Amphoton?* | + | | | |
| *Asaphellus* | | | + | |
| *Bathyurus?* | | | | + |
| *Briscoia?* | | + | | |
| *Clavagnostus* | + | + | | |
| *Cotalagnostus* | + | | | |
| *Diplagnostus* | + | | | |
| *Gallagnostus* | + | | + | |
| *Geragnostus* | | | + | |
| *Homagnostus* | | + | | |
| *Hypagnostus* | + | | | |
| *Hystricurus?* | | | + | |
| *Keithiella* | | + | | |
| *Ogyginus?* | | | + | |
| *Olenoides* | + | ? | | |
| *Parabriscoia*[1] | | + | | |
| *Phalacroma* | + | | | |
| *Prosaukia?* | | + | | |
| *Pseudagnostus* | | + | | |
| *Spinagnostus?* | + | | | |
| *Tomagnostus?* | + | | | |

Provided that the generic determinations are correct, the stratigraphic range of the series of strata at Cerrillo El Solitario should be Middle Cambrian to Middle Ordovician, but Rusconi follows another line of reasoning. In 1950 he referred the fossiliferous strata at Cerrillo El Solitario to the Upper Cambrian in saying: "En la fauna del Cerrillo El Solitario hay elementos vinculados a los del Ordovicio basal de otros naciones, pero los más son del cámbrico superior y hasta del cámbrico medio, motivos por el cual sigo creyendo que el horizonte Villavicense, que ha proporcionado los citados organismos corresponden, por lo menos, al cámbrico superior, siendo su fauna distinta de la del cámbrico de San Isidro" (Rusconi 1950 b, p. 85).

In 1951 Rusconi changed his mind and referred the strata to the late

[1] According to Lochman ("Treatise of Invertebrate Paleontology", vol. 0, p. 0254) *Parabriscoia* Kobayashi, 1935 is a synonym of *Elkia* Walcott, 1924.

Middle Cambrian without further ceremony, and this opinion was maintained in the Cambrian symposium of the 20th International Geological Congres in México ("El Sistema Cámbrico, su Paleogeografía y el Problema de su Base", Pt. 2, p. 759). Provided that this is correct, Rusconi's Upper Cambrian and Ordovician elements in the fauna must be accounted for, and the question of the correctness of determinations must be taken into consideration.

The following comments on Rusconi's genera do not comprise his new genera, which are known from Cerrillo El Solitario only, and, accordingly, without importance with regard to the discussion of stratigraphic correlation.[1]

*Amphoton?:* (Rusconi 1950 a, p. 84). Not figured. The occurrence of this Asiatic and Australian genus in Argentina is very improbable.

*Asaphellus:* (Rusconi 1952, Pl. 1, figs. 1—2). The figures show species of two different genera. The specimens differ clearly from *Asaphellus*, and the occurrence of this Tremadocian genus in association with Cambrian genera is very improbable.

*Bathyrus?:* (Rusconi 1950 b, p. 93). Not figured. The occurrence of this Middle Ordovician genus in association with Cambrian genera is very improbable.

*Briscoia?:* (Rusconi 1951, p. 26, fig. 22). The specimen differs greatly from this genus in the shape of its pygidial axis.

*Clavagnostus:* (Rusconi 1950 a, p. 83, fig. 3). This is certainly not *Clavagnostus* (new genus?).

*Cotalagnostus:* (Rusconi 1952, Pl. 1, fig. 12). The generic determination seems to be correct.

*Diplagnostus:* (Rusconi 1952, Pl. 1, fig. 10). The generic determination seems to be correct.

*Gallagnostus:* (Rusconi 1950 a, p. 83, fig. 2). The specimen should be referred to *Phoidagnostus* Whitehouse.

*Geragnostus:* (Rusconi 1950 a, p. 83, fig. 1). The specimens differ clearly from this Tremadocian genus in cephalic and pygidial outline, and in shape and proportions of the glabella and the pygidial axis.

*Homagnostus:* (Rusconi 1950 b, p. 94, fig. 9). This specimen differs greatly from *Homagnostus* in the shape of the pygidial axis and the posterior border; provided that the specimen is correctly figured, the species in question must be regarded as belonging to a new genus.

*Homagnostus:* (Rusconi 1951, p. 26, fig. 21). The specimen differs clearly from *Homagnostus* in the shape and segmentation of the pygidial axis.

*Hypagnostus:* (Rusconi 1952, Pl. 1, figs. 7—9). The generic determination may be correct.

*Hystricurus?:* (Rusconi 1951, p. 26, fig. 27). This very fragmentary specimen differs greatly from *Hystricurus* in the shape of the "glabella", which shows considerable resemblance to the pygidial axis of an agnostid trilobite.

[1] It should be noticed in this connection that most of the present writer's comments are given mainly with regard to Rusconi's figures, as circumstances beyond the writer's control prevented a study of the actual specimens.

*Keithiella?:* (Rusconi 1951, p. 26, fig. 25). The specimen differs clearly from *Keithiella* in the shape of the pygidial axis and the number of axial rings.

*Ogyginus?:* (Rusconi 1950 a, p. 84). Not figured. The occurrence of this Lower Ordovician genus in association with Cambrian genera is very improbable.

*Olenoides:* (Rusconi 1950 a, p. 83, fig. 10). Provided that the specimen (a pygidium) is correctly figured, it differs clearly from *Olenoides* in the shape of the axis and the lack of pleural furrows.

*Parabriscoia:* (Rusconi 1951, p. 26, fig. 23). As mentioned above (p. 34), *Parabriscoia* is a junior synonym of *Elkia* Walcott. The specimen differs from *Elkia* in the location of the pleural furrows.

*Phalacroma:* (Rusconi 1950 b, p. 94, fig. 5). Judging from the figure this may be *Cotalagnostus*.

*Prosaukia:* (Rusconi 1950 a, p. 82). Not figured; the description does not fit in with the characters of *Prosaukia*.

*Pseudagnostus:* (Rusconi 1950 b, p. 94, fig. 6). The short glabella, the lack of a preglabellar longitudinal furrow, and the shape of the pygidial axis clearly show that the specimen should not be referred to the Pseudagnostidae.

*Spinagnostus?:* (Rusconi 1952, Pl. 1, fig. 5). Provided that the specimen is correctly figured, it may be referred to *Spinagnostus*.

*Tomagnostus?:* (Rusconi 1951, p. 26, fig. 29). This "cranideo" is estimated to represent a pygidium of the new genus *Stigmagnostus* (p. 15).

It appears from the above comments that the agnostid genera *Cotalagnostus, Diplagnostus, Hypagnostus,* and *Spinagnostus* may be represented in Rusconi's material, and to these may be added *Phoidagnostus* (= *Gallagnostus* of Rusconi).

The stratigraphic range of many agnostid trilobites is well-known owing to Westergård's excellent monograph of 1946. In the Scandinavian-Baltic region *Cotalagnostus* ranges from the *Tomagnostus fissus* zone to the *Jincella brachymetopa* zone, *Diplagnostus* from the *Ptychagnostus punctuosus* zone to the *Lejopyge laevigata* zone, *Hypagnostus* from the *Tomagnostus fissus* zone to the *Jincella brachymetopa* zone, and *Phoidagnostus* is characteristic of the *Jincella brachymetopa* zone. *Spinagnostus* is known from the *Centropleura vermontensis* zone (St. Albans formation) of northwestern Vermont. Accordingly, the age of the strata of Cerrillo El Solitario appear to be late Middle Cambrian, and the "Upper Cambrian" and "Ordovician" genera in Rusconi's lists of fossils from this locality call for revision.

The material collected by the present writer contains representatives of nine agnostid genera, viz. *Agnostus, Baltagnostus, Clavagnostus, Diplagnostus, Kormagnostus, Oedorhachis, Peronopsis, Phoidagnostus,* and *Stigmagnostus.* The stratigraphic range of five of these genera is well-known in the Acado-Baltic province (Westergård 1946); their vertical distribution is shown in the following table (p. 37).

| Acado-Baltic agnostid genera from Cerrillo El Solitario | UPPER CAMBRIAN | MIDDLE CAMBRIAN | | | | | |
|---|---|---|---|---|---|---|---|
| | *Agnostus pisiformis* | *Lejopyge laevigata* | *Jincella brachymetopa* | *Triplagnostus lundgreni* and *Goniagnostus nathorsti* | *Ptychagnostus punctuosus* | *Hypagnostus parvifrons* | *Tomagnostus fissus* and *Ptychagnostus atavus* | *Triplagnostus gibbus* | *Paradoxides pinus* | *Paradoxides insularis* |
| | | | | | | | *Paradoxides paradoxissimus* | | | |
| | | | | *Paradoxides forchhammeri* | | | | | | *Paradoxides oelandicus* |
| *Agnostus* | + | + | + | | | | | | | |
| *Clavagnostus* | | + | + | | | | | | | |
| *Diplagnostus* | | + | + | + | + | | | | | |
| *Peronopsis* | | | + | + | + | + | + | + | + | |
| *Phoigagnostus* | | | + | | | | | | | |
| **Cotalagnostus* | | | + | | + | + | + | | | |
| **Hypagnostus* | | | + | + | + | + | + | | | |

* Genera not represented in the writer's material.

It clearly appears from the vertical distribution of agnostid genera shown in the above table that the age of the fauna of Cerrillo El Solitario is late Middle Cambrian and that the strata constitute a strati-

graphic equivalent of the Acado-Baltic *Paradoxides forchammeri* stage, most probably the *Jincella brachymetopa* zone.

The occurrence of *Bolaspidella* in the material is of special interest. This genus is characteristic of the so-called Pacific province of North America, and its presence in the Cerrillo El Solitario fauna must be regarded as an indication of stratigraphic and correlative importance. The species of *Bolaspidella* are dominant faunal elements in the late Middle Cambrian *Bolaspidella* zone although in the Upper Cambrian cratonic realms of Texas (Llano uplift), Montana-northern Wyoming, and in the Upper Cambrian intermediate realm of Vermont and Gaspé this genus penetrates into the *Cedaria* zone of the Dresbachian (Lochman & Wilson 1958). In the *Bolaspidella* zone of the Pacific province of North America the genus *Bolaspidella* is associated with *Baltagnostus*,[1] and this is also the case in the Cerrillo El Solitario fauna. As mentioned above, the Acado-Baltic agnostid genera in the Cambrian fauna of Cerrillo El Solitario constitute strong evidence that the strata of this locality should be correlated with the *Jincella brachymetopa* zone of the Acado-Baltic *Paradoxides forchhammeri* stage, and the association of these elements with the Pacific *Bolaspidella* and *Baltagnostus* indicates that the Cerrillo El Solitario strata, the *Jincella brachymetopa* zone, and the *Bolaspidella* zone should be regarded as stratigraphic equivalents.

It is well-known that during the greater part of the Cambrian period the Pacific and the Acado-Baltic provinces were very effectively separated from each other; for this reason it has been postulated that a barrier, the so-called New Brunswick geanticline, extended along the northwest margin of the Acadian geosyncline so as to prevent the mingling of the faunas from the two separate realms. However, Howell (1937) described the *Centropleura vermontensis* fauna from the St. Albans formation of northwestern Vermont in which *Centropleura* and another Acado-Baltic genus, *Elyx*, are found associated with Pacific ones, *inter alia Bolaspidella*. This fauna was placed by Howell & Duncan (1939, p. 5) as late Middle Cambrian, and it was regarded as a little younger than the *Paradoxides forchhammeri* fauna. However, in Scandinavian areas of continuous sedimentation (alum shale series) the *Paradoxides forchhammeri* stage constitutes the very top of the Middle Cambrian, and the youngest zone of this stage, the *Lejopyge laevigata* zone, is followed without hiatus by the lowermost zone of the Upper Cambrian, the *Agnostus pisiformis* zone; in view of this fact the youngest

[1] Lowermost part of the Riley formation (central Texas) and Conasauga shale (S. Appalachians).

possible Acado-Baltic stratigraphic equivalent of the St. Albans formation must be the *Lejopyge laevigata* zone of the *Paradoxides forchhammeri* stage. In consideration of the fact that *Centropleura vermontensis* appears to be very closely related to species in the *Jincella brachymetopa* zone of the Acado-Baltic province and that in Scandinavia species of *Elyx* have not been found above this level, the present writer is of opinion that the St. Albans formation should be regarded as a stratigraphic equivalent of the *Jincella brachymetopa* zone.

It is a remarkable fact that in northwestern Vermont and in the Mendoza region of Argentina invasion of late Middle Cambrian Acado-Baltic trilobite genera into the Pacific province took place simultaneously.

In addition to the Cerrillo El Solitario locality other Middle Cambrian occurrences are known from the Zonda region west-northwest of the city of San Juan and from the San Isidro region west of the city of Mendoza; these somewhat older Middle Cambrian occurrences belong to the *Glossopleura* zone, as pointed out by V. Poulsen (1958); thus the Middle Cambrian remained Pacific up to *Bolaspidella* time, when Acado-Baltic invasion changed the character of the fauna. The data at hand suggest a transgressive tendency in late Cambrian time leading to mingling of Pacific and Acado-Baltic faunas in the western hemisphere.

The palaeogeographical conditions in South America during the Cambrian are practically unknown owing to the lack of satisfactory evidence, but in the writer's opinion it seems probable that the Acado-Baltic invasion penetrated into the Mendoza region via the Jujuy embayment of Harrington & Leanza (1957, p. 42); the existence of this embayment in the northern Argentine has been ascertained by these authors on the basis of a magnificent fossiliferous series of Ordovician formations with a pronounced Acado-Baltic affinity.

## Zonal division in Cerrillo El Solitario

In 1956 Rusconi published a table, representing his interpretation of the Middle Cambrian sequence of strata in the Mendoza region; in this table he introduces a division of the Cambrian of Cerrillo El Solitario ("Horizonte Villavicense") into five zones, and a number of species are referred to each of them. Such zonal division had not been accomplished in 1955, when the present writer visited the locality, and owing to the fact that the expedition was about to leave the Argentine, it was necessary to concentrate on the collection of fossils from a greatly fossiliferous limestone bed on top of the

hill very close to the southern slope; therefore, it is not the writer's intention to take up a definite attitude with reference to the zonal division proposed by Rusconi; one observation, however, must be mentioned. The material described in the present paper contains well-preserved specimens of *Goycoia tellecheai* Rusconi, which was presented by Rusconi as characteristic of Zone 1, and specimens of *Phoidagnostus solitariensis* (Rusconi), which was presented as characteristic of Zone 4, are found associated with the former. This fact is mentioned only to indicate that further collection and study may be necessary in order to establish a safe basis for zonal division of the series of strata.

# References


Harrington, H. J. & Leanza, A. F. (1957): "Ordovician Trilobites of Argentina". — Dept. of Geol., Univ. of Kansas, Special Publication No. 1.

Howell, B. F. (1937): "Cambrian *Centropleura vermontensis* Fauna of northwestern Vermont". — Bull. Geol. Soc. America, Vol. 48, pp. 1147—1210.

Howell, B. F. & Duncan, D. (1939): "Middle-Upper Cambrian Transition Faunas of North America." — Bull. Wagner free Inst. Sci., Vol. 14, No. 1.

Hupé, P. (1953): "Classification des trilobites". — Ann. Paléont. (Paris), Vol. 39.

Lochmann, C. (1940): "Fauna of the basal Bonneterre Dolomite (Upper Cambrian) of southeastern Missouri". — Journal of Paleontology, Vol. 14, No. 1.

Lochman, C. & Duncan, D. (1944): "Early Upper Cambrian Faunas of Montana". — Geol. Soc. America, Special Papers, No. 54.

Lochman, C. & Wilson, J. L. (1958): Cambrian Biostratigraphy in North America". — Journal of Paleontology, Vol. 32, No. 2.

Palmer, A. R. (1954): "The Faunas of the Riley Formation in Central Texas". — Journal of Paleontology, Vol. 28, No. 6.

Poulsen, V. (1958): "Contributions to the Middle Cambrian Paleontology and Stratigraphy of Argentina". — Det Kongelige Danske Videnskabernes Selskab, Matematisk-fysiske Meddelelser, Vol. 31, No. 8.

Rasetti, F. (1944): "Upper Cambrian Trilobites from the Lévis Conglomerate". — Journal of Paleontology, Vol. 18, No. 3.

Raymond, P. E. (1924): "New Upper Cambrian and Lower Ordovician Trilobites from Vermont". — Proc. Boston Soc. Nat. Hist., Vol. 37, pp. 389—466.

Resser, C. E. (1937): "Third contribution to nomenclature of Cambrian trilobites". — Smiths. Misc. Coll., Vol. 95, No. 22.

Resser, C. E. (1938): "Cambrian System (restricted) of the Southern Appalachians". — Geol. Soc. America, Special Papers, No. 15.

Rusconi, C. (1950 a): "Trilobitas y otros organismos del Cámbrico de Canota". — Rev. Mus. Hist. Nat. Mendoza, Vol. 4, pp. 71—84.

Rusconi, C. (1950 b): "Nuevos Trilobitas y otros organismos del Cámbrico de Canota". — Rev. Mus. Hist. Nat. Mendoza, Vol. 4, pp. 85—94.

Rusconi, C. (1951): "Más Trilobitas Cámbricos de San Isidro, Cerro Pelado y Canota". — Rev. Mus. Hist. Nat. Mendoza, Vol. 5, pp. 3—30.

Rusconi, C. (1952): "Varias especies de Trilobitas del Cámbrico de Canota". — Rev. Mus. Hist. Nat. Mendoza, Vol. 6, pp. 5—17.

Rusconi, C. (1954): "Trilobitas Cámbricos de la Quebradita Obliqua, Sud del Cerro Aspero". — Rev. Mus. Hist. Nat. Mendoza, Vol. 7, pp. 3—59.

Rusconi, C. (1955): "Fossiles Cámbricos y Ordovícios al Oeste de San Isidro, Mendoza". — Rev. Mus. Hist. Nat. Mendoza, Vol. 8, pp. 3—64.

Rusconi, C. (1956): "Correlationes Cambro-Ordovicicas entre Mendoza y Norte America". — 20. Congresso Geológico Internacional, Mexico: "El Sistema Cámbrico su Paleogeografía y el Problema de su Base" (Symposium), Pt. 2, pp. 751—762.

Shaw, A. B. (1952): "Paleontology of Northwestern Vermont, 2. Fauna of the Upper Cambrian Rockledge Conglomerate near St. Albans". — Journal of Paleontology, Vol. 26, No. 3.

Walcott, C. D. (1912): "Cambrian Brachiopoda". — Monogr. U. S. Geol. Surv., Vol. 51.

Walcott, C. D. (1916): "Cambrian Geology and Paleontology 3, No. 5, Cambrian Trilobites". — Smiths. Misc. Coll., Vol. 64, No. 5.

Westergård, A. H. (1946): "Agnostidea of the Middle Cambrian of Sweden". — Sveriges Geologiska Undersökning, Ser. C., No. 477.

Whitehouse, F. W. (1936): "The Cambrian Faunas of North-Eastern Australia", Pt. 1—3. — Mem. Queensland Mus., Vol. 11, Pt. 1; Vol. 11, Pt. 3.

Indleveret til Selskabet den 1. april 1960.
Færdig fra trykkeriet den 11. august 1960.

# PLATES

## Plate 1


| | | | Page |
|---|---|---|---|
| Fig. | 1. | *Dicellomus* sp. ind., ventral valve, × 10 | 5 |
| - | 2. | *Orthotheca* sp., dorsal face, × 5 | 5 |
| - | 3—4. | *Agnostus exsulatus* n. sp. Fig. 3, cephalon (holotype), × 5; fig. 4, pygidium, × 5. | 6 |
| - | 5—6. | *Baltagnostus hospitus* n. sp. Fig. 5, cephalon, × 5; fig. 6, pygidium (holotype), × 5. | 7 |
| - | 7. | *Baltagnostus mendozensis* n. sp., two pygidia (the larger specimen is the holotype) × 5 | 8 |
| - | 8. | *Oedorhachis australis* n. sp., pygidium (holotype), × 5 | 13 |
| - | 9. | *Diplagnostus jarillensis* Rusconi?, cephalon, × 10 | 10 |
| - | 10. | *Kormagnostus? propinquus* n. sp., cephalon, (holotype), × 5 | 11 |
| - | 11—12. | *Stigmagnostus canotensis* (Rusconi) Fig. 11, cephalon, × 10; fig. 12, pygidium, × 5. | 15 |
| - | 13. | *Peronopsis ultima* n. sp., pygidium (holotype), × 10 | 13 |
| - | 14. | *Clavagnostus chipiquensis* (Rusconi), pygidium, × 10 | 9 |
| - | 15. | *Phoidagnostus solitariensis* (Rusconi), pygidium, × 5 | 14 |
| - | 16—17. | *Prometeoraspis canotensis* n. sp., dorsal and lateral views of cranidium (holotype), × 3 | 17 |
| - | 18. | Genus et sp. ind., librigena, × 1.5 | 32 |
| - | 19—24. | *Williamsina cortesi* n. sp. Fig. 19—21, dorsal, frontal, and lateral views of cranidium (holotype), × 3; fig. 22, librigena, × 3; fig. 23—24, dorsal and lateral views of pygidium, × 3. | 19 |
| - | 25—28. | *Williamsina mikkelseni* n. sp. Fig. 25—27, dorsal, lateral, and frontal views of cranidium (holotype), × 3; fig. 28, pygidium, × 3. | 21 |
| - | 29. | *Williamsina harringtoni* n. sp., pygidium (holotype), × 3 | 20 |


1


3

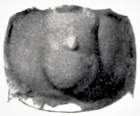
4


5


2

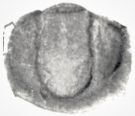
6


7

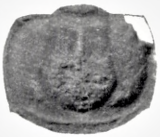
8

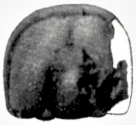
9


10


11


13


14

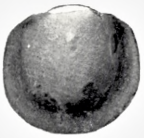
15


12


22

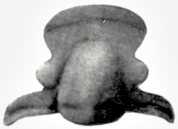
19


20


21


27


16


24


23


29


26


17


18


28


25

## Plate 2


| | | Page |
|---|---|---|
| Fig. 1. | *Williamsina ornata* n. sp., pygidium (holotype), × 3 | 22 |
| - 2— 8. | *Talbotinella communis* n. sp. Fig. 2, cranidium, × 1.5; fig. 3—5, dorsal, frontal, and lateral views of cranidium (holotype), × 1.5; fig. 6, librigena, × 1.5; fig. 7—8, dorsal and lateral views of associated pygidium, × 3. | 24 |
| - 9—12. | *Talbotinella leanzai* n. sp. Fig. 9—11, dorsal, lateral, and frontal views of cranidium (holotype), × 3; fig. 12, librigena, × 1.5. | 25 |
| - 13—15. | *Talbotinella rusconii* n. sp., dorsal, lateral, and frontal views of cranidium without posterior areas of fixigenae (holotype), × 1.5 | 27 |
| - 16—17. | *Bolaspidella lucieae* n. sp. Fig. 16, cranidium (holotype), × 15; fig. 17, librigena, × 10. | 28 |
| - 18—19. | Genus et sp. ind., dorsal and lateral views of fragmentary pygidium, × 1.5 | 33 |
| - 20. | Genus et sp. ind., librigena, × 1.5 | 33 |
| - 21—22. | *Canotaspis aliena* n. sp. Fig. 21, dorsal view of cranidium (holotype), × 10; fig. 22, lateral view of the same, × 14. | 29 |
| - 23. | *Goycoia brevicauda* n. sp., pygidium (holotype), × 1.5 | 31 |
| - 24. | *Goycoia tellecheai* Rusconi, large pygidium, × 1.25 | 30 |
| - 25. | *Goycoia pecoralis* n. sp., pygidium (holotype), × 1.5 | 32 |
| - 26. | Genus et sp. ind., fragmentary pygidium, × 1 | 32 |

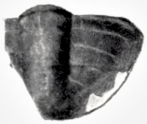
1


2


3


6

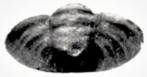
7


8


4


5

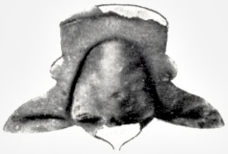
9


10


11


12


13


16


17


14


18


21


15


19


20


22


23


24

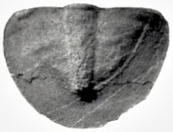
25


26

## Plate 3


Page

Fig. 1. *Williamsina ornata* n. sp., pygidium (holotype), showing surface markings on border, × 15 ..... 22

– 2. *Talbotinella communis* n. sp., cranidium, showing surface markings, × 7.5 ..... 24

1

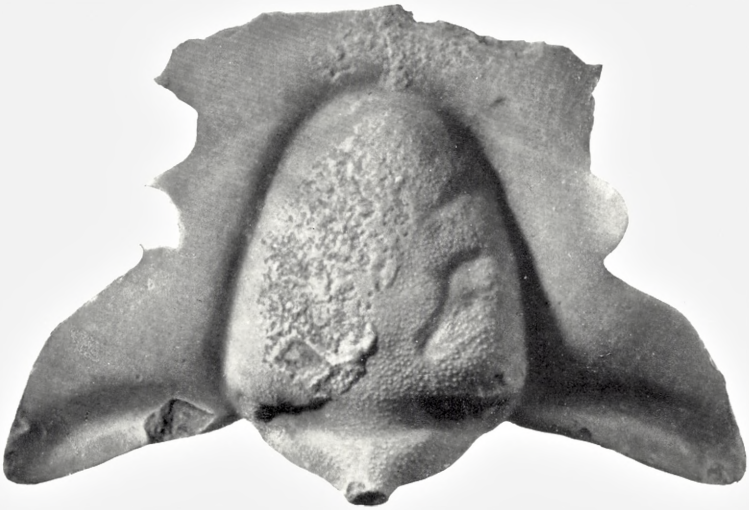

2

Matematisk-fysiske Meddelelser
udgivet af
Det Kongelige Danske Videnskabernes Selskab
Bind **32,** nr. 12

Mat. Fys. Medd. Dan. Vid. Selsk. **32,** no. 12 (1960)

# HALF LIVES OF FIRST EXCITED STATES OF EVEN NUCLEI OF Em, Ra, Th, U, and Pu

BY

R. E. BELL, S. BJØRNHOLM, AND J. C. SEVERIENS


København 1960
i kommission hos Ejnar Munksgaard

# CONTENTS


Pages

1. Introduction ..... 3
2. Experiments and Results ..... 5
   (a) $Th^{226}$ (72 keV), $Ra^{222}$ (111 keV), $Em^{218}$ (325 keV) ..... 6
   (b) $Th^{230}$ (53 keV), $U^{230}$ (51.7 keV) ..... 14
   (c) $Ra^{224}$ (84 keV) ..... 20
   (d) $Em^{220}$ (241 keV) ..... 21
   (e) $Em^{222}$ (187 keV) ..... 22
   (f) $Ra^{226}$ (68 keV) ..... 23
   (g) $Th^{234}$ (48 keV) ..... 24
   (h) $Ra^{228}$ (59 kev) ..... 29
   (i) $Th^{228}$ (57.8 keV) ..... 30
   (j) $Th^{232}$ (50 keV), $U^{232}$ (47 keV), $U^{234}$ (43 keV), $U^{236}$ (45 keV), $Pu^{238}$ (44 keV), and $Pu^{240}$ (43 keV) ..... 34
   (k) $U^{238}$ (45 keV) ..... 40
3. Discussion ..... 41

References ..... 48


## Synopsis


The half lives of the first excited states of eighteen even nuclei of Em, Ra, Th, U, and Pu have been measured, and an upper limit has been set for a nineteenth. The measurements were made by the delayed coincidence method, using a fast time-to-amplitude converter. The experimental half lives were all found to lie between 1.5 and $7.6 \times 10^{-10}$ sec. The results are used to calculate reduced transition probabilities, quadrupole moments, and deformation parameters for the nuclei concerned. Comparisons are made between these values and recent theoretical calculations. Agreement within 10 % or less is found. As by-products of the present work, upper limits have been set for the half lives of two excited states in $Th^{230}$ and $U^{233}$, and the calculated $E2$ conversion coefficients of Rose have been verified within about 15 % for this region of $Z$ and energy.



Printed in Denmark
Bianco Lunos Bogtrykkeri A-S

# 1. Introduction

The measurements to be described here constitute an experimental survey of the half lives of first excited states of even nuclei between $Em^{218}$ and $Pu^{240}$. This part of the periodic table is one of the two most prominent regions showing large stable deformations of the nuclei, the other one being the rare earth region extending roughly from samarium to wolfram. The even nuclei in these regions show the typical spectrum of rotation of a deformed axially symmetric structure, viz., a band of energy levels of character $0+, 2+, 4+, \ldots$ having energies closely given by

$$E = \frac{\hbar^2}{2\Im} I(I+1). \tag{1}$$

Equation (1) and the other equations to follow are conveniently collected in the review paper of ALDER *et al.*[1]). From the observation of these energy levels, the effective moment of inertia, $\Im$, is at once known. The actual amount of distortion of the nucleus cannot be deduced from $\Im$, however, without more detailed knowledge of the nuclear motion.

Experimentally, the nuclear quadrupole deformation is derived from measurements of the pure electric quadrupole transition rate between adjacent levels in the rotational band, usually between the $0+$ ground state and the $2+$ first excited state. This rate may be measured either by measuring the cross section for Coulomb excitation of the $2+$ state from the $0+$ ground state, or by measuring the half life, $T_{1/2}$, of the reverse gamma transition $(2+ \rightarrow 0+)$ in a radioactive source. Given this half life, the rate of gamma ray emission $(2+ \rightarrow 0+)$ is $T(E2;\ 2 \rightarrow 0) = (ln\,2)\ [(1+\alpha)\ T_{1/2}]^{-1}$, where $\alpha$ is the total conversion coefficient; then

$$T(E2;\ 2 \rightarrow 0) = \frac{4\pi}{75} \frac{1}{\hbar} \left(\frac{E}{\hbar c}\right)^5 B(E2;\ 2 \rightarrow 0), \tag{2}$$

where $B(E2;\ 2 \rightarrow 0)$ is the reduced transition probability. The quantity found in Coulomb excitation experiments is

$$B(E2;\,0\to2) = 5\,B(E2;\,2\to0) \tag{3}$$

on grounds of statistical weight. If this transition probability is due to rotation of a deformed nucleus of intrinsic quadrupole moment $Q_0$, we may find $Q_0$ from

$$B(E2;\,0\to2) = 5\,(16\,\pi)^{-1}\,e^2\,Q_0^2. \tag{4}$$

If the nuclear shape is spheroidal, we may use the distortion parameter $\beta$ given by

$$\beta = \frac{4}{3}\left(\frac{\pi}{5}\right)^{1/2}\frac{\Delta R}{R_0} = 1.06\,\frac{\Delta R}{R_0},$$

where $\Delta R$ is the difference between the major and minor semi-axes, and $R_0$ is the mean radius. The value of $\beta$ may now be calculated from $Q_0$ by the use of

$$Q_0 = 3\,(5\,\pi)^{-1/2}\,Z\,R_0^2\,\beta\,(1 + 0.16\,\beta + \ldots). \tag{5}$$

Thus, an experimental half life leads directly to an experimental $Q_0$ and $\beta$ for the nucleus in question.

The nuclear moment of inertia depends on the structure of the intrinsic nucleonic motion.

If the nucleons in the rotating nuclear field behaved as completely independent particles, the effective moment of inertia would be approximately that corresponding to rigid rotation,

$$\Im_{\text{rig}} = \frac{2}{5}\,\text{AMR}_0^2\,(1 + 0.31\,\beta + \ldots), \tag{6}$$

where A is the atomic number and M the nucleon mass. Residual interactions between the nucleons in addition to the interaction included in the average binding field give rise to correlations in the intrinsic motion, which reduce the moment.

In the other extreme, if the residual interaction were so strong as to break down the independent-particle motion completely, the effective moment of inertia would approach the hydrodynamic value, equivalent to a wave travelling irrotationally on the surface of a liquid drop. In that case,

$$\Im_{\text{irrot}} = \frac{2}{5}\,\text{AMR}_0^2\,\beta^2\,(0.89 + 0\,(\beta^2)). \tag{7}$$

In fact, the moments of inertia are found to lie between the extremes, their actual values furnishing information on the strength of the residual

interactions between nucleons. Recently, methods have been developed for incorporating effects of these residual interactions (the pairing correlations). It has thereby become possible to make a more detailed comparison between theory and experiment than was previously feasible. This question will be raised again in the discussion section of this paper.

Before the present work was done, transition probabilities had been well studied in the rare earth region both by Coulomb excitation and by lifetime measurements, while comparatively little was known of the heavy element region. Among the heavy even nuclides, half lives had been measured for the first excited states of $Em^{220}$, $Ra^{224}$, and $Ra^{226}$, and Coulomb excitation measurements existed for $Th^{232}$ and $U^{238}$. Details of these existing measurements are given later, in the experimental section of this paper. (The nuclides just mentioned are included in the present study, in one case with a different result ($Em^{220}$)). The reason for the lack of lifetime data is that the experimental half lives lie close to the limit of present day delayed coincidence techniques, around $10^{-10}$ sec for the low energies involved. The reason for the lack of Coulomb excitation data is that all the nuclides concerned are radioactive, and target preparation becomes difficult or impossible. Four Coulomb excitation results are available for odd nuclides in this region ($U^{233}$, $U^{235}$, $Np^{237}$, $Pu^{239}$).[1] We have avoided odd nuclides in this work for two reasons. First, the rotational transitions in odd nuclei contain strong $M1$ admixtures with the $E2$ part, thus shortening the experimental half lives to be measured, and rendering the interpretation less definite. Second, odd nuclei display effective moments of inertia 15 to 50 % greater than their even neighbours, owing to the presence of the extra odd particle.[1] They are therefore not immediately comparable with even nuclei.

## 2. Experiments and Results

The apparatus used for the half life measurements was a fast time-to-amplitude converter generally similar to that described by Green and Bell[2], but with a number of modifications. Some of these are described briefly in a paper by Bell and Jørgensen[3]. The circuit employed RCA-6342A photomultipliers and organic scintillators, often made of NE 102 plastic. In a typical measurement, an alpha emitter having a branch feeding the desired excited state was sandwiched between two organic scintillators, one detecting the alpha particles and the other the conversion electrons of the transition from the excited state to the ground state. The time-to-amplitude

converter then produces an output pulse spectrum that represents the distribution of time delays between the preceding alpha particles and the subsequent conversion electrons. (Occasionally, the preceding radiation was beta or gamma rays rather than alpha particles.) From this spectrum, observed with a 100 channel pulse analyzer, the half life of the excited state can be read off. In every case, the instrumental time resolution was good enough to allow the half life to be found directly from the logarithmic slope of the recorded time distribution.

The calibration of the pulse amplitude spectrum in terms of time is done by lengthening the cable delay from one of the counters by a measured amount, and observing the shift of the distribution along the amplitude scale. A standard error of 3 % has been adopted to take account of any errors in this procedure. The standard error in any particular measurement reported here varies with the circumstances, but the 3 % just mentioned forms a lower limit.

The individual sections to follow are arranged approximately in the chronological order in which the measurements were performed. All statements about the radioactive properties of the various sources are taken from standard compilations, usually STROMINGER, HOLLANDER, and SEABORG[4], except where separate references are given. Chemical and physical procedures for the preparation and mounting of the sources are given in each case.

### (a) $Th^{226}$ (72 keV), $Ra^{222}$ (111 keV), $Em^{218}$ (325 keV)

The measurements on these three excited states were made using a single source of $U^{230}$ and its descendants in equilibrium. The procedures will be described in detail, both because they are typical of those used in all the other cases, and because the $U^{230}$ source is the most complex one used in this study.

The activity was obtained from a source of $Pa^{230}$ (18 *d*), which decays to $U^{230}$ (21 *d*) by a 15 % beta branch. The $Pa^{230}$ had been made by a 65 MeV, 4 $\mu$amp-hour proton bombardment on 0.3 g of thorium metal.* The protactinium was separated from thorium and fission products by anion exchange. First it was absorbed on Dowex 1 from a 12 N HCl solution, allowing the thorium to pass through the ion exchange column. The protactinium was then eluted with a 2 N HCl solution. The procedure was repeated using

* We are indebted to Ing. ÅKE SVANHEDEN and the crew of the cyclotron of The GUSTAF WERNERS INSTITUTE, Uppsala, for carrying out the bombardment.

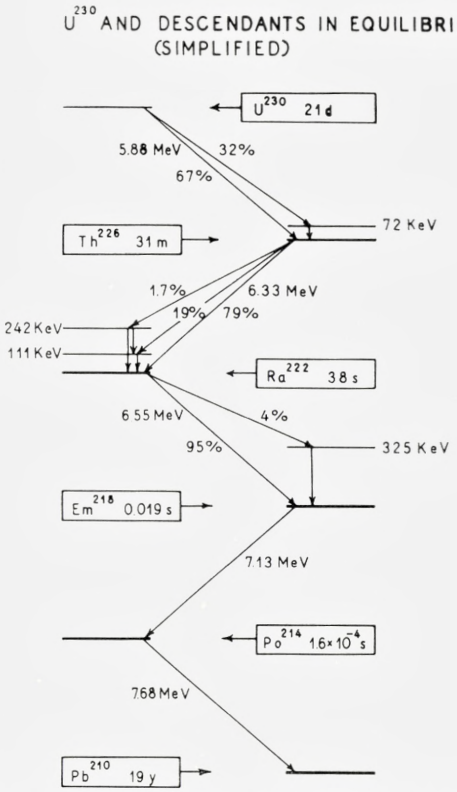


Fig. 1. A simplified decay scheme of $U^{230}$ and its descendants. All branches of less than 1% intensity are omitted.

a solution 9 N in HCl and 0.006 N in HF as eluant. Finally, a third cycle was made using the former eluant. The protactinium sample contained all the isotopes from $Pa^{228}$ to $Pa^{233}$, but only $Pa^{230}$ gives rise to a uranium daughter of any appreciable activity. After letting $U^{230}$ grow in for about three weeks, a separation of protactinium and uranium was performed. The activity was again absorbed on Dowex 1 from 12 N HCl and eluted with the above mentioned HCl-HF mixture, uranium remaining on the column. $U^{230}$ was eluted with a 0.5 N HCl solution and the purification cycle was repeated. After evaporation of the HCl solution the source was ready. No visible material was present, as should also be expected.

$U^{230}$ is the parent of a chain of five successive alpha decays, ending (for our purposes) with 19 year $Pb^{210}$. A simplified decay scheme of this

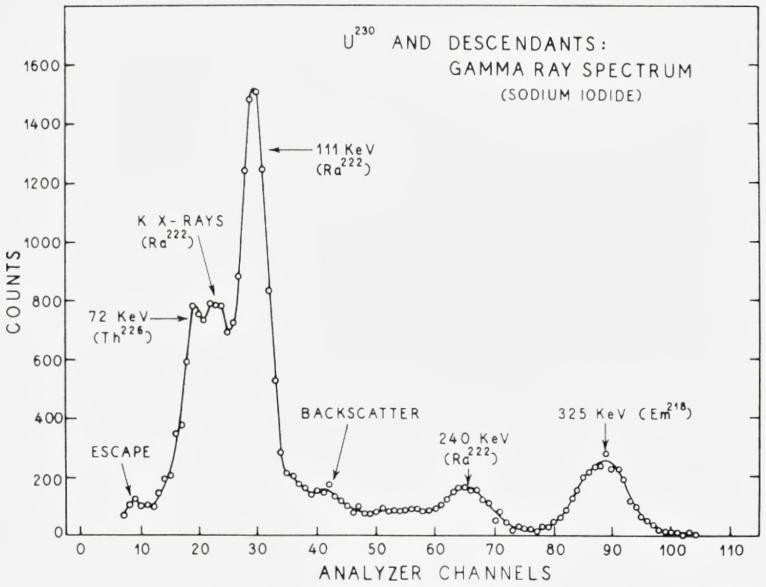


Fig. 2. The gamma ray spectrum of $U^{230}$ and its descendants, seen in a sodium iodide scintillation counter.

chain is shown in fig. 1, in which all branches of less than 1% intensity have been omitted. All the observations made on our $U^{230}$ source are consistent with this scheme in energy and intensity. Before the $U^{230}$ source was finally mounted, its X- and gamma-rays were observed with a sodium iodide counter. The result, fig. 2, shows radiations that are easily identified from fig. 1, and no others. Fig. 2 shows that the source is free of $Pa^{230}$, which has strong K X-rays and high energy gamma rays. The fact that the 325 keV gamma ray is the highest-energy one of appreciable intensity is used later in the measurement of $Em^{218}$.

The $U^{230}$ activity was deposited on a 0.020 mg/cm$^2$ plastic foil and covered with a 0.15 mg/cm$^2$ aluminium foil. This pair of foils was sandwiched between two discs of NE-102 plastic phosphor, each 20 mm in diameter and 2 mm thick, which in turn were coupled to two RCA-6342A photomultipliers. The whole assembly constituted a pair of independent $2\pi$ counters working on the same source. The total source strength in all five members of the decay chain was about $3 \times 10^4$ disintegrations per second.

The pulse height spectrum of one of the $2\pi$ counters is shown in fig. 3. The spectrum is dominated by a broad peak at about 250 keV equivalent

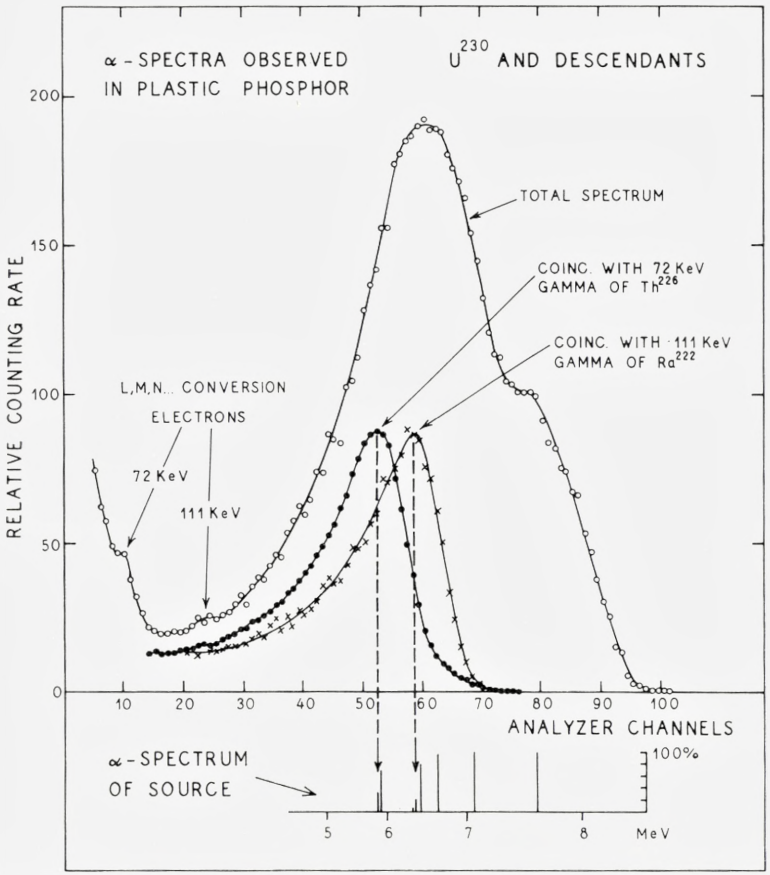


Fig. 3. The pulse height spectrum of $U^{230}$ and its descendants, seen in a 2 mm thick plastic phosphor. Two coincidence alpha spectra are also shown. A separate scale at the bottom shows the alpha energy scale.

*electron* energy, caused by the $\approx 6$ MeV alpha particles. This peak shows only faint signs of resolution into its component alpha energies. At lower energies there are slight indications of the LMN . . . conversion peaks of the 72 keV and 111 keV radiations of $Th^{226}$ and $Ra^{222}$, respectively. (The coincident alpha peaks in fig. 3 are discussed later.)

A pulse height window was set to cover the broad alpha peak in fig. 3, and was left there for all the subsequent observations. The counter so arranged may now be designated the alpha counter. The spectrum of pulses from the other scintillation counter (the electron counter) coincident

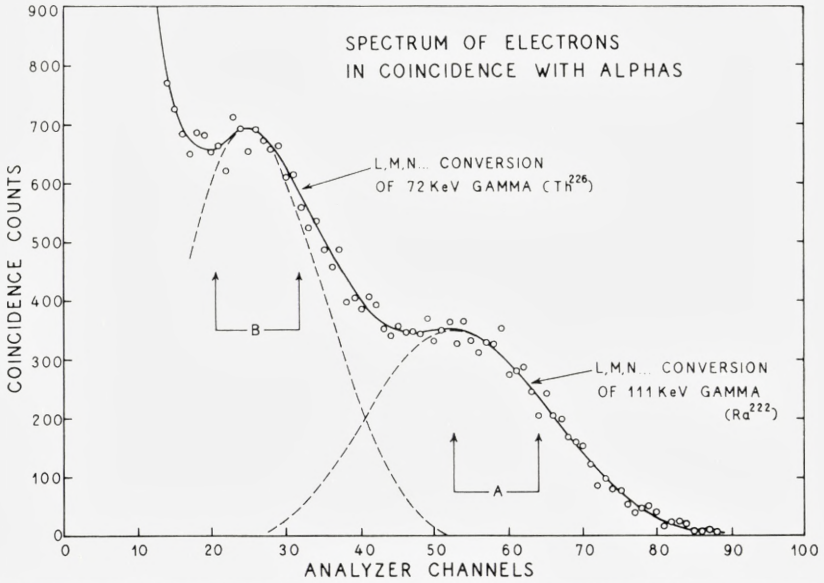


Fig. 4. The pulse height spectrum in a 2 mm plastic phosphor of conversion electrons in coincidence with alpha particles, for $U^{230}$ and its descendants. The dashed curves are illustrative only. The two pulse height windows A and B were used in the half life measurements.

with these alpha pulses is shown in fig. 4. Two broad peaks appear, corresponding to the LMN . . . conversion of the 72 and 111 keV transitions of $Th^{226}$ and $Ra^{222}$, respectively. Broken lines in fig. 4 indicate in a rough way how the two peaks may be separated.

The two pulse height windows A and B in fig. 4 enable us to detect the 111 and 72 keV transitions almost independently. For verification of this fact, we refer again to fig. 3. Here we have plotted the spectra of alpha pulses coincident with the 72 and 111 keV transitions. The two alpha peaks so revealed are clearly separate. It still cannot be excluded that some pulses from the 111 keV transition are mixed with those from the 72 keV transition, perhaps to the extent of a few percent. Fortunately the two transitions turn out to have half lives only about 30 % apart; the possible admixture effect has been taken into account by assigning fairly generous standard errors to the measured half lives.

The two coincident alpha peaks, plus the partially resolved high energy alpha group in the singles spectrum, allow us to attach a rough scale of alpha energies at the bottom of fig. 3, with the alpha spectrum of the source. The scale is non-linear, as expected for a plastic phosphor.

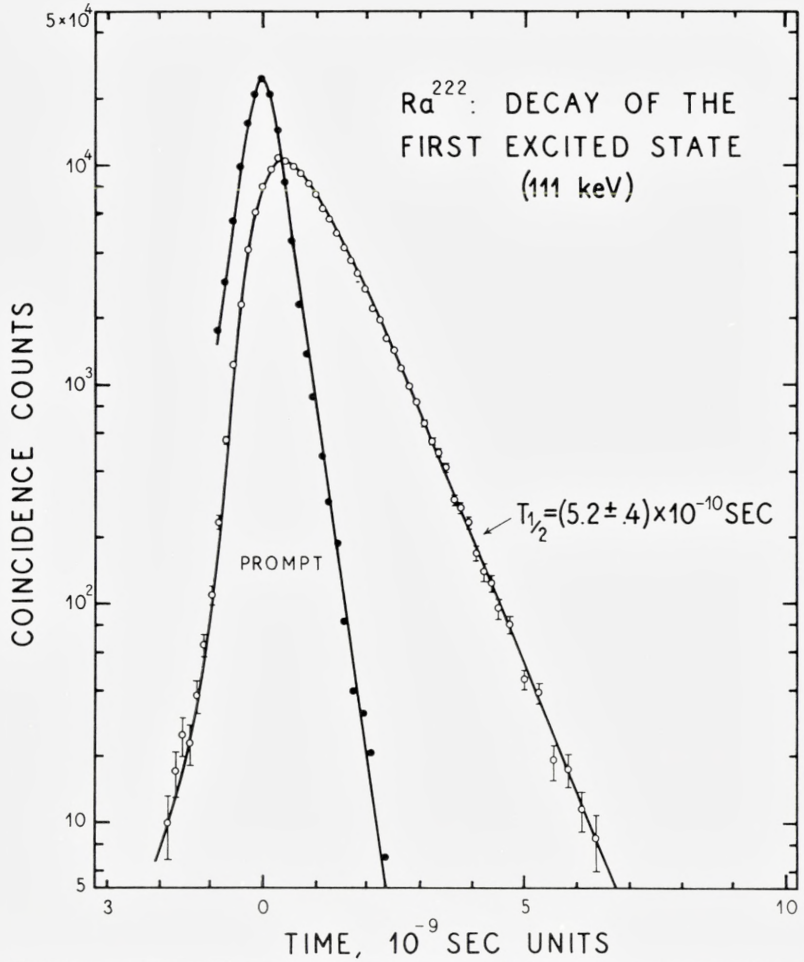


Fig. 5. The time analysis of the coincidences between alpha particles and conversion electrons of the 111 kev radiation of $Ra^{222}$. A prompt resolution curve is shown for illustrative purposes.

The time analysis of coincidences between alpha particles and the 111 keV radiation of $Ra^{222}$ (pulse height window A, fig. 4) is shown in fig. 5. The half life read from this curve is $(5.2 \pm 0.4) \times 10^{-10}$ sec. The prompt resolution curve shown in fig. 5 is included, for illustrative purposes only, to show that the slope of the 111 keV curve is real and not instrumental. This prompt curve was made by partially removing the aluminium foil separating the alpha counter from the electron counter, so that a little light from each alpha

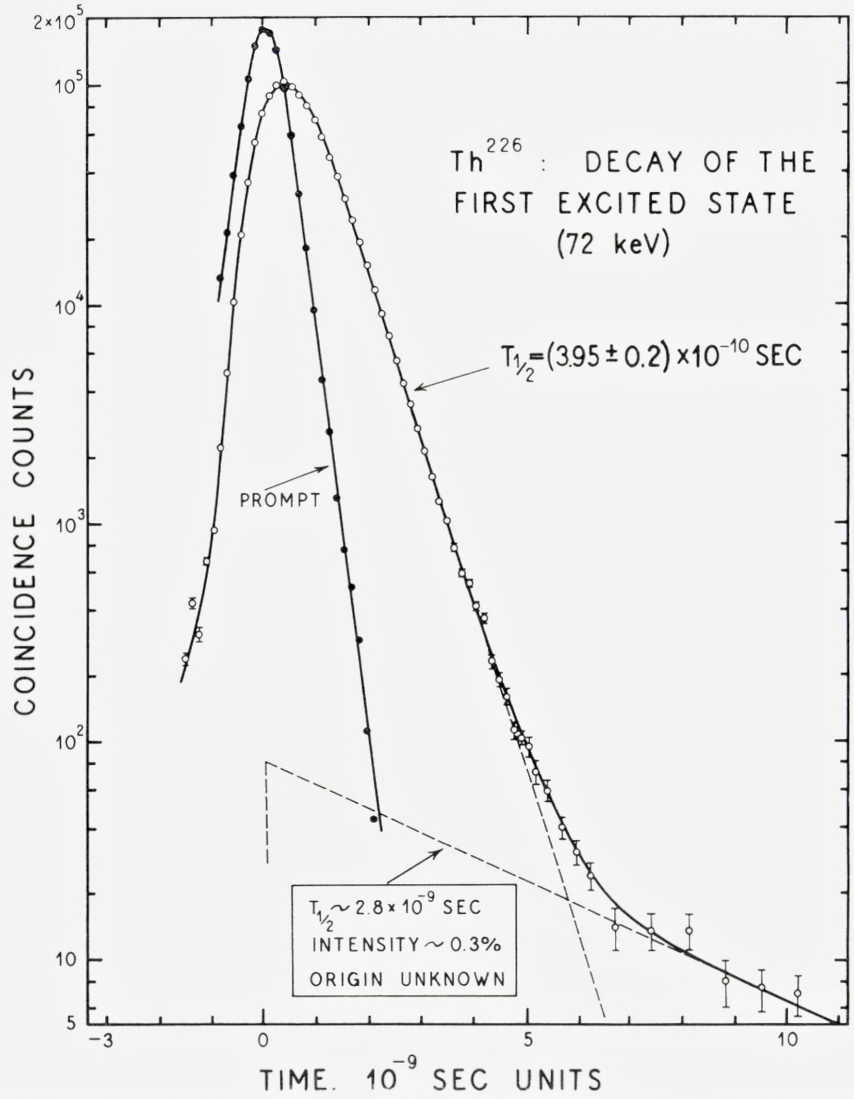


Fig. 6. The time analysis of the decay of the first excited state of $Th^{226}$. A weak component of longer half life has been subtracted. A prompt resolution curve is shown for illustrative purposes.

scintillation could enter the electron counter. In this way every alpha pulse is made to yield a true coincidence, with no change of discriminator settings. (No claim is made that this procedure yields a highly accurate prompt

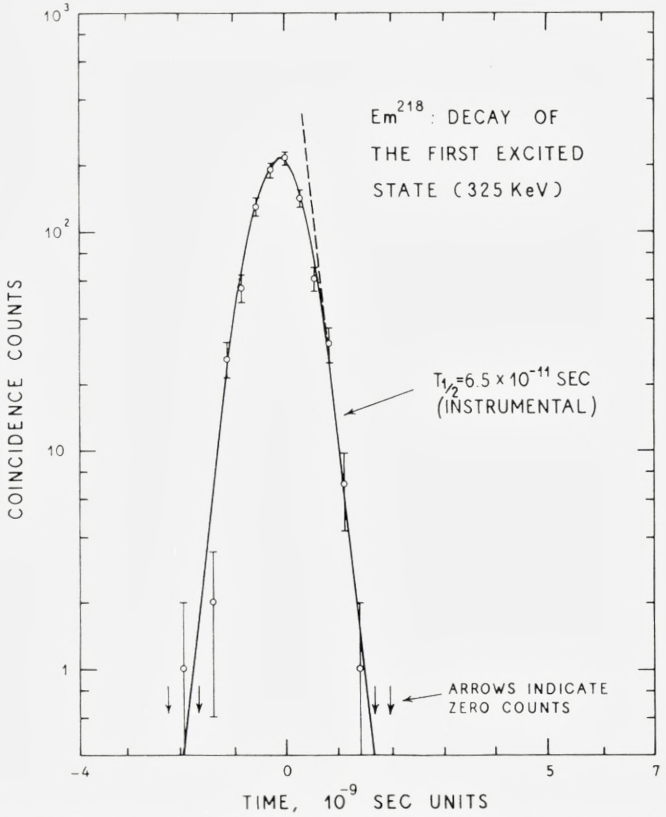


Fig. 7. The time analysis of the decay of the first excited state of $Em^{218}$. No half life longer than $6.5\times10^{-11}$ sec was observed, and the experimental limit has been taken as $8\times10^{-11}$ sec.

resolution curve; an accurate curve should be somewhat narrower and steeper than the one shown.)

The time analysis of the 72 keV radiation of $Th^{226}$ (pulse height window *B*, fig. 4) is shown in fig. 6. The half life read from this curve is $(3.95\pm0.2)\times10^{-10}$ sec. A prompt curve is also shown, made in the same way as that described in the previous paragraph. At the foot of the 72 keV curve there appears a weak component (total intensity 0.3 % of the 72 keV curve) with a half life of about $2.8\times10^{-9}$ sec. This component is so weak that its presence does not interfere with the accuracy of reading the main half life. Its origin could be in any one of several very weak radiations not shown in the decay scheme of fig. 1, or in some minor impurity in the source. We can

speculate that its energy must be low, because it appears in the 72 keV curve, but not in the 111 keV curve. It was not investigated further.

The final observation on the $U^{230}$ chain concerned the 325 keV first excited state of $Em^{218}$. For this measurement the electron counting crystal was removed and a 15 mm thick diphenylacetylene (DPA) gamma counter was put in place of it, shielded by enough aluminium to stop all electrons. By the use of auxiliary radioactive sources, this counter was biased to respond only to gamma rays above 250 keV. Reference to fig. 2 shows that this counter then detects only the 325 keV gamma ray of $Em^{218}$. The time analysis for this radiation is given in fig. 7. The curve shows only the instrumental resolution of the apparatus, with a slope on its right-hand edge corresponding to $T_{\frac{1}{2}} = 6.5 \times 10^{-11}$ sec. We may therefore state conservatively that the half life of the 325 keV level of $Em^{218}$ is less than $8 \times 10^{-11}$ second.

### (b) $Th^{230}$ (53 keV), $U^{230}$ (51.7 keV)

$Pa^{230}$ (18 *d*) decays both by electron capture to $Th^{230}$ (85 %) and by beta emission to $U^{230}$ (15 %). The electron capture decay to $Th^{230}$ is accompanied by plentiful high energy gamma rays (400 keV to 950 keV), many of which feed the first excited state at 53 keV. The beta decay to $U^{230}$ has no high energy gamma rays. Thus, coincidences between high energy gamma rays and low energy conversion electrons are due solely to the first excited state of $Th^{230}$. As we shall see, no such simple selection scheme applies to $U^{230}$, and the results for this nucleus are of lower accuracy.

The source of mixed protactinium activities mentioned in the preceding section (a) was used in the present measurement. The half lives of the protactinium isotopes are such that after a few weeks only $Pa^{230}$, and possibly $Pa^{233}$ (27 *d*), remain in the source. Under the bombarding conditions mentioned (65 Mev protons), the cross section for the formation of $Pa^{230}$ largely exceeds that of $Pa^{233}$, therefore the activity will be relatively pure $Pa^{230}$. The protactinium fraction from the protactinium-uranium separation already described could thus be used as source of $Pa^{230}$. The lifetime measurements were performed within one day after chemical separation, to avoid complications from the growth of $U^{230}$ (21 *d*) and its daughters.

In order to estimate the amount of $Pa^{233}$ present in the source, a comparison was made between the sodium iodide gamma spectrum of our $Pa^{230}$ source and that of a source of pure $Pa^{233}$ of roughly known strength. No $Pa^{233}$ was detected, and an upper limit of 10 % could be set for the abundance of $Pa^{233}$ in the $Pa^{230}$ source.

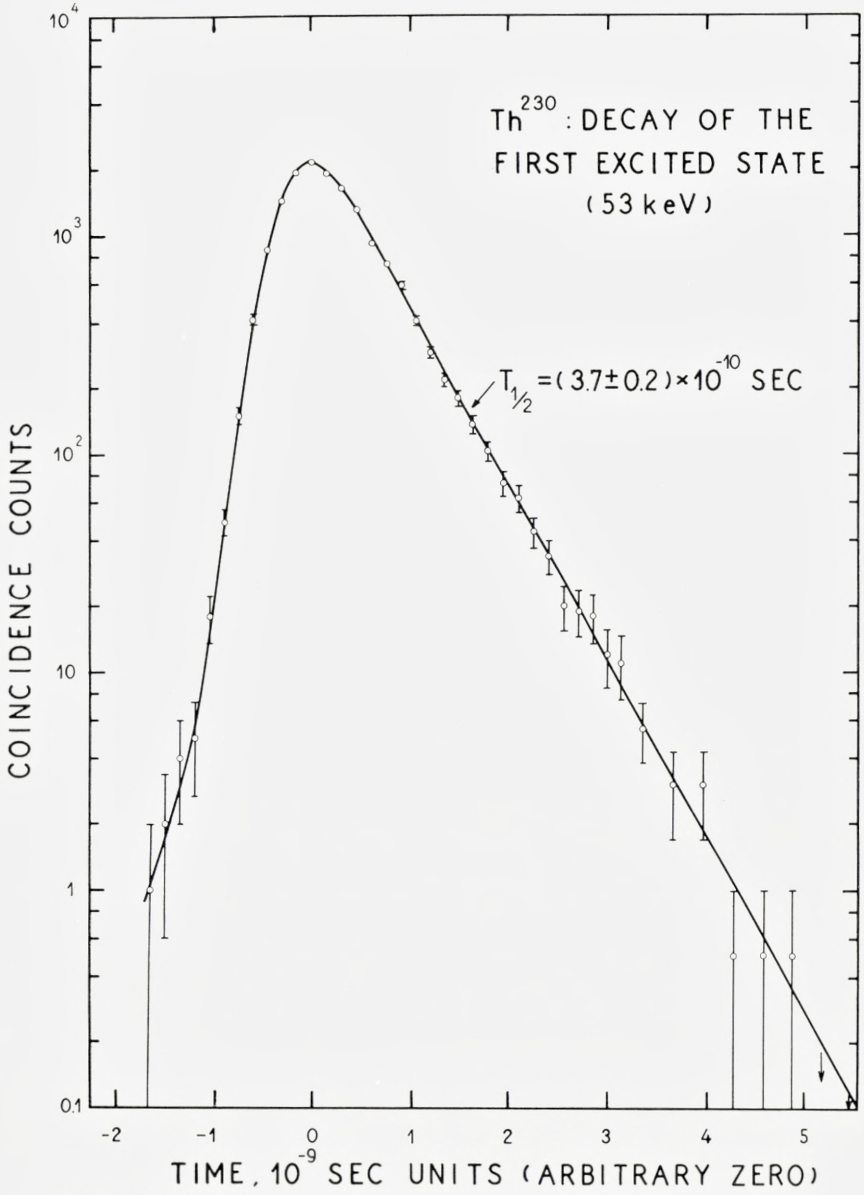


Fig. 8. The time analysis of the decay of the first excited state of $Th^{230}$.

As a control experiment, a lifetime measurement was made on a $Pa^{233}$ source in the same manner as for the $Pa^{230}$ source, described below. The yield of coincidences was small, and no half life in excess of $10^{-10}$ sec was present. We are thus assured that the $Pa^{230}$ results are not disturbed by the presence of a possible small impurity of $Pa^{233}$. A second control experiment consisted of a gamma-gamma coincidence experiment on the $Pa^{230}$ source before it was finally mounted, which showed that the intermediate states between high energy gamma rays in $Th^{230}$ have half lives less than $10^{-10}$ sec. As a result of these control experiments we can say definitely that the 508 keV level of $Th^{230}$ and the 313 keV level of $U^{233}$ have half lives less than $10^{-10}$ sec.

For the measurement of the $Th^{230}$ 53 keV half life, the source of $Pa^{230}$ was mounted on a 2 mm thick plastic phosphor. A 15 mm thick DPA gamma counter was placed next to this source, and adjusted to accept pulses from gamma rays above 600 keV, i.e., principally the $\approx 900$ keV gamma rays feeding the 53 keV state. The low energy electrons in the plastic counter in coincidence with these gamma rays showed a clean peak due to LMN... conversion electrons of the 53 keV transition, with even a hint of resolution of the MN... peak. A broad pulse height window was placed on this peak, and the coincidence resolution curve was measured. The result, fig. 8, shows a clean decay with a half life of $(3.7 \pm 0.2) \times 10^{-10}$ sec for the 53 keV state.

The measurement of the half life of the 51.7 keV excited state of $U^{230}$ is more difficult. The preceding radiation is the weak beta decay branch of $Pa^{230}$, with end point energy 360 keV, but this spectrum is overlain by conversion lines from the stronger electron capture branch. The gamma counter mentioned in the preceding paragraph was removed and a 2 mm plastic electron counter was substituted for it. The pulse spectrum of this counter showed evidence of discrete groups (conversion lines) in addition to the desired continuum, but the resolution was of course not good enough to enable us to choose any pulse height region that avoided the conversion lines. Under these conditions, the resolution curves will show a mixture of the desired $U^{230}$ lifetime and the unwanted $Th^{230}$ lifetime already measured. Several curves were measured with different biases on the beta counter (the bias on the original conversion electron counter remaining fixed), and the one with the best ratio of $U^{230}$ effect to $Th^{230}$ effect is shown in fig. 9. The curve was purposely run to a very high statistical accuracy; it shows the expected mixture of the known half life of the $Th^{230}$ excited state, $3.7 \times 10^{-10}$ sec, and a shorter half life due to the $U^{230}$ excited state. The resolution of this decay curve into its two components would be very difficult if it were not for the fact that we already know the longer half life accurately. The

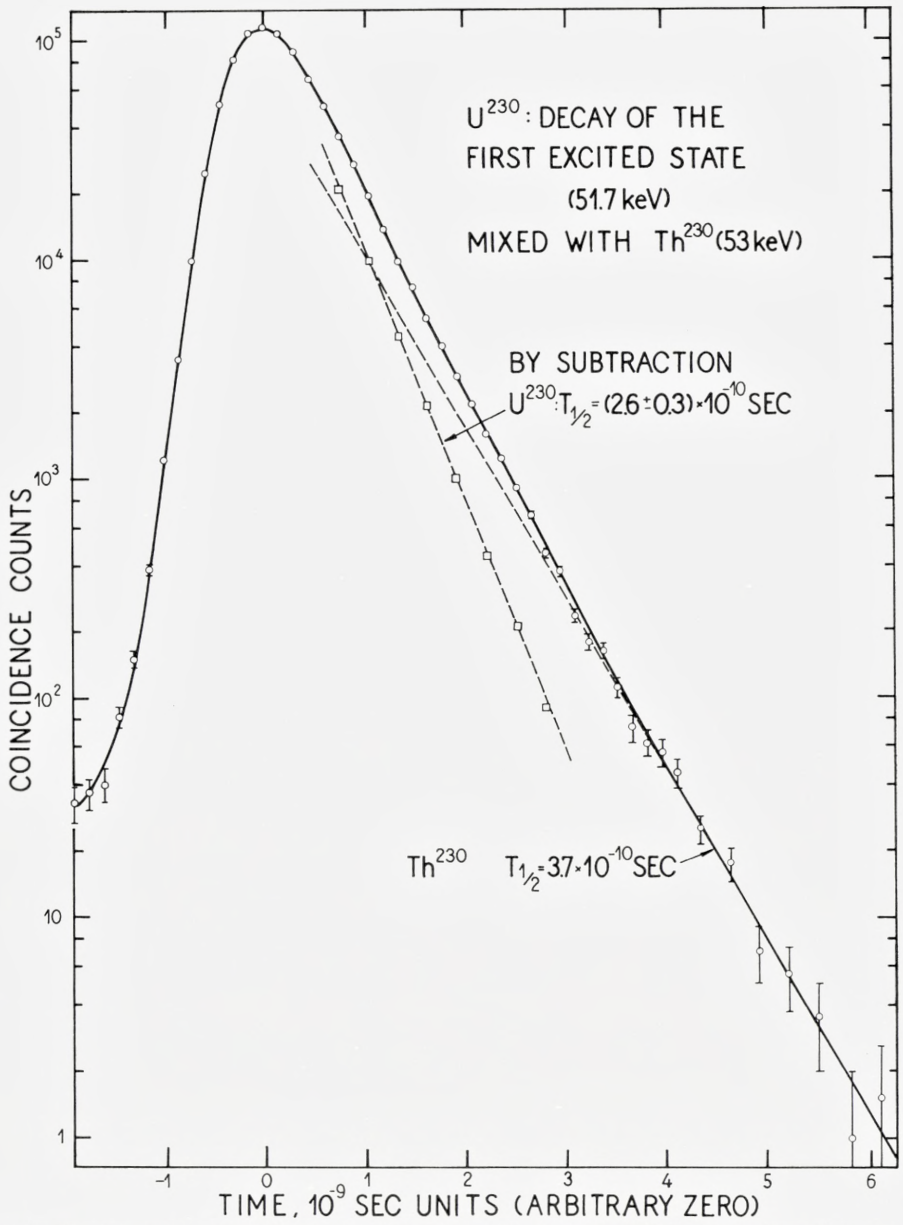


Fig. 9. The time analysis of the decay of the first excited state of $U^{230}$. The subtraction shown is assisted by prior knowledge of the longer half life (see section (b) and fig. 8).

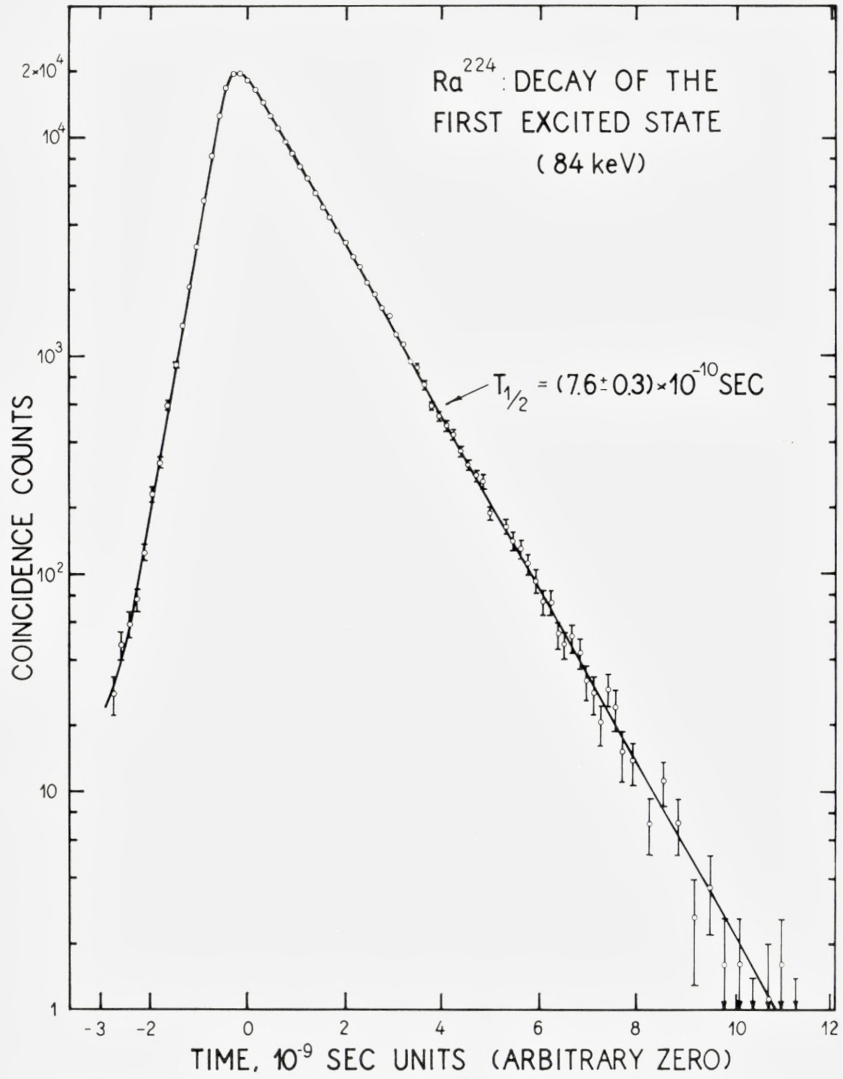


Fig. 10. The time analysis of the decay of the first excited state of $Ra^{224}$.

subtraction indicated by broken lines in fig. 9 yields a half life of $2.6 \times 10^{-10}$ sec for the first excited state of $U^{230}$. The error to be quoted in this value is to some extent a matter of judgement. Adjusting the position of the subtracted component ($Th^{230}$) causes a variation in the result for the half life

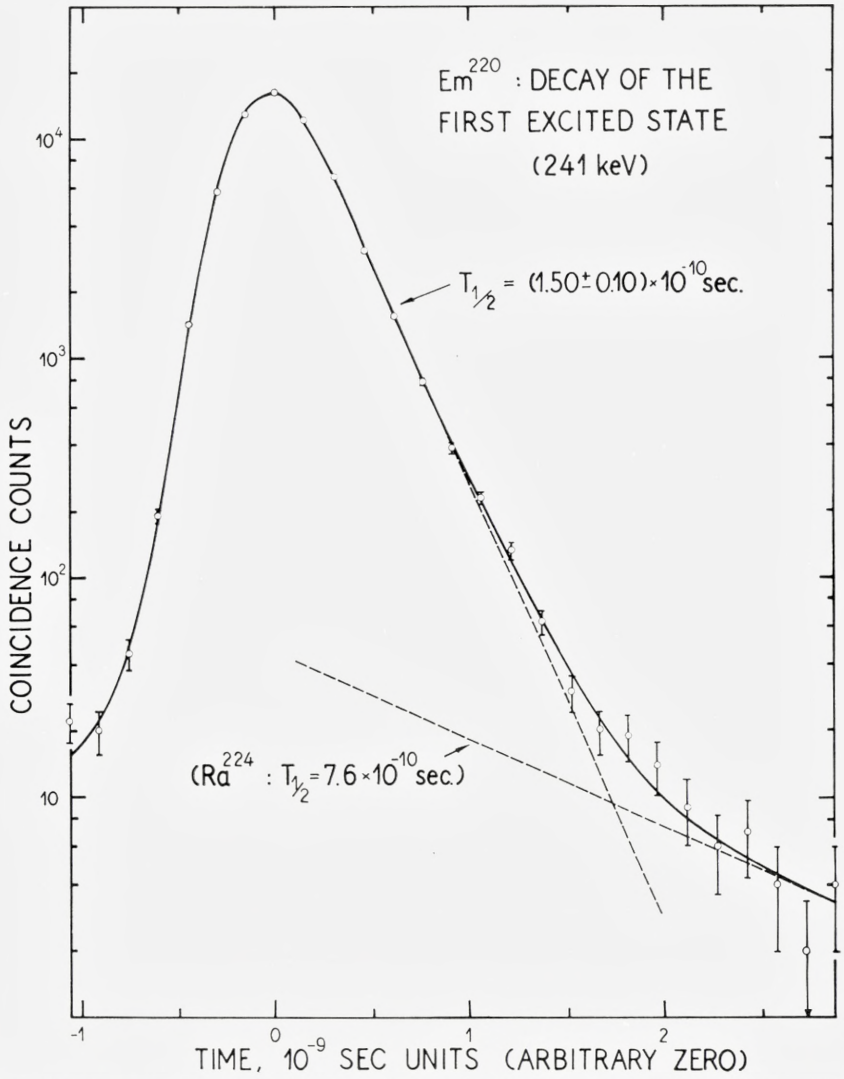


Fig. 11. The time analysis of the decay of the first excited state of $Em^{220}$. A small contribution from $Ra^{224}$ has been subtracted.

of the remainder ($U^{230}$); we take, as the limits of our standard error, the half lives outside which the remainder curve shows a distinct curvature. In this way we arrive at the value $(2.6 \pm 0.3) \times 10^{-10}$ sec. The fractional error quoted is larger than that of most of the other measurements in this series.

It would be worth while to have a better value for this half life. Since $Pa^{230}$ is the only radioactivity that populates the excited state of $U^{230}$ to an appreciable extent, the sole way to observe the $U^{230}$ decay alone is to use magnetic selection to resolve the radiations leading to $U^{230}$ from the stronger ones leading to $Th^{230}$. We were not equipped to do this at the time the source was available.

### (c) $Ra^{224}$ (84 keV)

The half life of this excited state has been measured previously by SIEKMAN and DE WAARD[5] both by the delayed coincidence method (centroid shift) and by the recoil method (Doppler shift of conversion line). Their results were $T_{\frac{1}{2}} = (7.5 \pm 1.5) \times 10^{-10}$ sec and $T_{\frac{1}{2}} = (7.0 \pm 1.0) \times 10^{-10}$ sec, respectively. SEVERIENS and RICHTER[6] have found a value $T_{\frac{1}{2}} = (6.0 \pm 1.6) \times 10^{-10}$ sec by another recoil method. VARTAPÉTIAN[7] finds $T_{\frac{1}{2}} = (8.4 \pm 0.7) \times 10^{-10}$ sec by delayed coincidences, again using the centroid-shift method.

The present measurement was made using a source of $Th^{228}$ (RdTh, 1.9 *y*), an alpha emitter having a 28 % branch to the 84 keV state of $Ra^{224}$. The source was prepared from a sample of $Th^{228}$ in equilibrium with its daughter activities. Of these $Ra^{224}$ (3.6 *d*) and $Pb^{212}$ (10 *h*) have the longest half lives. Once these two activities are removed, the remaining daughters soon die away. In order to prepare the $Th^{228}$ free of radium and lead, the activity was absorbed on a cation exchange column. The column was eluted with 7 N HCl, which removed lead and radium. Thorium was eluted with a 1 M ammonium lactate buffer of pH $\approx 3.4$. The volume of the resin filling of the ion exchange column was chosen to be very small (15 $\mu$l). The purified thorium activity was therefore present in a very small volume, $< 5$ $\mu$l, which was spread over an area of one square centimeter and dried. In this way a source thickness much less than 0.5 mg/cm$^2$ was assured.

All the measurements on the half life of the 84 keV state of $Ra^{224}$ were completed within 10 hours of the chemical separation, in order to minimize complications arising from the growth of the 3.6 day $Ra^{224}$ and its descendants. The source material was deposited on the surface of a piece of 10 mg/cm$^2$ plastic phosphor (NE 102), so that only alpha particles could produce large pulses with appreciable probability. The conversion electron counter was a 2 mm thick plastic phosphor separated from the alpha counter by a 0.15 mg/cm$^2$ aluminium foil. The spectrum of electron pulses in coincidence with alpha pulses showed a peak due to LMN... conversion of the 84 keV gamma ray, and a pulse height window was set on this peak.

The time analysis of the resulting coincidences is shown in fig. 10, and yields the result $T_{\frac{1}{2}} = (7.6 \pm 0.3) \times 10^{-10}$ sec for the 84 keV state of $Ra^{224}$. Within their errors, all the previously measured values agree with this one.

### (d) $Em^{220}$ (241 keV)

The source of $Th^{228}$ used for the measurement of the $Ra^{224}$ excited state (see the preceding section (c)) was allowed to stand for two days so as to accumulate an appreciable amount of the 3.6 *d* $Ra^{224}$ daughter and its descendants. $Ra^{224}$ is an alpha emitter having a 5 % branch to the 241 keV excited state of $Em^{220}$. For the measurement of this state, the alpha counter was left unchanged, and the electron counter was covered with 11 mg/cm$^2$ of aluminium, sufficient to stop all alpha particles and all electrons of energy lower than about 90 keV. The pulse spectrum of the electron counter in coincidence with alpha particles showed two clearly resolved peaks corresponding to K and LMN... conversion of the 241 keV gamma ray. The K/LMN... ratio was about 0.7, in agreement with expectation for an $E2$ gamma ray of this energy. A pulse height window was set on the LMN... peak, and the time analysis of the resulting coincidences is shown in fig. 11. The curve shows a decay with $T_{\frac{1}{2}} = (1.50 \pm 0.10) \times 10^{-10}$ sec, followed by a weak tail having a half life near the value $7.6 \times 10^{-10}$ sec appropriate to the 84 keV level of $Ra^{224}$, already measured. The tail is presumably due to a few 84 keV gamma rays dissipating their full energy in the electron counter. The presence of this tail does not in any case interfere with the evaluation of the main half life in fig. 11. The further descendants of $Ra^{224}$, extending to $Pb^{208}$, do not include any alpha emitters having appreciable branching to excited states with energies high enough to register in the electron counter. Two other runs, of lower statistical accuracy, were made on this excited state. In one of them, the pulse height window in the electron counter was moved from the LMN... peak to the K peak. In the other, the electron counter was replaced by a 15 mm thick DPA gamma counter biased to detect the 241 keV gamma rays. In both cases, the result was in agreement with that given above. A final check was made to ensure that the half life found was not dangerously close to the limit of resolution of the apparatus. For this purpose, the thin alpha counter was removed and replaced by a 2 mm plastic phosphor. The counters were reassembled and a 5 $\mu$C source of $Na^{22}$ was placed nearby. There was enough scattering between the counters of secondary electrons produced by the gamma radiation from this source

to give a small prompt coincidence counting rate, with the same biases on the counters as before. The resulting resolution curve had a slope on its right hand side corresponding to $T_{\frac{1}{2}} = 7.5 \times 10^{-11}$ sec, about as expected; thus, the measured half life is twice as large as the experimental limit at this energy. (The same conclusion might have been drawn from fig. 11 by noting that its left-hand side has a slope corresponding to a half life of $7 \times 10^{-11}$ sec.) We therefore give the value $T_{\frac{1}{2}} = (1.50 \pm 0.10) \times 10^{-10}$ sec for the 241 keV excited state of $Em^{220}$.

J. G. SIEKMAN[8] has measured this half life by the delayed coincidence method (centroid shift), using a resolving time of about $7 \times 10^{-9}$ sec. He measured coincidences between alpha particles and the K conversion line of the 241 keV gamma ray focused in a magnetic spectrometer. His result, $T_{\frac{1}{2}} = (3.1 \pm 1.1) \times 10^{-10}$ sec, differs from the present result by a factor of 2, but his lower limit of error is not far above our value.

### (e) $Em^{222}$ (187 keV)

$Ra^{226}$ (1620 *y*) is an alpha emitter having a 6 % branch to the 187 keV excited state of $Em^{222}$ (3.8 *d*).* The further descendants are the well-known radium series ending at $Pb^{206}$. $Ra^{226}$ free of its decay products was prepared in the following way. A few $\mu$g of $RaCl_2$ were dissolved in 0.1 N HCl and absorbed on a cation exchange column, which was then eluted with 7 N HCl. The drops coming out of the column were collected on separate counting discs and dried. These samples were counted in an alpha counter, and their decay was followed for 24 hours; in addition, their gamma activity was checked, using a sodium iodide scintillator and an oscilloscope displaying the pulse height spectrum. The radium fraction was clearly identified at the expected elution position; lead, bismuth, and (presumably) polonium were eluted first, followed by radium. The radium was found to be quite pure. It was stored in a solution of 0.1 N HCl through which air was bubbled, so that $Em^{222}$ and its short-lived daughters were prevented from growing in. The source was mounted just before the beginning of the lifetime measurements which were completed within 6 hours.

The $Ra^{226}$ source material was mounted directly on a 10 mg/cm$^2$ plastic phosphor, and covered with enough aluminium (6.3 mg/cm$^2$) to prevent any alpha particles from reaching the electron counter. The latter, as usual,

* While this manuscript was in preparation, FOUCHER published a value for the half life of this excited state. His value, $(3.5 \pm 1.0) \times 10^{-10}$ sec, is in good agreement with ours (R. FOUCHER, Comptes Rend. **249**, 2310 (1959)).

was a 2 mm thick plastic phosphor. The pulse spectrum of the electron counter in coincidence with alpha particles showed a large peak corresponding to LMN. . . conversion of the 187 keV gamma ray. A pulse height window was set on this peak. The time analysis of the resulting alpha-electron coincidences is depicted in fig. 12. The curve shows a clean decay, giving a value $T_{\frac{1}{2}} = (3.2 \pm 0.2) \times 10^{-10}$ sec for the 187 keV excited state of $Em^{222}$.

### (f) $Ra^{226}$ (68 keV)

The half life of the 68 keV excited state of $Ra^{226}$ has been measured by VARTAPÉTIAN and FOUCHER[9] using the delayed coincidence method (centroid shift), with resolving time $8 \times 10^{-9}$ sec. They found $T_{\frac{1}{2}} = (6.3 \pm 0.7) \times 10^{-10}$ sec.

The 68 keV level of $Ra^{226}$ is excited by a 24 % branch in the alpha decay of $Th^{230}$ (ionium, $8 \times 10^4$ *y*). This activity was obtained from a one year old source of $Th^{234}$ (24 *d*), containing some $Th^{230}$. The source was originally made by extracting thorium from reactor grade natural uranyl nitrate, and very carefully purifying the thorium fraction. In natural uranium, $U^{238}$ and $U^{234}$ are in radioactive equilibrium. $U^{238}$ gives rise to the $Th^{234}$ activity, while $U^{234}$ decays into $Th^{230}$. In view of the very long half life of $Th^{230}$, only a very small amount of activity will have grown in. From the alpha activity present in the source we concluded that the $Th^{230}$ had grown in for about two years, which appears reasonable. The alpha activity was 0.03 $\mu$C. In order to check the purity, an alpha spectrum was made, using a Frisch grid ionization chamber.* The spectrum showed only one group of alpha particles with energy 4.66 Mev, as expected (actually 4.68 and 4.61 Mev, unresolved). The beta activity ($Th^{234}$) was about 0.01 $\mu$C, but this contamination could not interfere with the measurements.

The procedure for measuring this half life was exactly the same as for the 84 keV level of $Ra^{224}$, described in (*c*) above. The time analysis for the present case is shown in fig. 13. This particular source was ideal in strength and thinness, and it yielded the best decay curve observed in this study. (Few radioactivities of whatever lifetime have had their decay plotted over five decades in a single experiment.) The half life found from this curve is $(6.3 \pm 0.2) \times 10^{-10}$ sec, the assigned error of 3 % being entirely due to uncertainty of the time-to-amplitude calibration. It is gratifying that the previous measurement of VARTAPÉTIAN and FOUCHER agrees exactly with this value.

* We are indebted to Mag. N. O. ROY POULSEN for making this measurement.

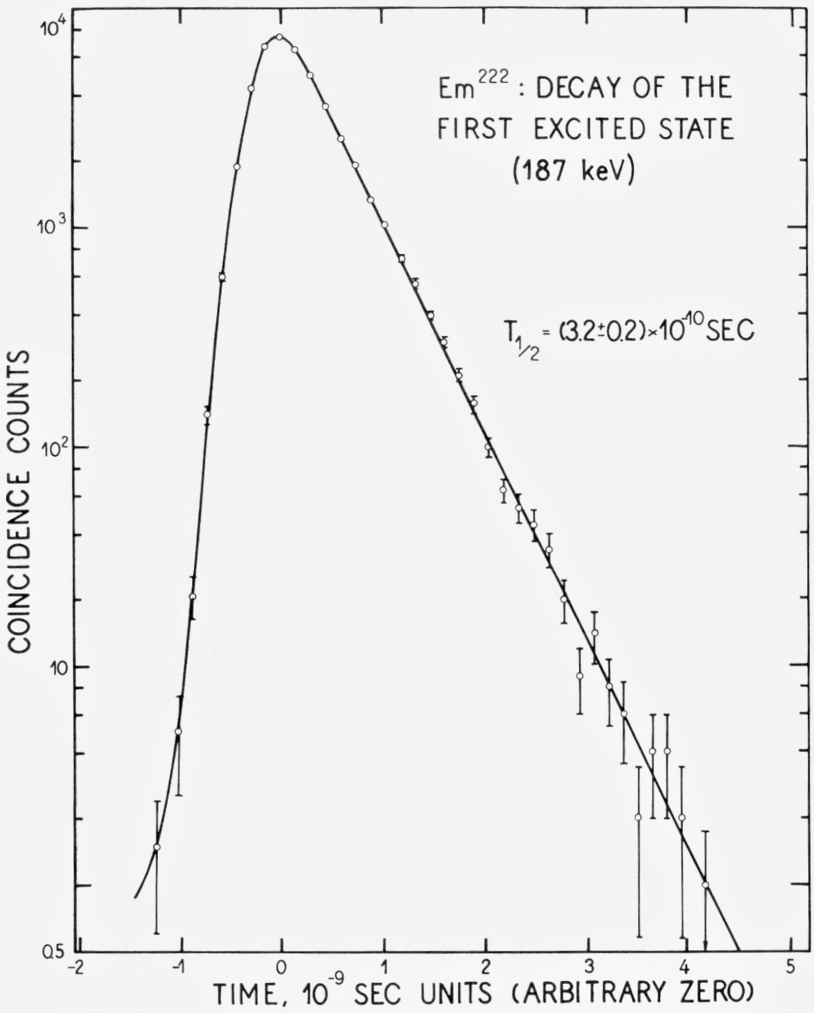


Fig. 12. The time analysis of the decay of the first excited state of $Em^{222}$.

### (g) $Th^{234}$ (48 keV)

The 48 keV excited state of $Th^{234}$ is excited by a 23 % branch in the alpha decay of $U^{238}$. The difficulty in using this source is that pure $U^{238}$ metal has a specific activity of only 12 disintegrations per second per milligram, and yet the source to be used must be thin both for $\approx$ 44 keV MN...

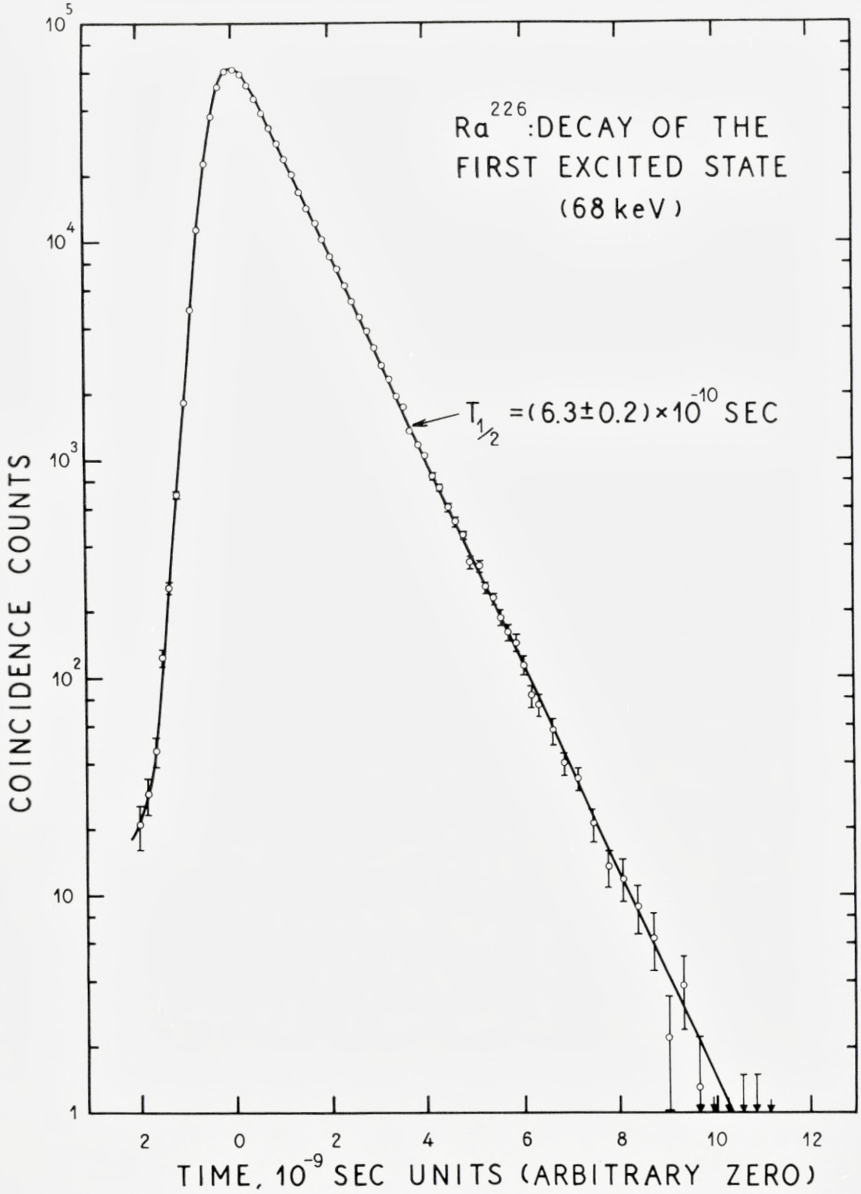


Fig. 13. The time analysis of the decay of the first excited state of $Ra^{226}$.

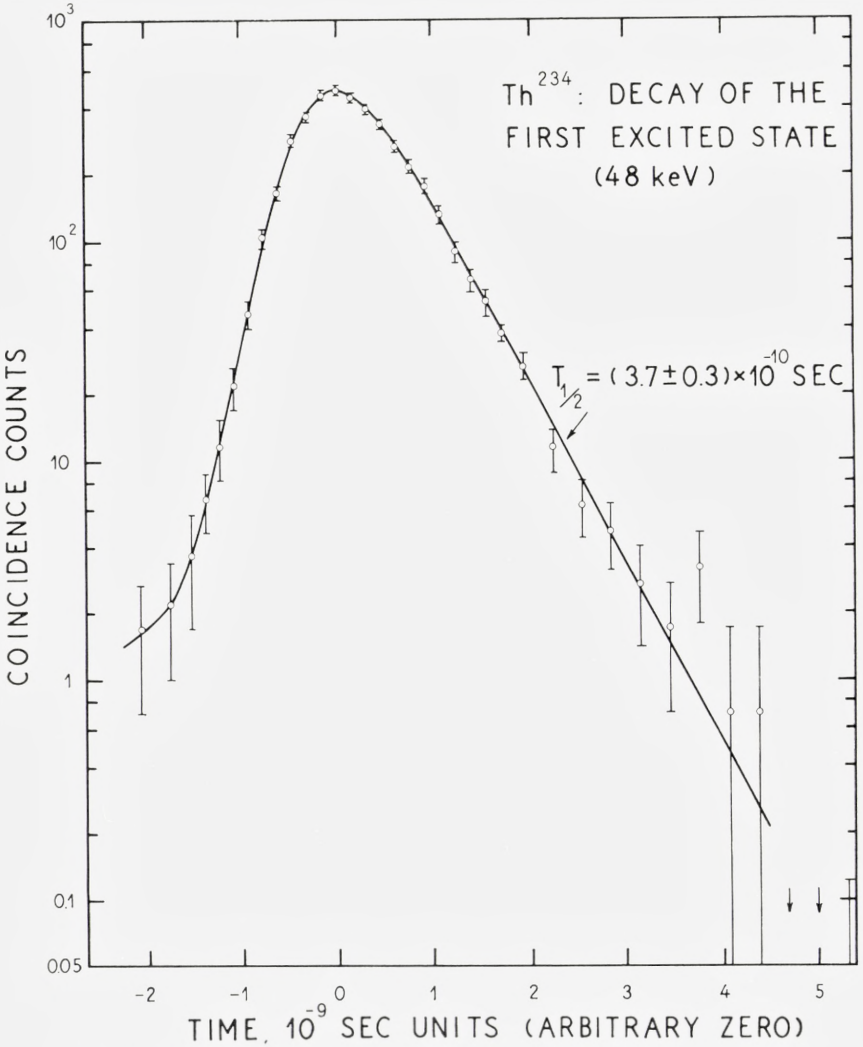


Fig. 14. The time analysis of the decay of the first excited state of $Th^{234}$.

conversion electrons and for 4 MeV alpha particles. A further difficulty lies in the presence of $U^{234}$ ($2.5 \times 10^5$ *y*), which exists in ordinary uranium in radioactive equilibrium with $U^{238}$. $U^{234}$ decays to $Th^{230}$, populating the 53 keV excited state of $Th^{230}$ with an intensity of 28 %. A measurement on ordinary uranium chemically freed of its decay products (except, of course,

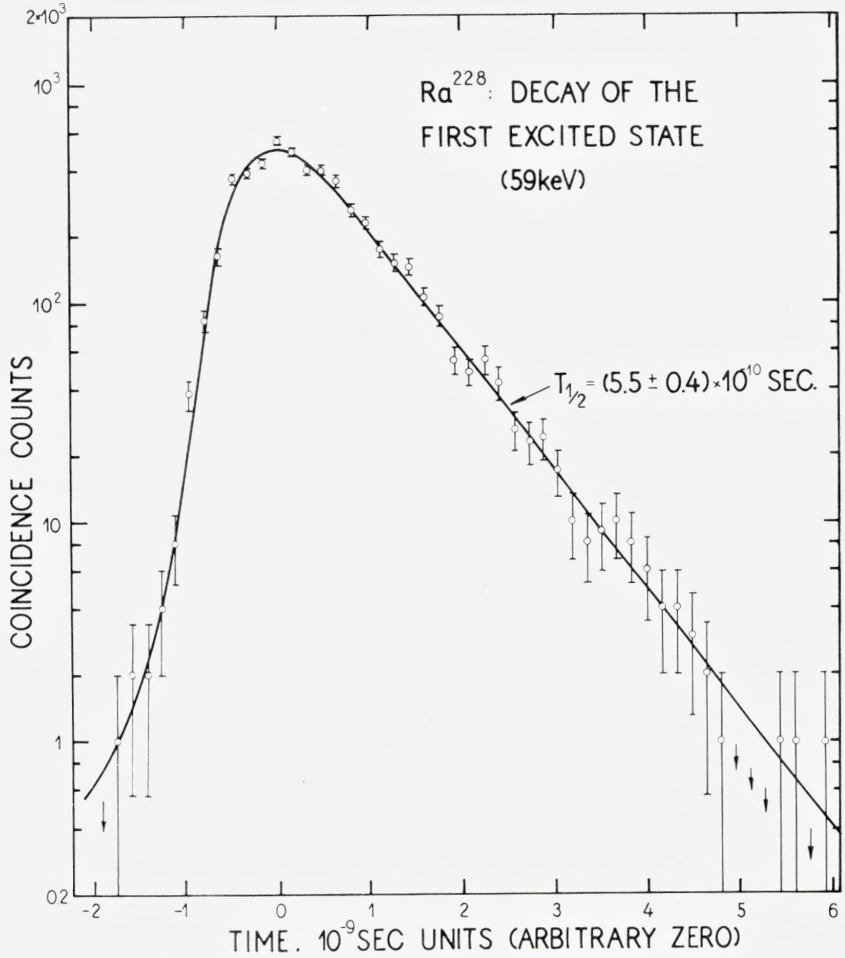


Fig. 15. The time analysis of the decay of the first excited state of $Ra^{228}$.

$U^{234}$) would give a mixture of the half lives of the $Th^{234}$ and $Th^{230}$ excited states.

The low specific activity must be accepted, implying very low counting rates in the experiment; the $U^{234}$ admixture difficulty was avoided by using a supply of uranium depleted in $U^{235}$ and hence *a fortiori* in $U^{234}$. The depletion figure for $U^{234}$ was not known for this uranium sample. It was determined by preparing duplicate sources of normal and depleted uranium, as described below, and measuring their alpha activity with a $2\pi$ propor-

tional flow counter. A source of $U^{238}$ alone, freed from all other radioactive products, should show a specific activity almost exactly half that of a source of normal uranium, the contribution from $U^{235}$ being only 2.5 %. The counting results showed that the abundance of $U^{234}$ in our depleted sample was approximately $^1/_7$ of the equilibrium amount. This amount would still be sufficient to require a correction in the measured result for the half life of the $Th^{234}$ excited state, if it were not for the fact that the half life of the $Th^{230}$ excited state, already measured, turns out to be exactly the same. We can therefore take the measured value for $Th^{234}$ without further correction. Before mounting the source, the uranium was freed of its decay products, $Th^{234}$ (24 *d*) and $Pa^{234}$ (1.1 *m*). The starting material, $UO_2$, was dissolved in concentrated nitric acid, and oxidised to the uranium (VI) state. The solution thus contained $UO_2(NO_3)_2$ which can be extracted into ether, leaving all thorium in the aqueous phase. From the ether phase a very small volume, corresponding to the desired amount of uranium, was taken out and added to about 200 $\mu$l of a 0.01 % solution of insulin in water.

This purified $UO_2(NO_3)_2$ solution was deposited on the surface of a 0.15 mg/cm² aluminium foil, which in turn was on the surface of a 10 mg/cm² plastic phosphor disc, 2 cm in diameter. The solution was spread as uniformly as possible over this area of $\approx 3$ cm², and evaporated to dryness, the insulin acting as a wetting agent and improving the evenness of the deposit. The total alpha activity of the source was about 6 disintegrations per second, implying a total mass of $U^{238}$ of about 0.5 mg, and an average thickness about 0.2 mg/cm². Non-uniformity of the deposit probably raised the effective thickness somewhat above this amount. The source was covered with a second 0.15 mg/cm² aluminium foil, and a 3 mm thick plastic phosphor disc to serve as electron counter. The apparently wasteful use of the layer of aluminium foil on both sides of the source was judged to be necessary in order to prevent absorption of scintillation light by the yellow $UO_2(NO_3)_2$ deposit.

The source produced a recognizable peak in the alpha singles spectrum (with, of course, very bad statistical errors), and an alpha-coincident electron spectrum extending to the correct maximum pulse height, but having no recognizable peak owing to source thickness effects. These results agreed with expectation. The total coincidence counting rate between the chosen alpha pulses and the chosen electron pulses was about one count per minute. The time analysis recorded in a 70-hour run is shown in fig. 14. The half life of the $Th^{234}$ excited state read from this curve is $(3.7 \pm 0.3) \times 10^{-10}$ sec; on account of the relatively large statistical errors, the assigned error is

somewhat larger than usual. (In assessing the drawing of the curve through the measured points, the reader should note that the last three plotted points on the right, all lying above the drawn curve, are balanced by two points, indicated by small arrows, which lie below the curve.)

### (h) $Ra^{228}$ (59 keV)

The 59 keV excited state of $Ra^{228}$ is excited by a 24 % branch in the alpha decay of $Th^{232}$. All the remarks just made about using $U^{238}$ as a source apply to an even greater extent to $Th^{232}$, whose specific activity is only 4 disintegrations per second per milligram. In addition, sources of thorium depleted in $Th^{228}$ (1.9 *y* radiothorium) are not readily available. There is one factor in favour of the thorium case, compared with uranium; the conversion electrons of the 59 keV transition are higher in energy than the corresponding ones from a $U^{238}$ source, because of the higher transition energy and lower atomic binding energies. Thus we may hope to use the *L* conversion electrons ($\approx$ 42 keV) as well as the MN. . . conversion electrons ($\approx$ 56 keV), gaining a factor of 4 in intensity.

The source used in the measurements was prepared in the Copenhagen isotope separator[10], through the kind cooperation of Ing. O. Skilbreid. The charge material for the ion source of the separator was 2 g of $ThO_2$ that had been chemically freed of its decay products (except, of course, $Th^{228}$). The ion source was run with a mixture of $CCl_4$ vapour and $Cl_2$ as the working gas, and produced a strong beam (50 to 100 $\mu$A) of $(Th^{232})^+$ ions. Since the nearest mass was four units away from $Th^{232}$, the separation was exceptionally clean. The ion beam struck a graphite plate placed 15 mm above the source holder, and metallic $Th^{232}$ sputtered from the graphite surface onto the source holder. This procedure involves a loss of a factor of 5 in separated material, but it makes it easier to get a uniform deposit over a large area, and it avoids the necessity of dissipating the ion beam power ($\approx$ 3 watts) in the source holder. Experience with the Van de Graaff targets prepared in this way has shown that the number of carbon atoms carried onto the target is negligible for our purposes. The separation proceeded for about 30 hours, the source holder being rotated periodically during this time to ensure uniformity. The source holder, as in the uranium case just discussed, was a 2 cm diameter disc of 10 mg/cm$^2$ plastic phosphor, covered with a 0.15 mg/cm$^2$ aluminium foil. The total activity of the source at the end of separation was about 2.4 disintegrations per second, implying a

total mass of 0.6 mg, or an average density of 0.2 mg/cm$^2$. Both visual inspection and rough alpha counting showed that the deposit was very uniform. Its appearance was that of a slightly tarnished bright metal.

The $Th^{232}$ source was mounted as in the $U^{238}$ case just discussed, and counter settings much the same were used. The advantages of electron energy and source uniformity outweighed the disadvantage in specific activity, however, and the coincidence counting rate was about three times better than for the uranium source, viz., 3 counts per minute. The time analysis was run for 45 hours, and the result is shown in fig. 15. The half life of the 59 keV excited state of $Ra^{228}$ is found to be $(5.5 \pm 0.4) \times 10^{-10}$ sec.

### (i) $Th^{228}$ (57.8 keV)

The 57.8 keV first excited state of $Th^{228}$ is strongly excited in the beta decay of $Ac^{228}$ (6.1 *h*). Two beta branches of maximum energy 2.1 and 1.8 MeV, totalling 25 % of the disintegrations, feed almost directly into the desired state. Further beta branches, of energy 1.1 MeV or less, feed higher excited states which then emit a variety of gamma rays. The half life of the 57.8 keV state was measured by analyzing coincidences between the high energy beta branches and the MN... conversion electrons of the 57.8 keV state, thus avoiding most of the prompt coincidences that would otherwise occur.

The $Ac^{228}$ activity was obtained from a sample of $Ra^{228}$ (MsTh 6.7 *y*), which was in partial equilibrium with its daughters. These are the same as the ones dealt with under $Ra^{224}$, section (*c*), plus of course $Ac^{228}$. Again a cation exchange procedure was used to prepare the source. The mixture of isotopes was absorbed from a very dilute hydrochloric acid solution (0.01 N) onto a cation exchange column which had previously been conditioned with a 0.05 M solution of $(NH_4)_2$EDTA (ethylene-diamino-tetraaceticacid-diammonium salt) (pH 4.7) and then washed with water. All activities were absorbed in a band on the top of the resin filling. The column was first eluted with 0.005 M $(NH_4)_2$ EDTA (pH 4.7) which removed thorium, lead, and bismuth, leaving radium and actinium behind. The concentration of the eluant was then increased to 0.05 M. This took out $Ac^{228}$. The fraction used had a purity of about 95 % by beta activity, the impurities being $Pb^{212}$ and $Bi^{212}$.

The $Ac^{228}$ activity was deposited directly on the surface of a plastic phosphor 3 mm thick, and had a surface density of about 100 $\mu$g/cm$^2$ (con-

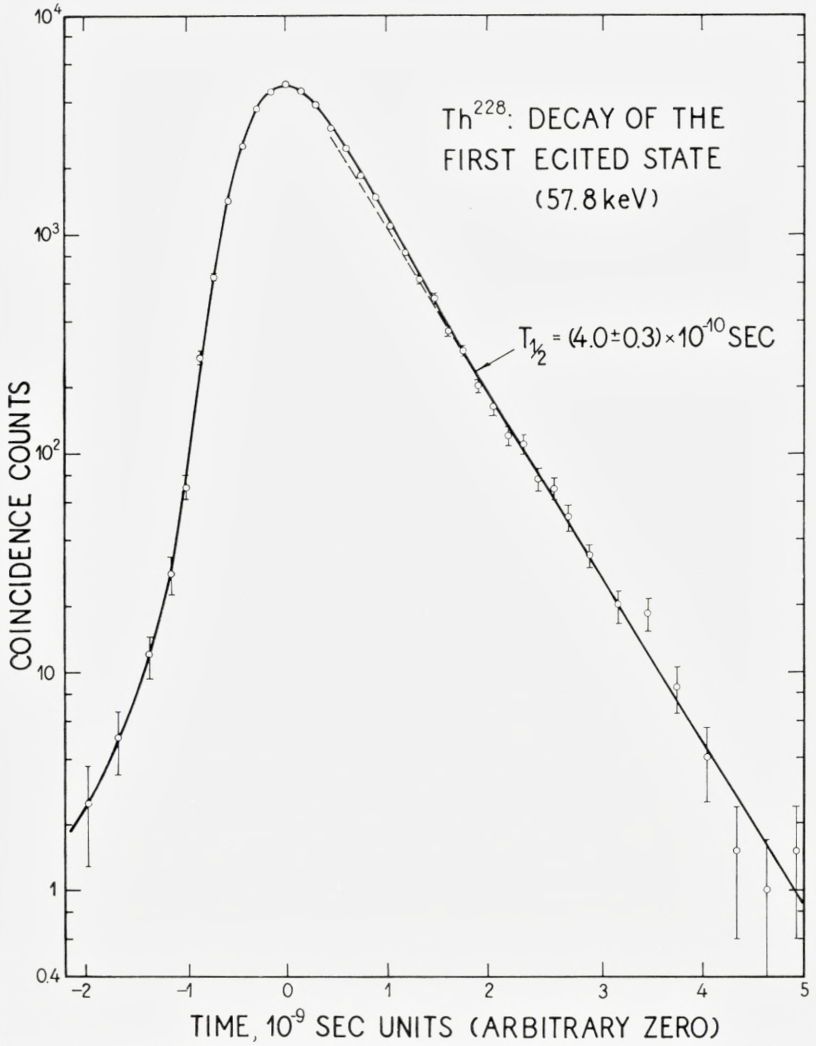


Fig. 16. The time analysis of the decay of the first excited state of $Th^{228}$. Note that a few prompt coincidences occur in this curve (see the text, section (i)).

sisting mainly of the organic eluant material). This phosphor detected the conversion electrons; it was covered with 30 mg/cm² of aluminium and then with a second 3 mm thick phosphor to serve as beta counter. Pulses from this counter lying between 1.0 and 1.6 MeV were accepted as the beta events. The spectrum of the conversion electron counter in coincidence with these

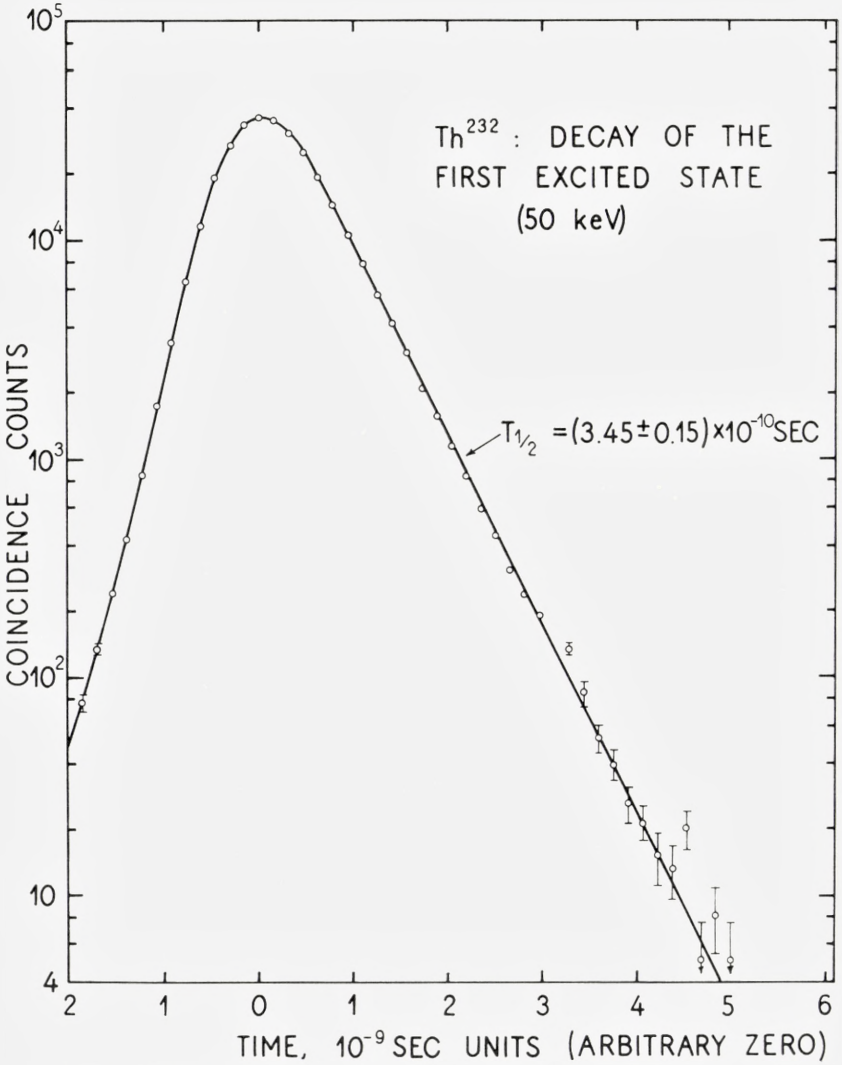


Fig. 17. The time analysis of the decay of the first excited state of Th$^{232}$.

pulses showed a peak from $L$ conversion of the 57.8 keV transition, with a bump on its upper energy edge due to MN... conversion electrons. In addition, there was a low background due to coincidences between nuclear beta rays detected in the conversion electron counter and high energy gamma rays detected in the beta counter. These coincidences would give rise to prompt events in the time analysis amounting to about 15 % of the

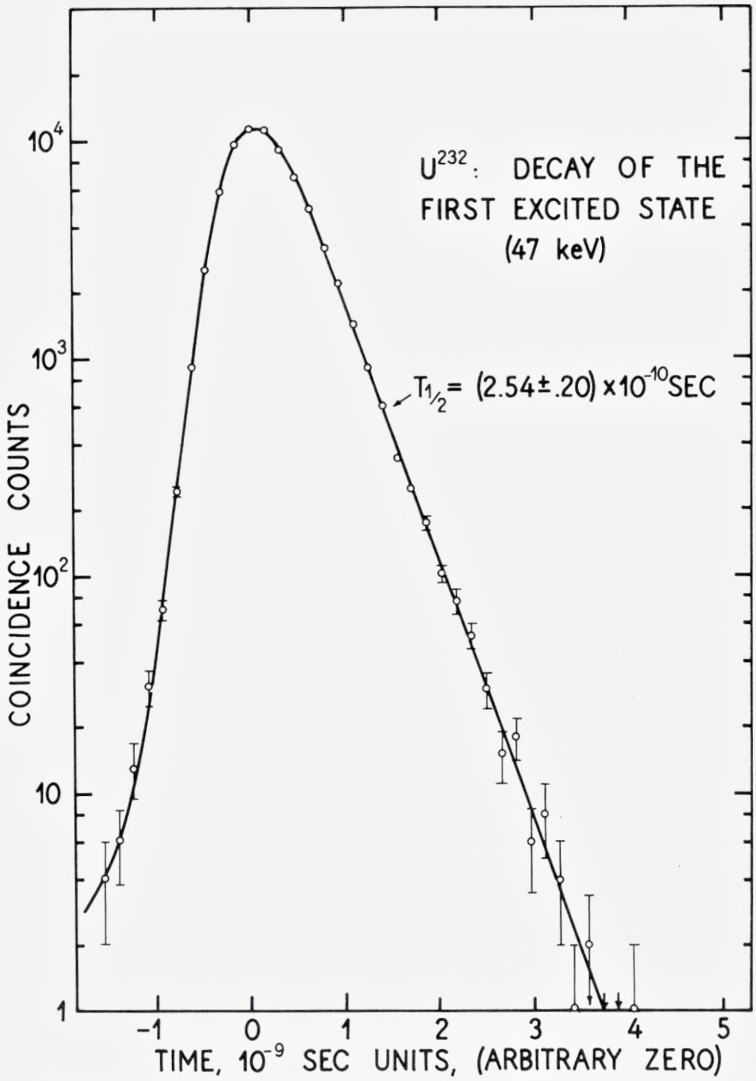


Fig. 18. The time analysis of the decay of the first excited state of $U^{232}$.

total. The time analysis, fig. 16, shows the expected small prompt component, together with a clean decay of half life $4.0 \times 10^{-10}$ sec. If the presence of the prompt coincidences had been ignored and a straight line drawn through the points, the half life would have appeared about 5 % lower. We assign a slightly larger than usual error, and give for the 57.8 keV excited state of $Th^{228}$ the value $T_{\frac{1}{2}} = (4.0 \pm 0.3) \times 10^{-10}$ sec.

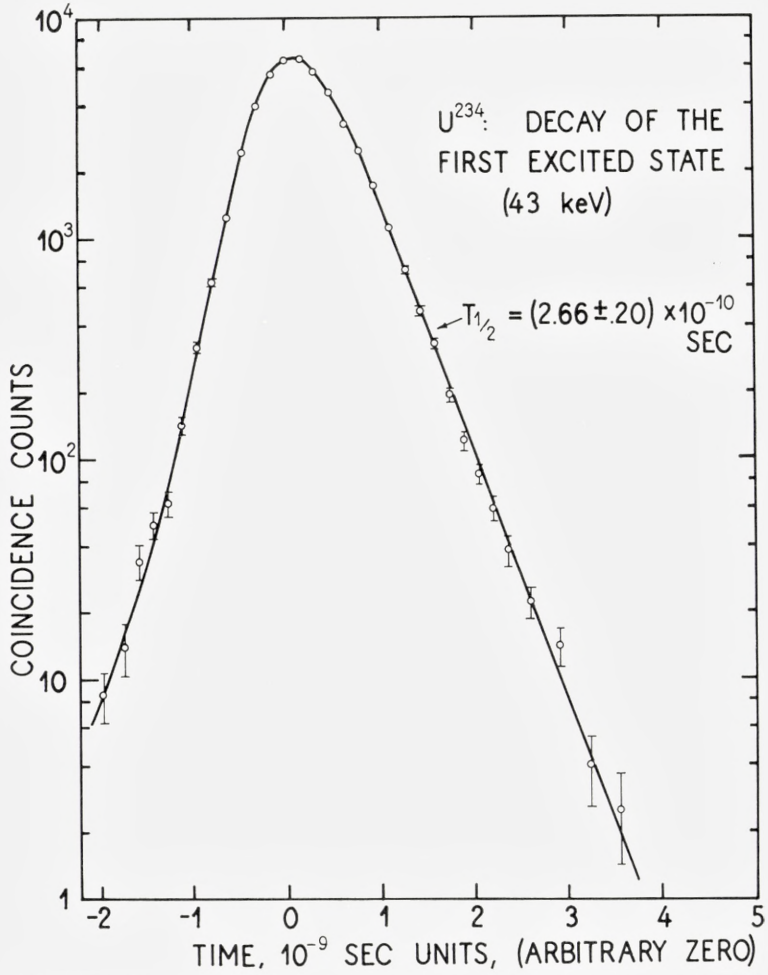


Fig. 19. The time analysis of the decay of the first excited state of $U^{234}$.

### (j) $Th^{232}$ (50 keV), $U^{232}$ (44 keV), $U^{234}$ (43 keV) $U^{236}$ (45 keV), $Pu^{238}$ (44 keV), and $Pu^{240}$ (43 keV)

These six excited states were studied in radioactive sources supplied through the kind cooperation of Dr. E. P. Steinberg of the Argonne National Laboratory. The parent source in each case is an alpha emitter with about 25 per cent branching to the first excited state of the daughter. (The parents

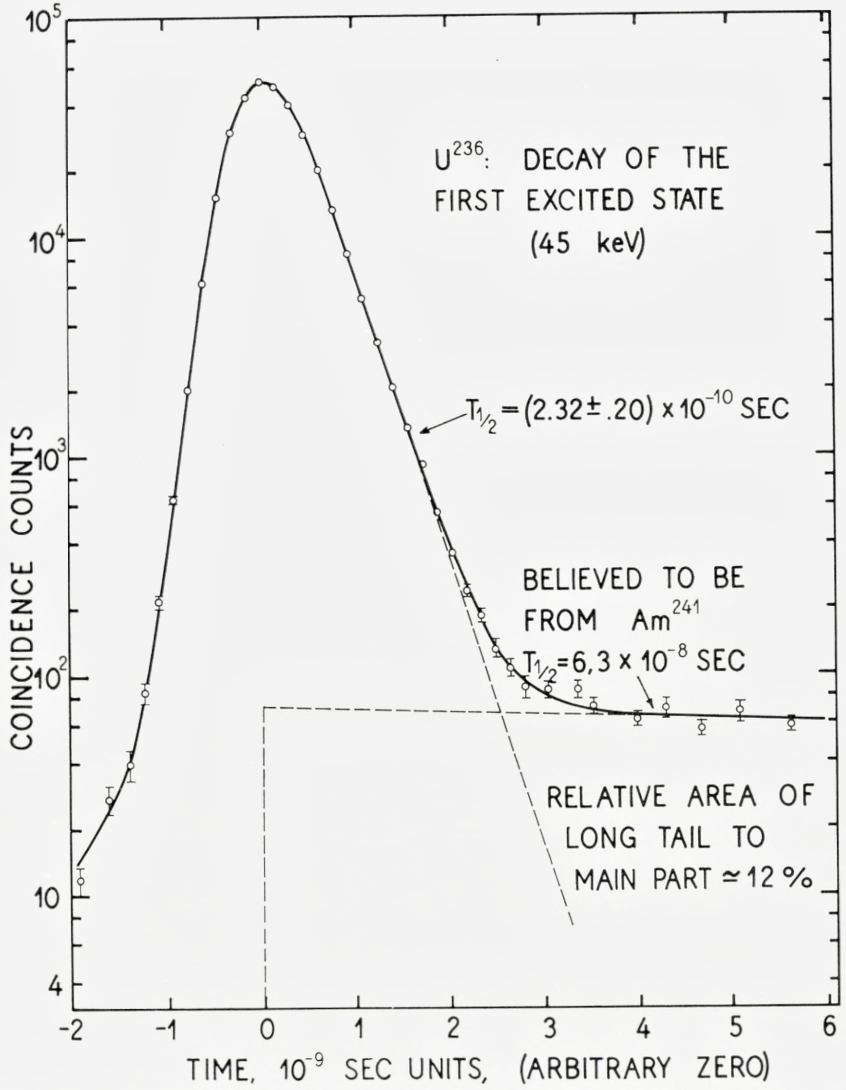


Fig. 20. The time analysis of the decay of the first excited state of $U^{236}$. A long lived contribution has been subtracted (believed to be from $Am^{241}$).

are, in order, $U^{236}$, $Pu^{236}$, $Pu^{238}$, $Pu^{240}$, $Cm^{242}$, and $Cm^{244}$). Each source was supplied already deposited on the surface of a 10 mg/cm$^2$ plastic phosphor, with an average strength of a thousand disintegrations per second. On

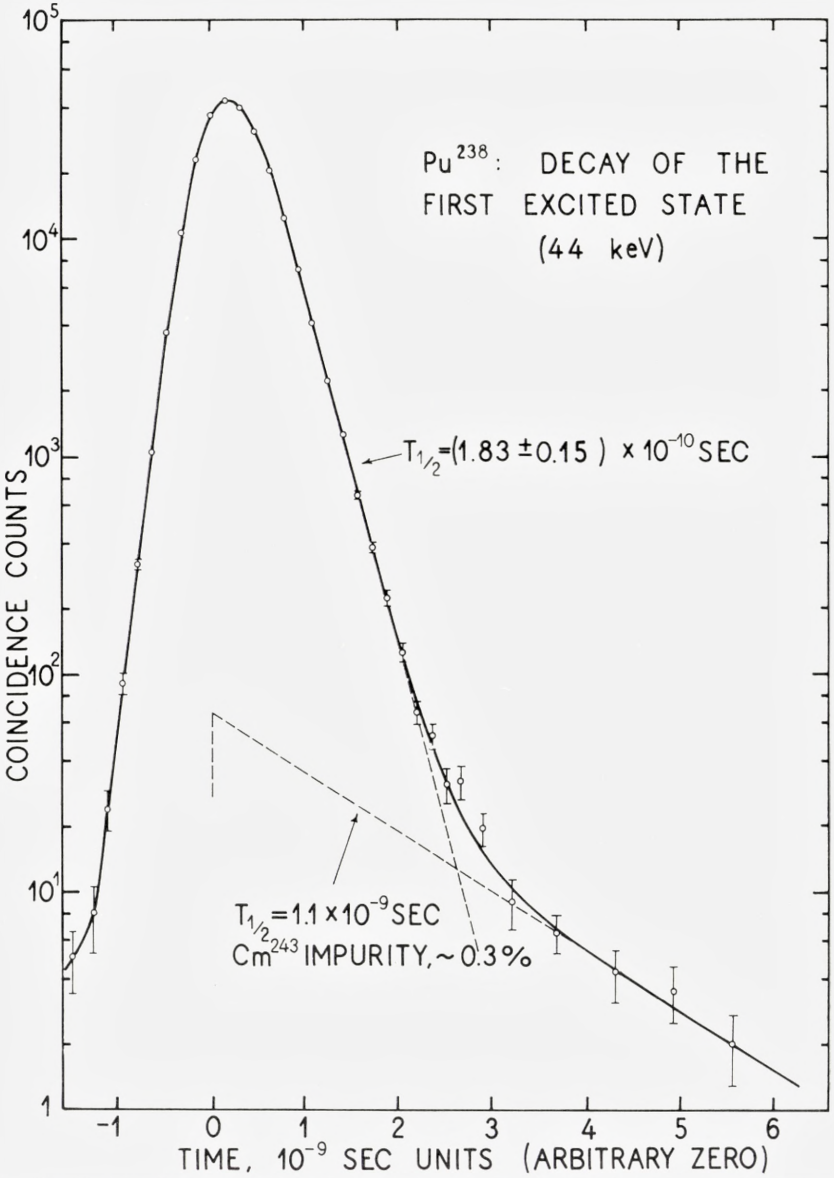


Fig. 21. The time analysis of the decay of the first excited state of $Pu^{238}$. A long lived impurity has been subtracted (believed to be from $Cm^{243}$).

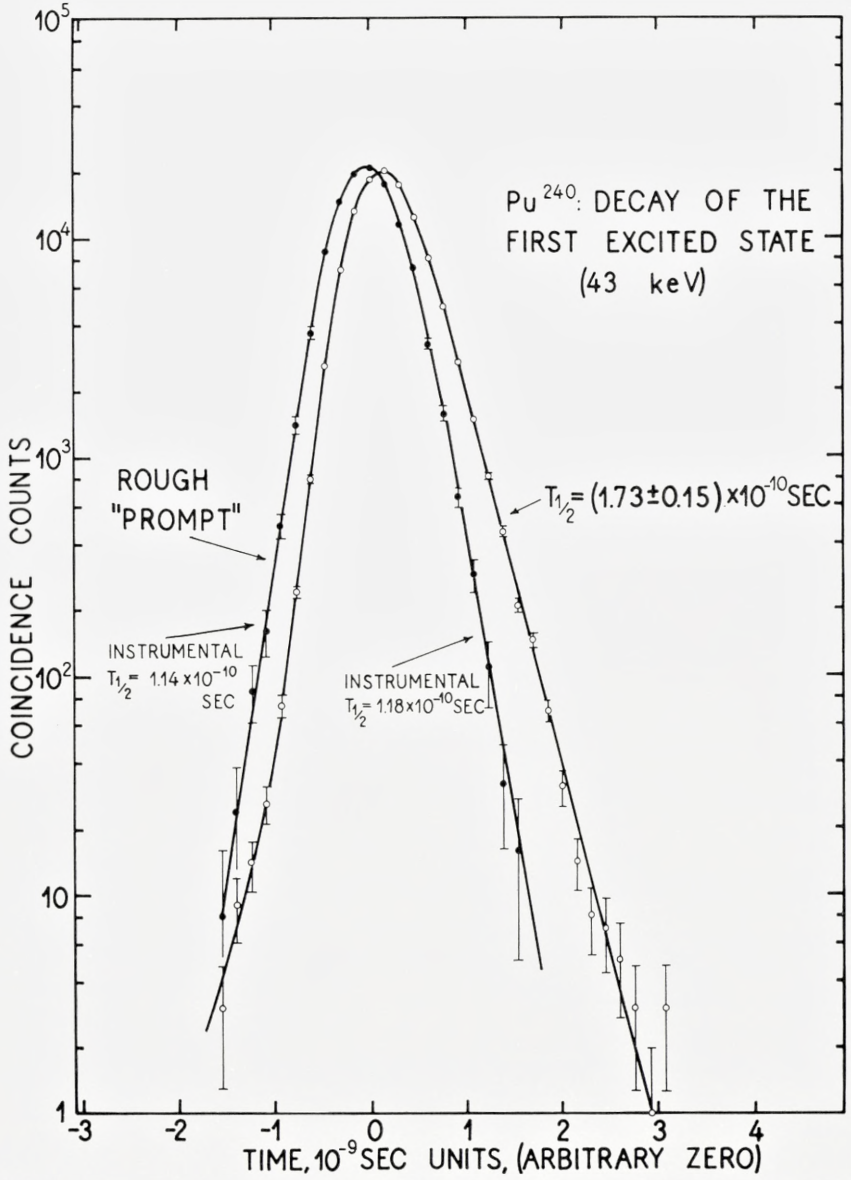


Fig. 22. The time analysis of the decay of the first excited state of $Pu^{240}$. A prompt curve is included for reference.

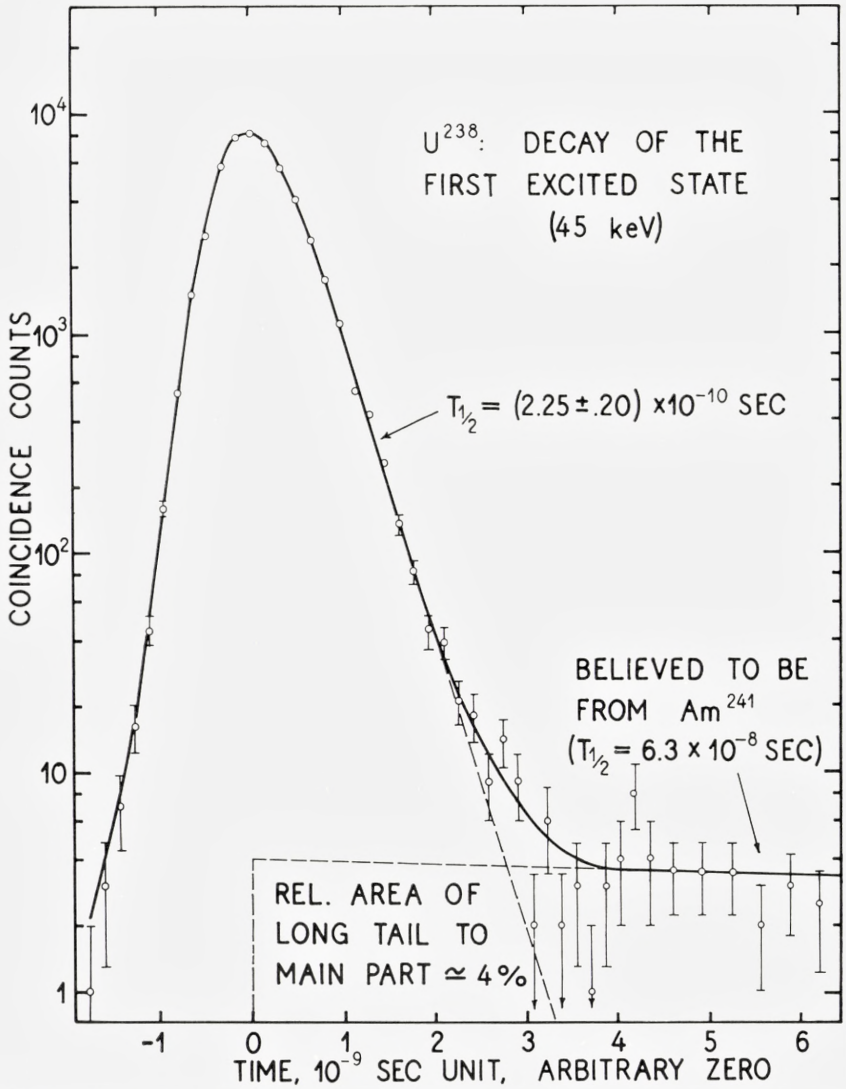


Fig. 23. The time analysis of the decay of the first excited state of $U^{238}$. A long lived contribution has been subtracted (believed to be from $Am^{241}$).

account of the small penetrating power of the LMN. . . conversion electrons, the thin phosphor on which the source was deposited was used in each case as the electron counter. The source deposit was covered with a

layer of 0.15 mg/cm$^2$ aluminium foil, and a second thin plastic phosphor was pressed against the foil to serve as an alpha counter. The conversion electron counter bias was set to accept energies from 30 to 50 keV, approximately. In this way the MN... conversion lines, and perhaps the upper edge of the $L$ conversion line, were detected. The alpha pulse height window covered the broad alpha peak in the usual way. No trouble was experienced with any of the sources, and the six measurements were completed in as many days.

The result for the 50 keV first excited state of $Th^{232}$ is shown in fig. 17. The half life is $(3.45 \pm 0.15) \times 10^{-10}$ sec. This nuclide is one of two for which the corresponding Coulomb excitation measurement has been made by SKURNIK *et al.*[11], the other being $U^{238}$.

The curves for $U^{232}$ (47 keV) and $U^{234}$ (43 keV) appear in figs. 18 and 19, with half lives $(2.54 \pm 0.20) \times 10^{-10}$ sec and $(2.66 \pm 0.20) \times 10^{-10}$ sec, respectively.

Fig. 20 shows the curve for $U^{236}$ (45 keV), measured from a parent source of $Pu^{240}$. The weak component of longer lifetime is tentatively identified as due to the presence of $Am^{241}$ impurity in the source. $Am^{241}$ (458 $y$) has an 85 % alpha branch to an excited state at 60 keV whose half life is known to be $6.3 \times 10^{-8}$ sec, consistent with our measured curve. It is a logical impurity in a $Pu^{240}$ source, because it can be formed by the beta decay of $Pu^{241}$ (13 $y$). The long lived component is subtracted in fig. 20, giving a half life for the 45 keV first excited state of $U^{236}$ of $(2.32 \pm 0.20) \times 10^{-10}$ sec. It is clear that exact knowledge of the half life of the subtracted component in fig. 20 is not required in any case.

Fig. 21 shows the curve for $Pu^{238}$ (44 keV), measured from a parent source of $Cm^{242}$. Again we have a longer lifetime due to an impurity, in this case $Cm^{243}$, which decays to an excited state of $Pu^{239}$ having a half life of $1.1 \times 10^{-9}$ sec. Making the subtraction, we arrive at a half life of $(1.83 \pm 0.15) \times 10^{-10}$ sec for the 44 keV state of $Pu^{238}$.

Fig. 22 shows the curve for $Pu^{240}$ (43 keV), with a comparison curve labelled "rough prompt". This prompt curve was made by the same technique of light leakage as that described in section ($a$) above. It was included at this point in the measurements because the $Pu^{240}$ excited state has the shortest half life of any of the transitions below 100 keV. The instrumental half lives read from the slopes of the two sides of the prompt curve lie between 1.1 and $1.2 \times 10^{-10}$ sec, while the half life of the 44 keV excited state of $Pu^{240}$ is $(1.73 \pm 0.15) \times 10^{-10}$ sec. Fig. 22 thus shows that we are still far enough from the instrumental limit to make a slope measurement of this

half life at this energy, but it also suggests that the still shorter half lives anticipated for the first excited states of curium and californium would be much more difficult to measure.

### (k) $U^{238}$ (45 keV)

The 45 keV first excited state of $U^{238}$ is excited by a 24 % branch in the alpha decay of $Pu^{242}$ ($3.8 \times 10^5$ *y*). The $Pu^{242}$ sample was also provided by the Argonne National Laboratory through the kindness of Dr. STEINBERG.

The sample contained 97.3 % $Pu^{242}$ by weight, but, owing to its long half life, the $Pu^{242}$ activity only represented 6.4 % of the total alpha activity; the main activity was $Pu^{238}$ (86 *y*). In this case, therefore, an isotope separation was essential. The alpha activity due to $Pu^{242}$ in the sample was 3,200 disintegrations per second, corresponding to 20 $\mu$g of plutonium. The ion source of the isotope separator could not be expected to work on such a small mass. The sample was therefore mixed with 1 mg of uranium oxide, and a procedure similar to the one described in section (*h*) was used, except that the activity was collected directly on a 0.15 mg/cm$^2$ collector foil of aluminium. The result was a source of $Pu^{242}$ 1 mm wide and 8 mm long, having 170 alpha disintegrations per second, corresponding to 5 % yield in the mass separation. The source was mounted in the usual way and counter settings similar to those of section (*j*) were employed. The delay curve is shown in fig. 23. It can be seen that there is a long-lived tail present in the distribution. This is believed to be due to small amounts of $Am^{241}$ (458 *y*) present in the source as an impurity. The presence of some $Am^{241}$ is reasonable, even in the mass-separated source, because its mass is adjacent to that of $Pu^{242}$. The $6.3 \times 10^{-8}$ sec half life produced by $Am^{241}$ has been discussed in section (*j*), under $U^{236}$ (see also fig. 20). The alpha decay energy of $Am^{241}$ (5.57 MeV) differs appreciably from that of $Pu^{242}$ (4.94 MeV), and it was possible to discriminate against $Am^{241}$ by using a narrow channel in the region of 5 MeV for the pulses from the alpha counter. The poor resolution of the plastic phosphor limits the effectiveness of this procedure, but the $Am^{241}$ contribution was reduced to 4 % (see fig. 23) from a value of 12 % when a wide window was used. After the usual subtraction, fig. 23 gives $(2.25 \pm 0.20) \times 10^{-10}$ sec for the half life of the 45 keV excited state of $U^{238}$. The corresponding Coulomb excitation measurement has been made for this nuclide[11].

## 3. Discussion

Before evaluating the experimental results, we consider how well the rotational model applies to them. In fig. 24 we have plotted the energy of the first excited state, $E_1$, and the ratio of the energy of the second excited state to that of the first excited state, $E_2/E_1$, as functions of $A$ for the nuclides of this study. For the rotational description to be valid, $E_1$ should be low and relatively independent of $A$. One suggested criterion[1] for what is meant by "low" is that $E_1$ should be below

$$E_1 \simeq 13\,\hbar^2/\Im_{\mathrm{rig}}. \tag{8}$$

This critical value of $E_1$ is calculated to be 109 keV for $Ra^{222}$, the left hand radium point in fig. 24; the experimental value of $E_1$ for the same nucleus is 111 keV. We may thus accept all the nuclides except the emanation isotopes as "rotational", on this criterion. Fig. 24 also shows that the values of $E_2/E_1$ for all the nuclides except the emanation isotopes are near the rotational value 3.33, as deduced from equation (1). For the emanation isotopes, the values of $E_2/E_1$ lie closer to the value 2.0, characteristic of vibrational excitations. (In any case their second excited states are of $2+$ character, rather than the $4+$ required in a rotational model.) Both of our criteria therefore suggest that the rotational description is not a good one for emanation isotopes, i.e., that the emanation isotopes are nearly spherical. We will nevertheless evaluate the emanation results in the same way as the others, enclosing the resulting values in brackets in tables and graphs as a warning. (The values of $B(E2;\,0\rightarrow 2)$ are correct, independent of assumptions about nuclear shape.)

We note that in this region the question of whether a nucleus is spherical or deformed is decided primarily by the proton number $Z$, the change from spherical to deformed occurring between $Z = 86$ (emanation) and $Z = 88$ (radium). In the rare earth region, the change occurs between neutron numbers $N = 88$ and $N = 90$. The calculated particle energy levels in a deformed potential of Nilsson[12] are consistent with these facts.

The first step in treating the experimental half lives is to calculate the values of $B(E2;\,0\rightarrow 2)$ in units of $e^2\times 10^{-48}\ \mathrm{cm}^4$ by means of

$$B(E2;\,0\rightarrow 2) = 282\,[T_{\frac{1}{2}}\,(1+\alpha)\,E_\gamma^5]^{-1}, \tag{9}$$

which follows from (2) and (3), with $E_\gamma$ in keV. The values of $E_\gamma$ are those quoted in the preceding experimental sections. The values of $\alpha$ were ob-

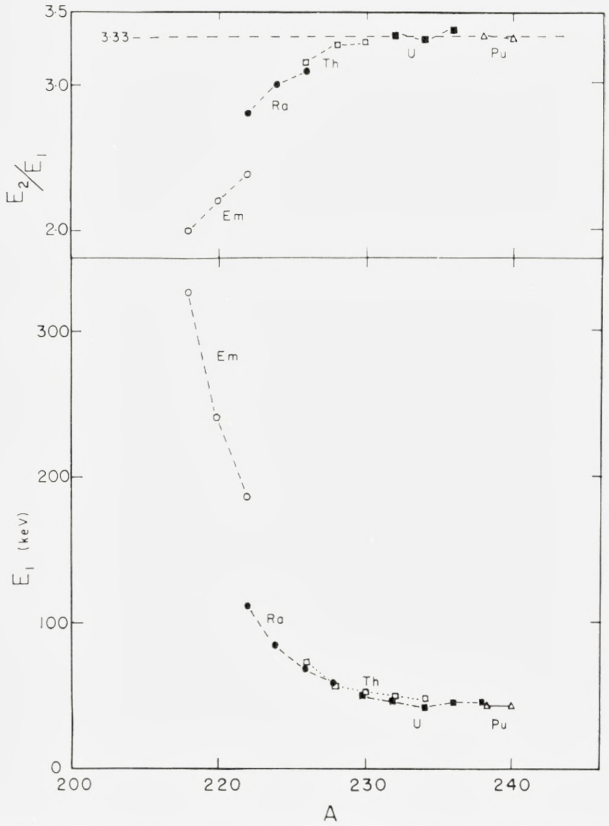


Fig. 24. (Lower part). The energy $E_1$, of the first excited states of each of the even nuclei used in this experiment, plotted as a function of A. The energies for the three Em isotopes are too high for a rotational description to apply (see the text).
(Upper part). The ratio, $E_2/E_1$ of the energies of the second and first excited states. The ratios for the three Em isotopes lie closer to the value 2.0 (vibrational excitations) than to 3.33 (rotational excitations). In addition, the second excited states in the Em isotopes are 2+, rather than 4+ as required on the rotational model.

tained by interpolation in the $K$ and $L$ conversion tables of Rose[13], with the additional assumption, based on experiment, that MN. . . conversion is always one-third of $L$ conversion. No additional error has been assigned for this procedure, because the results could be corrected if better conversion tables should become available. The energy values, $E_\gamma$, often have uncertainties of two per cent or so, and at first glance this error would appear to be serious, owing to the high power of $E_\gamma$ in (9). In fact, however, $\alpha$ is large compared with unity, and varies approximately as $E_\gamma^{-5}$. The factor

$(1+\alpha)\,E_\gamma^5$ appearing in (9) is therefore almost independent of energy, and moderate errors in the values of $E_\gamma$ contribute negligible errors to the final results. The same effect accounts for the fact, at first sight remarkable, that all the experimental half lives lie in the narrow range $1.5\times10^{-10}$ to $7.6\times10^{-10}$ sec. Moreover, most of this variation is due to actual variations in $B(E2)$ and to the variation of $\alpha$ with $Z$, rather than to variations in $E_\gamma$.

Table I lists the nuclides measured (col. 1), the values of $E_\gamma$ (col. 2), the measured half lives (col. 3), the values of $(1+\alpha)$ used in applying (9) (col. 4), and the resulting values of $B(E2;\ 0\rightarrow2)$ (col. 5). Column 6 gives the results for $B(E2;\ 0\rightarrow2)$ for $Th^{232}$ and $U^{238}$, measured by Coulomb excitation by Skurnik *et al.*[11]. The discrepancies between their values and ours are 13 %, quite consistent with the combined errors of measurement. These two Coulomb excitation measurements were made by observing inelastically scattered protons or deuterons from the target, and are independent of internal conversion coefficients. The agreement between the two pairs of values may be interpreted as an indirect verification, within 15 %, of the computed $E2$ conversion coefficients of Rose[13] for this region of $Z$ and energy. The conversion coefficients involved are large (cf. col. 4 of table I), and it is unlikely that direct measurements of them will furnish any closer check of Rose's values.

Column 7 of table I gives the values of $Q_0$ in units of $10^{-24}$ cm$^2$, derived from the $B(E2;\ 0\rightarrow2)$ values by means of

$$|Q_0| = [10.05\,B(E2;\ 0\rightarrow2)]^{1/2}, \tag{10}$$

which follows from (4). The errors shown for $Q_0$ and for $B(E2;\ 0\rightarrow2)$ in the table reflect only the errors assigned to the experimental half lives. Column 8 gives the values of $\beta$ calculated from $Q_0$ by means of (5). At this point it is necessary to choose a value for $R_0$, the average nuclear radius. We have used $R_0 = 1.2\,A^{1/3}\times10^{-13}$ cm, so as to agree with other workers in this field, particularly Mottelson and Nilsson.[12] In that case, (5) becomes

$$\beta = 3.12\left[\left(1+\frac{59\,Q_0}{ZA^{2/3}}\right)^{1/2}-1\right]. \tag{11}$$

The fractional errors in $\beta$ are closely the same as those in $Q_0$, ranging from 1.7 % to 5.5 %. Finally, column 9 gives the value of $\mathfrak{I}/\mathfrak{I}_{\mathrm{rig}}$, with $\mathfrak{I}$ calculated from the observed energy of the first excited state by means of (1), and $\mathfrak{I}_{\mathrm{rig}}$ calculated from (6), using the experimental values of $\beta$ and the

TABLE I.

| (1) Nuclide | (2) $E_\gamma$ (keV) | (3) $T_{\frac{1}{2}}$ ($10^{-10}$ sec) | (4) $1+\alpha$ | (5) $B(E2;\,0\to2)$ ($e^2\,10^{-48}\,\mathrm{cm}^4$) | (6) $B(E2;0\to2)$ from Coulomb excitation | (7) $Q_0$ ($10^{-24}\,\mathrm{cm}^2$) | (8) $\beta$ | (9) $\Im/\Im_{\mathrm{rig}}$ |
|---|---|---|---|---|---|---|---|---|
| $Em^{218}$ | 325 | $<0.8$ | 1.112 | $>0.875$ | .. | $(>2.97)$ | $(>.085)$ | $(<.081)$ |
| $Em^{220}$ | 241 | $1.50 \pm 0.1$ | 1.283 | $1.8 \pm 0.12$ | .. | $(4.26 \pm 0.14)$ | (0.121) | (0.106) |
| $Em^{222}$ | 187 | $3.2 \pm 0.2$ | 1.70 | $2.27 \pm 0.14$ | .. | $(4.79 \pm 0.15)$ | (0.136) | (0.135) |
| $Ra^{222}$ | 111 | $5.2 \pm 0.4$ | 7.36 | $4.37 \pm 0.34$ | .. | $6.63 \pm 0.26$ | 0.184 | 0.223 |
| $Ra^{224}$ | 84.4 | $7.6 \pm 0.3$ | 22.6 | $3.84 \pm 0.15$ | .. | $6.21 \pm 0.13$ | 0.171 | 0.291 |
| $Ra^{226}$ | 68 | $6.3 \pm 0.2$ | 59.6 | $5.17 \pm 0.17$ | .. | $7.22 \pm 0.12$ | 0.197 | 0.351 |
| $Ra^{228}$ | 59 | $5.5 \pm 0.4$ | 119.1 | $6.03 \pm 0.44$ | .. | $7.79 \pm 0.28$ | 0.212 | 0.400 |
| $Th^{226}$ | 72 | $3.95 \pm 0.2$ | 54.7 | $6.77 \pm 0.34$ | .. | $8.25 \pm 0.20$ | 0.220 | 0.330 |
| $Th^{228}$ | 57.8 | $4.0 \pm 0.3$ | 152 | $7.14 \pm 0.54$ | .. | $8.47 \pm 0.32$ | 0.225 | 0.403 |
| $Th^{230}$ | 53 | $3.7 \pm 0.2$ | 236 | $7.70 \pm 0.63$ | .. | $8.80 \pm 0.35$ | 0.233 | 0.433 |
| $Th^{232}$ | 50 | $3.45 \pm 0.15$ | 308 | $8.50 \pm 0.37$ | $9.7 \pm 0.5$ | $9.25 \pm 0.23$ | 0.243 | 0.450 |
| $Th^{234}$ | 48 | $3.7 \pm 0.3$ | 377 | $7.98 \pm 0.64$ | .. | $8.93 \pm 0.35$ | 0.233 | 0.467 |
| $U^{230}$ | 51.7 | $2.6 \pm 0.3$ | 330 | $8.90 \pm 1.00$ | .. | $9.46 \pm 0.52$ | 0.245 | 0.443 |
| $U^{232}$ | 47 | $2.54 \pm 0.2$ | 490 | $9.90 \pm 0.78$ | .. | $9.98 \pm 0.28$ | 0.257 | 0.470 |
| $U^{234}$ | 43 | $2.66 \pm 0.2$ | 758 | $9.50 \pm 0.72$ | .. | $9.77 \pm 0.38$ | 0.251 | 0.516 |
| $U^{236}$ | 45 | $2.32 \pm 0.2$ | 614 | $10.70 \pm 0.92$ | .. | $10.35 \pm 0.44$ | 0.263 | 0.485 |
| $U^{238}$ | 45 | $2.25 \pm 0.2$ | 614 | $11.05 \pm 0.98$ | $12.6 \pm 0.6$ | $10.52 \pm 0.48$ | 0.268 | 0.480 |
| $Pu^{238}$ | 44 | $1.83 \pm 0.15$ | 783 | $11.9 \pm 1.0$ | .. | $10.95 \pm 0.45$ | 0.271 | 0.493 |
| $Pu^{240}$ | 43 | $1.73 \pm 0.15$ | 880 | $12.6 \pm 1.1$ | .. | $11.26 \pm 0.48$ | 0.278 | 0.488 |

This is a compilation of the experimental results from the previous section. The experimental energy of the first excited $2+$ state is listed in column 2, the data coming from the nuclear tables of STROMINGER *et al.*[4] Column 3 lists the measured half lives and their absolute errors. Column 4 shows the quantity $(1+\alpha)$, where $\alpha$ is obtained from the tables of ROSE[13] by interpolation. The reduced transition probability, $B(E2)$, is shown in column 5. Column 6 gives the two available measurements from the Coulomb excitation data (by the kind permission of E. SKURNIK *et al.*[11]). The ground state quadrupole moments are listed in column 7. The deformation parameter $\beta$ is given in column 8. The last column gives the ratio of the moment of inertia to that of a rigid rotor, $\Im/\Im_{\mathrm{rig}}$.

value of $R_0$ mentioned earlier. The simplified formula under these conditions is

$$\Im/\Im_{\mathrm{rig}} = 2.15 \times 10^5\,[E_\gamma A^{5/3}(1+0.31\,\beta)]^{-1}. \qquad (12)$$

The experimental uncertainty in $\beta$ makes only a small contribution to the error in $\Im/\Im_{\mathrm{rig}}$, about comparable with the contribution from the uncertainty in $E_\gamma$. The values of $\Im/\Im_{\mathrm{rig}}$ thus have relative uncertainties of around two per cent.

Fig. 25 presents the results for $B(E2;\,0\to2)$ plotted as a function of $A$. An auxiliary ordinate scale on the right also shows the values of $|Q_0|$ for the

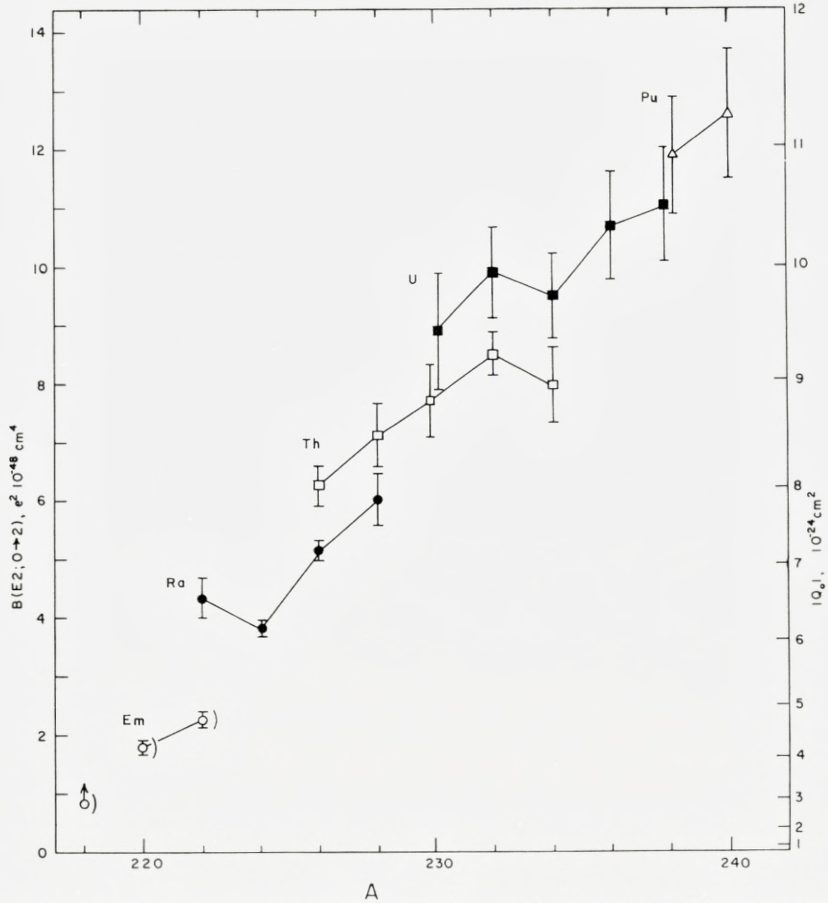


Fig. 25. The reduced transition probabilities, $B(E2; 0 \rightarrow 2)$, plotted as a function of A. The right-hand ordinate refers to the corresponding intrinsic quadrupole moments, $|Q_0|$, calculated assuming the rotational model. The errors shown are the absolute ones, the relative ones being smaller by about a factor $^1/_2$. The half-brackets on the Em points show that the right hand $|Q_0|$ scale should not be taken seriously as far as they are concerned.

same plotted points. The error bars on the points represent the estimated absolute standard errors (but with no allowance for errors in $\alpha$, as mentioned earlier). The relative errors can be taken as considerably smaller, perhaps by a factor 1/2. The plotted points have been joined in groups according to $Z$. It is clear that the $B(E2)$ or $Q_0$ values depend mainly on $Z$, with a residual tendency to increase with $N$. The detailed structure of the results, e.g., the low values at $A = 224$ and $A = 234$, is probably real, but we will not attempt any interpretation of these fine points.

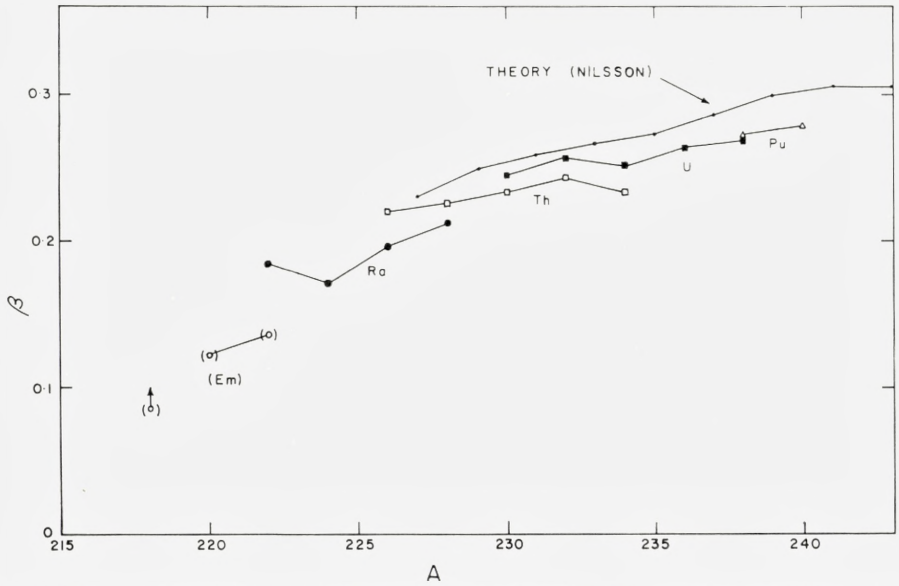


Fig. 26. The experimentally measured deformation parameters, $\beta$, assuming spheroidal nuclear shapes, plotted as a function of A. The theoretical curve is due to MOTTELSON and NILSSON[12]. The Em points have been placed in brackets as a warning (see the text).

Fig. 26 shows the experimental values of $\beta$ plotted as a function of $A$, together with a theoretical line due to NILSSON (reference 12). The theoretical values represent the deformations which yield minimum nuclear energy for a model of independent-particle motion in a deformed potential. The actual values refer to particular odd mass nuclei in this region, and are therefore not expected to reproduce the experimental values in detail. In addition, the residual interactions are expected to reduce the deformations somewhat. Quantitative calculations of this effect have not yet been published.* With these remarks in mind, the agreement between theory and experiment is seen to be very good.

We turn now to the moments of inertia. Fig. 27 shows the experimental values of $\mathfrak{I}/\mathfrak{I}_{\text{rig}}$, plotted as a function of $\beta$. The diagram also includes a set of experimental values for the even rare earths, taken from ELBEK, OLESEN and SKILBREID[14]. The experimental values are indicated by circles. Crosses refer to preliminary theoretical values calculated by S. G. NILSSON and O. PRIOR.** Theoretical and experimental points belonging to the same

* Such calculations are at present in progress (Z. L. SZYMANSKI, private communication).

** We are indebted to Dr. S. G. NILSSON for making available the results of these calculations prior to publication.

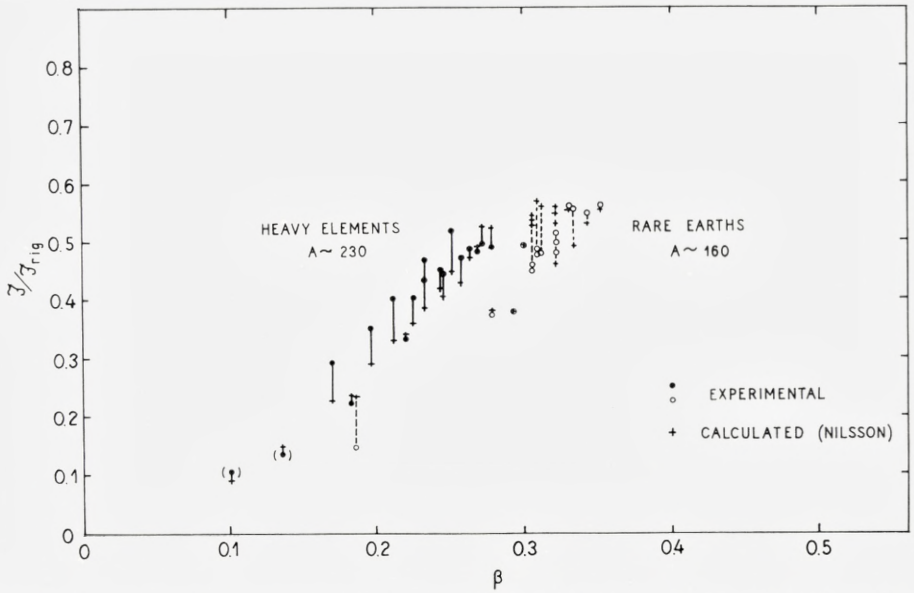


Fig. 27. The ratios of the moments of inertia to the rigid rotor moments of inertia, $\Im/\Im_{rig}$, plotted as a function of $\beta$. The results for even rare earth nuclei are taken from ELBEK, OLESEN and SKILBREID.[14] Two points for Em have been placed in brackets as a warning (see the text). Circles represent experimental points. Crosses are calculated values (see text).

nucleus are joined. The theoretical values have been calculated on the basis of individual-particle motion in a spheroidal field with pairing correlations added, using the general expressions derived by BELYAEV[15]. It is seen that the agreement between theory and experiment is quite satisfactory, especially in the heavy element region. The discrepancies found are on the average 10 %, while the experimental errors are of the order of 3 %.

We may summarize our conclusions by saying that recent theoretical calculations succeed very well in reproducing the general trends of the experimental results. The deviations between theory and experiment are of the order of 10 %, which is somewhat more although of the same order of magnitude as the experimental uncertainty. It remains to be seen whether a refinement of the theory and of the experimental accuracy will remove the discrepancies.

We wish to thank Professor NIELS BOHR for the excellent working conditions at his Institute. Essential help was received in the form of seven sources from Dr. E. P. STEINBERG of the Argonne National Laboratory, and two isotope separations by ing. O. SKILBREID. Most of the chemical mani-

pulations were ably performed by Mrs. HELLE NORDBY. We thank E. SKURNIK and B. ELBEK for supplying us with data in advance of publication. Valuable suggestions have been received from A. BOHR, T. HUUS, B. MOTTELSON, O. B. NIELSEN, and S. G. NILSSON.

Two of the authors (R. E. B. and J. C. S.) wish to thank the Institute for Theoretical Physics for its hospitality, and one (J. C. S.) wishes to thank the Ford Foundation for making his stay in Copenhagen possible.

*Institute for Theoretical Physics, University of Copenhagen.*
Radiation Laboratory, Department of Physics,
McGill University, Montreal.
Physics and Mathematics Branch, Division of Research,
U.S. Atomic Energy Commission, Washington 25, D.C.

## References

(1) K. ALDER *et al.*, Revs. Mod. Phys. **28**, 432 (1956).
(2) R. E. GREEN and R. E. BELL, Nuclear Instruments **3**, 127 (1958).
(3) R. E. BELL and M. H. JØRGENSEN, Can. J. Phys. **38**, 652 (1960).
(4) D. STROMINGER, J. M. HOLLANDER, and G. F. SEABORG, Revs. Mod. Phys. **30**, 585 (1958).
(5) J. G. SIEKMAN and H. DE WAARD, Nuclear Physics **8**, 402 (1958).
(6) J. C. SEVERIENS and F. W. RICHTER, Nuclear Physics **13**, 239 (1959).
(7) H. VARTAPÉTIAN, Comptes Rend. **246**, 1846 (1958).
(8) J. G. SIEKMAN and G. T. POTT, Physica **25**, 179 (1959).
(9) H. VARTAPÉTIAN and R. FOUCHER, Comptes Rend. **246**, 939 (1958).
(10) K. O. NIELSEN and O. SKILBREID, Nuclear Instruments **2**, 15 (1958).
(11) E. SKURNIK, B. ELBEK, and M. C. OLESEN, private communication. See also reference (1).
(12) B. R. MOTTELSON and S. G. NILSSON, Mat. Fys. Skr. Dan. Vid. Selsk. **1**, no. 8 (1959).
(13) M. E. ROSE, Internal Conversion Coefficients, North-Holland Publishing Co., Amsterdam, 1958.
(14) B. ELBEK, M. C. OLESEN, and O. SKILBREID, Nuclear Physics (to be published).
(15) S. T. BELYAEV, Mat. Fys. Medd. Dan. Vid. Selsk. **31**, no. 11 (1959).

Indleveret til selskabet 16. marts 1960.
Færdig fra trykkeriet 31. oktober 1960.

Matematisk-fysiske Meddelelser
udgivet af
Det Kongelige Danske Videnskabernes Selskabs
Bind **32,** nr. 13

Mat. Fys. Medd. Dan. Vid. Selsk. **32,** no. 13 (1960)

# SOUND PROPAGATION IN A DILUTE FERMI GAS AT ZERO TEMPERATURE

BY

K. GOTTFRIED AND L. PIČMAN

København 1960
i kommission hos Ejnar Munksgaard

# CONTENTS


| | Pages |
|---|---|
| I. Introduction | 3 |
| II. Formulation of the problem | 4 |
| A. The response to an external field | 4 |
| B. The propagation of density fluctuations | 8 |
| III. The undamped approximation | 13 |
| A. Collective frequency and cut-off momentum | 13 |
| B. Phonon contribution to ground state energy | 18 |
| IV. Attenuation of zeroth sound | 19 |
| A. Definition of the complex phonon energy | 19 |
| B. Corrections to the Fredholm denominator | 22 |
| C. The width | 28 |
| References | 30 |


## Synopsis


LANDAU has shown that a non-ideal Fermi gas at zero temperature can sustain collective oscillations of the acoustical type (zeroth sound). The present work concerns itself with the attenuation of zeroth sound in a dilute Fermi gas with repulsive interactions. The problem is formulated in terms of the Green function $\mathcal{G}$ which describes the propagation of density fluctuations through the system. The simplest approximation to $\mathcal{G}$ leads to Landau's dispersion law which is analyzed in some detail. The contribution of the phonons' zero point oscillations to the ground state energy is estimated, and shown to lead to a term which has an essential singularity at the origin of the coupling constant plane. The energy and width of the phonon are given by the poles in the spectral representation of $\mathcal{G}$, and the location of these poles is determined from the Fredholm solution of an approximate integral equation satisfied by $\mathcal{G}$. In this way it is shown that the width, divided by the displacement of the collective state above the single-particle continuum of the free gas, vanishes linearly in the long wavelength limit. It is also shown that in the limit of extreme dilution the correct damping can be obtained by merely taking the finite lifetime of single-particle excitations into account, and ignoring the dissipative effects of the non-instantaneous interactions between the particles in the medium. Finally, it is also argued that the Fredholm method is the natural tool for discussing many problems in the theory of collective motion.



Printed in Denmark
Bianco Lunos Bogtrykkeri A-S

# Introduction

LANDAU has shown [1] that a Fermi gas at the absolute zero of temperature can sustain collective excitations provided the inter-particle forces have a finite range and are predominantly repulsive. In the long wavelength limit he found that these excitations have a phonon spectrum, i. e., an energy proportional to their momentum, but that their velocity exceeds the classical sound velocity by $\sqrt{3}\,(1+\delta)$, with $\delta$ depending on the strength of the forces in a very non-analytic fashion. By examining the appropriate density matrix LANDAU has also shown that the mode in question can be described by a rather peculiar distortion of the Fermi sphere which is quite different from what one would expect for an ordinary sound wave, and in order to emphasize these distinctions he has called this motion zeroth sound. If the temperature of the system is raised, the damping of zeroth sound rapidly increases, as ABRIKOSOV and KHALATNIKOV have recently demonstrated [2].

In deriving the results just summarized, LANDAU employed the somewhat semi-classical theory of Fermi liquids which he previously developed [3]. This theory does not readily lend itself to a systematic study of corrections to lowest order results, nor is it clear what approximations have tacitly been made in order to arrive at these results. It is therefore of some interest that Landau's findings have been retrieved from the more general field-theoretic formulation of the many-particle problem by GALITSKII and MIDGDAL [4], and by GLASSGOLD, HECKROTTE and WATSON [5]. From this work it appears at first sight that Landau's approximations are essentially* the same as those invoked in the theory of plasma oscillation of an electron gas [6–9]. As these approximations are known to be strictly valid only in the high density limit for an electron gas [10], it is natural to ask whether Landau's results are characteristic of the approximations used, or whether they will also be found in a more accurate treatment.

In order to answer these questions we have investigated the corrections to Landau's results for the case of a dilute gas. This is the natural system

* We use the qualification "essentially" because Landau's treatment automatically includes a certain class of self-energy effects, and replaces the actual inter-particle potential by a scattering matrix.

to choose for this purpose, since one can hope to make systematic expansions in the small parameter $k_F a_0$ ($k_F$ being the Fermi momentum, and $a_0$ the scattering length associated with the inter-particle forces). One then finds a complex correction to the phonon energy, the imaginary part representing the decay (or damping) of the highly organized motion into more complicated excitations. This damping is found to vanish in the long wavelength limit, and Landau's conclusions are thereby substantiated.

Unfortunately our considerations cannot be applied to any existing physical system without greatly transcending our basic approximations. $He^3$ is, from our point of view, a very dense liquid, and a semi-phenomenological theory such as Landau's appears to us the only possible way of describing this system. Nuclear matter is a much more dilute Fermi gas, but in nuclear physics the problem of practical interest is the collective motion of a finite system, with the attendant breakdown of translational invariance. In view of these remarks, the work presented here constitutes a contribution to the mathematical physics, but not the theoretical physics, of many-body systems.

In Section II, the problem is formulated in a general way, and an integral equation for the Green function which describes the propagation of density fluctuations is derived. The phonon's dispersion law in Landau's approximation* is discussed in Section III, and the phonon contribution to the ground state energy is estimated; it is shown that the ground state energy has an essential singularity at $k_F a_0 = 0$. A systematic discussion of damping by means of the Fredholm theory is presented in Section IV. As we shall see, the Fredholm method is the natural tool for investigating the dispersion law of any collective motion, because it leads directly to the poles of Green's function in the complex energy plane. The method is, moreover, very practical because the diagonal terms in the Fredholm determinant exist in the many-body case, and do not have to be eliminated as in three-dimensional scattering problems.

## II. Formulation of the Problem

### A. The Response to an External Field

The most natural way to formulate the problem at hand is to ask for the response of the system to a time-dependent, externally applied field $F(t)$.** We shall assume that the resulting interaction Hamiltonian $W(t)$ is linear

* For an elementary account of this matter, see ref. [11].

** This approach has, of course, been used by many authors. Cf., e.g., references [12-14].

in $F(t)$, and that $F(t)$ can be made weak enough for the Born approximation to be valid. We shall, furthermore, assume that $F(t)$ interacts with the particles of the target one at a time, that is to say, we assume that $W(t)$ is a sum of one-particle operators. In the case of $He^3$, for example, an external field satisfying our requirements would be provided by a beam of light[15], a magnetic field, or perhaps by the interaction with cold neutrons.

Since $W(t)$ is assumed to be linear in $F(t)$, we can restrict ourselves to an external field having a single frequency $\omega$ and one wave number $\boldsymbol{q}$, in which case $W(t) = \{W_{q,\omega}\, e^{-i\omega t} + \text{h.c.}\}$. In terms of second quantized operators we shall write $W_{q,\omega}$ as*

$$W_{q,\omega} = \int (d^3x)\, e^{i\boldsymbol{q}\cdot\boldsymbol{x}}\, \psi^\dagger(\boldsymbol{x})\, [F^{(0)}_{q,\omega} + \sigma \cdot \boldsymbol{F}^{(1)}_{q,\omega}]\, \psi(\boldsymbol{x}). \tag{1}$$

$F^{(0)}_{q,\omega}$ and $\boldsymbol{F}^{(1)}_{q,\omega}$ are the parameters which characterize the interaction. Thus, if we apply a magnetic field $\{\boldsymbol{H}_{q,\omega}\, e^{i(\boldsymbol{q}\cdot\boldsymbol{x}-\omega t)} + \text{c.c.}\}$ to $He^3$, $F^{(0)}_{q,\omega} = 0$ and $\boldsymbol{F}^{(0)}_{q,\omega} = \mu \boldsymbol{H}_{q,\omega}$, with $\mu$ the magnetic moment of the $He^3$ nucleus, whereas for neutron diffraction

$$F^{(0)} \sim \frac{1}{4}(\alpha_s + 3\,\alpha_t),$$

$$\boldsymbol{F}^{(1)} \sim \frac{1}{4}(\alpha_t - \alpha_s)\, \sigma_n,$$

where $\alpha_s$ and $\alpha_t$ are the singlet and triplet scattering lengths, and $\sigma_n$ is the neutron's spin vector. If we choose the spin quantization axis of the target particles parallel to $\boldsymbol{F}^{(1)}$, we can rewrite eq. (1) as

$$W_{q,\omega} = \sqrt{2} \int d^3x\, e^{i\boldsymbol{q}\cdot\boldsymbol{x}}\, [F^{(0)}_{q,\omega}\, \varrho_0(\boldsymbol{x}) + F^{(1)}_{q,\omega}\, \varrho_1(\boldsymbol{x})], \tag{2}$$

with

$$\varrho_0(\boldsymbol{x}) = \frac{1}{\sqrt{2}} \left\{ \psi^\dagger_\uparrow(\boldsymbol{x})\, \psi_\uparrow(\boldsymbol{x}) + \psi^\dagger_\downarrow(\boldsymbol{x})\, \psi_\downarrow(\boldsymbol{x}) \right\}, \tag{3a}$$

$$\varrho_1(\boldsymbol{x}) = \frac{1}{\sqrt{2}} \left\{ \psi^\dagger_\uparrow(\boldsymbol{x})\, \psi_\uparrow(\boldsymbol{x}) - \psi^\dagger_\uparrow(\boldsymbol{x})\, \psi_\downarrow(\boldsymbol{x}) \right\}. \tag{3b}$$

The density operators $\varrho_0$ and $\varrho_1$ are, respectively, scalars and vectors in the total spin space of the target; if we restrict ourselves to transitions out of

* $\psi_s(\boldsymbol{x})$ destroys a particle with spin $s$ at the point $\boldsymbol{x}$, $\sigma$ is the Pauli matrix, $\int (d^3x)$ indicates integration over all space, and a sum over spin indices. Frequently, the spin variables are suppressed. Of course, eq. (1) is not the most general form $W_{q,\omega}$ can have, since we assume that the interaction is both local in $\boldsymbol{x}$-space and velocity-independent. A more general form for $W_{q,\omega}$ would only lead to tedious complications which are completely irrelevant to our consideration.

a ground state with total spin zero, this means that the states which can be excited by $\varrho_0$ and $\varrho_1$ are, respectively, singlets and triplets, and therefore incoherent.

We define the response of the system, $\Re(q\omega)$, to be the total transition rate out of the ground state $|0\rangle$ induced by the external field. Thus,

$$\Re(q\omega) = \Re_0(q\omega) + \Re_1(q\omega), \tag{4}$$

with ($\hbar = 1$)

$$\Re_\lambda(q\omega) = 4\pi |F^{(\lambda)}_{q,\omega}|^2 \sum_n \delta(\omega - E_n) |\langle n | \int d^3x \varrho_\lambda(\boldsymbol{x}) e^{i\boldsymbol{q}\cdot\boldsymbol{x}} | 0 \rangle|^2. \tag{5}$$

Here, $|n\rangle$ is an exact eigenstate of the system with excitation energy $E_n$.

For purposes of calculation, and also for intuitive considerations, it is very convenient to express $\Re_\lambda$ as a ground state expectation value. This may be achieved by introducing the autocorrelation function of the density fluctuations

$$\mathfrak{G}'_\lambda(q\omega) = -i\int_{-\infty}^{\infty} dt\, e^{i\omega t} \int d^3x d^3x' e^{-i\boldsymbol{q}\cdot(\boldsymbol{x}-\boldsymbol{x}')} \langle (\delta\varrho_\lambda(\boldsymbol{x}, t)\, \delta\varrho_\lambda(\boldsymbol{x}'))_+ \rangle_0, \tag{6}$$

where $(\ \ )_+$ is Wick's time ordering symbol. The time-dependent density fluctuation is defined as

$$\delta\varrho_\lambda(\boldsymbol{x}, t) = e^{iHt} \varrho_\lambda(\boldsymbol{x}) e^{-iHt} - \langle \varrho_\lambda(\boldsymbol{x}) \rangle_0,$$

where $H$ is the Hamiltonian of the target (in the absence of the external field). If $\omega \neq 0$, $\delta\varrho$ may of course be replaced by $\varrho$ itself in (6). Upon reintroducing the eigenstates $|n\rangle$ of $H$, (6) becomes

$$\mathfrak{G}'_\lambda(q\omega) = \lim_{\eta\to 0} \sum_n \left\{ \frac{|\langle n | \int d^3x e^{i\boldsymbol{q}\cdot\boldsymbol{x}} \varrho_\lambda(\boldsymbol{x}) | 0 \rangle|^2}{\omega - E_n + i\eta} - \frac{|\langle n | \int d^3x e^{-i\boldsymbol{q}\cdot\boldsymbol{x}} \varrho_\lambda(\boldsymbol{x}) | 0 \rangle|^2}{\omega + E_n - i\eta} \right\} + 2\pi i \delta(\omega) |\langle \int d^3x\, e^{i\boldsymbol{q}\cdot\boldsymbol{x}} \varrho_\lambda(\boldsymbol{x}) \rangle_0|^2. \tag{7}$$

Comparing eq. (5) with eq. (7), we have

$$\Re_\lambda(q\omega) = -4 |F^{(\lambda)}_{q,\omega}|^2 \operatorname{Im} \mathfrak{G}'_\lambda(q\omega) \tag{8}$$

if $\omega > 0$.

According to eq. (7), the poles of $\mathfrak{G}'_\lambda(q\omega)$ lie at the system's excitation energies (resonant frequencies), while the residues at these poles are pro-

portional to the transition probabilities for exciting the corresponding states. If the system is a free Fermi gas, these poles are confined to the region of the $q-\omega$ plane bounded by the curves $\omega = (q^2/2\,m) \pm qk_F/m$. The residues at these poles are squares of single-particle matrix elements, and therefore independent of the number of particles $N$.

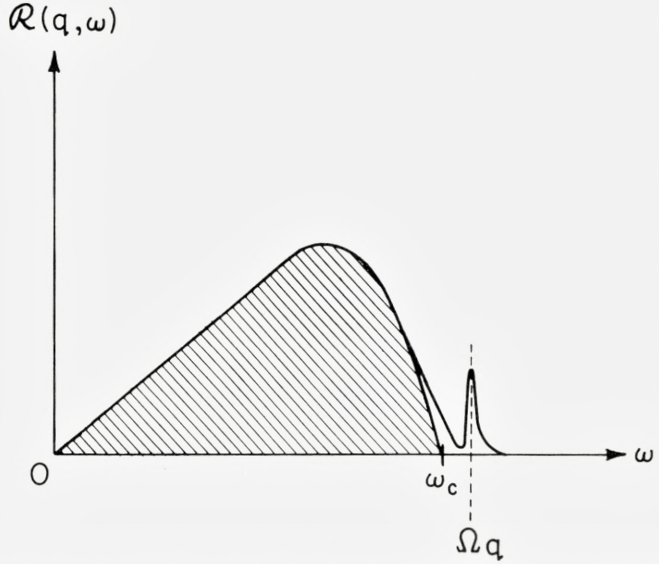


Fig. 1. The response as a function of $\omega$ for fixed $q$ is sketched here. The shaded portion show the response in the absence of interaction, and $\omega_c$ is defined by eq. (33). The collective resonanc is centered at $\Omega_q$.

When the interactions in the system are turned on, $\mathfrak{S}'_\lambda(q\omega)$ acquires singularities throughout the entire $q-\omega$ plane, the residues at these new poles being in general quite small if the interactions are weak. In the approximation of Landau (and Galitskii — Migdal), however, only a line of new singularities appears, but their residues are anomalously large. They therefore correspond to states having transition probabilities out of the ground state which are vastly greater than the single-particle probabilities mentioned earlier, and it is therefore natural to call these collective excitations.

A more accurate treatment exhibits the other singularities, and the the huge residues of order $N$ are spread over many poles in the vicinity

of the line of singularities discovered by Landau. For fixed $q$ and as a function of $\omega$, $\Re(q\omega)$ then has the form shown in Fig. 1, with the sharp resonance centered at $\Omega_q$ coming from the collective excitation.

## B. The Propagation of Density Fluctuations

We now turn to the evaluation of $\mathfrak{G}'_\lambda(q\omega)$. It is not possible, in general, to find an equation which determines $\mathfrak{G}'_\lambda(q\omega)$ itself*, and it is necessary to consider the most general 4-point propagator**

$$\left.\begin{aligned}\mathfrak{G}(p_1 s_1,\ p_2 s_2;\ p_3 s_3,\ p_4 s_4) = (2\pi)^{-8}\int d^4x_1 \ldots d^4x_4\, e^{-i\,(p_1\cdot x_1 - p_2\cdot x_2 + p_3\cdot x_3 - p_4\cdot x_4)}\\ \times\langle(\psi_{s_1}(x_1)\,\psi^\dagger_{s_2}(x_2)\,\psi_{s_3}(x_3)\,\psi^\dagger_{s_4}(x_4))_+\rangle_0 .\end{aligned}\right\} \quad (9)$$

The physical significance of the expectation value in eq. (9) is quite clear: when $t_1, t_2 > t_3, t_4$, it represents the probability amplitude for finding a "particle-hole" excitation superimposed on the true ground state at $(x_1, x_2)$, if such an excitation was originally prepared at $(x_3, x_4)$. The relationship between the function defined by eq. (9) and $\mathfrak{G}'_\lambda(q\omega)$ will now be given. First, note that translation invariance requires eq. (9) to contain the factor $\delta(p_1 - p_2 + p_3 - p_4)$; it is therefore convenient to introduce the variables

$$p = (p_1 + p_2)/2,\quad \bar{p} = (p_3 + p_4)/2,\quad P = p_1 - p_2,\quad P' = p_4 - p_3 . \quad (10)$$

Functions which describe singlet ($\lambda = 0$) and triplet ($\lambda = 1$) excitations can now be defined through

$$\delta(P - P')\,\mathfrak{G}_{1-\lambda}(p\bar{p}; P) = \sum_{s_1 \ldots s_4} \langle \lambda\, 0 \mid -s_1 s_2\rangle\, \mathfrak{G}(p_1 s_1,\ \ldots,\ p_4 s_4)\langle -s_3 s_4 \mid \lambda\, 0\rangle, \quad (11)$$

where $\langle \lambda 0 \mid s s'\rangle$ is the usual Clebsch-Gordan coefficient for spin 1/2. Again because of translation symmetry, it is more convenient to consider

* In Hubbard' spapers on the electron gas [7], an equation which employs the notion of irreducible polarization parts is derived for $\mathfrak{G}'(q\omega)$ itself. We, however, are concerned with strong, short-range forces, for which direct and exchange diagrams are of the same magnitude, and which, moreover, must be represented by a rather complicated pseudo-potential (see Figs. 3 and 4, and eq. (24)). Therefore, it does not appear to be possible consistently to define simple polarization parts, and a technique such as the one described here seems to be required.

** Our notation is: $x = (\boldsymbol{x}, t)$, $p = (\boldsymbol{k}, \varepsilon)$, $x \cdot p = \boldsymbol{x}\cdot\boldsymbol{k} - \varepsilon t$, and $\psi(x)$ is the Heisenberg operator $e^{iHt}\psi(\boldsymbol{x})\,e^{-iHt}$.

$$\mathfrak{G}_\lambda(\varkappa) = -i(2\pi)^3 \int d^4x\, e^{-i\varkappa\cdot x} \langle (\varrho_\lambda(x)\,\varrho_\lambda(0))_+ \rangle_0 , \tag{6'}$$

$\varkappa = (\boldsymbol{q}, \omega)$ being the 4-vector of momentum transfer; since $x = 0$, the relationship between eqs. (6) and (6') is simply $\mathfrak{G}'_\lambda(\varkappa) = (V/8\pi^3)\,\mathfrak{G}_\lambda(\varkappa)$, where $V$ is the volume of the system. Upon comparing eq. (6') with eqs. (9) and (11), we arrive at the required connection

$$\mathfrak{G}_\lambda(\varkappa) = \frac{1}{2\pi i} \int_+ d^4p \int_+ d^4\bar{p}\; \mathfrak{G}_\lambda(p\bar{p};\varkappa) . \tag{12}$$

The subscript "+" on the integral signs indicates that in carrying out hte integrations over the energy components of $p$ and $\bar{p}$ the contours are to be

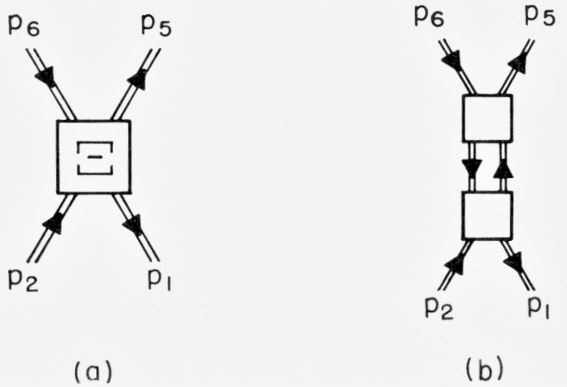


Fig. 2. The definition of $\Xi(15;\,26)$. Double lines represent the "dressed" propagator $G(p)$.

closed in the upper half plane; this prescription produces the correct sequence of equal-time field operators as demanded by eq. (6').

As Galitskii and Migdal have noted, the function defined by eq. (9) satisfies the identity[16–18]

$$\mathfrak{G}(12;34) = \mathfrak{G}^0(12;34) + G(1)\,G(2) \int \Xi(15;26)\,\mathfrak{G}(65;34)\,(d^4p_5)\,(d^4p_6); \tag{13}$$

here $G(p)$ is the one-particle Green function

$$G(p) = -i \int d^4x\, e^{-ip\cdot x} \langle (\psi(x)\,\psi^\dagger(0))_+ \rangle_0 , \tag{14}$$

and

$$\mathfrak{G}^0(12;34) = G(p_2)\,G(p_4)\,[\delta(p_2-p_3)\,\delta(p_1-p_4) - \delta(p_1-p_2)\,\delta(p_3-p_4)] .$$

The kernel $\Xi(15;\,26)$ is the sum of all diagrams of the type shown in Fig. 2(a) which *cannot* be reduced to diagrams like that shown in Fig. 2(b).

If the interparticle force $v$ is weak, the leading contribution to this kernel is just proportional to the matrix element $(15 \mid v \mid 26)$. When the forces are strong, but have a range small compared to the mean interparticle spacing, $\Xi$ can be expanded in powers of the free space scattering amplitudes. We postpone a more detailed discussion of $\Xi$ for a moment, because it is possible to effect a considerable simplification of eq. (13) on general principles*. Invariance considerations immediately lead to the conclusion that**

$$\left.\begin{aligned} &\Xi(p_1 s_1,\ p_5 s_5;\ p_2 s_2,\ p_6 s_6) \\ &= \delta(p_1 + p_5 - p_2 - p_6) \sum_{SM} \langle s_1 s_5 \mid SM \rangle \Xi_S(\tilde{p},\ \tilde{p}';\ \tilde{P}) \langle SM \mid s_2 s_6 \rangle, \end{aligned}\right\} \tag{15}$$

with

$$\tilde{p} = (p_1 - p_5)/2,\ \tilde{p}' = (p_2 - p_6)/2,\ \tilde{P} = p_1 + p_5.$$

Therefore, if we change variables according to eq. (10), employ eq. (15) and the inverse of relation (11), and integrate over $\overline{p}'$, we find that eq. (13) reduces to

$$\mathfrak{G}_\lambda(p;\varkappa) = \mathfrak{G}^0(p;\varkappa)\left\{1 + \int d^4p'\, R_\varkappa^{(\lambda)}(p \mid p')\, \mathfrak{G}_\lambda(p';\varkappa)\right\}, \tag{16}$$

with

$$\mathfrak{G}_\lambda(p;\varkappa) = \int_+ d^4\overline{p}\, \mathfrak{G}_\lambda(p\overline{p};\varkappa), \tag{17}$$

and $(\varkappa \neq 0)$

$$\mathfrak{G}^0(p;\varkappa) = G\left(p + \frac{1}{2}\varkappa\right) G\left(p - \frac{1}{2}\varkappa\right). \tag{18}$$

The kernel in eq. (16) is related to the functions defined by eq. (15) through

$$\left.\begin{aligned} R_\varkappa^{(0)}(p \mid p') &= 1/2\left\{3\,\Xi_1(Q_1, Q_2; Q) + \Xi_0(Q_1, Q_2; Q)\right\}, \\ R_\varkappa^{(1)}(p \mid p') &= 1/2\left\{\Xi_1(Q_1, Q_2; Q) - \Xi_0(Q_1, Q_2; Q)\right\}, \end{aligned}\right\} \tag{19}$$

with

$$Q_1 = (p - p' + \varkappa)/2,\ Q_2 = (p - p' - \varkappa)/2,\ Q = p + p'. \tag{19'}$$

*Eq.* 16 *is our basic equation*; its solution $\mathfrak{G}_\lambda(p;\varkappa)$, after integration over $p$, gives us the desired quantity $\mathfrak{G}_\lambda(\varkappa)$ from which we can immediately deduce the response. The reader will have noted that eq. (16) has the same

* In ref. [4], a homogeneous particle-hole wave equation is derived from eq. (13). As GELL-MANN and LOW [17] have pointed out, such a wave equation exists only if the eigenstate in question is a discrete one (e. g., the deuteron in the meson-nucleon system). In our problem, the collective mode is degenerate with a host of more complex excitations (i. e., it is damped), and so the Galitskii-Migdal equation (their eq. 40) only holds in the no-damping approximation. Our procedure is always valid, and is, in fact, just as easy to work with as the particle-hole wave equation.

** Here we assume that there are no tensor or spin-orbit forces, i. e., that the system's total spin vector is a constant of motion.

structure as the integral equation for a two-particle Green function in normal scattering theory. Loosely speaking, $\mathfrak{G}_\lambda(p;\varkappa)$ describes the propagation through the medium of a particle-hole pair with total 4-momentum $\varkappa$, relative 4-momentum $p$, and spin $\lambda$. It is impossible, however, to extract a complete orthonormal set of particle-hole wave functions from $\mathfrak{G}_\lambda(p;\varkappa)$.

It is of course not possible to solve eq. (16) with arbitrary kernels, and approximate solutions must be sought. But the approximation technique must be capable of producing resonances in the response, and ordinary perturbation theory is therefore ruled out. (In fact, as we shall see in the next section, the ground state energy itself has an essential singularity at the origin of the coupling constant plane.) The Fredholm method[19], on the other hand, constructs the solution as the ratio of two entire functions of the coupling parameter, and is therefore well defined even if $\mathfrak{G}_\lambda(\varkappa)$ is not an analytic function of the coupling constant. The Fredholm solution reads

$$\mathfrak{G}_\lambda(\varkappa) = \Pi(\varkappa) + \frac{1}{2\pi i}\frac{\mathfrak{N}_\lambda(\varkappa)}{\mathfrak{D}_\lambda(\varkappa)}, \tag{20}$$

with

$$\Pi(\varkappa) = \frac{1}{2\pi i}\int_+ d^4p\, G(p+\varkappa/2)\, G(p-\varkappa/2), \tag{21}$$

$$\mathfrak{N}_\lambda(\varkappa) = \sum_{n=1}^{\infty}\mathfrak{N}_\lambda^{(n)}(\varkappa),\quad \mathfrak{D}_\lambda(\varkappa) = 1 - \sum_{n=1}^{\infty}\mathfrak{D}_\lambda^{(n)}(\varkappa), \tag{22}$$

$$\mathfrak{N}_\lambda^{(1)}(\varkappa) = \int_+ d^4p \int d^4p'\, \mathfrak{G}^0(p;\varkappa)\, R_\varkappa^{(\lambda)}(p\,|\,p')\, \mathfrak{G}^0(p';\varkappa), \tag{23a}$$

$$\left.\begin{aligned}\mathfrak{N}^{(2)}(\varkappa) = \int_+ d^4p \int d^4p'd^4p''\, \mathfrak{G}^0(p;\varkappa)\, R_\varkappa^{(\lambda)}(p\,|\,p')\, \mathfrak{G}^{(0)}(p';\varkappa)\, R_\varkappa^{(\lambda)}(p'\,|\,p'')\, \mathfrak{G}^0(p'';\varkappa)\\ - \mathfrak{D}_\lambda^{(1)}(\varkappa)\, \mathfrak{N}_\lambda^{(1)}(\varkappa),\end{aligned}\right\} \tag{23b}$$

$$\mathfrak{D}_\lambda^{(1)}(\varkappa) = \int d^4p\, \mathfrak{G}^0(p;\varkappa)\, R_\varkappa^{(\lambda)}(p\,|\,p), \tag{23c}$$

$$\mathfrak{D}_\lambda^{(2)}(\varkappa) = -1/2\int d^4p\, d^4p' \begin{vmatrix} \mathfrak{G}^0(p;\varkappa)\, R_\varkappa^{(\lambda)}(p\,|\,p) & \mathfrak{G}^0(p;\varkappa)\, R_\varkappa^{(\lambda)}(p\,|\,p') \\ \mathfrak{G}^0(p';\varkappa)\, R_\varkappa^{(\lambda)}(p'\,|\,p) & \mathfrak{G}^0(p';\varkappa)\, R_\varkappa^{(\lambda)}(p'\,|\,p') \end{vmatrix}, \tag{23d}$$

etc.

We now return to a closer specification of $\Xi$, and thereby of the kernels of eq. (16). As stated in Section I, we shall be interested in the dilute gas, and so an expansion of $\Xi$ in terms of free scattering amplitudes is required. For this purpose, we introduce the $T$-matrix in the ladder approximation (see Fig. 3); this quantity plays the role of a non-singular pseudo-potential


Fig. 3. The $T$-matrix is represented by the shaded vertex, and the two-particle potential $v$ by the heavy dot. The $T$-matrix is the sum of all the diagrams shown. The single lines in this figure represent the free-particle propagator $G_0(p)$ defined by eq. (27).

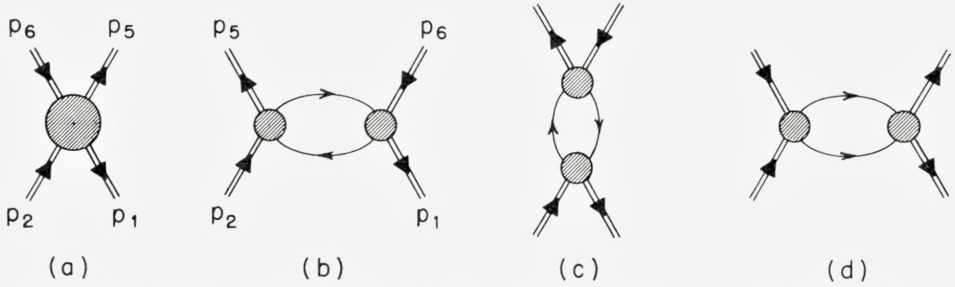


Fig. 4. The two lowest order diagrams contributing to the kernel $\Xi$ are shown in (a) and (b). The second order diagrams (c) and (d) are not to be counted because they are already included by the integral equations for $\mathfrak{G}(p;\varkappa)$ and the $T$-matrix.

in terms of which expansions can be carried out, the lowest contributions to $\Xi$ being those of Figs. 4(a) and (b). To each $T$-vertex there corresponds a factor $\langle \boldsymbol{k}_1 s_1 \boldsymbol{k}_2 s_2 \mid T(E) \mid \boldsymbol{k}_3 s_3 \boldsymbol{k}_4 s_4 \rangle$, where $\boldsymbol{k}_1 s_1$, $\boldsymbol{k}_2 s_2$ ($\boldsymbol{k}_3 s_3$, $\boldsymbol{k}_4 s_4$) are the momenta and spins of the lines leaving (entering) the vertex, and $E = \omega_1 + \omega_2 = \omega_3 + \omega_4$ is the sum of the energies entering or leaving the vertex. Now let $\boldsymbol{k} = (\boldsymbol{k}_1 - \boldsymbol{k}_2)/2$, $\boldsymbol{k}' = (\boldsymbol{k}_3 - \boldsymbol{k}_4)/2$, $\boldsymbol{K} = \boldsymbol{k}_1 + \boldsymbol{k}_2$, and

$$\langle \boldsymbol{k}_1 s_1 \boldsymbol{k}_2 s_2 \mid T(E) \mid \boldsymbol{k}_3 s_3 \boldsymbol{k}_4 s_4 \rangle$$
$$= \frac{\delta(\boldsymbol{k} - \boldsymbol{k}_3 - \boldsymbol{k}_4)}{(2\pi)^3} \sum_{SM} \langle s_1 s_2 \mid SM \rangle \langle \boldsymbol{k} \mid T_S(E, \boldsymbol{K}) \mid \boldsymbol{k}' \rangle \langle SM \mid s_3 s_4 \rangle .$$

We wish to express $\langle \boldsymbol{k} \mid T \mid \boldsymbol{k}' \rangle$ in terms of quantities which describe the free-space scattering. The most convenient parameters are the amplitudes $f_S(\boldsymbol{k} \mid \boldsymbol{k}')$, which are related to the center-of-mass differential cross sections for unpolarized particles through

$$d\sigma_{\boldsymbol{k}\leftarrow\boldsymbol{k}'} = \left\{ 1/4 \mid f_0(\boldsymbol{k} \mid \boldsymbol{k}') \mid^2 + 3/4 \mid f_1(\boldsymbol{k} \mid \boldsymbol{k}') \mid^2 \right\} \left(\frac{m}{4\pi}\right)^2 d\Omega .$$

If these $f$'s satisfy outgoing wave boundary conditions at infinity, then the relation

$$\langle \boldsymbol{k} \mid T_S(E, \boldsymbol{K}) \mid \boldsymbol{k}' \rangle = f_S(\boldsymbol{k} \mid \boldsymbol{k}') - \frac{m}{2} \int d^3k'' \frac{f_S(\boldsymbol{k} \mid \boldsymbol{k}'') f_S^*(\boldsymbol{k}' \mid \boldsymbol{k}'')}{\boldsymbol{k}'^2 - \boldsymbol{k}''^2 + i\eta}$$

$$+ 1/2 \int m\, d^3k'' \left\{ \frac{\Lambda_{\boldsymbol{K}}^{(+)}(\boldsymbol{k}'')}{mE - \frac{1}{4}K^2 - k''^2 + i\eta} - \frac{\Lambda_{\boldsymbol{K}}^{(-)}(\boldsymbol{k}'')}{mE - \frac{1}{4}K^2 - k''^2 - i\eta} \right\} f_S(\boldsymbol{k} \mid \boldsymbol{k}'') f_S^*(\boldsymbol{k}' \mid \boldsymbol{k}'') \quad (24)$$

gives the $T$-matrix correctly to second order in $f^{(20)}$. The other new symbols are

$$\Lambda_{\boldsymbol{K}}^{(\pm)}(\boldsymbol{k}) = \Theta_{\pm}(\boldsymbol{K}/2 + \boldsymbol{k})\, \Theta_{\pm}(\boldsymbol{K}/2 - \boldsymbol{k}).$$

with

$$\left.\begin{aligned} \Theta_+(k) &= 1 - \Theta_-(k) \\ &= \begin{cases} 1 & \text{if } k > k_F \\ 0 & \text{if } k < k_F \end{cases} \end{aligned}\right\} \quad (25)$$

The factor 1/2 in front of the integrals in eq. (24) is due to the fact that our amplitudes are already antisymmetrized: if primes denote unsymmetrized amplitudes, then

$$f_S(\boldsymbol{k} \mid \boldsymbol{k}') = f'_S(\boldsymbol{k} \mid \boldsymbol{k}') + (-1)^S f'_S(\boldsymbol{k} \mid -\boldsymbol{k}').$$

We are now in possession of the formal apparatus required for our investigation. We begin by summarizing the situation when damping is ignored.

## III. The Undamped Approximation

### A. Collective Frequency and Cut-off Momentum

The inhomogeneous term $\mathfrak{G}^0(p; \varkappa)$ of eq. (16) has branch cuts along the entire real axis of $\omega$, and therefore the solution of this equation must be expected to have the same analytic property, no matter what approximation for the kernel $R$ is used. In physical terms, therefore, eq. (16) has no undamped solutions. This is of course due to the fact that the single-particle

propagators $G$ which we have used describe "dressed quasi-particle" excitations which are themselves damped. If we are to get undamped solutions, we must therefore replace $\mathfrak{G}^0(p;\varkappa)$ by

$$\mathfrak{G}_f(p;\varkappa) = G_0\left(p+\frac{1}{2}\varkappa\right) G_0\left(p-\frac{1}{2}\varkappa\right), \tag{26}$$

where $G_0(p)$ is the free-particle propagator,

$$G_0(p) \equiv G_0(\boldsymbol{k},\varepsilon) = \frac{\Theta_+(k)}{\varepsilon-\frac{1}{2m}|\boldsymbol{k}|^2+i\eta} + \frac{\Theta_-(k)}{\varepsilon-\frac{1}{2m}|\boldsymbol{k}|^2-i\eta}. \tag{27}$$

The lowest order contributions to the kernels of eq. (16) are linear in the $f$'s, and therefore arise from Fig. 4(a). They are simply

$$R_\varkappa^{(0)}(p\,|\,p') = -\frac{1}{2}\,i\,(2\pi)^{-4}\left\{3\,f_1(\boldsymbol{Q}_1\,|\,\boldsymbol{Q}_2)+f_0(\boldsymbol{Q}_1\,|\,\boldsymbol{Q}_2)\right\}, \tag{28a}$$

$$R_\varkappa^{(1)}(p\,|\,p') = -\frac{1}{2}\,i\,(2\pi)^{-4}\left\{f_1(\boldsymbol{Q}_1|\,\boldsymbol{Q}_2)-f_0(\boldsymbol{Q}_1\,|\,\boldsymbol{Q}_2)\right\}, \tag{28b}$$

the $\boldsymbol{Q}$'s being the spatial parts of the 4-vectors defined by eq. (19′). The momentum transfer involved in these scattering amplitudes is $\boldsymbol{q}$, which is always small compared to $k_F$ (long wavelength disturbances). From eqs. (26) and (27) it follows that $|\boldsymbol{k}|$ and $|\boldsymbol{k}'|$ lie in the vicinity of $k_F$, and therefore $|\boldsymbol{Q}_1| \lesssim k_F$, $|\boldsymbol{Q}_2| \lesssim k_F$. Hence in the dilute gas, where the effective range is small compared to $k_F^{-1}$, we can replace the amplitudes in eq. (28) by their zero-energy limits. Since $f_1$ only contains states with odd angular momentum, we have

$$f_1 \to 0 \tag{29a}$$

in this limit, whereas

$$f_0 \to \frac{8\pi}{m}\,a_0, \tag{29b}$$

$a_0$ being the conventional $S$-wave scattering length[21]. With these simplifications eq. (16) becomes trivially soluble,

$$\mathfrak{G}_\lambda(\varkappa) = \frac{\Pi_0(\varkappa)}{1-(-1)^\lambda\,(a_0/2\pi^2 m)\,\Pi_0(\varkappa)}, \tag{30}$$

with

$$\Pi_0(\varkappa) = 1/2\pi i \int d^4p\, G_0(p+\varkappa/2)\, G_0(p-\varkappa/2). \tag{31}$$

Note that eq. (30) has the same structure as the Fredholm solution (20) of the complete equation.

According to our previous discussion, the resonant frequencies of the system are determined by the poles of $\mathfrak{G}_\lambda(\varkappa)$, i. e., in present approximation by the condition

$$1 = (-1)^\lambda \frac{a_0}{2\pi^2 m} \Pi_0(\varkappa). \tag{32}$$

The solution of this equation has been extensively discussed in the literature for the case of Coulomb interactions[7-9]. We recall that $\mathfrak{G}_\lambda(\varkappa)$ is an even function of $\omega$, and so we can confine ourselves to $\omega > 0$; it has a cut along the real $\omega$-axis when $\omega \leqslant \omega_c$, where

$$\omega_c = \frac{q k_F}{m} + \frac{q^2}{2m}. \tag{33}$$

This cut corresponds to a perturbed continuum of simple "particle-hole" excitations which is present whatever the forces, and is of little interest to us. If, however, $(-1)^\lambda a_0 > 0$, another *isolated* solution of eq. (32) can exist for $\omega > \omega_c$. This is because $\Pi_0(q, \omega)$ has the properties

$$\left.\begin{aligned} &\operatorname{Im}\Pi_0(q,\omega) = 0, \quad \Pi_0(q,\omega) > 0, \\ &\frac{\partial \Pi_0(q,\omega)}{\partial \omega} < 0, \quad \Pi_0(q,\omega) \xrightarrow[\omega\to\infty]{} 0, \end{aligned}\right\} \tag{34}$$

when $\omega > \omega_c$. The explicit form of eq. (32) for $\omega > \omega_c$ is

$$1 = (-1)^\lambda (k_F a_0 / \pi) A(q, \omega), \tag{35}$$

with

$$\left.\begin{aligned} A(q,\omega) &= -1 + \left\{ \frac{(\omega+\omega_0)(\omega-\omega_c)}{2q^3} \ln\left|\frac{\omega-\omega_c}{\omega+\omega_0}\right| + (\omega \to -\omega) \right\}, \\ \omega_0 &= q - q^2/2. \end{aligned}\right\} \tag{36}$$

In eq. (36) and all subsequent formulae of this section, momenta and energies are expressed in units of $k_F$ and $(k_F^2/m)$, respectively.

We are only interested in the case $a_0 > 0$, since for negative scattering lengths superconductivity is to be expected, and then the whole theory developed here is certainly not valid*. Thus we have a collective root only for spin singlet excitations. From eq. (35) we find that this root exists provided $q \leqslant q_c^0$, the cut-off momentum being given by

* Unlike Glassgold et. al. [6], we only find a complex root if $k_F a_0 < -\pi/2$. It is therefore clear that these pathological roots bear no simple relation to the occurrence of superconductivity, since they only appear when the forces are extremely strong.

$$q_c^0 = 0.736\, e^{-1/\xi}, \quad \xi = \frac{k_F a_0}{\pi}, \tag{37}$$

when $\xi \ll 1$. The collective root has the phonon form as $(q/q_c^0) \to 0$:

$$\Omega_q^0 \to q \left\{ 1 + 0.270\, e^{-1/\xi} \left[ 1 + 0.309\, (q/q_c^0)^2 + \ldots \right] \right\}. \tag{38}$$

A plot of the phonon energy in the weak coupling limit will be found in Fig. 5.

Another quantity of interest is the excitation probability of the collective state. We recall that this probability is proportional to the residue of $\mathfrak{G}_\lambda(\varkappa)$ at the phonon pole. A simple calculation yields

$$\Re_q \xrightarrow[q \to 0]{} \frac{50\, nq}{\xi^2}\, e^{-1/\xi} \tag{39}$$

for this residue, $n = (k_F^3/3\pi^2)$ being the density. Furthermore, $\Re_q \to 0$ as $q \to q_c^0$, as is to be expected.

A word concerning the accuracy of eqs. (37) and (38) is in order here. It is, of course, an easy matter to compute the leading correction terms to these expressions; for the extreme case $k_F a_0 = 1$ (i. e., $\xi = 1/\pi$), we then find that eqs. (37) and (38) are in error by 9 and 7 per cent, respectively. Furthermore, Fig. 5 reveals that eq. (38) reproduces the actual $q$-dependence quite well for the entire range below $q_c^0$. We therefore conclude that eqs. (37) and (38) adequately characterize the collective root in the present approximation for all reasonable values of the scattering length $a_0$.

On the other hand, once we depart from the extreme low-density limit ($\xi \to 0$), the approximation of eq. (29) must be modified, and then the simple solution (30) is no longer valid. We shall therefore resort to the Fredholm solution as given in Section II. If we retain the kernel given by eq. (28), we find that the $\lambda = 0$ secular equation is

$$1 - \frac{1}{16\pi^3} \left[ f_0(\boldsymbol{q}/2 \mid \boldsymbol{q}/2) - 3 f_1(\boldsymbol{q}/2 \mid \boldsymbol{q}/2) \right] \Pi_0(\varkappa) = 0 \tag{40}$$

instead of eq. (32). The contribution from the second Fredholm determinant, eq. (23d), has been neglected here because it already leads to a result of higher order in $\xi$ than we shall obtain from eq. (40). We now expand these forward amplitudes about $\boldsymbol{q} = 0$. Retaining terms up to $q^2$, we find that

$$1 = (\xi + q^2 \zeta)\, A(q, \omega) \tag{41}$$

replaces our previous eq. (35). Here,

$$\zeta = \frac{1}{4\pi} k_F^3 \left( \frac{1}{2} r_0 \, a_0^2 - a_0^3 - 3 \, a_1^3 \right), \tag{42}$$

$r_0$ being the $S$-wave effective range[21], and $a_1$ the $P$-wave scattering length (i. e., the $P$-wave phase shift $\delta_P \sim -(qa_1)^3$ as $q \to 0$). In deriving eqs. (41) and (42) we have only kept the real parts of $f_S$ $(\boldsymbol{q}/2 \,|\, \boldsymbol{q}/2)$. The imaginary parts of the amplitudes should not be taken into account in the present

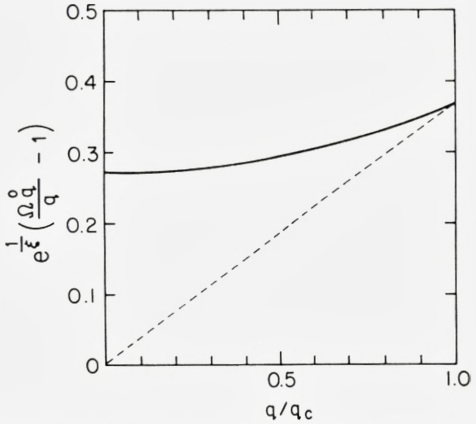


Fig. 5. The phonon energy $\Omega_q^0$ as a function of the momentum $q$ can be obtained from this graph. The abscissa shows $q$ divided by the cut-off momentum (the latter quantity being given by eq. (37)). The ordinate is

$$\left( \frac{\Omega_q^0}{q} - 1 \right) \exp(1/\xi),$$

where $\Omega_q^0$ is the solution of $1 = \xi A \left( q, \Omega_q^0 \right)$, i. e. it does not include the parameter $\zeta$ appearing in eq. (41). The present curve is therefore "universal" in the sense that it gives $\Omega_q^0$ or all $k_F a_0 \ll \pi$. The broken line indicates the top of the single-particle excitation continuum in these variables, i. e. $\left( \omega_c q^{-1} - 1 \right) \exp(1/\xi) = 0.368 \left( q/q_c^0 \right)$.

no-damping approximation; the reason for this will become clear in the following section (see discussion following eq. (58)).

From (4) we readily find that the cut-off momentum is now

$$q_c = q_c^0 \left\{ 1 + q_c^0 \left( 1 + \frac{1}{2\,\xi} \right) + \frac{\zeta}{\xi^2} (q_c^0)^2 + 0 \left( (q_c^0)^3 \right) \right\}, \tag{43}$$

whereas the collective state lies at

$$\Omega_q^0 = q \left\{ 1 + 2\,\varepsilon_0 \left[ 1 + \varepsilon_0 \left( 5 + \frac{2}{\xi} \right) + \left( \frac{\zeta}{\xi^2} + \frac{0.309}{(q_c^0)^2} \right) q^2 + \ldots \right] \right\}, \tag{44}$$

with $\varepsilon_0 = \exp(-2-\xi^{-1})$. *It is important to note that for all reasonable values of* $\xi$ *and* $\zeta$ *the cut-off* $q_c$ *lies well below the Fermi momentum.* For, even if we take a rather dense gas with $k_F a_0 = 1$, we find that $q_c^0 = 0.032$, and so the parameter $\zeta$, which contains the $P$-wave and the momentum-dependent part of the $S$-wave, has a very minute effect on eq. (43), the same being true of eq. (44).

### B. Phonon Contribution to Ground State Energy

The contribution of the phonons' zero point motion to the ground-state energy can be evaluated by using the variational principle and invoking the well-known connection between the frequency integral over the response and the equal-time pair correlation function in the ground state. The ground-state energy per particle is then[7]

$$(E_0/N) = \frac{i}{4\pi n}\int_0^{\xi}\frac{d\xi'}{\xi'}\int\frac{d^3q}{(2\pi)^3}\int_+ d\omega\ \ \frac{\xi' A(q,\omega)}{1-\xi' A(q,\omega)},$$

whence the contribution of the collective pole is

$$(E_0/N)_{\text{coll.}} = \frac{1}{2n}\int_0^{\xi}\frac{d\xi'}{\xi'}\int\frac{d^3q}{(2\pi)^3}\ \ \frac{\xi' \Re_q(\xi')}{2\pi k_F m},$$

where $\Re_q(\xi)$ is the residue at this pole. One obtains an upper limit to this integral by assuming eq. (39) to be valid for all $q$'s, and cutting the $q$-integration off at $q_c^0$. One then finds

$$(E_0/N)_{\text{coll.}} < 0.005\, e^{-5/\xi}(k_F^2/2m).$$

(The $\xi$-dependence of the exact result for $(E_0/N)_{\text{coll.}}$ is of the same form as this upper bound.) This contribution to the ground-state energy is, of course, completely negligible for all practical purposes. Nevertheless it does show that *the ground state energy of a hard sphere gas has an essential singularity at the origin of the coupling constant plane*, a result which is hardly surprising if one recalls that changing the sign of $\xi = k_F a_0/\pi$ leads to a drastically different physical system — the superfluid.

# IV. Attenuation of Zeroth Sound

## A. Definition of the Complex Phonon Energy

We now consider $\mathfrak{G}(\varkappa) \equiv \mathfrak{G}(q, z)$ as a function of the complex variable $z$, with $\omega = \mathrm{Re} z$. According to the spectral representation (7), $\mathfrak{G}(q, z)$ has the following properties: it is analytic throughout the plane except for poles and cuts along the real axis; across these cuts $\mathrm{Im}\,\mathfrak{G}$ is discontinuous while $\mathrm{Re}\,\mathfrak{G}$ is continuous; it is an even function of $z$; for $\omega > 0$, $\mathrm{Im}\,\mathfrak{G} < 0$ as $z \to \omega + i0$. We recall that eq. (7) follows directly from the definition of $\mathfrak{G}$, and therefore the preceding statements are generally valid. It is also clear that the excitation energies $E_n$ entering eq. (7) will extend to infinity, and that for a large system they must be expected to form a continuous spectrum. In our case, therefore, $\mathfrak{G}(q, z)$ should have cuts along the entire real axis*.

In the approximation considered in the last section, $\mathfrak{G}(q, z)$ was found to have a cut in the interval $-\omega_c \leqslant \mathrm{Re}\, z \leqslant \omega_c$, and simple poles at $z = \pm \Omega_q^0$. The manner in which these results will be modified by higher approximations can be seen most easily by retaining the simplest kernel in the low-density limit, eq. (29), but leaving the dressed single-particle propagators in the inhomogeneous term of eq. (16). Instead of eq. (30) we then have

$$\mathfrak{G}(q, z) \simeq \frac{\Pi(q, z)}{1 - (a_0/2\pi^2 m)\,\Pi(q, z).} \tag{45}$$

This solution already has the infinite cut, because $\mathrm{Im}\,\Pi(q, z)$ is discontinuous along the entire real axis. In fact, $\Pi(q, z)$ can be easily evaluated in terms of the spectral densities $\varrho_\pm(p, \varepsilon)$ appearing in the representation[4]

$$G(p, \varepsilon) = \int_0^\infty d\varepsilon' \left( \frac{\varrho_+(p, \varepsilon')}{\varepsilon - \mu - \varepsilon' + i\eta} + \frac{\varrho_-(p, \varepsilon')}{\varepsilon - \mu + \varepsilon' - i\eta} \right), \tag{46}$$

where $\mu$ is the separation energy (i. e., the chemical potential). According to eq. (21), therefore,

$$\Pi(q, z) = \int d^3p \int_0^\infty d\varepsilon \int_0^\infty d\varepsilon'\, \varrho_+(|\boldsymbol{p} + \boldsymbol{q}|, \varepsilon)\, \varrho_-(p, \varepsilon') \left( \frac{1}{z - \varepsilon - \varepsilon'} - \frac{1}{z + \varepsilon + \varepsilon'} \right). \tag{47}$$

The densities $\varrho_\pm(p, \varepsilon)$ are real and positive definite for real $\varepsilon$, and satisfy the relation

* Since we shall only interest ourselves in the singlet excitation ($\lambda = 0$) we drop the subscript $\lambda$ henceforth.

$$\int_0^\infty d\varepsilon \, [\varrho_+(p, \varepsilon) + \varrho_-(p, \varepsilon)] = 1 .$$

Thus, $\Pi(q, z)$ has the analytic properties listed in the preceding paragraph, and therefore the same holds for eq. (45). In other words, the poles at $z = \pm\Omega_q^0$ have now disappeared. However, since $-\operatorname{Im}\Pi(q, \omega + i0)$ is small (actually $0(f^2)$, as we shall see) when $\omega^2 > \omega_c^2$, the denominator of eq. (45) nearly vanishes if, for some $\Omega_q^2 > \omega_c^2$,

$$1 - (a_0/2\pi^2 m) \operatorname{Re}\Pi(q, \Omega_q) = 0 . \tag{48}$$

When this is the case, the discontinuity of $\mathfrak{G}(q, z)$, and *ipso facto* the response, will have sharp resonances (see Fig. 2) of approximately Lorentzian shape centered at $\operatorname{Re} z = \pm\Omega_q$, with $\Omega_q$ near $\Omega_q^0$ since $\operatorname{Re}(\Pi - \Pi_0)$ is also small. The parameters describing the line shape are then identified in the standard way with the energy $\Omega_q$ and width $\Gamma_q$ of the phonon. The solution $\mathfrak{G}(q, z)$ that we shall find can be used immediately to determine the actual shape of the absorption line (i. e., the deviations from the Lorentz form), but we shall confine ourselves to the evaluation of the parameters $\Omega_q$ and $\Gamma_q$.

As is well known[4, 9, 22], the occurrence of a resonance is associated with a pole in the analytic continuation of $\mathfrak{G}(q, z)$ from $\operatorname{Im} z > 0$, $\operatorname{Re} z > 0$, onto the next Riemann sheet in the lower half plane, the location of the pole being $z = \Omega_q - {}^1/_2 i\Gamma_q + 0\,(\Gamma_q^2/\Omega_q)$. This continuation can be effected easily by means of the Fredholm solution (20). All we need do is to evaluate $\mathfrak{D}(q, z)$ as a power series in $z$ about some point in the first quadrant of $z$—the obvious choice being the zeroth order collective frequency $\Omega_q^0 + i0$—and look for a root of $\mathfrak{D}(q, z) = 0$ with $\operatorname{Im} z < 0$. The Fredholm method has the additional advantage of providing $\mathfrak{D}(q, z)$ as a power series in the coupling parameter, since the kernel $R_\varkappa(p \mid p')$ of eq. (16) is itself such a power series. In this connection it is interesting to note that the Fredholm denominator $\mathfrak{D}(q, z)$ consists of terms which never appear in perturbation theory. The perturbation series is contained in the numerator $\mathfrak{N}$ of eq. (20), which does not enter into the determination of the pole.

The location of this pole will now be given. Let

$$\mathfrak{D}(q, z) = 1 - \xi A(q, z) - B(q, z), \tag{48}$$

where $A(q, z)$ is the function introduced in Sec. III A (cf. eqs. (35) and (36)), and $B(q, z)$ contains all the corrections, both those arising from higher order kernels and higher order Fredholm determinants, as well as those due to using dressed one-particle Green functions in the inhomogeneous term of eq. (16). Expansion of eq. (48) about $\Omega_q^0$ gives

$$\mathfrak{D}(q, z) \simeq -\xi (z - \Omega_q^0) \left. \frac{\partial A}{\partial z} \right|_{\Omega_q^0 + i0} - B(q, \Omega_q^0 + i0) + \cdots . \tag{49}$$

This expansion in $(z - \Omega_q^0)$ converges extremely well because $(z - \Omega_q^0)$ is presumably small compared to $(\Omega_q^0 - \omega_c)$, the zeroth order level displacement, and this latter quantity, it will be recalled, tends to zero exponentially as $\xi \to 0$. Therefore, if $\Omega_q^0$ is a meaningful approximation to the energy, eq. (49) provides an accurate representation of $\mathfrak{D}(q, z)$ for the $z$'s of interest to us. Except for terms which vanish exponentially, we thus have

$$\Omega_q = \Omega_q^0 - \frac{B(q, \Omega_q^0 + i0)}{\xi \left. \dfrac{\partial A(q, \omega)}{\partial \omega} \right|_{\omega = \Omega_q^0}} \tag{50}$$

for the location of the pole. If $q \ll q_c^0$ and $q_c^0 \ll 1$, (we shall confine ourselves to this domain throughout),

$$\left. \frac{\partial A(q, \omega)}{\partial \omega} \right|_{\Omega_q^0} \simeq \frac{1}{q - \Omega_q^0} \equiv -\frac{1}{D_q^0}. \tag{52}$$

Here, $D_q^0$ is the displacement of the collective state above the continuum of single-particle excitations in the approximation of Section III. Hence the "exact" displacement of this state is

$$\Omega_q - q = D_q^0 [1 + \frac{1}{\xi} B(q, \Omega_q^0 + i0)]. \tag{53}$$

In particular, therefore, the width $\Gamma_q$ divided by the zeroth order displacement is

$$\frac{\Gamma_q}{D_q^0} = -\frac{2}{\xi} \operatorname{Im} B(q, \Omega_q^0 + i0). \tag{54}$$

In the following pages we shall confine ourselves to a calculation of $(\Gamma_q / D_q^0)$, for which we require only $\operatorname{Im} B$. It is of course possible to consider the real part of the correction to $D_q^0$, but this is of rather less intrinsic interest, and is also much more difficult to compute in detail. Our calculations of eq. (54) will be found in the following section. Readers who are not interested in such details can, with but little loss of continuity, proceed directly to Section IV C.

### B. Corrections to the Fredholm Denominator

The complete Fredholm denominator, $\mathfrak{D}(q, z)$, was given in Section II B. To second order in the free space amplitude the kernel $R_{\varkappa}(p \mid p')$ has contributions from only two diagrams, those of Figs. 4(a, b); we call these kernels $R'$ and $R''$, respectively. Since we shall not go as far as fourth order, we only require the diagonal elements

$$\left.\begin{aligned} R'_{\boldsymbol{q}\omega}(\boldsymbol{p}\,\varepsilon \mid \boldsymbol{p}\,\varepsilon) = \frac{1}{(2\pi)^4 i}\, 1/2 \Big\{ & 3 \langle \boldsymbol{q}/2 \mid T_1(2\boldsymbol{p}, 2\varepsilon) \mid -\boldsymbol{q}/2 \rangle \\ & + \langle \boldsymbol{q}/2 \mid T_0(2\boldsymbol{p}, 2\varepsilon) \mid -\boldsymbol{q}/2 \rangle \Big\} \end{aligned}\right\} \tag{55}$$

and

$$R''_{\boldsymbol{q}\omega}(\boldsymbol{p}\,\varepsilon \mid \boldsymbol{p}\,\varepsilon) = -\frac{8}{(2\pi)^4 i} \left(\frac{a_0}{m}\right)^2 \Pi_0(0,0) + 0(a_0^3), \tag{56}$$

where $\Pi_0(\boldsymbol{k}, \omega)$ is given by eq. (31).

In computing the first Fredholm trace with eq. (56), we can replace $\mathfrak{G}^0(p; \varkappa)$ by $G_0(p + \varkappa/2)\, G_0(p - \varkappa/2) = \mathfrak{G}_f(p; \varkappa)$: the difference between $\mathfrak{G}^0$ and $\mathfrak{G}_f$ leads to terms of order $a_0^4$ in $\operatorname{Im} \mathfrak{D}$, and does not concern us. Therefore the contribution of $R''$ to eq. (23c) is

$$\int d^4p\, R''_{\varkappa}(p \mid p)\, \mathfrak{G}_f(p; \varkappa) = -\frac{1}{\pi^3} \left(\frac{a_0}{m}\right)^2 \Pi_0(0,0)\, \Pi_0(q, \omega). \tag{57}$$

Since $\omega > \omega_c$, $\operatorname{Im} \Pi_0(q, \omega) = 0$; furthermore, $\operatorname{Im} \Pi_0(\boldsymbol{k}, 0) = \operatorname{Im} \Pi_0(0, \omega) = 0$ for all $\boldsymbol{k}$ and $\omega$. Thus eq. (57) is real, and Fig. 4(b) therefore does not contribute to the damping in the present approximation.

Using the representation of the $T$-matrix given in eq. (24), the Fredholm trace of eq. (55) is found to be

$$\left.\begin{aligned} \mathfrak{D}^{(1)}(\varkappa) = 1/2 \int_{-\infty}^{\infty} \frac{d\varepsilon}{2\pi i} \int \frac{d^3p}{(2\pi)^3}\, G\left(p + \frac{1}{2}\varkappa\right) G\left(p - \frac{1}{2}\varkappa\right) \\ \times \Bigg\{ \left[ f_0\, \boldsymbol{q}/2 \mid \boldsymbol{q}/2) - 3 f_1(\boldsymbol{q}/2 \mid \boldsymbol{q}/2) \right] - \frac{1}{2} m \int d^3k \, \frac{\mid f_0(\boldsymbol{q}/2 \mid \boldsymbol{k}) \mid^2 - 3 \mid f_1(\boldsymbol{q}/2 \mid \boldsymbol{k}) \mid^2}{\frac{1}{4} q^2 - k^2 + i\eta} \\ + \frac{1}{2} m \int d^3k \left[ \mid f_0\, \boldsymbol{q}/2 \mid \boldsymbol{k}) \mid^2 - 3 \mid f_1(\boldsymbol{q}/2 \mid \boldsymbol{k}) \mid^2 \right] \\ \times \left[ \frac{\Lambda_{2\boldsymbol{p}}^{(+)}(\boldsymbol{k})}{2m\varepsilon - p^2 - k^2 + i\eta} - \frac{\Lambda_{2\boldsymbol{p}}^{(-)}(\boldsymbol{k})}{2m\varepsilon - p^2 - k^2 - i\eta} \right] \Bigg\}. \end{aligned}\right\} \tag{58}$$

The imaginary part of the first two terms inside the curly braces of eq. (58) vanishes in virtue of the optical theorem. Because of this, only the real parts of the $f$'s were retained in Section III. The third term of eq. (58) is already $0(f^2)$, and so we can use free propagators $G_0$ in computing its contribution to $\mathfrak{D}^{(1)}(\varkappa)$. Therefore

$$\left.\begin{aligned}\mathfrak{D}^{(1)}(q,\omega) = \frac{1}{16\pi^3}\Pi(q,\omega)\,\mathrm{Re}\,[f_0(\boldsymbol{q}/2\,|\,\boldsymbol{q}/2) - 3\,f_1(\boldsymbol{q}/2\,|\,\boldsymbol{q}/2)]. \\ +2\pi\xi^2 J(q,\omega),\end{aligned}\right\} \quad (59)$$

where $\Pi(q,\omega)$ is given by eq. (47), and

$$\left.\begin{aligned}J(q,\omega) = \int_{-\infty}^{\infty}\frac{d\varepsilon}{2\pi i}\int d^3k\,d^3p\,G_0(|\boldsymbol{p}+\boldsymbol{q}/2|,\,\varepsilon+\omega/2)\,G_0(|\boldsymbol{p}-\boldsymbol{q}/2|,\,\varepsilon-\omega/2) \\ \times\left\{\frac{\Lambda_{2\boldsymbol{p}}^{(+)}(\boldsymbol{k})}{2\varepsilon-p^2-k^2+i\eta} - \frac{\Lambda_{2\boldsymbol{p}}^{(-)}(\boldsymbol{k})}{2\varepsilon-p^2-k^2-i\eta} - \frac{\mathrm{P.V.}}{q^2/4-k^2}\right\}.\end{aligned}\right\} \quad (60)$$

In order to arrive at eq. (60) we have retained only the $S$-wave scattering in the effective range approximation (eq. (29)), and expressed momenta and energies in units of $k_F$ and $k_F^2/m$, respectively.

We proceed directly to the evaluation of $\mathrm{Im}\,J$. After carrying out the $\varepsilon$-integration, we find that

$$-\mathrm{Im}\,J(q,\omega+i0) = I_+(q,\omega) + I_-(q,\omega) \quad (61)$$

with

$$\left.\begin{aligned}I_+(q,\omega) \\ = \pi\int d^3p\,d^3k\,\Lambda_{2\boldsymbol{p}}^{(+)}(\boldsymbol{k})\,\Theta_-(\boldsymbol{p}-\boldsymbol{q}/2)\,\frac{\delta((\boldsymbol{p}-\boldsymbol{q}/2)^2-(p^2+k^2)+\omega)}{\omega-\boldsymbol{p}\cdot\boldsymbol{q}}\end{aligned}\right\} \quad (62_+)$$

and

$$\left.\begin{aligned}I_-(q,\omega) \\ = \pi\int d^3p\,d^3k\,\Lambda_{2\boldsymbol{p}}^{(-)}(\boldsymbol{k})\,\Theta_+(\boldsymbol{p}+\boldsymbol{q}/2)\,\frac{\delta((\boldsymbol{p}+\boldsymbol{q}/2)^2-(p^2+k^2)-\omega)}{\omega-\boldsymbol{p}\cdot\boldsymbol{q}}\end{aligned}\right\} \quad (62_-)$$

provided $\omega > \omega_c$. In proceeding further it is necessary to consider the integrals

$$\int d^3k'\,\delta(k^2-k'^2)\,\Lambda_{2\boldsymbol{p}}^{(\pm)}(\boldsymbol{k}') = 2\pi k\,\chi_\pm(p,k). \quad (63)$$

The functions $\chi_\pm$ vanish in certain domains:

$$\chi_+(p,k) = 0 \quad \text{if} \quad k^2+p^2 < 1, \quad (64_+)$$

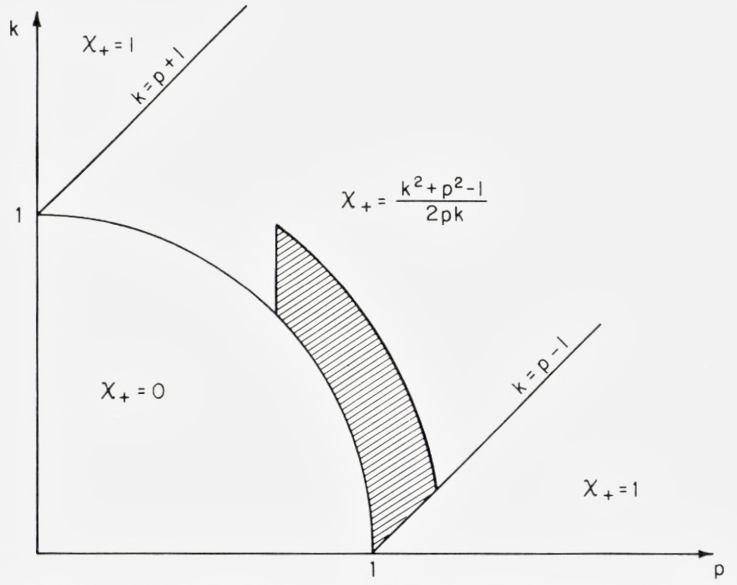


Fig. 6. The function $\chi_+(p, k)$ defined by eq. (63). The functional form of $\chi_+$ changes in the indicated manner upon crossing the heavy solid lines. The integrand of $I_+(q, \omega)$ lies within the shaded domain, which does not intersect the line $k = p + 1$ if $\omega_c \ll 1$.

$$\chi_-(p, k) = 0 \quad \text{if} \quad k^2 + p^2 > 1 . \tag{64_-}$$

The functional form of $\chi_+$ in the balance of the $k-p$ plane is shown in Fig. 6. Fortunately only one form of $\chi_+$, namely

$$\chi_+(p, k) = \frac{k^2 + p^2 - 1}{2pk}, \tag{65}$$

enters into our calculation if $\omega > \omega_c$, and $\omega_c \ll 1$. This can be proven as follows. From the step and delta functions in $I_+$ we have

$$1 \leqslant k^2 + p^2 \leqslant 1 + \omega , \tag{66a}$$

$$1 + q/2 \geqslant p \geqslant \sqrt{1-\omega} - q/2 . \tag{66b}$$

A lower bound on $k$ for fixed magnitude of $\boldsymbol{p}$ is

$$k^2 \geqslant (\omega + q^2/4 - pq) \equiv k_0^2 .$$

To show that $\chi_+$ always has the form given by eq. (65) we must have $k_0^2 \geqslant (p-1)^2$. However, by using eq. (66b) we find that

$$k_0^2-(p-1)^2 \geqslant \omega-\omega_c,$$

and so for $\omega > \omega_c$ we have the desired result.

The situation with respect to $I_-$ is quite different. From the $\delta$-function we have

$$q^2/4 - \omega - pq \leqslant k^2 \leqslant q^2/4 - \omega + pq.$$

On the other hand, $p < 1$ according to eq. (64_), and therefore

$$k^2 \leqslant \frac{1}{4} q^2 - \omega_c + q$$

if $\omega \geqslant \omega_c$. Since the right hand side of this inequality is negative, $I_- = 0$.

We therefore conclude that after the $\boldsymbol{k}$-integration eq. (61) reads

$$\left.\begin{aligned} -\operatorname{Im} J(q, \omega+i0) &= \pi^2 \int_{1-\omega \leqslant (\boldsymbol{p}-\frac{1}{2}\boldsymbol{q})^2 \leqslant 1} \frac{(\boldsymbol{p}-\boldsymbol{q}/2)^2+\omega-1}{\omega-\boldsymbol{p}\cdot\boldsymbol{q}} \frac{d^3p}{p} \\ &= \frac{2\pi^3}{p} \int_{1-\omega}^{1} ds \int_{\sqrt{s}-\frac{1}{2}q}^{\sqrt{s}+\frac{1}{2}q} dp \frac{s+\omega-1}{\omega+s-p^2-q^2/4}, \end{aligned}\right\} \quad (67)$$

with $s = (\boldsymbol{p}-\boldsymbol{q}/2)^2$. We are interested in the behaviour of the function defined by eq. (67) in the immediate neighbourhood of $q = 0$, $\omega = 0$, but for finite values of the velocity $v = \omega/q$. It is therefore convenient to make the transformation $y = (1-s)/q$, in which case eq. (67) reduces to

$$\left.\begin{aligned} -\operatorname{Im} J(q, vq+i0) &= \pi^3 q \int_0^v dy \sqrt{\frac{v-y}{1+q(v-y)-q^2/4}} \\ &\times \ln\left(\frac{v+\sqrt{1+q(v-y)-q^2/4}}{v-\sqrt{1+q(v-y)-q^2/4}}\right). \end{aligned}\right\} \quad (68)$$

In the long wavelength limit eq. (68) simply becomes

$$-\operatorname{Im} J(q, vq+i0) \xrightarrow[q\to 0]{} \frac{1}{2}\pi^3 q v^2 \ln\left(\frac{v+1}{v-1}\right), \quad (69)$$

provided $qv < (v-1)$.

Finally we come to the first term of eq. (59), i. e., to the evaluation of $\operatorname{Im} \Pi(q, \omega)$. From eq. (47) we have

$$-\operatorname{Im} \Pi(q, \omega+i0) = \pi \int d^3p \int_0^\omega d\varepsilon \varrho_+(|\boldsymbol{p}+\boldsymbol{q}|, \omega-\varepsilon) \varrho_-(p, \varepsilon). \quad (70)$$

One can readily compute the spectral densities $\varrho_{\pm}$ in perturbation theory, and for small $\omega$ and $q$ the further integrations demanded by eq. (70) can be easily carried through. The resulting expression is, however, linearly divergent as $\omega \to \omega_c$, and it is not possible to tell from the perturbation calculation itself whether this expression is still valid when $\omega = \Omega_q^0$, which, we recall, is extremely close to $\omega_c$ (cf. Section III A). A more accurate evaluation of eq. (70) is therefore required. With this purpose in mind, we ecall that

$$\varrho_{\pm}(p, \varepsilon) = -\mp 1/\pi \operatorname{Im} G(p, \mu \pm \varepsilon) \tag{71}$$

are immediate consequences of eq. (46). Upon introducing the selfenergy $\Sigma(p, \varepsilon)$ in the usual way[4],

$$G(p, \varepsilon) = \frac{1}{G_0^{-1}(p, \varepsilon) - \Sigma(p, \varepsilon)},$$

we see from eq. (71) that

$$\varrho_{\pm}(p, \varepsilon) = \mp \frac{1}{\pi} \frac{\operatorname{Im}\Sigma(p, \mu \pm \varepsilon)}{|G_0^{-1}(p, \mu \pm \varepsilon) - \operatorname{Re}\Sigma(p, \mu \pm \varepsilon)|^2 + |\operatorname{Im}\Sigma(p, \mu \pm \varepsilon)|^2}. \tag{72}$$

$\Sigma(p, \varepsilon)$ has been studied by GALITSKII[20] to order $f^2$. For $p \approx k_F$, $\varepsilon \approx \mu$, $\operatorname{Re}\Sigma(p, \varepsilon)$ is found to be a relatively slowly varying function and can, for our purpose, be thought of as having been absorbed into the definition of an effective mass $m^*$ and the energy $\mu$. These changes have no effect on $(\Gamma_q/D_q^0)$, however, and so we shall retain the "bare" mass $m$, and put $\mu = \mu_0 = (k_F^2/2\,m)$ hereafter. On the other hand, for $p \approx k_F$,

$$\operatorname{Im}\Sigma(p, \varepsilon) \simeq \left\{ \begin{array}{lll} -c^2(\varepsilon - \mu_0)^2 m/k_F^2 & \text{if} & \varepsilon > \mu_0 \\ c^2(\mu_0 - \varepsilon)^2 m/k_F^2 & \text{if} & \varepsilon < \mu_0 \end{array} \right\}, \tag{73}$$

with

$$c^2 = \pi \xi^2. \tag{74}$$

Putting eq. (73) into eq. (72), and this in turn into eq. (70), we have

$$\left. \begin{array}{l} L(q, \omega) \equiv -(k_F m)^{-1} \operatorname{Im} \Pi(q, \omega + i0) \\ = \dfrac{1}{\pi} \displaystyle\int d^3p \int_0^{\omega} d\varepsilon \, \frac{c^2 \Delta^2}{[1/2 + \Delta - (\boldsymbol{p} + \boldsymbol{q})^2/2]^2 + c^4 \Delta^4} \cdot \frac{c^2 \varepsilon^2}{(1/2 - \varepsilon - p^2/2)^2 + c^4 \varepsilon^4} \end{array} \right\} \tag{75}$$

where all momenta and energies in eq. (75) are again dimensionless, and

$$\Delta = \omega - \varepsilon.$$

Integrating over the orientation of $\boldsymbol{p}$ we have

$$\left.\begin{aligned} L(q,\omega) &= \frac{2}{q}\int_0^{\omega} d\varepsilon \int_{-\infty}^{\infty} p\,dp\, \frac{c^2\varepsilon^2}{(1/2-\varepsilon-p^2/2)^2+c^4\varepsilon^4}\ \mathrm{arctgt}\left(\frac{(p+q)^2/2-1/2-\Delta}{c^2\Delta^2}\right) \\ &= \frac{2}{q}\int_0^{\omega} c^4\Delta^2\varepsilon^2\, d\varepsilon \int_0^1 d\gamma \int_{-\infty}^{\infty} p\,dp\, \frac{(p+q)^2/2-1/2-\Delta}{[(1/2-\varepsilon-p^2/2)^2+c^4\varepsilon^4]\left\{c^4\varepsilon^4+\gamma^2[(p+q)^2/2-1/2-\Delta]^2\right\}}. \end{aligned}\right\} \quad (76)$$

The $p$-integral is now elementary, but the resulting expression is rather clumsy, and must moreover be handled with great care if one wishes to evaluate $L(q,\omega)$ when $\omega$ is in the immediate neighbourhood of $\omega_c$. If, however, the inequality

$$\frac{c^2\omega^2}{\omega-\omega^c} \ll 1 \quad (77)$$

is satisfied, a considerable simplification of the expression referred to becomes possible. Putting $\omega = \Omega_q^0$ in eq. (77), and using eqs. (37) and $(38)_q$ we have

$$\frac{c^2(\Omega_q^0)^2}{\Omega_q^0-\omega_c} \longrightarrow 2.73\, c^2\left(\frac{q}{q_c^0}\right) \quad \text{as} \quad \frac{q}{q_c^0}\to 0;$$

therefore eq. (77) is satisfied if $q \ll q_c^0$. When $q \to q_c^0$, the inequality (77) will of course break down at $\omega = \Omega_q^0$.

After carrying out the approximations permitted by eq. (77) we find that eq. (76) reduces to

$$\left.\begin{aligned} L(q,\omega) &= \frac{2\pi c^2}{q}\int_0^{\omega}\Delta^2\, d\Delta \int_0^1 d\gamma\left(\frac{\omega+q}{\gamma^2(\omega+q)^2+c^4\Delta^4}-(q\to -q)\right) \\ &\quad -\frac{2\pi c^4}{q}\,\mathrm{Im}\int_0^{\omega}\Delta^2\varepsilon^2\, d\varepsilon \int_0^1 d\gamma\left(\frac{1}{[\gamma(\omega+q)-ic^2\Delta^2]^2}+(q\to -q)\right) \\ &= \frac{8\pi}{3}\,\frac{c^2\omega^3}{\omega^2-q^2}+0(c^6). \end{aligned}\right\} \quad (78)$$

This is just the result one obtains by using perturbation theory for the spectral functions $\varrho_{\pm}$. The only thing that our calculation has achieved is the inequality

$$8.6\,\xi^2(q/q_c^0) \ll 1 \quad (79)$$

which must be satisfied if $L(q,\Omega_q^0)$ is to be given by eq. (78). If one wants

to compute the width as $q \to q_c^0$, a more accurate evaluation of eq. (76) is required.

Collecting our results from eqs. (59), (69), (75), and (78), we finally have

$$-\operatorname{Im} B(q,\ \Omega_q^0 + i0) \simeq \pi^4\, \xi^2 q \left(\frac{\Omega_q^0}{q}\right)^2 \ln\left(\frac{\Omega_q^0 + q}{\Omega_q^0 - q}\right) + \frac{2\,\pi\,\xi^3\, q^2}{3\, D_q^0}, \tag{80}$$

and according to eq. (54), the expression for the width follows immediately from this.

## C. The Width

In view of our calculation of the preceding subsection, it is instructive to break the leading contributions to $\Gamma_q$ into two partial widths, $\Gamma_q^{\text{dress}}$ and $\Gamma_q^{\text{int}}$. The former arises from "dressing" the single particle excitations, the latter from the modifications of the interaction law between the particles due to their immersion in the Fermi sea (cf. eq. (24)). Recalling our results of Sections III A and IV B, we find

$$\frac{\Gamma_q^{\text{int}}}{D_q^0} \simeq 2\,\pi^4 \left(\frac{q}{k_F}\right)(1 + 2\,\xi), \tag{81}$$

whereas

$$\frac{\Gamma_q^{\text{dress}}}{D_q^0} = 11.4\ \xi^2 \left(\frac{q}{q_c^0}\right). \tag{82}$$

At first sight it would appear that $\Gamma_q^{\text{int}} \gg \Gamma_q^{\text{dress}}$. This is somewhat fallacious, however, because $q$ must be less than $q_c^0$, and this cut-off momentum should be explicitly introduced in (81). When this is done, the more perspicuous expression

$$\frac{\Gamma_q^{\text{int}}}{D_q^0} = 144\ e^{-1/\xi} \left(\frac{q}{q_c^0}\right) \tag{83}$$

emerges.

It is quite clear that higher order corrections to the interaction kernel $\Xi$ (as well as higher order Fredholm determinants) will only append a power series in $\xi$ to eq. (83). The reason for the very great difference in the $\xi$-dependence of eqs. (82) and (83) is a result of the fact that $\Pi(q,\ \omega)$, which describes the one-particle damping, must grow very rapidly as $\omega$ tends to $\omega_c$, because for $\omega \leqslant \omega_c$ $\operatorname{Im} \Pi(q,\ \omega)$ does not vanish even if the system is free (see Fig. 1). On the other hand, the contributions resulting from the

corrections to the kernel $\Xi$ naturally do not display any dramatic increase as the single-particle excitation continuum is approached from above.

We therefore conclude that, in the limit $\xi \to 0$, the phonon damping which results from the fact that the one-particle excitations have a finite lifetime completely dominates the dissipation arising from the non-instantaneous nature of the interaction law between one-particle excitations. However, for more moderate values of $\xi = k_F a_0/\pi$ the large numerical coefficient in eq. (83) implies that $\Gamma^{\text{dress}}$ and $\Gamma^{\text{int}}$ can be of quite comparable magnitude.

Another lesson we have learned is that the Fredholm method is ideally suited to an investigation of the present type where one is mainly interested in the isolated poles of a Green function. It may perhaps be fruitful to apply this method to transport problems in a system with non-trivial interactions, such as $He^3$ [2].

## Acknowledgments

We take pleasure in expressing our gratitude to Professor NIELS BOHR and Professor AAGE BOHR for enabling us to enjoy the generous support and warm hospitality of the Institut for Teoretisk Fysik where the work reported herein was initiated. We should also like to thank Professor A. BOHR, Dr. J. GOLDSTONE, and Professor P. C. MARTIN for comments and suggestions. The work of the first-named author was supported in part by the United States Air Force Office of Scientific Research (ARDC), under contract number AF 49 (638)—589.

*Institute for Theoretical Physics*
*University of Copenhagen, Denmark*

*Harvard University*
*Cambridge, Mass.*

*Institut "Jozef Stefan"*
*Ljubljana, Yugoslavia*

## References


1) L. D. Landau, J. Exptl. Theoret. Phys. (U.S.S.R.) **32**, 59 (1957) [translation: Soviet Phys. JETP **5**, 101 (1957)].
2) A. A. Abrikosov and I. M. Khalatnikov, Repts. Prog. Phys. **22**, 329 (1959).
3) L. D. Landau, J. Exptl. Theoret. Phys. (U.S.S.R.) **30**, 1058 (1956) [translation: Soviet Phys. JETP **3**, 920 (1957)].
4) V. M. Galitskii and A. B. Migdal, J. Exptl. Theoret. Phys. (U.S.S.R.) **34**, 139 (1958)
[translation: Soviet Phys. JETP **7**, 96 (1958)].
5) A. E. Glassgold, W. Heckrotte and K. M. Watson, Ann. Phys. (N.Y.) **6**, 1 (1959).
6) D. Bohm and D. Pines, Phys. Rev. **92**, 609 (1953).
7) J. Hubbard, Proc. Roy. Soc. **A 240**, 539 (1957); **A 243**, 336 (1957).
8) K. Sawada, K. A. Brueckner, N. Fukuda and R. Brout, Phys. Rev. **108**, 507 (1957).
9) D. F. DuBois, Ann. Phys. (N.Y.) **7**, 147 (1959); **8**, 24 (1959).
10) M. Gell-Mann and K. A. Brueckner, Phys. Rev. **106**, 364 (1957).
11) J. Goldstone and K. Gottfried, Nuovo Cimento **13**, 849 (1959).
12) J. Lindhard, Mat. Fys. Medd. Dan. Vid. Selsk. **28**, no. 8 (1954).
13) D. Pines and P. Nozières, Nuovo Cimento **9**, 470 (1958).
14) P. C. Martin and J. Schwinger, Phys. Rev. **115**, 1342 (1959).
15) A. A. Abrikosov and I. M. Khalatnikov, J. Exptl. Theoret. Phys. (U.S.S.R.) **34**, 198 (1958) [translation: Soviet Phys. JETP **7**, 135 (1958)].
16) H. A. Bethe and E. E. Salpeter, Phys. Rev. **82**, 309 (1951).
17) M. Gell-Mann and F. E. Low, Phys. Rev. **84**, 350 (1951).
18) J. Schwinger, Proc. Nat. Acad. Science **37**, 452 (1951).
19) F. G. Tricomi, "*Integral Equations*", (Interscience Publishers, New York, 1957) pp. 64—76. P. M. Morse and H. Feshbach, "*Methods of Theoretical Physics*" (McGraw-Hill, New York, 1953) pp. 1018—1025.
20) V. M. Galitskii, J. Exptl. Theoret. Phys. (U.S.S.R.) **34**, 151 (1958) [translation: Soviet Phys. JETP **7**, 104 (1958)].
21) J. M. Blatt and J. D. Jackson, Phys. Rev. **76**, 18 (1949).
22) M. Gell-Mann and R. E. Peierls, *Proceedings of the 1958 International Conference on High Energy Physics* (CERN, Geneva) pp. 142—144.



Indleveret til Selskabet den 8. april 1960.
Færdig fra trykkeriet den 19. november 1960.

Matematisk-fysiske Meddelelser
udgivet af
Det Kongelige Danske Videnskabernes Selskab
Bind **32,** nr. 14

Mat. Fys. Medd. Dan. Vid. Selsk. **32,** no.14 (1960)

# OPTICAL HYPERFINE STRUCTURE OF NEON-21

BY

EBBE RASMUSSEN(†) AND V. MIDDELBOE

København 1960
i kommission hos Ejnar Munksgaard

Printed in Denmark
Bianco Lunos Bogtrykkeri A-S

## Introduction

The hyperfine structure in the spectrum of Neon-21 was investigated for the first time by KOCH & RASMUSSEN[1] more than ten years ago. In this investigation some of the hfs components of $Ne^{21}$ were masked by partially unseparated $Ne^{20}$. Nevertheless, it was still possible to obtain the following results: the nuclear spin of $Ne^{21}$ is $^3/_2$ (possibly greater) and the nuclear magnetic moment is negative. In recent years, both these observations have been confirmed by the use of modern experimental methods; thus, HUBBS & GROSOF[2] have established with certainty that $I = {}^3/_2$, and RAMSAY et al.[3] have determined the value of $\mu = -0.66176$ n.m.

In 1955, K. CLUSIUS, Zürich, kindly has sent one of us (E.R.) a very highly enriched $Ne^{21}$ sample (about 1 c.c. at atm. pressure). The spectroscopical investigation of the hfs of $Ne^{21}$ was resumed soon after the receipt of this generous gift in which the $Ne^{21}$ concentration had been enriched (from $0.3\,\%$ in natural Neon) to very nearly $99\,\%$ pure by repeated thermal diffusion. The renewed optical investigation led to a determination of the hfs splitting in a number of terms of the $Ne^{21}$ arc spectrum. In the case of the $2s_5$ term (Paschen notation), a precise determination of the hfs splitting has recently been obtained by RABI et al.[4] working with an atomic beam resonance method.

In many respects our spectroscopical procedure was much the same as that previously used, and it is given in detail, for example, in the description of some investigations on separated Krypton isotopes[5]. However, certain experimental modifications were necessary, partly because the Neon was provided in the gaseous state (Kr had been collected in Aluminium), and partly because of the large Doppler width of the spectral lines (twice that of Kr) in combination with the rather narrow splittings (one third those of Kr) — line broadening had now in fact become the limiting experimental factor.

## Experimental Modifications

Using the apparatus sketched in Fig. 1, the $Ne^{21}$ gas was transferred to a number of "seeds", i.e., closed glass tubes about $0.5 \times 1$ mm in diameter and a few centimetres long. Furthermore, the discharge tube was given

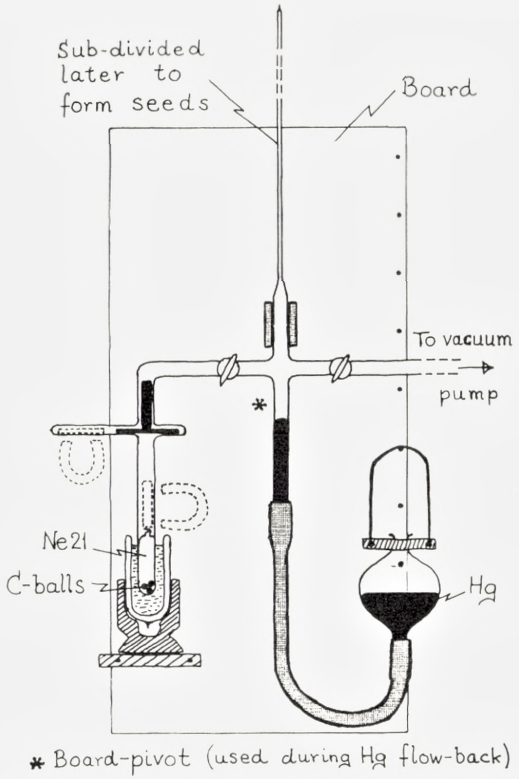


Fig. 1. Neon-21 transfer apparatus. Scale: approximately 1/10.

the modified shape shown in Fig. 2. Hereby it was possible to make use of a technique, developed many years ago[6], which consists in breaking open one or more seeds inside the sealed-off discharge tube.

Helium from Canada (free from Ne) was used as a carrier gas, and in order to reduce the broadening of the $Ne^{21}$ lines, the Helium pressure was kept lower than usual (2—3 mm Hg instead of 10), although this inevitably shortens the life of a discharge tube. The pressure of $Ne^{21}$ was estimated

at 0.1 mm Hg for each seed that was liberated. Up to three or four seeds were liberated consecutively during the life span of each discharge tube.

In an attempt to reduce the temperature of the liquid air used for cooling the discharge, the Dewar containing the cooling medium was closed with a large rubber stopper (penetrated by the U-shaped part of the discharge tube) and, during exposure, the pressure above the cooling medium was kept down at 15—20 mm Hg by means of continuous mechanical pumping via a $^1/_2$ inch exhaust pipe. On starting the pump, the liquid air would bubble violently for a short time, no doubt while its nitrogen content was boiling off,

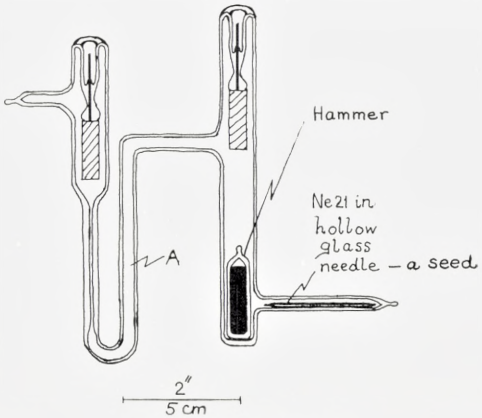


Fig. 2. Discharge tube.

but soon the remaining liquid (oxygen) became perfectly calm—presumably at a temperature of 60—65° K. A $^3/_4$ inch steel ball resting on the top of a $^1/_2$ inch bore through the rubber stopper constituted a combined refilling device and safety valve.

The Joule heat evolved in the He-Ne-gas was kept as low as possible by reduction of the discharge current to a minimum (1—2 mA). Furthermore, the discharge in the thin-walled part of the tube, "A" in Fig. 2, was spectographed instead of that in the capillary part of the tube normally used. These modifications, in connection with the lowered temperature of the cooling medium, reduced the Doppler width sufficiently (20—40 %) and made it just possible to resolve a number of the hfs components. This was only achieved, however, at the cost of a considerable loss in luminance.

The unavoidable reduction in the brightness of the discharge was compensated by a five- to ten-fold increase in the transmission of the Fabry-Perot interferometer. This was achieved by coating each quartz plate with

seven alternate layers of zinc sulphide and cryolite—instead of the silver layer normally used. Moreover, the resolving power of these multilayers was perfectly adequate in the whole of the spectral region (yellow-orange) that was investigated.

Finally, a new étalon spacer of optimum thickness (40 mm) was produced with a tolerance far better than 1 mil.

## Measurement of Line Structure Intervals

The spectroscopically resolved hyperfine structure (hfs) of seven $Ne^{21}$ spectral lines was measured. All the measured lines represent $1s-2p$ combinations, and their wavelengths are given in Table 1. Each measurable interval in the structure of these seven lines was determined 5—15 times, using the best out of 83 exposures.

Table 1.

| Wavelength Å. | Transition |
|---|---|
| 5852 | $1s_2-2p_1$ |
| 5881 | $1s_5-2p_2$ |
| 6030 | $1s_4-2p_2$ |
| 6074 | $1s_4-2p_3$ |
| 6266 | $1s_3-2p_5$ |
| 6598 | $1s_2-2p_2$ |
| 6717 | $1s_2-2p_5$ |

A plate showing three of the investigated spectral lines is reproduced on page 7.

The mean values of all the measured line intervals are collected in Table 2, and given there in units of $10^{-3}$ cm$^{-1}$. These values are believed to be correct to within 1—2 units. The sequence of the intervals given in the last column of Table 2 is in accordance with the *increasing* energy of the hfs components; in an interferogram (Plate 1, page 7), this corresponds to moving through a single order *away from* the centre of the photographic plate. In Table 2, the J-value of each term is noted directly below the term symbol in question.

At the bottom of Figs. 3—7, the hfs patterns of five of the measured spectral lines are shown. The height of each line pattern component is drawn

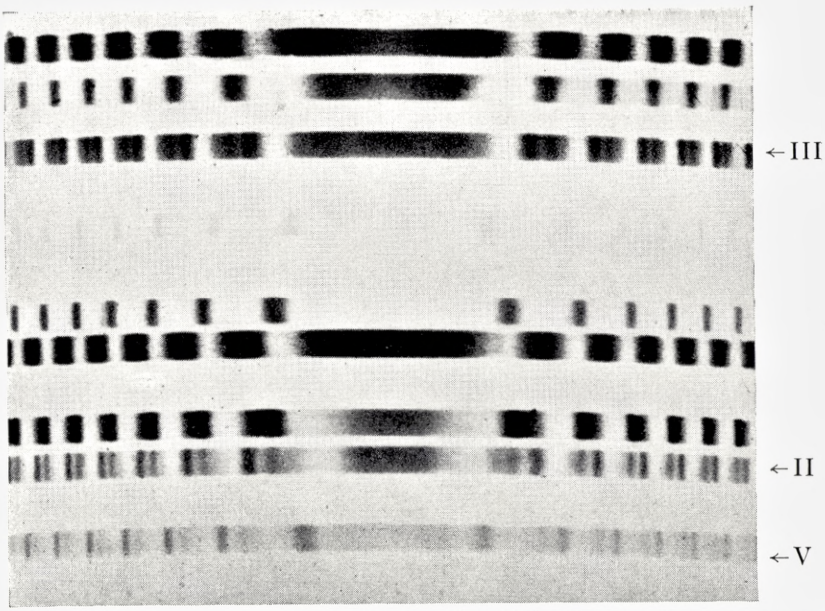


Plate 1. An interferogram of Neon-21. V: 6030 Å. II: 6074 Å III: 6266 Å. 6—7 orders are to be seen on each side.

TABLE 2.

| $Ne^{21}$ spectrum | Lower term | Upper term | Total line splitting $\times 10^{-3}$ cm$^{-1}$ | Measured intervals $\times 10^{-3}$ cm$^{-1}$ |
|---|---|---|---|---|
| Line I..... | $1s_2$ | $2p_1$ | 82 | 25 57 |
| | $J = 1$ | 0 | | |
| „ II..... | $1s_4$ | $2p_3$ | 66 | 27 39 |
| | $J = 1$ | 0 | | |
| „ III..... | $1s_3$ | $2p_5$ | 62 | 37 25 |
| | 0 | $J = 1$ | | |
| „ IV ..... | $1s_2$ | $2p_2$ | 88 | 27 61 |
| | $J = 1$ | 1 | | |
| „ V ..... | $1s_4$ | $2p_2$ | 71 | 29 42 |
| | $J = 1$ | 1 | | |
| „ VI ..... | $1s_5$ | $2p_2$ | 76 | 12 24 40 |
| | $J = 2$ | 1 | | |
| „ VII ..... | $1s_2$ | $2p_5$ | 89 | 54 35 |
| | $J = 1$ | $J = 1$ | | |

proportional to its calculated intensity, and the mean value of each interval that could be measured is given below the corresponding line pattern. $\nu$ stands for the wave number which, of course, is proporional to the energy.

### Determination of Term Component Separations

In the case of the spectral lines I, II, and III (Table 2), the line splittings are directly equal to the splittings of the terms $1s_2$, $1s_4$, and $2p_5$, respectively, because in each case the combining term has $J = 0$. In Figs. 3 and 4, the respective term diagrams of the two lines, I (5852 Å) and III (6266 Å), are

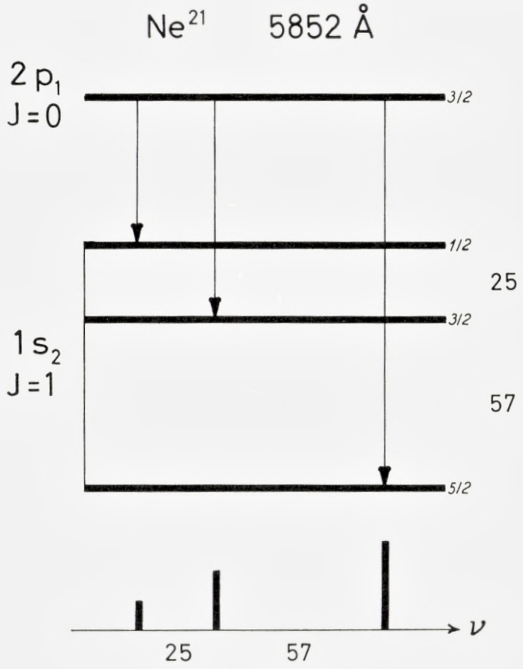


Fig. 3. Spectral line I.

given above the line patterns. In each term diagram the F-values are given directly to the right of the term components, and the separations are noted —also to the right—in between the hfs term components in question.

The term component separations that have been determined are noted in the third column of Table 3 (in units of $10^{-3}\,\mathrm{cm}^{-1}$). A separation is given there as positive, when the upper (i.e. more energetic) hfs component has the higher F-value.

In Table 2 a comparison between the lines I and IV on the one hand, and II and V on the other, shows immediately that the splitting of the term $2p_2$ is rather small. The separations between the $2p_2$ components can be estimated, for example, from the measured intervals of line V (6030 Å), by the following "trial and error" procedure (see Fig. 5). Assume the separations between the $1s_4$ components (already found from line II) to be correct, assign arbitrary separations to $2p_2$, construct the line structure pattern (bottom of Fig. 5) and determine the "centres of gravity" of the resulting groups of line components. The selected assignment of the $2p_2$ separations is that which results in intervals between the aforementioned centres of

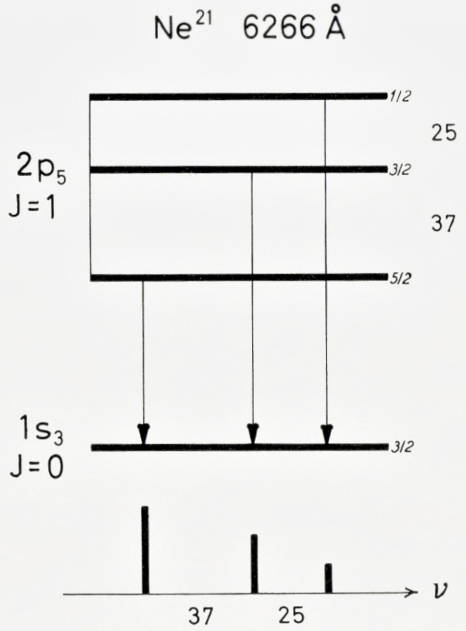


Fig. 4. Spectral line III, which can be compared with III in Plate 1.

gravity (dotted lines in fig. 5), that turn out to be equal to the observed values, viz., 29 and 42 units.

Using the trial and error method just described, the hfs separations of $2p_2$ were evaluated at 6 and 4 units, respectively. The relative uncertainty of the ratio of these two separations, i.e. 6:4, is naturally rather great, but the uncertainty of the total splitting, 10 units, is fair — maybe 20 %. The result is included in Table 3. The opposite sign of the splitting of this term

as compared with the other terms is analogous to what has previously been found for isotopes of other noble gases[5)7)].

Adopting the estimated values for the $2p_2$ separations and applying the trial and error method described above, the separations of the term

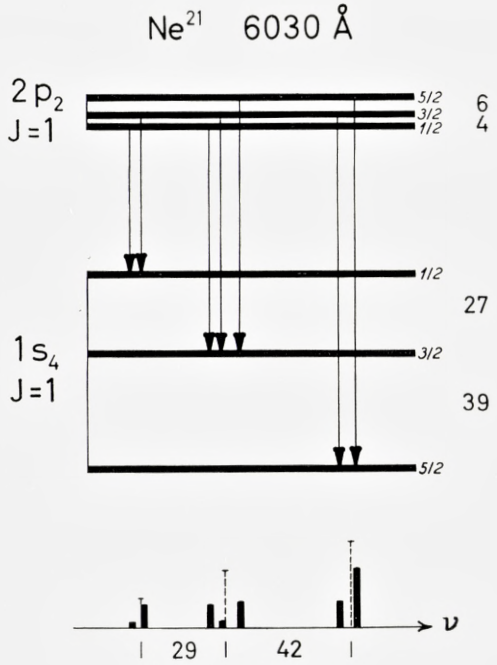


Fig. 5. Spectral line V.

$1s_5$ have been found from the measured intervals of line VI (5881 Å). The result is shown in Fig. 6, and given in Table 3 along with the observed separations of the other four terms.

Finally, line VII (6717 Å) gives a check on the hfs separations of the

TABLE 3.

| Term | $J$-value | Separations | | | Total |
|---|---|---|---|---|---|
| $1s_2$ | 1 | −57 | −25 | | −82 |
| $1s_4$ | 1 | −39 | −27 | | −66 |
| $2p_5$ | 1 | −37 | −25 | | −62 |
| $2p_2$ | 1 | (+6) | (+4) | | +10 |
| $1s_5$ | 2 | −36 | −20 | −10 | −66 |

terms $1s_2$ and $2p_5$. The measured splittings of these two terms, as determined from lines I and III, lead to the structure pattern of line VII shown at the bottom of Fig. 7. The resolution obtained spectroscopically permitted the measurement of the two intervals that are bounded by the two dotted lines

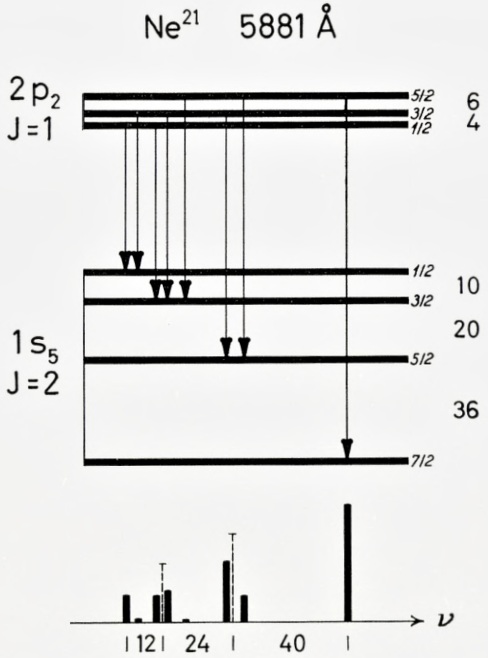


Fig. 6. Spectral line VI.

and the most energetic line component. By *calculation* from the previously determined splittings of $1s_2$ and $2p_5$ the magnitude of these two intervals is found to be equal to 52.5 and 35.5 units (total: 88 units). The corresponding directly *observed* values, as noted in Table 2, are 54 and 35 units (total: 89 units), which constitutes a satisfactory agreement.

## Theoretical Discussion

Assuming the following formula to be valid for the energy of an hfs term component

$$E = E_0 + a\frac{C}{2} + b\left[\frac{\frac{3}{4}C(C+1) - I(I+1)J(J+1)}{2I(2I-1)J(2J-1)}\right],$$

where $C = F(F+1) - I(I+1) - J(J+1)$, and using the value $I = {}^3/_2$, the interval factors (interaction constants) $a$ and $b$ in Table 4 have been computed (evaluated) from the hfs sparations given in Table 3. The $a$- and $b$-values in Table 4 should be experimentally correct to within 0.5—1 unit of $10^{-3}\,\mathrm{cm}^{-1}$.

The graphically evaluated $a$ and $b$ constant for the term $1s_5$ (see Fig. 8)

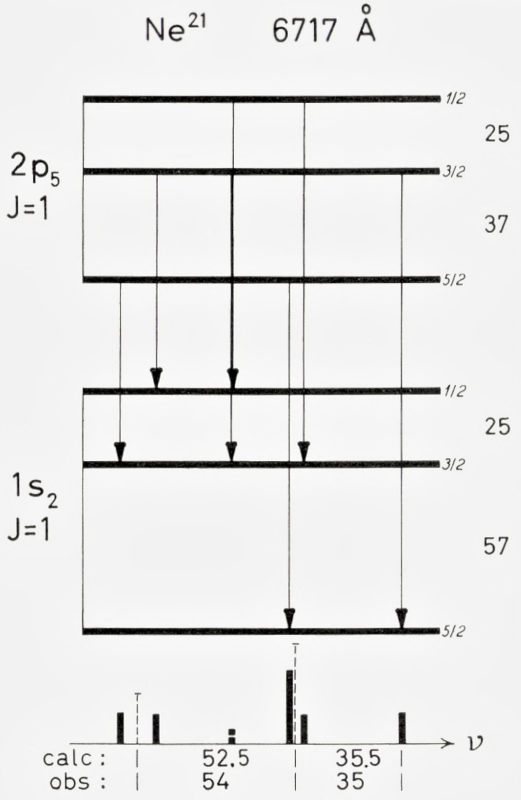


Fig. 7. Spectral line VII.

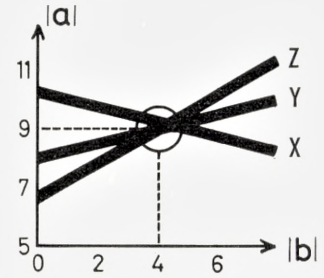


Fig. 8. Graphical evaluation of $a$ and $b$ from the following observed hfs separations of $1s_5$: 36 units (X), 20 units (Y), and 10 units (Z). The width of the graphical lines (X, Y, and Z) indicates the extent of the estimated experimental error.

may be used to re-calculate a set of mathematically consistent values for the hfs separations of this term. This procedure yields the separations 35, 20, and 10 in the optical units, or in Mc/sec: 1050, 600, and 300, which compares well with the high-precision values 1034.48, 599.44, and 303.93, measured by Grosof, Buck, Lichten, and Rabi. These latter values correspond to $a(1s_5) = -8.93$ and $b(1s_5) = -3.72$ in units of $10^{-3}\,\mathrm{cm}^{-1}$.

An analysis of the hfs separations may be performed in analogy to that of the Xe-[7] and Kr-spectra[5]. The most reliable determination of the nuclear quadrupole moment is obtained from the interval factors of the $1s_5$ term, which may be regarded as a rather pure configuration consisting of a $3s$ electron plus the ion in a $^2P_{3/2}$ state, corresponding to a "hole" of the $p_{3/2}$ type. Only the hole contributes to the quadrupole coupling. The determination of $Q$ involves an estimate of $\overline{r^{-3}}$ for the hole (cf., e.g., expressions (7) and (8) in ref. [7]), and this can be obtained either from the fine structure separation $\Delta$ of the ion (cf., e.g., expression (9) in ref. [7]) or from the magnetic coupling between the hole and the nucleus. The latter procedure, employed in ref. [4], involves as a first step an estimate of the magnetic

TABLE 4.

| Term | $a$ | $b$ |
|---|---|---|
| $1s_2$ | −21 | −3 |
| $1s_4$ | −16 | +1 |
| $1s_5$ | − 9 | −4 |
| $2p_2$ | +2.5 | (0) |
| $2p_5$ | −15 | +1 |

coupling of the $s$-electron, which, from the Fermi-Segré formula, is found to be $a(s) = -8.1$. Now, since $a(1s_5) = \frac{1}{4}\, a(s) + \frac{3}{4}\, a(P_{3/2})$, one finds $a(P_{3/2}) = -9.2$ as the interval factor value for the ion. This in turn leads to $\overline{a_0{}^3 r^{-3}} = 12.4$ (cf., e.g., equation 13 in ref. [7]). Using this value, GROSOF et al.[4] found $Q = +0.093$, with an estimated error of 10 % due to the uncertainty in $\overline{r^{-3}}$. Moreover, the Sternheimer correction arising from polarization effects has been neglected. On the basis of the empirical fine structure separation ($\Delta = 782\ \mathrm{cm}^{-1}$) one obtains the alternative estimate $\overline{a_0{}^3 r^{-3}} = 11.2$, if one assumes an effective nuclear charge of $Z_i = Z - 2 = 8$. Within the estimated uncertainty the two values for $\overline{r^{-3}}$ are consistent.

For the terms $1s_2$ and $1s_4$, the wave functions can be written in the form

$$\psi = c_1 \varphi(\tfrac{3}{2}, \tfrac{1}{2}) + c_2 \varphi(\tfrac{1}{2}, \tfrac{1}{2}),$$

which represents a superposition of states with the hole in the $p_{3/2}$ and $p_{1/2}$ levels, while the outer electron is in the $3s$ level. The coefficients $c_1$ and $c_2$ can be computed from the atomic $g$-factors as well as from the multiplet separations; these two determinations agree well and both give for the $1s_4$

term the alternative possibilities ($c_1 = 0.77$, $c_2 = 0.64$) or ($c_1 = 0.34$, $c_2 = 0.94$).

By means of the above-mentioned wave functions one can calculate the $a$- and $b$-factors for the terms $1s_2$ and $1s_4$ on the basis of those belonging to the $1s_5$ term, if one applies expressions given by CASIMIR[8] (cf. also ref. [7]). We first note that the sum of the interval factors for $1s_2$ and $1s_4$ is independent of $c_1$ and $c_2$, and given by

$$a(1s_2) + a(1s_4) = \tfrac{1}{4}\, a(s) + \tfrac{5}{4}\, a(P_{3/2}) + \tfrac{1}{2}\, a(P_{1/2})$$
$$b(1s_2) + b(1s_4) = \tfrac{1}{2}\, b(P_{3/2}) = \tfrac{1}{2}\, b(1s_5),$$

where $a(P_{1/2})$ is the interval factor for the $p_{1/2}$ hole. Assuming $a(P_{1/2}) = 5\, a(P_{3/2})$, holding for a non-relativistic $p$-electron, and using the above quoted values for $a(s)$ and $a(P_{3/2})$, one finds $a(1s_2) + a(1s_4) = -37$, which agrees well with the values in Table 4. Also the sum rule for the $b$-factors is seen to be fulfilled.

In the non-relativistic case, the individual $b$-factors involve the same combination of $c_1$ and $c_2$ as the $g$-factors, and for $1s_2$ and $1s_4$ one then has the following relation:

$$b = -3\,(g-4)\; b(1s_5).$$

Using $g(1s_2) = 1.034$ and $g(1s_4) = 1.464$, and $b(1s_5) = -3.7$, one obtains $b(1s_2) = -3.3$ and $b(1s_4) = +1.4$ in good agreement with the optically determined values.

The $a$-factors differ in accordance with the alternative sets of $c$-coefficients; both these $c$-sets (quoted above) can be derived from the Zeeman effect and from the multiplet separation. The first $c$-set gives $a(1s_2) = -22$ and $a(1s_4) = -15$, while the second $c$-set gives $a(1s_2) = -13$ and $a(1s_4) = -24$. Thus, the magnetic hfs splitting (Table 4, column $a$) provides strong evidence in favour of the first set ($c_1 = 0.77$, $c_2 = 0.64$).

The $p$-terms have a more complex structure since, for the terms considered, neither the ion nor the outer electron has a definite j.

## Acknowledgements

Sincere thanks are due to AAGE BOHR for valuable theoretical discussions, to ALFRED HERMANSEN for coating the interferometer plates with multilayers, and to POUL STREANDER for the painstaking construction of the Fabry-Perot étalon. Furthermore, financial support from the *Carlsbergfond* and the *Statens almindelige Videnskabsfond* is gratefully acknowledged.

*Physics Department,*
*University of Copenhagen*

*Isotope Laboratory, Physics Department*
*Royal Veterinary and Agricultural College,*
*Copenhagen*

## References

1) J. KOCH and E. RASMUSSEN: Phys. Rev. **76**, 1417 (1949).
2) J. C. Hubbs and G. M. GROSOF: Phys. Rev. **104**, 715 (1956).
3) J. T. LATOURETTE, W. E. QUINN and N. F. RAMSAY: Phys. Rev. **107**, 1202 (1957).
4) G. M. GROSOF, P. BUCK, W. LICHTEN, and I. I. RABI: Phys. Rev. Letters **1**, 214 (1958).
5) E. RASMUSSEN and V. MIDDELBOE: Mat. Fys. Medd. Dan. Vid. Selsk. **30**, no. 13 (1955).
6) E. RASMUSSEN (Dissertation): *De ædle Luftarters Spektrer*, 73 (1932).
7) A. BOHR, J. KOCH, and E. RASMUSSEN: Ark. f. Fys. **4**, 455 (1952).
8) H. B. G. CASIMIR: Teylers Tweede Genootschap, Haarlem (1936).

Indleveret til selskabet den 12. maj 1960.
Færdig fra trykkeriet den 5. september 1960.

Matematisk-fysiske Meddelelser
udgivet af
Det Kongelige Danske Videnskabernes Selskab
Bind **32**, nr. 15

Mat.Fys. Medd. Dan.Vid. Selsk. **32**, no. 15 (1960)

# ELECTROCHEMICAL INVESTIGATION OF THE TRANSITION FROM TETRAGONAL TO CUBIC CÆSIUM PLUMBO CHLORIDE

BY

CHR. KN. MØLLER

København 1960
i kommission hos Ejnar Munksgaard

## Synopsis

The cæsium halide concentrations for which $Cs_4PbX_6$ and $CsPbX_3$ (X = Cl or Br) together may be in equilibrium with aqueous solutions of CsX have been determined as a function of the temperature, and the range of stability for $CsPbX_3$ alone in equilibrium with such solutions at room temperature has also been obtained. Measurements at a series of temperatures of the e.m.f. of electrochemical cells, where crystalline $CsPbCl_3$ is involved in the electrode processes allow a determination of the entropy change, $\Delta S$, for the process $CsPbCl_3$(tetragonal) $\rightarrow$ $CsPbCl_3$(cubic). The value thus obtained is $\Delta S = 4.0$ cal/mol. degree. On the assumption that the process is essentially an order-disorder tranformation, an elementary calculation based on Boltzmann's relation gives $\Delta S = 4.1$ cal/mol. degree. The results are compared with those for $BaTiO_3$.



Printed in Denmark
Bianco Lunos Bogtrykkeri A-S

## Introduction

Perovskite-like crystals usually undergo a transition from slightly distorted cubic to true cubic structure at one temperature or another. Sometimes there is a simultaneous, great change in dielectric properties, e.g. in $BaTiO_3$ from a ferroelectric to a paraelectric state.[1] It has been suggested that these might be cases of "second order transitions", and the temperatures at which they occur are often named $\lambda$-points or Curie-points.

The term second-order transition was first used by EHRENFEST[2] to describe a type of transition for which the $G$-function and the entropy $S = -\left(\frac{\partial G}{\partial T}\right)_p$ are continuous, while $C_p = T\left(\frac{\partial S}{\partial T}\right)_p = -T\left(\frac{\partial^2 G}{\partial T^2}\right)_p$ shows a discontinuity. According to FRENKEL,[3] however, as true examples of such transitions have never been observed and are not likely to correspond to a stable equilibrium between two phases, it seems preferable to characterize a second-order transition in crystals with the following features:

A certain (super-)order of the atomic arrangement decreases *continuously*, though at an ever increasing rate until it vanishes completely at a certain temperature, $T_0$. The specific heat at constant pressure, $C_p$, shows an abnormal rise, reaching a finite or infinite peak value at $T_0$ and *rapidly dropping to its normal value as the temperature is raised beyond the point* $T_0$.

Hence, from a purely thermodynamic point of view transitions of the second order may be treated as a generalization of transitions of the first kind with the transition temperature $T'$ replaced by a certain temperature range $\Delta T$ about $T'$. The latent heat for the change is replaced accordingly by the integral $\int \Delta C_p \, dT$, where $\Delta C_p$ denotes the excess of the specific heat over its normal value. Also a first-order transition may be described as a limiting case of that of the second order with a specific heat anomaly $\Delta C_p$ represented by a delta-function.

[1] See e.g. H.D. MEGAW, *Ferroelectricity in Crystals*, Chapters 4 and 5. Methuen 1957.

[2] See e.g. E.A. GUGGENHEIM, *Thermodynamics*, p. 276—288. North-Holland Publishing Co. 1949.

[3] J. FRENKEL, *Kinetic Theory of Liquids*, Chapter II. Oxford 1946.

Throughout this paper we have adopted FRENKEL's point of view. It will then be understood that the two types of transitions should not be contrasted with one another, but only considered ideal extremes of actual thermodynamic transitions.

If we have a series of discrete first-order transitions taking place within a narrow temperature range and each separately represents only a small change of the entropy, it seems legitimate, from a purely thermodynamic point of view, to treat the total change as a second-order transition. It would appear futile to discuss whether the transition properly belonged to the one type *or* the other—the more so as there will often be unavoidable hysteresis phenomena.

The perovskite-like crystals of $CsPbCl_3$ and $CsPbBr_3$ undergo transitions from a tetragonal super-lattice to a primitive cubic lattice at 47 °C. and 130 °C., respectively, which fulfil some of the requirements for second-order transitions.[1] In the work referred to, no volume change was observed at the transitions, but a small anomaly (discontinuity) was found in the thermal expansion coefficient $\alpha = \frac{1}{V}\left(\frac{\partial V}{\partial T}\right)_p$ for $CsPbCl_3$. As there is a certain parallellism between changes of the latter and changes of the heat capacity at constant pressure,[2] $\Delta C_p$, this would indicate an anomaly in $C_p$ also. It was suggested that the observed transitions were connected with order-disorder transformations rather than drastic changes in the kinematic state of certain ions.

To reach a better understanding of the nature of these transitions it was chosen to study more closely the simultaneous changes in the thermodynamic functions, $G$ (thermodynamic potential) and $S$ (entropy) of $CsPbCl_3$. As the transition temperature here is only 47 °C. this can be done by ordinary wet chemical methods, e.g. by measuring the electric potential of electrochemical cells whose electromotive force depends on the chemical potential of crystalline $CsPbCl_3$ in equilibrium with an aqueous solution of CsCl. Before this could be done it was necessary to determine the range of stability of such systems.

In the following X means either Cl or Br.

[1] C.K. MØLLER, *The Structure of Perovskite-like Cæsium Plumbo Trihalides*, Mat. Fys. Medd. Dan. Vid. Selsk. **32** No. 2 (1959).

[2] See J. FRENKEL, *loc. cit.* p. 76.

## The Equilibrium of $CsPbX_3$ with Aqueous Solutions of CsX

When the concentration of CsX in aqueous solution changes from that of saturated to that of very dilute solutions the composition of the stable Pb-compounds in equilibrium with it changes from $Cs_4PbX_6$ through $CsPbX_3$ and $CsPb_2X_5$ to $PbX_2$. It follows from the phase rule that at a given temperature one definite Pb-compound will be in equilibrium with CsX-solutions over a certain range of CsX-concentrations; for two different Pb-compounds to be in equilibrium with the same CsX-solution at a definite temperature only one CsX-concentration exists. This will then be the concentration at which the composition of the precipitate changes at that temperature.

On this basis we have determined the equilibrium temperatures for the process $Cs_4PbX_6 \rightleftarrows CsPbX_3 + 3CsX(aq.)$ as a function of aqueous CsX-concentrations. A series of CsX-solutions of known concentrations were made. A few crystals of $CsPbX_3$ and $Cs_4PbX_6$ were placed side by side in a hollow microscope slide and a drop of one of the CsX-solutions added. A cover glass was quickly put over it, "sealed" to the microscope slide with paraffin oil to make a closed space from which no water could evaporate. The slide with its contents was placed upside down, i.e. with the liquid drop hanging down from its concave side, on a hot stage. By this procedure water condensation on the cover glass was avoided during heating of the specimen.

The crystals in the drop of CsX-solution were carefully watched through a microscope. If nothing happened, the specimen was slowly heated till changes of the crystals could be observed. This was much easier to see than one would think, and as a matter of fact even a first trial usually gave the transition temperature within 5°C. After heating to above this temperature, the changes occurring during cooling were observed and the temperature interval for the transition narrowed by subsequent experiments. As an example fig. 1 shows how the crystals in equilibrium with a certain CsCl-solution changed when the temperature was varied.

An alternative method was also used for the Br-compounds. It is based on the fact that $CsPbBr_3$ is strongly orange-coloured while $Cs_4PbBr_6$ is colourless. In a very small test tube attached to a thermometer a sample of $Cs_4PbBr_6$-crystals was placed, about 0.7 cc. of a CsBr-solution of known concentration was added, and the test tube well corked. The thermometer and the test tube with its contents were very slowly heated in a small water bath and the temperature at which the colour of the crystals suddenly turned orange was noted.

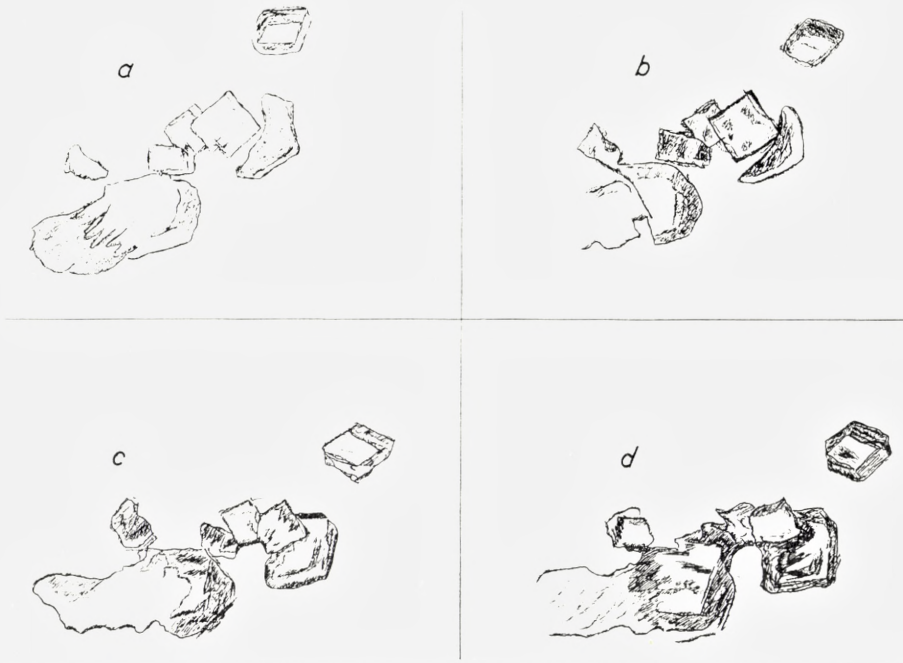


Fig. 1. Crystals of $Cs_4PbCl_6$(rhombohedral) and $CsPbCl_3$(cubic) in equilibrium with a CsCl-solution at different temperatures (drawn by means of an Abbe's drawing apparatus; magnification 100 ×).

| | | | | |
|---|---|---|---|---|
| a: | Time: | 0 ; | temp. | 22° C. |
| b: | – | 10 m; | – | 22° C. |
| c: | – | 85 m; | – | 19° C. |
| d: | – | 110 m; | – | 18° C. |

There was good agreement between the two methods, but the latter is by far the quickest where it can be applied. It is believed that the equilibrium temperatures (as a function of the CsX-concentrations) have been determined with an accuracy of ± 2°C. An obvious advantage of these methods is the small amount of material that is necessary, and for several purposes, e.g. when, as here, only an estimate of the stability range is required they may be of sufficient accuracy.

The cæsium halogenides used for the experiments were the very pure salts prepared by LANNUNG or prepared from his very pure Cs-alums by the method described by him.[1] $PbX_2$-compounds were precipitated from aqueous solutions of $Pb(NO_3)_2$ (Merck, "rein") and very pure HX, and recrystallized several times from hot, dilute solutions of HX (pH ≈ 1).

[1] A. LANNUNG, *Z. phys. Chem.* Abt. A. **161**, 255 (1932).

The compounds $CsPbX_3$ and $Cs_4PbX_6$ were precipitated from aqueous solutions of these materials as previously described.[1]

The compositions of the CsX-solutions were determined by evaporating to dryness (final temperature 120°C.) weighed samples of the solutions and then weighing the residues again.

As attainment of the equilibrium $2CsPbX_3 \rightleftarrows CsPb_2X_5 + CsX(aq.)$ was very sluggish, the CsX-concentrations for it to occur were determined only at room temperature and by the first of the two methods mentioned above.

## Stability Range of $CsPbX_3$

The results of the experiments mentioned above are reproduced in Table 1 and in figs. 2 and 3.

TABLE 1. Equilibrium concentrations and temperatures

| System | Aqueous CsX-conc. | | Equilibrium temp. $t_e$ °C. | Estimates of $\Delta H$ cal/mol. |
|---|---|---|---|---|
| | g CsX per 100 g $H_2O$ | $x_e$, mole fraction of $X^-$ or $Cs^+$ | | |
| $Cs_4PbCl_6 \rightleftarrows CsPbCl_3 + 3CsCl$ ..... | 151 | $12.2_0\ 10^{-2}$ | 63—64 | 6100 |
| | 144.5 | $11.8_0$ – | 58 | |
| | 141 | $11.5_8$ – | 49—50 | |
| | 135 | $11.2_0$ – | 45—46 | |
| | 122 | $10.3_4$ – | 31—32 | |
| | 113 | $9.7_3$ – | 20 | |
| $2CsPbCl_3 \rightleftarrows CsPb_2Cl_5 + CsCl$ ..... | 20 | $2.0_5$ – | $t_e \approx 58°$ | |
| | 15 | $1.5_5$ – | 20 | |
| $Cs_4PbBr_6 \rightleftarrows CsPbBr_3 + 3CsBr$ ..... | 109 | $7.7_8$ – | 69.5 | 16400 |
| | 87 | $6.4_1$ – | 51 | |
| | 75 | $5.6_3$ – | 43 | |
| | 67 | $5.0_9$ – | 37 | |
| | 55 | $4.2_5$ – | 24.5 | |
| $2CsPbBr_3 \rightleftarrows CsPb_2Br_5 + CsBr$ ..... | 23.5 | $1.9_1$ – | $t_e > 20°$ | |
| | 20.5 | $1.6_8$ – | 20 | |
| | 18.8 | $1.5_4$ – | $(t_e < 20°)$ | |

[1] C.K. MØLLER, *Mat. Fys. Medd. Dan. Vid. Selsk.* **32** Nos. 1, 2, and 3 (1959) and (1960).

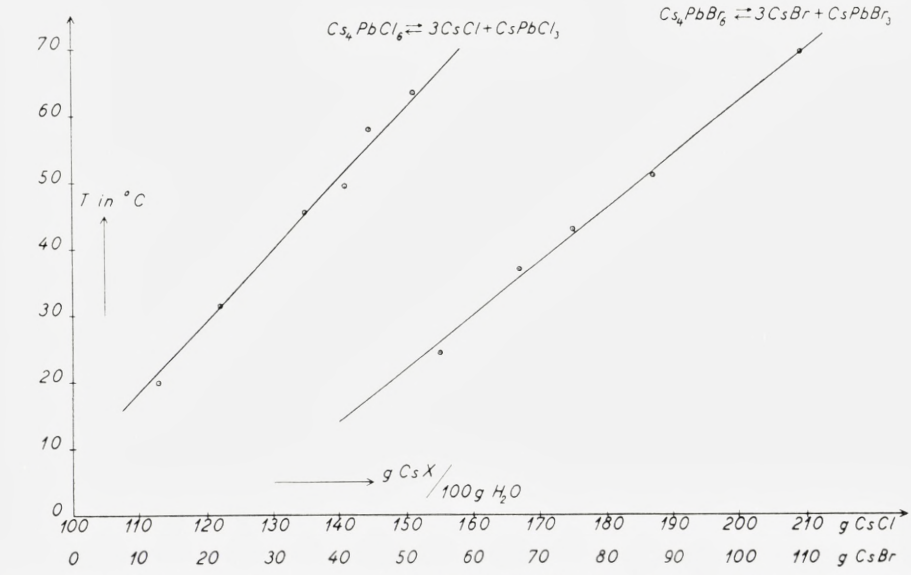


Fig. 2. The equilibrium temperature for $Cs_4PbX_6 \rightleftarrows CsPbX_3 + 3Cs^+ + 3X^-$ as a function of the aqueous CsX-concentration.—The lower horizontal scale refers to CsBr, the upper one to CsCl.

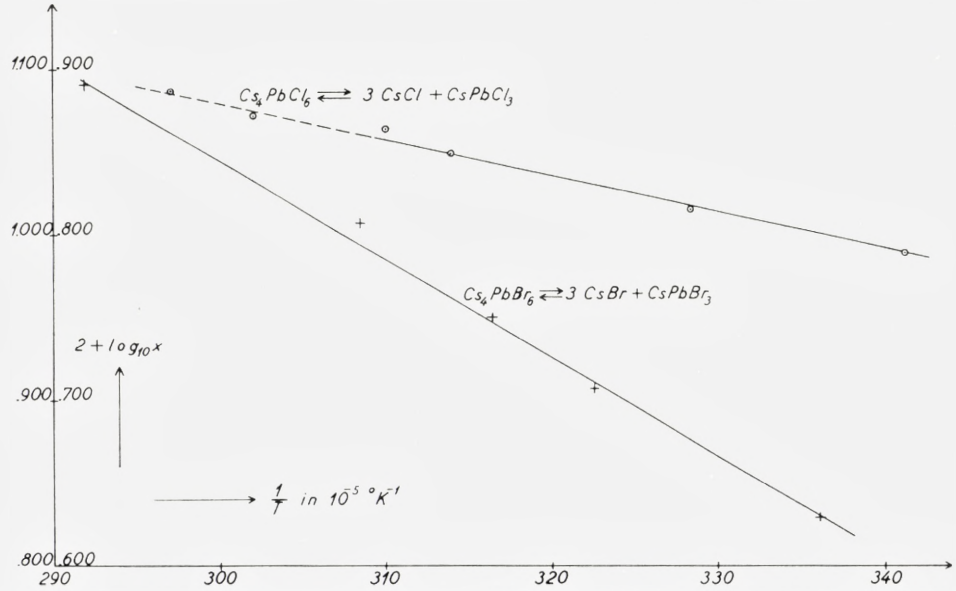


Fig. 3. $\mathrm{Log}_{10}\, x_e$ as a function of the inverse equilibrium temperature in °K. The left ordinate scale refers to CsCl, the right to CsBr.

Within the experimental uncertainty it appears that the CsX-concentrations for which the equilibrium

$$Cs_4PbX_6 \rightleftarrows CsPbX_3 + 3Cs^+ + 3X^- \qquad (1)$$

can be established, depend linearly on the temperature. If we neglect the temperature dependence of the chemical potentials of the crystalline solids and of the activity coefficients for CsX in solution we can estimate the heat of reactions for the above processes from VAN'T HOFF's relation expressed as follows:

$$(\log_e K =)\ 3\ \log_e x_e^2 = 13.815\ \log_{10} x_e = -\frac{\Delta H}{RT} + \text{const.}, \qquad (2)$$

where $x_e$ is the ionic mole fraction of $Cs^+$ or $Cl^-$ at the equilibrium (1), These estimates, which should not be considered very accurate, are given in the last column of Table 1.

In principle it should be possible to determine the entropy change for the reaction

$$\text{Tetragonal } CsPbCl_3 \rightleftarrows \text{Cubic } CsPbCl_3 \qquad (3)$$

from measurements of $\Delta H$ for (1) above as well as below the transition temperature (47°C.) for (3). Unfortunately it becomes increasingly difficult to obtain reliable values for the CsCl-concentrations as functions of the temperature above 55°C. because the solubility of the $CsPbCl_3$ becomes too great so that the actual CsCl-concentration is not accurately known; nor was in our case the temperature in the hollow microscope slide sufficiently well determined at higher temperatures. And finally it would be necessary to use CsCl-activities instead of concentrations in order to derive rather small entropy changes.

The sluggishness of the reaction

$$2\ CsPbX_3 \rightleftarrows CsPb_2X_5 + CsX(aq.) \qquad (4)$$

is presumably connected with the rather drastic changes of the PbX-coordination taking place here: In $CsPbX_3$ and $Cs_4PbX_6$, Pb is approximately octahedrally coordinated by the halogen ions, whereas the $CsPb_2X_5$-compounds are likely to contain $PbX_2$-"molecules".[1]

It is interesting that H.L. WELLS has described a dimorphous form of $CsPbBr_3$, said to be stable in a narrow CsBr-concentration interval close to the equilibrium for (4) with X = Br.[2]

[1] Cf. H.M. POWELL and H.S. TASKER, *J. Chem. Soc.* London, 1937, p. 119 and Ref. 1 on page 7.

[2] H. L. WELLS, *Z. anorg. Chem.* **3**, 203, (1893).

In this region we also have seen crystals which closely correspond to the characteristics given by WELLS: They were white, needle-shaped, showed parallel extinction, and on heating to 140–150° C. they turned orange-coloured. But it looks as if also $CsPbCl_3$ is dimorphous: Occasionally white needle-shaped crystals having parallel extinction can be seen in the CsCl-solutions when the concentration is only slightly higher than that corresponding to the equilibrium (4) with X = Cl. Although no *X*-ray diagrams have so far been obtained of the white needle-shaped crystals, it seems very tempting to guess that they are the Cl- and Br-analogues to the orthorhombic $CsPbI_3$-crystals[1] and thus represent one of the stages in changing the Pb-coordination.

## Principle of the Electrochemical Determination of the Entropy Change

Let us consider an electrochemical cell of the type

$$\mathrm{Pt} \mid \mathrm{Pb(Hg)} \mid \mathrm{PbCl_2} \mid \text{Aqueous solution of NaCl} \mid \mathrm{Hg_2Cl_2} \mid \mathrm{Hg} \mid \mathrm{Pt}, \quad (5)$$

where Pb(Hg) denotes a Pb-amalgam saturated with Pb. The chemical process when two faradays flow from the left to the right is:

$$\mathrm{Pb(Hg) + Hg_2Cl_2 \rightarrow 2\,Hg + PbCl_2} \quad (6)$$

Similarly, when the CsCl-concentration is kept within the limits for which $CsPbCl_3$ is stable, the chemical process accompanied by the flow of two faradays through the cell

$$\mathrm{Pt} \mid \mathrm{Pb(Hg)} \mid \mathrm{CsPbCl_3} \mid \text{Aqueous solution of CsCl} \mid \mathrm{Hg_2Cl_2} \mid \mathrm{Hg} \mid \mathrm{Pt} \quad (7)$$

is:

$$\mathrm{Pb(Hg) + Hg_2Cl_2 + CsCl(aq.) \rightarrow 2\,Hg + CsPbCl_3}\,. \quad (8)$$

Hence the difference in electromotive forces of the two cells, $\pi_6 - \pi_8$, is a measure of $\Delta G$ for the process

$$\mathrm{PbCl_2 + CsCl(aq.) \rightarrow CsPbCl_3} \quad (9)$$

and

$$\pi = \pi_6 - \pi_8 = \frac{1}{2F}\left\{\mu(\mathrm{CsPbCl_3}) - \mu(\mathrm{CsCl, aq.}) - \mu(\mathrm{PbCl_2})\right\}, \quad (10)$$

or

$$\mu(\mathrm{CsPbCl_3}) = 2F\pi + RT\log_e\left\{a(\mathrm{CsCl,aq.})\right\} + \mu(\mathrm{PbCl_2}) + \mu_0(\mathrm{CsCl,aq.}), \quad (11)$$

[1] Cf. Ref. 1 on page 7.

where $\mu_0$(CsCl,aq.) is independent of the CsCl-concentration. Hence it is not possible in this way to obtain absolute values of the chemical potential for $CsPbCl_3$ unless we know the activity of CsCl in aqueous solution and the chemical potential for $PbCl_2$. However, we shall not be particularly interested in absolute values of the potentials, but only in the changes of the chemical potential of $CsPbCl_3$ as a function of temperature. It seems safe to assume that $\mu(PbCl_2)$ and $\mu$(CsCl,aq.) vary only slowly with temperature so that any sharp or rapid variation of $\pi$ or, as experiments show that $\pi_6$ is a linear function of temperature within the temperature interval for the investigation, of $\pi_8$ is produced by similar changes in the chemical potential of $CsPbCl_3$.

The changes in $G$-function and in entropy of $CsPbCl_3$(cryst.) at 47°C. may therefore be obtained from the temperature variation of $\pi_8$ measured above as well as below 47°C.:

$$\Delta S = -\left(\frac{\partial \Delta G}{\partial T}\right)_p \simeq 2F\left\{\left(\frac{\partial \pi_8}{\partial T}\right)_{>47^\circ} - \left(\frac{\partial \pi_8}{\partial T}\right)_{<47^\circ}\right\}. \qquad (12)$$

If the CsCl-concentration in (8) is kept so high that a $Cs_4PbCl_6$-electrode may be used instead of the $CsPbCl_3$-electrode the reaction expressed in (1) can be examined in the same way. Furthermore, as $Cs_4PbCl_6$ is stable in a solution saturated with CsCl, the activity of CsCl in aqueous solution with concentration $m$ can be related to the chemical potential of CsCl in crystalline CsCl from measurement of the electric potential difference of such cells of which one contains a saturated CsCl-solution, the other a CsCl-solution of concentration $m$ as electrolyte. Unfortunately the $Hg_2Cl_2$-electrode turned out not to be reliable at such high CsCl-concentrations.

The diffusion potential in the cells mentioned above have been neglected because the CsCl-concentration in every case is much higher than the concentrations of $Pb^{++}$ and $Hg_2^{++}$ around the electrodes, so that they are practically "cells without transference".

## Experimental Details

Rather small electrode vessels requiring about 1 cc. of electrolyte were used. They were H-shaped with Pt-electrodes sealed into the bottom. A loose plug of cotton wool was placed between the two electrodes. The branch with Pb-amalgam also contained a small (glass-covered) magnetic stirrer as stirring here sometimes was necessary in order to obtain reproducible

measurements. The temperature of the cells was controlled within 0.02°C. by an oil thermostat.

The quality of the chemicals were as follows: Hg, cleaned in dilute nitric acid and distilled in vacuum; Pb-amalgam (always containing solid phase) made from distilled Hg and Merck's Pb pro analysi. Other Pb-compounds were prepared as mentioned above. Except for preliminary experiments, where rather impure CsCl was used, "AnalaR" or Lannung's spectroscopically pure CsCl was used (both giving the same results within the accuracy of the measurements).

The electrolyte solutions were made by adding a definite amount of water to a weighed sample of CsCl and the composition was checked after the often very long experiments by taking out a certain amount of the electrode solution, weighing it, and after evaporation of the liquid, weighing the residue again.

This final determination is considered to indicate the CsCl-concentration in the cells during the measurements, as it is difficult to avoid some evaporation while preparing the cells.

Measurements of the electromotive forces were made by the usual compensation method, using a precision potentiometer, a 2 volt lead accumulator, galvanometer, and a standard Cd-cell (E = 1.0184 volt at 20°C., checked occasionally by comparison with an International standard cell). The uncertainty presumably is not higher than 0.1 mV.

The cells with $Cs_4PbCl_6$, which required rather concentrated CsCl-solutions, did not give steady potentials (except when saturated with CsCl), and when the CsCl-content of the electrolyte solution was examined after the experiments it had often changed by 5–10 per cent. It was observed in such cases that the $Hg_2Cl_2$-electrode became grey or dark grey and had developed a hard, solid crust, suggesting the formation of double compounds according to the reactions:

$$\left.\begin{aligned} Hg_2Cl_2 &\rightarrow Hg + HgCl_2 \\ n\,CsCl + HgCl_2 &\rightarrow Cs_nHgCl_{n+2}\,. \end{aligned}\right\} \quad (13)$$

However, the cells with $CsPbCl_3$ and less concentrated CsCl-solutions seemed very reliable when stirred now and then. While equilibrium was very quickly re-established in the cells when going from one temperature to a higher one, they often showed 0.3–0.5 mV. higher potentials at 20°C. after cooling from 60°C. than when measured before heating to this temperature. This change may possibly be due to slow or irreversible diffusion processes, either in the electrolyte solution or in the $CsPbCl_3$-crystals. It might perhaps

also be due to evaporation even though the cells were well corked and immersed in oil; however, they showed no significant variation in potential when kept for several days at 60°C. (A change of 0.5 mV. would correspond to a little less than a two per cent change of the CsCl-concentration).

Table 2 shows examples of the daily variation of the potentials of some of the cells.

The averages of several measurements at each of a series of selected temperatures are given in Tables 3 and 4 for a number of cells of Type (7), some cells of Type (5), and one having $CsPb_2Cl_5$ instead of $CsPbCl_3$.

## Results

The variation of the measured potentials with the logarithm of the ionic mole fraction, $x$, of $Cs^+$ or $Cl^-$ in the cells (7) is shown in fig. 4 for different temperatures. It is seen that for a given temperature, and for the CsCl-concentrations considered, the potential $\pi_8$ is a nearly linear function of $\log_{10} x$ of the form

$$\pi_8 = \beta \log_{10} x + b \,. \tag{14}$$

The relation to be expected is from (8) and (10):

$$\pi_8 = 2.3026 \cdot \frac{RT}{F} \log_{10} (x f_{\pm}) + a = \alpha \log_{10} (x f_{\pm}) + a \,. \tag{15}$$

From Robinson and Stokes's tables of activity coefficients[1] it appears that $f_{\pm}$ should be practically independent of $x$ for the CsCl-concentrations used here. Hence, if the process in the cells really is the one expressed in (8) $\beta$ would be expected to be identical with the theoretical value $\alpha$—or nearly so. The smallness of the relative deviations:

$$\eta = \frac{\beta - \alpha}{\alpha} \tag{16}$$

shown in the graph fig. 5 in fact warrants the correctness of the assumption.

Before discussing the reason why $\beta$ and $\alpha$ are not identical it should be emphasized that the CsCl-concentrations in the cells have not been determined with any high accuracy—the relative uncertainty may indeed be as high as 2–3 per cent. (The original aim was only roughly to check the cell process, and hence no correction was made for the possible Pb-contents

[1] R.A. Robinson and R.H. Stokes, *Trans. Far. Soc.* **45**, 613 (1949).

TABLE 2. Examples of the daily variation in electromotive force of the cells.

| Date | Temp. °C. | E.m.f. in mV. of the cells | | |
|---|---|---|---|---|
| | | *P* | *R* | *S* |
| 30.11 a. m. | 20.00 | $577.0_4$ | $562.3_0$ | $529.2_8$ |
| – – – – | – | $577.0_2$ | $562.3_0$ | $529.2_5$ |
| – – p. m. | 30.00 | $576.1_8$ | $560.4_5$ | $530.1_3$ |
| – – – – | – | $576.1_5$ | $560.4_5$ | $530.4_0$ |
| 1.12 a. m. | – | $576.1_6$ | $560.5_6$ | $530.3_5$ |
| – – – – | – | $576.1_2$ | $560.5_2$ | $530.3_6$ |
| | | stirred | stirred | stirred |
| – – p. m. | – | $576.1_3$ | $560.4_8$ | $530.1_8$ |
| – – – – | – | $576.1_8$ | $560.5_5$ | $530.1_8$ |
| 2.12 a. m. | – | $576.1_5$ | $560.5_7$ | $530.2_7$ |
| 17.12 a. m. | 50.50 | $575.3_0$ | $558.3_5$ | $533.3_1$ |
| – – – – | – | $575.2_8$ | $558.3_4$ | $533.3_0$ |
| – – p. m. | 55.00 | $575.1_5$ | $557.9_5$ | $533.8_0$ |
| – – – – | – | $575.1_8$ | $557.9_3$ | $533.8_5$ |
| 18.12 a. m. | – | $575.1_5$ | $557.9_6$ | $533.8_5$ |
| – – – – | – | $575.1_5$ | $557.9_8$ | $533.8_8$ |
| | | stirred | stirred | stirred |
| – – p. m. | – | $575.1_9$ | $558.0_0$ | $533.9_0$ |
| – – – – | – | $575.2_3$ | $558.0_2$ | $533.9_0$ |

of the samples taken out from the cells). E. GÜNTELBERG[1] has shown that even with very pure materials small amounts of $Br^-$ or other unwanted ions in the cell solutions may be troublesome when very accurate e.m.f.-measurements have to be made. This effect has also been disregarded here.

The observed differences between $\beta$ and $\alpha$ would imply that the mean activity coefficient $f_\pm$ for the CsCl-concentrations considered was approximately given by:

$$\log_{10} f_\pm = \eta \log_{10} x + \sigma , \qquad (17)$$

where $\sigma$ may depend on the temperature, but not on $x$. This is not quite in accordance with the results given by ROBINSON and STOKES, but the the electrometric measurements by HARNED and SCHUPP[2] are in fact compatible with (17), and the value obtained for $\eta$ for this concentration interval is nearly the same as found here at 25°C., when regard is paid to the rather large uncertainty on $\eta$: $\pm$ 0.01.

[1] E. GÜNTELBERG, *Studier over Elektrolyt-Aktiviteter i vandige Opløsninger.* Dissertation, Copenhagen 1938.

[2] H.S. HARNED and O.E. SCHUPP, J. Am. Chem. Soc. **52**, 3886. (1930).

If we neglect the temperature variation of $\sigma$ in (17) an estimate of the partial molar heat of transfer, $Q$, from an infinitely dilute solution of CsCl in $H_2O$ to the CsCl-concentrations considered may be obtained from

$$\frac{\partial \log_{10} f_{\pm}}{\partial \left(\frac{1}{T}\right)} = 2.303 \cdot \log_{10}(x) \cdot \frac{\partial \eta}{\partial \left(\frac{1}{T}\right)} = \frac{Q}{R} \cdot \qquad (18)$$

We find $Q \simeq -R\, 2.303 \cdot 135 \cdot \log_{10}(x)$ which for a 2 molal CsCl-solution becomes $Q \simeq 900$ cal/mol.

The potentials $\pi_8$ for given CsCl-concentrations are shown as functions of the temperature in fig. 6; for comparison the results of measurements

TABLES 3, 4, and 5. Electromotive forces of cells with different electrolyte concentrations at a series of temperatures from 18°C. to 60°C.

Table 3.

| Cell | $K$ | $L$ | $M$ |
|---|---|---|---|
| g CsCl/100 g $H_2O$ | 41.5 | 64.0 | 52.2 |
| Temp. °C. | E.m.f. in mV. | | |
| 18.02 | $576.1_2$ | $585.7_4$ | $581.5_2$ |
| 25.00 | $575.4_8$ | $585.4_9$ | — |
| 32.05 | $574.9_2$ | $585.2_8$ | — |
| 39.00 | $574.4_7$ | $585.1_4$ | — |
| 40.00 | $574.4_0$ | $585.1_3$ | $580.3_6$ |
| 41.00 | $574.3_6$ | $585.1_1$ | $580.2_9$ |
| 42.00 | $574.3_5$ | $585.2_2$ | $580.3_1$ |
| 43.02 | $574.3_2$ | $585.2_4$ | $580.2_8$ |
| 44.00 | $574.3_3$ | $585.2_4$ | $580.3_6$ |
| 45.00 | $574.3_0$ | $585.2_8$ | $580.3_3$ |
| 46.00 | $574.2_6$ | $585.3_3$ | $580.3_0$ |
| 47.00 | $574.2_7$ | $585.3_5$ | $580.3_2$ |
| 48.00 | $574.2_5$ | $585.4_0$ | $580.3_6$ |
| 49.00 | $574.3_0$ | $585.4_1$ | $580.4_3$ |
| 50.00 | $574.2_9$ | $585.5_4$ | $580.4_8$ |
| 52.00 | $574.2_2$ | $585.8_4$ | $580.5_3$ |
| 55.00 | $574.2_2$ | $585.9_5$ | $580.6_0$ |
| 60.00 | $574.1_5$ | $586.3_1$ | $580.7_7$ |
| 20.00 | 576.30 | 585.1 | $581.8_5$ |
| $\left(\frac{\partial \pi_8}{\partial T}\right)_{>47^\circ} - \left(\frac{\partial \pi_8}{\partial T}\right)_{<42^\circ}$ | 0.075 | 0.100 | 0.080 mV/°C. |

Table 4.

| Cell | *P* | *T* | *R* | *U* | *S* |
|---|---|---|---|---|---|
| g CsCl/100 g $H_2O$ | 42.4 | 31.4 | 21.9 | 11.0 | NaCl, unsat. |
| Temp. °C. | E.m.f. in mV. | | | | |
| 20.00 ..... | $577.0_4$ | $569.8_5$ | $562.3_3$ | $552.7_5$ | $529.2_7$ |
| 30.00 ..... | $576.1_5$ | $568.9_3$ | $560.5_3$ | $551.1_5$ | $530.2_7$ |
| 40.00 ..... | $575.4_9$ | $567.8_4$ | $559.1_6$ | $549.6_5$ | $531.6_0$ |
| 43.50 ..... | $575.2_8$ | $567.6_6$ | $558.7_3$ | $549.3_3$ | $532.0_2$ |
| 47.03 ..... | $575.2_9$ | $567.4_0$ | $558.5_2$ | $548.9_1$ | $532.7_7$ |
| 50.50 ..... | $575.3_0$ | $567.2_6$ | $558.3_1$ | $548.6_2$ | $533.3_0$ |
| 55.00 ..... | $575.2_3$ | $567.1_9$ | $558.0_6$ | $548.2_5$ | $533.9_0$ |
| 60.00 ..... | $575.2_8$ | $567.1_9$ | $557.9_0$ | $547.8_5$ | $534.5_4$ |
| 20.00 ..... | $577.4_4$ | 570.2 | $562.8_3$ | 552.2 | $529.2_0$ |
| $\left(\frac{\partial \pi_8}{\partial T}\right)_{>47^\circ} - \left(\frac{\partial \pi_8}{\partial T}\right)_{<42^\circ}$ | 0.085 | 0.085 | 0.095 | mV/°C. | |

Table 5.

| Cell. | A NaCl, sat. |
|---|---|
| Temp. °C. | E.m.f. in mV. |
| 18.60 | $529.0_0$ |
| 25.60 | $530.0_0$ |
| 30.00 | $530.5_7$ |
| 36.98 | $531.5_0$ |
| 44.92 | $532.5_5$ |
| 46.40 | $532.7_5$ |
| 47.05 | $532.8_3$ |
| 47.40 | $532.8_5$ |
| 49.00 | $533.0_5$ |
| 54.62 | $533.7_6$ |
| 56.40 | $533.9_4$ |
| | B NaCl, sat. |
| 18.40 | $529.0_3$ |
| 26.45 | $530.0_5$ |
| 35.40 | $531.2_4$ |
| 41.26 | $532.0_4$ |
| 50.26 | $533.1_8$ |

on cells of Type (5) and on one cell with $CsPb_2Cl_5$ instead of $CsPbCl_3$ are also reproduced in this graph. The potentials of the latter cells show a smooth or linear dependence on the temperature without irregularities, but

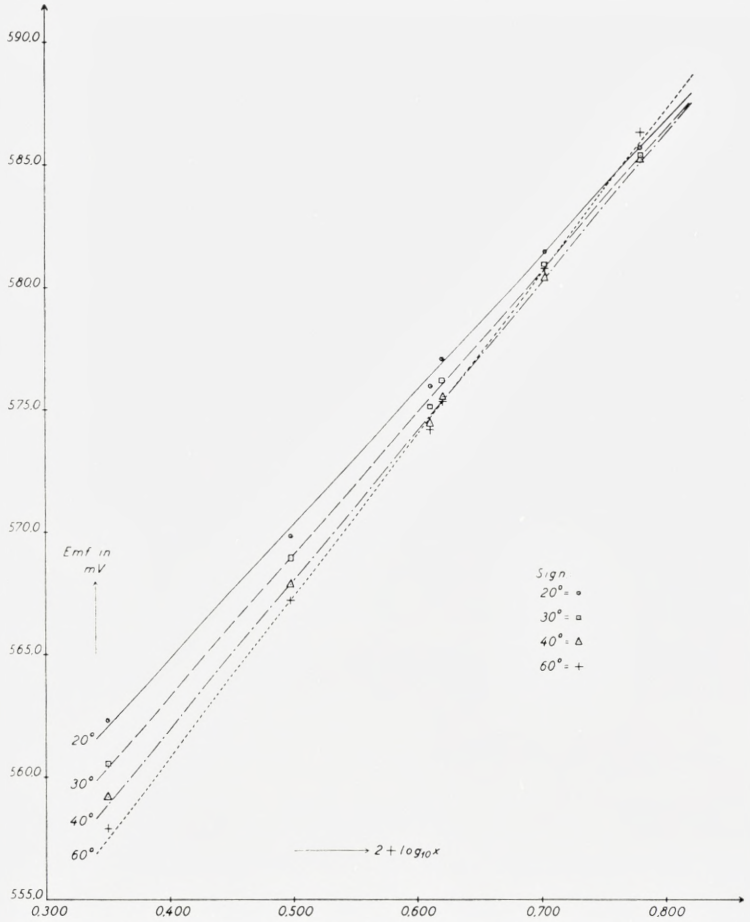


Fig. 4. The potential $\pi_8$ as a function of $\log_{10} x$, for given temperatures; $x$ is the ionic mole fraction of $Cl^-$ or $Cs+$.

the former exhibit a rather sharp (though continuous) change in the temperature region from about 40°C. to about 50°C. As the slope, too, changes continuously it is seen from (12) that the entropy function is continuous throughout the transition region as required for a second-order transition. It is interesting that the maximum variation of $G$ and $S$ appears to lie about

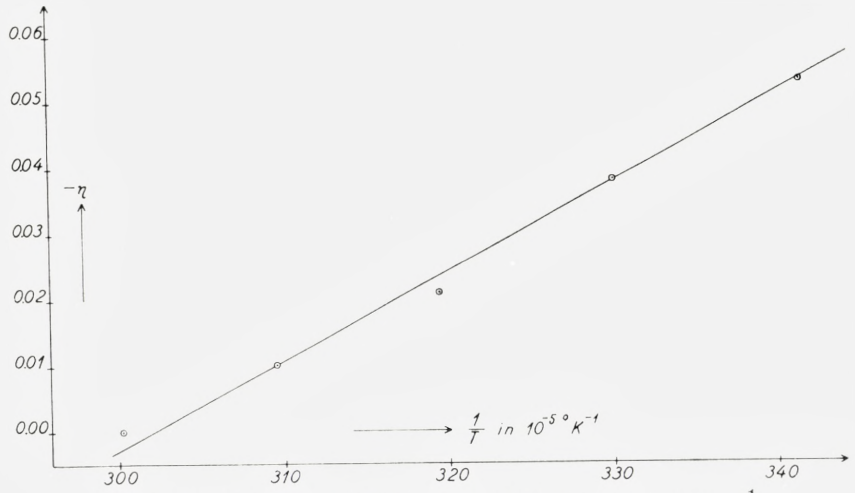


Fig. 5. $\eta$ as a function of the reciprocal absolute temperature, $\frac{1}{T}$.

44°C., whereas from the crystallographic investigation one gets an impression that the maximum changes occur just below 47°C.

From the slopes of the linear parts of $\pi_8$, i.e. below 42°C. and above 47°C., values are obtained for $\left(\frac{\partial \pi_8}{\partial T}\right)_{>47^\circ} - \left(\frac{\partial \pi_8}{\partial T}\right)_{<42^\circ}$ for some selected CsCl-concentrations in the cells. They are given in the last line of Tables 3 and 4 and do not seem to vary systematically with the CsCl-concentrations. Nor would such a variation be expected on the assumption that the changes in $\pi_8$ have to be referred to changes in the chemical potential of the crystalline $CsPbCl_3$. From the mean value of these numbers we calculate the total change in entropy for the transition (3):

$$\Delta S = 4.0 \pm 0.3 \text{ cal/mol. degree} \qquad (19)$$

## Discussion

The entropy change for a transition in the crystalline phase may be divided into two parts,[1] one of which originates from the changes in the configuration of the crystal, the other, called the "thermal entropy change", from changes in the frequency spectrum of the lattice vibrations. The *X*-ray analysis of $CsPbCl_3$ and $CsPbBr_3$[2] reveals practically no changes of the

[1] See e.g. A.J. DEKKER, *Solid State Physics*, p. 63. MacMillan 1958.
[2] Ref. 1 on page 4.

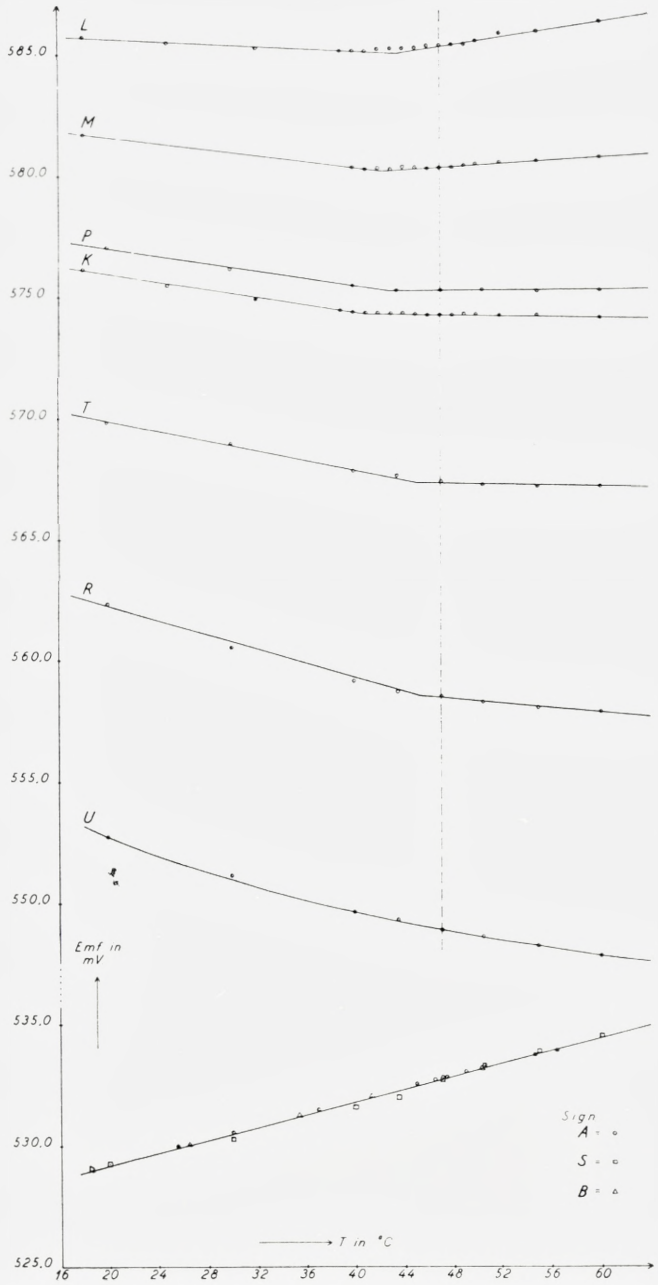


Fig. 6. Temperature variation of the electromotive forces for a number of cells with different electrolyte compositions. The letters refer to cells in the Tables 3, 4, and 5.

local atomic arrangements in these crystals during their respective transitions at 47°C. and 130°C., so that the lattice frequencies would be expected not to change very much here, and the vibrational or thermal contribution to the entropy may be considered unaltered. However, a superstructure which exists below the transition temperature, disappears above it, so that there must be a change in the configurational entropy. This change can be estimated as follows.

The axes of the primitive tetragonal unit cell all appear, from the *X*-ray analysis, to be twice as long as those of the cubic cell. As there is only one $CsPbX_3$-"molecule" in the latter, there must therefore be $2\times2\times2 = 8$ "molecules"—having different relative orientations—in the former. These eight situations for a $CsPbX_3$-unit in the tetragonal lattice become equivalent in the cubic structure because of transformation from one to the others, thus giving the latter an eight times larger thermodynamic probability than the former. (For a certain $CsPbX_3$-unit, which in the tetragonal crystal can have only one stable "configuration", there exist eight equivalent possibilities in the cubic crystals).

From BOLTZMANN's relation we therefore get:

$$\Delta S = R \log 8 = 4.11 \text{ cal/mol. degree.} \qquad (20)$$

The agreement of this with the experimental value obtained above lends some support to the interpretation given here.

Similar considerations would seem to apply to the transition observed in $BaTiO_3$ at 120°C.[1]. However, as the primitive, non-centrosymmetric unit cells below this temperature all have the same orientation, a strong electric polarization results, which gives a temperature-dependent, electrical contribution to the free energy. Above the transition the additional field is destroyed. It then follows that the observed entropy change $\Delta S = -\left(\frac{\partial \Delta G}{\partial T}\right)_p =$ 0.12 cal/mol. deg. may not be entirely due to change of the "configurational" entropy, but contains other contributions as well.

If in $BaTiO_3$-crystals the ions could occupy several close-lying potential minima these would be so close together that the barriers separating them would be very low and much narrower than in the $CsPbX_3$-crystals. Transitions to vibration states above or close to the barrier height may then easily occur at temperatures as low as 120°C., these minima thus losing their individuality, and there will be practically no configurational entropy change. (Compare the fact that the entropy of mixing for gases becomes

[1] Ref. 1 on page 3.

zero when the molecules to be mixed become identical). Nor will the vibrational entropy change drastically.

If the transition observed at 47°C. in $CsPbCl_3$ corresponded to a change from vibrational rotation to free rotation of the Cl- or Cs-ions, then, following FRENKEL[1] $C_p = T\left(\frac{\partial S}{\partial T}\right)_p$ immediately after the transition should be lower than before it sets in. This would imply that the second derivative of the $\pi_8$-versus-$T$ curves after 47°C. should be smaller than before, say, 42°C. No such change is indicated in the curves, but our measurements may not be accurate enough to show it. Further investigations of the transition by means of Raman- or infrared spectroscopy would appear interesting.

## Acknowledgements

I am highly indebted to Professor A. TOVBORG JENSEN, Ph.D., for his interest in this work and for the readiness with which rather expensive chemicals were placed at my disposal.

I also wish to thank Mr. K.J. PEDERSEN, Ph.D., for many helpful discussions.

[1] Ref. 3 on page 3.

Indleveret til Selskabet 16. maj 1960.
Færdig fra trykkeriet 18. november 1960.

Matematisk-fysiske Meddelelser
udgivet af
Det Kongelige Danske Videnskabernes Selskab
Bind **32,** nr. 16

Mat. Fys. Medd. Dan.Vid. Selsk. **32,** no. 16 (1961)

# THE EFFECT OF PAIR CORRELATION ON THE MOMENT OF INERTIA AND THE COLLECTIVE GYROMAGNETIC RATIO OF DEFORMED NUCLEI

BY

S. G. NILSSON AND O. PRIOR

København 1961
i kommission hos Ejnar Munksgaard

# CONTENTS


Page

Introduction ..... 3

I. The Hamiltonian Describing the Intrinsic Motion of Deformed Nuclei with the Inclusion of the Pair Correlation ..... 5

II. The Bardeen–Cooper–Schrieffer Trial Function and the Canonical Transformation of the Hamiltonian Considered to a Hamiltonian Describing Independent Quasi-Particles ..... 8

III. General Formula for the Moment of Inertia and the Collective Gyromagnetic Ratio in Terms of the Quasi-Particle Formalism ..... 13

IV. Numerical Calculations of the Moment of Inertia and the Collective Gyromagnetic Ratio ..... 17

a. Energy scale of the single-particle energies $\varepsilon_\nu$ and determination of the deformation $\delta$ ..... 17

b. The gap parameters $\Delta_n$ and $\Delta_p$ ..... 19

V. Details of the Numerical Calculations ..... 36

VI. Results of the Calculations ..... 37

a. Moments of inertia of even-even nuclei ..... 37

b. The collective gyromagnetic ratio $g_R$ ..... 47

Appendix I. On the Quasi-Particle Approximation ..... 52

Appendix II. Single-Particle Matrix Elements of $j_x$ ..... 58

List of References ..... 60


## Synopsis


The moment of inertia and the collective gyromagnetic ratio of even-even nuclei are calculated on the basis of wave functions that take a pairing interaction into account through the quasi-particle formalism. The results obtained theoretically are found to be in reasonable agreement with experiments. The strength of the characteristic pair-correlation matrix element to be employed is estimated on the basis of data on odd-even mass differences. The dependence of the calculational results on the central-field parameters, as e. g. the eccentricity and the single-particle energy scale, is discussed. Other possible effects with particular relevance to the odd-even mass difference and the experimentally occurring energy gap are also surveyed.



Printed in Denmark
Bianco Lunos Bogtrykkeri A-S

# Introduction

The regions of deformed nuclei are empirically characterized by the occurrence of rotational bands in the nuclear excitation spectra. The characteristic energy spacings within these bands exhibit the well-known $I(I+1)$ dependence. The occurrence of such collective rotational states is largely independent of the detailed character of the intrinsic motion.

If one writes the rotational energy in the form

$$E_{\mathrm{rot}} = \frac{\hbar^2}{2\Im} I(I+1), \tag{1}$$

the magnitude of the moment of inertia $\Im$, entering in the proportionality constant, provides, however, more of a test of the detailed nuclear model. For even-even nuclei two more intrinsic constants determine most of the properties of the low-lying states. One is the intrinsic quadrupole moment which determines the $E2$ transition strengths for gamma decay and for Coulomb excitation. The other constant, $g_R$, the gyromagnetic ratio of the collective flow, enters, for instance, when one measures the magnetic moment of a higher member of the ground-state rotational band. While $\Im$ measures the mass of the collective flow, $g_R$ is associated with the magnetic properties of the flow.

For odd-A nuclei, magnetic moments and decay probabilities within a rotational band also depend on some of the details of the odd-particle orbital in addition to the said quantities connected with the even-even ground-state band.

The present work is based on the "cranking model"[1]. This model corresponds to the approximation that the self-consistent field determining the single-particle orbitals is cranked around externally. The rotational energy of the system is then calculated as the extra energy necessary for the nucleons to follow a slow rotation. The cranking model applied on the basis of a completely-independent-particle description gives a value of the moment of inertia approximately equal to that of rigid motion, provided one chooses

the equilibrium value of the deformation of the nuclear field[2, 3]. The empirical values amount, however, to only 20-50 % of the rigid moment of inertia.

BOHR and MOTTELSON[2] gave general arguments to the effect that a residual short-range attractive interaction between the particles—the latter being assumed in the first approximation to move independently in a common field—would decrease the value of the moment of inertia. They also studied the effects explicitly in terms of a very simplified "two-particle model". The strength that such an additional interaction must have to reproduce the empirical situation was found to be of the order usually attributed to the short-range inter-particle force. It remained, however, to treat such an inter-particle force in the case of a large number of particles outside of closed shells.

Such an additional inter-particle force, the pair-correlation force, which allows a complete treatment even when many particles are involved, has recently been introduced into nuclear physics by BOHR, MOTTELSON and PINES[4, 3, 5], by BELYAEV[6], and by SOLOVIEV[7] and other authors of the Bogolubov school. These authors employ and adapt to nuclear physics the elegant and powerful methods developed by BARDEEN and others[8] to explain the phenomenon of superconductivity. Such a pairing interaction is first of all capable of explaining the empirically encountered energy gap in the spectra of even-even nuclei. For an example of the empirical occurrence of such a gap, take for instance the region of rare-earth nuclei $150 < A < 190$. The empirical average energy spacing of intrinsic excitations appears to be of the order of 150 keV (which seems to indicate a single-particle level density of about one level per 300 keV). In even-even nuclei in this region, however, there exist experimentally no excited states that are not of collective character below $\sim$ 1000 keV. Such an energy gap cannot be explained by the mere assumption of an additional diagonal pairing energy, effective between the pair of particles filling the degenerate orbitals $K$ and $-K$. This would indeed forbid the breaking of such a pair, but could not prevent low-lying two-particle excitations; the latter would occur with an average level density of one state per 300 keV or so, where about half the states would correspond to excited proton pairs and half to neutron pairs.

As pointed out, the pair-correlation interaction is capable of explaining this very conspicuous feature of even-even spectra. Expressed in terms of the single-particle states of the average nuclear potential, the pair-correlation interaction thus scatters pairs of particles from the originally filled lower-lying, doubly degenerate single-particle orbitals into the higher-lying levels which are left unoccupied according to the earlier description. The new

total intrinsic wave function that most effectively utilizes this additional type of interaction and represents the ground state is then a state with a diffuse Fermi surface. In this state there exists a particular correlation between all the scattering pairs of particles within the region of diffuseness of the Fermi surface. Any excited state which thus involves the formation of a state orthogonal to the ground state then necessarily spoils some of the correlation and is therefore associated with an excitation energy of at least about the width of the diffuseness of the Fermi surface.

The investigation reported in this paper appears to bear out the contention that the introduced pair-correlation interaction in the regions of deformed nuclei is capable of explaining quantitatively at the same time the occurrence and magnitude of the energy gap in the spectra of even-even nuclei, the even-odd-mass difference, and the magnitude of the moment of inertia associated with the collective rotation. A computation of the moment of inertia rather similar in scope to the one reported here has been carried through by GRIFFIN and RICH[9]. Also the investigations by MIGDAL[10] and by HACKENBROICH[11] contain some numerical results largely in line with the results obtained in the publication cited above as well as with those of the present paper.

A preliminary report of the present calculations was presented at the Conference of the Swedish Physical Society in June, 1959[12].

## I. The Hamiltonian Describing the Intrinsic Motion of Deformed Nuclei with the Inclusion of the Pair Correlation

The application of the quasi-particle formalism in the nuclear case is described in detail in the paper by BELYAEV[5]. For the reader's convenience we shall, however, give a short account of the most important results.

Let the Hamiltonian of the (static) self-consistent nuclear field be denoted $H_s$. The corresponding single-particle eigenfunctions are first characterized by the eigenvalue $K$ of the angular-momentum component along the nuclear axis. This component is a constant of the motion provided $H_s$ exhibits cylindrical symmetry. Furthermore, under the condition that the system is invariant under time reversal there always exist two states degenerate in energy, each of which is the time reverse of the other. Under the additional requirement of cylinder symmetry these may be labelled by the components of angular momentum $K$ and $-K$.

We define such a single-particle state as $|\nu\rangle$, where $\nu$ denotes both the $K$-value and the additional quantum numbers necessary for the complete specification of the state. It is sometimes convenient to consider such a state expanded in terms of eigenstates of the angular momentum $j$ as follows:

$$|\nu\rangle = \sum_j c_j^\nu \chi_K^j . \tag{2}$$

We then define the conjugate $|-\nu\rangle$ state, which corresponds to the nucleonic orbit with a completely reversed direction of motion compared with $|\nu\rangle$, as*

$$|-\nu\rangle = \sum_j (-)^{l+j-K} c_j^\nu \chi_{-K}^j , \tag{3}$$

where the phases of $\chi_K^j$ and $\chi_{-K}^j$ are defined in accordance with the conventions of CONDON and SHORTLEY[13]. As already pointed out, this definition of the conjugate state makes it equal to the time-reversed state $T|\nu\rangle$, possibly apart from a conventional phase. In the following we shall employ the relation

$$T|\nu\rangle = |-\nu\rangle, \tag{4}$$

which then fixes the arbitrary phase of $T$. We denote the eigenvalues of $H_s$ by $\varepsilon_\nu$. Furthermore we assume that both $\varepsilon_\nu$ and $|\nu\rangle$ can be taken with sufficient accuracy from the calculations by MOTTELSON and NILSSON[15, 16]. The remaining, most important features of the inter-particle forces, which correspond to the very short range components of these forces, may now (cf. references 3, 5, 6) be simulated by the said pair-correlation interaction. In its simplified form this interaction may be written in second-quantization language

$$H^{\text{pair}} = -G \sum_{\nu\nu'} a_{\nu'}^+ a_{-\nu'}^+ a_{-\nu} a_\nu . \tag{5}$$

Eq. (5) represents the limiting assumption that the residual force acts only when two particles move in a $J = 0$ state. The said force displays the main features of the $\delta$-force, although the latter has minor but non-negligible effects on pairs of particles in states of non-vanishing but small angular momentum.

In this notation a one-particle state is expressed as follows in terms of the creation operator $a_\nu^+$:

$$|\nu\rangle = a_\nu^+ |0\rangle. \tag{6}$$

* By redefinition of the spherical harmonics as $\hat{Y}_{lm} = i^l Y_{lm}$, where $Y_{lm}$ is the conventional spherical harmonic defined in accordance with the CONDON-SHORTLEY[13] phase conventions, the parity sign in (3) or $(-)^l$ may be absorbed into $|-\nu\rangle$ (see EDMONDS[14]). This parity sign is furthermore unimportant in our calculations.

With the inclusion of $H_s$ the total Hamiltonian takes the form

$$H = \sum_{\nu} \varepsilon_\nu (a_\nu^+ a_\nu + a_{-\nu}^+ a_{-\nu}) - G \sum_{\nu\nu'} a_{\nu'}^+ a_{-\nu'}^+ a_{-\nu} a_\nu . \tag{7}$$

The great advantage of the second-quantization formalism is that it automatically ensures compliance with the Pauli principle. This principle is built into the formalism by the usual anti-commutation relations which the $a_\nu$:$s$ are required to obey.

The obvious aim is now to find an eigenfunction of the Hamiltonian (7) that is in addition an eigenfunction of the number operator

$$N = \sum_{\nu} (a_\nu^+ a_\nu + a_{-\nu}^+ a_{-\nu}) . \tag{8}$$

BARDEEN et al. find a convenient but approximate eigenfunction of (7) at the cost of weakening the latter condition* and replacing it by a condition for the average value of $N$:

$$\langle \Psi | \, N \, | \Psi \rangle = n . \tag{9}$$

In conformity with the fact that the number of particles is conserved only on the average, the solution corresponds physically to an ensemble of nuclei having slightly different numbers of nucleons. The procedure for treating this new simplified problem is then to introduce an auxiliary Hamiltonian $H'$:

$$H' = H - \lambda N , \tag{10}$$

where $\lambda$, treated as a Lagrangian multiplier, takes the role of the chemical potential. Thus $\lambda$ represents the energy of the last added particle.

* A method for obtaining wave functions which fulfil this condition exactly has recently been discussed by B. BAYMAN[17].

## II. The Bardeen-Cooper-Schrieffer Trial Function and the Canonical Transformation of the Hamiltonian Considered to a Hamiltonian Describing Independent Quasi-Particles

BARDEEN et al. employ a trial wave function of the following type to minimize $H'$:

$$\Psi_0 = \prod_{\nu} (u_\nu + v_\nu a_\nu^+ a_{-\nu}^+) \mid 0 \rangle . \tag{11}$$

In eq. (11), $u_\nu$ and $v_\nu$ are free parameters, subject only to the normalization condition, which can be fulfilled by the requirement

$$u_\nu^2 + v_\nu^2 = 1 , \tag{12}$$

and to the auxiliary condition (9), which takes the form

$$n = 2 \sum_{\nu} v_\nu^2 \tag{13}$$

in terms of the parameters introduced.

The variational calculation leads to the equations[3, 6]

$$(\varepsilon_\nu - \lambda)\, 2\, u_\nu v_\nu - G \sum_{\nu'} u_{\nu'} v_{\nu'} (u_\nu^2 - v_\nu^2) - 2\, G\, v_\nu^2 u_\nu v_\nu = 0 . \tag{14}$$

The last term in (14) is small compared with the second (except in a region near the Fermi surface) and is usually neglected or assumed to be included in the self-consistent field energies $\varepsilon_\nu$*.

If one chooses to neglect the third term, one obtains for $u_\nu$ and $v_\nu$ the simple expressions

$$u_\nu^2 = \frac{1}{2}\left(1 + \frac{\varepsilon_\nu - \lambda}{E_\nu}\right), \tag{15 a}$$

$$v_\nu^2 = \frac{1}{2}\left(1 - \frac{\varepsilon_\nu - \lambda}{E_\nu}\right), \tag{15 b}$$

and for the energy of the ground state the expression

$$\langle H' \rangle + \lambda \langle N' \rangle = \sum_{\nu} \varepsilon_\nu\, 2\, v_\nu^2 - \frac{\Delta^2}{G} - G \sum_{\nu} v_\nu^4 , \tag{16}$$

* Concerning a method of accounting for this term by perturbation theory, see Appendix I.

where the third term is again of self-energy origin and is usually neglected as small compared with the second term (see the discussion below).

In eqs. (14) and (15) we have used the definitions

$$E_\nu = \sqrt{(\varepsilon_\nu - \lambda)^2 + \Delta^2} \tag{17}$$

and

$$\Delta = G \sum_\nu u_\nu v_\nu . \tag{18}$$

Provided the $\varepsilon_\nu$:$s$ (the single-particle energies of the deformed field) are given and $G$ is known, the auxiliary parameters $\lambda$ and $\Delta$ can be determined from eqs. (18) and (13). The interpretation of $v_\nu^2$ as the probability of the state $\nu$ being populated by a pair is borne out by eq. (13).

An equivalent way to obtain the ground-state energy given by eq. (16) and the corresponding wave function is provided by the BOGOLUBOV-VALATIN[8] transformation to quasi-particles (the creation operator of a quasi-particle is a linear combination of the corresponding particle operator and the operator creating a hole of opposite angular momentum)

$$\alpha_\nu = u_\nu a_\nu - v_\nu a_{-\nu}^+ , \tag{19 a}$$

$$\alpha_{-\nu} \equiv \beta_\nu = u_\nu a_{-\nu} + v_\nu a_\nu^+ . \tag{19 b}$$

In terms of $\alpha_\nu$ and $\beta_\nu$ the transformed Hamiltonian $H'$ is

$$H' = U' + H'_{11} + H'_{20} + H'_{\text{int}} \tag{20}$$

when written in its normal form, i. e. with $\alpha^+$, $\beta^+$ in front of $\beta$, $\alpha$. In terms of the quasi-particle operators, $U'$ is then a constant, $H'_{11}$ is an operator that can destroy and recreate one quasi-particle at a time (and, furthermore, contains only the particular combinations $\alpha_\nu^+ \alpha_\nu$ and $\beta_\nu^+ \beta_\nu$), while $H'_{20}$ can either destroy or create two quasi-particles. The operator $H'_{\text{int}}$ contains products of four-quasi-particle operators and can be split up into the terms $H'_{22}$, $H'_{31}$ and $H'_{40}$ (the notation should be obvious from the above). It is discussed in more detail by BELYAEV[6] and in Appendix I of the present paper.

The imposed condition that $H'_{20}$ vanishes identically leads to eq. (14), whereby $u_\nu$ and $v_\nu$ are determined. As $H'_{11}$ is a function only of the occupation number of the quasi-particles, we are then left with a system of non-interacting quasi-particles in the approximation that $H'_{\text{int}}$ may be neglected. Indeed, as far as the ground state, i. e. the no-quasi-particle state, is concerned, only $H'_{40}$ of the neglected $H'_{\text{int}}$ term has non-vanishing matrix

elements connected with this state. The magnitude of this coupling is thus a measure of the lack of generality of the trial function (11). In this respect the quasi-particle formalism forms a complement to the variational procedure. The effect of $H'_{40}$ on the ground-state wave function is fundamentally small of the order $\frac{G}{2\Delta}$. One may take the quantity*

$$\Omega_{\text{eff}} = \frac{2\Delta}{G} = \sum_{\nu} \frac{1}{\sqrt{\left(\frac{\varepsilon_\nu - \lambda}{\Delta}\right)^2 + 1}} \tag{21}$$

as a measure of the accuracy of the approximation. The definition may be less suitable in cases where the level density of single-particle states is very different above and below the Fermi surface. It is quite satisfactory for our purposes as the single-particle levels are rather evenly distributed in the cases treated here.

It should be noted at this point that the neglected term in (14) is also small of just this order $\frac{G}{2\Delta}$.

The ground state $\Psi_0$ of an even-even nucleus, given by (11), thus defines the quasi-particle vacuum; it will be denoted $|0\rangle\rangle$ in the following and is characterized by the condition

$$\alpha_\nu \Psi_0 \equiv \alpha_\nu |0\rangle\rangle = 0 . \tag{22}$$

We now turn to the ground state of an odd-A nucleide. The odd particle here occupies, say, the orbital $\varepsilon_{\nu'}$. This particle is entirely unaffected by the pairing force, which only scatters pairs of particles. The trial function of the ground state of such an odd-particle system is obviously

$$\Psi^{\text{odd}} = a^+_{\nu'} \prod_{\nu \neq \nu'} (u_\nu + v_\nu a^+_\nu a^+_{-\nu}) |0\rangle . \tag{23}$$

Now $u_\nu$ and $v_\nu$ are still given by eqs. (15), but the sums over states in eqs. (13) and (18), which determine $\Delta$ and $\lambda$, now exclude the "blocked" $\nu'$ state; furthermore, $n$ in (13) has to be replaced by $(n-1)$.

The effect on $\lambda$ is a trivial one; if $\nu'$ lies near the Fermi surface (as it must for the ground state of an odd system), $\lambda$ is not appreciably changed with respect to the "even" case of $n/2$ pairs. As $\Omega_{\text{eff}}$ terms in fact contribute to (18), the exclusion of one term appears again to imply an error of the order $\frac{1}{\Omega_{\text{eff}}}$, the

* The formula (21) gives values of $\Omega_{\text{eff}}$ about 5-10 for the actual calculations we have performed.

fundamental inaccuracy of the BCS-solution. If we neglect this blocking effect for the moment, we end up with the same $u_\nu$ and $v_\nu$ as in the "even" cases. Therefore we still have the same quasi-particle vacuum, and we may write $\Psi^{\text{odd}}$ in a form identical with (23):

$$\Psi^{\text{odd}} = \alpha^+_{\nu'} | 0 \rangle\rangle. \tag{23'}$$

The additional energy of this one-quasi-particle state compared with the vacuum state (the "even" case of $n/2$ pairs) is most easily obtained from

$$H'_{11} \equiv \sum_\nu \left\{ (\varepsilon_\nu - \lambda)(u_\nu^2 - v_\nu^2) + \Delta 2 u_\nu v_\nu - G v_\nu^2 (u_\nu^2 - v_\nu^2) \right\} (\alpha^+_\nu \alpha_\nu + \beta^+_\nu \beta_\nu). \tag{24}$$

The last term in (24) is small, again of the order $\frac{G}{2\Delta}$, compared with the sum of the first two terms, and often much smaller because of the factor $(u_\nu^2 - v_\nu^2)$. The neglect of this term thus amounts to an approximation of the same order as that due to the neglect of $H'_{40}$ etc. We then arrive at the simple relation

$$H'_{11} \simeq \sum_\nu E_\nu (\alpha^+_\nu \alpha_\nu + \beta^+_\nu \beta_\nu). \tag{24'}$$

The odd-even mass difference, which we have here defined as the difference in mass between an odd-system and the "even" system* having $n/2$ pairs and thus no orbital blocked, in this approximation simply equals $E_\nu$. This quantity is in turn very near to $\Delta$ for the ground state of the odd-n system, as $(\varepsilon_\nu - \lambda)^2$ is very small compared with $\Delta^2$ (usually of the order of a few per cent).

The spectrum of excited states of an odd-A nucleus is given in this approximation by the quasi-particle energies $E_\nu$. As the single-particle level density is of the order of one state per 300 keV on the average, compared with an average $\Delta$ of between 500 and 1000 keV, this would lead to a level density in odd-A nuclei of the order of one state per 50-100 keV for excitation energies smaller than $\Delta$, which is contrary to experience[16]. It appears that of the approximations made, involving terms of the order of $\frac{G}{2\Delta}$, the neglect of the blocking effects described on page 10 may be the most serious**, ***.

* i.e. a system described by eq. (11) treated formally as if $n$ were an even number.

** A comparison with the results of an exact diagonalization performed for a particular case of six levels and three pairs (corresponding to a $20 \times 20$ matrix) clearly bears out this contention.

*** This effect has also been studied recently by Soloviev[18].

One may estimate the change in $\Delta$ between the even and the odd case due to the blocking of one level by the odd particle as*

$$\Delta^{\mathrm{odd}} \simeq \Delta^{e} - \frac{1}{(\Delta^{e})^{2}} \left( \sum_{\nu \neq \nu'}{}' \frac{1}{E_{\nu}^{3}} \right)^{-1} . \tag{25}$$

In obtaining this formula we have neglected terms of the type $\sum_{\nu} (\varepsilon_{\nu} - \lambda) E_{\nu}^{-n}$ as being small compared with $\Delta \sum_{\nu} E_{\nu}^{-n}$. As is obvious from (25), the difference $(\Delta^{e} - \Delta^{\mathrm{odd}})$ depends somewhat on the cut-off of the sum over $\nu$ in $\sum_{\nu}{}' \frac{1}{E_{\nu}^{3}}$. The change in $\Delta$, leading to a change in $u_{\nu}$ and $v_{\nu}$ also for $\nu \neq \nu'$, also affects the odd-even mass difference. If one makes the same approximations as in deriving (25), one obtains for the odd-even mass difference $P$ the expression

$$P \simeq \Delta^{e} + \frac{1}{(\Delta^{e})^{2}} \left( \sum_{\nu \neq \nu'}{}' \frac{1}{E_{\nu}^{3}} \right)^{-1} + \frac{G}{4} \left( 1 - \frac{2}{\Delta^{e}} \frac{\sum_{\nu \neq \nu'}{}' \frac{(\varepsilon_{\nu} - \lambda)^{2}}{E_{\nu}^{4}}}{\sum_{\nu \neq \nu'}{}' \frac{1}{E_{\nu}^{3}}} \right). \tag{26}$$

In deriving (26) we have included the "self-energy" terms from (16). They give as a result the third term in (26). While the neglect of these terms leads to the relation $P > \Delta^{e}$ to first order in $\delta \Delta$, the inclusion of these and of terms of higher order results in a $P$ smaller than $\Delta^{e}$ by a magnitude of the order of $10\,\%$ in the present cases (see table II). The results of table II correspond to an exact inclusion of the blocking effect, but are generally in line with eq. (26).**

Of interest to us here are finally the lowest excited states in an even-even nucleus, which correspond to the excitations of two quasi-particles. Take as an example a state reached from the ground state by the $j_x$ operator considered in section III. Such a state is e. g.

$$\Psi_{\nu' - \nu''} \equiv \alpha_{\nu'}^{+} \beta_{\nu''}^{+} \mid 0 \rangle\rangle \equiv a_{\nu'}^{+} a_{-\nu''}^{+} \prod_{\nu \neq \nu', \nu''} (u_{\nu} + v_{\nu} a_{\nu}^{+} a_{-\nu}^{+}) \mid 0 \rangle . \tag{27}$$

* On account of the rapid convergence of the sum in eq. (25) the choice of the cut-off energies $\lambda \pm D$ is not very critical provided $D \gg \Delta$. Assuming a constant level density $\varrho$ and furthermore $\Delta \gg \frac{1}{\varrho}$, one obtains the estimate $\Delta^{\mathrm{odd}} \simeq \Delta^{e} - \frac{1}{2\varrho}$. The actual calculations, in which the "blocking" effects have been included exactly, indicate a difference in $\Delta$ between systems with even and odd numbers of particles of the order of $20\,\%$, as exhibited in table II. These results are roughly in agreement with eq. (25) and the estimate above.

** The arbitrariness in the choice of the cut-off energy enters (26) through the relation between $G$ and $\Delta$, which depends more critically on the cut-off energy than does eq. (25).

In the approximation implied by this equation (where, for $\nu \neq \nu' \nu''$, $u_\nu$ and $v_\nu$ are the same as in the no-quasi-particle ground state) the excitation energy is given simply by application of $H'_{11}$ as

$$\mathfrak{E}^{(\nu', -\nu'')} - \mathfrak{E}^{(0)} = E_{\nu'} + E_{\nu''} \geq 2\Delta . \tag{28}$$

As the reduction in the effective $\Delta$, i.e. in the diffuseness of the Fermi surface, is considerable in this two-quasi-particle state, owing to the blocking of two levels, one might be tempted to correct for this error in line with what is done above for the one-quasi-particle state, and write as an alternative to eq. (27)*

$$\Psi_{\nu'-\nu''} = a^+_{\nu'} a^+_{-\nu''} \prod_{\nu \neq \nu', \nu''} (u_\nu^{(\nu'\nu'')} + v_\nu^{(\nu'\nu'')} a^+_\nu a^+_{-\nu}) \mid 0 \rangle , \tag{27'}$$

where $u_\nu^{(\nu'\nu'')}$ and $v_\nu^{(\nu'\nu'')}$ are thus calculated from (14) with two single-particle levels blocked. The excitation energy of this state (27') must be calculated via the total energies (16) obtained from variational calculations applied to the excited state, respectively to the ground state. It is obvious that a quasi-particle description has no advantage if one wants to include the effects of blocking, as we should then be forced to assume a vacuum for the excited state different from that of the ground state.

## III. General Formula for the Moment of Inertia and the Collective Gyromagnetic Ratio in Terms of the Quasi-Particle Formalism

A derivation of the formula for the moment of inertia based on the cranking approximation has already been given in the quasi-particle formulation by BELYAEV[6]. The exposition of ref. 6 appears not explicitly to include the case of the single-particle angular-momentum component being equal to 1/2. Although the explicit inclusion of this case only amounts to a minor modification, we shall repeat the general lines of the derivation.

We first express $j_x$, the operator associated with the rotation of the field of an individual particle, in terms of creation and annihilation operators $a^+$ and $a$. By the indices $\nu$, $\nu'$ we denote combinations of states for which $K_\nu$

* It is easily verified that this state is orthogonal to the ground state.

and $K_{\nu'}$ *do not both* equal 1/2. The indices $\mu$, $\mu'$ are then reserved for combinations of orbitals that *both* have $K = 1/2$.

$$\left.\begin{aligned} j_x^{\mathrm{op}} = \sum_{\nu\nu'} \{ \langle \nu \,|\, j_x \,|\, \nu' \rangle a_\nu^+ a_{\nu'} \\ + \langle -\nu \,|\, j_x \,|\, -\nu' \rangle a_{-\nu}^+ a_{-\nu'} \} + \sum_{\mu\mu'} \{ \langle \mu \,|\, j_x \,|\, -\mu' \rangle a_\mu^+ a_{-\mu'} \\ + \langle -\mu \,|\, j_x \,|\, \mu' \rangle a_{-\mu}^+ a_{\mu'} \}. \end{aligned}\right\} \quad (29)$$

Employing the phase convention implied by eq. (4), one can readily prove the relations

$$\langle \nu \,|\, j_x \,|\, \nu' \rangle = -\langle -\nu' \,|\, j_x \,|\, -\nu \rangle \quad (30)$$

and

$$\langle \mu \,|\, j_x \,|\, -\mu' \rangle = \langle -\mu \,|\, j_x \,|\, \mu' \rangle. \quad (31)$$

To prove (30) one may for instance use the fact that the time reflection operator $T$ is a product of a unitary operator and the complex conjugation operator, to obtain

$$\langle \nu \,|\, j_x \,|\, \nu' \rangle = \langle T\nu \,|\, T j_x T^{-1} \,|\, T\nu' \rangle^*. \quad (32)$$

To arrive at (30) one has then only to employ the facts a) that $j_x$ is a Hermitian operator, b) that it changes sign under time reversal. To derive eq. (31) one must in addition use the fact that the matrix elements of $j_x$ are real in the representation employed here.

The next step is to transform eq. (29) by the canonical transformations (19a, b), using (30) and (31). We may then write

$$j_x^{\mathrm{op}} = (j_x)_{11} + (j_x)_{20}, \quad (33)$$

where $(j_x)_{11}$ thus first destroys and then creates a quasi-particle. It can therefore have no matrix elements with the ground state of an even-even nucleus, which is just the quasi-particle vacuum. On the other hand, $(j_x)_{20}$ creates a two-quasi-particle state from the quasi-particle vacuum $|0\rangle\rangle$:

$$\left.\begin{aligned} j_x^{\mathrm{op}} \,|\, 0 \rangle\rangle = \sum_{\nu\nu'} \langle \nu \,|\, j_x \,|\, \nu' \rangle (u_\nu v_{\nu'} - v_\nu u_{\nu'}) \, \alpha_\nu^+ \beta_{\nu'}^+ \,|\, 0 \rangle\rangle \\ + \sum_{\mu\mu'} \langle \mu \,|\, j_x \,|\, -\mu' \rangle (u_\mu v_{\mu'} - v_\mu u_{\mu'}) \frac{1}{2} (\alpha_{\mu'}^+ \alpha_\mu^+ + \beta_\mu^+ \beta_{\mu'}^+) \,|\, 0 \rangle\rangle. \end{aligned}\right\} \quad (34)$$

Now the two-quasi-particle states $\alpha_\nu^+ \beta_{\nu'}^+ |\, 0 \rangle\rangle$ and $\alpha_{\nu'}^+ \beta_\nu^+ |\, 0 \rangle\rangle$ both correspond to an excitation energy $E_\nu + E_{\nu'}$, measured with respect to the energy of the quasi-particle vacuum. These two states differ in their sign of the

angular-momentum component. Similarly, $\alpha^+_{\mu'}\alpha^+_{\mu}|0\rangle\rangle$ and $\beta^+_{\mu}\beta^+_{\mu'}|0\rangle\rangle$ both have the energy $E_\mu + E_{\mu'}$, but have $K = 1$ and $-1$ respectively. Thus the contributions from these transitions do not interfere. Although in eq. (34) the $\nu-$ and $\mu-$ sums do not at first glance appear quite symmetrical with respect to one another, their contributions to the moment of inertia are quite analogous. We finally obtain the following formula for the moment of inertia:

$$\left.\begin{aligned} \Im = 2\hbar^2 \Bigg\{ & \sum_{\nu\nu'} \frac{|\langle \nu | j_x | \nu' \rangle|^2}{E_\nu + E_{\nu'}} (u_\nu v_{\nu'} - v_\nu u_{\nu'})^2 \\ & + \sum_{\mu\mu'} \frac{|\langle \mu | j_x | -\mu' \rangle|^2}{E_\mu + E_{\mu'}} (u_\mu v_{\mu'} - v_\mu u_{\mu'})^2 \Bigg\} \qquad (K_\mu = K_{\mu'} = 1/2). \end{aligned}\right\} \tag{35}$$

Indeed the second term can be formally included in the first, provided one remembers to take also the matrix elements between $K = 1/2$ and $K' = -1/2$ into account. Really there is no asymmetry between the $\nu$ and $\mu$ terms, as to every $\langle \nu | j_x | \nu' \rangle$ transition there corresponds a $\langle -\nu | j_x | -\nu' \rangle$ transition, of which only the first is counted formally in (35); further, to every $\langle \mu | j_x | -\mu' \rangle$ transition counted in (35) there corresponds a $\langle -\mu | j_x | \mu' \rangle$ transition which is not written out explicitly in (35).

The collective rotation takes place perpendicularly to the nuclear symmetry axis and is associated with the collective angular momentum $\vec{R}$. In an odd-A nucleus $\vec{R}$ couples with the angular-momentum component $K$ of the odd particle to form the total angular momentum $\vec{I}$, the nuclear spin. On the other hand, in the ground state of an even-even nucleus we have simply $\vec{R} = \vec{I}$. The collective flow of protons and neutrons building up the $\vec{R}$ also gives rise to an instantaneous magnetic moment associated with the operator

$$\vec{\mu}_{\text{coll}} = \sum_i \vec{\mu}_i = \sum_i \left( g_s^i \vec{s}_i + g_l^i \vec{l}_i \right), \tag{36}$$

where the sum runs over the paired nucleons. One may express this magnetic moment in terms of a collective gyromagnetic ratio $g_R$ defined by the relation

$$\vec{\mu}_{\text{coll}} \equiv g_R \vec{R}. \tag{37}$$

(The definition is of course limited to matrix elements of the operator $\vec{\mu}_{\text{coll}}$ that are diagonal with respect to the intrinsic nuclear wave function.)

In the cranking approximation the gyromagnetic ratio $g_R$ takes the form[2]

$$g_R = \frac{\hbar^2}{\Im} \sum_{\beta}' \frac{\langle \Phi_\alpha | \mu_x | \Phi_\beta \rangle \langle \Phi_\beta | J_x | \Phi_\alpha \rangle}{\varepsilon_\beta - \varepsilon_\alpha} + \text{c. c.}, \tag{38}$$

where $J_x = \sum_i j_x^i$ is the angular-momentum operator associated with the rotation. As $\mu_x$ transforms under time reflection in the same way as $j_x$, the inclusion of the pair-correlation interaction is completely analogous to the procedure employed on pp. 13–15. We just give the final expression

$$g_R = \frac{\Im_p}{\Im} + (g_s^p - 1)\frac{W_p}{\Im} + g_s^n \frac{W_n}{\Im}, \tag{39}$$

where

$$\left.\begin{aligned} \frac{1}{2\hbar^2} W = &\sum_{\nu\nu'}' \frac{\langle \nu' | j_x | \nu \rangle \langle \nu | s_x | \nu' \rangle}{E_\nu + E_{\nu'}} (u_\nu v_{\nu'} - v_\nu u_{\nu'})^2 \\ &+ \sum_{\mu\mu'}' \frac{\langle \mu | s_x | -\mu' \rangle \langle -\mu' | j_x | \mu \rangle}{E_\mu + E_{\mu'}} (u_\mu v_{\mu'} - v_\mu u_{\mu'})^2. \end{aligned}\right\} \tag{40}$$

Thus, apart from the spin contributions (given by the last two terms of (39)) to the magnetic moment of the collective flow, $g_R$ is just the relative fraction contributed by the protons to the moment of inertia or, in other words, the effective charge of the collective flow. Of the last two terms of (39), $W_p$ is the sum over all proton states and $W_n$ the sum over all neutron states of the expression (40). The contribution from the terms containing $W$ is small and is largely cancelled, as $(g_s^p - 1)$ is very nearly of the same magnitude as $g_s^n$ and of opposite sign.

It has already been pointed out that the quasi-particle description used here involves the neglect of terms of the order $\frac{G}{2\Delta}$ at various stages. The errors connected with the neglect of $H'_{40}$ for the ground state and with the neglect of $H'_{40}$, $H'_{31}$ and $H'_{22}$ in calculating the excited two-quasi-particle states enter in a fundamental way, and they are also the errors that it is most difficult to correct for. On the other hand, the errors associated with the blocking effects may, in many respects, be the most severe. We have therefore attempted a programme taking this blocking fully into account through the use of (27′) instead of (27) as the form of the two-quasi-particle state. Including the said corrections, one obtains the following expression for the even-even moment of inertia:

$$\left.\begin{aligned}\Im = 2\hbar^2 \sum_{\nu'\nu''} \frac{|\langle \nu'' | j_x | \nu' \rangle|^2}{\mathfrak{E}^{(\nu'\nu'')} - \mathfrak{E}^{(0)}} (v_{\nu'}^{(0)} u_{\nu''}^{(0)} - u_{\nu'}^{(0)} v_{\nu''}^{(0)})^2 \\ \prod_{\nu \neq \nu'\nu''} (u_\nu^{(\nu'\nu'')} u_\nu^{(0)} + v_\nu^{(\nu'\nu'')} v_\nu^{(0)})^2 + (\text{terms involving } \mu' \text{ and } \mu'').\end{aligned}\right\} \quad (35')$$

In this formula the superscript 0 refers to the ground state, while the superscripts $\nu'$ and $\nu''$ refer to the states in which the single-particle orbitals $\nu'$ and $\nu''$ are blocked.

The modification of eq. (40) is completely analogous to that of (35).

## IV. Numerical Calculations of the Moment of Inertia and the Collective Gyromagnetic Ratio

### a. Energy scale of the single-particle energies $\varepsilon_\nu$ and determination of the deformation $\delta$

The relative order of the single-particle energies is probably rather well represented by the calculations of ref. 15. A minor readjustment of the energy differences within a shell, as may be suggested by the analysis of experimental nuclear spectra by MOTTELSON end NILSSON[16], does not very significantly affect either $\Im$ or $g_R$ of an even-even nucleus. Even though the level order is fairly well established, the total energy scale $\hbar\omega_0$ is determined from a condition on the extension of the nuclear matter which is somewhat arbitrarily formulated[15] as $5/3\langle r^2\rangle = R_0^2$, where, furthermore, the nuclear radius $R_0$ has been set equal to $1.2 \times A^{1/3}$ fermis. This then corresponds to choosing $\hbar\omega_0 = 41 \times A^{-1/3}$ MeV. As the uncertainty of $R_0$ must be regarded as being, say, of the order of 10 %, the inaccuracy of $\hbar\omega_0$ is probably larger than 20 %. Now the scale $\hbar\omega_0$ enters first of all in the energy denominator, so from this effect alone there appears at first glance to be an uncertainty in $\Im$ of, say, 20 %. However, the ratio $\frac{\Delta}{\hbar\omega_0}$, which determines the $u$ and $v$ values, obviously decreases when $\hbar\omega_0$ is increased, and vice versa. This effect largely cancels the first effect. Indeed, as seen from figs. 22 and 23, a 10 % decrease of $\hbar\omega_0$ results in a net change of $\Im$ by only $\pm 2$ % or less in the range of parameters used in these calculations.

Furthermore, the single-particle energy parameters $\varepsilon_\nu$ are also connected with the eccentricity parameter $\delta$. Indeed, for the use of the energy diagram

of ref. 15 it is necessary to know $\delta$. To obtain values of $\delta$ we have employed the empirical values of the quadrupole moments as determined from Coulomb-excitation data. We have made use of the measurements and compilations* of $Q_0$ recently made by ELBEK et al.[19] in the mass region $150 < A < 190$ (often denoted region I in the following) and by BELL et al.[20] in the region $A > 220$ (region II). The experimental values of the quadrupole moments in region I exhibit an estimated accuracy of the order of 3 % compared with one another[19]. The absolute uncertainty may be greater, however. In particular the values of ELBEK et al. appear systematically to be a few per cent lower on the average than those of most other authors, as pointed out in ref. 19.

Assuming a homogeneous charge distribution, one obtains the well-known relation between the intrinsic quadrupole moment and $\delta$

$$Q_0 = \frac{4}{5}\,\delta Z R_z^2 \left(1 + \frac{1}{2}\,\delta + \ldots .\right). \tag{41}$$

The main uncertainty connected with the use of this formula probably lies in the specification of the parameter $R_z$. We have, in using formula (41), put $R_z$ equal to the average nuclear radius $R_0$, which, as pointed out, is related to the energy scale $\hbar\omega_0$. Also the analysis by RAVENHALL[21] of electron scattering data indicates a proton charge distribution such that the charge radius $R_z$ defined as $[5/3 \langle r^2 \rangle]^{1/2}$ equals about $1.2 \times A^{1/3}$ fermis.

It turns out that $\delta$ is a most critical parameter in the calculation of the moments of inertia. The very large uncertainty in its determination is thus due mostly to the inaccurate knowledge of $R_z$, furthermore to the experimental inaccuracies in the $Q_0$ determination, and finally to the approximate assumptions underlying formula (41). Indeed, as the nucleonic wave functions are known in the pairing approximation, they may be used to calculate an expectation value of the quadrupole operator. For the quasi-particle vacuum, one obtains the simple relation[6]

$$Q_0 = \sum_{\nu} q^0_{\nu\nu}\, 2\, v^2_{\nu}, \tag{42}$$

where

$$q^0_{\nu\nu} = \sqrt{\frac{16\,\pi}{5}} \langle \nu | r^2 Y_{20} | \nu \rangle . \tag{43}$$

As the population numbers of the single-particle states as well as $q^0_{\nu\nu}$ are functions of $\delta$, eq. (42) provides a relation between $Q_0$ and $\delta$ in which,

* We are grateful to the authors cited for access to their values in advance of publication.

however, $\hbar\omega_0$ (and thereby $R_0$) enters as a parameter. Formula (42) should be considered somewhat of an improvement on (41). However, the preliminary calculations by SZYMANSKI and BÉS[22], until now limited to region I, indicate that the approximation (41) is accurate to within a few per cent in the entire region. This corresponds to a matter distribution displaying approximately the same eccentricity as the potential shape.

SZYMANSKI and BÉS go further to seek the equilibrium deformations $\delta_{eq}$. Using the relation (42), they then compare the magnitude and trend of the calculated $Q_0$ corresponding to $\delta_{eq}$ with the empirical $Q_0$-values. The preliminary results indicate deviations from the experimental values of the order of 20 %.

As pointed out, the use of formula (42) instead of (41) does not remove the uncertainty in the specification of the nuclear charge radius. The $\delta$ obtained from equilibrium calculations appears rather sensitive to details of the model, and therefore uncertain.

### b. The gap parameters $\Delta_n$ and $\Delta_p$

The moment of inertia is very sensitive to the choice of $\Delta_n$ and $\Delta_p$, the energy-gap parameters of neutrons and protrons. Thus a 10 % increase in the magnitude of $\Delta_n$ and $\Delta_p$ results in an average decrease in $\Im$ of the order of magnitude of 10 % (cf. figs. 20 and 21).

Now, $\Delta_n$ and $\Delta_p$ are determined from the average pair-correlation matrix elements $G_n$ and $G_p$ and the single-particle level density. The exact relation is given by eq. (18). A separate and independent treatment of neutrons and protons, which we have implied here, appears to be adequate in the two regions of deformed nuclei to which the calculations have been confined, as neutrons and protons fill different shells. The assumption that the pairing matrix element can always be set equal to a constant, $G$, is of course also approximate. Indeed, as the single-particle states on the average become less and less similar as they get more distant from one another in energy, it appears that the overlap of two such wave functions should on the average decrease with increasing energy difference. The contribution from the states far below and above the Fermi surface to the sum in (18) is thus effectively limited. This we may approximately simulate by including in the sums only a certain number of states nearest above and nearest below the Fermi surface. The effect of the arbitrariness in the choice of a cut-off point is less severe as outside of a certain region the inclusion of some extra terms beyond

the cut-offs in many respects corresponds only to a renormalization of $G$ (cf. refs. 5 and 6)*.

In our calculations we have included all states of the $N = 3, 4, 5$ shells ($N$ is the total number of oscillator quanta) for protons in region I (56 levels). Furthermore, we have taken into account all states of the $N = 4, 5, 6$ shells for protons in region II and neutrons in region I (64 levels), and finally all states of the shells $N = 5, 6, 7$ (85 levels) for the neutrons in region II. Compared with an earlier calculation in which only altogether 20 levels near the Fermi surface were taken into account, the inclusion of this great number of levels implied an increase in $\mathfrak{I}$ by an amount of the order of 10 % for nuclei at the beginning and the end of region I, provided $\Delta_n$ and $\Delta_p$ were kept the same in the two calculations. In the middle of region I the effect was even smaller. On the other hand, to obtain the same $\Delta$-value in the two cases we had to use $G$-values 30-50 % larger in the calculation in which the fewer levels were taken into account.

Kisslinger and Sorenson[23] have analysed systematically sequences of isotopes and isotones of single-closed-shell nuclei, such as the Pb and Sn isotopes, in terms of the known shell-model states with the inclusion of the pair-correlation interaction and a long-range $P^2$-force. They conclude that the strength of the pair correlation that best fits the data corresponds to $G = \frac{\text{const}}{A}$ with $G \times A = 17$-$28$ MeV when they take single-particle levels of one shell into account. They do not explicitly point out any systematic difference between the $G \times A$ values for neutrons and protons. Similar calculations by Bro-Jørgensen and Haatuft[23a] in progress, treating nuclei that exhibit low-lying vibrational states, also indicate that the values of $G \times A$ that best reproduce the experimental material lie between 20 and 25 MeV. Szymanski and Bés[22], taking always the 24 levels nearest to the Fermi surface into account, give $G_p \times A \simeq 32$, $G_n \times A \simeq 25.5$. Previously Mottelson[3] had suggested a value of $G \times A \simeq 25$-$30$ MeV, based on an analysis of nucleon-nucleon scattering data.

In the present calculations we have first attempted to obtain a direct estimate of the energy-gap parameters $\Delta_n$ and $\Delta_p$, based on empirical evidence other than the rotational-band spacing. We have then studied how well one value of $G_n \times A$ and one value of $G_p \times A$ can reproduce the empirical $\Delta_n$ and $\Delta_p$ values in both regions. The result of this analysis (cf. figs. 7-14) is discussed below.

* On examination of the effects of "blocking" it appears that the choice of the cut-off limits is much more critical e. g. in the determination of the odd-even mass difference (see section II).

TABLE I. *Parameters Defining the Single-Particle Level Spectrum Employed in the Calculations.*

| Region | | Treated shells | $\varkappa$ | $\mu$ | Energies to be found in reference: | Additional shifts in units of $\hbar\omega_0$ (in line with reference MN) | | |
|---|---|---|---|---|---|---|---|---|
| | | | | | | Case A | Case B | Case C |
| I | Protons $62 \leq Z \leq 74$ | N = 3 | 0.05 | 0.45 | N | — | — | The same as case A (plus some very small shifts of a few individual levels) |
| | | 4 | 0.05 | 0.55 | N | — | — | |
| | | 5 | 0.05 | 0.55 | * | h 11/2: −0.075<br>others: +0.1 | −0.075<br>— | |
| | Neutrons $90 \leq N < 112$ | N = 4 | 0.05 | 0.45 | N | — | — | |
| | | 5 | 0.05 | 0.45 | N | — | — | |
| | | 6 | 0.05 | 0.45 | N | i 13/2: unchgd.<br>others: +0.15 | —<br>— | |
| II | Protons $Z \geq 88$ | N = 4 | 0.05 | 0.55 | N | −0.38 | −0.15 | −0.20 (plus some very small shifts of a few individual levels) |
| | | 5 | 0.05 | 0.70 | MN | h 11/2: −0.2 | — | −0.05 |
| | | 6 | 0.05 | 0.45 | N | i 13/2: −0.35<br>others: unchgd. | −0.35<br>— | −0.35<br>— |
| | Neutrons $N \geq 138$ | N = 5 | 0.05 | 0.45 | N | −0.38 | 0.15 | −0.225 |
| | | 6 | 0.05 | 0.45 | N | i 13/2: −0.23 | — | −0.075 |
| | | 7 | 0.05 | 0.40 | MN | j 15/2: −0.06<br>others: unchgd. | −0.06<br>— | −0.06<br>— |

N: S. G. NILSSON [1955] ,ref. 15
MN: B. MOTTELSON and S. G. NILSSON [1958], ref. 16
*: S. G. NILSSON, unpublished calculations.

Regions I and II refer to the so-called rare-earth region ($150 < A < 190$) and the actinide region ($A > 220$) of elements respectively. The parameters $\varkappa$ and $\mu$ of columns four and five are defined in ref. 15. Note that we have employed only one $\varkappa$-value ($\varkappa = 0.05$). A few ad hoc changes have been made in the level scheme obtained on the basis of the parameters listed. These are indicated in columns seven, eight and nine for the cases A, B and C, which are discussed in the text. Case C should correspond to the level scheme that is in best agreement with the empirical data on level spectra of odd-A nuclei (cf. ref. 16).

When searching for empirical information from which estimates of $\Delta_n$ and $\Delta_p$ may be obtained, one first thinks of the empirical energy gap in the excitation spectra of even-even nuclei and of the odd-even mass differences. As pointed out on p. 13, the quasi-particle description gives an energy gap $\geq 2\Delta$, where $\Delta$ is the smaller of $\Delta_p$ and $\Delta_n$. Indeed, the gap should be very nearly equal to $2\Delta$, as pointed out in section 2. In region I the lowest excited states clearly identified as two-quasi-particle states occur in $Hf^{178}$ and $Hf^{180}$ at about 1150 keV, in $Er^{168}$ at about 1100 keV, in $Dy^{162}$ at about

1450 keV, and in $Gd^{156}$ at about 1500 keV. One would, however, be inclined to regard the empirical identification of such lowest-lying states merely as setting a lower limit on $2\Delta$. The neglected additional interactions, as for instance the fluctuating part of the long-range $P^2$-force which is not already included in the spheroidal field, would split apart the two-quasi-particle states lying very densely just above the energy gap. Furthermore, the inclusion of the $H'_{22}$ term of $H'_{\text{int}}$ would tend to pull some of these states down below $2\Delta$. An estimate of the magnitude of the depression due to this term is rather difficult as a large part of its effect is spurious (see Appendix I) and related to the fluctuations in the number of particles introduced by the BCS wave function. A somewhat better measure of the energy gap is probably provided by spectra in which a great number of higher-lying two-quasi-particle states are identified, as is the case in $W^{182}$. Here the level density becomes very high at $\simeq 1400$ keV, which seems to indicate a gap of such magnitude for this nucleus*. Finally there are also the effects associated with the effective reduction of $\Delta$ in the two-quasi-particle case due to "blocking", as discussed in section 2.

Thus a more detailed experimental study of even-even spectra above one MeV would be very informative. In particular one should be able to see whether the lowest-lying two-quasi-particle excitations correspond to broken neutron rather than broken proton pairs, as the evidence from mass differences suggests**.

Probably the best available information on the gap parameters can be obtained from the study of even-odd mass differences. The mass measurements by JOHNSON and BHANOT[25] are the main source of empirical knowledge in region I, while the extensive compilation, based on many empirical sources including beta and alpha systematics, by FOREMAN and SEABORG[26] covers region II. We have also exploited systematics of beta-decay energies in region I, where more extensive binding-energy data are available for neutrons only.

The total binding energies of, for instance, a series of isotopes having an even value of $Z$, exhibit a smooth variation with $N$ for all even-even nucleides and a parallel smooth variation with $N$ for the odd ones. According to the present theory, the displacement should correspond to the quasi-particle energy of the last nucleon.

Consider first the neutrons. We have defined the empirical odd-even mass difference $P_n$ by the formula***

* We are grateful to Professor B. R. MOTTELSON for an enlightening discussion of this point.

** Indeed a recent analysis by C. GALLAGHER[24] of beta-decays populating higher-lying states of even-A nuclei in region I appears to lend support to this supposition.

*** This quantity would more correctly be labelled $P_n$ $(Z, N-1/2)$.

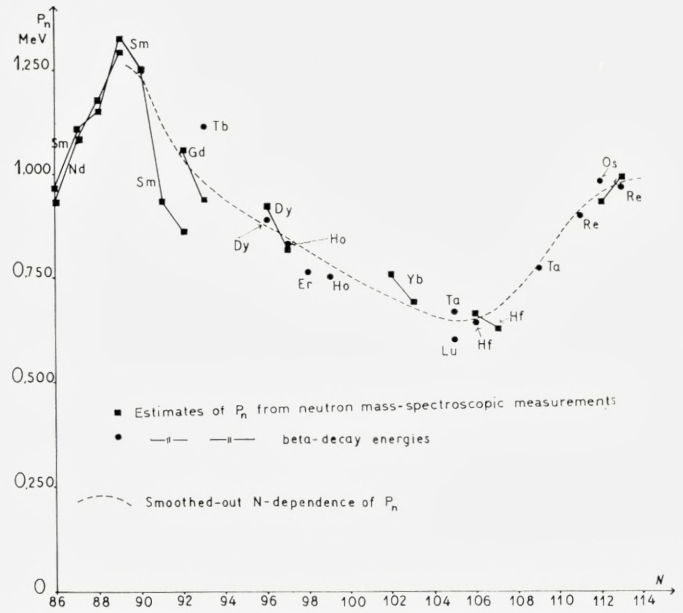


Fig. 1. *The odd-even mass difference parameter $P_n$ for neutrons in region I ($150 < A < 188$).* The squares refer to mass-spectroscopic measurements by JOHNSON and BHANOT[25], while the circles refer to beta-decay energy data. The dashed curve represents averaged values used in the moment –of– inertia calculation.

Added in proof: Recently published more complete mass-spectroscopic measurements by BHANOT, JOHNSON and NIER[30] give 100–200 keV lower $P_n$-values in the region $N = 108$–$112$; see furthermore fig. 28.

$$\left.\begin{aligned} P_n(Z, N) &= \frac{1}{4}\{-E(Z, N+1)+3E(Z, N)-3E(Z, N-1)+E(Z, N-2)\} \\ &= \frac{1}{4}\{-S_n(Z, N+1)+2S_n(Z, N)-S_n(Z, N-1)\}, \end{aligned}\right\} \quad (44)$$

where the neutron separation energy $S_n(Z, N)$ is related to the total binding energies $E(Z, N)$ by the formula

$$S_n(Z, N) = E(Z, N) - E(Z, N-1). \quad (45)$$

Analogous relations hold for the proton binding energy. Eq. (44) thus corrects for a second-order $N$-dependence of the mass valley. In fig. 2 of the present paper the values of $P_n$ have been extracted from FOREMAN and SEABORG's binding energies by means of eq. (44). This figure may be compared with fig. 3 of ref. 27, where the same data have been exploited, but the following relation has been used:

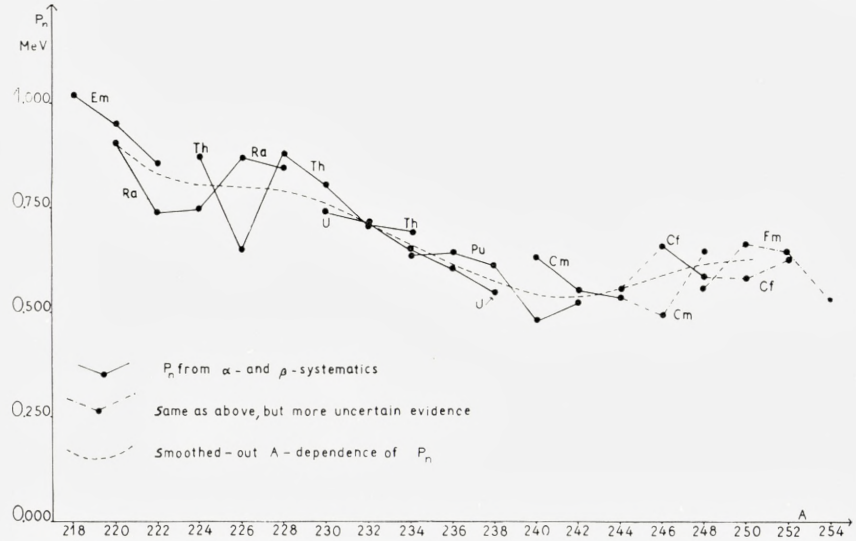


Fig. 2. *The odd-even mass difference parameter $P_n$ for nuclei in region II ($A > 224$).* The circles correspond to data collected by FOREMAN and SEABORG[26]. The dashed curve represents the smoothed-out values of $P_n$ on which the calculations were based.

$$P_n(Z, N) = \frac{1}{2}\{S_n(Z, N) - S_n(Z, N-1)\}, \qquad (44')$$

which allows only for a first-order $N$-dependence of the masses. The use of (44) appears to give smaller fluctuations. In region I, where the data are meagre, the difference between (44) and (44′) also appears significant. The values of $P_n$ derived from (44) turn out usually 50-100 keV higher than those obtained by the use of eq. (44′).

In region I, as already pointed out, the beta-decay energy systematics are a valuable complementary source of information. From a comparison of sequences of odd isobars connected by beta decay or electron capture one obtains an estimate of $(P_p - P_n)$, as an odd-$Z$ isobar corresponds to a proton quasi-particle state and an odd-$N$ nucleide to a neutron quasi-particle state. In addition to using beta-decay energies from isobars it turns out to be advantageous to study also elements having $(N-Z)$ = constant (isodiaspheres[28]) or $(3N-Z)$ = constant. Indeed, one could employ any systematic cut through the mass valley other than those mentioned. For isobars, usually only a few energy differences are known. In particular, electron capture energies are very uncertain; furthermore the elements soon get very shortlived as one moves away from the stability minimum. Contrary to iso-

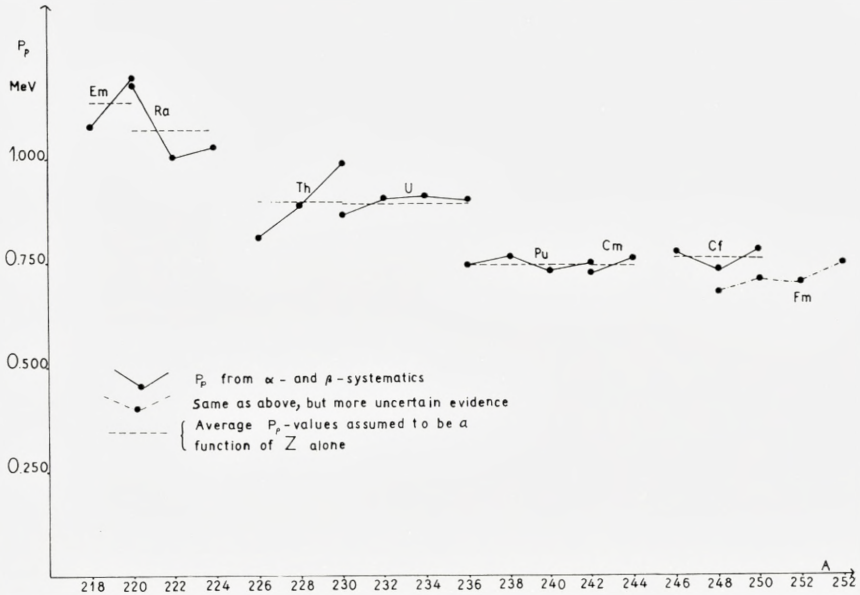


Fig. 3. *The odd-even mass difference parameter $P_p$ for nuclei in region II.* For further explanation see fig. 2.

bars, which correspond to lines of elements almost perpendicular to the direction of the mass valley, isodiaspheres, as well as elements corresponding to $(3N-Z)$ = constant, represent cuts exhibiting a small inclination to the direction of the valley. Such lines thus contain many more studied nucleides. On the other hand, for instance isodiaspheres also correspond to an averaging over a larger region of elements.

A collection of such available data on $(P_p - P_n)$, mostly taken from Nuclear Data Sheets[29] and ref. 16, is given in fig. 4. The diagram shows clearly that $P_p$ is rather consistently much greater than $P_n$ in region I. This is also the case in region II, where the evidence is more complete (cf. figs. 2 and 3). The difference is of the order of 100 keV in region I and about 150-200 keV in region II. Fig. 4 also indicates a trend in the value of $(P_p - P_n)$ from 0-50 keV around $A = 155$ up to 150-200 keV around $A = 175$, and then a decline towards zero again beyond $A = 180$. However, it must be borne in mind that the uncertainty of these energy differences is probably more than 50 keV. If the mass valley were exactly parabolic in shape, the beta energies would lie on straight lines. There is, however, a systematic curvature, especially conspicuous for isodiaspheres, which we have in some

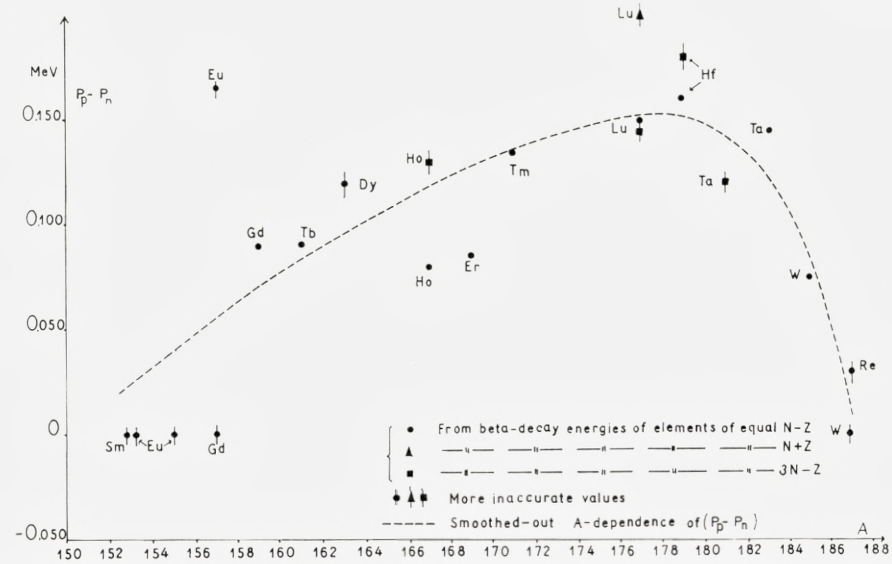


Fig. 4. *The difference $P_p - P_n$ for nuclei in region I from beta-decay energy systematics.* The circles correspond to cuts through the mass valley characterized by (N—Z) being constant (isodiaspheres), the triangles to series of isobars, and the squares to series of elements with $(3N-Z)$ equal to a constant. Uncertainties associated with the points are of the order of 50-100 keV.

measure taken into account graphically by drawing smooth curves through the points. This deviation corresponds to a higher-order $(N-Z)$-dependence of the mass-valley*.

Furthermore, a study of beta decay energies of even-$A$ nucleides gives a measure of $(P_p + P_n)$. However, a study of the available wealth of mass data in region II indicates clearly that there is an additional coupling energy[27, 28] between the odd neutron and the odd proton that makes the mass difference between the odd-odd and even-even nuclei smaller than $P_p + P_n$. We define such an empirical coupling energy $R_{np}$ as

* The somewhat astonishing conclusion that empirically $P_p$ is greater than $P_n$ is suggested already by the fact that of the stable odd-A elements the odd-N nucleides are more numerous than the odd-Z ones in the mass regions of interest here. For instance, among the elements $A = 153, 155, \ldots, 185$ there are 10 odd-N nucleides and seven odd-Z ones. If we assume the distribution of masses to lie on the parabolic surfaces

$$M(I) = M_0 + \frac{1}{2} b (I - I_s)^2 + \begin{Bmatrix} P_n \\ P_p \end{Bmatrix},$$

where $I = N - Z$, the probability of the odd-N nucleide being stable is apparently

$$\frac{1}{2}\left(1 + \frac{P_p - P_n}{2b}\right).$$

For the elements mentioned above one then obtains the estimate $(P_p - P_n) \simeq 100$ keV as an average for the whole region.

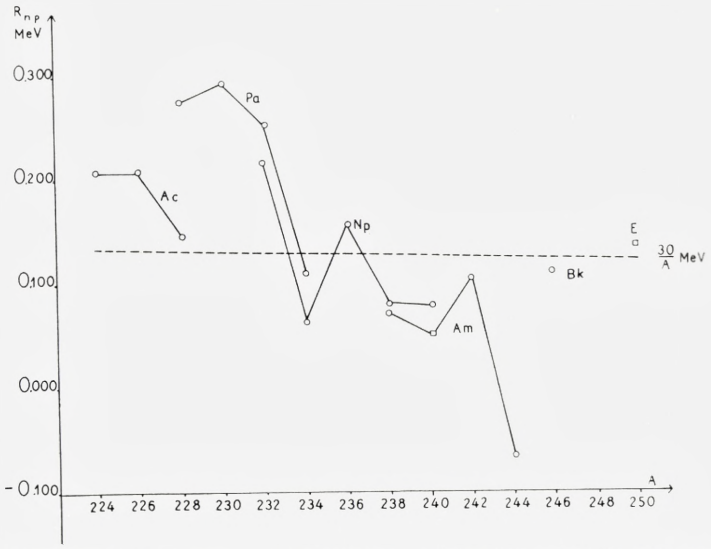


Fig. 5. *Coupling energies $R_{np}$ between the odd proton and the odd neutron in odd-odd nuclei.* The experimental binding energies of series of nucleides, as given in ref. 26, are exploited by means of eq. (46) of the present article for a determination of $R_{np}$. The uncertainty in the obtained values of $R_{np}$ is at least of the order of 50 keV. The squares in fig. 5 correspond to particularly uncertain points.

$$R_{np}(Z, N) = \frac{1}{8}\{ [-S_n(Z+1, N) + 2S_n(Z, N) - S_n(Z-1, N)] + [-S_p(Z, N+1) + 2S_p(Z, N) - S_p(Z, N-1)]\}, \quad (46)$$

where $(Z, N)$ refers to the odd-odd nucleus. Values of $R_{np}$ are collected in fig. 5. As expected, there are great fluctuations (to some extent probably indicating a difference between the overlaps of the neutron and proton orbitals in the different cases). However, $R_{np}$ appears to be greater than zero in almost all the cases. On the inclusion of the data from other regions of elements, as collected e. g. in ref. 28, one might conclude that, on an average,

$$R_{np} \simeq \frac{20-30}{A} \text{ MeV}. \quad (47)$$

This correction has been employed in region I in obtaining the values of $P_p + P_n$ from beta-decay systematics. The corrected energies have then been used together with the smoothed-out $(P_p - P_n)$-values of fig. 4 in obtaining the $P_n$-values exhibited in fig. 1.

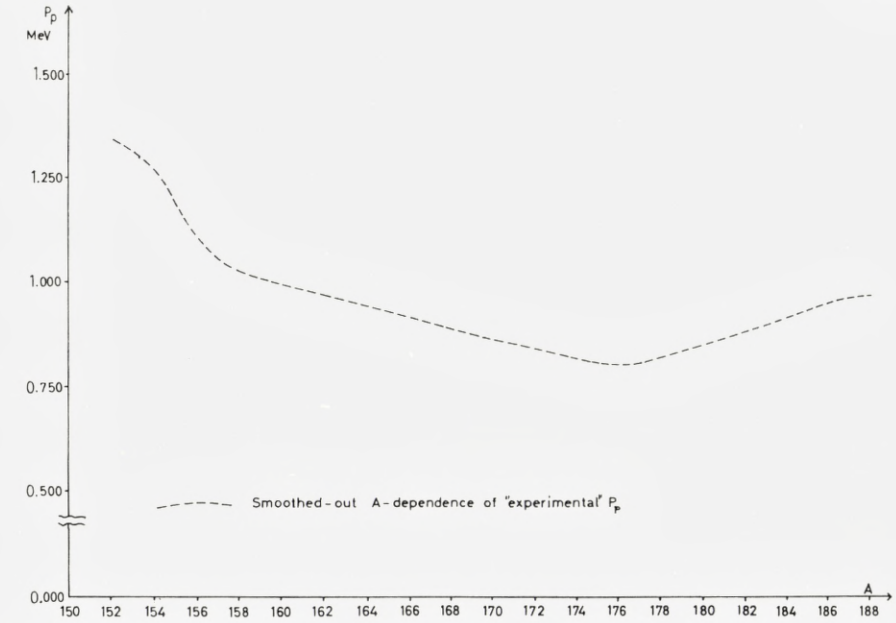


Fig. 6. *Average empirical values of the proton odd-even mass difference parameter* $P_p$ *in region I used in the calculations.* This dashed curve is obtained by addition of the smoothed-out $(P_p - P_n)$-function of fig. 4 to the averaged $P_n$-values of fig. 1.

Note added in proof: The recent mass-spectroscopic measurements by BHANOT, JOHNSON and NIER[30] allow more accurate $P$ -values as displayed in fig. 29. The deviation from fig. 6 is notable only for A > 180.

The main problem now concerns the relation between $P$ and $\Delta$. It has already been discussed in some detail in section 2, where it is pointed out that, if one assumes the same quasi-particle vacuum for the odd and the even case, this leads to $P = \Delta$. The results of a calculation that allows for the fact that the odd particle blocks the scattering of the pairs by its presence and thereby changes the occupation numbers also of the other single-particle levels, are exhibited in table II. This calculation gives the result that $P$ is smaller than $\Delta$ by a magnitude of the order of 10 % on the average, both for neutrons and protons. The relation between $P$ and $\Delta$ is unfortunately very uncertain as, first, the correction is somewhat dependent on the cut-off, secondly, an important contribution comes from the "self-energy" term displayed in eq. (26), thirdly, still other effects of the order $\frac{G}{2\Delta}$ are neglected, some of which are discussed in Appendix I. In the calculations presented in this article we have simply started from the assumption $\Delta_n = P_n^{\exp}$ and $\Delta_p = P_p^{\exp}$ (or rather some smoothed-out experimental values of $P_n^{\exp}$ and $P_p^{\exp}$).

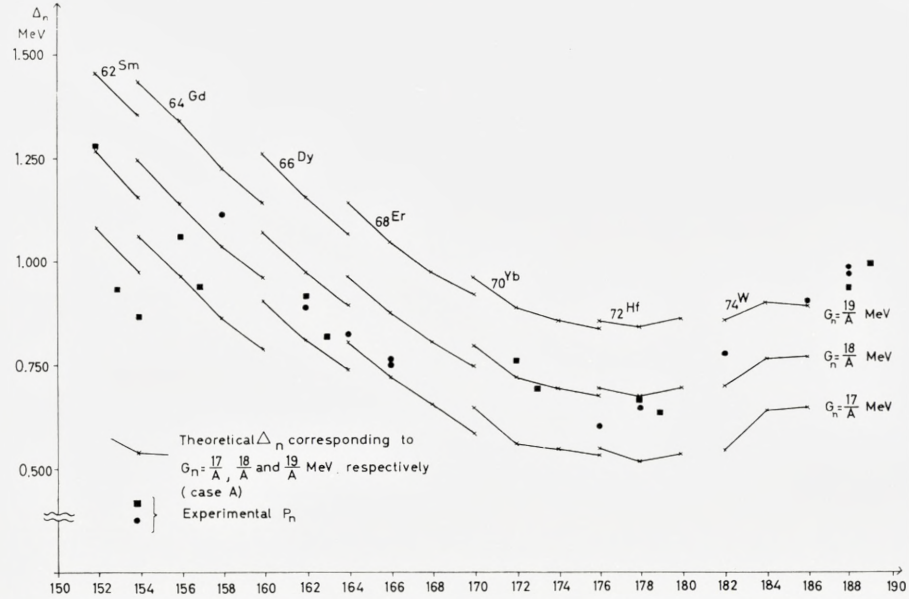


Fig. 7. *The relation between values of $\Delta_n$ and $G_n$ in region I obtained in the calculations.* For details of the single-particle spectrum employed, denoted as "case A", see table I. The points exhibited for comparison refer to the $P_n$-values of fig. 1.

In figs. 7-10 and 11-14 we have compared the values of $\Delta_n$ and $\Delta_p$ obtained in the detailed calculations corresponding to constant values of $G_n$ and $G_p$ with the empirically given values of $P_n$ and $P_p$. It is found that values of $G_n \times A \simeq 18$ MeV and $G_p \times A \simeq 25$-$26$ MeV both in region I and II and for a given set of $\varepsilon_\nu$:$s$, denoted case A, reproduce rather well the "empirical" trends. For an alternative set of $\varepsilon_\nu$:$s$, denoted case B, we find instead that $G_p \times A \simeq 16$-$17$ MeV and $G_n \times A \simeq 23$ MeV give the best fit. It seems plausible that case A represents rather well the situation in region I, while region II is presumably better described by a set of $\varepsilon_\nu$:$s$ intermediate between case A and case B and probably closest to case B (cf. case C of table I). Still the similarity of the $G$-values used in the two regions appears encouraging*.

* One might also point out in connection with figs. 7-14 that the illustrated relation between $G$ and $\Delta$ appears to be described rather well by the expression $\Delta \sim e^{-\frac{1}{\varrho G}}$, where $\varrho$ is the single-particle level density. The conditions for this relation to hold are that the level density is roughly constant, that there is approximately the same number of levels above and below the Fermi surface, that $\varrho G \langle\langle 1$, and furthermore that $\Delta \rangle\rangle d$, which is implied by the replacement of sums by integrals in obtaining the expression above ($d$ is the magnitude of the cut-off energy above and below the Fermi surface).

TABLE II. *The Odd-Even Mass Difference Parameter P when the Effect of Blocking due to the Odd Particle is Included, Referring to Odd-N Nuclei in Region I* (TABLE IIa) *and Region II* (TABLE IIc) *and to Odd-Z Nuclei in Region I* (TABLE IIb) *and Region II* (TABLE IId).

TABLE IIa

| Nucleide | $G_n \times A$ (MeV) | $\Delta_n^e$ (keV) | $\Delta_n^{\text{odd}}$ (keV) | $\frac{\Delta_n^e - \Delta_n^{\text{odd}}}{\Delta_n^e}$ (%) | $P_n^{\text{theor.}}$ (keV) | $\frac{\Delta_n^e - P_n^{\text{theor.}}}{\Delta_n^e}$ (%) | $P_n^{\text{exp}}$ (keV) |
|---|---|---|---|---|---|---|---|
| $^{91}_{64}Gd^{155}$ | 17 | 1047 | 895 | 15 | 977 | 7 | 1145 |
| | 18 | 1215 | 1068 | 12 | 1122 | 8 | |
| | 19 | 1396 | 1247 | 11 | 1294 | 7 | |
| $^{93}_{64}Gd^{157}$ | 17 | 958 | 796 | 17 | 868 | 9 | 990 |
| | 18 | 1122 | 960 | 14 | 1028 | 8 | |
| | 19 | 1303 | 1134 | 13 | 1232 | 5 | |
| $^{95}_{66}Dy^{161}$ | 17 | 895 | 744 | 17 | 874 | 2 | 904 |
| | 18 | 1050 | 887 | 16 | 1046 | 0 | |
| | 19 | 1231 | 1049 | 15 | 1276 | —4 | |
| $^{97}_{66}Dy^{163}$ | 17 | 809 | 643 | 21 | 837 | —3 | 846 |
| | 18 | 965 | 802 | 17 | 986 | —3 | |
| | 19 | 1141 | 969 | 15 | 1150 | —1 | |
| $^{99}_{68}Er^{167}$ | 17 | 711 | 516 | 27 | 618 | 13 | 787 |
| | 18 | 859 | 677 | 21 | 730 | 15 | |
| | 19 | 1030 | 846 | 18 | 903 | 12 | |
| $^{101}_{70}Yb^{171}$ | 18 | 783 | 557 | 29 | 733 | 6 | 732 |
| | 19 | 946 | 732 | 23 | 881 | 7 | |
| | 20 | 1121 | 914 | 18 | 1048 | 7 | |
| $^{103}_{70}Yb^{173}$ | 18 | 699 | 397 | 43 | 531 | 24 | 684 |
| | 19 | 869 | 604 | 30 | 736 | 15 | |
| | 20 | 1049 | 811 | 23 | 926 | 12 | |
| $^{105}_{72}Hf^{177}$ | 18 | 677 | 374 | 45 | 503 | 26 | 659 |
| | 19 | 845 | 581 | 31 | 704 | 17 | |
| | 20 | 1022 | 786 | 23 | 892 | 13 | |
| $^{107}_{72}Hf^{179}$ | 18 | 677 | 375 | 45 | 488 | 28 | 690 |
| | 19 | 846 | 585 | 31 | 701 | 17 | |
| | 20 | 1021 | 790 | 23 | 893 | 13 | |
| $^{109}_{74}W^{183}$ | 18 | 733 | 529 | 28 | 700 | 5 | 788 |
| | 19 | 883 | 692 | 22 | 849 | 4 | |
| | 20 | 1040 | 858 | 18 | 997 | 4 | |
| $^{109}_{74}W^{183}$ (1.1 $\delta$) | 18 | 686 | 452 | 34 | 613 | 11 | 788 |
| | 19 | 839 | 623 | 26 | 785 | 6 | |
| | 20 | 997 | 796 | 20 | 945 | 5 | |

TABLE IIb

| Nucleide | $G_p \times A$ (MeV) | $\Delta_p^e$ (keV) | $\Delta_p^{odd}$ (keV) | $\frac{\Delta_p^e - \Delta_p^{odd}}{\Delta_p^e}$ (%) | $P_p^{theor.}$ (keV) | $\frac{\Delta_p^e - P_p^{theor.}}{\Delta_p^e}$ (%) | $P_p^{exp}$ (keV) |
|---|---|---|---|---|---|---|---|
| $_{63}Eu^{153}$ | 24 | 1270 | 1041 | 18 | 1149 | 10 | 1309 |
| | 25 | 1421 | 1185 | 17 | 1320 | 7 | |
| | 26 | 1586 | 1337 | 16 | 1532 | 3 | |
| $_{65}Tb^{159}$ | 24 | 1098 | 854 | 22 | 982 | 11 | 1013 |
| | 25 | 1244 | 991 | 20 | 1157 | 7 | |
| | 26 | 1409 | 1133 | 20 | 1399 | 1 | |
| $_{67}Ho^{165}$ | 24 | 985 | 713 | 28 | 834 | 15 | 925 |
| | 25 | 1127 | 856 | 24 | 1001 | 11 | |
| | 26 | 1285 | 1000 | 22 | 1226 | 5 | |
| $_{69}Tm^{169}$ | 24 | 917 | 613 | 33 | 742 | 19 | 883 |
| | 25 | 1060 | 771 | 27 | 918 | 13 | |
| | 26 | 1220 | 922 | 24 | 1151 | 6 | |
| $_{71}Lu^{175}$ | 24 | 883 | 644 | 27 | 821 | 7 | 809 |
| | 25 | 1025 | 770 | 25 | 1015 | 1 | |
| | 26 | 1208 | 895 | 26 | 1369 | −13 | |
| $_{73}Ta^{181}$ | 24 | 839 | 632 | 25 | 830 | 1 | 869 |
| | 25 | 951 | 733 | 23 | 945 | 1 | |
| | 26 | 1078 | 844 | 22 | 1100 | −2 | |
| $_{75}Re^{185}$ | 25 | 822 | 496 | 40 | 715 | 13 | 937 |
| | 26 | 948 | 661 | 30 | 860 | 9 | |
| | 27 | 1090 | 815 | 25 | 1040 | 5 | |
| $_{75}Re^{187}$ | 25 | 803 | 476 | 41 | 718 | 11 | 961 |
| | 26 | 923 | 638 | 31 | 854 | 7 | |
| | 27 | 1057 | 790 | 25 | 1012 | 4 | |

Column one identifies the nucleide; column two lists the chosen G-values; columns three, four and five give the corresponding $\Delta$-values for the even and the odd case, and the relative difference in per cent. Column six shows the calculated P-value, which is compared with the corresponding $\Delta$-value of the even case in column seven. The last column gives the averaged experimental $P$-value corresponding to the first diagrams of the present article. (Note that here the so-called "even" case corresponds to a nucleide having $n/2$ pairs and no single-particle state blocked.)

The result that $G_p$ comes out considerably larger than $G_n$ is in agreement with the fact that near the Fermi surface the velocity of the protons is smaller than that of the neutrons owing to the Coulomb repulsion. Now the $S$-wave phase shift, with which the pair-correlation force is directly associated, falls off rapidly with increasing relative energy because of the increasing importance of the repulsive core. This in turn follows from the fact that particles of higher velocity may penetrate closer to each other*.

* The authors are indebted to Professor B. R. MOTTELSON for valuable comments on this point.

TABLE IIc

| Nucleide | $G_n \times A$ (MeV) | $\Delta_n^e$ (keV) | $\Delta_n^{odd}$ (keV) | $\frac{\Delta_n^e - \Delta_n^{odd}}{\Delta_n^e}$ (%) | $P_n^{theor.}$ (keV) | $\frac{\Delta_n^e - P_n^{theor.}}{\Delta_n^e}$ (%) | $P_n^{exp}$ (keV) |
|---|---|---|---|---|---|---|---|
| $^{139}_{90}Th^{229}$ | 16 | 639 | 534 | 16 | 627 | 2 | 777 |
| | 17 | 781 | 666 | 15 | 746 | 4 | |
| | 18 | 935 | 810 | 13 | 909 | 3 | |
| $^{141}_{90}Th^{231}$ | 16 | 587 | 410 | 30 | 504 | 14 | 737 |
| | 17 | 732 | 585 | 20 | 642 | 12 | |
| | 18 | 890 | 758 | 15 | 791 | 11 | |
| $^{141}_{92}U^{233}$ | 16 | 573 | 400 | 30 | 491 | 14 | 687 |
| | 17 | 714 | 570 | 20 | 625 | 12 | |
| | 18 | 869 | 738 | 15 | 777 | 11 | |
| $^{143}_{92}U^{235}$ | 16 | 532 | 351 | 34 | 438 | 18 | 639 |
| | 17 | 669 | 519 | 22 | 568 | 15 | |
| | 18 | 825 | 687 | 17 | 723 | 12 | |
| $^{145}_{94}Pu^{239}$ | 16 | 488 | 311 | 36 | 397 | 19 | 561 |
| | 17 | 615 | 464 | 25 | 514 | 16 | |
| | 18 | 767 | 620 | 19 | 680 | 11 | |
| $^{147}_{94}Pu^{241}$ | 17 | 576 | 416 | 28 | 473 | 18 | 543 |
| | 18 | 725 | 573 | 21 | 626 | 14 | |
| | 19 | 927 | 734 | 21 | 976 | −5 | |
| $^{149}_{96}Cm^{245}$ | 17 | 529 | 351 | 34 | 440 | 17 | 574 |
| | 18 | 665 | 505 | 24 | 558 | 16 | |
| | 19 | 839 | 669 | 20 | 777 | 7 | |

TABLE IId

| Nucleide | $G_p \times A$ (MeV) | $\Delta_p^e$ (keV) | $\Delta_p^{odd}$ (keV) | $\frac{\Delta_p^e - \Delta_p^{odd}}{\Delta_p^e}$ (%) | $P_p^{theor.}$ (keV) | $\frac{\Delta_p^e - P_p^{theor.}}{\Delta_p^e}$ (%) | $P_p^{exp}$ (keV) |
|---|---|---|---|---|---|---|---|
| $_{91}Pa^{231}$ | 22 | 846 | 713 | 16 | 782 | 8 | 896 |
| | 23 | 949 | 814 | 14 | 887 | 7 | |
| | 24 | 1059 | 919 | 13 | 1008 | 5 | |
| $_{93}Np^{237}$ | 22 | 742 | 593 | 20 | 676 | 9 | 821 |
| | 23 | 841 | 690 | 18 | 779 | 7 | |
| | 24 | 949 | 792 | 17 | 904 | 5 | |
| $_{95}Am^{241}$ | 22 | 615 | 400 | 35 | 579 | 6 | 745 |
| | 23 | 718 | 526 | 27 | 693 | 3 | |
| | 24 | 832 | 648 | 22 | 827 | 1 | |
| $_{95}Am^{243}$ | 22 | 601 | 383 | 36 | 563 | 6 | 745 |
| | 23 | 702 | 508 | 28 | 676 | 4 | |
| | 24 | 813 | 630 | 23 | 802 | 1 | |

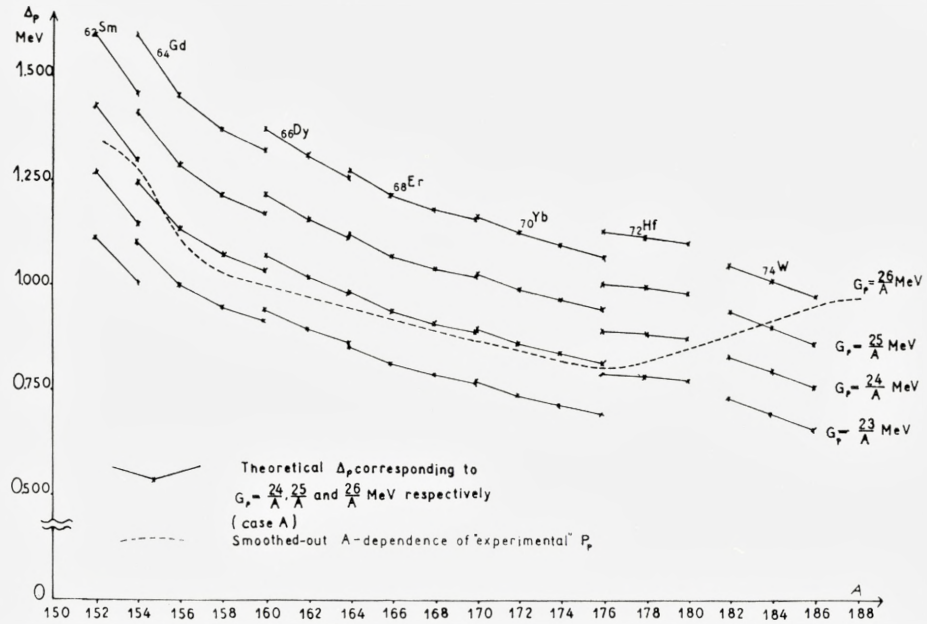


Fig. 8. *The relation between $\Delta_p$ and $G_p$ in region I* (case A). The "empirical" dashed curve refers to the averaged $P_p$ curve of fig. 6.

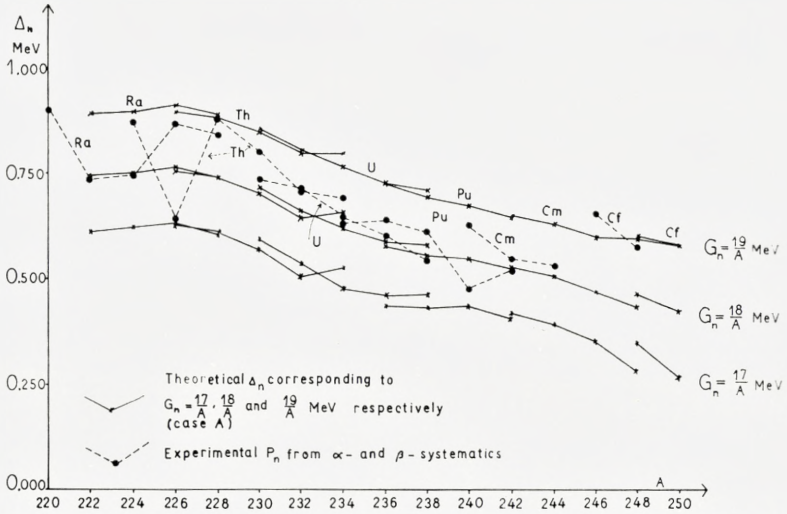


Fig. 9. *The relation between $\Delta_n$ and $G_n$ in region II* (case A). The exhibited points refer to the $P_n$-values of fig. 2.

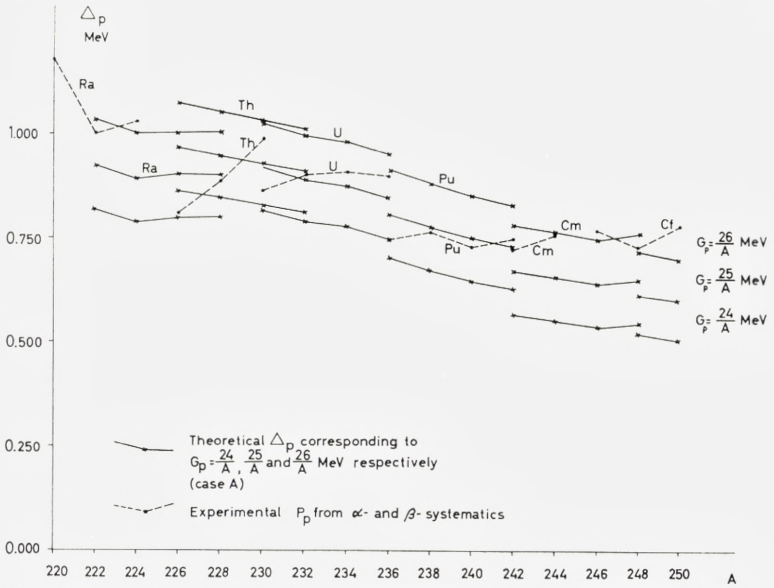


Fig. 10. *The relation between $\Delta_p$ and $G_p$ in region II* (case A). The exhibited points refer to the $P_p$-values of fig. 3.

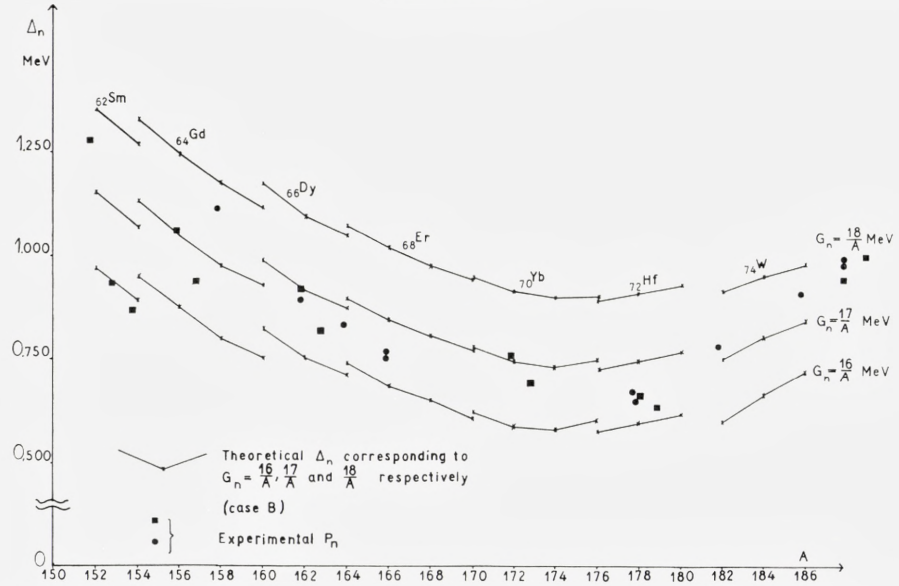


Fig. 11. *The relation between $\Delta_n$ and $G_n$ in region I as obtained in the calculations* (case B). For details about the single-particle spectrum employed in these calculations, denoted as "case B", see table I. The points exhibited for comparison refer to the $P_n$-values of fig. 1.

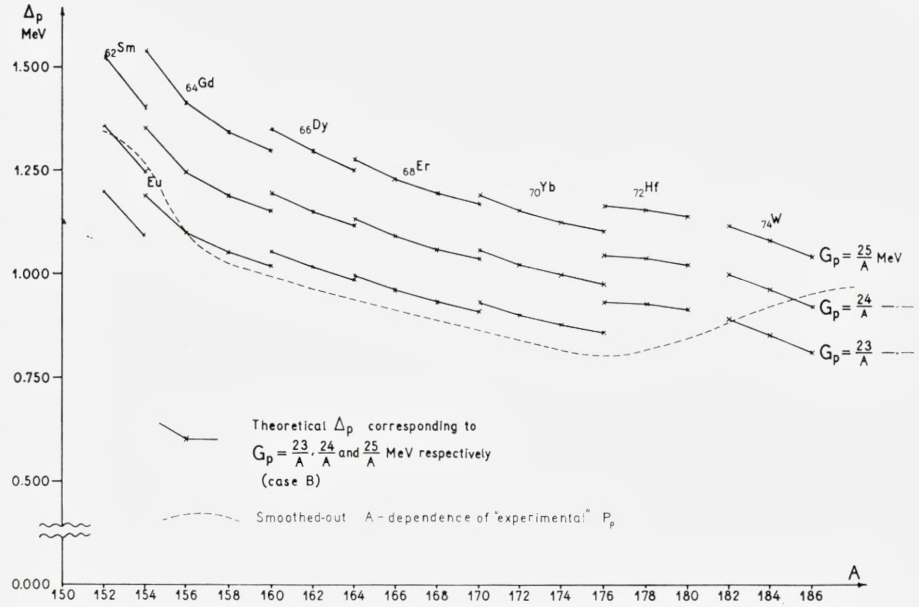


Fig. 12. *The relation between $\Delta_p$ and $G_p$ in region I* (case B). The "empirical" dashed curve corresponds to the $P_p$-values of fig. 6.

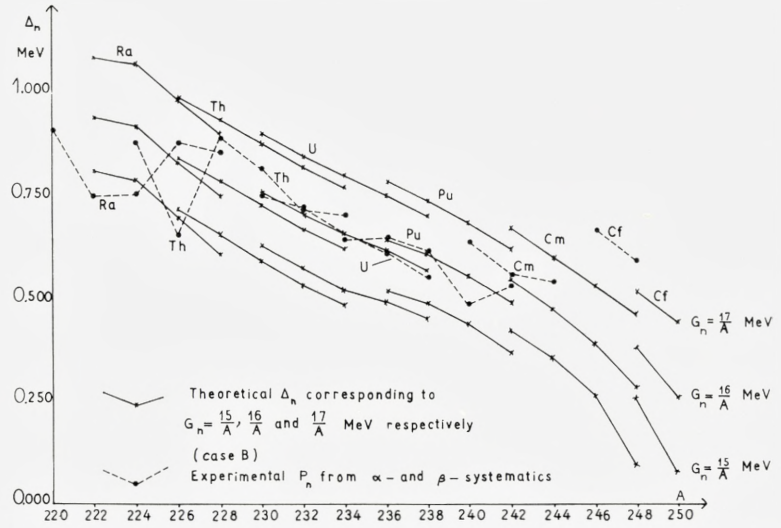


Fig. 13. *The relation between $\Delta_n$ and $G_n$ in region II* (case B). The exhibited points refer to the $P_n$-values given in fig. 2.

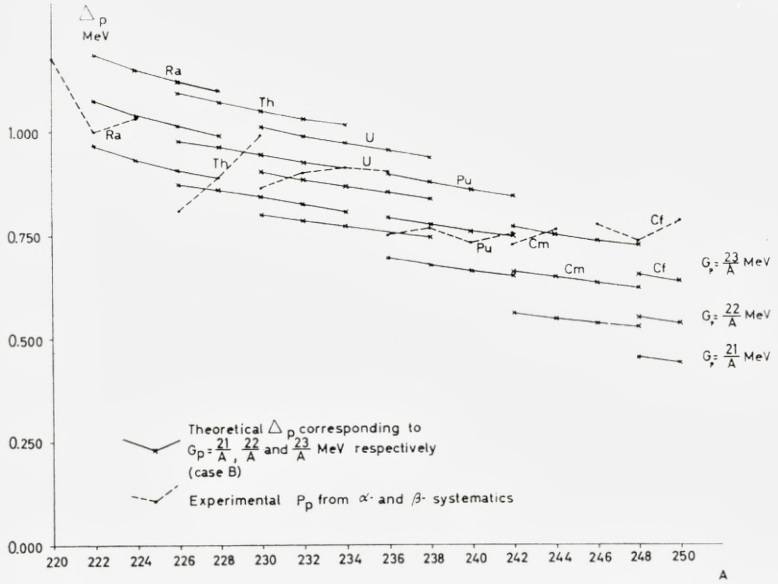


Fig. 14. *The relation between $\Delta_p$ and $G_p$ in region II* (case B). The exhibited points refer to the $P_p$-values given in fig. 3.

## V. Details of the Numerical Calculations

The numerical calculations were performed on the SMIL electronic digital computer of the University of Lund. In the first programme used* the $\varepsilon_\nu$:$s$ were stored in the computer for three different eccentricities, $\delta = 0.20$, 0.25 and 0.30, in region I and for $\delta = 0.20$ and 0.25 in region II. Furthermore the computer was provided with a set of four different $\Delta_n$ and $\Delta_p$ values, covering the whole region of variation of these parameters. For each value of $\delta$ and $\Delta$ the computer was instructed to find the correct $\lambda$ fulfilling the condition (13) for the sequence of given $Z$ and $N$ values of the elements of regions I and II. About 1000 different matrix elements of $s_x$ and $j_x$ were also stored, connecting all single-particle states up to and including the $N = 7$ shell in terms of the wave functions of ref. 15 and computed for three, respectively two, different values of the eccentricity. When the $u$:$s$ and $v$:$s$ had been determined for each $\lambda$, $\Delta$ and $\delta$, SMIL went on to compute $\mathfrak{I}_n$, $W_n$, $\mathfrak{I}_p$, $W_p$, $G_n$, $G_p$, the total energy, the fluctuation in the number of particles, etc. All this information was printed. A subroutine was then used

* The programme was constructed by Dr. C. E. Fröberg, Director of the Institute of Numerical Analysis of the University of Lund.

to interpolate $\Im$ and $W$ for specific values of $\delta$ and $\Delta$, by means of all the points computed, and also to find the relation between $\Delta$ and $G$ for the given eccentricities, as exhibited in figs. 7-14.

In a later programme designed also for the treatment of moments of inertia of odd-$A$ nuclei (see Appendix III), where the correct position of the chemical potential with reference to the level populated by the odd particle is very critical, we employed a different procedure. According to this latter programme the interpolation between $\varepsilon_\nu$:$s$, stored in the memory for a few deformations, to the correct deformation is performed first.

## VI. Results of the Calculations

### a. Moments of inertia of even-even nuclei

The values of the calculated moments of inertia of even-even nuclei, corresponding to the sets of single-particle states $\varepsilon_\nu$ as given in table I (cases A and B), as well as to the eccentricities exhibited in figs. 15 and 16, and to the $\Delta$-values equal to the $P$-values of figs. 1, 2, 3, and 6, are displayed in fig. 17 (region I) and in fig. 18 (region II). All the empirical and some of the calculated values are listed in table III, where the appropriate references of the former are also given. A correction to the empirical values for the rotation-vibration interaction is not employed for the plotted values of figs. 17-25. Information on this point is incomplete, but the effect is of some importance at the beginning of regions I and II, and its inclusion amounts to a depression in $\Im$ of a few per cent, as can be studied in table III, thus very slightly improving the agreement with the theoretical calculations. In region I the quantity $\frac{2}{\hbar^2}\Im$ in case A lies consistently $\sim 10$ MeV$^{-1}$ below the experimental values. The calculations corresponding to case B (which case implies that the ad hoc raise of the shells above $Z = 82$ and $N = 126$, assumed according to case A, is very largely diminished) give values of $\Im$ above those of case A, particularly at the end of the region. Nevertheless, the overall variation over the nucleides is probably less favourable than in case A. Furthermore, in case B the single-particle states of the above-lying shells are allowed to come down further than is tolerable on the basis of the detailed knowledge[16] about the odd-A nuclear excitation spectra at the end of region I. Thus case A appears more realistic*.

* The interest in including case B lies, however, apart from its giving an estimate of the effects of the inaccuracies of the single-particle level scheme, in the fact that fewer ad hoc changes in the single-particle spectra are made in that case. Such changes are dangerous as they lead to violations of the sum rules otherwise fulfilled by any consistent model.

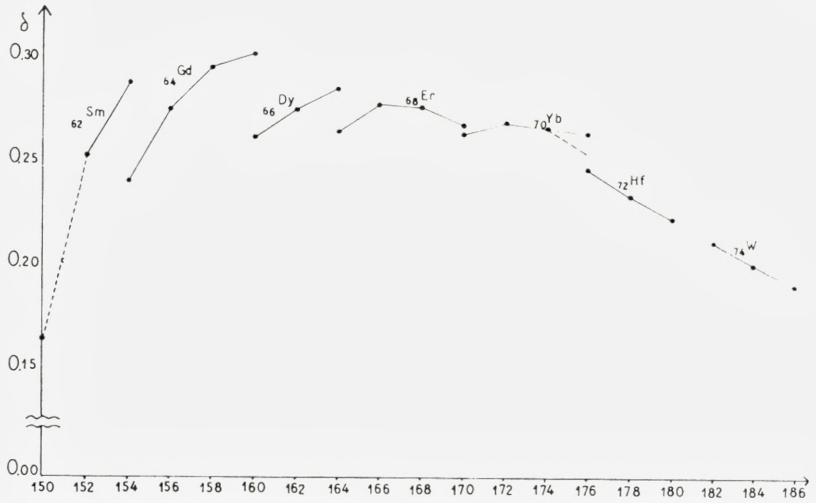


Fig. 15. *Values of the eccentricity parameter $\delta$ in region I used in the calculations.* The values of $\delta$ are obtained by means of eq. (41) from the quadrupole moments given by ELBEK et. al.[19], assuming $R_z = 1.2 \times A^{1/3}$ *f*. Note that the dashed line ending at $Yb^{176}$ represents a slight ad hoc correction of the $Yb^{176}$ point. Such a correction is in line with the level diagram of ref. 15.

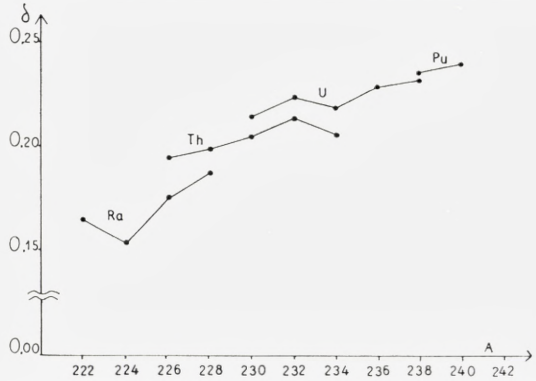


Fig. 16. *Values of the eccentricity parameter $\delta$ in region II used in the calculations.* For references to the experimental data see BELL et al.[20] and STROMINGER, HOLLANDER and SEABORG[44]: The detailed fine structure of the A-dependence of $\delta$ appears less regular than in fig. 15, and some of the variations may be due to experimental uncertainties.

In region II both the calculations, corresponding to case A and case B, give results very much below the empirical energy moments, particularly at the beginning of the region, even when the vibration-rotation correction for the empirical values is applied.

Unfortunately, however, both $\delta$, $\Delta_n$ and $\Delta_p$ are known too inaccurately

TABLE III. *Experimental and Theoretical Values of the Moment of Inertia and the Collective Gyromagnetic Ratio in Region I* (TABLE IIIa) *and Region II* (TABLE IIIb).

The nucleides are identified from columns one and two. Column three shows the experimental values of the moment of inertia based on the excitation energy of the first rotational states as found, e. g., in refs. 44 and 46. Column four gives the inertia values that include the correction for the rotation-vibration interaction. These values have been taken from ref. 45. Columns five, six and seven show the values of the parameters $\delta$, $\Delta_n$ and $\Delta_p$ assumed in the calculations. The values of $\delta$ given in parentheses are extrapolated. Of the quantities listed in the last columns, the theoretical quantities $\overset{\circ}{\Im}$ and $W$ are defined from eqs. (A II-10) and (40). The indices $n$ and $p$ refer to neutrons and protons respectively. Columns 10 and 13 (respectively 14) give the final theoretical values of the moment of inertia and the collective gyromagnetic ratio. In table III a, columns 8-13 refer to "case A", only column 14 to "case B". For experimental values of $g_R$ see refs. 33 and 40.

TABLE IIIa

| Nucleide | A | $\frac{2}{\hbar^2}\Im_{\mathrm{exp}}$ $(\mathrm{MeV})^{-1}$ | $\frac{2}{\hbar^2}\Im^{\mathrm{corr}}_{\mathrm{exp}}$ $(\mathrm{MeV})^{-1}$ | $\delta$ | $\frac{\Delta_n}{\varkappa\hbar\omega_0}$ | $\frac{\Delta_p}{\varkappa\hbar\omega_0}$ | Case A: $\frac{2}{\hbar^2}\overset{\circ}{\Im}_n$ | Case A: $\frac{2}{\hbar^2}\overset{\circ}{\Im}_p$ | Case A: $\frac{2}{\hbar^2}\Im$ | Case A: $\frac{2}{\hbar^2}W_n$ | Case A: $\frac{2}{\hbar^2}W_p$ | $g_R$ Case A | $g_R$ Case B |
|---|---|---|---|---|---|---|---|---|---|---|---|---|---|
| Sm | 152 | 49.2 | 47.3 | 0.254 | 3.254 | 3.502 | 22.98 | 13.20 | 38.9 | 0.619 | 0.327 | 0.341 | 0.344 |
| | 154 | 73.2 | | 0.289 | 2.720 | 3.329 | 33.67 | 16.41 | 53.9 | 0.951 | 0.436 | 0.295 | 0.299 |
| Gd | 154 | 48.8(a) | 46.8 | 0.242 | 3.269 | 3.329 | 21.28 | 13.19 | 36.9 | 0.567 | 0.361 | 0.367 | 0.378 |
| | 156 | 67.4 | 66.7 | 0.277 | 2.731 | 2.886 | 32.45 | 17.83 | 53.9 | 0.949 | 0.553 | 0.333 | 0.339 |
| | 158 | 75.5 | 75.0 | 0.297 | 2.479 | 2.705 | 38.38 | 20.10 | 62.9 | 1.160 | 0.654 | 0.319 | 0.326 |
| | 160 | 79.7 | | 0.303 | 2.320 | 2.651 | 41.42 | 20.82 | 67.0 | 1.273 | 0.687 | 0.307 | 0.311 |
| Dy | 160 | 69.0(a) | 68.5 | 0.263 | 2.489 | 2.651 | 34.18 | 17.98 | 55.5 | 1.064 | 0.584 | 0.318 | 0.325 |
| | 162 | 74.4 | 74.0 | 0.277 | 2.330 | 2.574 | 38.54 | 19.09 | 61.6 | 1.208 | 0.634 | 0.311 | 0.310 |
| | 164 | 81.8 | | 0.287 | 2.176 | 2.501 | 41.09 | 19.99 | 65.4 | 1.183 | 0.677 | 0.304 | 0.309 |
| Er | 164 | 66.7 | | 0.266 | 2.339 | 2.501 | 37.26 | 18.93 | 59.9 | 1.168 | 0.601 | 0.306 | 0.324 |
| | 166 | 74.5 | 74.1 | 0.279 | 2.185 | 2.448 | 40.59 | 19.92 | 64.7 | 1.181 | 0.640 | 0.303 | 0.313 |
| | 168 | 75.2 | 75.0 | 0.278 | 2.046 | 2.403 | 41.85 | 20.30 | 66.4 | 1.079 | 0.658 | 0.309 | 0.315 |
| | 170 | 75.6 | | 0.269 | 1.905 | 2.358 | 44.25 | 20.38 | 68.7 | 1.118 | 0.665 | 0.296 | 0.298 |
| Yb | 170 | 71.2 | 70.9 | 0.265 | 2.053 | 2.358 | 41.07 | 20.48 | 65.4 | 1.066 | 0.627 | 0.313 | 0.329 |
| | 172 | 76.2 | 76.0 | 0.270 | 1.913 | 2.289 | 44.35 | 21.59 | 70.1 | 1.119 | 0.661 | 0.308 | 0.322 |
| | 174 | 78.5 | | 0.268 | 1.806 | 2.224 | 45.15 | 22.10 | 71.4 | 1.236 | 0.687 | 0.305 | 0.303 |
| | 176 | 73.1 | | 0.265 | 1.788 | 2.190 | 41.41 | 21.62 | 67.1 | 1.163 | 0.700 | 0.324 | 0.305 |
| Hf | 176 | 67.9 | 67.5 | 0.248(b) | 1.812 | 2.190 | 43.88 | 16.95 | 64.3 | 1.228 | 0.578 | 0.245 | 0.301 |
| | 178 | 64.4 | 64.1 | 0.235(b) | 1.795 | 2.250 | 39.74 | 15.34 | 58.2 | 1.149 | 0.553 | 0.245 | 0.285 |
| | 180 | 64.3 | 64.1 | 0.224(b) | 1.997 | 2.338 | 33.14 | 14.30 | 50.1 | 0.876 | 0.517 | 0.280 | 0.292 |
| W | 182 | 60.0 | 59.6 | 0.213(b) | 2.004 | 2.455 | 32.67 | 11.65 | 46.8 | 0.850 | 0.412 | 0.231 | 0.254 |
| | 184 | 54.1 | 53.6 | 0.202(b) | 2.358 | 2.558 | 25.12 | 10.81 | 38.1 | 0.610 | 0.375 | 0.284 | 0.285 |
| | 186 | 49.0 | | 0.194(b) | 2.659 | 2.651 | 18.41 | 10.23 | 30.6 | 0.434 | 0.340 | 0.352 | 0.334 |

(a) J. O. RASMUSSEN and K. S. TOTH, Phys. Rev. *115*, 150 (1959).
(b) from B. ELBEK, unpublished.

TABLE IIIb

| Nucleide | | $\frac{2}{\hbar^2}\Im_{exp}$ | $\frac{2}{\hbar^2}\Im^{corr}$ | $\delta$ | $\frac{\Delta_n}{\varkappa\hbar\omega_0}$ | $\frac{\Delta_p}{\varkappa\hbar\omega_0}$ | Case B | | | | | |
|---|---|---|---|---|---|---|---|---|---|---|---|---|
| | A | $(MeV)^{-1}$ | $(MeV)^{-1}$ | | | | $\frac{2}{\hbar^2}\overset{\circ}{\Im}_n$ | $\frac{2}{\hbar^2}\overset{\circ}{\Im}_p$ | $\frac{2}{\hbar^2}\Im$ | $\frac{2}{\hbar^2}W_n$ | $\frac{2}{\hbar^2}W_p$ | $g_R$ |
| Ra | 226 | 88.5 | 86.2 | 0.176 | 2.377 | 3.179 | 35.14 | 9.14 | 46.5 | 0.841 | 0.041 | 0.14 |
| | 228 | 102 | | 0.188 | 2.354 | 3.188 | 41.84 | 11.55 | 56.1 | 1.033 | 0.141 | 0.16 |
| Th | 226 | 83.2 | 81.1 | 0.195 | 2.377 | 2.665 | 40.24 | 18.98 | 62.2 | 0.990 | 0.389 | 0.29 |
| | 228 | 103.6 | 103.1 | 0.199 | 2.354 | 2.673 | 43.55 | 19.82 | 66.5 | 1.097 | 0.428 | 0.28 |
| | 230 | 113.2 | 112.9 | 0.205 | 2.281 | 2.681 | 48.82 | 21.11 | 73.3 | 1.217 | 0.487 | 0.27 |
| | 232 | 120.5 | | 0.214 | 2.134 | 2.689 | 55.96 | 23.05 | 82.9 | 1.321 | 0.576 | 0.26 |
| | 234 | 125 | | 0.206 | 1.990 | 2.696 | 58.33 | 21.27 | 83.2 | 1.337 | 0.495 | 0.23 |
| U | 230 | 116.1 | | 0.215 | 2.281 | 2.673 | 51.25 | 24.58 | 79.7 | 1.341 | 0.666 | 0.30 |
| | 232 | 127.1 | 126.8 | 0.224 | 2.134 | 2.680 | 59.08 | 26.15 | 89.6 | 1.510 | 0.728 | 0.28 |
| | 234 | 137.9 | 137.9 | 0.219 | 1.990 | 2.687 | 62.32 | 25.23 | 91.8 | 1.499 | 0.691 | 0.26 |
| | 236 | 132.5 | | 0.229 | 1.860 | 2.695 | 68.44 | 26.99 | 100.2 | 1.545 | 0.759 | 0.26 |
| | 238 | 133.9 | | 0.232 | 1.741 | 2.703 | 73.76 | 27.48 | 106.2 | 1.662 | 0.778 | 0.25 |
| Pu | 236 | 134.4 | | (0.230) | 1.860 | 2.252 | 70.04 | 35.25 | 110.3 | 1.703 | 1.072 | 0.32 |
| | 238 | 136.1 | 136.1 | 0.236 | 1.741 | 2.258 | 74.92 | 36.25 | 116.5 | 1.707 | 1.103 | 0.32 |
| | 240 | 139.9 | 139.5 | 0.240 | 1.652 | 2.264 | 79.50 | 36.85 | 122.0 | 1.777 | 1.124 | 0.30 |
| | 242 | 134.8 | | (0.242) | 1.642 | 2.271 | 78.83 | 37.14 | 121.8 | 1.723 | 1.132 | 0.31 |
| Cm | 242 | 142.5 | | (0.243) | 1.642 | 2.259 | 80.80 | 36.88 | 123.6 | 1.793 | 1.003 | 0.30 |
| | 244 | | | (0.243) | 1.698 | 2.265 | 76.82 | 36.87 | 119.6 | 1.655 | 1.001 | 0.31 |
| | 246 | 139.9 | | (0.243) | 1.804 | 2.271 | 71.02 | 36.85 | 113.7 | 1.349 | 0.999 | 0.34 |
| | 248 | 138.3 | | (0.225) | 1.891 | 2.277 | 69.94 | 36.48 | 112.2 | 1.221 | 0.990 | 0.34 |
| Cf | 248 | | | (0.240) | 1.891 | 2.332 | 68.03 | 34.30 | 108.0 | 1.277 | 0.894 | 0.33 |
| | 250 | 142.2[a] | | (0.225) | 1.922 | 2.339 | 69.09 | 34.28 | 109.1 | 1.200 | 0.893 | 0.33 |

(a) Van den Bosch, Diamond, Sjöblom, and Fields, Phys. Rev. **115**, 115 (1959).

to admit any further definite conclusions. An increase of $\delta$ by about 20 % corresponding to the use of an $R_z = 1.08 \times A^{1/3}$ fermis in eq. (41) raises the curves by amounts that can be studied in fig. 19. A decrease in $\Delta_n$ and $\Delta_p$ by 10-20 % is certainly admissible within the inaccuracy of the experimental data, particularly in view of the uncertain relation between $P$ and $\Delta$*. The effect of choosing 20 % smaller $\Delta$-values may be studied in figs. 20 and 21.

* The recent very detailed and inclusive study of relative nucleidic masses by EVERLING, KÖNIG, MATTAUCH, and WAPSTRA[31], based on all relevant information available, indicates that a few per cent smaller $P_n$-values should be chosen at the end of region I.

Added in proof: The recent more complete mass-spectroscopic data published by BHANOT, JOHNSON and NIER[30] lowers the values of $\Delta_n$ and $\Delta_p$ to be used for $_{74}W$ by up to 10–20 % as exhibited in fig. 28. The adoption of these new $\Delta$-values would considerably improve the agreement with theory for the $W$-isotopes.

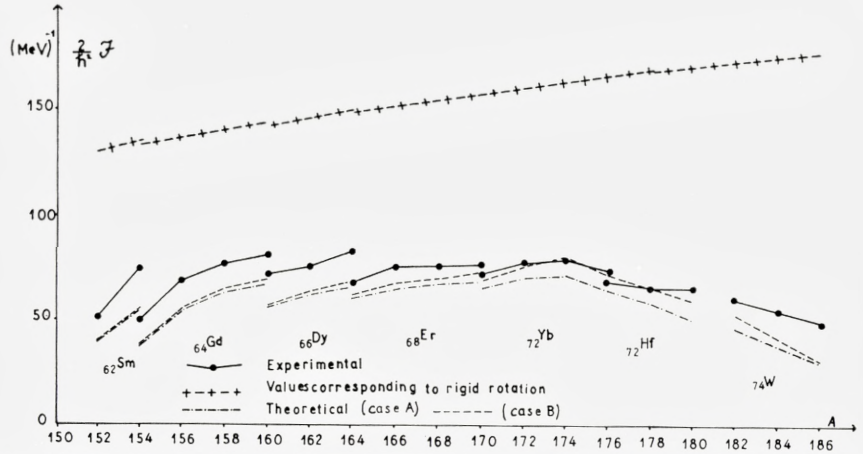


Fig. 17. *Moments of inertia of even-even nuclei in region I.* The figure exhibits by the crossed line the rigid moment of inertia corresponding to $R_0 = 1.2 \times A^{1/3} f$. The empirical values given as filled circles do not include any correction for the rotation-vibration interaction. The dashed and dot-and-dash lines refer to calculations corresponding to the choice of $\Delta_p = P_p$ and $\Delta_n = P_n$ with an assumed single-particle level spectrum $\varepsilon_\nu$ as given according to the alternative cases A and B of table I.

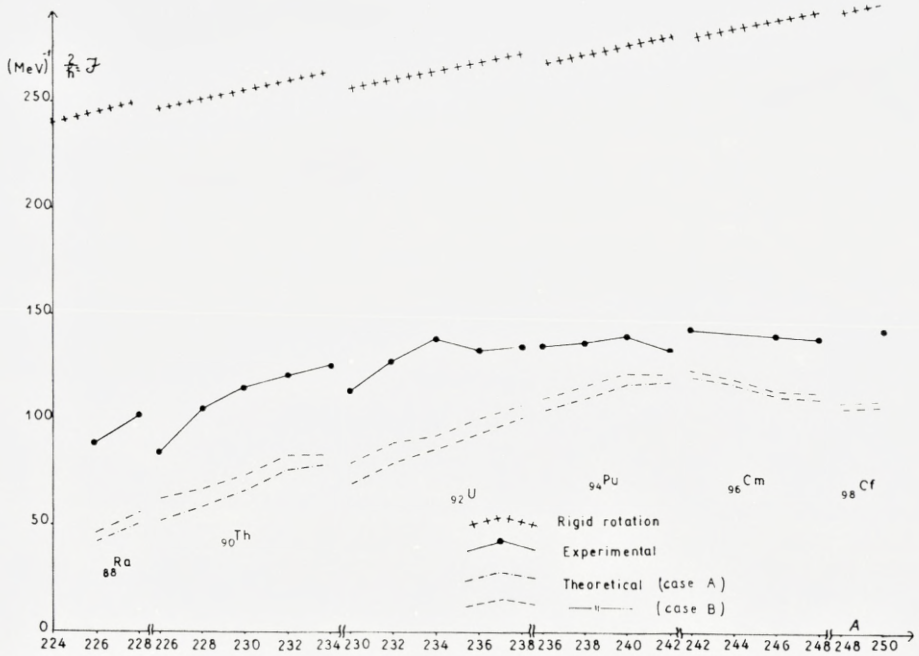


Fig. 18. *Moments of inertia of even-even nuclei in region II.* For explanation see fig. 17.

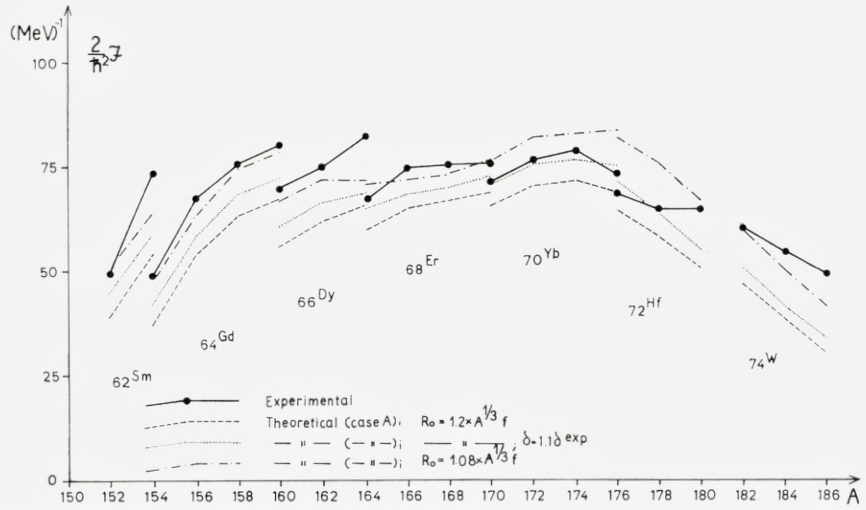


Fig. 19. The *dependence of the calculated moment of inertia for nuclei in region I on the eccentricity parameter* $\delta$. Note that the dot-and-dash line corresponds to $\delta$ as obtained from the experimental $Q_0$-values of eq. (41) with the charge radius $R_z$ chosen equal to $1.08 \times A^{1/3} f$.

It may also be of interest to note the great dependence on the type of wave functions employed in calculating the matrix elements of $j_x$ and $s_x$. Thus the use of "asymptotic"[15] matrix elements, i. e. the employment of nucleonic wave functions corresponding to the limit of very large eccentricities, gives values considerably above the experimental points in region I and of the same order of magnitude as the experimental values in region II. As can be seen from fig. 25, the variation with $(N, Z)$ is much less favourable than in the calculations where the more accurate nucleonic wave functions have been employed.

It may be argued that the use of the more detailed and realistic wave functions is consistent with the fact that we employ the level scheme of ref. 16 and the empirical estimate of the eccentricity parameter $\delta$.

The greater magnitude of $\Im$ when the asymptotic wave functions are employed corresponds to the fact that while a very large fraction of the whole $j_x$ coupling strength lies between nearby states in the representation of the detailed wave functions, some of this strength and the strength connecting very far-away states is collected in states 2-3 MeV distant in the asymptotic case. When $\Delta \to 0$, the results are not very different in the two cases. In the case treated here the factor containing $u$ and $v$ cuts down the contribution from the very close-lying states most drastically (by a factor of

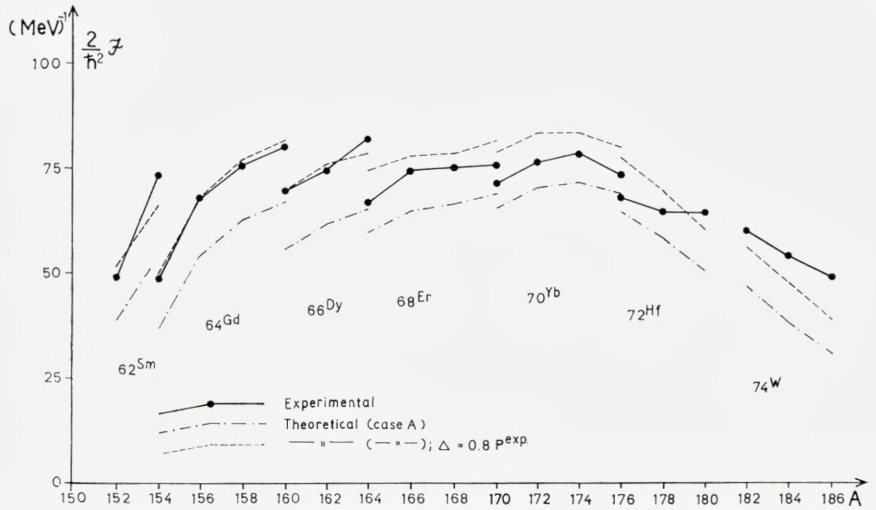


Fig. 20. *The dependence of the calculated moment of inertia for nuclei in region I on the chosen values of* $\Delta_n$ *and* $\Delta_p$.

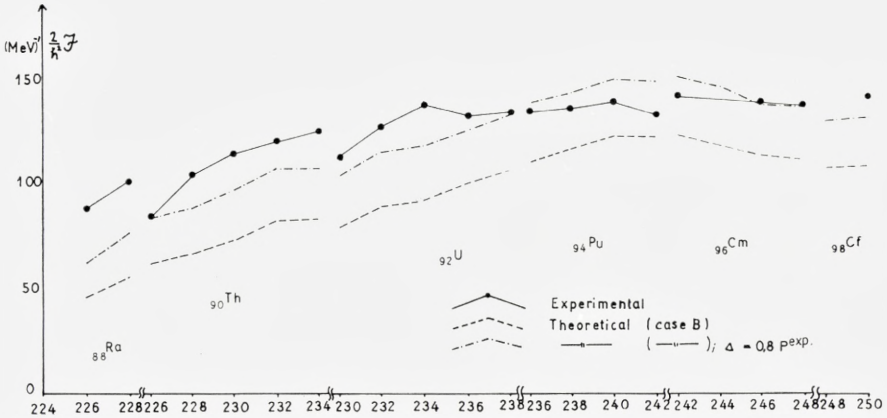


Fig. 21. *The dependence of the calculated moment of inertia for nuclei in region II on the chosen values of* $\Delta_n$ *and* $\Delta_p$.

five or so). This cancellation therefore affects the asymptotic case less than the other.

In summary, we can only conclude first that, compared with the independent-particle value, the agreement in the magnitude of $\mathfrak{I}$ is rather good; in particular the "fine structure" of the A-dependence of $\mathfrak{I}$ is well reproduced.

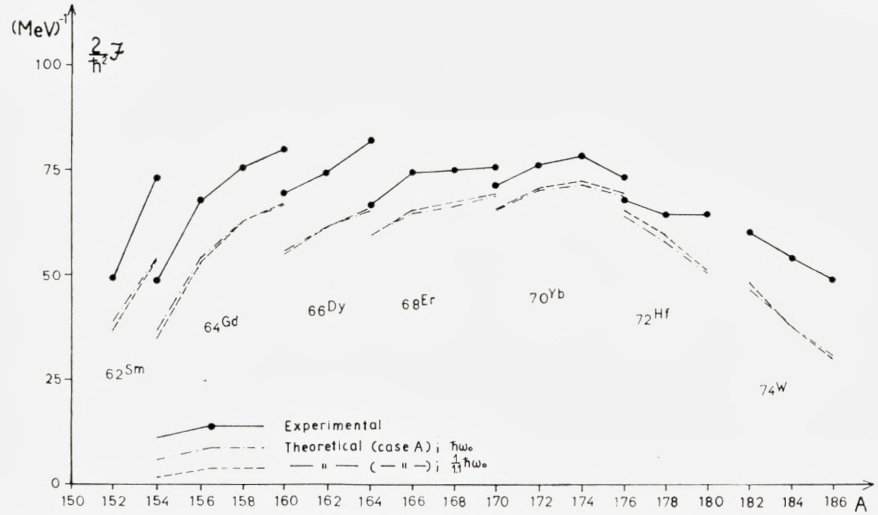


Fig. 22. *The dependence of the calculated moment of inertia for nuclei in region I on the choice of the energy scale parameter* $\hbar\omega_0$.

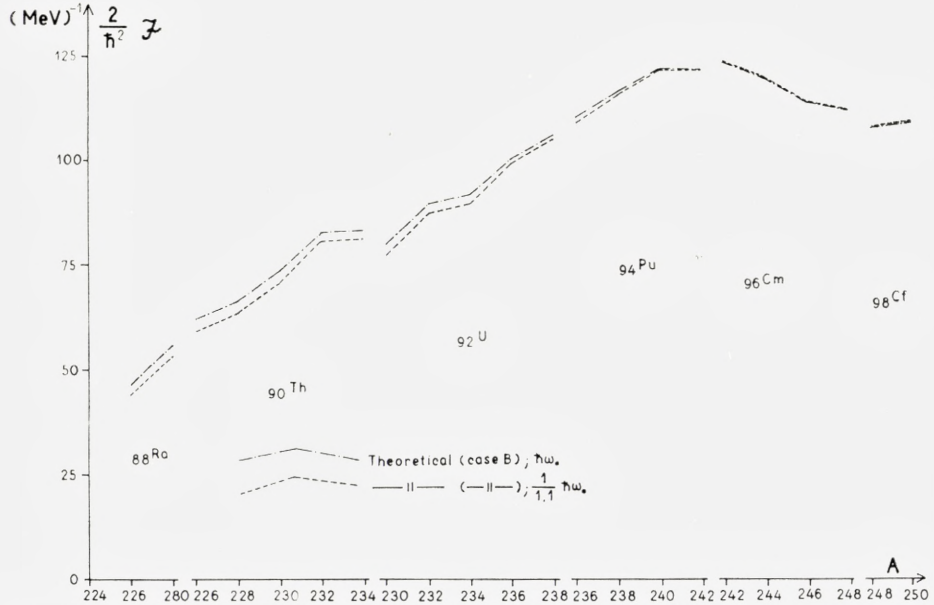


Fig. 23. *The dependence of the calculated moment of inertia for nuclei in region II on the choice of the energy scale parameter* $\hbar\omega_0$.

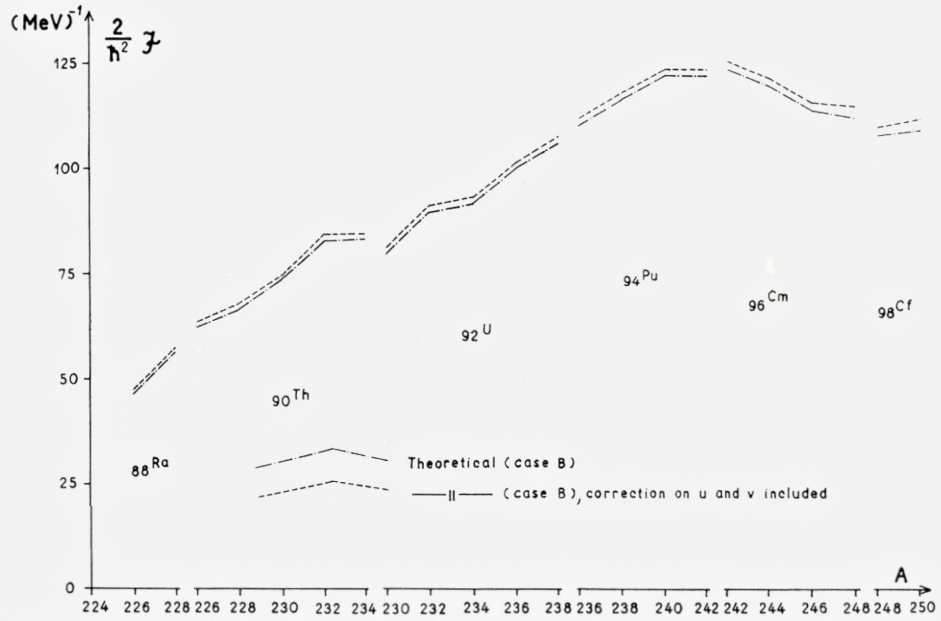


Fig. 24. *Correction of the moment of inertia due to the inclusion of the otherwise neglected* $H'_{20}$ *terms in the calculation of* $u$ *and* $v$ (cf. (A I-6) etc.).

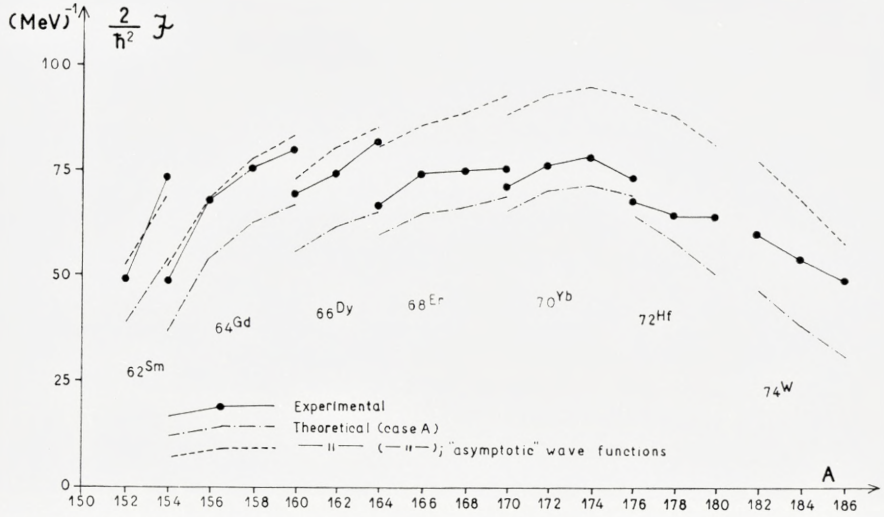


Fig. 25. *The theoretical values of the moment of inertia when the asymptotic wave functions are used,* compared with the case in which the more detailed wave functions of ref. 15 are employed.

The fine-structure variation appears largely a function of $\delta$*, which latter in the calculation is taken in turn from the accurate quadrupole determinations of refs. 19 and 20. The systematic deviation between the results of the present calculations and the empirical values may very well lie within the inaccuracies of the parameters $\delta$ and $\Delta$ and may also depend critically on the insufficient accuracy of the nucleonic wave functions**.

There are, however, also other effects which might be responsible for the deviation. They are connected with the limitations in the form of the interaction Hamiltonian assumed and with the approximate character of the BCS solution** corresponding to the given Hamiltonian.

As pointed out in connection with eq. (5), the assumed type of nucleonic interaction, given by that equation, admits scattering of pairs solely in $K = 0$ states. In particular, the scattering in the $K = 1$ state, that is the intermediate two-quasi-particle state in the cranking formula, is neglected. The inclusion of such an interaction would probably tend to depress somewhat the lowest-lying $K = 1$ states. By that effect alone the energy denominators of eq. (35) would be somewhat cut down and $\Im$ correspondingly increased.

The inclusion of such effects is of interest also for the following reason: In the limit of an infinite nucleus, $A \to \infty$, the level density of single-particle states increases proportionally to $A$. As $G$, owing to the decreasing overlap, tends to zero as $\frac{1}{A}$, thus $\Delta$ in this limit goes towards a constant[6]. Finally, all the contributing states $\varepsilon_\nu$ are swallowed up by the energy gap, and the term containing $u$ and $v$ makes $\Im$ vanish identically in this limit. This consideration of the limiting behaviour of the solution appears to bear out the contention that some terms are missing in the Belyaev expression which would contribute the irrotational moment in the limit considered[10]. It remains to be shown, however, whether the terms present e. g. in the $\delta$-force, but neglected in the pairing interaction, can bring about the expected behaviour in the limit of $A \to \infty$***.

* This is also concluded from an analysis of experimental data in ref. 19.

** The effect of the usually neglected terms in (14) and (24), largely taken care of by eqs. (A I-6)–(A I-8), was included in one calculation. It was found to increase $\Im$ by only a few per cent, however (cf. fig. 24). Note added in proof: Calculations employing the expression (35′) for the moment of inertia so far performed for neutrons of $Sm^{152}$, $Gd^{156}$, $Dy^{160}$, and $W^{182}$ render a moment of inertia 6, 3, 2, and 16 per cent, respectively, lower than calculations on the basis of eq. (35), under the assumption of the same value of $G_n$. According to table II a calculations that take blocking into account in addition require slightly larger $G$-values to fit the odd-even mass difference. The preliminary results thus indicate that, all in all, the inclusion of the complicated „blocking effects" leads to values of the moment of inertia of the order of 10% lower. The disparity with empirical findings is therefore increased.

*** The present calculations by PRANGE[32] appear to support such a supposition.

### b. The collective gyromagnetic ratio $g_R$

The calculated value of $g_R$ for even-even nuclei is exhibited in figs. 26 and 27. As $g_R$ is approximately equal to $\frac{\Im_p}{\Im_n + \Im_p}$, it is less sensitive to e. g. an increase in $\delta$, which affects $\Im_p$ and $\Im_n$ in very much the same way. That the value of $g_R$ comes out smaller than the ratio $\frac{Z}{Z+N}$ is largely due to the fact that we have employed a value of $\Delta_p$ considerably larger than $\Delta_n$. Furthermore, "fine structure" effects in figs. 26 and 27 are due in particular to the fact that it is mainly the nucleons outside of closed shells $(z, n)$ that contribute to $\Im_p$ and $\Im_n$, whence the relevant ratio of comparison should be $\frac{z}{z+n}$ rather than $\frac{Z}{Z+N}$. The former ratio exhibits a much faster variation within a sequence of isotopes at the beginning and the end of shells. At the end of the shells the holes play the parts of the particles at the beginning of the shells, and so the trend of $g_R$ within a series of isotopes is reversed. Fig. 26 also exhibits a comparison with experimental values of $g_R$ for even-even nuclei, taken from a recent compilation by BODENSTEDT[33] *. The experimental errors are very large, as indicated in the figure. The values to the left correspond to measurements by GOLDRING and SHARENBERG[34], involving an angular-distribution measurement of the $E2$ gamma radiation emitted in the decay of the first rotational state. This state has been reached by Coulomb excitation and, during its very short lifetime, it is under the influence of a strong external magnetic field. Owing to paramagnetic effects connected with the unfilled atomic $4f$ shell the strength of this field is very much increased at the nucleus, which enhances the angular effects studied. However, as the atomic configurations are not known with sufficient accuracy, the interpretation of the angular-distribution measurements in terms of $g_R$ becomes very uncertain. Indeed, on the basis of new atomic wave functions calculated by KANAMORI[35] and SÜSSMANN[36], BODENSTEDT et al[33] have adjusted the values of $g_R$ originally given[34]. The experimental points on the right side in fig. 26 are based on very similar experiments[37], involving, however, a population of the rotational state by beta decay instead of by Coulomb excitation.

In view of the uncertainties of the experimental values, the agreement with the present calculations cannot be considered unsatisfactory.

* We are very much indebted to Dr. BODENSTEDT for his kind permission to quote his values of $g_R$ in advance of publication.

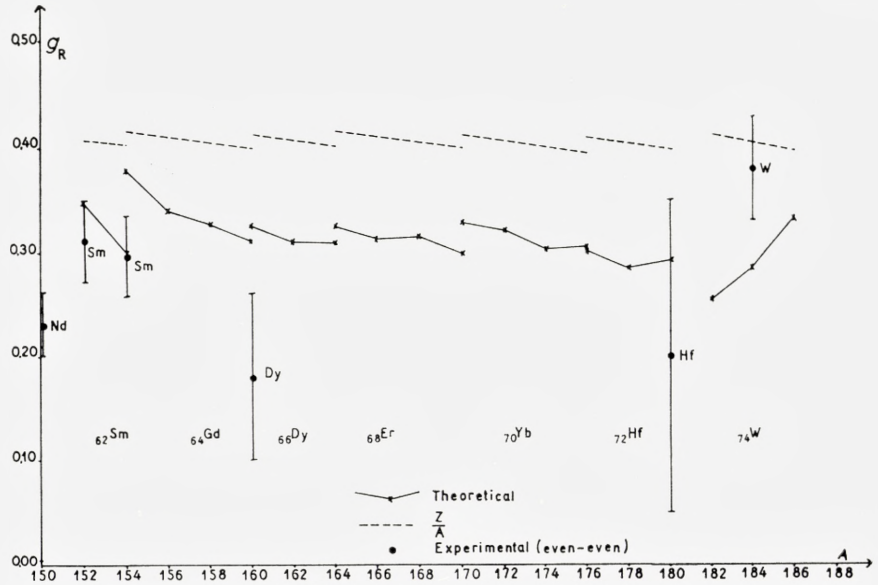


Fig. 26. *Collective gyromagnetic ratios of even-even nuclei in region I.* The theoretical values corresponding to the single-particle level scheme of "case B", $\Delta_n = P_n$, $\Delta_p = P_p$, and $R_0 = R_z = 1.2 \times 10^{-13}$ *f.*, are represented by the solid line. The measured $g_R$-values, with experimental errors as listed by BODENSTEDT[33], are exhibited for comparison. (The calculated values of $g_R$ corresponding to "case A", which can be found in table III b, show rather slight deviations from those of "case B".) Note added in proof: A recent measurement by BODENSTEDT et al. on $Er^{166}$ renders, with employment of the new $\langle r^{-3} \rangle$ values for 4 f electrons calculated by JUDD and LINDGREN (UCRL-9188, unpublished), a very accurate value of $g_R = 0.32 \pm 0.02$. This is in excellent agreement with the theoretical results. (Private communication from D. SHIRLEY.) Furthermore, a recent measurement by Stiening and Deutsch (Phys. Rev. Letters *6*, 421 (1961)) gives $g_R = 0.36 \pm 0.06$ for $Gd^{154}$.

Turning now to odd-A nuclei, many data are available from magnetic-moment measurements and $M1$ branching ratios within the ground-state rotational bands. From such information $g_R$ and $g_K$ may be determined. In the limit in which the Coriolis coupling (and furthermore the difference in $\Delta$ between the odd and the even nucleide) may be neglected, this $g_R$ is simply the same as that of the adjacent even-even nucleus. The effect of the Coriolis force, coupling the near-lying one-quasi-particle states, can now be accounted for in first approximation by a renormalization of $g_K$ and $g_R$ with respect to their adiabatic values[38]. An analysis of the experimental material in terms of the simple unperturbed formulae therefore yields the renormalized values $g'_R = g^\circ_R + \delta g_R$ and $g'_K = g^\circ_K + \delta g_K$, where

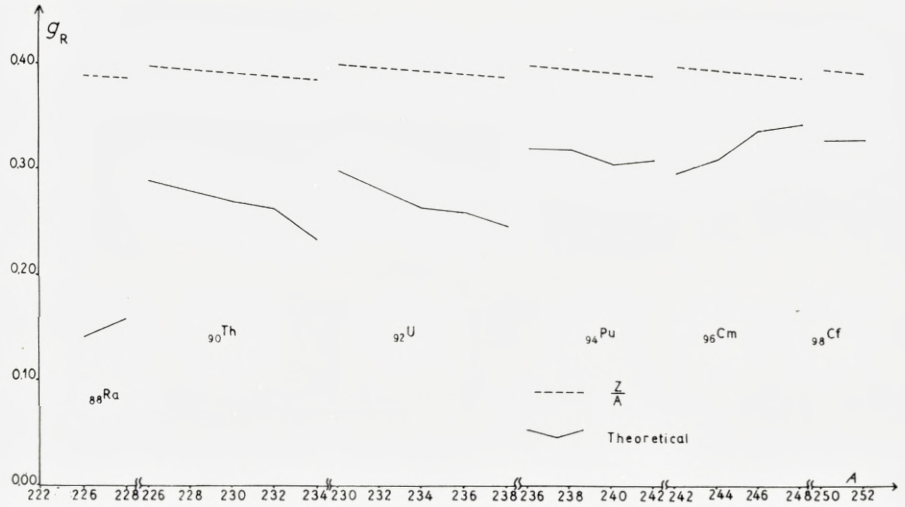


Fig. 27. *Collective gyromagnetic ratios of even-even nuclei in region II.* The theoretical values represented by the solid line correspond to the single-particle level scheme of "case B", and $\Delta_n = P_n$, $\Delta_p = P_p$. The dashed line represents the ratio $Z/A$ corresponding to "homogeneous flow".

$$\delta g_R(\nu) = \frac{\delta \Im^{(1)}(\nu)}{\Im}(g_l - g_R) + \frac{\delta W^{(1)}(\nu)}{\Im}(g_s - g_l). \tag{48}$$

In eq. (48) $\delta \Im^{(1)}$ is the contribution of the odd particle to the moment of inertia connecting the one-quasi-particle state $\nu$ with other states of the same kind. If the quasi-particle formulation is sufficiently accurate to estimate this difference, $\delta \Im^{(1)}(\nu)$ should be very nearly equal to the odd-even difference in moments of inertia[39]. Some of this difference, however, might be due to the effects of blocking. Blocking effects contributing to $\delta g_R$ may also be included in eq. (48) through $\delta \Im^{(1)}$. Similarly, $\delta W^{(1)}(\nu)$ is the contribution to the expression $W$ of the odd particle occupying the orbital $\nu$.

Now $\delta \Im^{(1)}$ is always a positive quantity. This is normally the case also with $\delta W^{(1)}$. As the first term always dominates, in all cases of practical interest $\delta g_R$ is positive for protons ($g_l = 1$, $g_s = 5.56$) and negative for neutrons ($g_l = 0$, $g_s = -3.83$). Indeed, in their analysis of the empirical values of $g_R$ and $g_K$ for odd-A nuclei BERNSTEIN and DE BOER[40] find values of $g_R$ for odd-N nuclei on the average 0.1 magneton lower than those for the odd-Z nuclei. This is qualitatively in agreement with (48). One might now attempt to apply (48) as a correction to the values found by the straightforward analysis, in order to obtain the unperturbed values $g_R^0$. If one inserts

in this formula for $\delta\mathfrak{I}^{(1)}$ the empirical odd-even differences in the moment of inertia and estimates the somewhat smaller second term by its "asymptotic" expression[15], one usually finds too large corrections $\delta g_R$. Now, the spin matrix elements empirically turn out to be systematically much smaller (about 50 %) than those calculated from the single-particle wave functions. This is evidenced e. g. by the plots of magnetic moments (theoretical and experimental) exhibited in ref. 16. This reduction may be explained in terms of the spin polarization effect[41] whereby e. g. in the case of an odd proton the spin-dependent part of the two-nucleon interaction tends to align the spins of the neutrons parallel to, and the spins of the other protons antiparallel to, the direction of the odd-proton spin. This polarization then effectively diminishes the magnetic dipole strength. Even with a 50 % reduction of the latter term the correction factor $\delta g_R$ still appears somewhat too large. In view of the uncertainty of the correction $\delta g_R$, clearly one cannot point to a definite disagreement with the theoretical $g_R$-values. One might tentatively say, however, that the experimental $g_R$-values are on the whole 10-20 % smaller than the calculated ones[42].

## Acknowledgements

In this work we have profited greatly by valuable suggestions and generous advice from Professors A. Bohr and B. Mottelson, and by discussions with other members of the Copenhagen group. We are deeply indebted to Professor C. E. Fröberg and Mr. J. Bohman of the Institute of Numerical Analysis in Lund for working out the large computational programme for SMIL. It is a pleasure for us to acknowledge the excellent working conditions of the Institute of Theoretical Physics in Lund and of NORDITA – Nordisk Institut for Teoretisk Atomfysik – in Copenhagen. We are also grateful to NORDITA and the Swedish Council for Atomic Research for financial support.

*NORDITA, Copenhagen, and*
*The Institute of Theoretical Physics,*
*The University of Lund, Sweden*

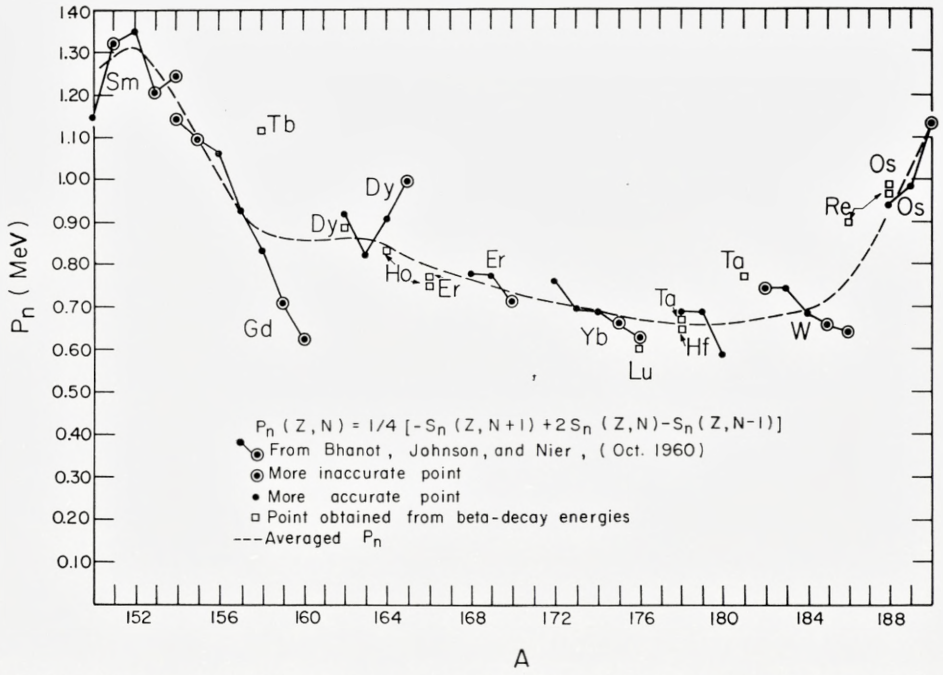


Fig. 28 (added in proof). Represents a revision of fig. 1 by the inclusion of recently published (Oct. 1960) mass-spectroscopic data, ref. 30.

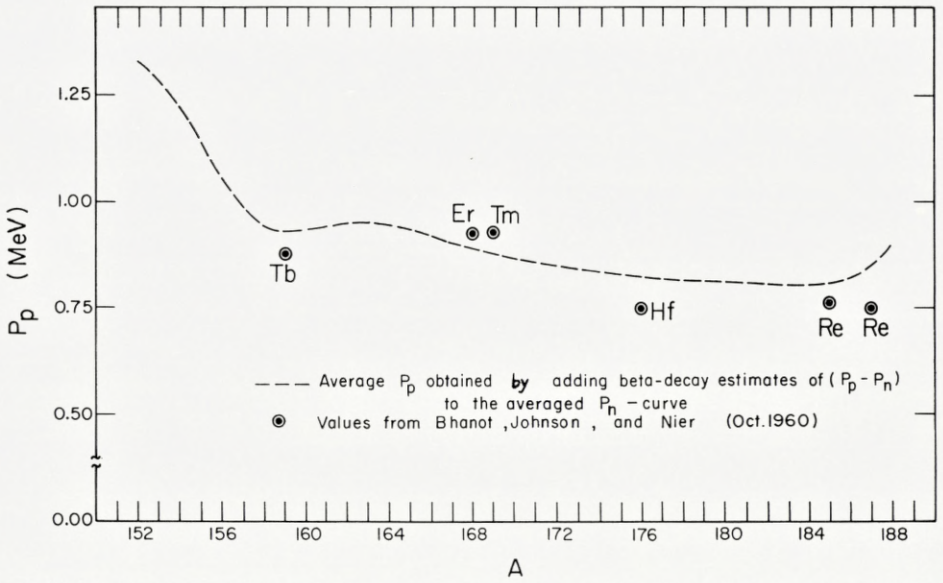


Fig. 29 (added in proof). Empirical values of $(P_p - P_n)$ are added to the averaged $P_n$-function of fig. 28 in obtaining the dashed curve of this figure. The latter curve may then be compared with the six points of the figure which are based directly on masses of isotones as listed in ref. 30.

# Appendix I

## On the Quasi-Particle Approximation

The calculations reported in the main text rest on various approximations leading up to the simple quasi-particle formulation employed. We will start the discussion from the Hamiltonian (7) as given, including its diagonal parts. The trial wave function (11) and, analogously, the canonical transformation (19) introduce a non-conservation in the number of particles, leading to wave functions describing an ensemble of nuclei rather than a specific nucleide. Some problems, in particular the occurrence of spurious states, are associated with the resulting fluctuations in the number of particles. We will defer till later a few remarks on the relevance of these fluctuations to our present problems. First we will discuss the various approximations of relative magnitude $\frac{G}{2\Delta}$ that have to do with the neglect of $H'_{\text{int}}$ etc.

The Hamiltonian (7) after the canonical transformation (19a, b) takes the form (20). Of interest here are the explicit expressions of the $H'_{\text{int}}$-terms $H'_{22}$, $H'_{31}$ and $H'_{40}$. These have all been listed by BELYAEV[6], but we give them here for the sake of completeness and in a form that is particularly simple as we have limited ourselves to the case of a constant matrix element $G$.

We first consider the problem of odd-even mass differences. The ground state of the odd system is affected by $H'_{31}$ in contrast to the even ground state. This interaction is of the form

$$H'_{31} = G \sum_{\nu} (u_\nu^2 - v_\nu^2)\, \alpha_\nu^+ \beta_\nu^+ \sum_{\nu'} u_{\nu'} v_{\nu'} (\alpha_{\nu'}^+ \alpha_{\nu'} + \beta_{\nu'}^+ \beta_{\nu'}) + \text{c. c.} \qquad \text{(A I-1)}$$

The effect of $H'_{31}$ on a one-quasi-particle state is therefore

$$H'_{31}\, \alpha_{\nu'}^+ \mid 0 \rangle = + G \sum_{\nu} (u_\nu^2 - v_\nu^2)\, u_{\nu'} v_{\nu'}\, \alpha_\nu^+ \beta_\nu^+ \alpha_{\nu'}^+ \mid 0 \rangle . \qquad \text{(A I-2)}$$

The depression $-\delta E^{(1)}$ of the ground state $\nu'$ due to $H'_{31}$ is given in lowest-order perturbation theory by

$$\delta E^{(1)}(H'_{31}) \simeq \quad G^2 \frac{1}{8} \sum_{\nu}{}' \frac{1}{E_\nu} \left(1 - \frac{\Delta^2}{E_\nu^2}\right). \qquad \text{(A I-3)}$$

Using (18), one easily obtains an upper limit to $\delta E^{(1)}$:

$$\delta E^{(1)}(H'_{31}) \leq \frac{G}{4}. \qquad \text{(A I-4)}$$

This perturbation estimate is actually rather accurate as the close-lying lower levels have small matrix elements because of the factor $(u_\nu^2 - v_\nu^2)$. We have computed (A I-3) numerically for some nuclei scattered over region I and have there obtained results between 50 and 80 % of the upper limit in (A I-4).

Furthermore, the $H'_{40}$-term is of the form

$$H'_{40} = G \sum_{\nu\nu''} u_\nu^2 \, v_{\nu''}^2 \, \alpha_\nu^+ \, \beta_\nu^+ \, \alpha_{\nu''}^+ \, \beta_{\nu''}^+ + \text{c. c.} \tag{A I-5}$$

This couples the quasi-particle vacuum with four-quasi-particle states and the one-quasi-particle state with five-quasi-particle states. In both cases $H'_{40}$ thus creates four new quasi-particles. Therefore, the first-order contribution is the same in the two cases within this formalism, except that in the second case the state $\nu'$, with which one quasi-particle is associated, is excluded in the sum. An estimate of the difference in depression due to $H'_{40}$ indicates that this energy difference is less than or of the order of $\frac{G}{4}$, i. e. a few tens of keV.

Furthermore, there is the effect of the neglect of the last term in eqs. (14), leading to the expressions (15) for $u_\nu$ and $v_\nu$, which approximation is also of the order $\frac{G}{2\Delta}$.

It is of course possible to take the neglected term in eqs. (14) into account in an approximate way by treating it as a perturbation. The modified form of the population parameter $v_\nu^2$ is then

$$\tilde{v}_\nu^2 = \frac{1}{2}\left(1 - \frac{\widetilde{(\varepsilon_\nu - \lambda)}}{\tilde{E}_\nu}\right), \tag{A I-6}$$

where

$$\widetilde{(\varepsilon_\nu - \lambda)} = (\varepsilon_\nu - \lambda_0)\left(1 + \frac{\mathring{G}}{2\mathring{E}_\nu}\right) \tag{A I-7}$$

and

$$\tilde{E}_\nu = \sqrt{\widetilde{(\varepsilon_\nu - \lambda)}^2 + \Delta^2}. \tag{A I-8}$$

The quantities of the unperturbed case, given by eqs. (15 a, b), (17) and (18), are denoted by an index zero in the relations above. Obviously, $v_\nu^2$ is not at all affected at $\varepsilon_\nu = \lambda_0$, and the correction also tends to zero for $|\varepsilon_\nu - \lambda_0|$ very large, while the largest correction occurs for $|\varepsilon_\nu - \lambda_0| \sim G$. On the assumption that the unperturbed solutions $\mathring{u}_\nu$ and $\mathring{v}_\nu$ fulfil (13) exactly, the perturbed

$u_\nu$ and $v_\nu$ given by (AI-6) correspond to a small error in the number of particles:

$$\delta n \simeq -\frac{\mathring{G}}{2} \Delta^2 \sum_\nu \frac{\varepsilon_\nu - \lambda_0}{\mathring{E}_\nu^4}, \tag{AI-9}$$

which error may easily be compensated for ad hoc.

Furthermore, in terms of this same approximation, the expression for $H'_{11}$ is simply

$$H'_{11} \simeq \sum_\nu \tilde{E}_\nu (\alpha_\nu^+ \alpha_\nu + \beta_\nu^+ \beta_\nu). \tag{AI-10}$$

Thus (AI-10) is formally identical with (24′) although the last terms of (14) and of (24) have been included to obtain (AI-10). The energy gap is still associated with the same $\Delta$. This $\Delta$, however, now corresponds to a somewhat different value of $G$ according to eq. (18), as $u_\nu$ and $v_\nu$ are slightly changed. It may also be pointed out that the modification of $v_\nu^2$ brought about by this perturbation method is largely equivalent to a small renormalization of $G$. The effect on the moment of inertia of the inclusion of the perturbation terms discussed may be studied in fig. 24.

As far as the odd-even mass differences are concerned, the total result of the effects discussed should normally not exceed an order of magnitude of 50 keV. There remain effects due to fluctuations in the number of particles (see below), and the effects of the change of the quasi-particle vacuum due to the blocking by the odd particle, discussed in the main text.

It may be appropriate in this connection to make a few comments on the two-quasi-particle states and the empirical energy gap in even-even nuclei. The $H'_{11}$-term gives an excess energy of the lowest two-quasi-particle states compared with that of the ground state:

$$\delta E^{(2)}(H'_{11}) = 2 E_\nu, \tag{AI-11}$$

which is just twice the uncorrected value of the odd-even mass difference. Most important among the neglected $H'_{\text{int}}$-terms is here probably $H'_{22}$, which we write out explicitly below:

$$\left.\begin{aligned} H'_{22} = -G \sum_\nu \sum_{\nu'} \{ &(u_\nu^2 u_{\nu'}^2 + v_\nu^2 v_{\nu'}^2) \alpha_\nu^+ \beta_\nu^+ \beta_{\nu'} \alpha_{\nu'} \\ &+ u_\nu v_\nu u_{\nu'} v_{\nu'} (\alpha_\nu^+ \alpha_{\nu'}^+ \alpha_{\nu'} \alpha_\nu + \beta_\nu^+ \beta_{\nu'}^+ \beta_{\nu'} \beta_\nu + 2 \alpha_{\nu'}^+ \beta_\nu^+ \beta_\nu \alpha_{\nu'}) \}. \end{aligned}\right\} \tag{AI-12}$$

It gives rise to matrix elements of the following type (we here denote the two-quasi-particle state* $\alpha_\nu^+ \beta_\nu^+ |0\rangle\rangle$ by $|\nu - \nu\rangle\rangle$):

* We here limit ourselves to two-quasi-particle states in which the two-quasi-particles refer to the same orbital $\nu$.

$$\langle\langle - \nu\nu \,|\, H'_{22} \,|\, \nu - \nu \rangle\rangle = - G \qquad \text{(A I-13)}$$

$$\langle\langle - \nu'\nu' \,|\, H'_{22} \,|\, \nu - \nu \rangle\rangle = - G(u_\nu^2 u_{\nu'}^2 + v_\nu^2 v_{\nu'}^2) \quad (\nu' \neq \nu). \qquad \text{(A I-14)}$$

There is thus first a negative diagonal element which is of the order of 5-10% of the energy gap in our case. Even more important, however, appears the effect of the non-diagonal matrix elements (A I-14) connecting the rather dense-lying two-quasi-particle states with one another. The factor $(u_\nu^2 u_{\nu'}^2 + v_\nu^2 v_{\nu'}^2)$ can also be written as $\frac{1}{2}\left(1 + \frac{(\varepsilon_\nu - \lambda)\,(\varepsilon_{\nu'} - \lambda)}{E_\nu\, E_{\nu'}}\right)$. It has a value close to 1/2 when $\varepsilon_\nu$ and $\varepsilon_{\nu'}$ refer to single-particle levels near the Fermi surface, as one would expect to be the case with the lowest-lying two-quasi-particle states. Thus the factor containing $u$ and $v$ causes no considerable reduction in the matrix elements. Furthermore, there are a number of states that are rather close-lying. The effect of the $H'_{22}$ terms therefore at first sight appears disastrous to the whole concept of the energy gap; in fact it is very largely spurious, however. To illucidate this point it is useful to refer to the "degenerate model", where all the single-particle states $\varepsilon_\nu$ are degenerate in energy[5]. In this case all $u$:$s$ and $v$:$s$ are equal. Therefore, all off-diagonal matrix elements of $H'_{22}$ are equal, and their value lies between $\frac{G}{2}$ and $G$; let us call them $G\varkappa$, where $\varkappa$ depends on the shell-filling parameter $\frac{n}{\Omega}$:

$$\varkappa = 1 - \frac{n}{\Omega}\left(1 - \frac{1}{2}\frac{n}{\Omega}\right). \qquad \text{(A I-15)}$$

If we diagonalize the $H'_{22}$-matrix with respect to the two-quasi-particle states, we find that the state $\Psi_s = \sum_\nu \alpha_\nu^+ \beta_\nu^+ \,|\, 0 \rangle\rangle$ exhausts the strength of the matrix apart from what is associated with the difference between the terms (A I-13) and (A I-14). The contribution to the energy in the state $\Psi_s$ is $[-G - (\Omega - 1)\varkappa G]$. The depression due to the $H'_{22}$ interaction should thus amount to something of the order of half or more of the energy gap*. This state $\Psi_s$ is, however, just the lowest spurion occurring in the degenerate model, as is demonstrated by Bohr and Mottelson in ref. 5. Its occurrence as a BCS state is connected with the extra degree of freedom introduced through the ensemble of states having slightly different numbers of particles. In the non-degenerate case, to the extent to which there is an energy gap at all, there must be a certain number $\Omega'$ of states $\varepsilon_\nu$ lying within a distance $\Delta$ above and below $\lambda$.

* Indeed the exact inclusion of couplings in higher orders brings this state all the way down to the ground state[5] (communication from B. Mottelson).

The $K = 0$ quasi-particle states associated with these levels now all fall densely above the energy gap. In between them, all matrix elements given by eq. (A I-14) are roughly constant. With respect to these states we have a matrix representation of $H'_{22}$ of the same type as that with respect to the $\Omega$ two-quasi-particle states in the degenerate case. The state that absorbs most of the strength of the coupling of $H'_{22}$ between the near-lying two-quasi-particle states is largely spurious in analogy with the degenerate case.

There also remain to be discussed effects that have to do with the number of particles of the BCS wave function. The first effect, which is related to the variation in the *average* number of particles in the quasi-particle approximation, is of very small magnitude, and we include it only for the sake of completeness. The relative difference in the number of particles between a two-quasi-particle state $|\nu{-}\nu\rangle\rangle$ and the ground state is

$$\langle\langle\, \nu-\nu\,|N|-\nu\nu\,\rangle\rangle-\langle\langle\, 0\,|N|\,0\,\rangle\rangle = 2(u_\nu^2 - v_\nu^2) = 2\,\frac{\varepsilon_\nu - \lambda}{E_\nu}. \qquad \text{(A I-16)}$$

Similarly, comparing the ground state of an odd-A nucleus with the even-even nucleide corresponding to the vacuum state, one obtains for the difference in the average number of particles

$$\langle\langle\, \nu\,|N|\,\nu\,\rangle\rangle-\langle\langle\, 0\,|N|\,0\,\rangle\rangle = u_\nu^2 - v_\nu^2. \qquad \text{(A I-17)}$$

Provided $\varepsilon_\nu$ lies near the Fermi surface, as is the case for the ground odd-A state and the lowest excited even-even state, the deviation $\delta n$ is rather small*. Now the solutions of $H' = H - \lambda N$ are stationary with respect to variations in the number of particles. That is to say, the quasi-particle solution corrects for the error in the number of particles $\delta n$ by subtraction of an energy $\delta n \times \lambda_0$, where $\lambda_0$ refers to the quasi-particle vacuum. However, a small increase in the number of particles raises $\lambda$ by $\dfrac{d\lambda}{dn} \times \delta n$. A good estimate of the error due to this effect should be

$$\delta E^{(1)}(\delta n) = \pm\,\frac{1}{2}\,\frac{d\lambda}{dn}\,(\delta n)^2, \qquad \text{(A I-18)}$$

where the plus sign corresponds to $\varepsilon_\nu < \lambda$ and the minus sign to $\varepsilon_\nu > \lambda$. In the cases treated in the present investigation the error from this source in

* It is thus apparent that in comparing odd-even mass differences of e. g. isotopes one should compare the odd-A nucleide with the average of the two adjacent even-even nucleides; this average is the appropriate quasi-particle vacuum in the odd-A case.

odd-even mass differences should be of the order of $\pm$ 5 keV. This effect obviously concerns also the energies of the two-quasi-particle states. The effect on the lower-lying excitations, according to eqs. (A I-16) and (A I-17), is twice that in the odd-A case, i. e. of the order of 10 keV. The higher-lying two-quasi-particle states are shifted by amounts of the order of a few hundred keV owing to this effect.

Furthermore there is an effect that is due to the fluctuations in the number of particles of the Bardeen wave functions. We introduce a mean square deviation defined by

$$\sigma_N^2 = \langle N^2 \rangle - \langle N \rangle^2. \tag{A I-19}$$

For the ground state we have

$$\langle\langle 0 | N^2 | 0 \rangle\rangle - \langle\langle 0 | N | 0 \rangle\rangle^2 = \sum_{\nu} 4\, u_\nu^2\, v_\nu^2. \tag{A I-20}$$

In the calculations performed for the regions of deformed nuclei a typical value of $\sigma_N$ is 3. The fluctuations are somewhat smaller for a one-quasi-particle state, where

$$\langle\langle \nu | N^2 | \nu \rangle\rangle - \langle\langle \nu | N | \nu \rangle\rangle^2 = \sum_{\nu \neq \nu'} 4\, u_\nu^2\, v_\nu^2, \tag{A I-21}$$

which for the odd-A ground state is smaller by about one than the expression (A I-20). In the actual cases this leads to a $\sigma_N$-value about 5 % smaller. The actual wave function thus corresponds to an ensemble of nucleides with slightly different numbers of particles. Thus, for instance, the BCS wave function corresponding to $U^{236}$ contains a very large fraction of $U^{234}$ and $U^{238}$ and also of $Th^{234}$ and $Pu^{238}$*. Now on the average the variation in the total energy of nucleides, as one moves between the shells, is expected to be somewhat concave upwards (at least if $\Delta_n$ and $\Delta_p$ are kept constant over the Bardeen ensemble). This effect in the Bardeen approximation would therefore cause a greater reduction of the binding energy of the state that displays the larger mean square deviation in the number of particles. An estimate of the influence this will have on the odd-even mass differences requires, however, a somewhat more detailed study of the parameters of the self-consistent field as functions of $N$ and $Z$.

* One would think that this effect would iron out in the theoretical results the rather detailed dependence on $Z$ and $N$ exhibited by the experimental moment of inertia. That this is not the case is due to the fact that the mixed-in components correspond to fictitious nuclei having all parameters except $\lambda$ in common with the $(Z_0 N_0)$-nucleus in question, such as $\Delta_n$, $\Delta_p$ and in particular the eccentricity parameter $\delta$. As the dependence of $\Im$ on $\lambda$ alone is weak, the fluctuations are therefore unimportant in this respect.

# Appendix II

## Single-Particle Matrix Elements of $j_x$

As pointed out in Appendix A of ref. 15, the interactions between the (spherical) harmonic oscillator shells $N$ and $N+2$ due to the quadrupole deformation of the potential can easily be taken into account if one first transforms to the slightly distorted coordinates $\xi \sim x\sqrt{\omega_x}$ etc. as defined in eq. (A5) of the reference cited. The wave function given in the tables of that reference should then be considered as expressed in these distorted coordinates, in terms of which we have

$$l_x = a\, l_x^t - b\, f_x^t, \tag{A II-1}$$

where

$$l_x^t = -i\left(\eta\frac{\partial}{\partial\zeta} - \zeta\frac{\partial}{\partial\eta}\right) \tag{A II-2}$$

and*

$$f_x^t = -i\left(\eta\frac{\partial}{\partial\zeta} + \zeta\frac{\partial}{\partial\eta}\right). \tag{A II-3}$$

A similar relation holds for the $y$-component, while

$$l_z = l_z^t.$$

The exact expressions for $a$ and $b$ are given in (A13) of ref. 15. The expansions up to the lowest order in $\delta$ are

$$a = 1 + \frac{1}{8}\delta^2 + \ldots \tag{A II-4}$$

$$b = \frac{1}{2}\delta + \ldots \tag{A II-5}$$

The operator $l_x^t$ now connects states only within the $N$-shell of these new coordinates, while $f_x^t$ connects the shells $N$ and $N+2$. This is most easily seen if we express $l_x^t$ and $f_x^t$ in terms of the operators $\Gamma_z$, $R$ and $S$ defined in ref. 43. Thus

$$l_+^t = \sqrt{2}\,[S\,\Gamma_z^* - R^*\,\Gamma_z] \tag{A II-6}$$

$$l_-^t = \sqrt{2}\,[S^*\,\Gamma_z - R\,\Gamma_z^*] \tag{A II-7}$$

* Such an operator $f_x$ is encountered e. g. in the theory of elasticity.

$$f_+ = \sqrt{2}\,[R^*\,\Gamma_z^* - S\,\Gamma_z] \tag{AII-8}$$

$$f_- = \sqrt{2}\,[R\,\Gamma_z - S^*\,\Gamma_z^*]\,. \tag{AII-9}$$

We have defined $f_+$ as $f_x - if_y$ and $f_-$ as $f_x + if_y$; $f_+$ is then associated with an increase in $\Lambda$ by one unit. The operator $\Gamma_z^*$ gives rise to an increase in $n_z$ by one unit, $R^*$ and $S^*$ both raise $n_\perp$ by one unit, but $R^*$ also raises $\Lambda$ by one unit while $S^*$ lowers $\Lambda$ by one unit. From these relations it is obvious that $\vec{l}^t$ connects states with the same $N$ while $\vec{f}^t$ has elements only between states with $N$ values different by two. The matrix elements in the asymptotic representation are also trivially obtained from these relations.

In evaluating the contribution from $\vec{l}^t$ to the moment of inertia it proved essential, however, to employ the exact wave functions of ref. 15, as is discussed in the main text.

On the basis of eq. (AII-1) one may write the expression for the moment of inertia in the form

$$\Im = \mathring{\Im}\,(1 + \frac{1}{4}\,\delta^2) + \Im_f\,, \tag{AII-10}$$

where $\mathring{\Im}$ is the moment of inertia obtained when the coupling of the quadrupole part of the nuclear potential between the shells $N$ and $N+2$ is neglected. The term $\Im_f$ represents solely the contribution of the term $\vec{f}^t$ in (AII-1). It only amounts to about 5 % of the whole moment of inertia. As the states connected by $\vec{f}^t$ lie two shells apart, the pairing effects are negligible. The detailed level order within the shells is also unimportant for an estimate of this small correction term. In the case of a pure-harmonic-oscillator model one finds

$$\Im_f = \frac{1}{4}\,\delta^2\,\Im_{\mathrm{rig}} = \frac{1}{4}\,\Im_{\mathrm{irrot}}\,. \tag{AII-11}$$

In addition, the effect of the coupling between the shells is manifested in the correction term $\frac{1}{4}\,\delta^2\,\mathring{\Im}$. This term is associated with the extra nodes in the wave functions of one shell that are due to this coupling; it is smaller than $\Im_f$ by a factor $\dfrac{\Im}{\Im_{\mathrm{rig}}}$.

## List of References


(1) D. R. Inglis, Phys. Rev. **96**, 1059 (1954); **97**, 701 (1955).
(2) A. Bohr, B. R. Mottelson, Mat. Fys. Medd. Dan. Vid. Selsk. **30**, no. 1 (1955).
(3) B. R. Mottelson, Nordita Publ. no. 20 (1959); Cours de l'Ecole d'Eté de Physique Théorique des Houches (Dunod, Paris, 1959).
(4) Bohr, Mottelson and Pines, Phys. Rev. **110**, 936 (1958).
(5) A. Bohr and B. R. Mottelson, to be published.
(6) S. T. Belyaev, Mat. Fys. Medd. Dan. Vid. Selsk. **31**, no. 11 (1959).
(7) V. G. Soloviev, J. Exp. Theor. Phys. USSR **35**, 823 (1958); Nucl. Phys. **9**, 655 (1958/59).
(8) Bardeen, Cooper and Schrieffer, Phys. Rev. **108**, 1175 (1957).
N. N. Bogolyubov, J. Exp. Theor. Phys. USSR **34**, 58 and 73 (1958); Nuovo Cimento **7**, 794 (1958);
J. G. Valatin, Nuovo Cimento **7**, 843 (1958).
(9) J. J. Griffin and M. Rich, Phys. Rev. Letters **3**, 342 (1959) and Phys. Rev. **118**, 850 (1960).
(10) A. B. Migdal, Nucl. Phys. **13**, 655 (1959); Exp. Theor. Phys. USSR **37**, 249 (1959).
(11) H. Hackenbroich (1960), to be published.
(12) S. G. Nilsson and O. Prior, Report at the Conference of the Swedish Phys. Soc., Stockholm, 1959, Ark. Fys. **16**, 541 (1960).
(13) E. U. Condon and G. H. Shortley, *The Theory of Atomic Spectra* (Cambr. Univ. Press, London, 1935).
(14) A. R. Edmonds, *Angular Momentum in Quantum Mechanics* (Princeton Univ. Press, Princeton, New Jersey, 1957).
(15) S. G. Nilsson, Mat. Fys. Medd. Dan. Vid. Selsk. **29**, no. 16 (1955); cf. the parallel work by K. Gottfried, Phys. Rev. **103**, 1017 (1956).
(16) B. R. Mottelson and S. G. Nilsson, Mat. Fys. Skr. Dan. Vid. Selsk. **1**, no. 8 (1959); cf. the parallel investigation by Stephens, Asaro and Perlman, Phys. Rev. **113**, 212 (1959).
(17) B. F. Bayman, Nucl. Phys. **15**, 33 (1959).
(18) V. G. Soloviev, Report D-545, Dubna, USSR (1960).
(19) Elbek, Olesen and Skilbreid, Nucl. Phys., in the press, and private communication.
(20) Bell, Bjørnholm and Severiens, Mat. Fys. Medd. Dan. Vid. Selsk. **32**, no. 12 (1960).
(21) D. G. Ravenhall, Revs. Mod. Phys. **30**, 430 (1958).
(22) Z. L. Szymanski and D. Bés, to be published.

(23) L. S. KISSLINGER and R. A. SORENSEN, Mat. Fys. Medd. Dan. Vid. Selsk., **32**, no. 9 (1960).
(23a) J. BRO-JØRGENSEN and A. HAATUFT, private communication.
(24) C. GALLAGHER, private communication.
(25) W. H. JOHNSON and V. B. BHANOT, Phys. Rev. **107**, 1669 (1957).
(26) B. M. FOREMAN and G. T. SEABORG, J. Inorg. Nucl. Chem. **7**, 305 (1958).
(27) B. A. KRAVTSOV, J. Exp. Theor. Phys. USSR **36**, 1224 (1959); cf. Akad. Nauk USSR **65**, 461 (1958).
(28) Cf. A. H. WAPSTRA, *Handb. d. Physik* XXXVIII/I (Springer Verlag, Berlin, Göttingen and Heidelberg, 1958).
(29) Nuclear Data Sheets, published by the National Bureau of Standards, Washington, U.S.A.
(30) BHANOT, JOHNSON and NIER, Phys. Rev. **120**, 235 (1960).
(31) EVERLING, KÖNIG, MATTAUCH and WAPSTRA, Nucl. Phys. **18**, 529 (1960).
(32) R. E. PRANGE, private communication.
(33) E. BODENSTEDT, to be published.
(34) G. GOLDRING and R. P. SCHARENBERG, Phys. Rev. **110**, 701 (1958).
(35) J. KANAMORI and K. SUGIMOTO, J. Phys. Soc. Japan **13**, 754 (1958).
(36) G. SÜSSMAN, to be published.
(37) BODENSTEDT, MATHIAS, KÖRNER, GERDAU, FRISIUS, and HOVESTADT, to be published; G. MANNING and J. D. ROGERS, Nucl. Phys. **15**, 166 (1960).
(38) A. KERMAN, Mat. Fys. Medd. Dan. Vid. Selsk. **30**, no. 15 (1956).
(39) O. PRIOR, Ark. Fysik, **14**, 451 (1959).
(40) J. BERNSTEIN and J. DE BOER, Nucl. Phys., **18**, 40 (1960).
(41) B. R. MOTTELSON, *Selected Topics in the Theory of Collective Phenomena in Nuclei*, Internat. School of Phys., Varenna (1960).
(42) J. DE BOER, private communication.
(43) B. R. MOTTELSON and S. G. NILSSON, Nucl. Phys. **13**, 281 (1959).
(44) STROMINGER, HOLLANDER and SEABORG, Revs. Mod. Phys. **30**, 585 (1958).
(45) MARKLUND, VAN NOIJEN and GRABOVSKI, Nucl. Phys. **15**, 533 (1960).
(46) J. M. HOLLANDER, Phys. Rev. **103**, 1591 (1956).

Indleveret til Selskabet den 16. september 1960.
Færdig fra trykkeriet den 22. marts 1961.